Karl-Heinz Witte, Wolfgang Engelmann, Anders Johnsson

Models for biological rhythms (with Scilab/Xcos)

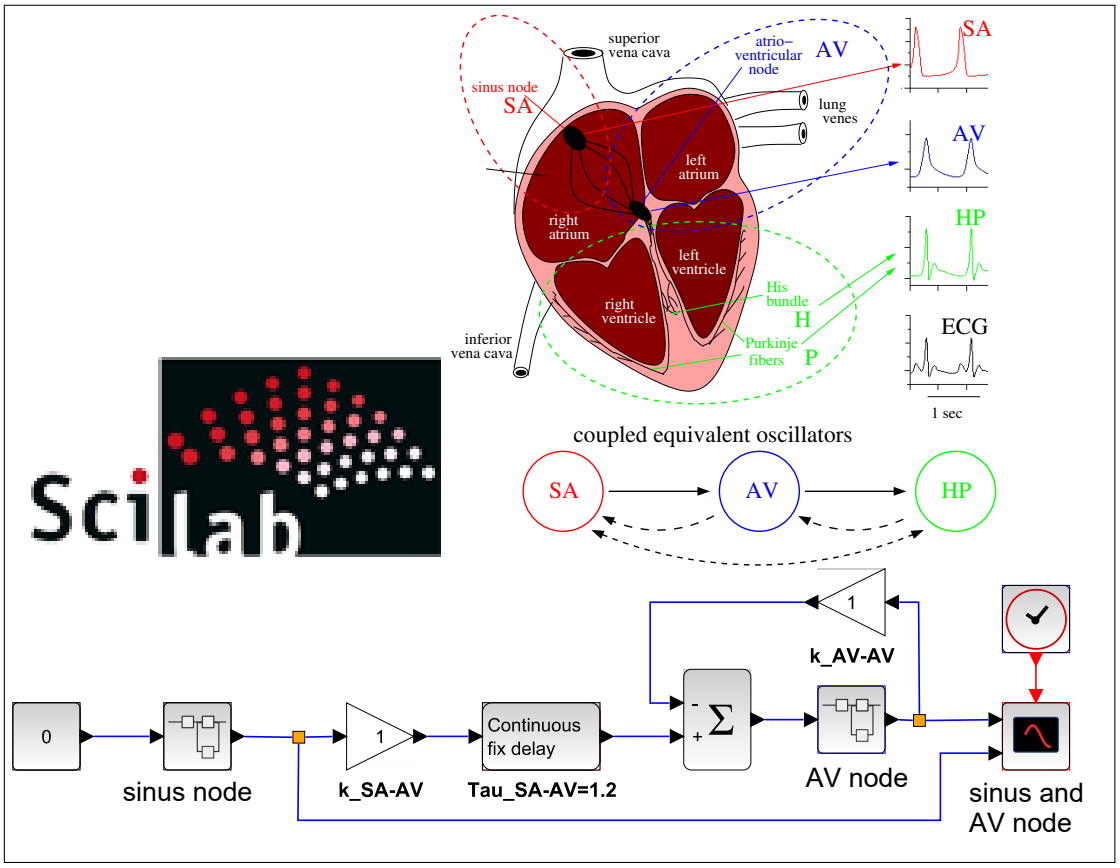

The water in a jug is sparkling; the water in the sea is dark. The small truth has words that are clear; the great truth has great silence.

Rabindranath Tagore

Models for biological rhythms (with Scilab/Xcos)

Karl-Heinz Witte, Wolfgang Engelmann(†)
and Anders Johnsson

Oct 25, 2025

Hochschule RheinMain, Universität Tübingen and Norwegian
University of Science and Technology

In memory of our Co-author, long-time friend and colleague Wolfgang Engelmann, who passed away suddenly and unexpected on 1 July 2023 and dedicated his life to research on biological rhythms

Contents

List of Figures

List of Tables

Listings

Preface

Recently one of the authors, Karl-Heinz Witte, a physicist with much experience in modelling, and Wolfgang Engelmann, a biologist who worked on circadian and other rhythms in organisms, wrote a book entitled “How to stop a biological clock: Point of singularity" (Engelmann-Witte-2021). It contained also in a newer version a chapter on models. It turned out, however, that the methods and the content of the book would overload the scope of that book. So we decided, to concentrate on models and experimental results of biological rhythms in a separate book. Anders Johnsson joined us. He worked in Biophysics and on biological rhythms at the Department of Physics, University of Trondheim in Norway.

The authors were teaching and researching at universities and have been active in the field for many years. We had thus intensive contact with colleagues and students who were eager to learn about this research field. We thankfully appreciate all knowledge we acquired in this interaction with persons around us[1] in the preparation of the book (see acknowledgements on page 289).

After having retired we thought it might be helpful for those students who are interested in both, the field of biological rhythms as well as the way of modelling oscillations, if we wrote a book about this interdisciplinary field. We included in the title of the book also the name of the program for performing the model building, indicating, that we want the reader to learn also methods of constructing models in an understandable way. We have chosen the program *Scilab* which is not difficult to learn and which is free of charge.

Besides conveying the experience of our engagement with the topic we also have compiled literature which should review the more recent development of modelling in the field.

The book is intended for readers, who want to know more about biological rhythms, what they are and what they are for, how they can be described and modelled, and how one might gain perhaps a deeper knowledge of the mechanisms. However, the interested reader will certainly pose new questions concerning it - since nature will never be understood completely!

We hope, the book finds interested readers for the field of biological rhythms and for the way of modelling them. The importance of this field and of circadian rhythms has been attested by the Nobel Prize in Physiology or Medicine in 2017 given to three researchers in this field (see Nobel Price 2017 and Young 2018).

In Chap. 1 (Introduction) the aims of the book and the structure of its contents are outlined.

[1] among others also two User Groups

1 Introduction: Biological rhythms

The rapidly growing research field between the life sciences and mathematics/informatics is attracting professional researchers as well as students. Building models of nature and simulating them on more and more advanced data machines provides a rich area for multidisciplinary learning and research in many fields.

When we use the concept of 'model' we think of a mathematical - theoretical models, represented by equations, block schemes etc. Sometimes an alternative meaning can be used - in biology/physiology, where for instance Guinea pigs are used as animal models for studying human deseases or physiology.

In the present book we focus on the field of *rhythmic processes* in life sciences and *models* for these processes. The rhythms will be of quite different character, but the general interest for so called biological clocks will be emphasised. The periods of these "clocks" can be about 24 h. However, another main topic in this book will be more rapid rhythms, e.g. the heart rhythm with its period in the second regime. Furthermore rhythms with longer periods (annual rhythms, predator-prey rhythms) will be discussed.

We hope, that presenting models of these biological rhythms can lead to a greater understanding of the systems and that the reader can deduce useful new experimental approaches. An indispensable part of rhythm modelling is the simulation of the models (see Chap. 6) and the comparison with experimental results. We will work with the simulation tool Scilab, which is simple to install and learn (see Chap. 5).

The structure of the book can be presented by giving a short overview of the various chapters and some of their sections. After this introduction we will present in Chap. 2 examples illustrating the diversity of rhythms such as circadian rhythms, i.e. rhythms with period length in the 24 h range (see Sect. 2.2). As will be demonstrated in subsection 2.2.1, circadian rhythms are among others a tool for survival (subsection 2.2.2), and the timing device for using the daylength to induce physiological processes such as flowering and other events to occur at certain seasons (subsection 2.2.3). In Chap. 2 are also more rapid rhythms presented (Sect. 2.3: The heart beat of mammals (subsection 2.3.1), the lateral leaf movements of the *Indian telegraph plant* (subsection 2.3.2), rotating growth movements in plants, often with periods of the order of 1 h (subsection 2.3.3), and rhythms in glycolysis (subsection 2.3.4); finally chemical oscillators, often with periods of the order of seconds, are described in subsection 2.3.5.

The stability of the various rhythms should also be mentioned. On the one hand, this relates to the dependence on their own parameters and, on the other, the influence of external factors. Chap.3 will therefore describe the stability of the rhythms with regard to temperature fluctuations, external disturbances and coupling between similar individual oscillators.

Rhythms and their orchestration in humans are so important in our view, that we have a special Chap. 4 for it. It is shown, that circadian rhythms are significant for humans and some elementary models for them are presented (Sect. 4.1; more models are found in later sections).

subsection 3 of this Chap. are about adaptation of the rhythms to different light-dark schemes and misalignment in humans, Sect. 4.2 treats the consequences for jet-lag, shift work and social jet-lag, Sect. 4.3 is about the best school time, chronotypes and daylight saving time. We discuss furthermore in Sect. 4.4 sleep models, metabolism, and medical aspects.

In the Chap. 5 we are dealing with basics of modelling in several sections. We start in Sect. 5.1 which introduce the use of Scilab to simulate models Why and how models are used is treated in Sect. 5.2, what kind of models exist in Sect. 5.3), general properties in modelling systems are explained in Sect. 5.4, and the way networks are deduced from differential equation is described in 5.5. The chapter ends with the description of various feedback models and of the properties of nonlinear nets (Sect. 5.6 with several subsections).

Chap. 6 contains an extended look at modelling and simulation of rhythms with a Sect. 6.1 on shifting circadian rhythms by external perturbations leading to phase shifts, a Sect. 6.2 discussing generally how circadian rhythms are entrained (also treated more specifically later) e.g. by external LD cycles (which might also be somewhat shorter or longer as 24 h).

In other subchapters of Chap. (6) some oscillator properties of special interest are presented, namely the possibility of stopping an oscillator by using a special treatment (Sect. 6.3.1) and temperature robustness of the period of circadian rhythms in Sect. 6.4.

There are of course quite a number of models for rhythms described in the literature, and some of them will be presented in Chap. 7, emphasising overall system models. This chapter ends with a subsection, in which rhythms in the heart are modelled and the topic is extended in relation to an earlier section.

Another important aspect is treated in Chap. 8 and deals with coupled cells/oscillators and modelling of multi-oscillatory systems. Several examples are given: The guard cells in plants control rhythmic transpiration through openings (stomata) in the leaves (subsection 3.3.2), rotation and rhythmic growth is often found in shoots and roots of plants and models for them are presented (see Sec. 2.3.3). In this chapter it is asked, whether we can model such very diverse rhythms and oscillators and we will look at system properties such as lumped models vs. multicellular models.

In Section 9.3tests of and predictions from models are mentioned. Results from some models which test arrhythmicity, splitting etc are referred to and it is stressed again, that both lumped models and multi-oscillator models are useful. Chaos theory and other new approaches in the modelling of biological rhythms are examples. The molecular mechanisms of biological rhythms and their genetic background should not be forgotten (see.9.3Chap.). We hope, that the reader will appreciate this exciting and vivid area of rhythm research.

The Appendices (see Chap. 9) contain extensions from earlier chapters with, e.g. algorithms, and a playground (9.1), where several models from the literature are proposed for exercises. Examples are the predator-prey model, how a Siberian hamster looses its circadian rhythm, the effect of compact light pulses and flashes, a simple simulation of coupled oscillators based on the Pavlidis model (Bergman, Johnsson, Karlsson 1973). Scilab examples used in the book allow you to run and play them and also extend and vary them.

2 Examples and observations of biological rhythms

Biological rhythms are found in all forms of life and at various levels of organisation such as cells, tissues, organs, organisms, populations. If we restrict us to examples of circadian rhythms, they were found in prokaryots such as bacteria (Eelderink-Chen et al. 2021) and cyanobacteria (Johnson, Mori, Xu 2008), in unicellular algae (e.g. cell division of *Euglena* (Malinowski, Laval-Martin, Edmunds 1985), in the phototactic behaviour (i.e. light induced movement) of the green alga *Chlamydomonas*, in the glow rhythm of *Lingulodinium polyedrum*, in plants (see e.g. Section 2.3.3), in fungi (see the paragraph on page 44), and in animals (see e.g. subsection 2.2.2).

Oscillations exist in tissues and organs, for instance in the human heart (see subsection 2.3.1). Other examples are the movement of the lateral leaflets in the telegraph plant (see page 2.1 and subsection 2.3.2), furthermore the so called circumnutation (rhythmic pendular or circular growth of plant seedlings, see subsection 2.3.3 and in more detail in subsection 3.3.4), the electric activity of an eye nerve in a marine snail (page 26 in subsection 2.2.4) dealing with circadian rhythms in the eye.

Circadian rhythms are also important for humans, as mentioned before, in fact so important that we have a special Chap. 4 for it.

2.1 Types of rhythms

There are many kinds of rhythms in organisms. In this book we will focus mainly on *circadian rhythms*, but mention also rhythms with shorter periods called *ultradian rhythms* (subsections 2.3.2, 2.3.3, 3.3.2. We furthermore refer to work on an *annual rhythm* in a beetle (see page 49).

Let's begin with a remarkable example, the Telegraph plant *Codariocalyx motorium*[1]. In many plants the leaves can move rhythmically in such a way, that they are positioned horizontally during the day and vertically during the night (see How plants grow and move). This is caused either by an alternating growth of the upper and the lower side of the leaf during different times of the day or by a special join (so called *pulvinus*).

In the case of the Telegraph plant a leaf consists of a larger terminal leaflet and two smaller lateral leaflets. The terminal leaflet moves up for the day and down for the night. The lateral leaflets show a fast *ultradian* rhythm with a period length in the minute range (see Fig. 2.1 and How plants grow and move). These movements arise due to water driven volume changes in the tissue of the pulvini (indicated by heavy black areas situated at the base of the leaves in figure 2.1. For more details see subsection 2.3.2.

[1] earlier name *Desmodium gyrans*

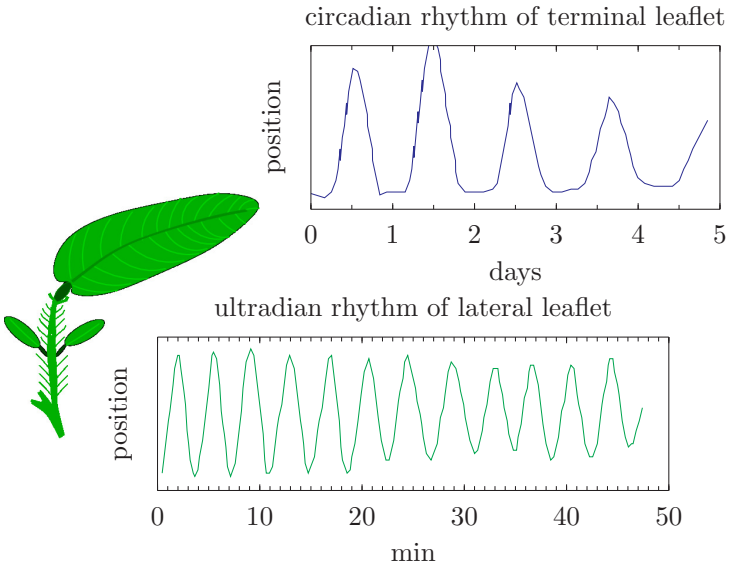

Figure 2.1: *To the left: A schematic drawing of a leaf of* Codariocalyx *with the larger terminal leaflet and two smaller lateral leaflets below it (joints dark green). To the right: The upper curve shows a diagram of the circadian up- and down movement of the terminal leaflet (x-axis days), and the lower curve a diagram of the movement of one of the two lateral leaflets (x-axis: min)*

2.2 Circadian rhythms: What they are for and how they might have evolved

In this section we try to answer the question, why (and how) circadian rhythms evolved during the evolution of life on earth. The adaptive value of a circadian rhythm is considerable. They enable organisms to prepare for changes in the daily light and temperature conditions thus adjusting better to the 24 h time structure of the environment. Circadian rhythms are the basis of *photoperiodic* timing where the light/darkness relation assures that growth, development, reproduction, dormancy and many more events occur at the appropriate time of the year (see for an example subsect. 2.2.3).

We will discuss a few examples, namely the circadian clock of *Cyanobacteria* as a molecular tool for survival (see subsect. 2.2.1), the eclosion rhythm of the fruit fly *Drosophila pseudoobscura* out of the pupal case (see subsect. 2.2.2), the photoperiodic reaction and the petal movement of the flaming Katy *Kalanchoë blossfeldiana* (see subsect. 2.2.3), and the circadian rhythm observed in eyes (see subsect. 2.2.4) with a special look at the compound action potentials in the eye nerve of marine snails (subsect. 2.2.4). We mention also an interesting case of a plasmodial rhizopod *Thalassomyxa australis* found at a beach in Australia, which could illustrate how circadian rhythms might have evolved (see subsect. 2.2.5).

2.2.1 The circadian clock of Cyanobacteria, a tool for survival

Even if we focus on circadian rhythms in higher organisms in this book, it is proper the mention rhythmic oscillations also in more 'primitive' organisms (like bacteria). Until the mid-1980s, it was common thought that only cells with nuclei had circadian rhythms. But it was later found that e.g. cyanobacteria (a phylum of photosynthetic eubacteria) have well-documented circadian rhythms (see e.g. review Johnson, Mori, Xu 2008). Temperature robustness was also documented (e.g. Onai K, K, M 2004).

These bacteria are prokaryots - i.e. lack nuclei (see Prokaryots) They are almost ideal organisms to study the mechanism of circadian control systems and to understand the advantage of possessing such a clock, because they are smaller, constructed more simple and the metabolism is much less complicated when compared to that of the eukaryots. There is only one ring-like chromosome and the genome is smaller. The regulation of transcription and translation is simpler and better known as is the case in eukaryots. The most often discussed models for biological clocks, valid for Drosophila, humans and higher organisms (see chapter 3) rely heavily on the molecular mechanisms in the nuclei.

Many laboratories study *Cyanobacteria* with molecular biological methods. The smaller genome allows to use saturating mutagenesis of those genes, which are necessary for the function of the circadian clock (Mackey, Golden 2007). Furthermore, in the meantime the genome of some cyanobacteria has been sequenced completely (Hess 2011).

The species *Synechococcus elongatus* and its strain PCC 7942 has been used for numerous studies, and many mutants which differ in their clock properties are available (Golden, Ishiura, Kondo 1997).

Since photosynthesis[2] and respiration[3] occur in the same cellular compartment (Mullineaux 2014), it must be ensured that these biochemically incompatible processes take turns at the right time (e.g. day/night, see Kim, Kaur et al. (2020)). That is taken care off by the circadian clock.

It was demonstrated in cultures of several *Synechococcus* mutants with different periods of their circadian clocks kept in LD cycles[4] which matched or did not match their periods, that the mutants with a period matching that of the LD had a better reproductive fitness and out competed the populations of other mutants that had different clock periods (Ouyang et al. 1998). This enhancement of fitness in the competition experiments was successfully simulated (Gonze, Roussel, Goldbeter 2002).

In the cyanobacteria three key proteins form a molecular clockwork mechanism. The protein structures have been determined, KaiA, KaiB, and KaiC. Deletion of any of the respective genes will result in arrhythmicity of the system. Kai BC complex and Kai A transcript are numerous. In the case of negative feedback regulation, Kai BC is repressed by overexpression of KaiC. This results in the elimination of the loss of rhythmicity.

By incubating *in vitro* a mixture of the three cyanobacterial proteins, KaiA, KaiB, and KaiC, and ATP Kondo and his colleagues reconstituted the robust circadian rhythm of the phosphorylation level of KaiC (Nakajima M et al. 2005). This finding indicates that protein-protein interactions and the associated hydrolysis of ATP suffice to generate the circadian rhythm. The in vitro

[2] the splitting of water by light to fix and store carbon
[3] the burning of the stored glycogen
[4] that is, cycles of, say 15:15 LD and thus with a period of 30 h

rhythm was even temperature stable, indicating that a temperature-compensation mechanism is encoded in the characteristics of the three Kai proteins and the nature of their interactions. We will come back to temperature compensation of period length or *period robustness* in a later chapter (Serct. 3.2). (see e.g. M. 2022)

We end this subchapter by emphasizing that in modern chronobiology there is a keen interest in the question of the evolutionary development of the biological rhythms (e.g. Bhadra U, MP 2017). In a later chapter (Sect. 3.3) we will come back to some evolutionary aspects in connection with discussion on temperature robustness of rhythms.

2.2.2 Eclosion rhythm in a fruitfly population

Rhythmic events can be observed also in populations[5]. Well studied is the eclosion rhythm of *Drosophila pseudoobscura* flies out of their pupal case (see in Engelmann: Flying clocks). This species lives in dry areas of the southern parts of the United States. In the last larval stage the insects crawl into the soil to a depth at which the time cues of the environment (daily LD, temperature differences, and humidity) are not felt any more. Here a pupal case is formed in which the metamorphosis takes place: The larva changes into the completely different structure of a fly.

It is of vital importance for the fly after eclosing from the puparium to arrive at the surface of the soil in the early morning when humidity is still high. This protects the fly from drying out before the cuticle has hardened. Since metamorphosis takes about seven days at 20°C, the time of eclosion must be precisely timed, since, as mentioned, no 24 h time cues are available for the fly in the soil. It is therefore not astonishing, that the circadian clock of this fruitfly species is almost exactly 24 h, independent of the soil temperature (see Sect. 3.2). For circadian rhythms this is unusual; their periods are usually close to, but not exactly 24 h. The flies eclose during early morning, but those flies, which were not yet developed, eclose in a time window on the next morning or on later days, until all flies have emerged.

We are here dealing with a rhythm, which can be observed only in populations, since each fly can eclose just once[6].

2.2.3 Photoperiodic induction and flower clock of the Flaming Katy *Kalanchoë*

The flaming Katy *Kalanchoë blossfeldiana* is a plant endemic to Madagascar. It belongs to the family of the *Crassulaceae*. The plants are found there in all warm, arid, rocky areas with long dry seasons. It flowers during the time of the year at which the days become shorter and the rainy season in Madagascar has ended.

This *short day plant* has been studied not only for its photoperiodic reaction, but also for the petal movement rhythm of the flowers[7]. They open in the morning and close in the evening. But even without an LD under a constant weak green light (which is for the flower like darkness)

[5] Another example for a population rhythm is the bioluminescence of *Lingulodinium polyedrum*, a dinoflagellate, since numerous individual cells are involved (see in Cellular Clocks and Roenneberg, Colfax, Hastings 1989; Roenneberg, Colfax, Hastings 1989). The rhythm can, however, also be observed in individual cells (Krasnow et al. 1981)

[6] Individual fruitflies do possess also circadian clocks, see Engelmann: Flying clocks

[7] which can be recorded even in flowers broken off from the inflorescence in a cuvette with sugar water.

and at constant temperature the rhythm continues; however, the period length is not any more exactly 24 h, but about 22 h. This shows, that an internal clock controls the petal movement (see Fig. 2.2).

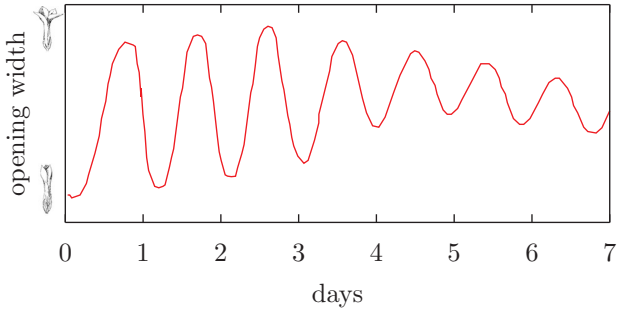

Figure 2.2: *Left:* Kalanchoë *flower closed (down, during the night) and open (up, during the day). Curve: The opening width of the flowers changes rhythmically after transferring the flowers from a 12:12 h LD into weak continues green light. The period is 22 h, indicating the control by a circadian clock*

Bünning (1936) had the idea, that a circadian clock measures the length of the day (or night) and allows the photoperiodic reaction to occur if the proper LD has been reached during the season. The ambient light has two functions: It entrains the circadian clock and, depending on the photoperiodic constellation of the season (long days or short days) and the photoperiodic situation of the organism (for instance long day plant/animal or short day plant/animal) induces the photoperiodic reaction, or not (see the book Bio-Calendar).

2.2.4 Rhythms in the eye

Circadian clocks belong to one of the most fascinating adaptations of creatures to the environment. The organisms can thus not only predict the day-night cycle, but also use it for measuring the daylength and thus determine the season. Since the period length is not exactly 24 h long, the clock has to be corrected each day by environmental signals (light, temperature). This entrainment (or phase-locking) by light is complicated by the fact, that the photoreceptors themselves are in many cases under circadian control (their transcription, feedback of the clock to inputs of the light, see Devlin (2002)).

To determine the season, the photoperiodic signals of the environment are transferred to the pineal organ in mammals, where they are decoded as melatonin secretion. Studies in mice mutants suggest, that two different molecular oscillators note the onset or the end respectively of the light period and use it for measuring the daylength and to inform the organism (Oster, Maronde, Albrecht 2002).

Circadian clocks have possibly evolved together with light perceiving molecules long before photoreceptor cells and eyes specialised. Structural homologies between those molecules, which are the component parts of the clock mechanism, and phylogenetically old photopigments suggest, that modern clock proteins evolved during the course of evolution from primitive light

sensitive proteins (Crosthwaite, Dunlap, Loros 1997). The function of opsines - a group of light sensitive proteins - can easily be altered, for instance, by exchanging single amino acids in such a way, that they adapt to the light situation in the environment. A circadian feedback system might have evolved from primitive photopigments, which were able to affect their own transcription. Such events might have occurred several times with different photopigments as outputs and might have been the cause for the various clock mechanisms, which are found among the different lines of organisms. Eyes evolved at least 40 times independently of each other in the course of phylogeny (Land, Fernald 1992).

A network of hierarchically organised circadian clocks in the retina of mammals controls many of the physiological, cellular and molecular rhythms (Doyle, Menaker 2007, see also Brainard, Hanifin 2005 and Morin, Allen 2006). Rods and cones are responsible for seeing forms, but a special population of retinal ganglia cells senses, whether light or darkness prevails in the environment. These detectors of lightness are bipolar cells and use melanopsin as a photopigment (see Reeth et al. 1997 and overview Nayak, Jegla, Panda 2007). They are distributed all over the retina and project via a special pathway, the retinohypothalamic tract (RHT), to the SCN (Supra Chiasmatic Nucleus; more on the SCN on page 57). Glutamate serves as the neurotransmitter and entrains the pacemaker in the SCN. They are connected with each other as adding or as averaging processors (Foster, Argamaso et al. 1993; Foster, Hughes, Peirson 2020).

The rods (night vision) and cones (day vision) of the vertebrate eye are not, as other cells of the body, renewed during the course of time. Instead the disks in the tip of the outer segment (arranged like a stack of coins) are shed and renewed at the base of the cones. This internal renewal, called *disk shedding*, is under circadian control and occurs at times when the photoreceptors are not used. Rods are therefore regenerated in the morning, and cones in the evening (McMahon, Iuvone, Tosini 2014).

Another well studied example for a circadian control in eyes are certain marine snails such as *Aplysia* and *Bulla*. Their eyes serve primarily to receive light, but they contain also neurons which control the firing of the eye nerve. A circadian action potential results, the so called "compound action potential" (CAP, Jacklet 1969). It can be recorded for an extended time even at the eye nerve of *isolated* eyes. The processes in the resting and in the excited nerve are well known. Electrical and pharmacological treatments can selectively influence these events. Since both eyes of an animal behave very similar, one of it can serve as a control. The cellular mechanisms of these circadian rhythms can therefore be studied quite accurately. The circadian rhythm is very precise and temperature robust. The locomotor activity of the animals (*Aplysia* is day active, *Bulla* night active) has a parallel course to the CAP rhythm (overviews: Jacklet 1989; Colwell, Khalsa, Block 1992; Koumenis, Eskin 1992; Whitmore, Block 1996; Herzog, Block 1999 and in Engelmann, Witte (2016)).

The eyes of *Bulla* contain besides about 1000 larger and smaller photoreceptor cells circa 130 neurons, which are called *basic retinular neurons* (BRN). Their axons run together with 2000 others in the optic nerve to the neuropil. The CAPs are produced by synchronous firing of the BRN population. Intracellular recordings show, that the membrane potential and the conductivity proceed in a daily pattern: During the subjective day time the membrane potential is low, during the subjective night high. In the hyperpolarized state (subjective night) there are inward directed rectifying K^+ channels, leakage channels and Cl^- channels in an open state.

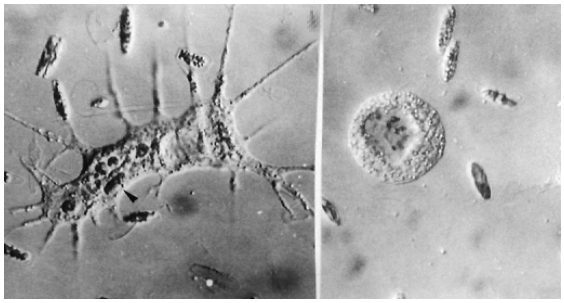

Figure 2.3: Thalassomyxa australis *changes its form rhythmically between an active phase with pseudopodia (left) and a resting stage (right). Diatoms as food*

The CAP rhythm can be entrained in at least two ways: Via a photic path by the LD, and an efferent entrance allows additionally that the brain influences the CAP rhythm. Light shifts the phase of the CAP rhythm by different amounts and in different directions (to earlier or later times) depending on the phase of the circadian system. A phase response curve describes this effect (for *Bulla* see Block et al. 1984 for *Aplysia* Corrent, Eskin, Kay 1982).

The rhythm of these marine snails was simulated with the feedback model of Johnsson, Karlsson 1972 by Benson, Jacklet 1977. The organisation of the retina of *Bulla* was modelled by Block et al. 1984.

2.2.5 The ancient clock of *Thalassomyxa*

We have seen in the preceding subsections three cases which are representative for the importance of circadian rhythms. Here we would like to speculate a bit about the question, how circadian rhythms might have evolved.

Grell (1985) discovered at the west coast of Australia a marine rhizopod, which he named *Thalassomyxa australis*. It belongs to the naked amoeba. It changes its form rhythmically between a resting stage, in which it lies like a hat on the substrate, and a phase, in which it crawls with pseudopodia over the substrate, while feeding and digesting unicellular marine algae (Fig. 2.3). The movie "The change of phases of *Thalassomyxa australis* (Promycetozoida)" (see Thalli movie)[8] shows its biology and this change in form. At a temperature of 22°C the period length is 25 h, at 10°C it amounts to 90 h, at 28°C it iso only 18 h. The dependency is shown in Fig. 2.4.

Since the period of the rhythm is not temperature robust, and since an LD cycle or a temperature change does not entrain it in the usual way (Fig. 2.5, Förster, Engelmann 1988; Smietanko et al. 1988), we are not dealing with a circadian rhythm in the strict sense.

We might be dealing with a precursor of a circadian clock, a kind of ancient clock (German: "Ur-Uhr"), which does not yet possess all the characteristic properties of "modern" circadian clocks, i.e. the temperature robustness of the period length, and the entrainment to LD cycles. Evolution could have found it important to develop entrainment to three simultaneous parameters: an LD variation in combination with temperature variations and mechanical perturbations (see Förster, Engelmann 1988). Whether and how they could an be deduced from existing ultradian rhythms, which did or did not or do possess temperature robustness, is speculative (see Fig. 2.6 from Silyn-Roberts, Engelmann 1986). The discussion on the origin of biological rhythms must also

[8]The movie can be used without charge for personal use, but not offered in the Internet or passed to outsider

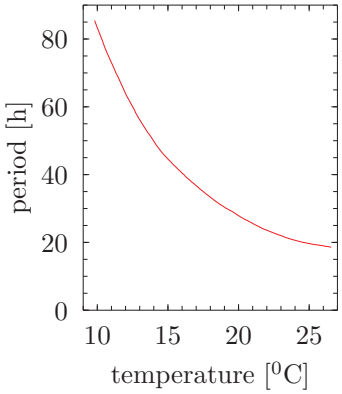

Figure 2.4: *The change between an active phase and a resting stage of* Thalassomyxa australis *depends on the temperature of the sea water. Period length is plotted on the y-axis, temperature of the sea water on the x-axis, in which the amoebae were kept. After Silyn-Roberts, Engelmann 1986*

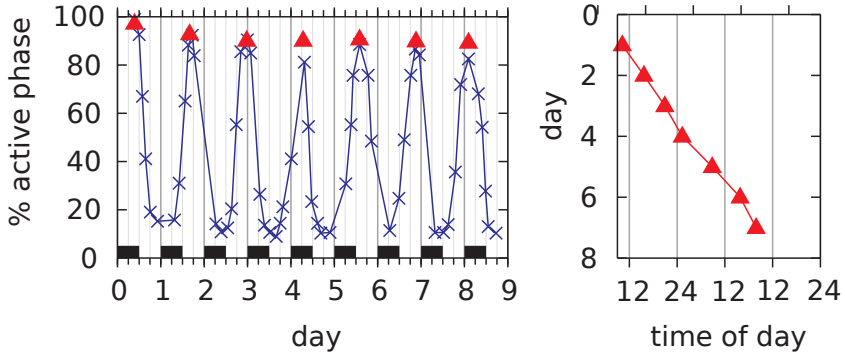

Figure 2.5: *Recorded values (×) and fitted curve (blue) in left part shows percentage of* Thalassomyxa amoeba *in its active phase during 8 days and the maxima (▲). The change in form of* Thalassomyxa australis *can not be entrained by a 12:12 h LD cycle (see the position of the maxima (▲) with respect to the grid marking the L/D transition) and the right part, where the maxima (▲) are delayed about 5 h from day to day. If the rhythm would be entrained, they should lie exactly below each other. After Förster, Engelmann 1988; Smietanko et al. 1988*

take into consideration that relevant oscillations have been demonstrated *in vitro* - both short term and circadian oscillations (see subsections 2.2.1, 2.3.4 and 2.3.5). In fact even temperature robustness could be verified in some of those experiments. Could such in vitro oscillations spontaneously have turned up in nature? For the time being we can only speculate!

2.3 Ultradian rhythms

More rapid rhythms are called *Ultradian rhythms* and their period length is considerably shorter than circadian ones. Many organisms have both circadian and ultradian rhythms and it seems to be a natural and versatile feature. It is present in the *Codariocalyx* plant, the leaf movement rhythms of which are described below (subsect. 2.3.2), the transpiration rhythms of various plants (subsect. 3.3.2), and in animals. We describe in this Section five of them, the heart rhythm in humans (subsect. 2.3.1 and more details and modelling of it in Section (7.5)), fast

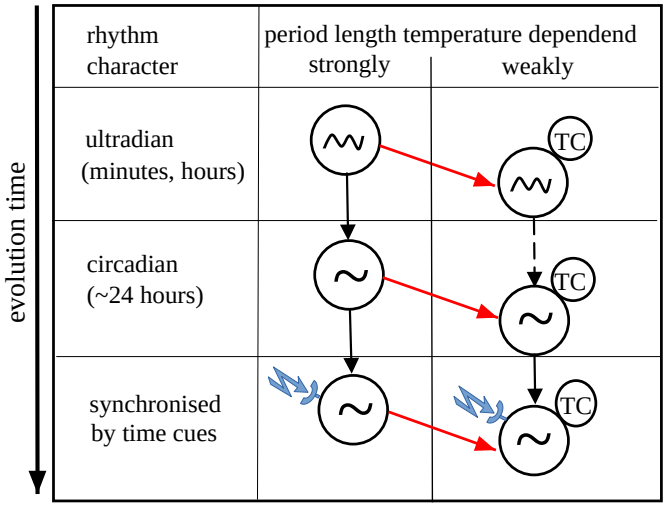

Figure 2.6: *Speculation on the evolution of circadian rhythms from ultradian rhythms to circadian ones which can be entrained and are temperature robust (TC). First column: Character of rhythm; second column: period length (~~ ultradian, ~ circadian rhythm, strongly dependent on temperature left sub-column, weakly dependent right sub-column. Red arrows: hypothetical development of temperature compensation; blue arrows hypothetical adaptation and possible synchronisation to external time cues like LD programs, mechanical perturbations etc. Observe that in this 'thought experiment' the circadian rhythms might have existed before they were developed to synchronize directly to external time signals like LD-programs From Silyn-Roberts, Engelmann 1986*

leaf movements (subsect. 2.3.2), circumnutations (subsect. 2.3.3), glycolysis (subsect. 2.3.4), and chemical oscillations (subsect. 2.3.5; for ultradian rhythms see also Brodsky Buch).

2.3.1 Rhythms in the human heart

The heart of mammals consists of the two atria which serve as "injection chambers", and the two ventricles as "pumps" (see Fig. 2.7). The contractions of the heart begin in the atria and take over in the ventricles. A wave of electric impulses run over the muscle cell of the heart tissue and coordinate the four chambers. The muscle fibres contract, if the internal potential of the cells is temporarily depolarised by an action potential. After a refractory phase the cells repolarise again.

Especially the cells in the sinus node at the upper rim of the atrium are pacemaker for this stimulation, and the atrioventricular node[9] serves as a further pacemaker. It triggers via the Purkinje fibres the contraction of the ventricular muscle (see Fig. 2.7).

The natural frequency of the sinus node determines the heart beat. Under resting conditions it is about 1 sec. Neuronal impulses from the brain, from various ganglia, and from internal organs can speed up or speed down the heart beat. This occurs normally in the whole heart

[9] A heavily branched neuronal network with exceptional fast conduction of electric pulses

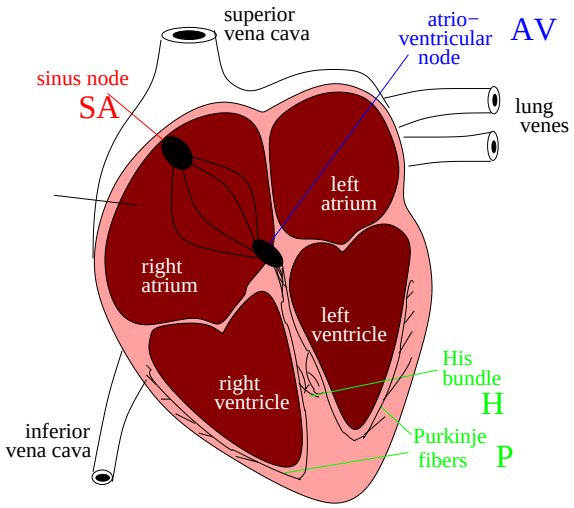

Figure 2.7: *Sketch of heart section.Left and right atrium are “injection chambers" and left and right ventricles are “pumps". Blood low in oxygen reaches the heart via the inferior and superior vena cava and from there via the lung veins to the lung, where the blood is again supplied with oxygen (see Heartfunction). Electric pulses are produced in the sinus node (SA) which is the primary pacemaker and synchronise the contractions of the atrium. The impulses reach the atrioventricular node (AV) and via the stem of His bundle (H) and the Purkinje fibres (P) the musculature of the main chambers. They make sure that they contract in the right beat rhythm (see Heart stimulation)*

synchronously. In the case of cardiac infarction, unusual high hormone or ion concentrations, chemical stress, physical damage, or a strong electric stroke, the synchronisation might fail.

Since the heart plays such an important role also in modelling, we present the topic in more details in a special Sect. (7.8).

2.3.2 Leaf movements: *Codariocalyx motorium*

We mentioned already the Indian Telegraph plant *Codariocalyx motorium* (earlier name *Desmodium gyrans*) with its terminal leaflets moving in a day-night rhythm, whereas the lateral leaflets show a fast "ultradian" rhythm (see page 21).

The ultradian rhythm of the lateral leaflets could be stopped by applying an electric current pulse of a certain strength at a critical phase (Johnsson, Boström, Pedersen 1993). This corresponds approximately to the situation in the heart (see subsect. 2.3.1), where an electric pulse can have the same effect with fatal consequences for the person. A 150 sec[10] long pulse of a 27 MHz[11] radio frequency[12] also stopped the oscillation of the lateral leaflets for some time or completely (Ellingsrud, Johnsson 1993).

[10] second
[11] megahertz
[12] power density $S = 0.53\,W/cm^2$

2.3.3 Circumnutations

So called circumnutations - usually with rhythms in the min to h range - are wide spread in plants. Seedlings, stalks, peduncles and roots do often not just grow straight, but in waves and in spirals. Darwin studied them intensively and he and his son published the results in a book (Darwin, Darwin 1880). An overview is found in Engelmann_2009:Book, in Stolarz 2009 and for roots in Loshchilov et al. 2021 and Yokawa, Baluška 2018. For an introduction the lecture Circumnutation Lecture is recommended.

The heliotropic movement of sunflower stalks is a well known (but often misunderstood[13]) example. Another example is the gravitropic pendulum of sunflowers. It can be triggered by laterally tilting seedlings, thus exposing them to gravity. Three concepts are presented by Stolarz 2009, which try to explain these movements. The first one is from Darwin. He thought, that circumnutation is endogenous, i.e. originates in the plant organ. The second concept was proposed by Johnsson, Israelsson 1968 and says, that circumnutations come about by the influence of gravity, i.e. are exogenously induced. The third concept was the result of studies in space under microgravity conditions. In spite of the virtual absence of gravity circumnutations were still present, although with smaller amplitudes (Johnsson, Solheim, Iversen 2009). The oscillations had thus *also* an endogenous origin.

During the elongation of plant seedlings circumnutations are often observable. Neugebauer recorded the hypocotyls of the Thale cress *Arabidopsis* and the sand rock-cress *Cardaminopis arenosa* seedlings with imaging analysis methods in three dimensions and analysed the development of the seedlings in time and space (see Neugebauer Thesis). Using "time windows" of growth and "natural markers" which can be seen on the hypocotyl, regions of the hypocoytyl could be distinguished in which growth and the circumnutations occur (the upper part of the hypocotyl), from regions without growth (a short movie can be viewed under Circumnutation). With a special analysis software of Winfried Hellrung virtual plants were generated, which helped to understand, where and how circumnutations develop at the seedling (see subsect. 3.3.4 and Fig. 3.14).

2.3.4 Glycolysis-oscillator

Another important ultradian reaction sequence is the so-called glycolysis oscillator.

As a small introduction one should point out that biological cells can produce energy in three ways: By photosynthesis, by respiration, and by glycolysis. Glycolysis is used by organisms which live without oxygen (such as yoghurt-fungi, bacteria in pickled cabbage, parasitic worms, red blood cells, diving vertebrates, see Winfree 1980). During the glycolysis process, one glucose molecule is ultimately converted to pyruvate and ATP as energy carrier (4 ATP is produced, but 2 of them are used in the process itself).Nine different enzymes participate in this reaction chain, outlined in Fig. 2.8.

The glycolysis reactions in yeast (*Saccharomyces cerevisiae*) have been the target of much research for different reasons, and Duysens, Amesz 1957 found that glycolysis in yeast does not always proceed uniformly but rhythmically under certain conditions. Typically the period

[13] because the movement takes place *before* the flowers are formed; *afterwards* the flowers point in an East direction (see e.g. Kutschera, Briggs (2016))

of the rhythm is in the range of 1 min to 1 h. The glycolysis-oscillations can be observed also in cell free extracts (Hess, Boiteux 1971). It is interesting that such pure extracts can exhibit the same oscillations as found in the living cell system. We will later see that also even more complicated oscillatory systems can exist both *in vivo* and *in vitro*.

Oscillatory chemical reactions are often described by negative feedback models, much in line of what we will mentioned later. In fact, feedback is so central in the modelling that it will be treated repeatedly in later chapters. This is true for different levels of complexity, at the molecular level, the cellular level and at the organism level (and in industry, sociology etc as well).

For the timing and coordination of metabolic events some organisms use also ultradian clocks which like circadian clocks are temperature robust, but in most ultradian oscillators such as leaf movements, circumnutations etc the period length is affected by the temperature and they can not be entrained by external time cues in a 24 h measure.

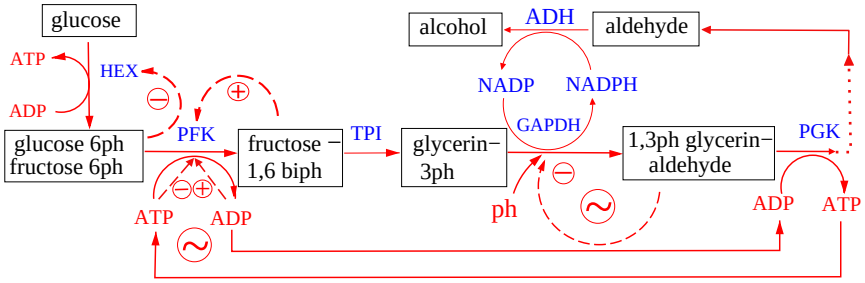

Figure 2.8: Course of glycolysis in yeast and feedback of substrate on enzymes. With ~ the positions are marked at which oscillations are easy to detect. →: flow. Broken arrow: Feedback path. +: Activation, -: Inhibition. HEX: Hexokinase, ATP: Adenosin triphosphate, ADP: Adenosin diphosphate, PFK: Phosphofructokinase, TPI: Triose phosphate-isomerase, GAPDH: Glycerine aldehyde/-phosphate-dehydrogenase, ph: Phosphate, PGK: phosphoglycerokinase, ADH: Aldehyde-dehydro/-genase, NADP: Nicotinamide-dinucleotide-phosphate. After *Chance, Pye, Higgins 1967; Edmunds 1988*

With oxygen-pulses the phase of the glycolysis-rhythm can be shifted. If the pulse is given with a certain strength in a critical phase, the rhythm disappears. (the phenomenon will be discussed in Sect. 3.1).This indicates that the limit cycle describing the oscillating system is based on two state variables only (see page 292 - The time crystal - in Winfree 1980).

In fast growing cells of *Schizosaccharomyces pombe* an ultradian clock controls cell division. A rhythm with a period length of 40 to 44 min is found. This rhythm is temperature-compensated and independent of growth rate (Kippert, Lloyd 1995). It continues for at least 18 h without damping. This is an indication for inter-cellular communication.

2.3.5 Chemical oscillations

Chemical oscillators are interesting and demonstrate in an impressive way how even relatively simple chemical systems can oscillate. They are fundamental for biological clocks and we will go often into chemical details later (e.g. the Goodwin oscillator in Sect. 7.3).

Oscillations can occur in pure chemical-biochemical systems. *In vitro* chemical oscillators demonstrate convincingly that even relatively simple inorganic systems can oscillate. Therefore we will, as a start, briefly describe one of these chemical oscillations, the Belousov-Zhabotinskii reaction. This reaction was discovered by Belusov in 1958 and studied in detail by Zhabotinskii (see Zhabotinsky reaction). As in most of the ultradian rhythms the period length of this chemical oscillator depends strongly on the temperature of the solution. At 10^0C higher temperature the period length is half as long.

We will then discuss a more complicated biochemical reaction - both for their importance in biological rhythms and also as an introduction to a deeper treatment later in the book (see subsubsection 2.3.5.2).

According to the laws of thermodynamics, in all spontaneously occurring chemical reactions in a homogeneous, closed system, the free enthalpy[14] decreases. Oscillatory reactions should therefore not be expected to occur. However, at certain conditions the concentration of intermediates can oscillate around the expected values in a stationary state (Fig. 2.9). For this to happen the reaction must not be in equilibrium (and energy can, therefore, be supplied for oscillations to occur during a limited period of time).

If the system has energy available (is "open"), thermodynamics does not pose any restriction on the existence of oscillatory chemical reactions.

2.3.5.1 The Belousov-Zhabotinskii reaction

Belousov noted that potassium bromate, cerium(IV) sulfate, malonic acid, and citric acid in dilute sulfuric acid, the ratio of concentration of the cerium(IV) and cerium(III) ions oscillated, causing the colour of the solution to oscillate between a yellow solution and a colourless solution. This is due to the cerium(IV) ions being reduced by malonic acid to cerium(III) ions, which are then oxidised back to cerium(IV) ions by bromate(V) ions[15].

A general Belousov Zhabotinskii (BZ) reaction (several different reaction schemes are discovered) consists of two main reactions A and B, which influence each other only slightly, since A consists of reactions between ions and molecules with paired electron spins (singlets), B consists of reactions between radicals. Whether A or B dominates depends on the concentration of Br^-. At high concentrations A dominates, at low concentrations B. A uses Br^-; in this way the reaction B is induced. B produces Br^-; in this way A is induced (Fig. 2.11). For more details see Winfree 1980 and a more general description see Tyson 2022..

The same chemical reactions are responsible for a wave pattern. It is found after pouring the solutions in a flat dish and keeping it undisturbed. In this case the diffusion of bromine ions plays a role, because the solution is not stirred (Fig. 2.10. Here a figure from Wikipedia shows

[14] a thermodynamic property of a system defined as H = U + PV (H enthalpy, U internal energy of system, P pressure exerted on the system by its environment, V volume of the system)

[15] For a description of the BZ oscillation and its history see Tyson 2022

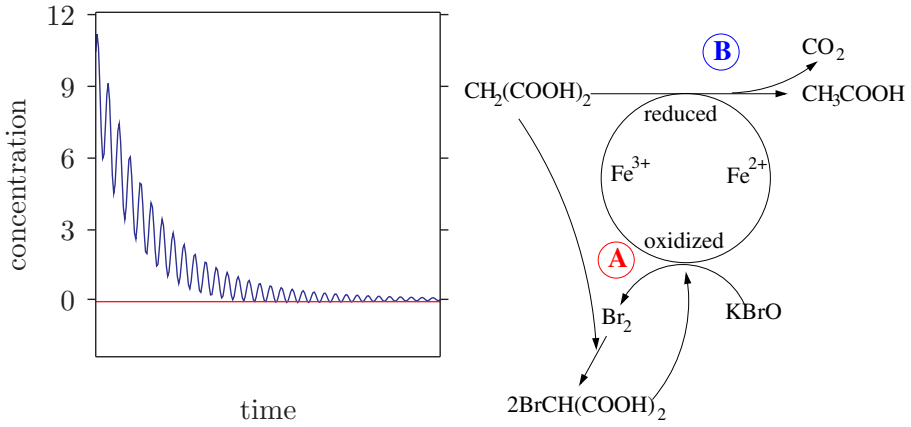

Figure 2.9: *Left: Course of a chemical oscillation in a closed system, before the equilibrium (horizontal red line) is reached. On the y-axis the concentration (arbitrary unit) of an intermediate is plotted (after Degn 1972). Right: Reaction scheme of the Belousov-Zhabotinsky-reaction with the two main reactions A and B.*
Reaction A: Bromide and potassium bromate (KBrO) form together with malonic acid $CH_2(COOH)_2$ bromine malonic acid. The ferroin indicator is first blue, due to the trivalent iron (bromate oxidizes Fe^{2+} to Fe^{3+}). If bromate disappears, Fe^{2+} is formed. The ferroin indicator turns red.
Reaction B: Bromine malonate is concentrated enough to reduce Fe^{3+} to Fe^{2+}. Acetic acid , (CH_3COOH) is formed aswell as CO_2 (gas bubbles!) and bromide, which inhibits reaction A. In this way the formation of bromine malonate is stopped, reaction B comes to a halt. After Winfree 1980

a photo sequence of a the BZ type reaction where the solution oscillates between blue and red and the period is about 30 sec).

Another example for a chemical oscillation is the Briggs-Rauscher oscillation, known as the iodine clock (see Iodine clock and for modelling Machado, Faria 2009), which can be observed also spatially (see spatial iodine clock). It was discovered by Landolt in 1886. It exists in several variations, which each involve iodine species (iodide ion, free iodine, or iodate ion) and redox reagents in the presence of starch. The two mixed colourless solutions turn suddenly dark blue, which is due to tri-iodide-starch complex formation and cycle back to colourless, until the reagents are depleted.

For demonstrating chemical oscillators see Engelmann1999.

2.3.5.2 Calcium ion oscillation

The calcium ion (Ca^{2+}) is a very important constituent in cells of organisms. It functions in processing signals via so called transduction pathways, in contraction of all muscle cell types, in fertilisation, and so on. The calcium status is also important for maintaining the potential differences across excitable cell membranes.

But the concentration of cellular Ca^{2+} has also been found to show ultradian oscillations in a

Figure 2.10: *Belousov-Zhabotinsky-reaction as a changing wave pattern in a Petri dish. First the solution is red (ferroin indicator* Fe^{2+}*) . By a disturbance at one place bromine ions are used up, bromate oxidizes* Fe^{2+} *to* Fe^{3+} *(ferroin indicator turns blue). Bromine ions diffuse into the surrounding and in this way the red area turns into blue. If the bromine malonate has reduced* Fe^{3+} *(bromine ions are formed), the area turns red again. The pictures show at a late situation the pattern changes at 0, 80, and 160 seconds). Released into the public domain by its author, J. Krieger at German Wikipedia Zhabotinsky wave pattern*

number of cell systems, for instance in the pollen tube[16] growth (Hepler, Lovy-Wheeler 2006; Holdaway-Clarke et al. 2003) (see Pollentube paper and Pollentube oscillation). It displays some unique features:

1. It is extremely fast (up to 1 cm per h in corn)
2. It is highly polarised (growth confined to the tip)
3. A guidance mechanism determines the direction of growth
4. The pollen tube growth rate oscillates with a period of 15 - 50 s
5. The intracellular Ca^{2+} and H^+ gradients and extracellular fluxes of Ca^{2+} oscillate with the same period (see Fig. 2.11).

During this process Ca^{2+} ions and protons play an important role: A high proton concentration or low pH (eg 4.5 to 6.5) facilitates both pollen germination and tube growth, and the intracellular calcium and proton gradients and extracellular fluxes of these ions oscillate with a period of 15 - 50 s. This is identical to the oscillation in the rate of pollen tube growth[17]

Much effort has been concentrated upon modelling these Ca^{2+} oscillations. We will study one minimal model in Chap. 8 based on the work of Goldbeter, Dupont, Berridge 1990 (see Section 7.4 and Fig. 7.21). Simulations of Ca^{2+} oscillations in one single cell will then be followed by studies of the behaviour when two oscillating cells are coupled, and, finally, networks of several coupled cells will be studied (see Chap. 8).

[16] which delivers the two sperm cells to the embryo sac, and is thus essential for reproduction in higher plants

[17] As a leading event for the Ca^{2+} oscillation, the rise in pH -presumably controlled by a proton ATPase on the apical plasma membrane- might be the prime regulator of pollen tube growth.

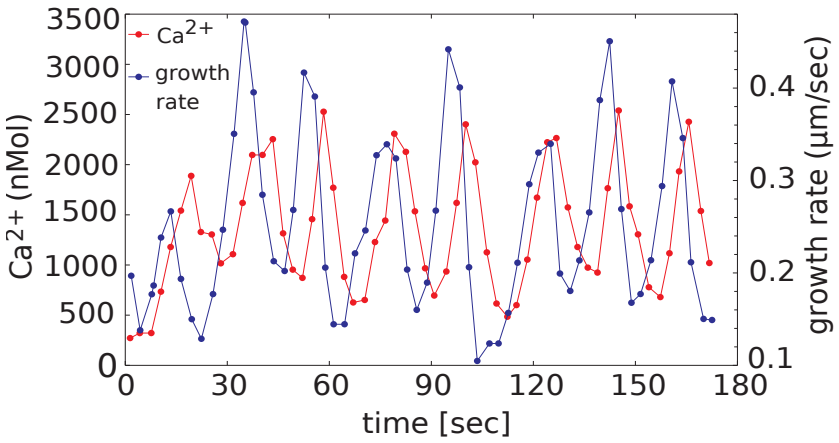

Figure 2.11: *Oscillation of intracellular* Ca^{2+} *(nM, blue, left ordinate) and growth rate (µm/s), red, right ordinate) of lilly pollen tube growth. The calcium oscillations (nM) vary with a period length of about 21 s, the growth rate (µm/s) shows here a somewhat longer period length of about 28 s. Modified from (Hepler, Lovy-Wheeler 2006)*

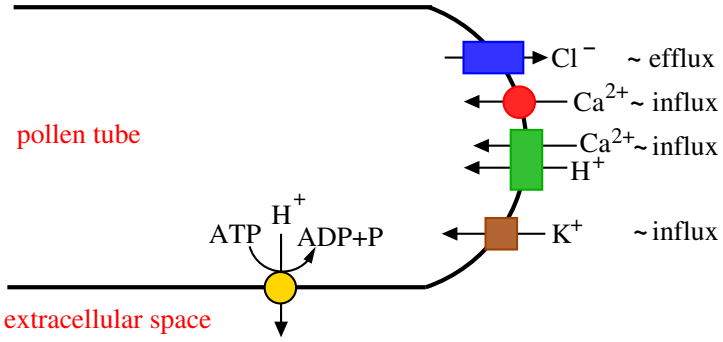

Figure 2.12: *Scheme of* Ca^{2+} *and other ion dynamics at the pollen tube tip after Fig. 1 e of Holdaway-Clarke et al. (2003). Oscillations (~) are observed in the* Cl^- *efflux, the* Ca^{2+}, Ca^{2+}/H^+, *and the* K^+ *influx in pollen tube. Blue:* Cl^- *- channel, Red* Ca^{2+}*: channel, Green. non-specific cation channel such as for* Ca^{2+} *and* H^+*,Bbrown.* K^+ *channel, Yellow* H^+*ATPase- channel.*

3 Influencing rhythms and their oscillators by external events

Biological rhythms are usually entrained by external factors of the environment such as the periodic alterations of light and darkness or temperature changes. The oscillators can be influenced also by single events such as a light pulse applied while the organism is in darkness or by a dark pulse while in light. Or the pacemaker has to adapt to a new time zone if the organism is actively changing it in e.g. migratory birds or humans by using flights to the East or West (see Fig. 4.3). If an oscillating system such as a circadian rhythm is shifted in its position by a flight covering time zones, the oscillation can change immediately or after so called *transients*, where it takes some time, until a steady state oscillation is established. In most practical cases one is interested in measuring the phase change between the perturbed and the unperturbed oscillation *after the transients*.

This is an important point particularly in some biological experiments where the experimental time available can be limited, and it is, therefore, tempting to judge the phase shift of the oscillation before the transient disappeared[1]. If so, it should be specified that the phase shift is not acquired for the steady state oscillations.

A more typical situation is an organism in an 12:12 h LD or in another LD cycle, e.g. a 16:8 h LD during the summer. If the rhythm is due to a circadian oscillator, it should continue to run at least for some time if the organism is released in constant conditions of DD or LL for some days without other entraining conditions such as temperature changes. If it is not running under these conditions, the LL or the DD might damp the rhythm. Alternatively, there is no oscillator, but the organism reacts to the L/D change directly. This is called masking (Mrosovsky 1999)[2]. In an LD cycle of e.g. 11:11 h or 13:13 h the rhythm might still show a 22 h or 26 h rhythm, but released in constant conditions (CC) it will not oscillate anymore if masking was working. If a circadian oscillator was at work, it will after the release oscillate with a circadian period, i.e. close to 24 h. However, there is a limit of entrainment, beyond which the oscillator will not entrain (called *range of entrainment*, see subsect. 6.2.2).

According to Bittman (2021) in both cases the oscillator was synchronised[3], but only in

[1] This happened in the history of the chronobiological science, while studying a possible temperature dependence of the circadian rhythm of the eclosion rhythm of *Drosophila* flies from their pupal cases. It was erroneously concluded by Bünning 1936, that the period length was depending on the environmental temperature, because he did not wait long enough until the transients were gone. This was corrected by Pittendrigh (Pittendrigh 1954) and he established the temperature compensation of this circadian rhythm.

[2] Example: street light, where a sensor switches the lamps on. The light is not entrained, but occurs synchronously with the onset of darkness

[3] Synchronisation (syn = with, chronos = time) means to occur at the same time. It does not require even a single oscillator and does not need to result from entrainment

the latter case entrained[4], because an internal oscillator was at work. The value of having a circadian rhythm is, to achieve an appropriate phase control with respect to the environment, and to ensure an optimal timing of internal events.

It should be mentioned, that synchronisation and entrainment is also found in non-circadian rhythms (such as ultradian, lunar, or annual rhythms). It is also important, to note, that besides light other external factors such as pulses or cycles of temperature or of electrical and magnetic fields can synchronise or entrain.

Single pulses applied to an oscillating system are able to shift the phase of a rhythm by different amounts and by delaying or advancing the oscillator, depending on the phase at which the pulse was given. The result of those treatments can be visualised in so called phase response curves[5] (PRC, see Fig. 6.8), which are discussed in respect to modelling in more detail in Sect.6.1. The perturbation can cause a delay of the oscillation, or its contrast, an advance. The PRC gives information about the magnitude and position of the perturbation to reach the effect.

Here are a few more examples of entrainment by non-24 h external rhythms:

The range of entrainment is determined by the degree of resonance between the organism's free-running period and the period of the external LD cycle. If the two period length are close, it promotes individual fitness, as shown in strains of the cyanobacterium *Synechococcus* matching the period of the LD cycle. They will out compete strains whose free run period is not concordant (Ouyang et al. 1998; Woelfle et al. 2004). Similar results were obtained in pitcher-plant mosquitoes (*Wyeomyia smithii*), raised in a non resonant LD cycle, which had a lower fecundity (Bradshaw, Holzapfel 1990), in hamsters (Martino et al. 2008), in mice (Spoelstra et al. 2016), in *Drosophila* (Pittendrigh, Minis 1972), and in ants (Lone et al. 2010). This improved fitness in the competition experiments was successfully simulated.

The free run period of humans was estimated to be near 25 h, but has later been corrected to ~24.2 h, as outlined by Duffy, Wright 2005. They used a forced desynchrony protocol which avoids the confounding influence of self-selected sleep-wake/light-dark cycle.[6]. The range of entrainment in humans is from 23.81 to 24.31 h (Czeisler, Duffy et al. 1999) or even broader (Duffy, Czeisler 2009). Small daily adjustments are necessary to entrain the clock to the 24 h cycle of the day[7] (Duffy, Wright 2005; Forger 2017). If the driving cycle is outside this range of entrainment, the clock fails to follow it and sleep, metabolism, and behaviour is impaired.

This is testified by the effects of on-watch schedules on the seafarer or personal on submarines and commercial vessels leading to increased health risks and decreased cognitive performance. Since the thirteenth century it was traditional to use a 4 h on and 8h off watch schedule in maritime crews. The watch schedule of the US board vessel crews was replaced by a 6 h on and

[4] Entrainment is used in physics for a situation in which two or more oscillators match period. The oscillators may be organised hierarchically or may have a more equivalent coupling relationship whereby they influence one another mutually to set period and phase

[5] The term "phase response curve" was created by Lo DeCoursey in 1960. The activity rhythms of her flying squirrels, kept in constant darkness, responded to pulses of light applied at different phases of the rhythm differently. The response curve shows the direction of the phase shifts - advances or delays - and the magnitude of the shifts.

[6] first described by Kleitman 1939. He used light-dark cycles several hours shorter or longer than 24 h and low light intensities during waking. The human clock cannot entrain to this scheme and the periods measured via the core temperature were close to 24 h.

[7] entrainment occurs when $n \cdot \tau - m \cdot T + \Delta\varphi = 0$ where n and m are integers, see subsect. 6.2.1

12 h off routine (18 h sections) of the three shift Sections. In contrast, most officers stand watch on a four-section schedule with 6 h on and 18 h off in 24 h sections (Guo et al. 2020).

3.1 Stopping a clock: Arrhythmicity

Besides temperature compensation, another special feature of circadian clocks is, that their oscillation can be stopped by a special treatment. This is interesting in itself, but also important, because models have to take care of this feature (see Section 6.3). We will first mention several rhythms of organisms in which arrhythmicity could be induced which are compiled in table 3.1:

Among unicellular algae the cell division of *Euglena* (see Euglena illustration) can be made arrhythmic by a special light pulse, so that the cells divide now continuously and not in certain time windows, which are opened by the circadian clock (Malinowski, Laval-Martin, Edmunds 1985).

Likewise, in the green alga *Chlamydomonas* the rhythm in the phototactic behaviour is suppressed by a specific light pulse and a singular state is reached (Johnson, Kondo 1992), and finally in *Lingulodinium polyedrum*, a dinoflagellate, a critical amount of anisomycin (300 nM) can stop the glow rhythm (Taylor, Dunlap, Hastings 1982).

A further example for suppressing a circadian rhythm is the conidia formation of the red bread mould *Neurospora crassa*, a fungus of the phylum Ascomyceta which was intensively studied in respect to the molecular processes producing these oscillations (Lakin-Thomas 2019; Hurley, Loros, Dunlap 2015; Baker, Loros, Dunlap 2012; Lakin-Thomas, Bell-Pedersen, Brody 2011). The rhythm of the conidia formation can be stopped by an increase in temperature at a critical phase or by a short LP (or in other cases by a temperature pulse or electric current pulse or pulse of a substance, again applied at a critical phase; see e.g. Fig. 1 respectively 2 in Huang, Wang, Liu 2006). The data lead to the assumption, that FRQ, a clock protein of *Neurospora crassa*, is a state variable of the circadian clock. This was confirmed by using a genetic trick, in which a promoter was used, which can be induced by quinine acid (Aronson et al. 1994)). In this way frq could be induced at certain times. A 2 h treatment with quinine acid between DD 26 and 27 suppressed indeed the conidia rhythm for 3 to 4 days.

Neurospora crassa can be used to produce enzymes in bioreactors. The production in darkness is, however very small. The fungus can be kept in a state of high metabolism by keeping the culture in a 11:11 h LD change (Cockrell et al. 2015). Almost all clock genes are thereby up-regulated and the circadian rhythm disappears. In this way the production of enzymes reaches industrial rates, because the negative feedback of the circadian oscillator is gone.

Finally we come back to the circadian rhythm of petal movements in the Flaming Katy *Kalanchoë blossfeldiana* mentioned already in subsect. 2.2.3 where photoperiodism was discussed. Normally the opening and closing of the flowers is synchronised by a *Zeitgeber* of the environment such as the 24 h LD cycle. If the plants (or the cut off flowers) are kept under constant temperature and in weak green light (which is like darkness), the flowers continue to move rhythmically, but the period is 22 h (see Fig. 2.2).

Light pulses can shift the rhythm. With a special light pulse arrhythmicity can be induced: The flowers stay in a state of medium opening, and a new light pulse induces the movement anew (see Fig. 3.1 and How to stop a biological clock: point of singularity).

Species	type of R	AR induced in	AR induced by	AR induced at	reference
Euglena	circadian	cell division	LP 300 lx	xx	[8]
Chlamydomonas	circadian	phototaxis		xx	[9]
Lingulodinium polyedrum	circadian	glow rhythm	anisomycin 300 nM	xx	[10]
Neurospora crassa	circadian	conidia bands	LP, TP↑, ElP, quinineP 2 h	DD 26-27	[11], [12]
Kalanchoë blossfeldiana	circadian	petal movement	R LP 230 $\mu W cm^{-2}$ 130 min	DD 54	[13]
Drosophila pseudoobscura	circadian	eclosion rhythm	LP	DD ?	[14]
Phodopus sungorus	circadian	body temperature R	LP	LP 1 at 4 on d 12, LP 2 at 22 on d 22	[15]
Anthrenus verbasci		circ pupation R	4 wk LD 16:8 P	9 wk after LD 12:12 onset	[16]
Avena sativa	ultradian	transpiration R	LP	xx	[17]

Table 3.1: *Arrhythmicity induction in various species. Overview and references. Abbreviations used: R rhythm, LP light pulse, TP temperature pulse, ElP electric pulse, DD continuous dark, wk week, d days, h hour, min minute, lx lux, nM nanoMol. See also Engelmann, Witte 2016.*

[8] Malinowski, Laval-Martin, Edmunds (1985)
[9] Johnson, Kondo (1992)
[10] Taylor, Dunlap, Hastings (1982)
[11] Huang, Wang, Liu 2006
[12] Gonze, Leloup, Goldbeter 2000, Upadhyay, Brunner, Herzel 2019
[13] Engelmann, Johnsson, Karlsson 1971
[14] Winfree 2001
[15] Steinlechner, Stieglitz, Ruf 2002
[16] Numata, Miyazaki, Ikeno 2015
[17] Prytz 2001

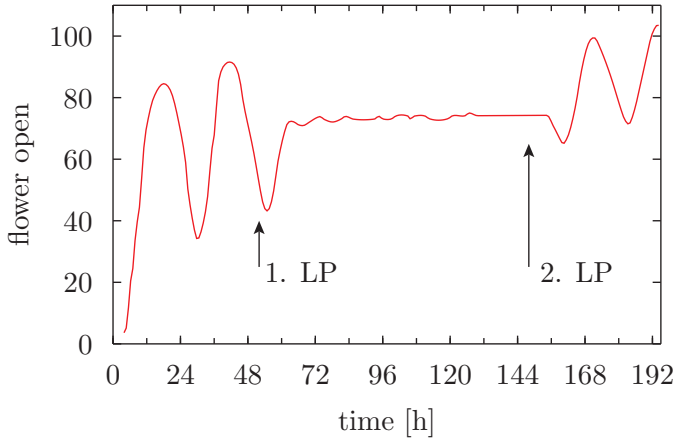

Figure 3.1: *A special pulse of red light of* 230 $\mu W\,cm^{-2}$ *and 130 min duration induces arrhythmicity in* Kalanchë *flowers, if this pulse is given 52 h after the onset of continuous darkness (first light pulse). A second LP induces the rhythm again*

These results can be simulated with a feedback model of Johnsson and Karlsson proposed a feedback model, which is describe in Section 7.1 (see there Fig. 3.2 and Johnsson, Karlsson 1972; Karlsson, Johnsson 1972). This model allows not only to simulate the experimentally found phase shifts of the rhythm by light pulses, but also by temperature pulses. A critical test of the model was, whether it would predict the suppression of the rhythm by a special light pulse, as described above. That was indeed the case (see Section 7.1).

On page 110 of Section 6.1 in Chap.6 methods are proposed which help to determine the location of the point of singularity.

More recent studies on humans showed, that the reaction of the circadian system towards light does not only depend on the time of application, the intensity and the duration of exposure. At a critical strength at a certain phase the system could be pushed into a singularity, which results in a "stop" of the circadian clock. The results are important for the treatment of certain sleep disturbances, because the human clock can be shifted to any arbitrary time in one to three days by a suitable light applications (Czeisler, Dijk 1995).

3.2 Temperature robustness of circadian period

As mentioned already, temperature robustness[18] is a necessary property of circadian clocks. To find out, how it is realised on the molecular biological level, one can for instance search for mutants, in which temperature robustness is impaired. This has been done e.g. in the fungus *Neurospora crassa* (Lakin-Thomas, Bell-Pedersen, Brody 2011 and more details on page 44).

[18] often called *temperature compensation*, but this implies already a certain mechanism responsible for this feature; therefore we prefer *temperature robust(ness)* and use it in the book - without always saying, that the *period* is meant the length of which is robust

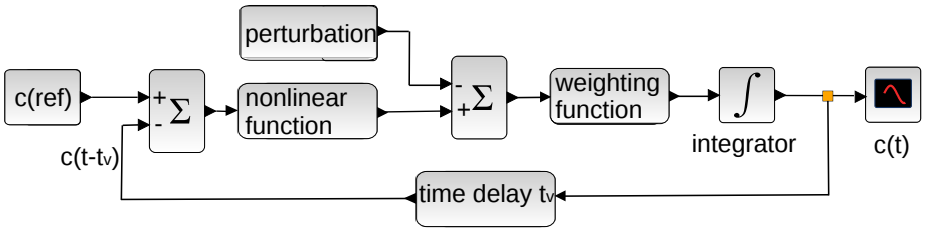

Figure 3.2: *Feedback model of Johnsson and Karlsson to simulate the* Kalanchoë *flower clock. A reference value c_{ref} is compared with the current value c_t(c denoting the oscillating variable). If the two values differ from each other, the error signal $c_{ref} - c_t$ is amplified by a non linear function f (see Fig. 7.2), weighted in a weighting function H (the preceding values influence the current value with varying weight), and after integration a new current value is compared again with the reference value. The size of the concentration c_t fluctuates periodically, if the functions are supplied with the right parameters. After Johnsson, Karlsson 1972. See also the more detailed Scilab model in Fig. 7.1 and the function blocks in Fig. 7.2*

However, the overall picture of temperature robustness is not yet clear. Three views are discussed in the literature:

1. According to Johnson, Egli (2014) temperature robustness of circadian clocks belongs to a general phenomenon, namely the *compensation of metabolism*; without it the metabolism would destabilise the precision of the clock (Pittendrigh, Caldarola 1973). An example is the sugar metabolism in *Neurospora* (Sancar, Sancar, Brunner 2012). It might be, that circadian clock mechanisms posses a metabolic sensor (via ATP?), which converts the circadian rate constant into an intracellular metabolic rate.

2. In the *network model* the temperature robustness is explained by assuming, that in spite of the period determining processes being temperature sensitive the changes in rate compensate each other (overview Kurosawa, Iwasa 2005 and Hong, Conrad, Tyson 2007). However, there are some difficulties with this model: Many mutations, in which the period is influenced, do not affect the temperature robustness (Hong, Conrad, Tyson 2007).

3. Therefore Kidd, Young, Siggia (2015) propose a *signal path model*, which is discussed on page 46.

After these general remarks regarding the temperature robustness of circadian rhythms we present in the following some examples of temperature robustness, namely the red blood cells of mammals[19] (page 43), some prokaryotes (page 44), the bread mould *Neurospora crassa* (page 44), the Thale cress *Arabidopsis thaliana* (page 45), the fruit fly *Drosophila* (page 45), and examples

[19] Red blood cells in mammals are unique amongst vertebrates as they do not have nuclei when mature; this provides more space for haemoglobin

Species	type of R	observed in	reference
erythrocytes	circadian	Casein kinase 1	[20]
Synechococcus	circadian	ATPase KaiC	[21]
Neurospora crassa	circadian	conidia bands	[22]
Ostreococcus tauri	circadian		[23]
Arabidopsis thaliana	circadian	conidia bands	[24]
Aplysia, Bulla	circadian	CAP-R	[25]
Drosophila	circadian	eclosion rhythm	[26]
mammalian cultured cells	circadian		[27]
Anthrenus verbasci		circ pupation R	[28]
Schizosaccharomyces pombe	ultradian	cell division	[29]

Table 3.2: *Temperature robustness in various species. Overview and references. Abbreviations used: R rhythm, CAP compound action potentials. In the footnote a first reference, and a second one for models, if available*

from vertebrates (page 48). Table (3.2) contains an overview of temperature compensation in various species and references in footnotes.

Human red blood cells (RBCs) are the most numerous cell type in the human body. They exhibit robust circadian rhythms, which have been described in isolated human RBCs under constant conditions (Beale et al. 2019). An adaptive advantage of circadian rhythms in RBC might be the daily variation in CO_2, osmotic homeostasis or cardiovascular events (Henslee et al. 2017).

RBCs lack nuclei, that is, they do not use transcription and translation. Transcription and translation are, however, claimed to lead to circadian rhythms by means of feedback loops in nucleated organisms. Thus, in this particular case the circadian rhythm and temperature robustness must be based on another principle. Casein kinase 1 (CK1[30]) is a candidate.

Inhibiting CKs in RBCs with staurosporine lengthened period, and a more specific inhibitor of CK1 abolished temperature independence. CK1 phosphorylates clock protein targets, such

[20] Beale et al. (2019)
[21] Johnson, Kondo (1992)
[22] Lakin-Thomas, Brody, Coté (1997) and Upadhyay, Brunner, Herzel (2019)
[23] O'Neill, Ooijen et al. (2011) and Dixon et al. 2014
[24] Huang, Wang, Liu 2006 and Avello, Davis, Pitchford 2021
[25] Koumenis, Eskin 1992 and Benson, Jacklet 1977, Block et al. 1984
[26] Pittendrigh 1954 and Kidd, Young, Siggia 2015
[27] Tsuchiya et al. 2016
[28] Numata, Miyazaki, Ikeno 2015
[29] Kippert, Lloyd 1995
[30] CK1ε and CK1ϑ are essential in the genetic transcription-translation (and post-translation) feedback loops that generate circadian rhythm in mammals. The *Drosophila* homolog of CK1ε double-time dbt is 86% identical to human CK1ε. Its protein product DBT plays a role in phosphorylating PER in *Drosophila*, and its mammalian homologs play a similar role

as PER[31] in mammals and FRQ[32] in fungi (references in Beale et al. 2019). The temperature independence is an intrinsic property of CK1 and due to a specific domain. It is present across the eukaryotic kingdom and independent of the presence or absence of the TTFL[33], and functions in nucleated and non-nucleated cells. The CK1 behaviour is similar to the KaiC[34] phosphorylation in cyanobacteria (see page 44 and subsect. 2.2.1) and may be functionally analogous to it (O'Neill, Ooijen et al. 2011).

That transcriptional oscillations are not essential for circadian rhythms was known already not only from human red blood cells (O'Neill, Reddy 2011), but also from the alga *Ostreococcus tauri* studied by O'Neill, Ooijen et al. 2011, and from other organisms (Lakin-Thomas 2006; Woolum 1991). They all are entrained by relevant environmental cues, they free run with an approximately 24 h period, and they are temperature robust.

Circadian rhythms with temperature robustness and entrainability by Zeitgeber (e.g. the daily LD cycle) are present also in **prokaryots** such as Cyanophyceae and well studied (Johnson, Mori, Xu 2008). Essentially all genes are regulated by the circadian system. The underlying circadian mechanism consists of both a posttranslational (PTO) and a transcriptional/translational feedback loop (TTFL). The PTO can be reconstituted *in vitro* with three purified proteins (KaiA, KaiB, and KaiC) and ATP added[35]. These three core oscillator proteins have been crystallised and structurally determined. Biochemical, biophysical, and structural studies have helped to understand this circadian oscillator with its long time constant, precision, and temperature robustness. The slow but between 25° and 35°C temperature insensitive ATPase hydrolysis of KaiC is the source of the temperature robust 24 h period with a Q_{10} of 1.2 (Wiegard et al. 2020). In KaiC3, a KaiC homolog, the ATPase activity is lower than that of the KaiC and its hydrolysis is not temperature robust any more. In mutants at position 402 of KaiC the enzymatic activity changed from 15 h (0.6 d) to 158 h (6.6 d). However, temperature robustness of the KaiC ATPase activity was still maintained (Ito-Miwa et al. 2020). The long period is due to a changed KaiC structure.

Temperature independence of clock speed in fungi (*Neurospora crassa*) has been studied and discussed by many researchers. Like most organisms *Neurospora* adjusts its lipid composition to changes in growth temperature by increasing the degree of unsaturation of its fatty acids at low temperature (Lakin-Thomas, Brody, Coté 1997). Membrane fluidity or phase transition behaviour is thus maintained over a range of temperatures. Mutations that affect temperature robustness of the circadian rhythm are defective in lipid synthesis suggesting that lipid metabolism is involved and that FRQ is involved in membrane function.

The group of Ruoff has also worked intensively on clarifying the cause of temperature robustness in *Neurospora crassa*. In an earlier model (Ruoff, Christensen, Sharma 2005) the stability of FRQ is supposed to determine period length as well as temperature robustness. They were able to describe the partial loss of temperature robustness in two *frq* mutants by using the Goodwin oscillator (see Section 7.3) and incorporating the experimentally obtained activation energies of FRQ degradation for these into the model. In the publication of Ruoff, Zakhartsev,

[31] mutation PERIOD
[32] mutation FREQUENCY
[33] transcription-translation feedback loop
[34] KaiC protein
[35] A simple animation is here: Cyanobacterial clock

Westerhoff 2007 temperature robustness is regarded as a pathway phenomenon rather than the result of a single-enzyme property and they identify reaction networks that exhibit temperature robustness.

A dynamic model of the circadian clock of *Neurospora crassa* that incorporates its key components and their transcriptional and post-transcriptional regulation was presented by Tseng et al. 2012. It accounts for a wide range of clock characteristics including a periodicity of 21.6 h in constant conditions, arrhythmicity in constant light, resetting by brief light pulses, and entrainment to LD cycles. Temperature robustness was supposed to be achieved by simultaneously increasing the translation of frq RNA and decreasing the nuclear import of FRQ protein. Mutations in the clock components frq, wc-2, chrono(chr) and period-3 alter temperature robustness. How transcriptional and posttranscriptional processes could act to increase or decrease period as a function of temperature and how this might lead to temperature robustness is described by Upadhyay, Brunner, Herzel 2019: The phosphorylation state of FRQ and the WC proteins dictates their activity and stability. Mutations or chemicals affecting FRQ stability affect temperature robustness (references in Tseng et al. 2012), whereby conformation changes and the localisation of FRQ at different temperatures are important[36].

In plants the circadian clock of the Thale cress *Arabidopsis thaliana* is well studied and clock models are analysed by Avello, Davis, Pitchford (2021). They constructed three minimal clock models with interactions between the clock components and three-node feedback loops which were robust to temperature variation. They describe also the response to LD conditions. Further simulations in more realistic scenarios distinguish between entrainment and temperature robustness. They reveal temperature robustness as a property which arises from multiple temperature-dependent interactions (Avello, Davis, Ronald et al. 2019). An evening-phased protein contributes to temperature robustness (Jones et al. 2019). It is co-expressed with components of the evening complex consisting of ELF3, ELF4, and LUX. The evening complex regulates also the expression of PRR9 and PRR7, which are important components of the temperature robustness mechanism.

How robust the clock is in individual root cells under constant conditions and how clock timing is coordinated across the plant was studied by Gould et al. 2018. They found robust single cell oscillations, albeit desynchronised, and observed a wave of clock activity going down, and one going up the root. They also find cell-to-cell coupling of the clock, especially in the root tip. This coupling and the observed period differences between them generate the observed waves. The results reveal a spatial structure of the plant clock. That is in contrast to the central clock of mammals. It was also pointed out (Shalit-Kaneh et al. 2018), that the plant circadian network is more complex than those found in animals and fungi. The multiple feedback loops of the plant clock shall help to ensure rhythmicity under adverse environmental conditions. That might have been the case even in some unicellular green algae as the earliest arising plant circadian oscillators. The complexity of the plant circadian network may have provided rhythmic robustness for the environmental extremes to which sessile plants are subjected.

Temperature robustness in insects was studied intensively, especially in *Drosophila*. At

[36] A mathematical model for *Neurospora* was proposed by Akman et al. 2008 which shows, that temperature changes the balance between the transcription of a shorter and a longer form of FRQ. It takes into account experimental results and applies not only for the wild type, but also for mutations. A simple mechanism uses FRQ-isoforms, which switch to the period of the controls

this point it is appropriate to mention how temperature robustness of circadian oscillators was found. Already Kalmus (Kalmus 1935; Kalmus 1940) and Bünning in 1936 (Bünning 1936) studied the eclosion rhythm of *Drosophila* flies out of the puparium. They verified the endogenous nature of it, but missed to note the temperature robustness of the event, because only the first cycle after the transfer to the other temperatures was observed. The length of this cycle does indeed depend on the temperature, but the following cycles are temperature robust, as was later reported by Pittendrigh (1954) who used *Drosophila pseudoobscura* for his studies.

As we know by now, circadian clocks are characterised by three properties: they run in constant conditions with a period of ~24 h, are entrained by environmental cycles of light and temperature, and are temperature independent, meaning they do not speed up at higher temperatures. However, there are fundamental differences between the central brain clock which regulates daily activity rhythms, and peripheral clocks which are dispersed throughout the body of insects (and also vertebrates). By using a set of luciferase reporter genes, it was shown by Versteven, Ernst, Stanewsky 2020 that *Drosophila peripheral* clocks are self-sustained but over-compensated, i.e., they slow down with increasing temperature. In contrast, *central* clock neurons in the fly brain, both in intact flies and in cultured brains, show accurate temperature robustness.

Drosophila melanogaster is an excellent model organism to study the molecular basis of the circadian clock and its robustness against ambient temperature fluctuations. The molecular mechanism of the circadian clock of *Drosophila* is quite complicated as shown simplifed in Fig 3.3 and explained in .Molecular mechanism of Drosophila

From two clock proteins, PER and TIM, a number of arrhythmic, slow, and fast clock mutants are known, the free running period τ of which is influenced by temperature, as reported by Singh et al. 2019. They all map to the same region of TIM. The authors tested, if this region is indeed important for temperature robustness by generating a collection of new mutants using targeted mutagenesis of specific gene regions and the CRISPR/Cas9 technology, followed by behavioural screening. Twenty new *tim* mutant alleles were obtained with various impairments of temperature robustness. The mutations included short in-frame insertions, deletions, or substitutions of a few amino acids. The exact mechanism of how these mutations affect TIM function is as yet unknown, but in silico analysis suggests they affect a putative nuclear export signal and phosphorylation sites of TIM.

A model was presented by Kidd, Young, Siggia 2015 (see Fig. 3.4), in which the oscillator is temperature robust but is still entrained by environmental temperature cycles (temperature changes as small as 1° C are sufficient). A temperature insensitive core oscillator is coupled to an adaptive temperature signalling pathway, a temperature sensor consisting of a gene circuit that responds only to temperature changes. A temperature change rescales the amplitude of the oscillation but leaves phase relationships and shapes unchanged. The authors show experimentally that this prediction is satisfied by the *Drosophila* clock.

This network model approach poses, however, difficulties. Many mutations in circadian genes affecting period do not affect temperature robustness. This is difficult to explain in models where temperature robustness relies on a careful balance of rates. Furthermore, experiments suggested that specific signalling pathways exist which sense temperature; removing them prevents phase shifting of the clock due to temperature changes.

Instead of assuming, that the entire circadian clock is temperature sensitive, in the *signalling*

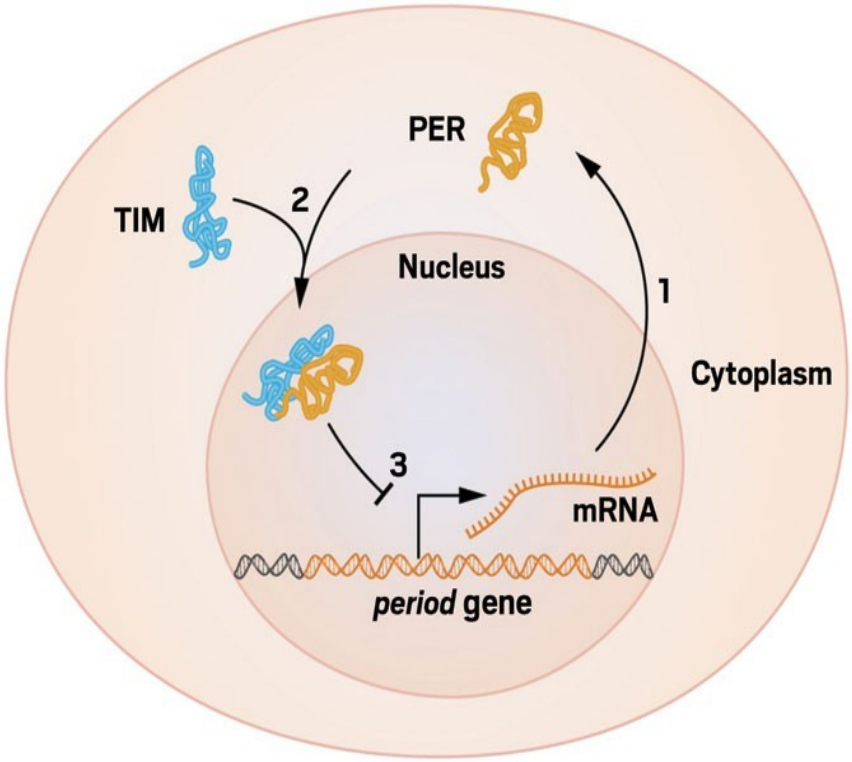

Figure 3.3: *A simplified illustration of parts of feedback control in the oscillatory system of the Drosophila biological clock. In the nucleus of the cell the period-gene builds up period-mRNA which leaves the nucleus (1) and PER-protein is formed in the cytoplasm. The PER-protein forms a dimer with TIM- protein (2) and can then be transported into the nucleus. Here the period-gen is affected (3) and the production of mRNA is diminshed/inhibited. PER is degraded an the period gene can be active again. This feed back circuit is basic in the builing up of the circadian rhythm (after Price announcement Nobel committee 2017 Nobel Price 2017)*

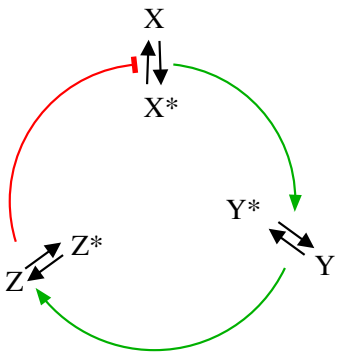

Figure 3.4: *Simple model for temperature robustness of an oscillator (Kidd, Young, Siggia 2015). mRNA isoforms X/X* are translated into proteins Y/Y*, which are converted into a second form Z/Z*, which represses transcription of X/X*. Each half of an isoform pair can be reversibly converted into the other (e.g. $X \leftrightarrows X^*$). It plays the same role as the other but has a different degradation rate.*

pathway model (Kidd, Young, Siggia 2015) the period determining processes in the core circadian clock are all independently temperature robust. A special pathway is responsible for circadian temperature sensation. This type of model as first suggested by Francois, Despierre, Siggia 2012 is consistent with the amplitude model by Lakin-Thomas 2006, in which an increase in amplitude and an increase in rate at high temperatures cancel each other.

Temperature independence of circadian oscillators was studied in a number of different organisms by Ruoff, Christensen, Sharma 2005 using models, among them *Drosophila*. The model shows, however, poor entrainment properties, especially under extended LD cycles, which suggests that parts of the LD tracking or sensing system are not well represented.

Central brain clocks regulate daily activity rhythms, whereas peripheral clocks are dispersed throughout the body of insects and vertebrates. Using a set of luciferase reporter genes, Versteven, Ernst, Stanewsky 2020 showed that *Drosophila peripheral* clocks are self-sustained but over-compensated, i.e., they slow down with increasing temperature. In contrast, *central* clock neurons in the fly brain, both in intact flies and in cultured brains, show accurate temperature robustness. This reveals a fundamental difference between central and peripheral clocks. It applies probably also for vertebrate clocks.

In a recent publication a new proposal of obtaining temperature robustness is introduced by Gibo, Kurosawa (2019). They first mention 3 older hypotheses to explain temperature robustness, namely the *temperature-amplitude coupling hypothesis* (temperature-sensitive amplitudes in gene activity rhythms can result in a stable period by generating larger amplitudes at higher temperatures), the *balance hypothesis* (temperature robustness arises from a balance between period-shortening and period-lengthening reactions), and the *critical-reaction hypothesis* assuming that critical reactions with rates stable to temperature establish the circadian period.

They afterward propose a new hypothesis, according to which the *waveform of the circadian oscillation* that is more nonsinusoidal at higher temperatures is essential for temperature robustness of the circadian rhythm. They used the transcription-translation oscillator model of *Drosophila* and mammals, and the post-translational oscillator of cyanobacteria (three proteins KaiA, KaiB, and KaiC and ATP) for their model. The waveform of the oscillation may also be important for the *entrainment* of circadian rhythms.

We mention furthermore some papers in which temperature robustness has been studied in **vertebrates** (mammals). Van Gelder, Buhr 2016 point out, that environmental temperature cycles are a universal entraining cue for all circadian systems at the organismal level with the exception of homeothermic vertebrates. In the homeotherms the resistance to temperature entrainment is a property of the SCN network and not a cell-autonomous property of mammalian clocks. This differential sensitivity to temperature allows the SCN to drive circadian rhythms in body temperature, which can then act as a universal cue for the entrainment of cell-autonomous oscillators throughout the body. Pharmacological experiments show that network interactions in the SCN are required for temperature resistance and that the heat shock pathway is integral to temperature resetting and temperature robustness in mammalian cells. It is suggested that the evolutionarily ancient temperature resetting response can be used in homeothermic animals to enhance internal circadian synchronisation.

Why vertebrates possess multiple, functionally overlapping homologous of the core clock genes was asked by Erzberger et al. 2013. They find, that this genetic redundancy strengthens

Figure 3.5: *Carpet beetle* Anthrenus verbasci. *Imago 1.7-3.5 mm long. Larva 4-5 mm long, front view right. Larvae feed on keratin and chitin (dead insects, animal hairs and feathers). Vermin in insect collections. Imago feeds on nectar and pollen. Mating between end of May and begin of June. Oviposition in human closure or in bird nests, tree holes and the like, civilisation follower. Live expectancy depends on environmental conditions and amounts to 1 to 3 years, two weeks of it as adult. From Carpet beetle*

the circadian clock and leads to an entrainment range three times as narrow as that of other organisms. Using genetically modified mice lacking one set of clock homologous and exposing them to non-24 h LD cycles they find that the mutant mice have a wider entrainment range than the wild types. The entrainment range relates inversely to the amplitude of the oscillator and the mutant mice have weaker circadian clocks than wild types.

Circadian gene expression rhythms are also temperature robust in *cultured cells of mammals* (Tsuchiya et al. 2016). They generated mutant cells with altered period length to analyse temperature robustness properties of the mammalian circadian clock using CRISPR-mediated genome editing for the genotype-phenotype analysis of the intracellular circadian clockwork in mammals.

Finally, a **temperature resistant annual rhythm** is mentioned in the pupation of the varied carpet beetle *Anthrenus verbasci* (Miyazaki, Nisimura, Numata 2009 and Fig. 3.5). It is entrained by the change in daylength (photoperiod), as it occurs in nature during the course of the year (see Fig. 3.6) and achieved by phase resetting of the circannual oscillator in response to photoperiodic changes. The authors showed, that a circadian system is involved in this photoperiodic time measurement by using the so called Nanda-Hamner protocol (Nanda, Hamner 1962).

It was furthermore shown, that this circannual rhythm is temperature robust (Miyazaki, Nisimura, Numata 2012). Thus, it fulfilled the same requirements known from circadian rhythms: It is self-sustained, exhibits temperature robustness of the periodicity, and is entrainable to environmental changes. A circannual phase response curve to a photoperiod pulse (a long-day pulse superimposed for 4 weeks over constant short days) displays a weak (type 1) or a strong (type 0) phase resetting, depending on the duration of the pulse (Numata, Miyazaki, Ikeno (2015).

Arrhythmic pupation could be induced by choosing the photoperiodic pulse at a specific time of the year and by selecting a duration of the pulse between the one leading to a weak and a strong phase resetting (Numata, Miyazaki, Ikeno (2015) and Fig. 3.7).

We are thus dealing with a self-sustaining biological oscillator with a period of about a year (circannual clock) analogous to the circadian clock. The authors discuss the general

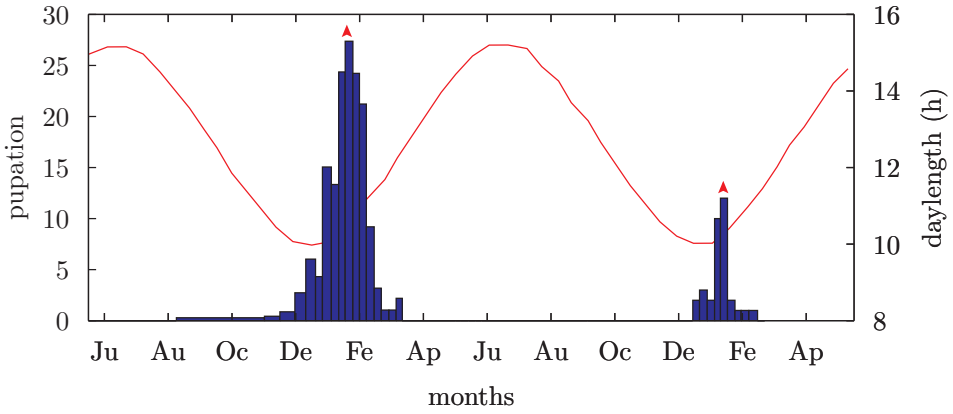

Figure 3.6: *Entrainability of the circannual pupation rhythm of* Anthrenus verbasci *at* 20^0 *C: Blue boxes number of pupations, red triangles are medians of pupation). Larvae kept under natural daylength (red curve shows duration of photophase in Osaka, Japan (*35^0 *N) including 1 h of twilight). x axis June (Ju) to June in 3rd year. After (Miyazaki, Nisimura, Numata 2014).*

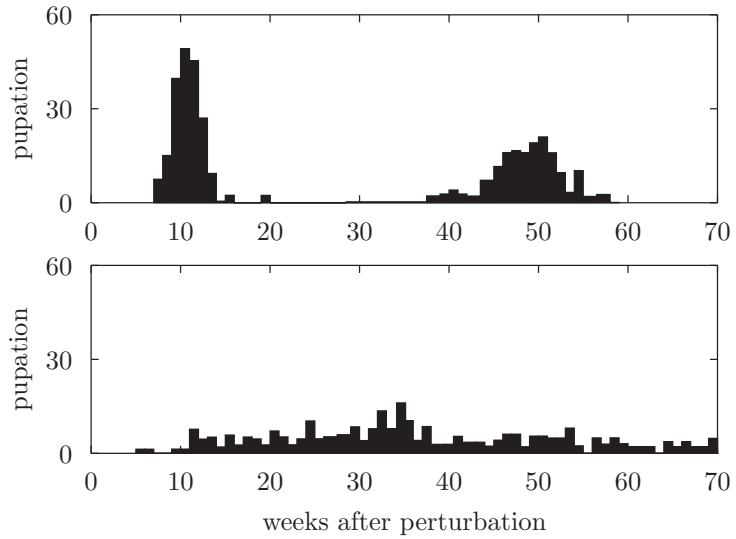

Figure 3.7: *Arrhythmicity of circannual pupation rhythm in* Anthrenus verbasci *induced by a 4-week long-day pulse of LD 16:8 applied nine weeks after exposing larvae to LD 12:12 (below). Without this pulse, circannual rhythmicity was shown with a period of approximately 40 weeks under constant short-day conditions of LD 12:12 (top) (Miyazaki, Nisimura, Numata 2009; Miyazaki, Nisimura, Numata 2014; Numata, Miyazaki, Ikeno 2015)*

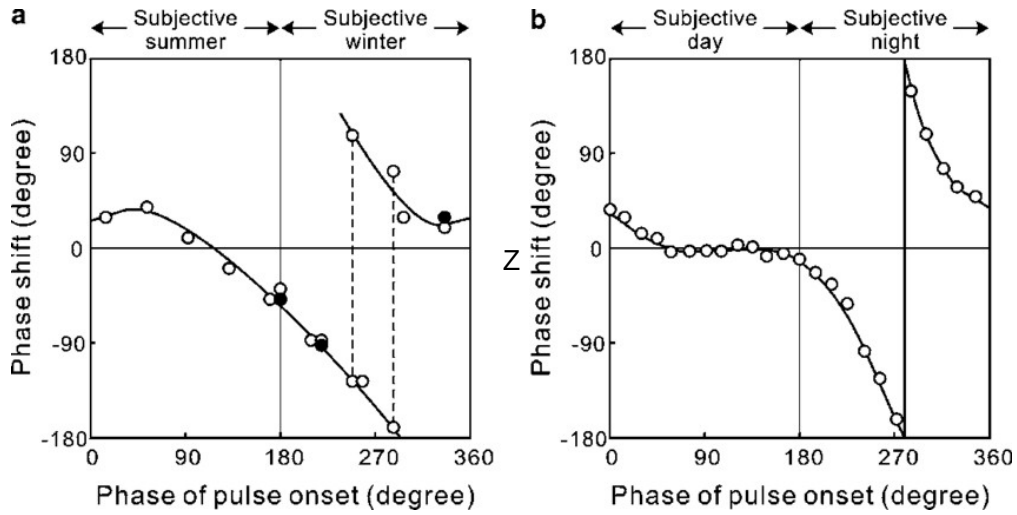

Figure 3.8: *Phase Response Curve(PRC), annual and daily. To the left: annual PRC from* Anthrenus verbasci *in response to 4-week long-day pulses), see (Numata, Miyazaki, Ikeno 2015) To the right; daily PRC from Drosophila psudoobscura, see (Pittendrigh 1967).*

characteristics of the physiological mechanisms underlying circannual rhythmicity by referring also to other organisms Numata, Miyazaki, Ikeno (2015).

Since this annual rhythm has the same features as circadian rhythms, namely, it can be entrained to an external rhythm (instead of daily), it is robust to the external temperature ("temperature robust"), it can be phase shifted (by long days during the otherwise prevailing short days), and arrhythmicity can be induced by a special treatment), one could use models which are developed for simulating circadian rhythms by just changing the time scale (years instead of days, see Fig.3.8).

3.3 Examples for interacting oscillators in cells

In this section we present a few examples of rhythms which are observed in tissues/organs with interacting cells, namely the petal movement in a plant (subsect. 3.3.1), guard cells (subsect. 3.3.2), pulvini for leaf movements (subsect. 3.3.4), and circumnutation of plant shoots (subsect. 3.3.4). How to model coupled oscillators is described in Chap. 8.

3.3.1 Example 1: *Kalanchoë* rhythmic petal movement

The *Kalanchoë* petal movement rhythm (mentioned already in another context in subsect. 2.2.3) is based on the circadian turgor changes of many motor cells in more than a dozen layers above the lower epidermis. These epidermis cells form a so called plaster epithelium as shown in Fig. 3.9 and the motor cells shrinking and swelling leads to the closing and opening of the flowers (Fig. 3.10).

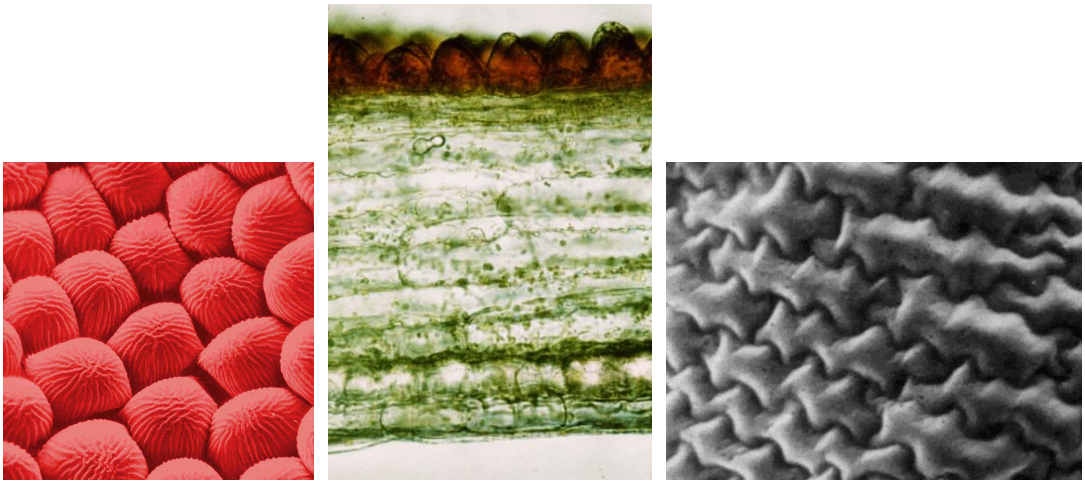

Figure 3.9: *Section through a* Kalanchoë *petal (center) with upper epidermis (plaster epithelium, red, seen from above at the left) and lower epidermis (plaster epithelium, right). Between the upper and lower epidermis are about 15 layers of motor cells, which extend, if the turgor increases. The upper epidermis cells are also able to extend. The cells of the lower epidermis do not extend, but this epidermis can be bent up and down, depending on the turgor of the motor cells (see Fig. 3.10).*

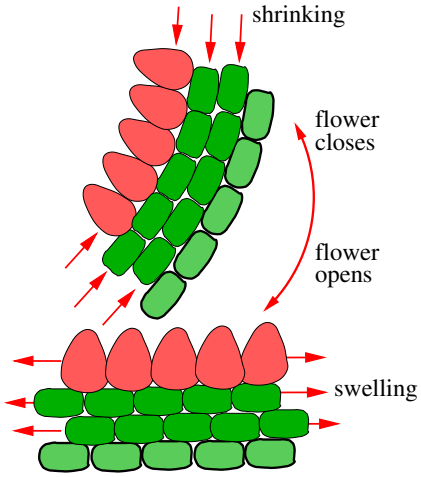

Figure 3.10: *Motor cells (= green parenchyma cells, only 2 of the 15 layers shown) of* Kalanchoë. *The papilla cells (red) of the upper epidermis do also shrink and swell. Lower epidermis. light green: Bendable bearing. At high turgor the cells extend and the petals open. At lower turgor the cells shrink and the petals close.*

3.3.2 Example 2: Guard cells

The structure and function of the motor cells of the *Kalanchoë* petals (see subsect. 3.3.1) resembles that of the *guard cells of stomata*. Their walls are wrapped by cellulose microfibrils, which prevent the cells from becoming thicker, but allow them to extend in the longitudinal direction (see Fig. 3.11). As a result they are opening if water enters the guard cells due to osmotic regulation[37], and they close, if water flows out of the guard cells. The neighbour cells of the guard cells - the subsidiary cells - exert pressure on the guard cells, and play thus also a role in the control of the stomatal opening.

The opening of the stomata of plant leaves allow gas exchange between the cavity below the guard cells and the environment. In this way CO_2 can be taken up for photosynthesis and water vapour transpired to the atmosphere. A more detailed discussion of the physiological aspects of the guard cells regulation will be given in Sect. 7.5.

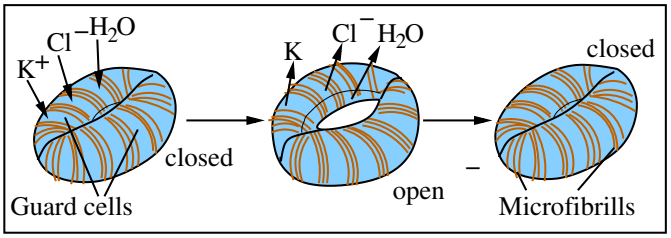

Figure 3.11: *Closed guard cells (left) start to open by influx of* K^+ *and* Cl^-*, which increases the turgor and* H_2O *uptake. Open guard cells (center) start to close by loosing* K^+*,* Cl^-*, and* H_2O *which leads to a low turgor and a closed stoma (right). Cellulose microfibrils (brown) are wrapped around the walls in such a way, that the cells can't become thicker, but are able to extend in the longitudinal direction.*

3.3.3 Example 3: Leaf movements by pulvini

If we would add a number of guard cells next to each other, we would obtain a ring of cells and if we stack many such rings on top of each other cylinder formed pulvinus model would result (see Fig. 3.12).

In all the three presented cases the cells changed their length reversibly. In the next subsect. Circumnutations in hypocotyls of seedlings are described, where the cells elongate only, but do not shrink.

3.3.4 Example 4: Circumnutation

Plants react quite sensitive to gravity in order to grow adequate and to position themselves in their environment. However, during this growth the sides of e.g. a cylindrical hypocotyl do often not elongate simultaneously, but the growth zone is turning: Seen from above the tip of the organ circles or swings. In tendrils these so called circumnutations are especially

[37] stomata open if the turgor in the guard cells increases and they close if the turgor decreases

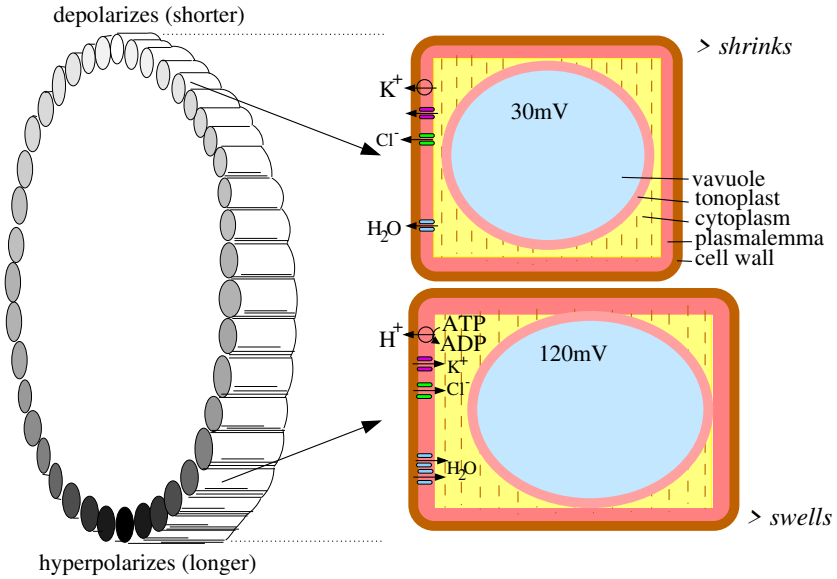

Figure 3.12: *A ring of motor cells illustrates the bending and lifting of leaves or leaflets by a pulvinus, which would consist of many such rings next to each other. In reality there would furthermore be not just one, but further cell rings inside the one shown here. But the principle can be demonstrated: Depolarised cells (upper right) loose* K^+, Cl^-, *and water and the turgor decreases. As a result, the vacuole shrinks and the cell shortens. At the same time the lower cells hyperpolarise (by a H+-ATPase pump in the outer cell membrane), gain* K^+, Cl^-, *and water, and the turgor increases, which leads to a lengthening of the cells (right figure). In connection with cellulose microfibrils (indicated by small brown lines), which allow stretching only in the longitudinal direction, the pulvinus and the leaf connected to it would move upward. After some time (in the case of the terminal leaflet of* Codariocalyx motorium *after 12 h, in the case of the lateral leaflets after some min, depending on the temperature) the upper cells would hyperpolarise and the lower depolarise: The pulvinus and the leaflets would bend down.*

pronounced and help winding plants to find a hold. Circumnutationen are wide spread and known from winding and non-winding dicots, monocots, gymnosperms and even from fungi and bacteria. Roots can also nutate ('root waving').

The period length of circumnutation is temperature dependent and lies between the minute and hour range in various species; in some cases the circumnutations show different frequencies in the same plant (see Neugebauer). In Chap. 1 (*The circumnutating movements of seedling plants*) of Darwin, Darwin 1880 the authors are elaborating on the subject.

Nutational movements shown in Fig. 3.13[38] present results of the thesis of Neugebauer using *Cardaminopsis* seedlings. He used imaging methods and analysed with Winfried Hellrung the elongation and direction of the hypocotyl growth. In Fig. 3.14 four stages of the elongating (and nutating) hypocotyl are shown and below the result of the imaging analysis. The vertical

[38] and in a movie in How plants grow and move

lines represent the ultradian movements, the stepped increase in size the circadian modulation of the elongation (during 4 days). The colour coding indicates the position of the pixel wise recorded vertical natural markers on the hypocotyl and the right image explains the position with a colour circle. This behaviour has been modelled by Winfried Hellrung as described in the mentioned publication and shown in Fig. 3.15.

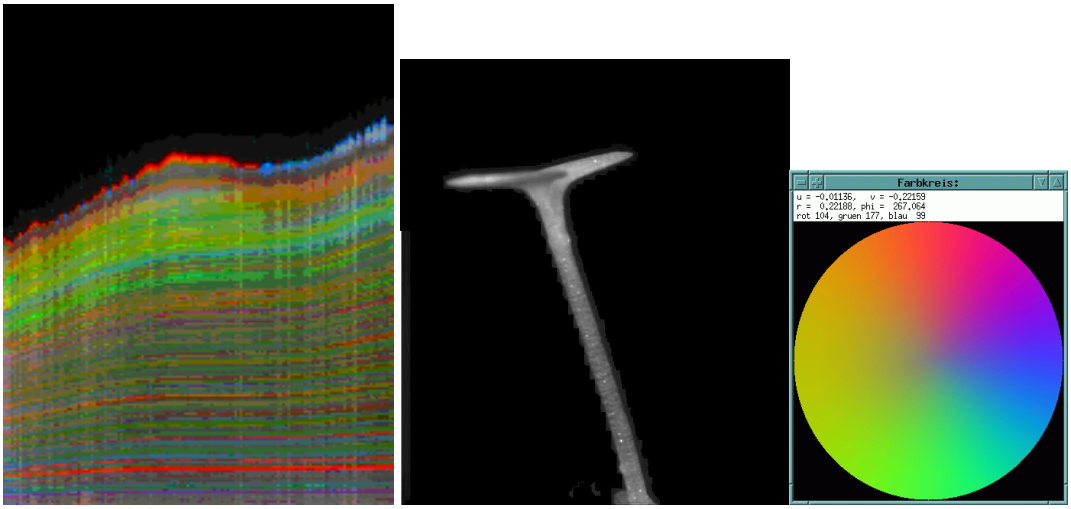

Figure 3.13: Left picture: From two pictures (x and y directions) of the growing seedling a three dimensional plant was calculated and transferred into straight line. The bendings were colour coded for all locations of the hypocotyl using the colour circle in the right picture (it represents the bending direction by the colour -yellow: Bending towards the camera, blue: away from the camera, red: to the left, green: to the right- and the amount of bending by the colour saturation). Center: Plant at the end of recording. From *Neugebauer*

For this purpose we assign a colour circle onto a cross Section through the seedling (Fig. 3.13).

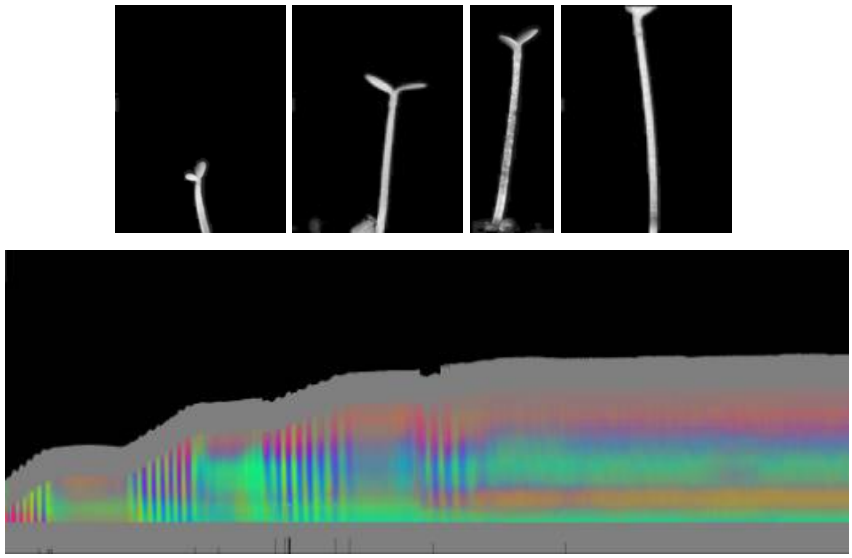

Figure 3.14: *Top: Hypocotyl of* Cardaminopsis *seedling in 4 stages of its elongation. This occurs in nutational movements as shown in a movie in How plants grow and move and in the Fig. 3.15. The vertical lines represent the ultradian. helical, movements, the step wise increase in height of curve the circadian modulation of the elongation. After Neugebauer.*

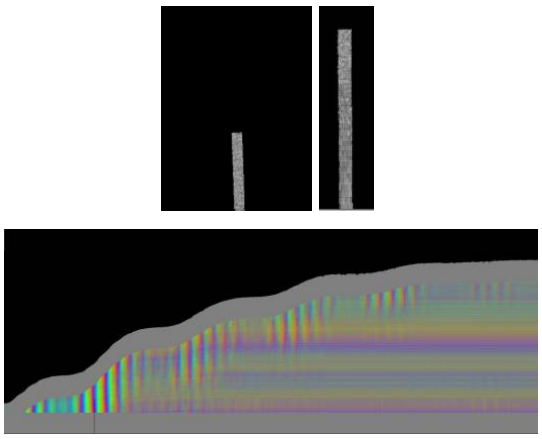

Figure 3.15: *Above: Two stages of* simulated *hypocotyl of* Cardaminopsis *seedling. Below: Color representation of bending of hypocotyl stem as a function of time. Elongation occurs in nutational movements (as shown e.g. in a movie in the publication How plants grow and move) . In the pattern the vertical lines represent the ultradian movements, the increase in size shows a wavy form, due to the circadian modulation of the elongation. The results of the simulation are quite similar to the recorded movements in Fig. 3.14. After Neugebauer.*

4 Significance of rhythms for humans

The natural light[1] has given the frame for the activity of our ancestors for millions of years. They were active mainly during the day and slept at night. With artificial light, especially the electric light, this changed. Its significance for our health and our life quality was discussed e.g. in a workshop (Münch et al. 2020). It turned out, that there is a big uncertainty about the optimal conditions of natural light for physiological and psychological processes (1), that the recording methods and evaluations for daylight should be known better (2), and that the interdisciplinary cooperation should be closer (3). In the workshop it was proposed, how this could be improved in the long run.

Circadian rhythms control numerous instances in the body humans such as sleep and wake, the cardiovascular system, metabolism, the immune system, reproduction, behaviour, alertness and mood. As in other vertebrates these processes are controlled by the SCN as the main pacemaker.

The SCN[2] is located in the hypothalamus above the optic chiasma and controls many circadian rhythms in the body including neuronal and hormonal activities (see Fig. 4.2 and Hastings, Maywood, Brancaccio (2019)). It receives its information about the ambient light conditions in the environment via the retinohypothalamic tract (RHT) from the retina in the eyes and is thus entrained to the 24 h day (see Fig. 4.1 and Fig. 4.2, and Foster, Hughes, Peirson 2020).

The circadian system of mammals consists besides the SCN as a master pacemaker of further circadian oscillators in the brain and of local clocks in the whole body. The cells of the pancreas for instance possess clocks, which are entrained by meal times, neuronal, endocrine and temperature signals, and they control various physiological processes including metabolism. They regulate the transcription of genes, which are involved in stimulating the secretion of insulin, in order to provide glucose. Irregular meal times, shift work or jet-lag can disturb the metabolism and lead e.g. to insulin shortage (hypoinsulinemia). For a mathematical model which describes this pancreas controlled circadian glucose homeostasis see Woller, Gonze 2018. They used data from experiments on rodents.

4.1 Human clocks - an outline

At this point it is again appropriate, to point out the significance of models in chronobiology (see Beersma (2005) and later chapters). Models for the circadian rhythm of humans were among others proposed by the Kronauer team and were further developed during the years. An older

[1] direct, strayed and reflected sun light. Depending on the latitude, time of day and season, and environment (buildings, vegetation), the radiation density and spectral composition changes

[2] It consists of about 20 000 neuronal oscillators and other cell types which put out peptides such as vasopressin and the vasoactive intestinal peptide, and neurotransmitters. It interacts with other nuclei of the brain

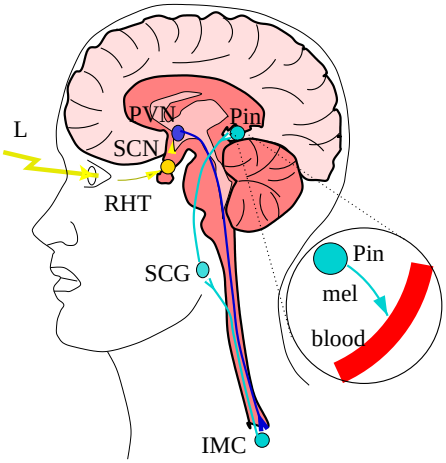

Figure 4.1: *Photoendocrine system in humans consists of the retina in the eye, that perceives light of the environment via special ganglia cells.*
The light information (L, yellow) is transmitted via the retinohypothalamic tract (RHT, yellow) to the suprachiasmatic nucleus (SCN, yellow), which is the main circadian control site. Efferents (yellow arrow)) transmit the cues via the paraventricular nucleus (PVN, blue) and the intermediolateral column (IMC, light blue, in the spinal cord) to the superior cervical ganglion (SCG, light blue). Postganglionic fibres stimulate by norepinephrine the melatonin (mel, night hormone) production in the pineal gland (Pin, light blue). Via the blood system melatonin feeds back to the SCN with its cellular endogenous clocks (see inset scheme).
Drawn by one of the authors (WE) after a figure in Stehle et al. 2011 and in Forskning och Framsteg .

model (Kronauer, Czeisler et al. 1982) does describe quite precisely, how strong light (above 4000 lx) given over a longer time (about 5 h) influences phase and amplitude, but it could not describe correctly more recent results, according to which shorter and weaker illuminations were effective. Therefore the authors proposed a newer model (Jewett, Kronauer 1998), in which a dynamic stimulus processor (process L) mediates between the light stimulus and the traditional circadian pacemaker as a self excited limit cycle oscillator (process P). With this model phase shifts by short and long light pulses and arbitrary intensities can be simulated. The model makes predictions, which should be tested (Kronauer, Czeisler et al. 1982).

The VP-oscillator in Kronauer's model was replaced by a limit cycle oscillator of higher order (Jewett, Forger, Kronauer (1999)), with which the amplitude in the neighbourhood of the singularity would recover more slowly and in the neighbourhood of the limit cycle faster. The maximal sensitivity for light is now about 4 h before the body temperature minimum and the critical phase 0.8 h later as compared to Kronauer's earlier model. The new model shows a direct effect of the light on the circadian period: With increasing light intensity the period decreases, which is in accordance with the Aschoff rule[3].

Special findings in the circadian system such as late sleep under free run conditions compared with those under entrained conditions, internal desynchronisation between circadian rhythms and the sleep-wake cycle and bicircadian (48-50 h) sleep-wake cycles could all be explained with the coupled oscillator model of Kronauer, Czeisler et al. (1982), but the physiological basis was unclear. Phillips, Czeisler, Klerman (2011) tried to elucidate with a physiological model of hypothalamic and brain stem nuclei the mechanisms, which are responsible for internal desynchronisation.

Indic et al. (2005) compared two models, which describe phase and amplitude dynamics.

[3]The free run period of night active animals is longer in LL than in DD; in day active animals it is shorter in LL than in DD (LL = continuous light, DD = continuous dark)

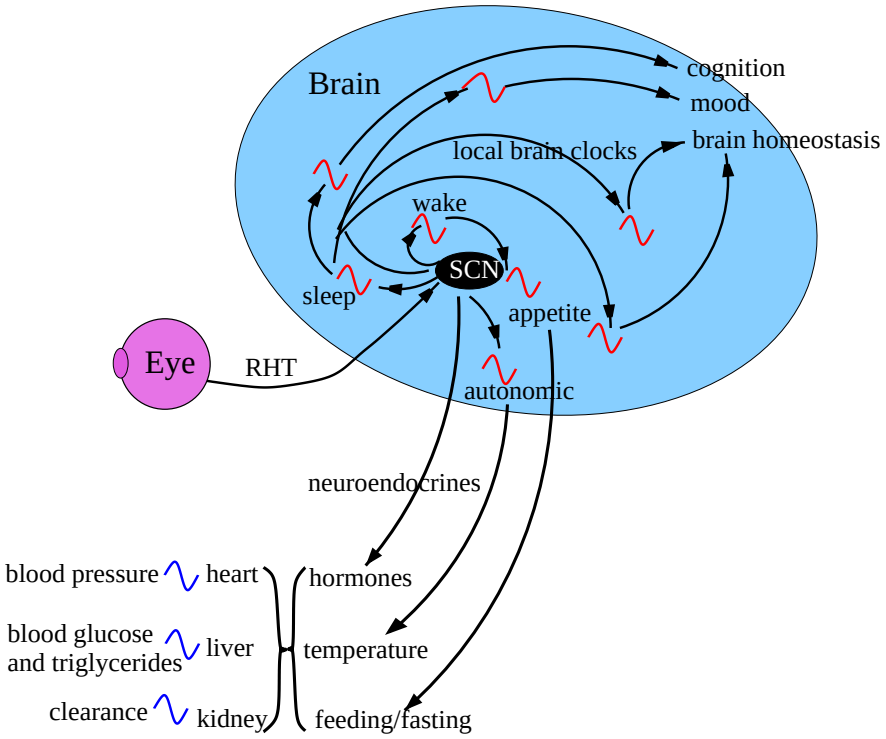

Figure 4.2: *Circadian rhythms and suprachiasmatic nucleus. The SCN as a central pacemaker receives signals from the eye about the LD conditions of the environment via the retino-hypothalamic tract RHT and its neuroendocrine and autonomic outputs lead via hormones, temperature and feeding/fasting routes to a circadian control of e.g. blood pressure in the heart, glucose and triglyceride control in the liver, and xenobiotic clearance in the kidney. The SCN furthermore influences other circadian centres in the brain which are responsible for the circadian control of cognition, mood and brain homeostasis (after Hastings, Maywood, Brancaccio (2019), simplified)*

They differ in their prediction, how fast phase and amplitude recover, if the amplitudes of the oscillation are small. If the biological processes, which are responsible for the rhythms, are brought in, more computational effort is necessary. Two models for mammals, one of it by Leloup, Goldbeter (2003) and Leloup, Goldbeter (2004) and the other one by Forger, Peskin (2003) with 19 respectively 73 differential equations have been published. It has been reduced to a model with two differential equations only, which still describes the most important properties of a biological clock, namely an about 24 h period, entrained by the LD cycle, the phase response curve and the amplitude recovery after a corresponding disturbance. This simplifies the mathematical analysis considerably. It can be used, to couple oscillators for mammals with each other and to understand the dynamics.

Kronauer, Gunzelmann et al. (2007) published the results of a symposium, at which models for circadian rhythms in humans were debated and stresses, that a close collaboration is

needed between those researchers, which work experimentally, and those, which construct mathematical models.

Many biological systems consist of a large number of dynamical units. To model them means either to simplify them on a coarse scale, or to use large computations. However, the Ott-Antonsen and Watanabe-Strogatz method (Ichiki, Okumura 2020) allows to bridge these different approaches and simplify the analysis by reducing the model (Bick et al. 2020). It still describes the dynamics for the subpopulations in the oscillator network via few collective variables. The model links microscopic and macroscopic descriptions of the underlying system, but are still simple enough to analyse without great computational effort. A similar approach is taken by Hannay, Booth, Forger 2019, who integrate measurements in single cells, tissue, and at the behavioural scale, allowing to develop accurate low-dimensional models for human circadian rhythms.

Recently *system biology is used as a sup*plement of molecular biology, to understand the various components of a system and the network of the interactions, so that it can be better controlled and new systems with adequate structures and the underlying dynamic principles be build (Ueda 2007). Circadian clocks of mammals were used as a model system with clock controlled genes and cis-elements, transcription and post-transcription loops (with functional genomics), with parameter changes of the clock components, disturbances of the clock and the special singular behaviour. To the model belong also phase shifts, nonlinear behaviour, temperature robustness of the period, and entrainment; furthermore, how clocks interact with the environment, how e.g. light changes are represented internally, how the day length is photoperiodically perceived. The singular behaviour of biological clocks can also be studied in a biological way as a system (Ukai, Kobayashi et al. 2007).

For better understanding the property, to become arrhythmic after a special pulse given at a certain time point, the photoreceptor melanopsin was introduced in mammalian cells. In this way they became light sensitive. The cellular clocks could indeed be brought into a singular state by a critical light pulse. Theoretical considerations show, why the singular behaviour occurs in various organisms. It is assumed, that desynchronisation is the most probable mechanism for arrhythmicity. The *in vitro* and *in silico* findings are confirmed by *in vivo* observations, according to which desynchronisation is responsible for the decrease in amplitude of the rhythms in the suprachiasmatic nucleus after a critical light pulse (Ukai, Ueda 2010).

A further model explains, how in flights crossing time zones the circadian system entrains slowly to the new time zone (Gander, Kronauer, Graeber 1985). How fast this resynchronisation occurs depends on the number of time zones which are crossed, on the flight direction (east or west) and on the strength of the Zeitgeber in the destination area (Gander, Kronauer, Graeber 1985). Differences in the adaptation depend mainly on the individual period length of the passengers.

Furthermore models for shift work are important (see page 62). The aim is, to find an optimal arrangement of the work times, which take into account the needs of the shift worker as well as the industries, hospitals etc.. For this, time schedules were developed, which shall avoid strong conflicts with the circadian system of the worker (Czeisler, Moore-Ede, Coleman 1982). To test these specifications in respect to the rhythm of the shift workers in the respective shifts the two-oscillator model of Kronauer, Czeisler et al. (1982) was used (Kostreva, McNelis, Clemens 2002). The most adequate shifts are those, in which the rhythm is close to the free run rhythm

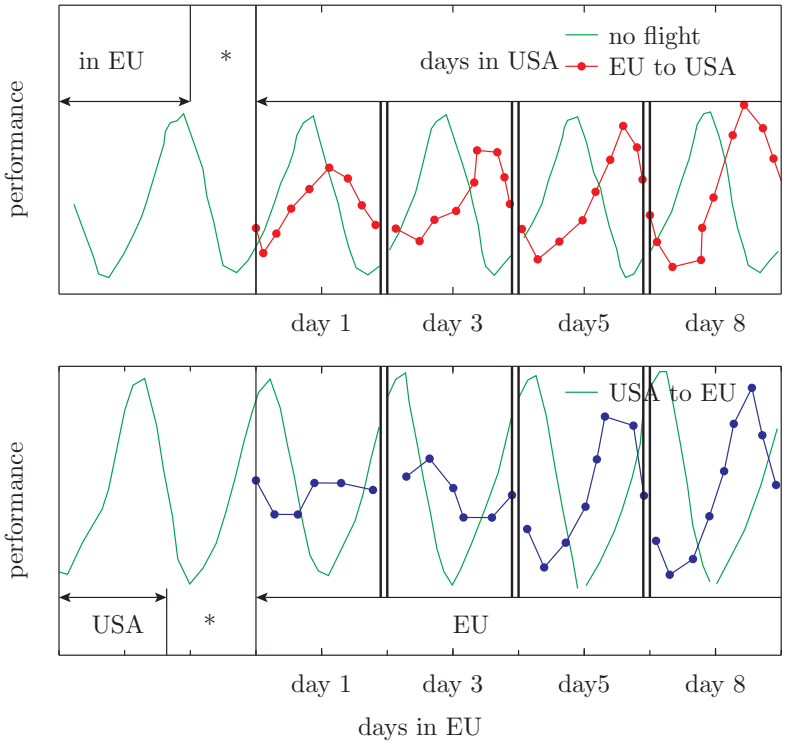

Figure 4.3: *Phase shifts by 8 h of the circadian performance rhythm of a pilot in a flight simulator. Top, red curve: Performance after a simulated 8 h flight from Europe to the USA and back, bottom, blue curve. After about 5 days the amplitude is normal again. Green curves show the normal performance rhythm without flight (extrapolated from preflight data). The travel time is marked by *. After a figure in Forskning och Framsteg, which was taken there from Ref 8*

and the rotation patterns should be slow, forward changing in a 2-week alternation, and contain two recovery days per week.

Wang et al. (2004) modelled periodic oscillators of biological networks with multiple genes, proteins and time delays by using multiple timescale networks. *Fast* reactions formed a positive feedback-loop network, *slow* reactions a cyclic feedback-loop network in the multiple timescale network. It applies to the modelling, analysing and designing a wide variety of biological systems.

4.2 Jet-lag, shift work, and social jet-lag

The ability and nowadays often used possibility to travel to other time zones leads to temporary symptoms such as tiredness, sleeplessness and other physiological, psychological, and cognitive troubles called *Jet-lag*. After the flight the phase of the LD cycle of the new environment differs from the internal time, and our body clock and the new local time are not anymore synchronised with each other. These symptoms of circadian dissonance can occur not only after eastward or westward flights across multiple time zones (see Fig. 4.3), but are encountered also during *northern or southern flights* when no time zones are crossed. The reasons are, that daylength also influences synchronization, as shown byDiekman, Bose 2018.

Using a model of the human circadian pacemaker these authors studied the process of reentrainment to the LD cycle of the time zone in the flight destination. They calculated the reentrainment time for flights between any two points on earth and at any time of the day

and year. Their results explain for instance, why most people experience a worse jet-lag after eastward flights than westbound ones. This East-West asymmetry depends not only on the circadian period of the air passenger's circadian clock being larger than or less than 24 h, but also on the daylength, as mentioned above. Why synchronisation is faster in westward flights was studied in a model based on the microscopic dynamics of individual pacemaker cells in the SCN (Lu et al. 2016). A simplified model by Kuramoto 1984 was used to model the large number of coupled phase oscillators in the individual cells of the SCN with heterogeneous intrinsic frequencies and external periodic forcing. The model parameters were estimated from previous biological experiments.

How fast resynchronisation occurs depends not only on the flight direction, but also on the number of time zones crossed and the strength of the time cues in the destination area (Gander, Kronauer, Graeber 1985).

It takes longer to resynchronise oscillators in peripheral tissues, organs and other oscillators in the brain as compared to the oscillators in the SCN. But even in the SCN the circadian oscillators in the cells do not resynchronise immediately (Harrison, Gorman 2015).

What can be done against jet-lag and the sleep problems connected with it is presented by Cingi, Emre, Muluk 2018. Non-pharmacological interventions for jet-lag such as light treatment, exercise, diet are explained by Bin, Postnova, Cistulli 2019. The results of these authors and of others can help air passengers to minimise jet-lag on transmeridian and translatitudinal journeys. An app program of Olivia Walsh, which is based on the method of Serkh, Forger (2014), could also bear a helping hand.

Of practical value are the results of jet-lag studies also for athletes and participants in Olympics. Thus, Lok et al. 2020 found for swimming that the timing of physical performance over the day can decide over the time difference between gold and silver medal in 40%, silver and bronze medal in 64%, and bronze or no medal in 61% of the finals. The fastest swim times occurred in the late afternoon around 17:12 h.

Phase shifting due to air travels is also important for the outcome of horse races. Horses are extremely sensitive to sudden changes in photoperiod and can benefit from them, as found by Tortonese et al. 2011. The light seems to adjust their phase shift to the new condition quite fast. This is not the case for humans. Thus for horse races in areas with different LD conditions the scheduling for the horses and riders has to be different if tournaments are on stake.

Jetlag symptoms are typical also for shift workers. Whereas the body clock has to adapt to the external time after a flight only once, it is at shift work more frequently dissociated with the locale time. This leads often to health problems (Reid et al. 2018).

Shift work is quite common in many branches[4] and the number of shift workers is increasing. Thus, in Germany according to Eurostat the number of people working between 18:00 and 23:00 has increased from 15.5% in 1992 to 25.2% in 2016, and the total number of shift workers increased from 11.5% to 17.4%. In the United States there are 20% shift workers (Deng, Kohn et al. 2018).

Approximately 5-10% of the workers suffer under shift work caused disorders. These disorders result from altering the sleep-wake schedule in relation to the external environment called *chronodisruption* (Kolbe, Oster 2019). They are often accompanied by metabolic disturbances

[4]Early, late, and night shifts are offered in either 2-shift, 3-shift or more shift schedules

such as overweight and type-2 diabetes, the development of the metabolic syndrome (Guerrero-Vargas et al. 2018), and a higher risk for mental illnesses (Chellappa 2020; Brown, Martin et al. 2020; Torquati et al. 2019; Zhao et al. 2019). Shift work sleep disorders are discussed by Deng, Kohn et al. 2018; Kerkhof 2018.

Fortunately shift work can be studied also by using animal models such as rodents. Genetic disruption of circadian clocks in rodents leads to metabolic dysregulations comparable to what is observed in shift workers (Kolbe, Oster 2019). They also pointed out how important clocks in tissues are for the metabolic regulation. Mistimed meal times can easily disrupt metabolic health (see also Guerrero-Vargas et al. 2018).

The chronotype (see page 66) should also be mentioned in connection with shift work, since morning types, particularly older workers, are less tolerant to it in respect to evening types, and they experience more sleep disturbances than non-shift workers (Hulsegge et al. 2019).

To find optimal working times, models were used, which take care of the needs of the shift workers and of the industry. For this time schedules were developed, which avoid strong conflicts with the circadian system of the workers (Czeisler, Moore-Ede, Coleman 1982).

Since light is the most important time cue for entraining the circadian system to the 24 h solar cycle, an accurate method to estimate circadian period from field data was developed by Woelders et al. 2017 who measured activity and light received in individuals which were unrestricted in their daily routines. This method may be important when optimising individual light treatment for shift work and jet-lag applications and for designing personalised chronotherapy. The findings from similar simulation studies by St Hilaire et al. 2020 using a mathematical model combined with sleep-wake and light exposure data helped to design shift work schedules with enhanced circadian alignment, which will improve sleep, alertness, and performance (see also Lunn et al. 2017).

Generally, health problems due to shift work can be avoided by providing an optimal work environment and ergonomical improvements, by avoiding, that the circadian system is disrupted by wrongly applied Zeitgeber, the most important of which is light. But diet and exercise are also time cues for circadian clocks in many tissues. The results of work by (Potter, Wood 2020) can help shift workers to adapt better to their work schedules by realising the importance of light and diet timing, the composition of food, and to improve their lifestyle (see also Gupta, Roth et al. (2019) and Woller, Gonze (2018)).

Shift work disrupting the circadian system has been classified as probably carcinogenic by the *International Agency for Research on Cancer*. It is caused by work overlapping with the individual subjective night (Fritschi et al. 2018). The authors used data from women working during their biological night with increased risk of breast cancer. The risk did not depend on the chronotype.

Shift worker suffer often under sleep disorder. Different strategies can be used to help them and guidelines based on biomathematical models of alertness are presented (see Darwent, Dawson, Roach (2012)). A mouse model was used by Barclay et al. 2012 to study its disruptive effect on metabolism. Walbeek et al. 2019 tried to increase the circadian flexibility in rodents using dim light at night by rhythm bifurcation and by changing the day length. If such protocols would work also in shift workers, it might facilitate to align their internal time with the external demands.

A similar approach was chosen by Noguchi, Harrison et al. 2020 using mice to overcome the

limited flexibility of the SCN to adjust to new LD cycles. They used atypical 24 h LDLD cycles leading to bifurcation (see Bifurcation) and resulting in faster resetting of behaviour, as predicted by a mathematical model (Noguchi, Leise et al. 2017). Such a non-invasive and simple light manipulation might also be applicable for shift work or jet-lag.

Another way is to alter diet and meal timing during night shifts, as reported by Gupta, Centofanti et al. 2019. Eating a large meal during the night shift impairs cognitive performance and increases sleepiness; shift workers should opt for a snack at night.

Shift work increases the risk of cardiovascular disease, as shown by Skornyakov et al. (2019) after dissociating effects of circadian misalignment from those of sleep displacement and altered physical activity patterns, whereby time of day, sleep/wake state, and physical activity have to be taken into account.

Shift workers sleep less than day workers (Richter et al. 2020). 20–40% of them have difficulties initiating and maintaining sleep. They use often alcohol as a self-medication, but this further impairs sleep quality and increases sleepiness at work. Nurses aged over 50 years are an important risk group. Preventive programs and alternative sleep aids are urgently needed.

Shift work leads also to sleep disorder such as insomnia or excessive sleepiness, to metabolic disorders, such as insulin resistance, diabetes, dyslipidemia, and metabolic syndrome, and it has been implicated in weight gain and cognitive impairment. Sleep schedules, timed bright light exposure, timed melatonin administration, and stimulants or drugs promoting alertness can be used to manage shift work sleep disorder (Burman 2017). Mukherji et al. (2015) tried to understand the molecular mechanisms causing these pathologies. Using mice, they revealed how metabolic alterations due to shifting the eating schedule from the active phase to the rest phase creates a misalignment between the central and peripheral circadian clocks. The metabolic syndrome is similar to that observed in shift workers.

In a number of conferences problems due to shift work and suggestions for solving them have been addressed (see for instance Roach et al. 2018).

Related to these problems is the social jet-lag (a circadian misalignment) which shift worker experience, if the time structure of workdays and free days differ. This affects especially older shift workers (Hulsegge et al. 2019).

Social Jetlag: There are two main problems in the modern societies which are due to the introduction of electric light allowing activities to be extended into the night: Irregular time schedules for sleeping and eating, and social jet-lag, a measure of circadian misalignment between an individual's circadian clock and social time. Social jet-lag is measured as the time difference between the midpoint of sleep during work/school days and on free (weekend) days. It might lead to chronic sleep loss and a number of health problems including obesity (Roenneberg, Allebrandt et al. 2012). Obesity has reached crisis proportions in industrialised nations and is also wide spread among children (Skjåkødegård et al. 2020; Johnson, Reid et al. 2020), adolescents (Zwart et al. 2018) and adults (Kim, Kaur et al. 2020).

Irregular time schedules for sleeping and eating disrupts the circadian system and could result in increased cardiometabolic risk (Zuraikat et al. 2020) and other major chronic diseases (McMahon, Burch et al. 2019). Synchronisation of feeding and sleeping behaviour with environmental cycles are recommended (Mota et al. 2019). Regular sleep habits together with healthy dietary patterns (Mediterranean food) prevents obesity, especially among young adults (Zerón-Rugerio, Cambras, Izquierdo-Pulido 2019).

Social jet-lag does not depend on chronotype, but they are related, since evening types tend to have a larger social jet-lag (Silva et al. 2016; Wong et al. 2015).

The economic effects of social jet-lag are discussed by Giuntella, Mazzonna (2019).

4.3 School time, chronotypes and daylight saving time

For many pupils school begins nowadays too early. In the preindustrial time most people slept between 20:00 and 6:00 and could therefore easily start at 8:00[5]. But nowadays they do not go to bed early enough, because they are engaged in the evening with watching TV or being active otherwise. This leads to social jet-lag (see page 64). It is at the expense of a restorative sleep, which is extremely important for their health and for the consolidation of the learned by the short term memory in the precortex (see Sect. 4.4). During puberty the time to go to sleep is additionally shifted into the night[6]. The daylight saving time (DST) adds another hour to the discrepancy between social and body time (see page 68 and Walker 2018), which increases the social jet-lag still further (the *limping time*).

The consequences are a misalignment of the circadian system with the solar time and not enough sleep primarily due to the early school begin (Crowley, Eastman 2018). Bright light in the morning (and later in the afternoon) can help to correct this misalignment of the circadian system in postpubertal adolescent by advancing the circadian clock, as shown by Crowley, Eastman (2017). The blue part of the spectrum of this morning light is important, since it removes the sleep hormone melatonin rapidly. Lack of short wavelength light in the morning delays the circadian clock, as shown for 8th-grade students by Figueiro, Rea 2010 using field data. Blue light in the evening should be avoided[7], since it is effectively delaying the circadian clock (Touitou, Point 2020).

Social jet-lag is associated with later schedules of meals and snacks and higher consumption of food throughout the day and together with the misalignment of food behaviour it can lead to obesity, which is a serious thread to the health of school children (Zwart et al. 2018; Skjåkødegård et al. 2020). If feeding behaviour, sleeping and waking hours would be better synchronised with environmental cycles, the negative impacts of these factors on health could be reduced or avoided (Mota et al. 2019; Mathew, Hale, Chang 2020).

Favourable sleep times are important for physical activities of preadolescent (Stoner et al. 2018) and adolescent (Aoki et al. 2020), their health (Palafox et al. 2019) and their school performance (Zerbini, Merrow 2017). Late chronotypes (*owls*) are especially discriminated, since the chronotype effect on grades is strongest in the morning, but disappears in the afternoon. Strategies against the mismatch between the adolescent circadian clock and the school clock could involve: Advance the sleep timing by adequate light schedules (see above), delayed school begin, and performance tests later in the day.

[5] Today only 23% of the US Americans would wake up before 7:00 without help by an alarm clock, as inferred from their sleep wake time on days off. Therefore 78% of the working population has to use an alarm clock during the winter and 72% during the summer.

[6] Crowley, Fournier, Eastman (2018) tested the hypothesis, that the free-running circadian period was getting longer during this time, but found it was similar to the one in adults.

[7] including LED and smartphone displays

Chronotypes: As mentioned already, there are different chronotypes in humans. The morning types, the *larks,* are wide awake in the morning and tired early in the evening. The evening types or *owls* get into gears late and stay awake late into the evening. Most people belong to the indifference type (or called also *doves*). You probably know already to which type you are belonging[8]. If not, you could use the Munich questionnaire to find out your chronobiological phase type (see https://humansleepproject.org/de/chronotyp).

Why are there these different types? As a guess: People used to live together in groups in nature, often in uncertain environments. It was important for the group, to have watchman in the night as well as in the early morning, to allow the members of the group to sleep safely.

The chronotype is mainly regulated by the circadian clock, caused by genetic variations in clock genes[9] and by environmental influences (Wittmann et al. 2006). A missense variant of the PER2 gene[10] and common in European populations, is associated with the later chronotype and a longer circadian period (Chang, Duffy et al. 2019).

The various chronotypes live so to speak in different geographical latitudes, that is, in their own chronobiological time zone (Roenneberg, Winnebeck, Klerman 2019). Whereas the inhabitants of Chicago live physically there, their body clock runs, depending on the chronotype, in such a way, as they would live East or West of Chicago in a virtual time zone. This difference was small at the time artificial light was not available: The virtual time zone of the *larks* was somewhat more East, the one of the *owls* more West, and that of the *doves* was right in the centre of the city.

Today about 36% of the inhabitants of Chicago live physically and chronobiologically ±30 min in the true solar time, 24% would live further East, 18% further West (Nebraska), 12% still further West (between Denver and San Francisco), and 10% in the Pacific between San Francisco and Tokyo. All of them must, however, work or attend school in Chicago.

This worsens, if the social clock is switched to DST, Daylight Saving Time. Now people have according to the true sun clock to work in Nova Scotia, Canada, that is 1 h earlier. Our social time limbs in many cases behind the local time (*limb time*). Actually our society ought to considerate the various prototypes (larks, doves, owls), especially in the case of pupils (see page 65).

Chronotypes and health aspects: The different chronotypes are confronted with various health problems. Evening types are more likely to develop health problems.

In the Finnish population sleep has become insufficient and sleep duration has decreased since 2007 especially in women and younger adults (Merikanto, Partonen 2020). Eveningness has increased especially in older adults and in men. All this is alarming, since the health status has deteriorated and caused more strain to the public health. The authors urge to prevent this circadian misalignment in the future. Again in the Finish population it was found that evening types tend to have unhealthier behaviours and increased morbidity and mortality as compared with morning types (Maukonen, Havulinna et al. 2020). A higher genetic risk score

[8] There is a fourth chronotype, the bimodal type, associated with female gender, young age and lower BMI, may be influenced by social and environmental factors (Tempaku et al. 2017).

[9] But there is no change in the patterns of clock gene expression on workdays and the day after holiday in the morningness group, and social jet-lag moves the peak time of expression after holiday from early to late workday (Takahashi et al. 2018).

[10] PER2 is a core component of the molecular clock work

was associated with the evening chronotype. In an earlier study of this group (Maukonen, Kanerva et al. 2016) it was reported that unhealthy diet is associated with obesity, and that evening types eat more often unhealthier food as compared to morning types. The evening chronotypes were more often smokers, physically less active and health was adversely affected than in the other chronotypes. However, the chronotype was not associated with obesity.

Health and longevity can be predicted to a certain degree by the chronotype (Basnet et al. 2017). In the Finnish adult population the evening types had a higher chance to develop depression, get gallstones, and chronic obstructive pulmonary disease whereby the underlying mechanisms remain unclear. Among evening types mental illness is more frequent (Taylor, Hasler 2018). This association may be related to neural processes. The chronotype-mental health relationship was studied by Melo et al. 2017 in bipolar disorder patients. The circadian rhythm pattern was more frequently disrupted in evening types and during the depressed period, whereas during mania irregular rhythms were observed.

The impact of chronotype, social jet-lag and sleep duration on health and work ability was investigated by Yong et al. 2016. With increasing social jet-lag and shorter sleep duration the work ability index decreased, while chronotype was not associated with it. The authors suggest, that circadian misalignment, but not chronotype per se, may be critical for health. Longer sleep may override the adverse effects of social jet-lag.

Chronotypes and personality profiles: Jankowski, Linke (2020) were interested in personality profiles[11] associated with morningness-eveningness. They tried to understand the behaviours and mental states of chronotypes among school pupils aged 13–19 years. Evening chronotypes tend temperamentally to anger[12] (Thomas et al. 2020).

Wittmann et al. (2006) investigated phase shift effects on the internal circadian rhythm. Late chronotypes who experience the most severe circadian misalignment benefit from phase advances in the morning *and* in the evening, but early chronotypes exacerbate circadian misalignment by evening exercise. Thus, personalised exercise timing based on chronotype could lessen circadian misalignment in young adults. Associations of chronotype, well being, and stimulant consumption are strongest in teenagers and young adults up to an age of 25 years. The highest correlation exists between chronotype and smoking, which is significantly higher in late chronotypes of all ages. This is most probably caused by social jet-lag and not due to different chronotypes. The authors strongly suggest to adapt work and school schedules to the chronotype.

Sex moderates sleep quality in relationship with social jet-lag, but not for the association between sleep quality and chronotype, as reported by Raman, Coogan 2020 for young adults.

Chronotype and shift work: The chronotypes among day workers, rotating shift workers, including night shift work and how it was associated with age and sleep duration was examined

[11] Personality type refers to the psychological classification of different types of individuals. Personality types are sometimes distinguished from personality traits, with the latter embodying a smaller grouping of behavioral tendencies. Types are sometimes said to involve qualitative differences between people, whereas traits might be construed as quantitative differences. According to type theories, for example, introverts and extroverts are two fundamentally different categories of people. According to trait theories, introversion and extroversion are part of a continuous dimension, with many people in the middle. In contrast to personality traits, the existence of personality types remains extremely controversial

[12] amongst five domains of emotionality-distress, emotionality-fearfulness, emotionality-anger, activity and sociability

by Schuster, Oberlinner, Claus 2019. Compared to day workers, rotating shift workers were later chronotypes and slept longer. With older age, this difference increased, while the difference in sleep duration decreased.

More flexible work hours adapted to chronotype could be of advantage especially for older employees. Courses and health campaigns could help to better adjust the sleep patterns to the work hours.

Daylight Saving Time (DST) was temporarily introduced in various countries of the moderate zones. For reasons and the history see Daylight-saving-time. The DST is 1 h earlier than the standard time (= time zone) and is valid during the half year of summer (or somewhat longer), serving as the legal time[13].

Concerning the advantages and disadvantages and alternatives see Daylight-saving-time. There is also mentioned the negative consequences of the DST on health and psyche. The circadian rhythm of the organism is impaired and sleep researchers and chronobiologists plead for keeping the standard time permanently. How the circadian clock, the social clock, sun clock, time zones and DST interact is discussed by Roenneberg, Winnebeck, Klerman (2019).

The DST intensifies the difference between sun clock and social clock and thereby also the body clock. The social jet-lag is increased with severe consequences for health. Thus in one time zone the additional 1 h evening light shortens the sleep duration by 19 min. Is has significant consequences for our health (obesity, diabetes, coronary cardiovascular problems, breast cancer) and for economy (Giuntella, Mazzonna 2019). Especially late chronotypes suffer under the DST (Merikanto, Partonen 2020; Wittmann et al. 2006; Pilz et al. 2018).

Implications of the DST, a global experiment with 1.5 billion people, are social jet-lag and circadian disturbances with shortened sleep. Although this is almost compensated during the weekend by a longer sleep, but during the week it is too short and during the weekend too long. Furthermore the different meal times on weekdays and on weekends can lead to obesity and metabolic problems (Mathew, Hale, Chang 2020). Further consequences of the DST: In one night in March sleep is shortened by 1 h. Hospital recordings show, that the number of heart attacks and the amount of traffic accidents has increased.

In 2018 the population of the EU was questioned about the DST. 84 %, especially Germans, wanted to get rid of the DST. A slight majority preferred DST during the whole year. And what says the science? The question was ill expressed. With the DST we change only the social time, since the day length stays the same. Although we come home earlier, we have to start work and school earlier.

Scientific results speak strongly against a change from standard time to permanent DST. The social jet-lag is increased, if DST is effective over the whole year instead of 8 months. The body clock would be still later in the winter as compared to the summer.

One solution would be, to keep to the standard time and to adjust the countries and regions closer to their sun time. The social clock time would correspond to the local sun clock and thus more to the body clock. There would be no disadvantages: Those who prefer the summer time with long evenings could shift their individual working time or school time accordingly. The

[13] The central European summer time begins at the last Sunday in March at 2:00 CET; the hour counting is advanced by one h from 2:00 to 3:00 h. It ends at the last Sunday in October at 3:00 CET by putting the counting on a hold for one h: from 3:00 to 2:00. Remember the memory hook *Spring forward, fall back.*

decisions should be made by the employers and in the schools in order to respect the personal, biological, and social requirements.

4.4 Sleep, metabolism, medical aspects

Sleep is extremely important for our performance and health. Shortage of sleep can make us sick. The shorter the sleep, the higher is the danger to gain weight (costs: 2 billion US$ per year (Brum et al. 2020; Skjåkødegård et al. 2020)), to contract type-2-diabetes (costs: 375 billion US$), and life exspectancy is shortened by 10 years (Giuntella, Mazzonna 2019). The immune system is also affected by sleep deficiency. Sleep cleans and restores our brain during the night by the *glymphatic system*[14] (Plog, Nedergaard 2018; Jessen et al. 2015). Drugs such as coffee, alcohol and nicotine are toxic for sleep (see Walker 2018). Short sleep duration, sleep problems, and obesity during childhood correlate, as studied by Krietsch et al. (2019) (for sleep duration and obesity in children see aslo Skjåkødegård et al. 2020). Children with heavy adipositas showed a later mean sleep duration during the school nights (36 min) and weekend nights (39 min) as compared to children with normal weight. They had also more sleep problems. According to Chaput et al. (2020) earlier sleep timing and regularity in sleep patterns with consistent bedtimes and wake-up times are favourably associated with health and should be encouraged (see also Fischer et al. (2020) and Zuraikat et al. (2020)). More studies such as the one by Stoner et al. 2018 find associations between sleep duration, sleep disturbances, and social jet-lag (see page 64) with adiposity in children. There is furthermore an association between social jet-lag and poor quality sleep in late chronotypes of both sexes (Raman, Coogan 2020).

A sleep model of Borbely und Daan (Daan, Beersma, Borbely 1984) (see also Skeldon, Derks, Dijk 2016; Skeldon, Dijk, Derks 2014; Jewett, Forger, Kronauer 1999) consists of a sleep dependent process S, a circadian rhythm dependent process C and the sleep requirement (sum of S and C, see Fig. 4.4). The process S reflects the sleep pressure, which depends on the length of the wake time. It increases exponentially and reaches an upper threshold, the maximum of the sleep requirement. During sleep, S is diminished and reaches after about 8 h a lower threshold. After 16 h wake time during the day the sleep requirement is high. Process C is controlled by the circadian clock and is stimulated by the activity of the SCN. Ambient light activates the SCN, and the SCN neurons display a circadian pattern. Since the SCN regulates the melatonin secretion of the pineal organ, the process C can be measured by the concentration of this hormone in the blood. A number of studies allude to it, e.g. the one of Mithani, Fink (2019) with a sleep model especially for nurses.

This model was extended by introducing three neuronal populations which are interacting (Héricé, Patel, Sakata 2019). The activity of each population determines the current state, namely wakefulness, rapid-eye-movement (REM)[15] sleep or non-REM (NREM) sleep. This model provides further insights into the mechanisms of sleep-wake regulation. In a workshop

[14] there exists even an ocular glymphatic clearance (Rangroo Thrane et al. 2020)

[15] see Héricé, Patel, Sakata 2019 for the physiological basis of REM sleep, namely pons and many components in the hypothalamus, midbrain, and medulla and the sleep-regulating circuits. Included are computational studies of the sleep-wake cycle which emphasise the REM sleep regulation

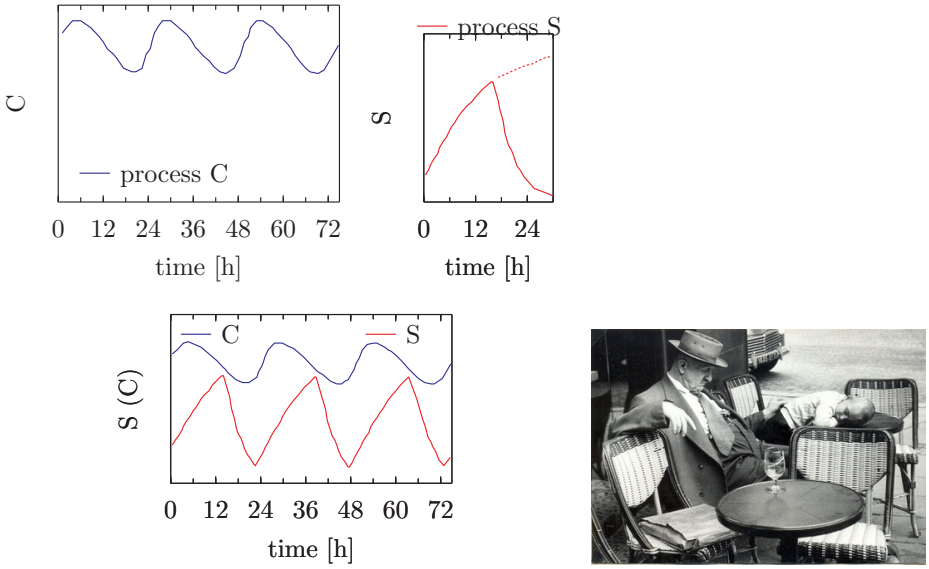

Figure 4.4: *Two process model of the sleep regulation.*
A circadian rhythm (process C, sleep dependant, blue curve) and a homeostatic process S (sleep dependent, red curve) interact with each other. A threshold for falling asleep (when the red curve hits the blue one) and a threshold for waking up (the red curve touches a threshold in its lowest point) are thereby important. The model was tested in rats and in humans. After Daan, Beersma, Borbely (1984). Photp: Sleep siesta in Paris, *snapped by Anders Johnsson*

the models of sleep regulation were discussed and how it influences our behaviour (Borbely et al. 2016).

The later sleep onset during late adolescence begins in middle childhood (by 19 min age 8, by 38 min age 12, by 89 min age 17 (Kuula et al. 2018)), and Skeldon, Derks, Dijk (2016) take care of it in their model, including the advanced sleep in later life. According to Phillips, Clerx et al. (2017) who model REM sleep, the academic performance is poorer under delayed sleep. A countermeasure against delayed sleep is blue light therapy in the morning, applied in a home setting, which phase advances the circadian rhythm as well as sleep timing (Geerdink et al. 2016; Crowley, Eastman 2015).

The connection between sleep, circadian rhythms and learning is treated by Heller, Ruby 2019. The circadian clock does not only time the propensity for sleep, but also learning and memory performance. Memory consolidation occurs during sleep and the circadian system interacts critically with it, as shown in experiments by Dodson, Zee 2010 using mice and Siberian hamsters. The latter can be made arrhythmic *permanently* by a light treatment advancing the rhythm on one day and delaying its phase on the next day. In this stage hamsters cannot learn anymore. The authors hypothesise, that the circadian system dampens neuroplasticity during sleep in order to stabilise memory during transfer to long-term memory. Sleep and the circadian systems play integrated roles in memory consolidation and do not just influence it separately and coincidental.

Sleep models should take care of consequences resulting from sleep disorders (see Abbott, Reid, Zee 2015 and Martinez, Carmo Sfreddo Lenz 2010), but regard also the large interindividual variability in the timing of sleep and circadian rhythms (Swaminathan, Klerman, Phillips 2017).

Therapies (Dodson, Zee 2010) such as light treatment (Gooley 2008; Fahey, Zee 2006) and other practical advice are available (Bjorvatn, Pallesen 2009; Morgenthaler et al. 2007). These models should also describe and simulate the effects of shift work (Rempe et al. 2018; Wehrens et al. 2012) and jet-lag (Cajochen 2005).

Circadian alignment of sleep, meal patterns and physical activities are essential for metabolic health and body weight management. Misalignment affects the architecture of sleep, disturbs insulin metabolism, leptin-, ghrelin and gut-peptide concentrations leading to metabolic disturbances (Westerterp-Plantenga 2016).

The neural systems that regulate sleep/wake states in mammals and their circadian timing mechanisms was reviewed by Scammell, Arrigoni, Lipton 2017. They also outline key models for REM and non-REM sleep, and how dysfunction in the circuits can give rise to sleep disorders.

Sleep models have been used also for mammals: By Cardon et al. 2018 for elephants and sloths, by (Phillips, Savenkova, Karatsoreos 2015) for mice, by (Gandhi et al. 2015) for zebrafish, by (Dubowy, Sehgal 2017) for *Drosophila*, to give a few examples.

4.4.1 Metabolism:

Rhythms are also widespread in metabolism. We restrict us to circadian rhythms and the timing of nutrition (*chrononutrition*). What we eat depends on many factors and influences our gut microbiota[16]. On the other hand, gut bacteria influence also our eating behaviour. This relation was quantified by Di Stefano et al. (2019) using gut metabolic modelling and statistical estimators, to describe their dynamic interplay. They also studied the impact of shift work on the dynamics of chrono-nutrition. Taking into account also the social aspects allowed them to develop metabolic models and how they affect human health.

The nutrient metabolism is under circadian control. If the circadian rhythms are disrupted by lifestyle, work schedule, eating pattern, and social jet-lag, intestinal dysbiosis might occur with increasing risk of obesity, metabolic syndrome, cardiovascular disease, diabetes, cancer, and inflammatory bowel disease. There are mathematical models for understanding the interplay between peripheral clocks and metabolism. They could help to correct metabolic dysfunction (Bae et al. 2019).

How the life style such as sleeping time and duration and dietary pattern has changed in the last decades and how it affects public health reports Pot 2018. Main concerns are irregular eating, breakfast skipping, and late night eating. The chronotype plays an important role. Thus, *owls* are likely to eat late and tend to consume fewer and larger meals. It is associated with lower HDL-cholesterol levels, more sleep apnea and higher stress hormone levels. The BMI was associated with night eating (Baron et al. 2017). Mediterranean diet (see Mediterranean diet) and avoiding social jet-lag helps to prevent obesity (Zerón-Rugerio, Cambras, Izquierdo-Pulido 2019).

[16] ecological communities of commensal, symbiotic and pathogenic microorganisms; microbiome are the microorganisms; metabolome refers to the complete set of small-molecule chemicals within a biological sample (cell, organelle, organ, tissue, or an entire organism

A special kind of irregular eating pattern, but widely distributed, is the later meal times at the weekend as compared to the working days. In parallel to the social jet-lag this has been termed eating jet-lag. It was found by Zerón-Rugerio, Hernáez et al. 2019 to be associated with an increased body mass index independent of the amount and content of the food, and of the chronotype if the eating jet-lag was 3.5 h or more. This finding could be included as a warning to prevent obesity among the general population.

Circadian disruption in shift workers also affect nutrition and well being (Mohd Azmi et al. 2020). Thus, the risk of obesity and diabetes may be related to food intake at adverse circadian times, e.g. if it is too early in the morning in early morning shift workers (Stothard et al. 2020). These workers represent the highest percentage of shift workers in the US. In addition to shortage of sleep, the eating pattern being out of synchrony with the circadian clock leads to desynchrony of the central and peripheral oscillators (Oosterman, Wopereis, Kalsbeek 2020). Different strategies are described to promote synchrony within and between organs involved in metabolism.

Night shift work and, often connected with it, too short sleep has been found to lead to obesity, and obesity is associated with increased mortality and comorbidities. In night shift workers social jet-lag was increased too (Brum et al. 2020).

Strategies to minimise the metabolic impacts of shift work have been discussed by Kervezee, Cermakian, Boivin 2019. Most of the rhythmic metabolites were misaligned with the circadian system during the night shift, which could be the cause of adverse metabolic health effects observed in these shift workers. According to Voigt et al. 2014 the circadian disorganisation due to shift work and jet-lag can affect the intestinal microbiota which may have implications for inflammatory diseases.

Circadian disruption in shift workers on chrononutrition was observed by Mohd Azmi et al. 2020, since the biological clock of an individual is often altered during night shifts. This affects the psychosocial well-being and the circadian nutritional intake of the worker. Metabolic disorders such as hypertension, dyslipidemia, dysglycemia, and abdominal obesity might develop. The authors review how to prevent the metabolic disorders and how to maintain sound psychological condition in shift workers.

Too short sleep and social jet-lag has also been linked to obesity (Roenneberg, Allebrandt et al. 2012). The time of eating and sleeping should be considered when designing interventions for weight management, since otherwise obesity might result (Goheer et al. 2021).

4.4.2 Medical aspects:

In this part medical aspects of the functioning of the circadian clock and its importance for human health are alluded (Klerman, Brager et al. 2022). To begin with an example, administering the same drug at the same local time[17] to two people can have quite different effects, depending on the chronotype (see Sect. 4.3) of the two persons. The reason is, that one person might be an owl, going to bed late and rising in the morning late, if possible. The other person might be a lark, rising early and going to bed early. At the same local time they are therefore in different

[17] Solar time: refers to time derived from the geophysical LD schedule set by the sun. Social time: refers to local time, as on a watch or computer. Derived from combination of solar time and social considerations > circadian time: refers to time of our personal circadian clock

phases of their circadian clock. This is understandable, since the effect of a drug does often differ during the course of the daily cycle (a field called *chronopharmacology* (Arendt 2018)). Therefore a personalised medicine which takes this into account is advocated by Klerman, Rahman, St Hilaire 2020.

A disrupted circadian clock has been found to cause health problems leading even to tumourigenesis and cancer progression (Vitale et al. 2018; Verlande, Masri 2019; Erren, Lewis 2019; Ashok Kumar et al. 2019). On the other hand, cancer affects the circadian clock (Morgan et al. 2019; Kinouchi, Sassone-Corsi 2020) and oncogenic processes directly weaken circadian rhythms (Sulli, Lam, Panda 2019). By using mice, Shilts, Chen, Hughey (2018) found that a systemic disruption of the clock due to multiple oncogenes can promote tumour growth also in humans. For an epigenetic link between the molecular circadian clock and cancer see Hernández-Rosas, López-Rosas, Saavedra-Vélez 2020, for lung cancer, a malignant tumour with increasing incidence worldwide see Qiu et al. (2019), for breast cancer see Samuelsson et al. (2018), for thyroid cancer, which represents the most common malignancy of the endocrine system see Malaguarnera et al. (2020). According to Deng, Yang 2019 an abnormal expression of *Per* genes and disruption of circadian rhythms can lead to the occurrence and development of cancer. Clock genes contribute to carcinogenesis by altering the expression of clock controlled and tumour related genes downstream of many cellular pathways (Li 2019).

Pharmacological modulation of circadian clock genes can lead to new therapeutic options, and a well functioning clock suppresses cancer (Davis et al. 2019). For instance, it was reported by Rogers et al. 2020 that bright light in the morning can be used against cancer in children in which circadian rhythm disturbances are common. It was recommend to study the molecular mechanisms of the circadian clock and the role of clocks in physiology and pathophysiology in order to better understand the causes of cancer and to enhance chemotherapies by using chronotherapy to treat them (Keshvari et al. 2020). For cancer chronotherapy a comprehensive analysis of the circadian clock across different cancer types and proposed potential clinical treatments was performed by Ye et al. 2018. How clock genes affect the development of tumours and their prognosis showed Angelousi et al. 2019.

Sleep disturbances are a further field, in which intensive research in respect to the circadian system is going on. The 'delayed sleep-wake phase disorder' is an example (Wilson et al. 2018).

5 Scilab simulations and basics for modelling rhythms

Models can principally be quite different. They can describe the events in words and illustrations without going into the quantitative relations. Others are presented as block diagrams and use concepts of the control theory. Still others are purely mathematical and describe the variables by differential equations.

In the following we discuss, why models for rhythms are used (Sect. 5.2), what kind of models exist (Sect. 5.3), describe, how networks are build in the form of block diagrams by using differential equations (Sect. 5.5), and how such feedback models are generally and specifically treated (Sect. 5.6).

In all these cases Scilab/xcos can be applied successfully (see Sect. 5.1). Scilab is a comprehensive and very powerful program for applications in numeric mathematics and for simulating dynamical systems. It was developed at the *Institut national de recherche en informatique et en automatique* (INRIA) in France since 1990 and was taken over in 2003 by the *Scilab consortium*. In July 2008 the Scilab consortium fused with the *Digiteo Foundation*; since July 2012 the editing and development is in the hands of Scilab Enterprises. The book of Campbell, Chancelier, Nikoukhah (2006) is recommended to become acquainted with the program.

5.1 Scilab/Xcos: A short introduction

With Xcos, a tool of Scilab[1], dynamic systems can be simulated. An editor presents a graphic surface, on which functional blocks can be arranged, which are selected from a palette and connected with each other. Besides the functional blocks offered, own blocks can be created. Examples of Buchbeispiele Faes can be download from the Internet at Examples Scilab. Further information is available under Scilab further infos or by entering in the Internet the search term *Scilab xcos tutorial*, e.g. Xcos Introduction.

The program Scilab can be downloaded from https://www.scilab.org/download and is free of charge. Select a *Scilab*-Version - *Linux 64 bits (tar.xz)* and store it in e.g. the Download folder of your Linux distribution, unpack it there and use the folder Scilab-xxxx.xx (xxxx.xx is the curent version-number) for working. Use a terminal for this folder and enter *./bin/scilab* which starts the program[2]. The Scilab console appears with a left, middle and right part, and (behind it) a *palette browser* (containing various elements for building a model) and an empty window

[1] Xcos is a graphical editor for Scilab to design hybrid dynamical systems models. Models can be designed, loaded, saved, compiled and simulated. We use also Zcos, which is a Scilab XML (Extensible Markup Language) to display hierarchically structured data in the format of a text file. It can be read by humans as well as by machines

[2] The easiest way is to klick on the xcos or zcos file. The program will show the model structure. Alternatively the program can also be started via the toolbar or the icon

untitled - Xcos for the model building (in which desired elements can be drawn from the palette and wired for a model) or for working with a model.

We will now build a simple model, using an outline from a talk "Modellbildung mit Scilab/Xcos mit Beispielen aus der Biorhythmik" which one of the authors (Karl-Heinz Witte) gave at the *Tübix 2015* in Tübingen (Beispiele-aus-Biorhythmik and Vortrag von Karl-Heinz Witte, in German, sorry). Let us start with the construction of a first degree low pass filter[3], which consists of two elements, a step function and a continuous transfer function unit  . These elements were selected from the proper icons of the palette with a mouse click and drawn to the model building window. They can be shifted by a click into the icon - a green cross will appear and moved with the pressed mouse button. Click in the black triangle of the step function and create a line to the continuous transfer function unit by keeping the button pressed. The dashed line turns into a solid one[4] if you click afterwards somewhere on the model window.

Since we want to see the results of our model, we insert an oscilloscope icon and a clock generator and connect[5] them with the output of the continuous transfer function element (see Fig. 5.1). bar.

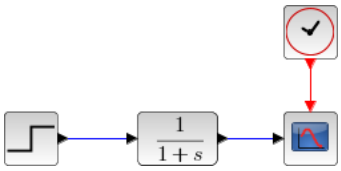

Figure 5.1: *Low pass filter consisting of a step function and a continuous transfer function* $1/(1+s)$*. A clock generator for scanning the results is included, so that not all results need to be displayed for each calculation step for data reduction.*

If we want to see the *step function* in addition to the *step function response*, we add a mux element[6] to see now both functions (see Fig. 5.2). To create the upper blue line it is important to know, that one has to click *first* on the upper input of the mux and then draw the connecting line to the connection of the two model elements. As soon as this line is hit, it will turn green and a small yellow box occurs, which marks the connection. Running the model (remember: click on ▷ in the menu bar) will show both curves simultaneously in the window (see Fig. 5.3).

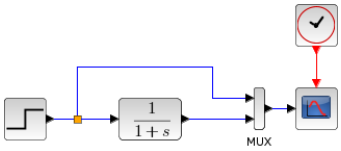

Figure 5.2: *Low pass filter consisting of a step function, a continuous transfer function* $1/(1+s)$ *with oscilloscope and clock generator*

The talk at the *Tübix 2015* continued with the predator prey model (see Fig. 5.26 in our book), how to construct a network from differential equations (see Sect. 5.5), the feedback model of Karlsson and Johnsson (see Sect. 7.1), the feedback model of Lewis (see Sect. 7.2), and leads to more advanced models describing the heart beat and its ECG signals (see Sect.7.8).

A few notes to the model building: Text can be added to the elements by clicking onto a block with the *right* button > format > edit > text setting (size, name, kind). The text will occur

[3] with a cut off frequency of 0.3 Hz, after Butterworth

[4] this connection is a regular signal

[5] this connection is an activation signal

[6] mux is not a multiplexer, but a kind of bus. Icon: 

underneath the block, but can be moved with the mouse. There the size and colour can also be set (use the slider).

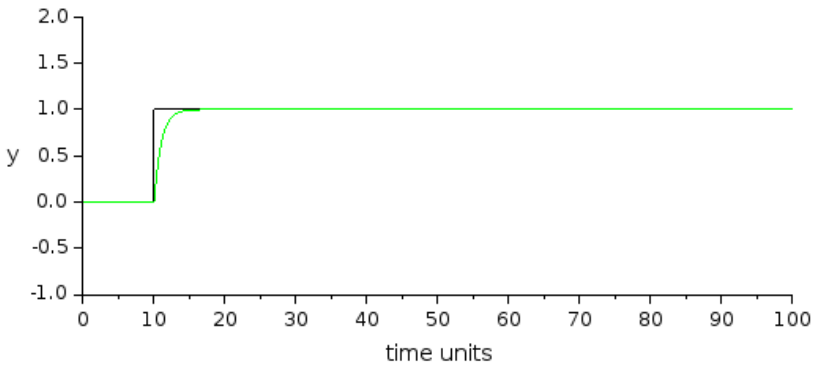

Figure 5.3: *Output x of the low pass filter in Fig. 5.6 (green curve) and the step function (black curve); time units arbitrary, e.g. in hours. (The green curve partially overwrites the black curve.)*

5.2 Why and how are models for rhythms used?

"*A useful model should be minimally complex to account for an existing set of data and maximally specific about what its parameters mean in physiological terms. It should not aim at completeness. The essence of a model's usefulness is in being a simplification of nature, rather than in approaching the complexity of nature itself.*" (Box 1 in Daan, Beersma (1984)).

The concept of "model" is nowadays used in different meanings: Chemical models, animal models etc. We will utilise it mainly as concepts of control system models and mathematical models. We will describe the methods in more detail in this book and will in addition show how they can be the basis for simulations.

Even if the models are simplifications they can improve handling of the processes and the systems and, furthermore, they can be used to predict features of the processes and indicate tests to further studies.

Models are liked to be used when complicated processes should be described and understood. Rhythmic processes in organisms constitute such complicated processes as discussed in Chap. 1.

Models can be used to study systems in computer simulations cheaply, which are experimentally difficult to tackle. They allow to decide between contradictory empirical results, to put forward hypotheses, to plan new experiments, and to intervene in circadian rhythms (Asgari-Targhi, Klerman 2019).

Quite a number of circadian rhythms can be stopped (see Sect. 3.1), if they are perturbed in a special way. Another feature of circadian rhythms is their temperature robustness, as outlined in Sect. 3.2. A suited model must of course take care of these properties.

5.3 What kind of models exist?

We will present various models of rhythms in Chap. 7 and 8, which are frequently used and mentioned in the literature. The models in Chap. 7 are designed for single oscillators, whereas in Chap. 8 coupled oscillators are treated. In Sect. 7.1 of Chap. 7 a feedback model of Johnsson and Karlsson is presented, which is based on control theory (Karlsson, Johnsson 1972). We will use it extensively and apply it to various rhythms (see Sect. 7.1). Derived from it is a feedback model by Lewis and Saunders (see Sect. 7.2), which describes for instance the locomotor activity of insects, but can also be used for photoperiodic phenomena (Lewis, Saunders 1987). Very frequently the VP oscillator is used to model rhythms (see Sect. 7.6). It was developed by Van der Pol, a Dutch electric engineer at the Philips company, in order to model oscillations in vacuum tubes. The VP equation is often used in physics and biology, e.g. by FitzHugh (1961) and Nagumo, Arimoto, Yoshizawa (1962) who modified the equations for describing action potentials of neurons. A modified version of the VP model was presented and used by Wever for his work on circadian rhythms in humans (Sect. 7.7 and Wever (1979)). In Sect. 7.3 the Goodwin oscillator and in Sect. 7.4 the Goldbeter oscillator are treated. The Cowan approach (Sect. 7.5) has been used to describe rhythmic transpiration in plants, and the role of stomata and their guard cells. Stomatal coupling is already hinting to Chap. 8, where coupling of oscillators is treated. But before there is a section which treats in detail the simulation of rhythms in the heart. It was mentioned already (see subsect. 2.3.1) and it will describe, how to simulate the heart beat (Sect. 7.8) of Chap. 7.

In Chap. 8, which describes coupled oscillators, there is a Sect. 8.1 with two and another Sect. 8.2 with several nets presented, and in Sect. 8.3 coupled oscillators involved in the transpiration by plant leaves are described. In subsect. 8.3.1, 8.3.2, and 8.3.3 we go into more details of this topic. Sect. 8.4 deals with rhythms in cylindric systems, starting with two oscillators (subsect. 8.4.1), rings of 6 cells (subsect. 8.4.2), 50 cells (subsect. 8.4.3), and 200 cells (subsect. 8.4.5).

In trying to use these models for circadian rhythms, we have to take care also of special characteristics such as the phase shifting (Sect. 6.1), synchronisation (Sect. 6.2), entrainment, temperature robustness (Sect. 3.2) and the possibility to induce arrhythmicity by certain treatments (Sect. 3.1).

5.4 General properties in modelling systems

To explain the general properties in modelling systems, one should distinguish between *linear* and *non-linear nets*. Linear nets can be described in the following way:

1. In this system only first order derivatives and two variables (x1 and x2) are used. In more complex systems additional variables can of course be added.

2. The *superposition principle*[7] is valid; the overall signal can be obtained at different nodes

[7]The superposition principle can be described by this analogy: If, e.g., the 6 molar concentration of a substance is doubled, it doesn't make any difference whether one subdivides it in a 1 molar and 5 molar part, each one doubles and subsequently totals (2 times 1 molar and 2 times 5 molar gives 12 molar) or directly doubles (6 molar times 2 gives also 12 molar). This does not work, however, if the net is saturated at 5 molar. The result would be 2 times 5 molar totalling 10 molar. Here the superposition principle would not hold and the net would be non-linear.

by dividing a stimulating signal and adding each of the corresponding individual signals at nodes. The same would have been obtained, if the stimulating signal would not have been divided and the total signal were directly produced.

Linear nets are easier to analyse, but most nets found in nature are complicated and non-linear. They can, however, be described by the simpler linear nets by *linearising around a working point*, and thus be calculated more easily; at least approximations can be generated.

Hence for linear nets the following relation is valid

$$y(x_a + x_b) = y(x_a) + y(x_b) \tag{5.1}$$

$$x_a + x_b \rightarrow \text{linear system} \rightarrow y(x_a + x_b)$$

Examples for the modules of linear networks are shown in Fig. 5.4[8].

Figure 5.4: *Top row: Adder, subtracter, proportional element*
Lower row: Integrator, delay element (a continuous fix delay specifically controls the next execution time when the last execution finishes), low pass filter

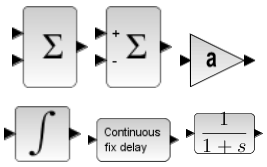

Linear nets are describable in the following way:

- as a linear differential equation system 1st order: e.g.

$$\frac{dx_1}{dt} = a \cdot x_1 + b \cdot x_2, \quad \frac{dx_2}{dt} = c \cdot x_1 + d \cdot x_2 \tag{5.2}$$

- as differential equations in matrix form::

$$\vec{X}' = \underline{\underline{A}} \cdot \vec{X} \tag{5.3}$$

with e.g.

$$\vec{X} := \begin{bmatrix} x_1 \\ x_2 \end{bmatrix}, \vec{X}' : \begin{bmatrix} dx_1/dt \\ dx_2/dt \end{bmatrix} \text{ and } \underline{\underline{A}} := \begin{bmatrix} a & b \\ c & d \end{bmatrix} \tag{5.4}$$

where by X is a system respectively an internal signal and A a coefficient matrix.

[8] The *delay element* leads to a continuous fixed delay, and a *low pass* element causes, that changes of the input signal are possible only with a maximal build up rate; or in the frequency range: without damping only spectral components up to a certain maximal cutoff frequency are transferred.

- as *one* differential equation of higher order, here second order, e.g. in

$$\frac{dx_1}{dt} = a \cdot x_1 + b \cdot x_2, \quad \frac{dx_2}{dt} = c \cdot x_1 + d \cdot x_2 \tag{5.5}$$

  If the 2nd equation above is solved for x_1 and this is inserted in the 1st equation, we obtain

$$\frac{d^2x_2}{dt^2} - (a+d) \cdot \frac{dx_2}{dt} + (a \cdot d - b \cdot c) \cdot x_2 = 0 \tag{5.6}$$

- as a functional diagram (see Fig. 5.5).

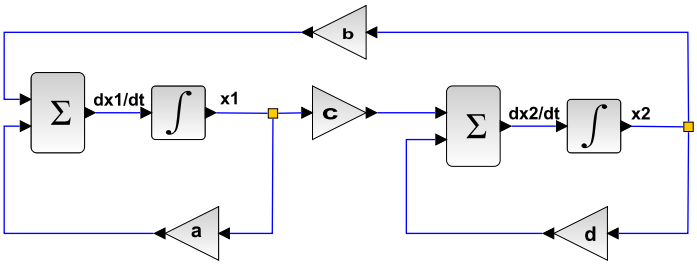

Figure 5.5: *Functional diagram of a linear network, where the left part corresponds to the left term and the right part to the right term in Eq. 5.6*

In a linear net a *point of singularity around zero* can occur:
For the stationary case (point of singularity) it would hold:

$$\vec{X}' = 0 = \underline{\underline{A}} \cdot \vec{X} \tag{5.7}$$

For this X value no oscillation is possible, i.e.

$$\frac{dx_1}{dt} = 0 = ax_1 + bx_2, \frac{dx_2}{dt} = 0 = c \cdot x_1 + d \cdot x_2 \tag{5.8}$$

Possible solutions are either

1. $x_1 = 0$ and $x_2 = 0$ or
2. $a \cdot d - b \cdot c = 0$ respectively $det(\underline{\underline{A}}) = 0$, i.e.

$$x_2 = -\frac{a}{b}x_1 = -\frac{c}{d}x_1 \tag{5.9}$$

Here one should note, that x_1 or x_2 do not need to have special values, but have only to stay in a definite relation to each other, which is determined by the system parameters a to d. Hence, a to d (independent of x_1 and x_2) has only to attain a specific value (independent of $x_1$and x_2) .

5.5 How to derive a network from a differential equation

Often models are proposed in the literature as functional equations, e.g. as a differential equation. How they can be displayed in Scilab will be shown here , using the VP-oscillator as an example. This oscillator is frequently used for simulations of biological rhythms. It can take different forms and be elaborated, but in this presentation of it we will use the simplest and basic form. At the same time it will be shown how to derive a network from a mathematical functional equation, here a differential VP equation. The differential equation normalised to a dimensionless time τ is:

$$x'' + \varepsilon \cdot (x^2 - 1)x' + x = 0 \tag{5.10}$$

To derive a network from the equation, different steps are used:

1st step: The differential equations are solved for the highest derivative, i.e.:

$$x'' = -\varepsilon \cdot (x^2 - 1)x' - x \tag{5.11}$$

2nd step: To get the left part (x'') of Eq. 5.11 we combine two integrators in series. The output of the second one is the variable x (see Fig. 5.6 below), the input to that integrator is then x'. The input to the first integrator must then be x'', which we were looking for. Since x'' is just the left part of the equation it must, furthermore, be the sum of two terms (see Eq. 5.11). We therefore provide the first integrator with the sum of two terms by adding a summand to its input.

In the next step we will extend the Fig. 5.6 to get the complete functional diagram for the Eq. 5.11. $x = \int x'dt$ is represented by an integrator, the right part $(-\varepsilon \cdot (x^2 - 1)x' - x)$ by an adder and a subtracter: From the differential equation results a functional diagram (1st part, Fig. 5.6)

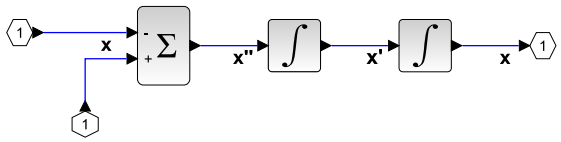

Figure 5.6: *Functional diagram (1st part) of the VP-oscillator. To get the left part (x´´) of the Eq. 5.11 we combine two integrators in series. The output of the second one is the variable x (see Fig. 5.7 below), the input to that integrator is then x´. The input to the first integrator must then be x´´, which we were looking for. Since x´´ is just the left part of the equation it must, furthermore, be the sum of two terms (see Eq. 5.11). We therefore provide the first integrator with the sum of two terms by adding an adder to its input.*

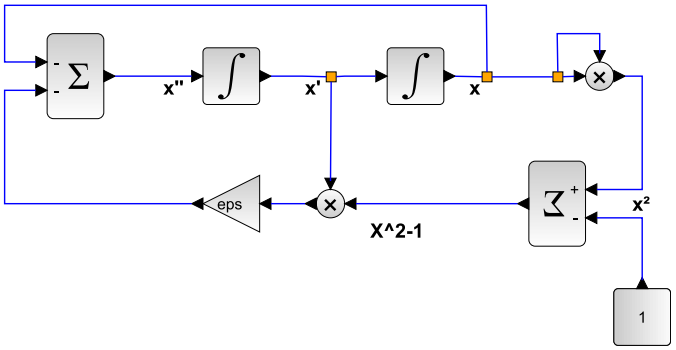

Figure 5.7: *Functional diagram (2nd part) of the VP-oscillator (see Fig. 5.8)*

3rd step: The input signal of the adder is obtained from the system signals x and its derivative with the help of further functional blocks. The result of the functional diagram shows Fig. 5.7.

With the Scilab-program the VP-oscillator can be simulated (see Fig. 5.8) and the time course of the functions visualised at certain nodes (see the figures 5.9 and 5.10).

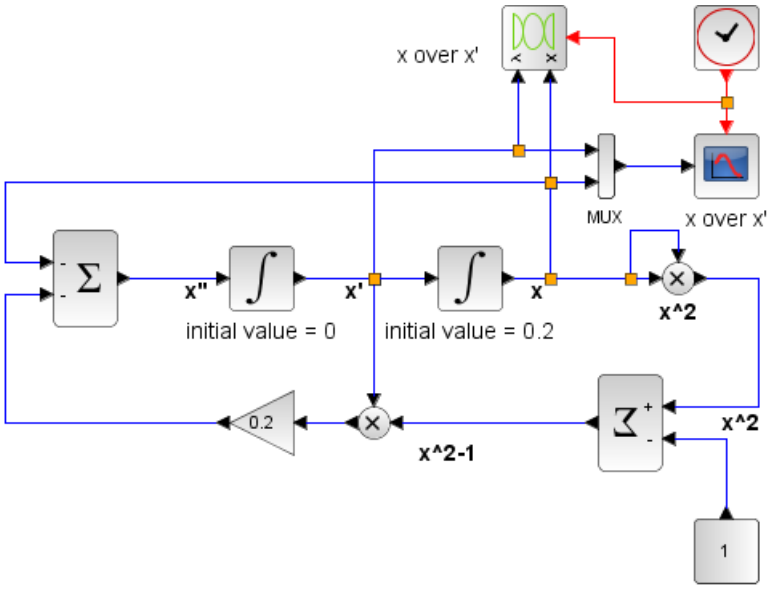

Figure 5.8: *Functional diagram of the VP-oscillator in Scilab with ε= 0.2 and initial value of x = 0.2*

The point of singularity of the VP-oscillator is obtained, if the differential Eq. 5.10 of second order is transformed in two differential equations of first order and the two corresponding derivatives are set to zero again. This can easily be done by first transforming the variables x into x_1 and x' into x_2. Then one finds the singularities from the condition that the first derivatives should be equal to zero, i.e. $x_1' = 0$ and $x_2' = 0$. The equations can only be solved if

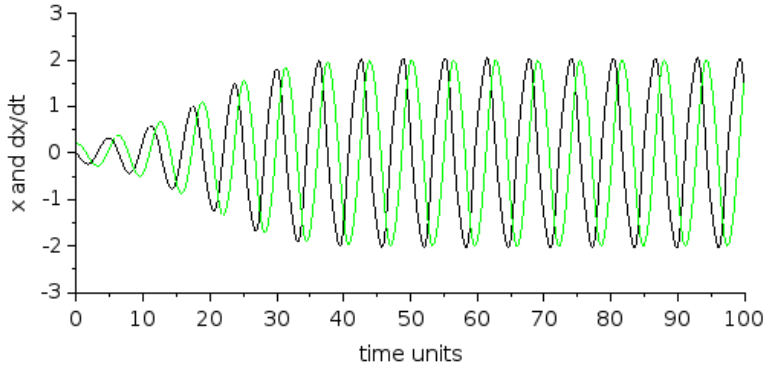

Figure 5.9: *Signal x (black) and its derivative x' (green) in the simulation example of the VP-oscillator in Fig. 5.8 with ε = 0.2. Arbitrary time units, e.g. in hours*

the singularities are $x_1^s = 0$ and $x_2^s = 0$.

$$\begin{aligned} x' = x_1' &= x_2 \\ x_2' &= -\varepsilon \cdot (x_1^2 - 1)x_2 - x_1 \end{aligned} \tag{5.12}$$

and if one looks for the values of $x_1 = x_1^s$ and $x_2 = x_2^s$, at which the first derivative disappears. As can be seen, the equation can only be satisfied, if $x_1^s = 0$ and $x_2^s = 0$

The VP-oscillator therefore has its *point of singularity in the origin of the coordinate system* and the resulting oscillation is symmetric for positive and negative values of x symmetric. In the x_1/x_2 plane the trajectory corresponds to an oval (see Fig. 5.9 and 5.10). It can be seen in Fig. 5.9 of the simulation with Scilab/Xcos, that the amplitude of the oscillation, which lies initially in the point of singularity $x = x_1 = x_1^s = 0$ and $x' = x_1' = x_2 = x_2^s = 0$, does not remain on this value, but increases and approaches after some time the constant value of 2. Thus this point of singularity is *not stable*.

Once this value is reached, the system begins to oscillate again. Whether this is not only the case in this simulation model, but generally so, can be tested by linearising the non-linear differential equation system of the VP-oscillator (Eq. 5.12) around the point of singularity and by checking, whether the Eigenvalue of this linearised system has a positive real part, which leads to a solution with increasing amplitude. The linearisation by breaking up the Taylor series after the first element gives:

$$\begin{aligned} x_1' &\approx f_1(x_1^s, x_2^s) + \frac{\partial f_1}{\partial x_1}_{|x_1^s, x_2^s} \triangle x_1 + \frac{\partial f_1}{\partial x_2}_{|x_1^s, x_2^s} \triangle x_2 \\ x_2' &\approx f_2(x_1^s, x_2^s) + \frac{\partial f_2}{\partial x_1}_{|x_1^s, x_2^s} \triangle x_1 + \frac{\partial f_2}{\partial x_2}_{|x_1^s, x_2^s} \triangle x_2 \end{aligned} \tag{5.13}$$

with

$$\begin{aligned} f_1(x_1, x_2) &:= x_2 \quad , & \triangle x_1 &:= x_1 - x_1^s \\ f_2(x_1, x_2) &:= -\varepsilon \cdot (x_1^2 - 1)x_2 - x_1 \quad , & \triangle x_2 &:= x_2 - x_2^s \end{aligned}$$

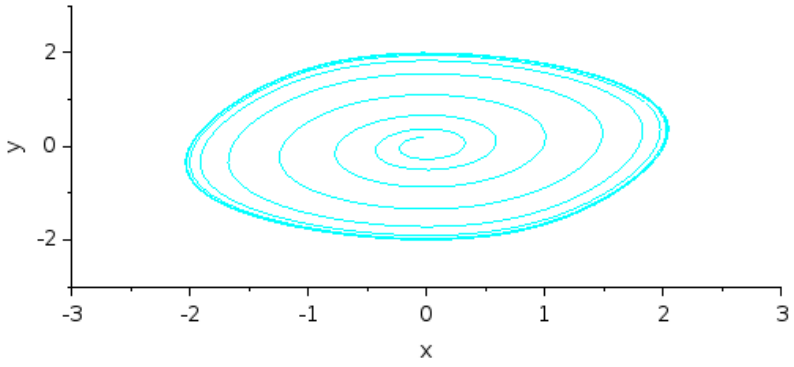

Figure 5.10: *Time derivative of the signal x as a function of x itself (xy diagram) in a simulation example of the VP-oscillator in Fig. 5.8 with ε = 0.2*

Applied to the VP differential equation system 5.12 one gets in the point of singularity because of $x_1^s = x_2^s = 0$ (and therefore also $f_1(x_1^s, x_2^s) = f_2(x_1^s, x_2^s) = 0$) for the linearised system in matrix form:

$$\underbrace{\begin{pmatrix} x_1' \\ x_2' \end{pmatrix}}_{\vec{x'}} = \underbrace{\begin{pmatrix} 0 & 1 \\ -1 & \varepsilon \end{pmatrix}}_{\underline{\underline{A}}} \cdot \underbrace{\begin{pmatrix} x_1 \\ x_2 \end{pmatrix}}_{\vec{x}} \tag{5.14}$$

A linear differential equation system can be easily solved in the frequency domain, because the differential equation becomes an algebraic equation. Fourier transformation of $\vec{x}$ and $\vec{x'}$ yields to:

$$p \cdot \vec{X} = \underline{\underline{A}} \cdot \vec{X} \tag{5.15}$$

whereby $\vec{X}$ is the Fourier transformed of $\vec{x}$ and $p = \sigma + j\omega$ is the complex frequency with the real part σ and the imaginary part ω. σ is the damping and ω the angular frequency of a cosine oscillation $\sim \exp(\sigma t) \cdot \cos(\omega t)$. Rearranging Eq. 5.15 one obtains:

$$\left(\underline{\underline{A}} - p \cdot \underline{\underline{E}}\right) \cdot \vec{X} = \vec{0}, \quad \underline{\underline{E}} : \text{ unit matrix} \tag{5.16}$$

Except for the trivial solution $\vec{X} = \vec{0}$ the last Eq. 5.16 is only fulfilled, if the expression in the brackets disappears, i.e.

$$\underline{\underline{A}} - p \cdot \underline{\underline{E}} = \begin{pmatrix} 0 & 1 \\ -1 & \varepsilon \end{pmatrix} - p \cdot \begin{pmatrix} 1 & 0 \\ 0 & 1 \end{pmatrix} = \underline{\underline{0}}, \quad \underline{\underline{0}} : \text{ zero matrix}$$

This is an eigenvalue for the matrix $\underline{\underline{A}}$, the solution of which can be found by the conditions for

the corresponding determinate

$$\det\left(\underline{\underline{A}} - p \cdot \underline{\underline{E}}\right) = \det\begin{pmatrix} -p & 1 \\ -1 & \varepsilon - p \end{pmatrix} = 0$$

In this way one obtains the Eq.

$$p^2 - \varepsilon \cdot p + 1 = 0$$

with the solution

$$p_{1/2} = \frac{\varepsilon}{2} \pm \sqrt{\left(\frac{\varepsilon}{2}\right)^2 - 1} \tag{5.17}$$

For $0 < \epsilon < 2$ the pole locations $p_{1/2}$ are complex and possesses a positive real part, which means, that the oscillation is gaining amplitude (see Fig. 5.9). For $\epsilon < 0$, the real part is negative and the oscillation is fading. For $|\epsilon| > 2$ no oscillation develops in this linearised system (Eq. 5.14), since the poles are truly real. The point of singularity around the coordinate origin at $x_1^s = x_2^s = 0$ is unstable, since in this point an increasing cosine oscillation develops, which is illustrated by the course of the signal in the Scilab/Xcos simulation in Fig. 5.9 for $\varepsilon = 0, 2$. However, this result does not mean, that for $\epsilon > 2$ an oscillation in the non linear system can not occur 5.12. In this case a „limit cycle“ forms, in which the oscillation is not any more sinusoidal (see e.g. Fig. 7.34 for ϵ =5)

The amplitude of the sinusoidal oscillation of the VP-oscillator can be determined easily in the linear range and approximated, if one assumes, that it does not change too fast in respect to the oscillation and that the oscillation increases only to such an amount, that is stays in the linear range of the characteristic. As an approximation a sinusoidal oscillation with *one* frequency can be chosen, e.g.

$$x(\tau) = \hat{x}(\tau) \cdot \cos(\tau), \text{ with } \tau := \omega_0 t \tag{5.18}$$

This approach can be put into the VP differential Eq. 5.10. Because of the assumed small amplitude changes and the linear range the arising harmonics with small amplitudes can be neglected (see for instance Van der Pol (1927) and Pfeifer (1966)). This leads again to a differential equation, but now for the amplitude of the cosine oscillation $\hat{x}(t)$:

$$\frac{d\hat{x}^2}{dt} = -\omega_0 \varepsilon \left(\hat{x}^2 - \frac{\hat{x}^4}{4}\right) = 0 \tag{5.19}$$

and the solution with

$$\hat{x}(t) = \frac{2}{\sqrt{1 + e^{-\omega_0 \varepsilon (t - t_0)}}} \tag{5.20}$$

can be determined (t_0 is an integration constant, which depends on the initial conditions). An amplitude is obtained, which reaches the final value 2 with increasing time τ, as illustrated e.g. by the results of the simulations in Fig. 5.9.

Retrospectively the alteration of the amplitude with time can be calculated and, it can be tested, whether our assumption was correct, namely, that it does not change so fast in respect

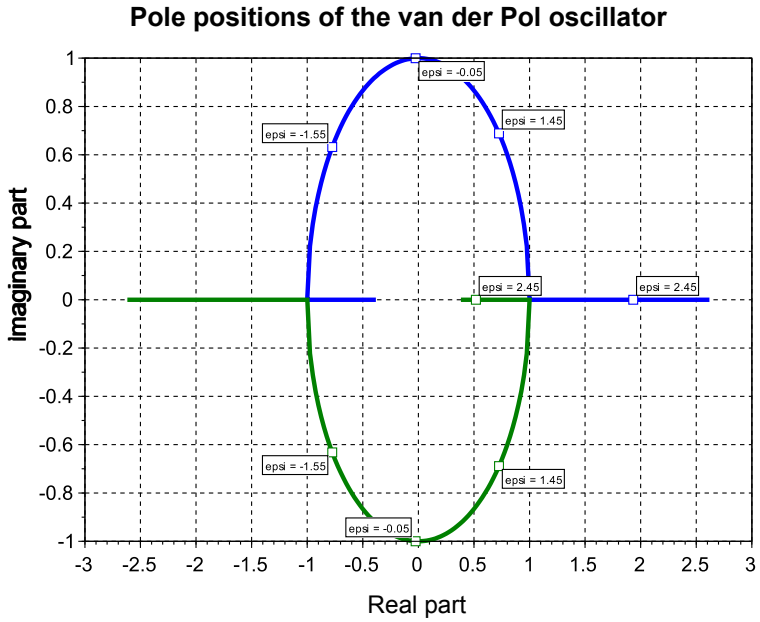

Figure 5.11: *Stability check of the VP-oscillator in Fig. 5.7 and in Fig. 5.8 respectively. x-axis: real part, y-axis: imaginary part.*
In this figure the poles of the linearised *system are shown in the point of singularity at* $x_1^s = x_2^s = 0$ *as a function of the parameter* ϵ *as a parameter curve in the range of* $\epsilon = -3$ *to* 3. *The blue curve is for the positive root in Eq. 5.17, the green one for the negative. Both curves together result in an oval, except for the real part. x-axis- .*

to the oscillation. If the Eq. 5.20 is differentiated in time, it follows:

$$\frac{d\hat{x}(t)}{dt} = \omega_0 \frac{\varepsilon\, e^{-\omega_0 \varepsilon (t-t_0)}}{\sqrt{\left[1 + e^{-\omega_0 \varepsilon (t-t_0)}\right]^3}} = \omega_0 \varepsilon\, e^{-\omega_0 \varepsilon (t-t_0)} \cdot \left(\frac{\hat{x}(t)}{2}\right)^3$$

The alteration of the amplitude $\hat{x}(t)/dt$ is proportional to the time t, the current value of the amplitude $\hat{x}(t)$ and the variable ε. Since t_0 is the original value of t and therefore $t - t_0 > 0$ still holds, we obtain the largest value for the amplitude change, if $t = t_0$ and if the amplitude has reached its maximal value $\hat{x}_{max} = 2$. In this case we have

$$\left.\frac{d\hat{x}(t)}{dt}\right|_{max} = \varepsilon. \tag{5.21}$$

and it follows, that the parameter ε should be chosen *as small as possible.*

5.6 General feedback networks

In general feedback nets the set value $c(t)_{Ref}$ is compared with the actual concentration $c(t)$ and the difference is used as a correction which controls the further synthesis of a desired substance; the result is again compared with the set value. Thereby two instances can be distinguished:

1. In the forward branch F_V the difference between the actual and the desired value is generated, e.g. for changing the concentration and with modifications (for example with low-pass filtering) and a certain time constant
2. in the backward branch F_R a delay occurs for e.g. decreasing the concentration. The signal reaches thus again the forward branch.

A graphical display of this model shows Fig. 5.15. For obtaining an oscillation, the following conditions must be fulfilled:

If a signal z is given to an input (e.g. the change of the set value of the concentration in form of an impulse), the back feeding signal f_{Ra} (e.g. the concentration to be compared at the input) has to be at least as large as the input signal z, to prevent the system from damping out.

From these two conditions follows, if the model is not in the time domain , but in the frequency domain:

1. The value of the product of the forward and backward amplification $|F_V \cdot F_R|$ must be larger than 1.
2. The phase of the back feeding signal (e.g. a sinus oscillation) must equal the input signal or must be the multiple of its period length.

This is possible also in the case of non-linear oscillators, if they can be linearised in order to study their oscillating behaviour in the stationary state in the x and y respectively in the phase diagram (see e.g. Fig. 5.10 for a VP-oscillator), where they form a circle in the stationary state.

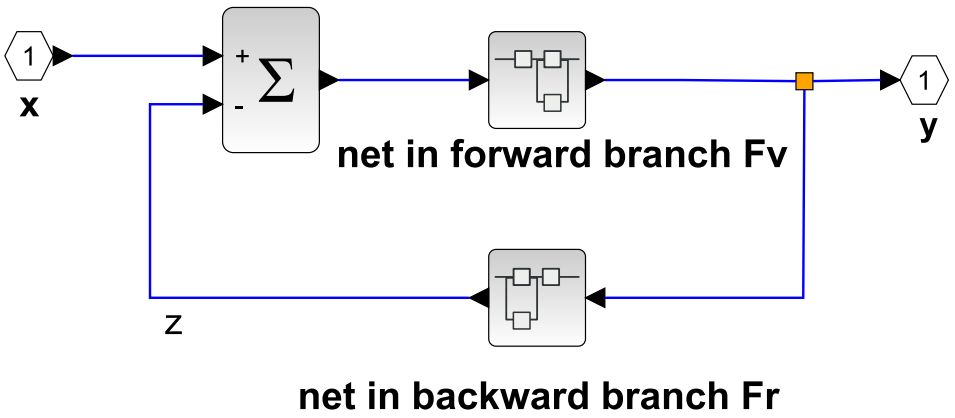

Figure 5.12: *General feedback model to generate an oscillation. In the forward branch* F_V *the signal in a superblock is influenced and changed again in the feedback branch* F_R *in a superblock ; it finally reaches the subtractor and the loop is closed and again run through.*

Further necessary conditions for *all* nets are:

- The oscillation occurs always around a point of singularity.
- In the case of *linear* nets the point of singularity lies at $\vec{X} = 0$, i.e. the oscillation occurs always around the origin.

5.6.1 Simple Feedback model with a delayer

In this model a delay is only present in the backward branch and a pulse is applied to the input (see Fig. 5.13). Its form and size are not changed, but at the comparison at the input its polarity is changed. This leads to a negative pulse, and in the next cycle, due to the change of polarity, becomes positive (see Fig. 5.14). Altogether the period length is twice as large as the delay time .

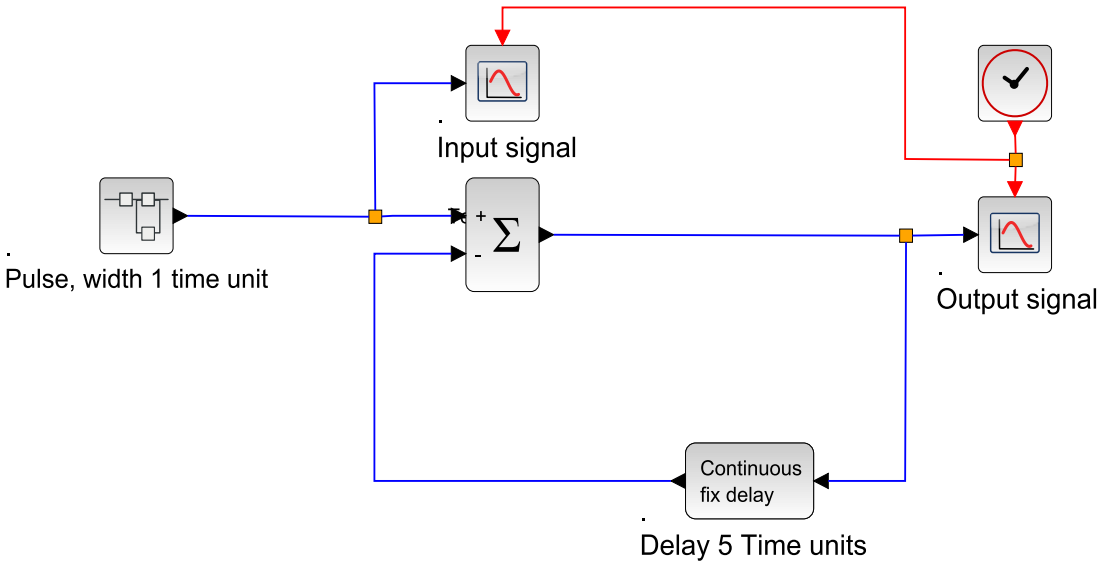

Figure 5.13: *Example for a feedback model consisting of one delayer.*

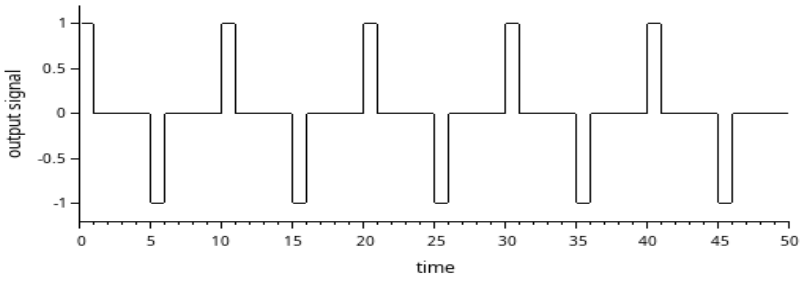

Figure 5.14: *Output signal of the simple feedback model with one delayer only as shown in Fig. 5.13. The period length is twice as long as the delay time of the delayer.*

5.6.2 Feedback model with delayer and integrator

In this model the forward branch contains a damping element, which reduces the difference signal (between input and back coupled signal) by a about third, and an integrator. In the backward branch is again a delay inserted.

At the input a pulse is applied with the duration of one time unit (see Fig. 5.15). Its form is again not changed, but its size is, in order to prevent the resulting oscillation from becoming too much amplified by the integrator at each cycle; it is thus limited. This amplification is, however, frequency dependent and decreases with higher frequencies. The higher frequency fractions of the rectangular pulse are not sufficiently amplified, and do therefore not occur any more in the output oscillation.

The integrator does, however, not only amplify the oscillation, but delays it also by one fourth of the period length (independent of the frequency of the remaining part of the oscillation). Since during the comparison of input and feedback signal the sign of the feedback signal is reverted, a total delay of half the period of the input signal results, due to the delay of the integrator and the delay element. Since the integrator delays already by a fourth of the period length, the delay element has to delay the period length only by another fourth, in order to bring about a total delay of half a period length. This results in a period length, which is *four times* as large as the delay time (see Fig. 5.16).

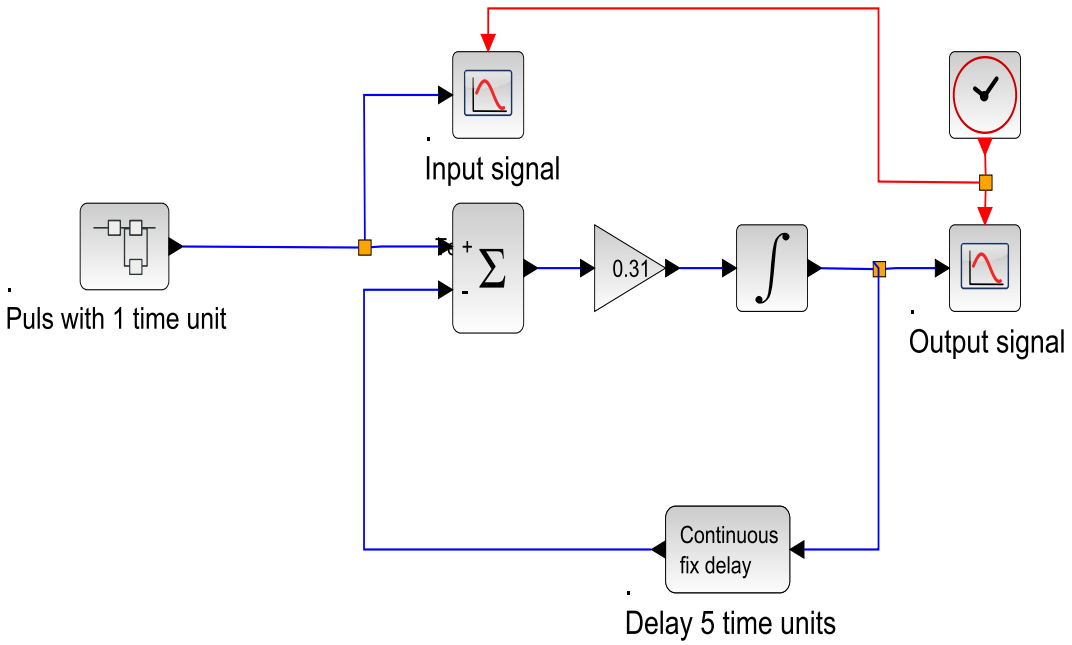

Figure 5.15: *Example for a feedback model consisting of a delayer, which has a delay of 5 time units (e.g. hours, days), and an integrator*

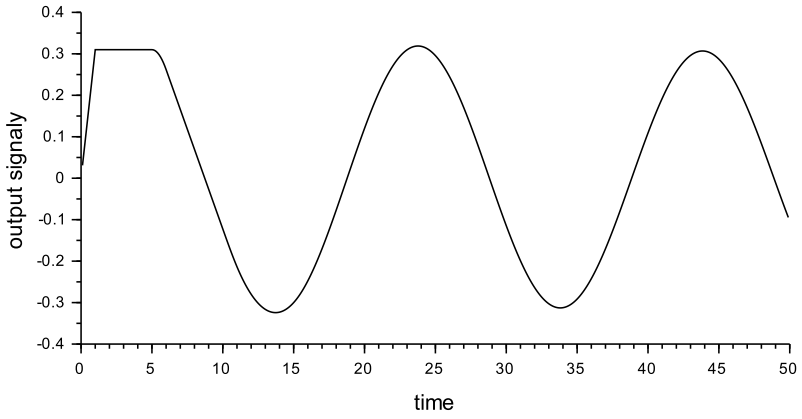

Figure 5.16: *Output signal of the simple feedback model consisting of a delayer and an integrator according to Fig. 5.15.*

5.6.3 Feedback model with two integrators

This model contains an integrator in the forward as well as in the backward branch.

At the input again a pulse with the duration of one time unit is applied (see Fig. 5.17). This pulse is not influenced by a damping element, but due to the filter effect of the integrator here too only the primary oscillation is filtered out (see Fig. 5.18). Each integrator leads to a phase change by 90°, i.e. in the forward and backward branch one obtains a total of 180°. A further 180° phase turn is induced due to the negative sign of the feedback, thus leading to a total of 360°. Therefore no further delay is needed, as was the case in the two preceding models, in order to get oscillations by the system. This time the circuit is purely linear and the transfer function $G(j\omega)$ is a function of the frequency f between the input and output signal X_a and X_e in the frequency domain ($\omega = 2\pi f$ is the angular frequency):

$$G(j\omega) = \frac{X_a(j\omega)}{X_e(j\omega)} = \frac{j\omega}{1 + (j\omega)^2} = \frac{j\omega}{1 - \omega^2} \tag{5.22}$$

This shows, that due to the filter effects of the two integrators a bandpass occurred, which shows a pole for $\omega = \omega_0 = \pm 1$ and possesses there the highest amplification. In the time domain one obtains than at this frequency a sinusoidal pulse answer, i.e. the oscillator oscillates with the frequency f_0, and the period length T_0 is

$$f_0 = 1/2\pi \approx 0.159\,Hz \quad \text{und } T = 2\pi \approx 6,28\,Sek. \tag{5.23}$$

which can be seen also from the course of the signal at the simulation in Fig. 5.18. If the derivative of the output signal is plotted as a function of the output signal, an ellipse is obtained (see Fig. 5.19).

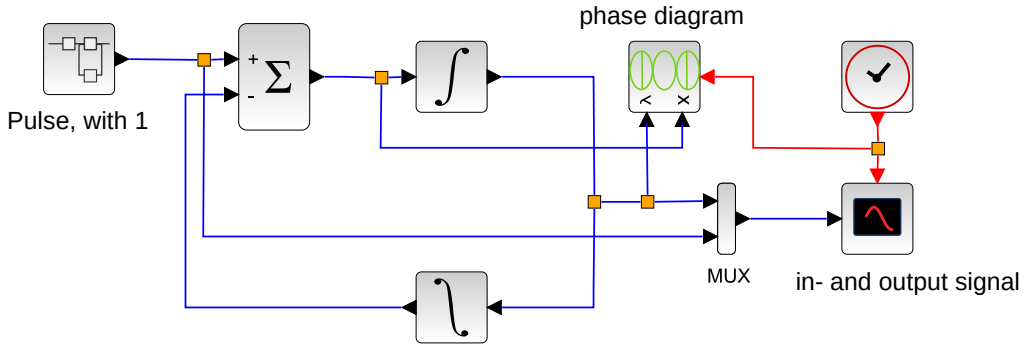

Figure 5.17: *Example of a feedback model with an integrator in the forward as well as in the backward branch*

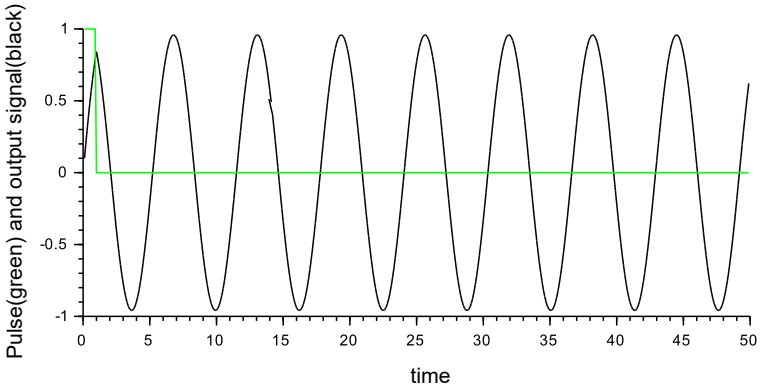

Figure 5.18: *Output signal of the simple feedback model with integrator in the forward as well as in the backward branch according to Fig. 5.17, MUX: multiplexer; pulse width 1 unit.*

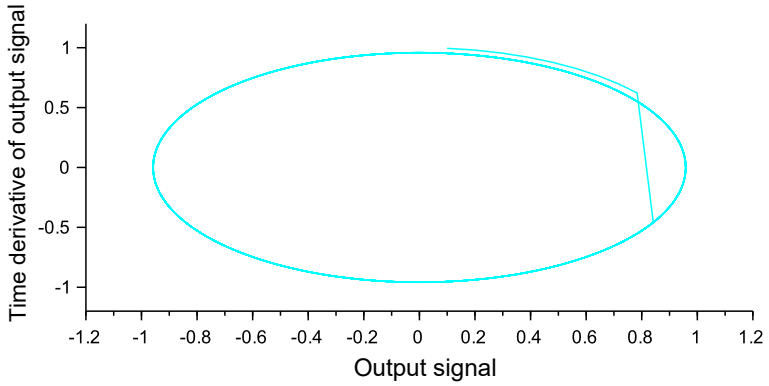

Figure 5.19: *Phase diagram of the simple feedback model with an integrator in the forward as well as in the backward branch according to Fig. 5.17*

With a damping parallel to the integrator in the feedback branch not only the amplitude, but also the frequency of the sinusoidal oscillation of the output signal changed (see e.g. figures 5.20 and 5.22). For the transfer function $G(j\omega)$ as a function of the frequency f between the output and input signal X_a and X_e in the frequency domain one obtains now from the system theory the relation:

$$G(j\omega) = \frac{X_a(j\omega)}{X_e(j\omega)} = \frac{j\omega}{1 + \varepsilon j\omega - \omega^2} \tag{5.24}$$

And for the frequency f_S of the oscillation at $\varepsilon < 2$:

$$f_S = \frac{1}{2\pi}\sqrt{1 - \left(\frac{\varepsilon}{2}\right)^2} \tag{5.25}$$

It matches for $\varepsilon = 0$ the Eq. 5.23 ($f_S = f_0$). If a damping exists ($\varepsilon > 0$), the oscillator frequency is the smaller, the larger ε becomes. For $\varepsilon \geq 2$ *no* oscillation exists.

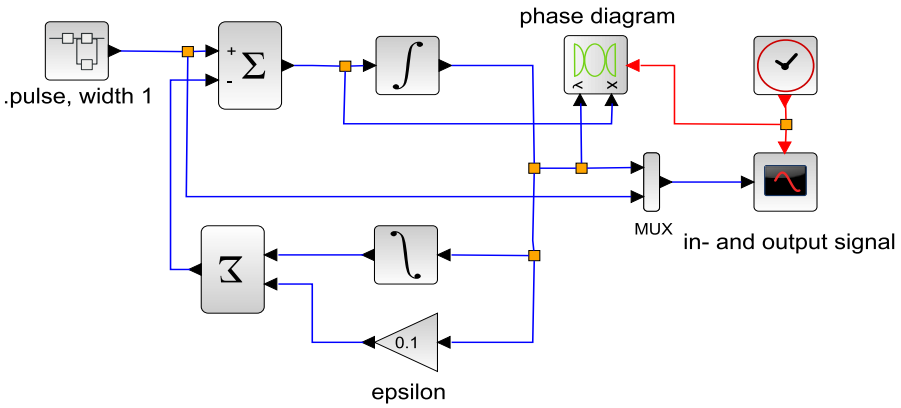

Figure 5.20: *Example of a feedback model with integrators in the forward as well as in the backward branch, and a damping unit parallel to the integrator in the feedback branch*

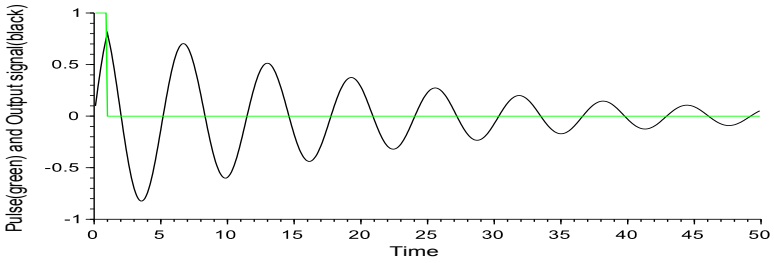

Figure 5.21: *Output signal of the simple feedback model with an integrator in the forward as well as in the backward branch according to the Model with damping, see Fig. 5.20*

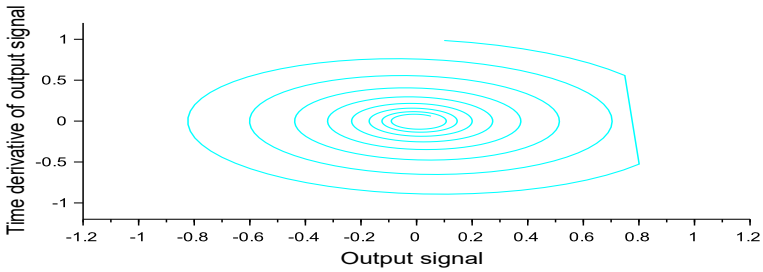

Figure 5.22: *Phase diagram of the simple feedback model with an integrator in the forward as well as in the backward branch according to the Model with damping, see Fig. 5.20*

5.6.4 The nyquist stability criterion

To investigate the stability of a linear system with feedback, it is not necessary to consider the transmission behaviour of the closed loop, but it is sufficient to determine the properties of the open loop (see Fig.5.12).The transfer function of the closed system results in

$$G(p) = \frac{Y(p)}{X(p)} = \frac{Fv(p)}{1 + Fv(p) \cdot Fr(p)} \text{ with } p = \sigma + j\omega$$

If the transmission in the forward and reverse branches $F_v(p)$ and $F_r(p)$ is stable, the overall system only becomes unstable when the denominator of G(p) vanishes:

$$G0(p_k) := Fv(p_k) \cdot Fr(p_k) = -1 \tag{5.26}$$

$G0(p)$ is the transfer function of the open feedback system.$p_k$is the critical value at which instability occurs. You can interpret the condition 5.26 in such a way that the two-dimensional complex p-plane is mapped onto the complex $G0(p)$ plane, which is also two-dimensional. This is a conformal mapping in which the angular trueness is retained. This means that the points p_k, which are then all mapped through $G0(p_k)$ to the point "-1" in the $G0(p)$-plane, must also lie to the left of the $j\omega$-axis in $G0(p = j\omega)$ if they lie to the left of the $j\omega$ axis in the p-plane (see Fig.5.23).

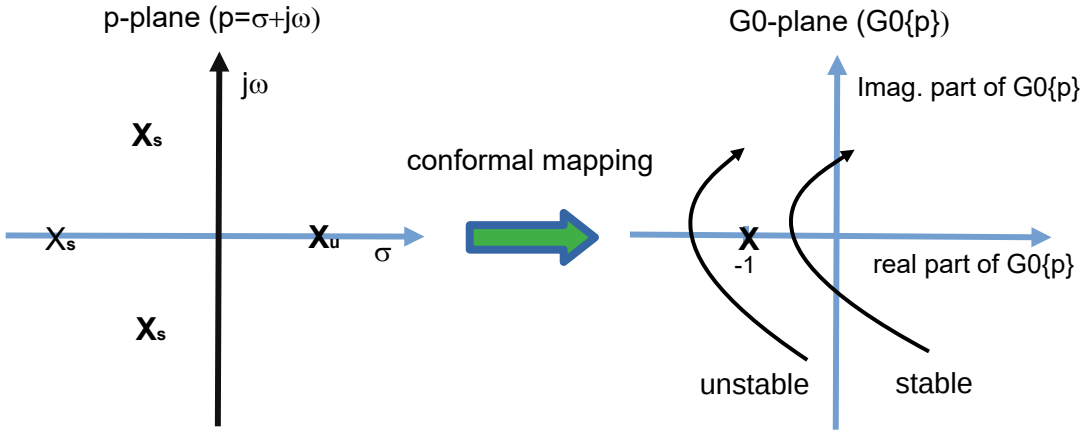

Figure 5.23: *Conformal mapping of the P-plane to the $G0(p)$-plane with specification of the zeros of $1 + G0(p) = 0$. In the p-plane, the zeros of a stable system (X_s) and those of an unstable system (X_u) are shown. The imaginary axis in the P-plane ($p = j\omega$) is mapped onto a curve (locus curve) in the G(p)-plane ($G(j\omega)$).*

The system is stable if the zeros of $1 + G0(p) = 0$ have a negative real part, i.e. lie in the left P-plane. If the imaginary axis of the P-plane is traversed from $\omega = -\infty$ to $+\infty$, these zeros lie to the left of the imaginary axis in a stable system. In an unstable system, they have a positive real part and are located on the right-hand side when traversing the imaginary axis from $-\infty$ to $+\infty$.

In the case of a conformal mapping with angular fidelity, this property is also retained in

the $G0(p)$-plane. This means that the zeros in a stable system lie to the left of the locus curve $G0(p = j\omega)$ if it runs from $\omega = -\infty$ to $+\infty$ and to the right in an unstable system. The zero points p_k in the P-plane are all mapped to the point -1 in the $G0(p)$-plane (regardless of whether they are in the left or right P-half-plane) (see eq.5.26) Therefore, with this Nyquist stability condition, it is only necessary to investigate whether the point -1 is to the left or right of the locus curve $G0(p)$ when ω is traversed from $-\infty$ to $+\infty$. If it lies to the left of this locus curve, the system is stable; if it lies to the right, it is unstable (see figure 5.23). However, the system must be linear and time-invariant and must be described by a fractionally rational function of $G(p)$. Therefore:

> The Nyquist plot provides an intuitive visualization of how the open-loop dynamics relate to closed-loop stability, particularly in systems with feedback. By interpreting the encirclements around the point -1, one can ensure robust stability or identify potential instabilities.

Example for an Feedback-Oscillator with two integrators and damping: The feedback model with an integrator in the forward branch and an integrator with damping losses in the reverse branch as shown in Fig.5.20 results in:

$$Fv(j\omega) = \frac{1}{j\omega} \text{ and } Fr(j\omega) = \frac{1}{j\omega} + \varepsilon$$

and

$$G0(j\omega) = Fv(j\omega) \cdot Fr(j\omega) = -\frac{1 + \varepsilon j\omega}{\omega^2}$$

The corresponding locus curve of $G0(j\omega)$ with $\varepsilon = -0.2$ and $f = \omega/2\pi$ from 0.05 to 20.0 can now be determined with the help of Scilab according to listing5.1:

Listing 5.1: *Illustration of the locus curve of the open feedback system with $G0(j\omega)$ with two integrators and attenuator according to Fig.5.20*

```
//
eps=-0.2; // positive values for an unstable system
freqmin=0.05;
freqmax=20.0;
s = poly(0,"s");
G0 = syslin('c',[1+s*eps],[s^2]);
nyquist(G0,freqmin,freqmax,,%f);
xlabel(_("Re{G0(f)}"), "fontsize",5); ylabel(_("Im{G0(f)}"), "fontsize",5)
title('Nyquist␣diagram','color','black', "fontsize",5);
```

The corresponding locus curves of $G0(j\omega)$ are shown in Fig.5.24. It can be seen quite clearly that in the stable system the point $G0(j\omega_k) = -1$ lies to the left of the locus curve when it is traversed from f=0.05 to 20.0 and to the right of it in the unstable system..

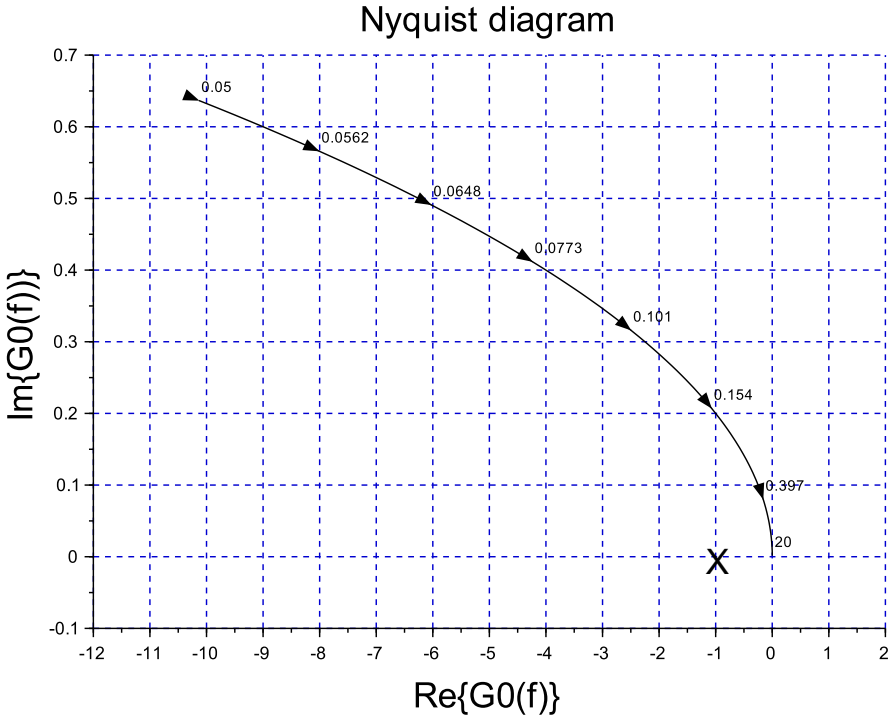

a)

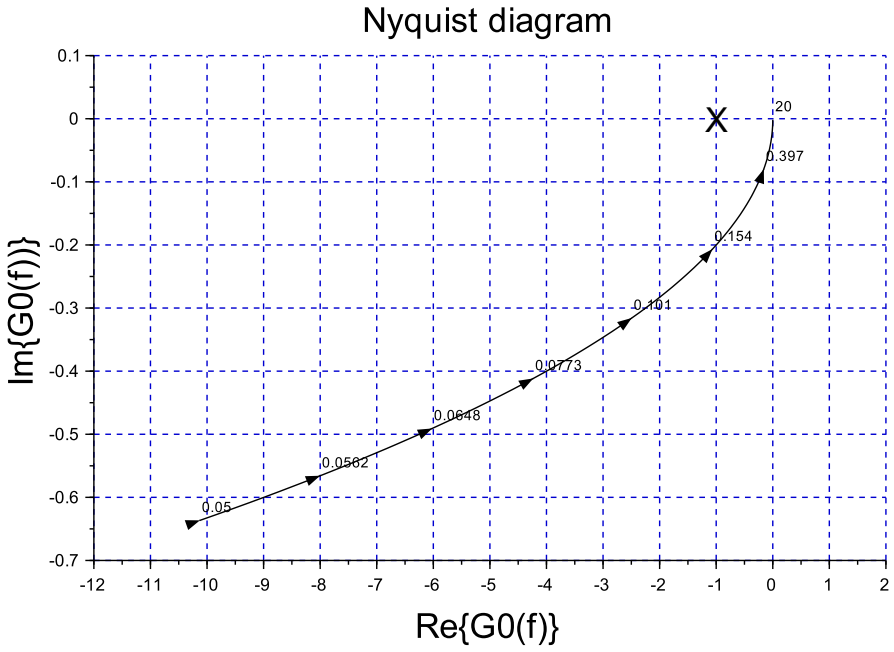

b)

Figure 5.24: *Nyquist diagram $G0(j\omega)$ for feedback system with two integrators and damping element according to Fig.5.20. In a) $\varepsilon = -0.2$ and system unstable; in b) $\varepsilon = 0.2$ and system stable. The Frequency f is indicated at the points on the locus curves.*

5.6.5 Properties of non-linear nets

The general description of a non-linear net occurs via a non-linear differential equation with a non-linear function f:

$$X' = f(X) \tag{5.27}$$

and the stationary case (point of singularity) would be:

$$X' = 0 = f(X) \tag{5.28}$$

This is a non-linear algebraic equation. In contrast to the linear equations *the superposition principle does not* hold *here.*

Examples for non-linear *network element*s are shown in Fig. 5.25.

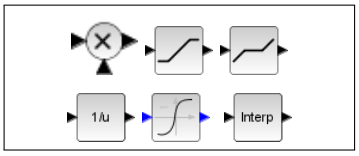

Figure 5.25: *Upper row: Multiplier, limiter, minimal value element. Bottom row: Inverter, integrator, nonlinear characteristic line from a table*

An example for a non-linear net is the **predator-prey model**, which can be described by the Eq.

$$\frac{dx_1}{dt} = a \cdot x_1 - b \cdot x_1 \cdot x_2, \quad \frac{dx_2}{dt} = c \cdot x_1 \cdot x_2 - d \cdot x_2 \tag{5.29}$$

where x_1 is the prey and x_2 the predator. The propagation rate of the prey is *a*, the killing rate of the prey is b, the birth rate of the predator is *c*, the death rate of the predator is *d.* The functional diagram is shown in Fig. 5.26.

For the points of singularities holds:

$$\frac{dx_1}{dt} = 0 = a \cdot x_1 - b \cdot x_1 \cdot x_2 = x_1(a - b \cdot x_2) \tag{5.30}$$

$$\frac{dx_2}{dt} = 0 = c \cdot x_1 \cdot x_2 - d \cdot x_2) = x_2(c \cdot x_1 - d) \tag{5.31}$$

where x_1 is the prey and x_2 the predator. The solution is

1. x_1=0 and x_2=0 or
2. $x_1 = \frac{d}{c}$ and x_2=$\frac{a}{b}$

The ratio of the coefficients a and b must equal the value of x_2 and the ratio of the coefficients d and c must equal the value of x_1, in order to reach a point of singularity.

The predator-prey functional diagram is shown in Fig. 5.26 for a particular simulation, where *no* point of singularity is obtained. The changes of the population size of prey and predator are

shown in Fig. 5.27. Fig. 5.28 displays the phase diagram, in which the number of prey is plotted against the number of predators.

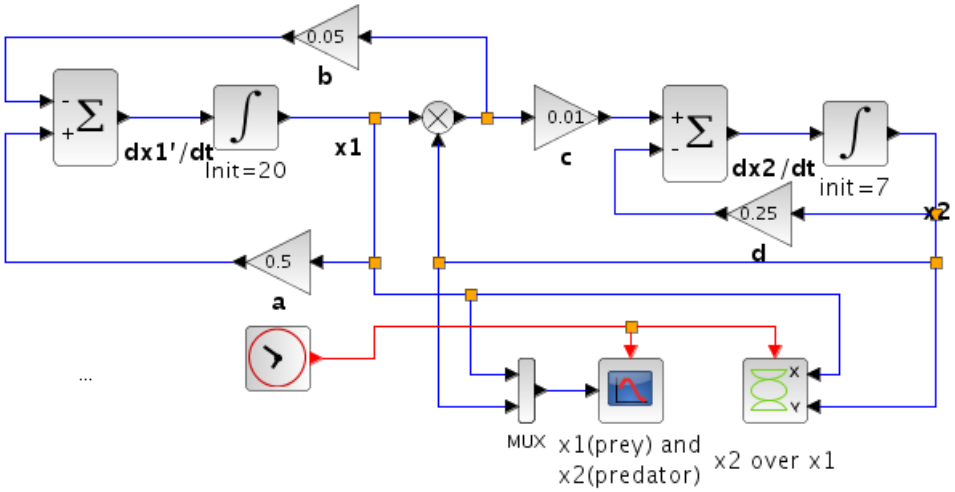

Figure 5.26: *Functional diagram of the predator-prey model of a linear network, where the left part corresponds to the term in Eq. 5.30 and the right part to the term in Eq. 5.31. The propagation rate of the prey is a, the one of the predators is b, death rate of the prey is c, the one of the predators is d. Simulation example for* $a = 0.5$, $b = 0.05$, $c = 0.01$, $d = 0.25$, $int = 20$ *for the initial values of the prey and* $int = 7$ *for the initial values of the predators (as given in the integrator). CLOCK_ is a clock generator for a uniform display of the time course of the prey and the predator population; the multiplexer MUX allows two inputs in CSCOPE, and CSCOPXY further to the right allows the output of two signals, where one is the prey (x1), and the other the predator (x2). The curves and the phase diagram obtained by the simulation are shown in Fig. 5.27.*

If the initial values are changed according to the Eq. 5.30 and 5.31 in such a way, that the conditions for the point of singularity are fulfilled, i.e. $a/b = 10 = x_2 = int = 10$ and $d/c = x_1 = int = 25$ (int: initial values for predator and prey), the number of predator and prey stays constant (see Fig. 5.28).

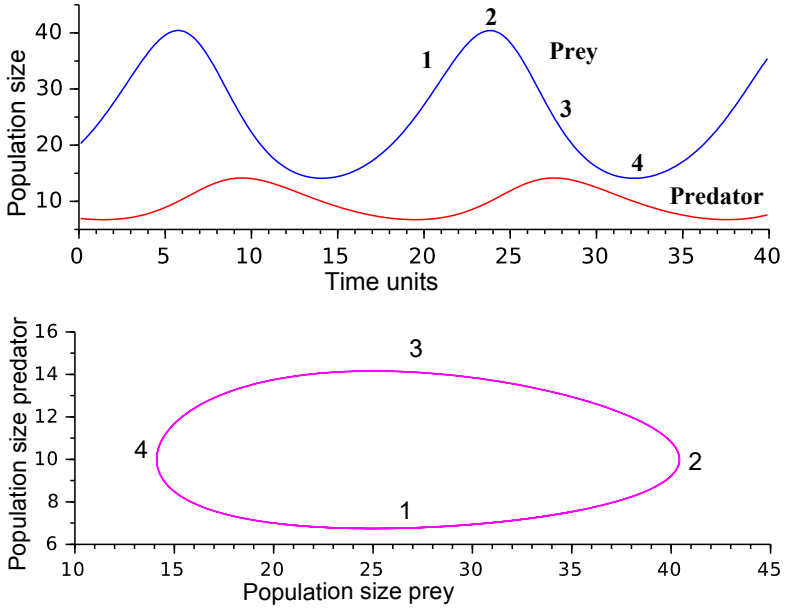

Figure 5.27: *Top figure: Changes of the population size of prey (blue curve) and predator (red curve) after simulation with the model in Fig. 5.26. The population size of the prey increases first (1), and with it -but time delayed, also the population size of the predator (2). Then the prey population decreases (3) and finally also the predator population (4).*
Bottom figure: Phase plane in which the number of predators is plotted against the number of prays. The resulting trajectory goes around the stable singularity with predator value 10 and prey value 25. In this singularity point no oscillations are shown, as demonstrated in Fig. 5.28.

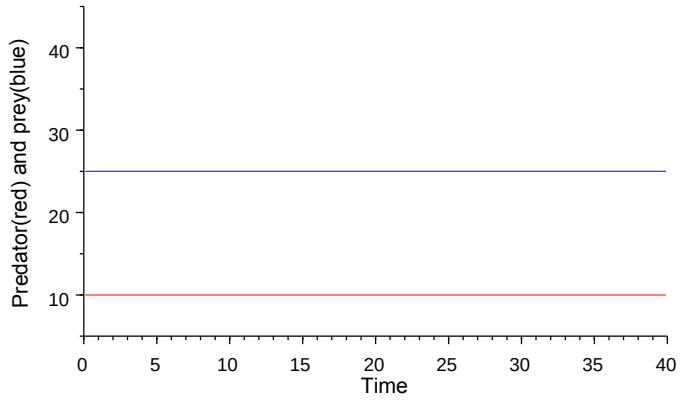

Figure 5.28: No *oscillation in a predator-prey population at the point of singularity, i.e.* $a/b = 10 = x_2 = int = 10$ *and* $d/c = x_1 = int = 25$ *(int: initial values for predator and prey). The population size of the prey (top) and the predator (bottom) in Fig. 5.26* does not change.

5.6.5.1 Approximation using the harmonic balance and the description function

The harmonic balance approximation consists of approximating the continuous oscillations of a non-linear feedback dynamic system by a harmonic oscillation. The non-linear subsystem in a feedback network with a non-linear characteristic curve in the feedback branch as in Fig.5.29 is represented by the description function..

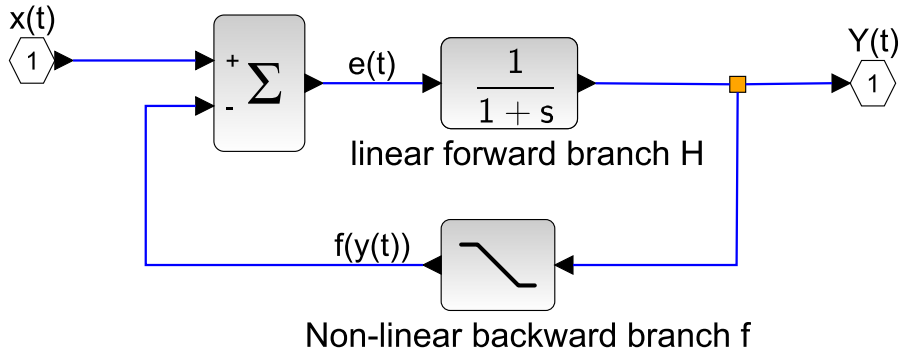

Figure 5.29: *General feedback network with static non-linear part in the feedback branch*

This approximation assumes that the signals of the system are approximately periodic and sinusoidal and that harmonics generated by the non-linearity are attenuated by the linear parts of the system to such an extent that they can be neglected. When decomposing the signal f(y(t)) at the output of the non-linearity into a Fourier series, only the DC component and the fundamental wave are taken into account. This means:

$$\begin{aligned} f(y(t)) &= a_0 + \sum_{n=1}^{\infty} a_n \cdot \cos \omega t + b_n \cdot \sin \omega t, \text{ with } \omega = \frac{2\pi}{T}, \text{ T:Period length} \\ &\approx a_0 + a_1 \cdot \cos \omega t + b_1 \cdot \sin \omega t \end{aligned} \tag{5.32}$$

The coefficients of the Fourier series a_0, a_1 and b_1 to be taken into account are of course now also dependent on the amplitude of the input signal y(t), e.g. if the output amplitude is limited in the case of a saturation characteristic and the fundamental oscillation is also damped as a result. This can now be indicated by a linear function that specifies these Fourier coefficients as a function of the input amplitude. The input signal is usually a sinusoidal signal with

$$y(t) = A \cdot \sin \omega t$$

The approximation of the output signal without DC component is then

$$f_1(t) = a_1 \cdot \cos \omega t + b_1 \cdot \sin \omega t$$

The description function F(A) now indicates how the amplitude of the fundamental oscillation specified by the Fourier coefficients a_1 and $b_1$changes as a function of the amplitude A of the sinusoidal input signal y(t), which can be summarised by complex representation of the Fourier

series with

$$y(t) = \Re\left\{\underbrace{-j \cdot A \cdot e^{j\omega t}}_{\overrightarrow{y(t)}}\right\}$$

$$f_1(t) = \Re\left\{\underbrace{(a_1 - j \cdot b_1) \cdot e^{j\omega t}}_{\overrightarrow{f_1(t)}}\right\}$$

and

$$F(A) := \frac{\overrightarrow{f_1(t)}}{\overrightarrow{y(t)}} = \frac{a_1 - j \cdot b_1}{-j \cdot A} = \frac{b_1}{A} + j\frac{a_1}{A} \tag{5.33}$$

$\overrightarrow{y(t)}$ is the complex representation of the input signal and $\overrightarrow{f_1(t)}$ that of the fundamental wave.

In principle, the fundamental wave can also exhibit a phase shift in relation to the input signal, which becomes clear through a non-vanishing imaginary part of the description function F(A). However, this is not the case with a saturation characteristic.

- The non-linear part in the backward branch can now be approximated by a linear part, which, however, depends on the amplitude of the fundamental oscillation of the output signal y(t) (see Fig.5.30)..

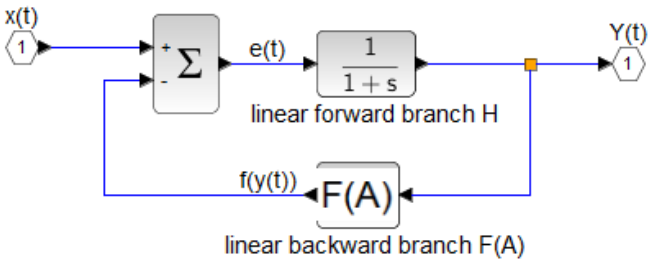

Figure 5.30: *General feedback network with static non-linear part approximation of the system in Fig. 5.29 according to harmonic balance with description function F(A) in the feedback branch*

The coefficients of the fundamental a_1 and b_1 in the equation of the linear function F(A)

5.33 result according to the Fourier series 5.32 to

$$a_1 = \frac{2}{T} \int_{-T/2}^{T/2} y(t) \cdot \cos \omega t \, dt \tag{5.34}$$

$$b_1 = \frac{2}{T} \int_{-T/2}^{T/2} y(t) \cdot \sin \omega t \, dt$$

These coefficients can

- be calculated and catalogued analytically, see e.g.Lutz, Wendt 2021 , or
- determined by simulation using Scilab/Xcos for any non-linear characteristic curve,see e.g. Fig. 5.31 .

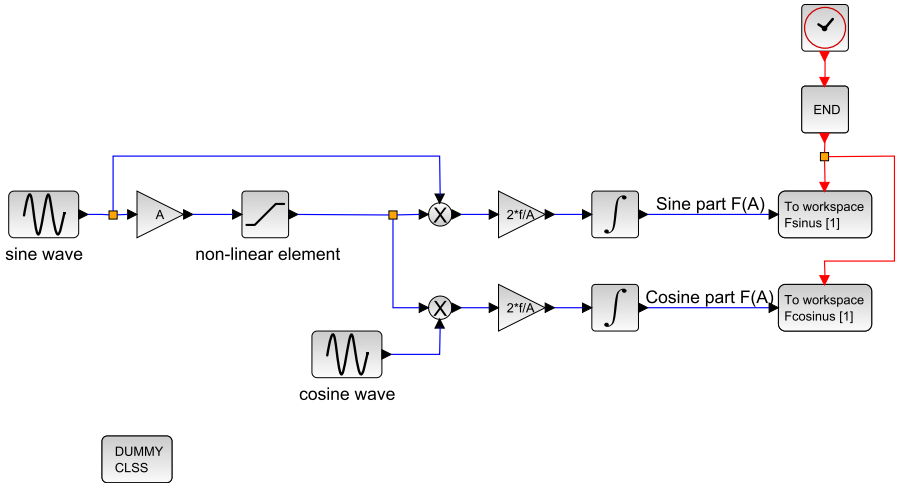

Figure 5.31: *Calculation of the description function F(A) with the help of Xcos for a non-linear characteristic curve. The end of the simulation is reached when one period of the sinusoidal oscillation of the input signal has ended (Endtime = T=1/f)*

This is particularly favourable if it is not a standardised characteristic curve, e.g. an asymmetrical saturation characteristic curve as shown in Fig.5.32.

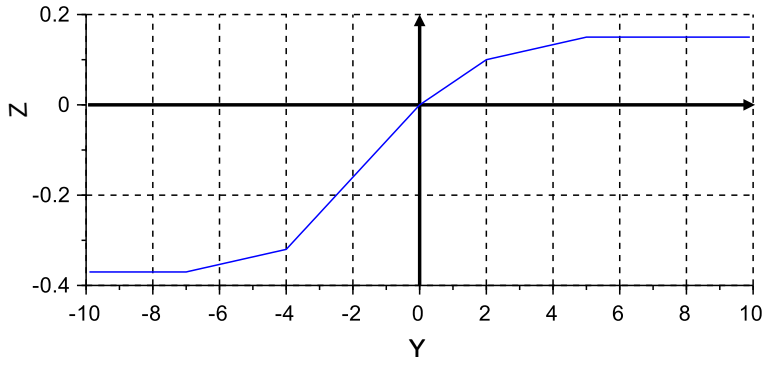

Figure 5.32: *Example of a asymmetrical saturation curve*

The description function F(A) as a function of the input amplitude A of a sinusoidal signal $y(t) = A \cdot \sin \omega t$ can then be determined using the small Scilab script such as Listing 5.2

Listing 5.2: *Scilab script for Determing the description function F(A) of the asymmetrical saturation characterisic curve 5.32 with the help of the Xcos model 5.31. This can also be determined as a function of the frequency.*

```
// Loading the library blocks and the simulation system
loadXcosLibs(); loadScicos();
//
importXcosDiagram("Modellname.zcos") // replace it with your Xcos-Modell name
//
typeof(scs_m) //diagram structure
//
// This diagram posesses 3 context variables:
//   A: Amplitude (standard value: 0.5)
//   f: Angular frequency (Standard value: 0.2)
//   EndTimed: End of simulation time (Standard value: 1/f)
//
scs_m.props.context; //imbedded definition
//
// First batch simulation with the imbedded parameter of the diagrams
printf("First␣simulation␣with␣internal␣standard␣values␣of␣the␣Xcos␣circuit\n")
scicos_simulate(scs_m);
Fsin=Fsinus.values;
Fcos=Fcosinus.values;
printf("Amplitude:␣0.5,␣frequency:␣0.2␣Hz,␣EndTime:␣1/f,␣Fsinus:␣%6.2f␣.,␣
    Fcosinus:␣%6.2f\n", Fsin, Fcos)
//
// selected changes of amplitude and frequency
printf("Then␣simulation␣with␣parameter␣variation␣of␣Xcos␣circuit\n")
A1=0.001 // min. Amplitude
A2=10    // max. Amplitude
AN=50    // number of calculation points
DA=(A2-A1)/AN // Amplitude steps
Af=[A1:DA:A2]
f1=0.1   // min. Frequency
f2=1.0   // max. Frequency
fN=5     // number of frequency points
```

```
Df=(f2-f1)/5 // frequency steps
ff=[f1:Df:f2]
printf("Ampl. Start: %6.2f, End: %6.2f, Diff: %6.2f, Freq. Start: %6.2f, End:
    %6.2f, Diff: %6.2f\n", A1, A2, DA, f1, f2, Df)
Fsinf=zeros(size(ff,2),size(Af,2))
Fcosf=zeros(size(ff,2),size(Af,2))
for j=1:size(ff,2)
  Context.f=ff(j)
  EndTime=1/ff(j)
  Context.EndTime=EndTime
//   Context.EndTime=1/ff(j)
  for i=1:size(Af,2)
    Context.A=Af(i)
    scicos_simulate(scs_m,Context);
    Fsin=Fsinus.values;
    Fsinf(j,i)=Fsin;
    Fcos=Fcosinus.values;
    Fcosf(j,i)=Fcos;
    if modulo(i-1,4) == 0 then printf("Freq.: %5.2f,Ampl.: %5.2f,Fsin: %6.2f,
        Fcos: %6.2f\n", ff(j), Af(i), Fsin, Fcos); end
  end
end
//
// Readout of results
//
scf(1);
for j=1:size(ff,2)
plot2d(Af,Fsinf(j,:)) // real part of F(A)
end
xgrid()
title("Describing function F(A,f)","fontsize",5);
xlabel("Amplitude A","fontsize",4);
ylabel("N(A,f) Real-Part","fontsize",4)
//
scf(2);
for j=1:size(ff,2)
plot2d(Af,Fcosf(j,:)) // imaginary part of F(A)
end
xgrid()
title("Describing function F(A,f)","fontsize",5);
xlabel("Amplitude A" ,"fontsize",4);
ylabel("F(A,f) Imag-Part","fontsize",4)
//
scf(3);
surf(Af,ff,Fsinf) //real part of F(A), 3d
title("Describing function F(A,f)","fontsize",5);
xlabel("Amplitude A","fontsize",4);
ylabel("Frequency f/Hz","fontsize",4);
zlabel("F(A,f) Real-Part","fontsize",4)
xgrid()
//
scf(4);
surf(Af,ff,Fcosf)  //imaginary part of F(A), 3d
title("Describing function F(A,f)","fontsize",5);
xlabel("Amplitude A","fontsize",4);
ylabel("Frequency f/Hz","fontsize",4);
zlabel("F(A,f) Imag-Part","fontsize",4)
xgrid()
```

In the case of a saturation characteristic, the imaginary part of the characteristic shown above in Fig. 5.32 disappears approximately, which is why only the real part is shown. In

addition, the description function F(A) does not depend on the frequency, which is why only the two-dimensional representation is shown in Fig..5.33 .

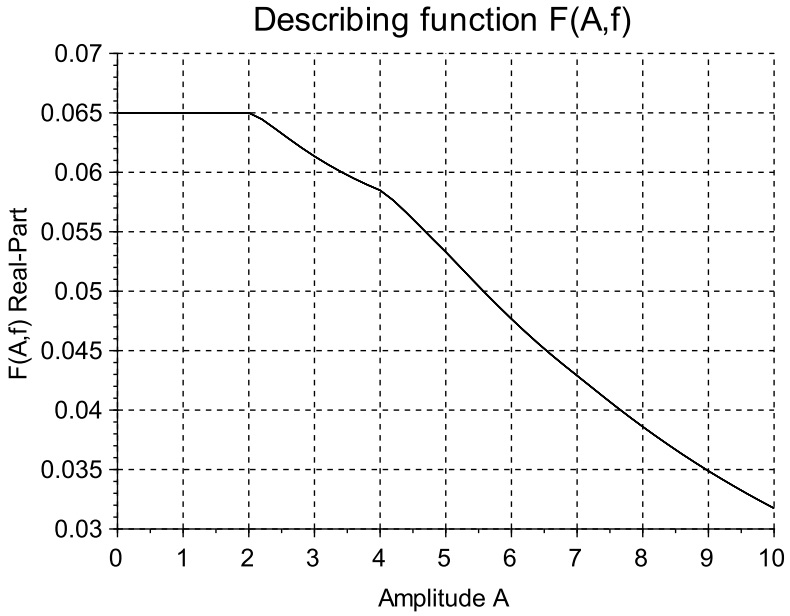

Figure 5.33: *Describing function F(A,f) for the example of an asymmetrical saturation characteristic curve according to Fig. 5.32 for f=0.1 to 1.0. This shows that in this case the description function does not depend on the frequency of the input signal.*

The condition that a stationary oscillation exists is that the feedback output signal generates the same signal again at the output without an additional input signal, in frequency domain with the complex frequency p according to the feedback model in Fig:5.12

$$Y(p) \cdot (-Fv(p)) \cdot Fr(p) = Y(p) \text{ mit } p = \sigma + j\omega$$

resp.

$$Fv(p) \cdot Fr(p) = -1 \tag{5.35}$$

In the harmonic balance approximation, this oscillation condition for non-linear feedback is only analysed for the fundamental wave. It can therefore be replaced by the linear description function F(A,f), which, however, depends on the amplitude A of the feedback signal y(t), i.e:

$$Fv(p) \cdot F(A, f) = -1 \tag{5.36}$$

For an undamped oscillation for $p = j\omega$ it is obtained when the locus curves of $Fv(j\omega)$

and $-1/F(A, f)$ intersect, i.e.

$$Fv(j2\pi f) = -\frac{1}{F(A, f)}$$

This makes it possible to determine approximately at which amplitude of the fundamental A and the frequency f of the output signal y(t) the feedback system becomes unstable and oscillates.
An Example of a stability analysis using the harmonic balance method with the aid of the description function F(A) of the saturation function in Fig.5.32 and the transfer function $H = 0.5/((0, 1 + j\omega) * j\omega) + 10 \cdot (1 - j)$. shows Fig.5.34.
Listing 5.3 shows the small Scilab script to calculate this curve..
Another example can be found in subsec.7.1.1 in the stability analysis for the non-linear Karlsson/Johnsson model

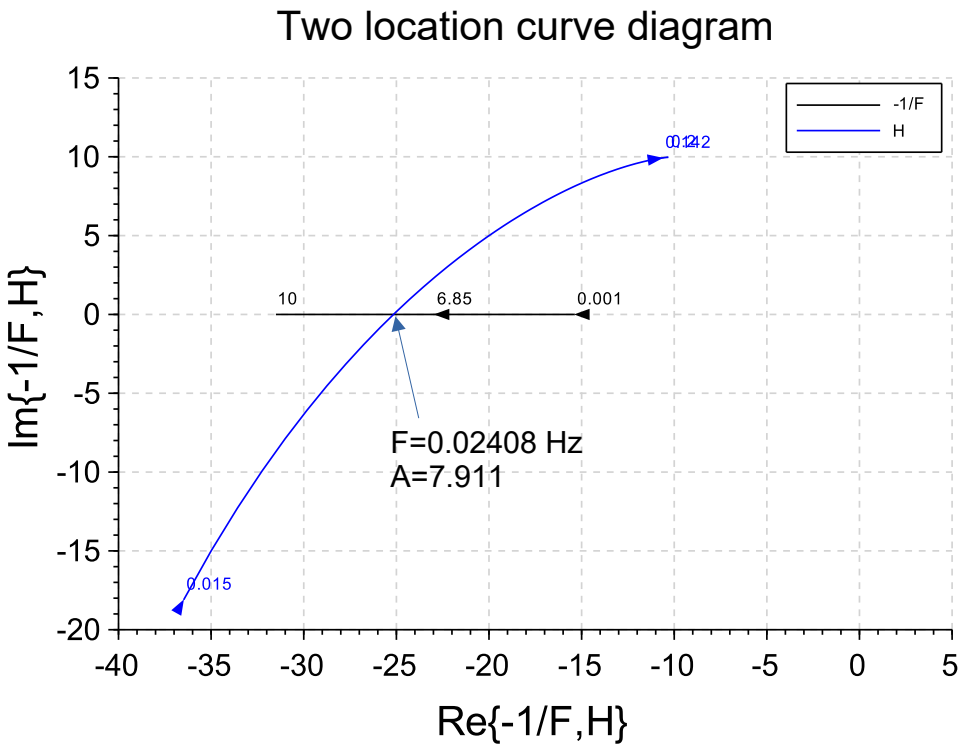

Figure 5.34: *Example of a stability analysis using the harmonic balance method. With the aid of the description function F(A) of the saturation function and the transfer function H and with the help of the two location curve diagram, the intersection of the two curves -1/F and H shows that the critical point can be reached when the amplitude A of the fundamental is approx. 7.911 and the frequency is 0.024 Hz.*

Listing 5.3: *Scilab script for determing the two locus curve diagram in Fig.5.34*

```
//Determination of the description function f
//
//Xcos-Modell load, replace it with your Model in Xcos
loadXcosLibs(); loadScicos();
importXcosDiagram("Modellname.zcos")
typeof(scs_m) //diagram structure
//
// This diagram posesses 3 context variables:
//   A: Amplitude argument of the description function(standard value: 6.0)
//   f: Frequency (Standard value: 0.2)
//   EndTimed: End of simulation time (Standard value: 1/f)
//
scs_m.props.context; //imbedded definition
A1=0.001 //Startvalue of the input amplitude
A2=10 //Endvalue of the input amplitude
nA=200 //number of amplitude points
dA=(A2-A1)/nA
Af=A1:dA:A2; //Amplitude range of A
f=0.2
printf("Ampl. Start: %6.2f, End: %6.2f, Diff: %6.2f, Freq.: %6.2f\n", A1, A2,
    dA, f);
  Context.f=f
  EndTime=1/f
  Context.EndTime=EndTime
for i=1:size(Af,2)
  Context.A=Af(i)
  scicos_simulate(scs_m,Context);
  Fsin=Fsinus.values;
  Fsinf(i)=Fsin;
  Fcos=Fcosinus.values;
  Fcosf(i)=Fcos;
  if modulo(i-1,4) == 0 then printf("Ampl.: %5.2f, Fsin: %6.2f, Fcos: %6.2f\n",
      Af(i), Fsin, Fcos); end
end
Fsinfni=-1./Fsinf //negative inverse of F(A) for Nyquist diagram
//
// Determination of the linear transfer function H
//
f1=0.015; // Start value of frequency
f2=0.200; // End value of frequency
nf=200;   // number of frequency points
df=(f2-f1)/nf;
freq=f1:df:f2;
om=2*%pi*freq;
H=0.5*(1./((0.1+%i*om).*(%i*om)))-10.0+%i*10; //replace it with your function H
//
// Representation of zwo curve nyquist diagram
//
scf(1);
nyquist([Af;freq],[Fsinfni';H],["-1/F";"H"],%f) // 2 location curve diagram
xlabel(_("Re{-1/F,H}"), "fontsize",5); ylabel(_("Im{-1/F,H}"), "fontsize",5)
title('Two location curve diagram','color','black', "fontsize",5);
```

6 Modelling and simulation of some oscillator properties of special interest

In this chapter we will focus on four aspects in modelling rhythms[1]:

1. Shifting the phase of a rhythm (mentioned before at various places, and treated in more detail in Sect. 6.1) simulating the behaviour of rhythms and oscillators under the influence of - especially - light pulses, both single ones and repeated. This will involve discussions both of theoretical and practical importance.

2. Synchronising rhythmic events (see Sect. 6.2) and entraining oscillators by giving repetitive perturbations (subsect. 6.2.1), whereby the range of entrainment is of special interest (subsect. 6.2.2).

3. Perturbation experiments have also been important in the discussion of possibilities to stop circadian clocks and other oscillators. This was discussed in Sect. 3.1 and will be described for modelling this feature (Sect. 6.3).

4. Finally, as described in Sect. 3.2, the astonishing fact that circadian rhythms show roughly the same period at different temperatures (at least in a certain temperature interval) - we denote it as *temperature robustness* of circadian rhythms - will be taken up again in Sect 6.4 for modelling it.

Any realistic model of circadian rhythms have to meet these features.

6.1 Shifting circadian rhythms by external perturbations

As mentioned already on page 38 in Sect. 3.1, a perturbation by, e.g. a light pulse can cause a delay of the oscillation, or its contrast, an advance. Giving the perturbation in different phases of the oscillation and plotting the resulting delays and advances in a so-called Phase Response Curve, PRC, provides a convenient representation of the magnitude and position of the perturbation to reach the effect. If φ denotes the phase shift in a perturbed sine wave, $sin(\omega t + \varphi)$, a positive φ denotes an advance, a negative one a delay in comparison to the control sine wave $sin(\omega t)$. A typical PRC is shown in Fig. 3.8 (right part), where the advance phase shifts are plotted along the positive y - axis, while delay phase shifts are plotted along the negative delay axis. The curve represents phase shifts due to light pulses in the case of the circadian eclosion rhythm of the fruit fly *Drosophila pseudoobscura* (Pittendrigh, Minis 1964)

[1] They are significant for circadian rhythms but concern basically also ultradian rhythms

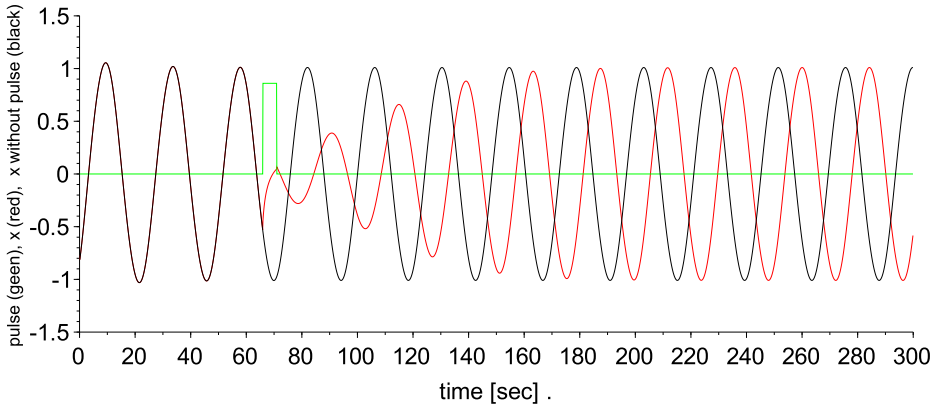

Figure 6.1: *A rectangular pulse (green) was applied in the case of a VP oscillator simulation with* $\varepsilon = 0.2$ *(black curve control). The length of the delay can be estimated by the times of the zero crossings of the curves and amounts to about 8 h*

By altering different internal parameters of a system such as its amplification factors, its losses, or its temperature, the form of the oscillation, the period length, the time of the onset of the oscillation or the end of the oscillation can be influenced. The heartbeat, for instance, can be stopped before a bypass surgery by hypothermia and medications and after ward induced again to beat by other medications and by increasing the temperature. Also a strong blow at the chest during a football game might stop the heart beat, and it needs an electroshock for resuming its normal rhythm (see page 220).

To valuate such changes of the rhythm it helps to see, how the oscillating system reacts to those perturbations. An external light or temperature pulse can be used and it can be checked, how the form of the oscillation has changed after the perturbation in respect to the unperturbed oscillation.

In this connection it is quite helpful to study the time of the maximum or the zero crossing of the oscillation, since it allows to determine critical perturbations (e.g. when the oscillation can be stopped completely, see Sect. 3.1). The phase shifts due to a perturbation can be described, as done before, by a PRC. It reflects for instance the phase change as a function of the time at which the perturbation (e.g. a pulse) occurred, or the strength of the perturbation (e.g. the height of the pulse; see Fig. 6.1).

In the PRC the alteration of the time of the zero crossing or of a maximum of an oscillation as compared to an unperturbed system is plotted as a function of the perturbation time respectively its phase. In Fig. 6.1 as an example the oscillation of an unperturbed system is shown in black, the one of the perturbed systems in red, and the perturbing pulse in green. The phase shift after the perturbation is the normalised[2] time difference between the red and the black curve. To determine it, the Scilab model shown in Fig. 6.2 can be used. In the model the oscillation of the perturbed system is compared with the unperturbed system, and in the superblock “phase

[2] i.e. the time difference divided by the the period of the oscillation

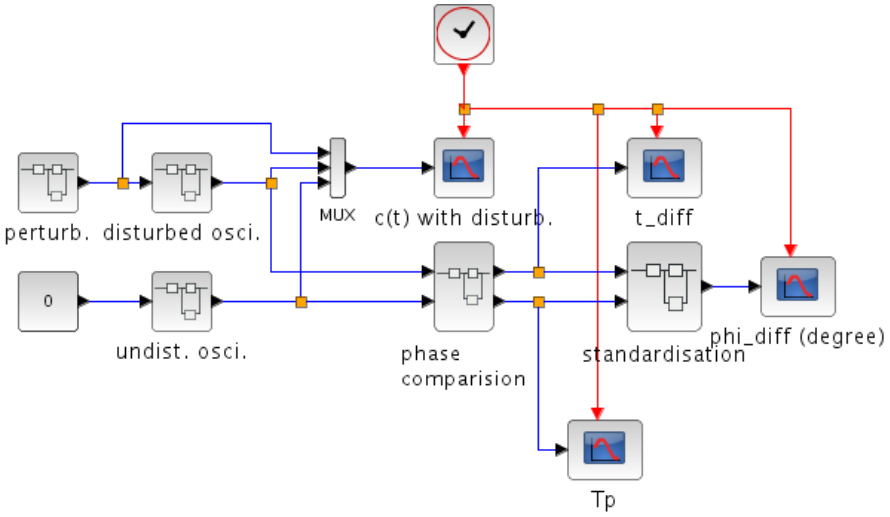

Figure 6.2: *Determination of the phase shift due to a perturbation of an oscillating system (osci) by using a Sciab/Xcos model. c(t) is the output signal, Tp the period length of the unperturbed signal and t_diff the time difference of the zero crossing between the perturbed and the unperturbed signal. In the block „phase comparison“ the period length and the time difference is determined, and in the block „standardisation“ the phase change is standardised for a full period to 360° (±180°). MUX is a multiplexer, phi_diff is phase difference in degrees (from 0 to 360°)*

comparison” the time difference is obtained. After standardising to the period length (superblock “standardisation”) one obtains the phase changes. The superblocks “phase comparison” and “standardisation” are shown in Fig. 6.3 and Fig. 6.4.

As an example for obtaining a PRC we use the simple VP oscillator shown in Fig. 5.8. The corresponding superblock “osci” in Fig. 6.2 is displayed in Fig. 6.5.

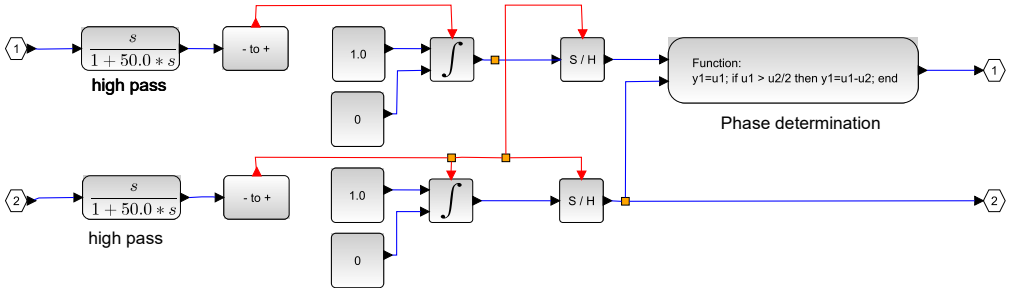

Figure 6.3: *Superblock "phase comparison" in Scilab/Xcos for determining the time difference of the zero crossing of two signals in Fig. 6.2, which suppress the lower frequencies of the signal (only* steep signals *are passing, e.g. steep zero crossings).*
At first the DC-parts of the signal are suppressed by high pass filters, the first blocks to the left. It suppresses the lower frequencies of the signal and only steep signals are passing, e.g. steep zero crossings. Next, the zero crosses are identified and the time differences of the zero crossings of the two input signals calculated. In the block „phase determination" this time difference is corrected, if it exceeds half of the period length. In this case it is assigned to the next period, but with a negative sign (i.e. an advance).

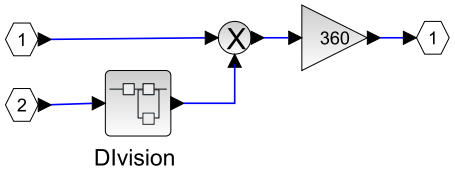

Figure 6.4: *Superblock „standardisation" in Fig. 6.2 from -180° to 180°*

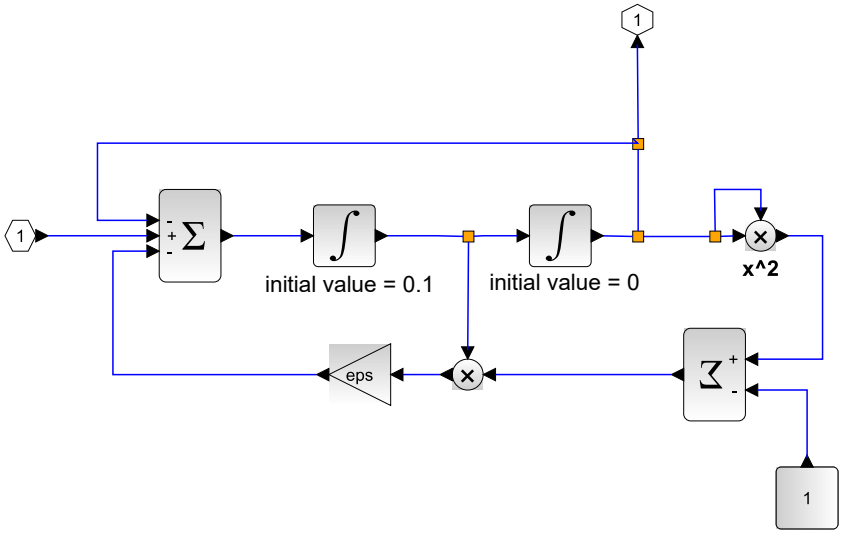

Figure 6.5: *Superblock „osci" in Fig. 6.2*

How the VP oscillator reacts to a rectangular pulse is shown for instance in Fig. 6.6 with the pulse applied in a different position of the oscillations than in Fig. 6.1. If the time of the application of the pulse is varied, one obtains the various differences of the times of the extreme value or zero crossings in respect to the unperturbed VP. Plotting the differences as a function of the application times leads to the PRC as shown in Fig. 6.1. Thereby the standardised values are used and not the direct time differences of the extreme values or zero crossings, whereby a phase shift by a full period corresponds to a phase shift of 360°. Using phase instead of time facilitates also comparisons between oscillations with different periods, from different organisms etc.

To avoid changing the parameters for each pulse time and the following simulations sequentially, one can use a Scilab script, which carries this out (see the Listing. 6.1).

Listing 6.1: *Scilab script for obtaining a PRC as shown in Fig. 6.8 with simulations of the Xcos-circuit according to Fig. 6.7*

```
loadXcosLibs(); loadScicos() ;// Loading the Xcos-model
importXcosDiagram("VanPol_Puls-SB-PRC_sb_V5_batch.zcos");
typeof(scs_m) //Diagram structure
t_p=128; h_p=3; b_p=1; eps=4.0; Tend=300; //Context variable :
Context.t_p=t_p; Context.h_p=h_p ; Context.b_p=b_p ; Context.eps=eps; Context.Tend=Tend
    ;
scs_m.props.context; funcprot(0);
printf("First␣simulation␣with␣internal␣standard␣values␣of␣Xcos␣circuit\n");
scicos_simulate(scs_m);
phi_diff=phi_diffEnd.values;
printf("eps:␣%5.2f,␣pulse␣height:␣%5.2f␣,pulse␣width:␣%5.2f␣,␣pulse␣onset:␣%6.2f␣sec\n"
    , eps, h_p, b_p, t_p)
printf("impulse␣onset:␣%5.2f␣sec,␣phase␣diff.:␣%5.2f␣degre.␣\n", t_p, phi_diff)
printf("then␣simulation␣with␣parameter-variation␣of␣the␣Xcos␣circuit\n")
t_p1=120; t_p2=132; dt_p=(t_p2-t_p1)/100; ft_p=[t_p1:dt_p:t_p2]; fphi_diff=zeros(size(
    ft_p))
for i=1:size(ft_p,2) //Variation of pulse time
Context.t_p=ft_p(i);
scicos_simulate(scs_m,Context);
phi_diff=phi_diffEnd.values; fphi_diff(i)=phi_diff;
if modulo(i-1,4) = 0 then printf("impulse␣onset:␣%5.2f␣sec,␣phase␣diff.:␣%5.2f␣degrees.
    ␣\n", ft_p(i), phi_diff); end
end
scf(1); plot2d(ft_p,fphi_diff); xgrid() //PRC-plot
title("PRC␣of␣the␣VP␣oscillator,␣eps␣=␣"+string(eps),"fontsize",5);
xlabel("time␣(sec)","fontsize",4);
ylabel("phase␣difference␣(degree)","fontsize",4)
```

For this purpose the respective parameter (here the time, at which the pulse is applied) is altered and the simulation with the Xcos-model performed. To avoid generating each time for a parameter value the oscilloscope pictures according to the Xcos circuit in Fig. 6.2, the oscilloscope has been removed from the circuit (see Fig. 6.7). The phase shift itself is stored in the workspace of Scilab by using the block „To workspace“ and can be processed by a Scilab script and finally plotted at the end of all simulations. This occurs at the output of the block „standardisation“, where the oscilloscope can not simply be exchanged by the block „To workspace“; for internal reasons of Scilab the oscilloscope has to be replaced by a „trash“, which serves as a "rubbish bin“ for the icon.

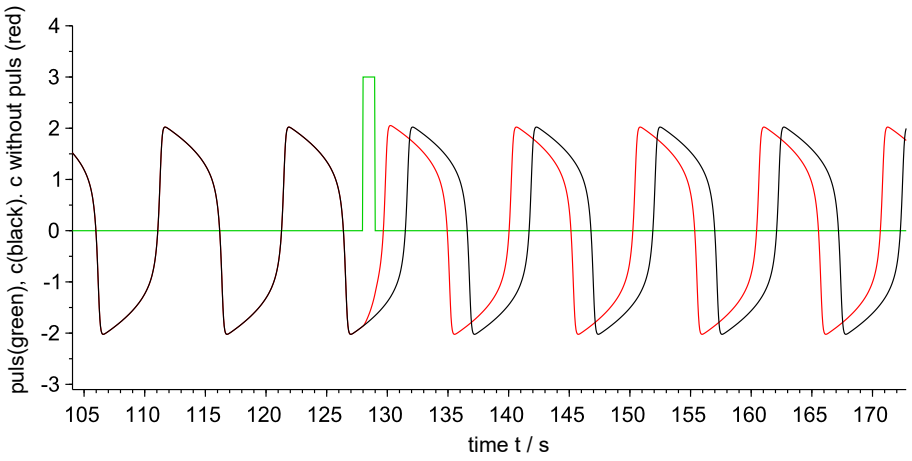

Figure 6.6: *Reaction of a VP oscillator (with $\epsilon = 4$) to a rectangular pulse (green) simulation based on the the schemes in Fig. 6.2 and 6.5.*
Due to this perturbation the maximum and/or the next zero crossing is reached earlier, which leads to an advance of the perturbed (red curve) oscillation with respect to the unperturbed (black curve) oscillation. For a smaller non-linearity (with a VP oscillator $\epsilon = 0.2$) the maximal amplitude is reached earlier after the pulse. The transient time is also smaller (see Fig. 6.1).

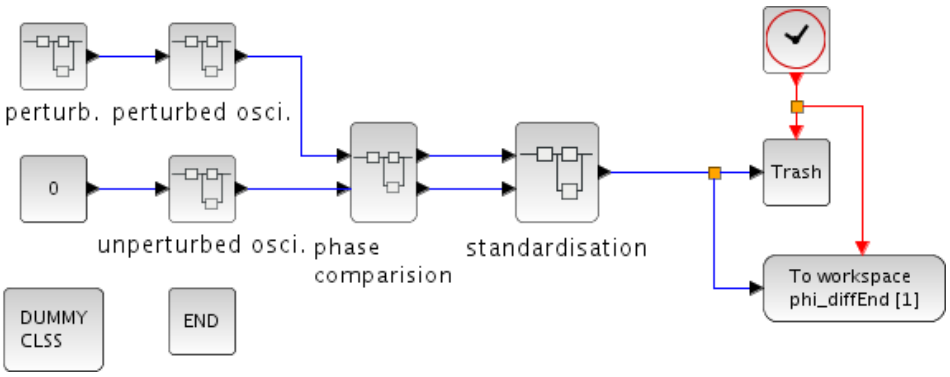

Figure 6.7: *Determination of the phase shift as in Fig. 6.2, but without oscilloscope. The block* DUMMY CLSS *is necessary for the simulation, to avoid a Scilab crash. The block* END *allows to determine the simulation time from outside, e.g. in a script.*

From the generated PRC in Fig. 6.8 one can see, that the pulse perturbation of ca. 126 sec alters the phase strongly. Here a small deviation of the time of the pulse application suffices, to generate quite large differences in behaviour of the oscillations. Therefore one could at this point study whether an additional variation of the pulse height and/or width could bring the system in a singular point and the oscillation to a halt. For this a similar Scilab script as in Lst.

6.1 is used, in which not only the time of the pulse application is varied, but also its height (see Lst. 6.2). The corresponding phase shift is colour coded and supplemented with „contour lines“ representing identical phase differences (see Fig. 6.9).

Listing 6.2: *Scilab-Skript for getting the colour coded phase response contour in Fig. 6.9 by varying the pulse begin and its hight*

```
loadXcosLibs(); loadScicos();// loading the Xcos-model
importXcosDiagram("Dateiname.zcos"):
typeof(scs_m) //diagram-structure
// onset values for pulse begin and its hight
t_p=128;   // pulse begin
h_p=3;     // pulse hight
// standard values
b_p=1;     // pulse width
eps=4.0;   // parameter of VP-osci.
Tend=300; // end of simulation
//context variable for  Xcos model:
Context.t_p=t_p;
Context.h_p=h_p;
Context.b_p=b_p;
Context.eps=eps;
Context.Tend=Tend ;
scs_m.props.context; // Xcos-model connection
funcprot(0); // no warning, if function is redefined
//
printf("first simulation with internal standard values of Xcos-circuits");
scicos_simulate(scs_m); phi_diff=phi_diffEnd.values;
printf("eps: %5.2f, pulse hight: %5.2f , pulse width: %5.2f ,, pulse begin: %6.2f sec.\n"
    , eps, h_p, b_p, t_p);
printf("pulse begin: %5.2f sec., phase diff.: %5.2f degree. \n", t_p, phi_diff);
//
printf("afterward simulation with parameter variation of Xcos-circuit\n")
t_p1=120;
t_p2=132;
dt_p=(t_p2-t_p1)/40;
ft_p=[t_p1:dt_p:t_p2];
h_p1=0.1;
h_p2=12.0;
dh_p=(h_p2-h_p1)/40
fh_p=[h_p1:dh_p:h_p2];
fphi_diff=zeros(size(fh_p,2),size(ft_p,2)):
//
for j=1:size(fh_p,2) //variation of pulse hight
  Context.h_p=fh_p(j)
  for i=1:size(ft_p,2) //variation of pulse time
    Context.t_p=ft_p(i)
    scicos_simulate(scs_m,Context);
    phi_diff=phi_diffEnd.values; // Xcos-adoption of result
    fphi_diff(j,i)=phi_diff; // storage in 2D-field
    if modulo(i-1,4) == 0 then
      printf("pulse begin: %5.2f sec., pulse hight: %5.2f, phase diff.: %5.2f degree. \n
          ",ft_p(i),fh_p(j), phi_diff);
    end
  end
end
scf(1);
xset("colormap",jetcolormap(64)); // colour scale fix
fphi_diffmin=min(fphi_diff);
fphi_diffmax=max(fphi_diff);
colorbar(fphi_diffmin,fphi_diffmax) // colour coded 2D-diagram plotting
```

```
Sgrayplot(ft_p,fh_p,fphi_diff', strf="021") // plot contour line at -120, -60, 0, 30,
    60 and 120 degrees
contour2d(ft_p,fh_p,fphi_diff',[-120.0,-60.0,-30.0,0.0,30.0,60.0,120.0]); // labeling
    of the graphic
title("PRC-pulse begin and ampl. of VP-osci., eps = "+string(eps),"fontsize",5);
xlabel("pulse time (sec.)","fontsize",4); ylabel("Imp.-Amp.","fontsize",4)
```

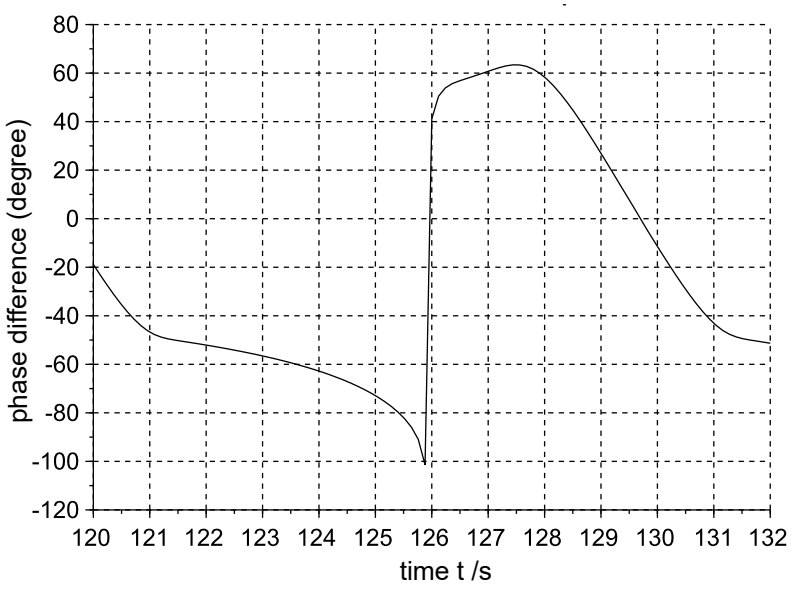

Figure 6.8: *PRC of the VP oscillator with $\epsilon = 4$ (ϵ is a parameter of the VP-Oscillators and determines the non-linearity; up to $\epsilon = 1$ the oscillation is sinusoidal) according to Fig. 6.5*
A superblock with the corresponding VP-oscillator, which is part of the circuit in Fig. 6.2) has been used when applying a perturbation (rectangular pulse with height=3 and duration=1) in the interval 120-132 of the simulation. Perturbations were applied at different times in the interval which represents ca. one period of oscillation. The phase shifts are given in degrees (1 oscillatory period corresponds to 360 degrees), advances upwards, delays downwards

One can see from Fig. 6.9, that for a pulse perturbation of ca. 126 sec not a singular *point* is obtained, but rather a singular *bar* (for a pulse height of ca. 3.9 to 7.6). In this range the phase shift changes strongly when varying the start time of the pulse. If, however, the pulse height is further increased, the *bar* bends to the left. If the pulse is applied in the time interval 129 to 130 sec, the phase in this range of the VP oscillator is quite insensitive towards perturbing pulses. This is the range with the steepest increase of the oscillation (see Fig. 6.6).

An alternative evaluation of the phase shift due to a pulse can be obtained by using the extended display of the derivation y = dx/dt as a function of x (see e.g Fig. 5.10 for the VP oscillator). One can see, that in the case of a small non-linearity with $\epsilon = 0.2$ the oscillation converges spirally from a small initial value in the xy plane to a final amplitude of about 2 and becomes circular. This non-linear cyclic oscillation is called limit cycle with a radius of about 2.

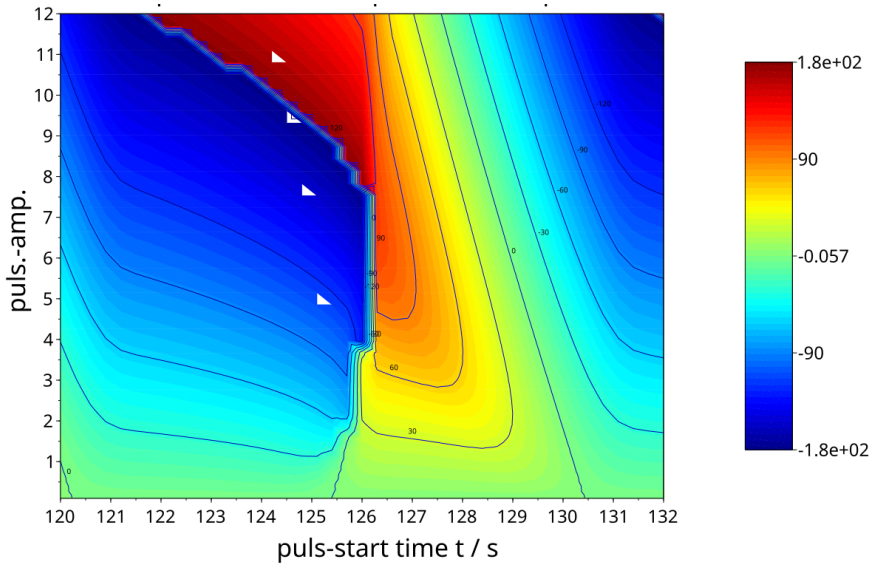

Figure 6.9: *Colour supplemented PRC contour map of the VP oscillator (VP-Osci, with $\epsilon = 4$) with different pulse heights.*
Phase shifts were calculated according to Fig. 6.5 in the case of a perturbation by a rectangular pulse of a width of 1. Pulses were given in the time interval 120 to 132 sec of the simulation, as in Fig. 6.8 , but now with different strengths. The phase-shifts caused by the perturbation are shown by the colour (scale of it to the right) as a function of pulse height (y-axis) and the start of the pulse applied (x-axis). Pulse duration = 1 sec.

If the initial value would have been such that it was located on the trajectory, the oscillation would not spiral, but loop on the limit cycle (see Fig. 6.10).

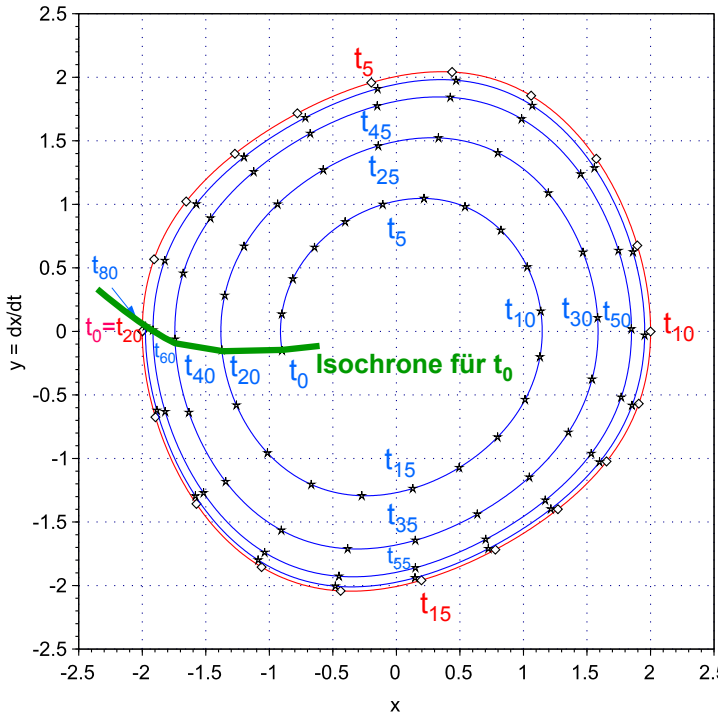

Figure 6.10: *xy diagram of the VP oscillator outlined in Fig. 5.8 with $\epsilon = 0.2$ for two initial conditions.*
One initial conditions is on the limit cycle trajectory with the initial values $x = -2$ and $y = 0$ (red trajectory),The period length is 6.3 sec. 20 time points per period are marked (on the red limit cycle with diamonds, on the blue oscillation with stars). At each fifth mark a time mark t_i is added. The time mark t_5 for instance means, that here one fourth of the period has passed. Four periods are calculated (from 0 to 25.2 sec). On the limit cycle, however, only one period is marked, since later periods of course coincide with the first one.

If the pulse is added to the input of the VP oscillator, the output value x of the oscillation will generally not belong to the limit cycle, and the oscillation will - similar to the smaller initial value (blue curve in Fig. 6.10) – approach the limit cycle perhaps after several periods. But at which location will it approach the limit cycle? One can see in Fig. 6.10, that at the time mark t_0 on the red trajectory (also marked t20 since the period is 20 sec.) an other xy pair of values is approaching, but they belong to the blue curve and not before the time mark t80 of the blue curve (that is after 4 periods) the values are equal. Not before the time mark t_{80} is reached (that is after 4 periods) the values are equal. We keep in mind that we are looking for a location, respectively the time or phase on the limit cycle, which is reached *after* a pulse (principally after an unlimited number of periods). In the example in Fig. 6.10 one recognises, that the time t_0 differs from the one on the blue curve. But one could also ask:

Where is the limit cycle reached, if the initial value of the oscillation is arbitrary?

The answer to this question can be approached by introducing the concept of *isochrons* i.e. curves that connect points in the x-y plane that have 'identical times' or *phases*. The term isochron was used and elaborated in the circadian context by Winfree 1967; Winfree 1980. And we can exemplify it with the VP oscillator in Fig. 6.10, where part of the isochron for t=t0 (equivalent to phase = 0) is outlined in green colour. Observe that we have derived the (green) isochron from calculated trajectories fairly close to the limit cycle. We could have used trajectories outside the limit cycle as well, and also approached closer to the centre of the limit cycle. The result would then have been as shown in Fig. 6.11.

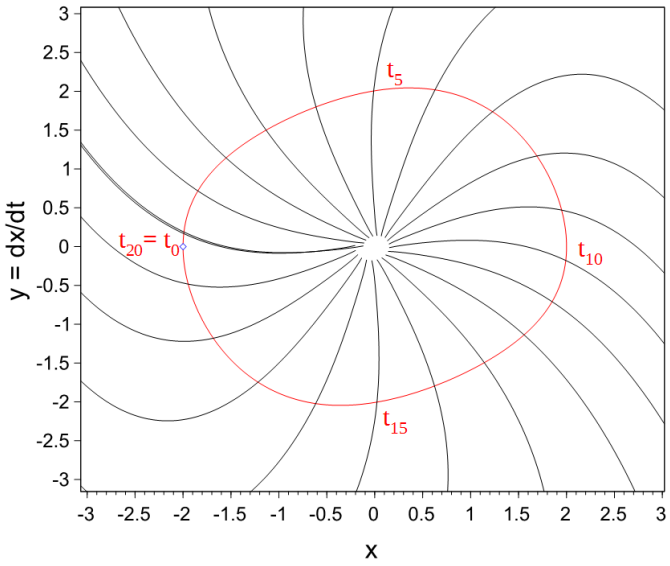

Figure 6.11: *xy diagram with isochrons of the VP oscillator in 5.8 with ε=0.2 and trajectories, after Fig. 6.10. The isochrons were generated with a Matlab program of Izhikevich 2007 transformed to Scilab (see Lst. 6.3)*

Listing 6.3: *Isochron calculation, see (Izhikevich 2007)*

```
function dx = F(t,x) //diff-eq. of the VP oscillator
dx(1)=x(2);
dx(2)=eps*(1-x(1)^2)*x(2)-x(1);
dx=dx';
endfunction
// isochron of a planar dynamic system x''=F(t,x)
global eps
mode(0); ieee(1); funcprot(0); eps=0.2; //work flow parameter
x0 = [-2;0]; T = phases($); tau = T/600; m = 200; k=5;
phases = 0:0.314:2*%pi; // time resp. phase values
t = 0:tau:T; t0=0; lc = ode("stiff",x0,t0,t,F);// forward integr.
dx = (max(lc') - min(lc'))'/m; // spacial resolution
center = (max(lc') + min(lc'))'/2; // centre of limit cycle
iso = [x0-(m^0.5)*dx,x0+(m^0.5)*dx]; // onset at x0
for t = 0:-tau:-(k+1)*T // backward integration
for i = 1:size(iso,2)
diso = F(t,iso(:,i)); // derivation dF/dt according to diff. eq.
```

```
iso(:,i) = iso(:,i) - tau*diso'; // one step further
end;
i = 1;while i<=size(iso,2) // remove too large values
if or(bool2s(abs(iso(:,i)-center)>(1.5*m)*dx)) then
iso = [iso(:,1:i-1),iso(:,i+1:$)]; // remove if limit violation
else i = i+1;end;
end;
i = 1; while i<=(size(iso,2)-1)
d = sqrt(sum(((iso(:,i)-iso(:,i+1)) ./dx) .^2)');// standardising
if d > 2 then // add a point in the centre
iso = [iso(:,1:i),(iso(:,i)+iso(:,i+1))/2,iso(:,i+1:$)];
end;
if d < 0.5 then // remove a point
iso = [iso(:,1:i),iso(:,i+2:$)];
else i = i+1;end;
end;
if(pmodulo(-t,T)<=tau/2)&(-t<k*T+tau)then
a = gca(); delete(a.children); // refresh monitor
plot(lc(1,:),lc(2,:),"r",x0(1),x0(2),"bd");// limit cycle
set(gca(),"auto_clear","off");
end;
if min(abs(pmodulo(-t,T)-phases))<tau/2 then
plot(iso(1,:),iso(2,:),"k-"); // draw isochrons
end;
end;
set(gca(),"auto_clear","on");
```

To repeat: All simulations with starting point on the same isochron, will be positioned (after transients) on the limit cycle at identical phase. Of course, the number of periods until the trajectory reaches the limit cycle can vary, dependent on the position of the starting point, but the phase achieved at the limit cycle will be the same for all oscillations starting at the isochron.

We observe that the isochrons converge into an area where they approach each other – or do they in fact converge into a point? We will discuss the nature of this *singularity* in several chapters, but it can be useful to describe the situation already here. In this area the isochrons lie very close to each other and it might be difficult to separate them from each other. The effect of starting oscillators in this region will therefore be difficult to predict. Noise, uncertainties and measurement errors will lead to ambiguities as to which isochron that is relevant and the experiments (simulations?) could, therefore, end up uncontrollably at different isochrons. At this (noisy?) meeting area of the isochrons all phases are represented!

The problems arising with biological oscillators that are forced into their singularity area have fascinated many investigators: do singular points/areas exist in physiology? Do cellular or multicellular oscillators stop oscillating there? What phase is achieved? We discuss some of the problems and results in this book (see Sect. 3.1 and 6.3).

With this isochron calculation the PRC can be obtained. Fig. 6.12 shows as an example, how a phase shift by two pulses is obtained, in which the switch from one isochron to another one is studied. This allows even, to determine that pulse, which puts the oscillation into the singular point. If this point is stable, the oscillation stops completely. In the case of a simple VP oscillator this is, however, not the case. Phase shifts of other pulses (triangle or trapeze) can not be studied in this way. In those cases the Xcos circuit according to Fig. 6.2 can be used, which allow arbitrary perturbation signals at the input of an oscillator.

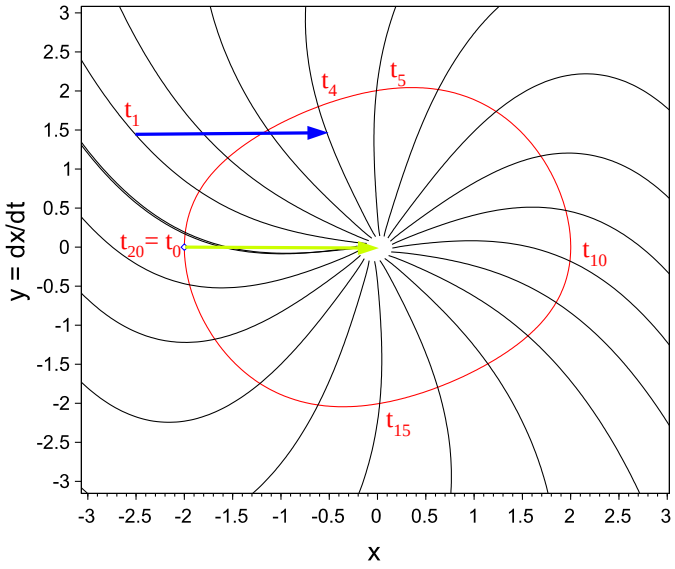

Figure 6.12: *xy-diagram with isochrons (cf. Fig. 6.11) and showing perturbations by pulses given to the VP oscillator.*
The blue arrow shows a pulse at time t_1 with the height of 2.0, which shifts the x value from -2.5 to about -0.5. In this way it is switched from the isochron for t_1 to the isochron for t_4. That means, the oscillation has after transients "jumped" on the limit cycle from time t_1 to time t_4: The phase has leapt. The bright green arrow points to the pulse at time t_0 with a height of 2.0, which shifts the x value from -2.0 to the zero point area. In this way the point of singularity of the VP oscillator is reached and, the oscillation disappears. It is, however, according to the investigations mentioned in Section 5.5, unstable, and after a while the oscillation begins again. The phase shifts obtained are, however, undefined and can change strongly even at small variations.

6.2 Synchronisation, entrainment, range of entrainment

How external influences synchronise circadian rhythms was already treated in Chap. 3. Here we come back to it again and concentrate on modelling the effects of repetitive signals/perturbations.

We will start by discussing models for how repetetive light signals given to retina can affect the human SCN oscillator. Then we will shortly treat the well known 'jet lag' where the external LD signals to the human clocks change their phase during, for example, a transmeridian flight

According to a model of Forger, Jewett, Kronauer (1999) photoreceptive molecules in the retina are transferred from a standby state into an active condition. This results in a signal burst which finally leads to a phase shift of the neuronal oscillators in the SCN, if the light is entraining the pacemaker. It is not the amount of active and inactive photopigments, but the conversion which leads to the signal. This is shown in Fig. 6.13. If $\alpha(I)$ is the conversion rate from the free to the used molecules, whereby (I) is the light intensity, and n the probability for a pigment molecule to be in the active state, the recycling rate is given by β. The dynamics can be described by the Eq.

$$\frac{dn}{dt} = \alpha(I) \cdot (1 - n) - \beta n \tag{6.1}$$

which resembles the gating variables in the Hodgkin-Huxley-modell for the neurons of the squid. After activation of the photoreceptor molecule a signal B is send to the circadian clock, which is proportional to the rate, with which the photoreceptor molecules are activated, i.e. $B \sim \alpha(I)(1 - n)$.

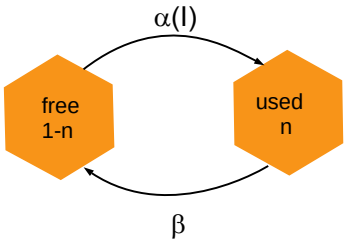

Figure 6.13: *Behaviour of a photoreceptor, $\alpha(I)$ is the conversion rate from the free to the used molecule, (I) is the light intensity, and n the probability for a pigment molecule to be excited by a photon. β is the recycling rate*

However, the light sensitivity of the circadian clock changes during the course of the day. This could also be due to the photoreceptors, if the signal transferring molecule for B is a part of the circadian clock and is able to oscillate, i.e. $B \sim \alpha(I)(1 - n) \cdot f(\vec{x})$, where the sensitivity f depends on the n state variables of the pacemaker in vector $\vec{x} = (x_1, x_2, \ldots, x_n)$.

The environmental influence on the circadian system was already studied by Wever (1963). To study, how light influences this system, more detailed models could be developed (Forger, Jewett, Kronauer (1999) and Kronauer, Czeisler et al. (1982)). A modified VP oscillator (see Sect. 7.6) was used, the free run period of which was $\tau_x = 24.2$ h, and the influence of light was taken into account by adding the signal B (Forger, Jewett, Kronauer (1999)):

$$\frac{dx}{dt} = \left(\frac{\pi}{12}\right)\left[x_c + \mu\left(x - \frac{4x^3}{3}\right) + B\right] \tag{6.2}$$

$$\frac{dx_c}{dt} = \left(\frac{\pi}{12}\right)\left[-\left(\frac{24}{\tau_x}\right)^2 x + Bx_c\right] \tag{6.3}$$

Later the authors changed the model in such a way, that the Aschoff rule was incorporated, according to which the free run period in day active animals is shortened, if the intensity of the constant light is increased, and in night active animals lengthened, see Aschoff (1981). For the modified model they obtained finally:

$$\frac{dx}{dt} = \frac{\pi}{12}(x_c + B) \tag{6.4}$$

$$\frac{dx_c}{dt} = \frac{\pi}{12}\left[\mu\left(x_c - \frac{4x_c^3}{3}\right) - x\left\{\left(\frac{24}{0.99669\tau_x}\right)^2 + kB\right\}\right] \tag{6.5}$$

$$\frac{dn}{dt} = 60\left[\alpha(I)(1-n) - \beta n\right] \tag{6.6}$$

$$B = G(1-n)\alpha(I)(1-0.4x)(1-0.4x_c) \tag{6.7}$$

$$\alpha(I) = \alpha_0\left(\frac{I}{I_0}\right)^p \tag{6.8}$$

with $\mu = 0.23$, $\tau_x = 24.2$ (circadian period in h), $\beta = 0.0075$, $G = 19.875$, $\alpha_0 = 0.16$, $p = 0.6$, $k = 0.55$, $I_0 = 9500$ (I_0 and I are light intensities in lx). The corresponding Scilab/Xcos-model is shown in Fig. 6.15, in which some parameters have been combined.

As a first application Fig. 6.16 shows the results of a simulation, in which a rectangular LD 16:10 h (that is a period of 26 h) is applied after 52 h, whereby the maximal value was 86 000 lx and the endogenous period was 24.2 h. It turned out, that it was synchronised (locked in) by the external 26 h LD after a transient time, and a constant phase relationship was obtained. Thus not only the period, but also the phases were synchronised.

As a second example the phase shift of 6 h during a west bound flight from e.g. Berlin to New York shall be studied with the aim, to find out, how long it takes, until the organism has adapted to the new situation. The circadian system was examined in a control without time shift under an 16:8 h LD with 10 000 lx during the LP and compared with the situation of the same day-length, but a 6 h time shift 90 h after onset of the simulation, see Fig. 6.17. The result is shown in Fig. 6.19. The human organism adapts and entrains with the 24 h rhythm of the entraining LD (red curve). Interestingly the maximum of the human rhythm is shifted towards the middle of the rectangular pulses, whereas in the control without the shift it is more left to the maximum. It will probably take more days until it is in the same phase relation as the control: Here a stable phase relation was obtained after 60 h (2.5 d). This is probably still too much for some activities (e.g. the flight personal). Studies are available which help to shorten this time (for instance, to prepare for the flight already before travelling by adjusting the time to go to bed). There are even apps for smartphones available, which give recommendations.

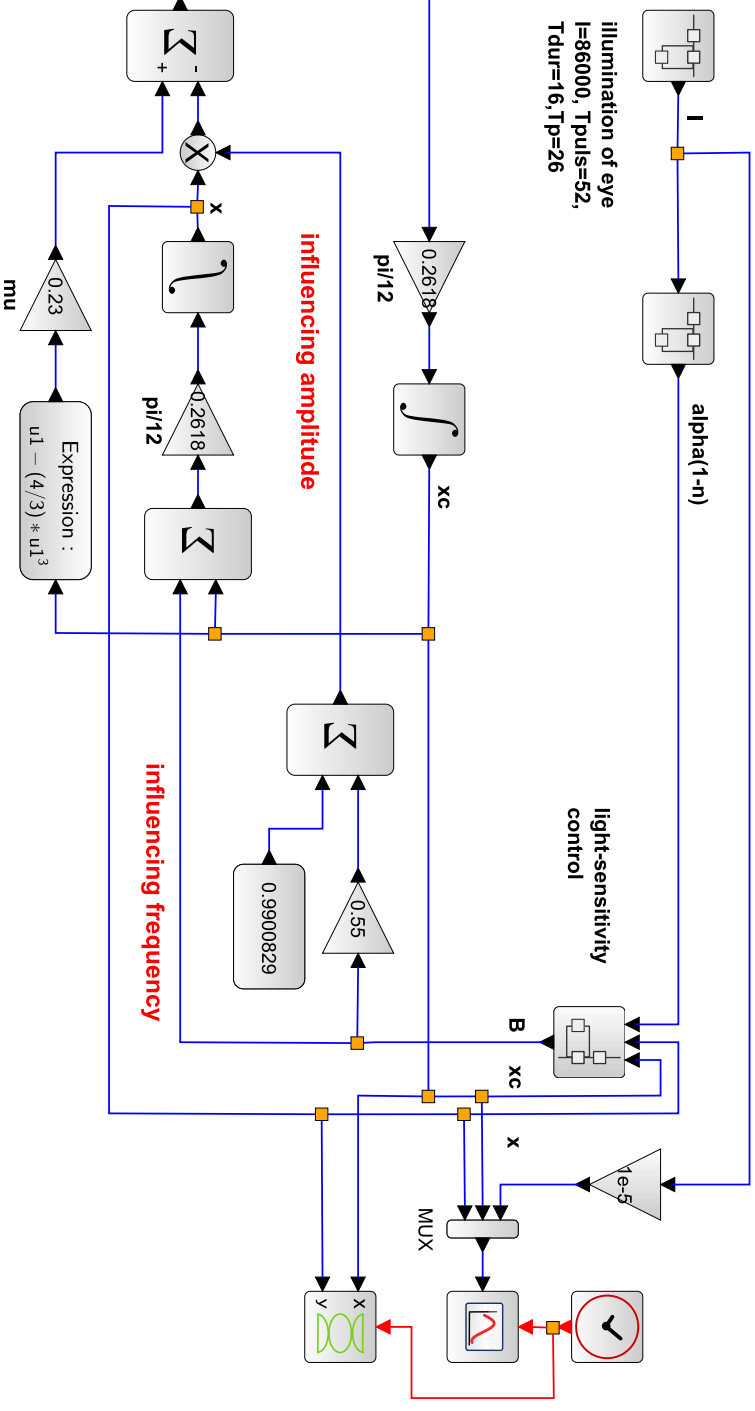

Figure 6.14: *Model of circadian rhythm after Forger, Jewett, Kronauer (1999) according to Eq. 6.4 to 6.8 Parameters: $\mu = 0.23$, $\tau_x = 24.2$ (circadian period in h), $\beta = 0.0075$, $G = 19.875$, $\alpha_0 = 0.16$, $p = 0.6$, $k = 0.55$, $I_0 = 9500$ (I_0 and I are light intensities in lx). The expression $\left(\frac{24}{0.99669\tau_x}\right)^2$ in Eq. 6.5 was calculated for $\tau_x = 24.2$ h and combined to one constant. The light perception in the retina and the control of the light sensitivity are shown in Fig. 6.15*

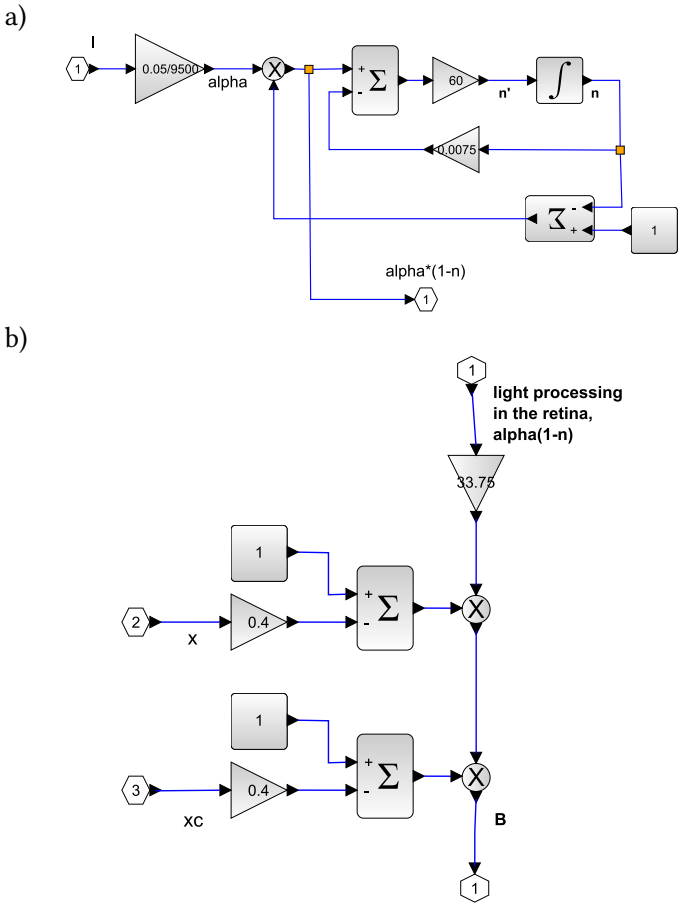

Figure 6.15: *Superblocks for Fig. 6.14: a) shows the light perception in the retina, b) the control of the light sensitivity*

Circadian misalignment is caused by a daily sleep-wake behaviour which is not aligned with the circadian system. It can adversely affect the health status and mood. We are mentioning a few publications in which the authors used models to simulate circadian misalignment.

A feedback controller for the time-optimal (re)entrainment in the Jewett-Forger-Kronauer circadian rhythm model i.e., computing the lighting schedule to drive a misaligned circadian phase to a reference circadian phase as quickly as possible, was developed by Julius, Yin, Wen 2019. It refers to work of Serkh, Forger 2014 on misalignment of human activity, as caused by rapid trans-meridian travel, but also from work and social schedules. Their schedules outperform other recently proposed schedules and are more robust to noise in light and to inter-individual variations in the endogenous period.

Liberman et al. (2018) built a simple mathematical model to simulate circadian polymorphism (PER3 variants) relations to mood disorders and their effects on circadian misalignment. This is important, since anxiety and other mood disorders (major depressive disorder, seasonal affective disorder) affect nearly one-fifth of the world population and disproportionately young

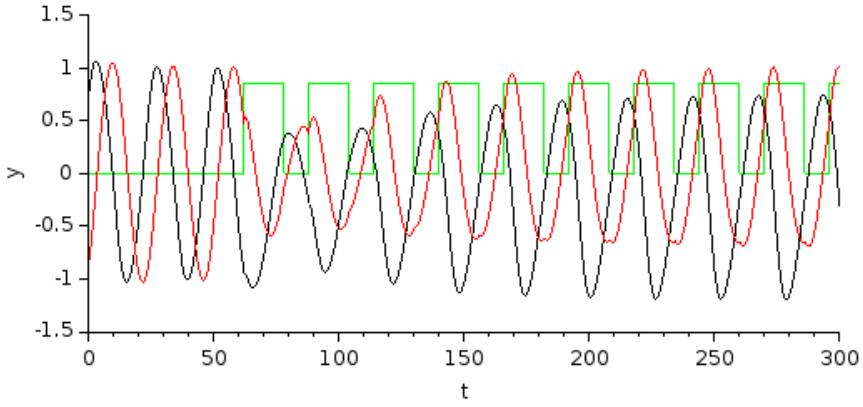

Figure 6.16: *Influence of an LD cycle on the circadian system of humans based on the model of Forger, Jewett, Kronauer (1999) using the Scilab/Xcos model in Fig. 6.14.*
x-axis: t in h; green curve: 16:10 h LD; red curve: first component of the complex reaction to the LD (green); black curve: associated second component

adults. The structure of their model is user-friendly and can be applied for further studies of the relationships among clock varieties, circadian misalignment, and mood disorders.

An arousal dynamics model (Postnova, Lockley, Robinson (2018)) predicts objective performance and subjective sleepiness propensity. It consists of a physiologically based flip-flop switch between the wake- and sleep- active neuronal populations and a dynamic circadian oscillator. The model predicts more accurately sleep under normal conditions and during circadian misalignment, caused by shift work and jet-lag. Further examples are in the Sections 4.2, 4.3, and 4.4.

6.2.1 Entrainment of oscillators by external inputs

Entrainment is usually possible only in certain period range around the natural frequency of the oscillator. As an example: humans have a clock with an 'intrinsic' period close to 24 h. In experiments under weak light (corresponding to candle light) alternating with darkness, given at a period of 23.5, 24 or 24.6 hours, the subjects synchronized to the 24 h rhythm but not the 23.5 h or the 24.6 h rhythms. (Wright et al. 2001: https://pubmed.ncbi.nlm.nih.gov/11717461/) . The last two periods were thus outside the so- called range of entrainment for the oscillator in this experiment (with the chosen light, temperature parameters etc.). Of course, the range of entrainment can change if the pulse conditions are changed – stronger light could, for example, synchronize in a wider period range.

If man visits the planet Mars, they have to adapt to the 24.65 h day prevailing there. Under the low light conditions of about 450 lux, available for the astronauts living there, this would be outside the range of entrainment. Sleep would be impaired and health harmed. Scheer et al. (2007) tested this situation experimentally using a 24.6 h Mars day model and a 23.5 day, which

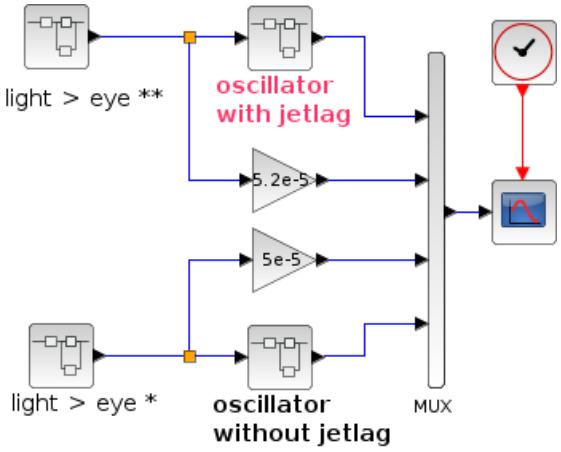

Figure 6.17: *Experimental setup for simulating the jet-lag duration.*
*Based on the model of Forger, Jewett, Kronauer (1999) using the Scilab/Xcos model superblocks for the oscillators (as presented in Fig. 6.14). The source of the light is shown in Fig. 6.18. Setup for light > eye** (top row): light intensity I 10 000 lux; period length of pulses Tp 24 h;. Setup for light > eye* (bottom row): same as above, but without jet-lag JL*

is often provided for short space flights of astronauts. The circadian period was judged by determining melatonin and cortisol in the blood plasma and by measuring the body temperature. After the Mars days has ended, the internal rhythm was lengthened (which is called *after-effect*). This shows, that the period of the circadian system can be plastic. This finding is also of interest for treating certain sleep disturbances such as *advanced sleep phase* or *non-24 h sleep*.

6.2.2 Range of entrainment

Circadian rhythms can be entrained to a certain degree also by external LD cycles, which are e.g. somewhat shorter or longer than 24 h. The period span (or frequency span) in which entrainment is possible is called the range of entrainment.

An et al. 2021 developed a two-step model with three coupled oscillators, the cyclic environment (providing the Zeitgeber), the SCN (representing the master clock), and the peripheral clocks. The entrainment consists of two steps (see Fig. 6.20). In the first step, the SCN clocks are entrained to the Zeitgeber during a one-hour window from 30 min before until 30 min. after dusk. In the second step, the peripheral clocks are aligned to the SCN clocks with a time offset. The model can be applied not only to humans, but also to other species such as *Neurospora* and *Drosophila*.

The model shows that the free-run period is circadian and is entrained by environmental signals. It describes periodic orbits and gives analytical solutions of the range of entrainment. The model uses also the rate of entrainment, which is the decay/recovery time after a phase shift such as jet-lag. Their values depend also on the initial conditions of the three oscillators and present the three-dimensional parameter spaces, illustrating the various behaviours of the

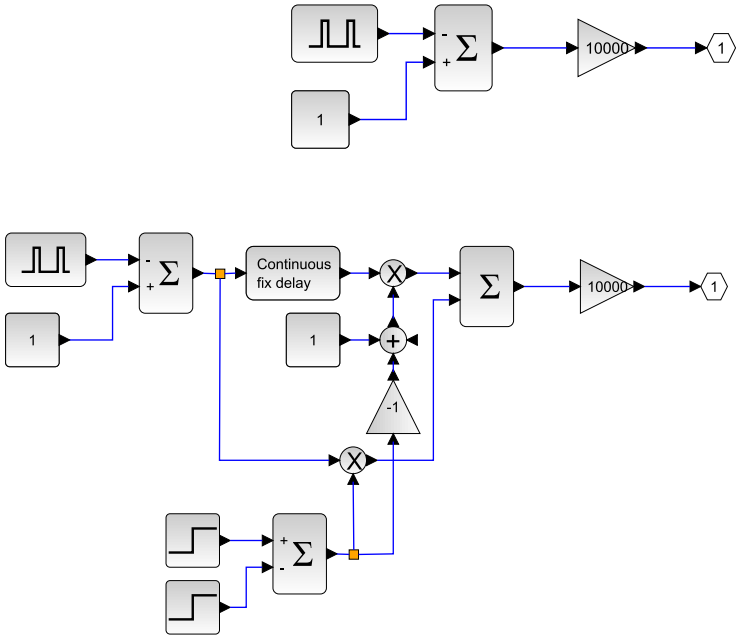

Figure 6.18: *Superblocks modeling the light sources in Fig. 6.17: a) shows the light source without jet-lag, b) with jet-lag*

phase of entrainment. Also these model findings can be used to diagnose and treat patients with sleep disorders caused by shift work or jet-lag.

Gu, Yang, Ruan 2017 used a mathematical model from Poincare, to describe the entrainment range of the SCN by the difference in the amplitudes of the circadian oscillations in the neurons of the ventrolateral and the dorsomedial subgroup. The ventrolateral subgroup receives the light information from the retina and relays it to the dorsomedial subgroup. They found, that the maximal entrainment range is obtained when the difference is equal to a critical point. If the difference is smaller, the entrainment range of the SCN increases, while if the difference is larger, the entrainment range decreases. The findings may explain the diversity of the entrainment ranges among species. The authors used clinical data of 12 subjects with various period length. Under weak light only one subject entrained after a long time and 3 out of 4 did not entrain. The model is sensitive to diagnose how people react to different cycling conditions and can be used to treat patients with sleep disorders caused by shift work or jet-lag.

Gu, Yang, Wang 2017 in a further publication showed, that the entrainment range in mammals depends on the coupling strength of the neurons in the SCN. It decreases with increasing coupling strength, provided that all the neuronal oscillators are identical. However, the SCN neurons differ in their intrinsic periods following a normal distribution in a range from 22 to 28 h which affects the ability of the SCN network to entrain. The dispersion of coupling strengths determines the diversity in the free-run periods, while the dispersion of intrinsic periods determines the diversity in range of entrainment (Gu, Le et al. 2013).

Entraining Zeitgeber are not only the LD cycles, but also temperature cycles consisting of

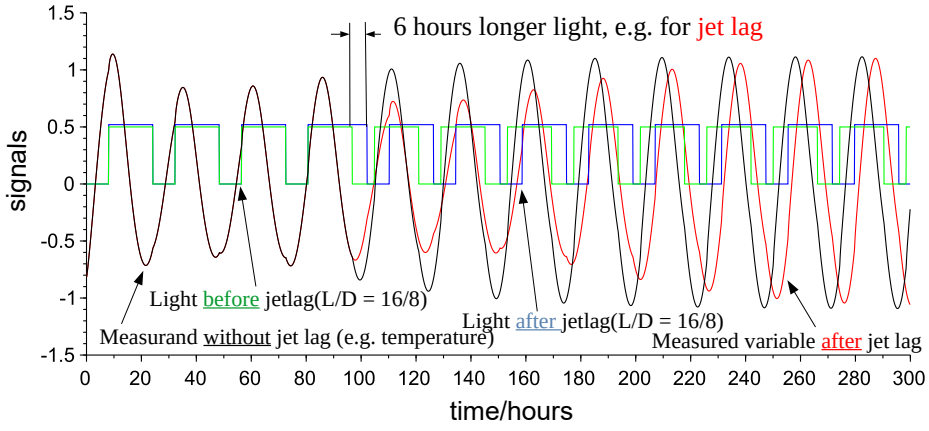

Figure 6.19: *A phase shift (jet-lag) by 6 h of a 16:8 h LD cycle was simulated with the model after Forger, Jewett, Kronauer (1999) and a Scilab/Xcos-model after Fig. 6.14 (red curve) and compared with the unshifted control (black curve).*

higher and lower sections or fasting-feeding periods. The range of entrainment for the latter was studied by Hamaguchi et al. (2015) in peripheral molecular clocks of mice for cycles shorter than 24 h. The PER2::LUCIFERASE rhythm was measured in vivo at different feeding cycles with periods ranging from 24 to 15 h. These peripheral clocks entrained to the feeding cycle from 24 to 22 h, but not to those from 21 to 15 h.

That peripheral clocks have a wider range of entrainment as compared to the SCN oscillators was reported by Abraham et al. 2010. In a theoretical and experimental study, they tried to find out which oscillator qualities determine the entrainment range. They uncovered phase and amplitude in the SCN and the lung and observed, that the ratio between Zeitgeber strength and oscillator amplitude (1) and the rigidity of the oscillator system (2) determine the entrainment properties. Coupling among oscillators affects both qualities and results in increased amplitude and rigidity. This explains, why lung clocks entrain to a larger entrainment range, whereas SCN clocks do not. Pharmacological inhibition of coupling in the SCN increases the range of entrainment. Apparently coupling-induced rigidity in the SCN filters environmental noise and creates a robuster circadian system.

In vertebrates multiple, functionally overlapping homologous of the core clock genes are present. The range of entrainment is in vertebrate clocks three times as narrow as that of other organisms. Erzberger et al. 2013 tried to find out, whether this is due to the genetic redundancies of the clock genes. They recorded the locomotor activity of genetically modified mice lacking one set of clock homologous and found, that the entrainment range was wider than in the wild types. Using the forced oscillator model they could show that mutant mice have weaker circadian clocks than wild types. This suggests that genetic redundancy strengthens the circadian clock leading to a narrow entrainment range in vertebrates.

In birds the circadian system is more complex than in mammals. Instead of one master clock in the SCN, the pacemaker of birds involves the interplay between the pineal and oscillators in

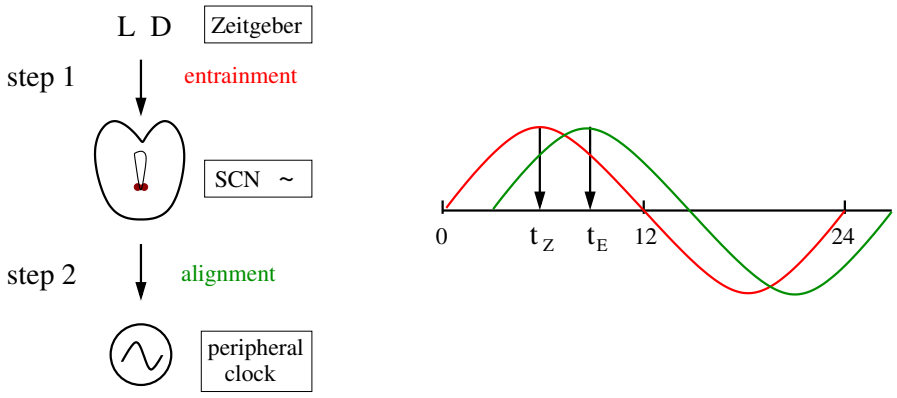

Figure 6.20: *Two step model showing phase relations.*
Left: Step 1: SCN clock entrained by Zeitgeber (LD) during entrainment *window. Step 2: Peripheral clock (~) aligned to the SCN clocks (*alignment*). After An et al. 2021.*
Right: Evolution of phase angles illustrated by sine curves. Red line: Zeitgeber clock. Green line: peripheral clock. Phase angle Ψ *is here* $\pi/2$ *and is the phase difference* $\Psi = t_z - t_E$*. Positive* Ψ*: advanced phase. Negative* Ψ*: delayed phase.Phase angle* Ψ *is negative in the figure and of the order of 3 h, i.e. a delay of about 3 h*

the hypothalamus. Woller, Gonze 2013 proposed a mathematical model for the circadian system of birds. It uses Goodwin-like equations (see Sect. 7.3) and is based on the resonance between the pineal and hypothalamic oscillators. Consistent with experimental results, self-sustained oscillations are produced due to mutual inhibitory coupling of the two oscillators, although the individual oscillators exhibit damped oscillations. The model simulated successfully the effect of melatonin, which couples the pineal and the hypothalamus oscillators. It also simulates the effects of light-dark cycles, of the entrainment range, of synchronisation after jet lag, and of entrainment under different photo-periods.

Whereas similar oscillators generally synchronise with each other and take up a common frequency with or without a fixed phase difference (see Chap. 8), entrainment by the originator influences an oscillation or several in a group in a directed way. This is for instance the case in the rhythm of the heart, where the sinus node sets its own frequency and with it also the one of the AV node and the His bundle, although the frequency of the AV node and the His bundle would be lower without the influence of the sinus node (see subsect. 7.8.3). To study these influences it is often not sufficient to determine the Eigenvalues of the linearised mathematical equations, but to use methods which take into account also non-linearities. For such studies the following prerequisites would be helpful (e.g. in the case of neurons):

1. The oscillation of a single oscillator can be controlled by an external signal (for instance a current, a potential, ion concentrations) in a certain range (example: a VCO ("voltage controlled oscillator") in an electronic circuitry (see e.g. Tietze, Schenk, Gamm (2019) and Best (2003))

2. An individual oscillator can be adjusted (or readjusted) to the frequency or phase of an

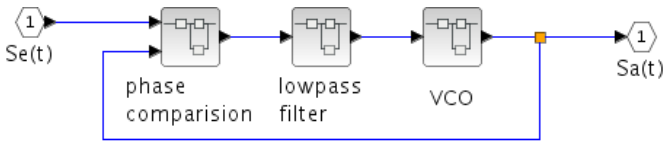

Figure 6.21: *Phase servo loop (PLL resp. VCON) with phase comparison, low pass filter, and variable oscillator step (VCO) after Hoppensteadt (1997), Pikovsky, Rosenblum, Kurths (2001) and Best (2003)*

external signal (frequency or phase control), as for instance by an "analogue phase locked loop" (APLL, see Glass, Mackey (1979), Best (2003) and Tietze, Schenk, Gamm (2019)) or in the "voltage controlled oscillator neuron model" (VCON, see Hoppensteadt (1997)).

Fig. 6.21 shows the principle of such a phase comparison (which is a basic procedure for example in many electronic devices using phase comparisons between two signals). One central component is the Voltage Controlled Oscillator, the frequency of which can be controlled by an applied voltage. The phase φ_a of the oscillator signal $s_a(t)$ is compared with the phase φ_e of an external signal $s_e(t)$ and the internal oscillator (VCO) is, depending on the difference of these two phases (perhaps after filtering), controlled in such a way, that the phase deviation $\Delta\varphi = \varphi_a - \varphi_e$ is minimised. The phase comparison can be realised for instance by a simple multiplication of the two input signals by the phase servo loop $s_e(t)$ and $s_a(t)$. If both of these signals are sinusoidal, e.g. with

$$s_a(t) = \hat{S}_a \sin(\omega_a t + \varphi_a) \text{ and } s_e(t) = \hat{S}_e \cos(\omega_e t + \varphi_e) \tag{6.9}$$

one obtains according to the addition theorem for the product:

$$\begin{aligned} s_a(t) \cdot s_e(t) &= 0.5 \cdot \hat{S}_a \hat{S}_e \{\sin([\omega_a - \omega_e]\, t + \varphi_a - \varphi_e) \\ &+ \sin([\omega_a + \omega_e]\, t + \varphi_a + \varphi_e)\} \end{aligned} \tag{6.10}$$

As a result two sinus oscillations arise, whereby one of it contains the difference between the angular frequency $\omega_a - \omega_e$ and the difference phase $\varphi_a - \varphi_e$, and the other the sum of the angular frequency $\omega_a + \omega_e$ and the phase $\varphi_a + \varphi_e$. This latter sine oscillation is suppressed by the low pass filter, which causes, that at the input of the controllable oscillator only the cosine oscillation with the difference frequency and phase is obtained. If the external and the internal oscillation have nearly the same frequency, i.e. $\omega_a - \omega_e \approx 0$ (called lock-in), one obtains at the input of the controllable oscillator (VCO) a signal $s_{VCO}(t)$ with

$$s_{VCO}(t) \sim 0.5 \cdot \hat{S}_a \hat{S}_e \sin(\varphi_a - \varphi_e) \quad \text{for } \omega_a \approx \omega_e \tag{6.11}$$

By a simple multiplication of the input signal with the internal signal of the VCOs one can thus produce (with nearly the same frequencies) after low pass filtering a control signal for the VCO, which increases around the zero point of the phase difference (where the difference increases), and which decreases, if the difference decreases, because for small arguments of the sine holds:

$$\sin(\varphi_a - \varphi_e) \approx \varphi_a - \varphi_e = \Delta\varphi \quad \text{for } \Delta\varphi \ll 1 \tag{6.12}$$

This signal can be used to control the VCO in such a way, that the phase difference $\Delta\varphi$ disappears. At the same time the frequency of the VCO is controlled and it locks in the frequency of the external signal. However, it can not only lock in to the input frequency, but also to a multiple or a whole number part, i.e. the input frequency could be half of the frequency of the VCO. The phase difference could thereby also be reduced to zero. Each second maximum of the external frequency could, for instance, coincide with the VCO, and in between could occur a phase difference as in the case of a swing, which is kicked only at every second oscillation.

However, in many models multiplications of an external signal with an internal signal are not used. How is then entrainment obtained ? The answer lies in the non-linearity, which these models use (e.g. the VP oscillator). Looking for instance at the VP oscillator in Fig. 6.5, an external signal is not multiplied with an internal signal, but *added*. After integrating the sum, it is *squared*. Besides constant parts one obtains also a product of the two signals similar to the Eq. 6.10. If, for instance, $s_a(t)$ and $s_e(t)$ in eq. 6.9 are added and squared, one obtains:

$$\begin{aligned}(s_a(t)+s_e(t))^2 &= s_a(t)^2 + 2s_a(t)s_e(t) + s_e(t)^2 \\ &= \hat{S}_a\hat{S}_e\{\sin([\omega_a-\omega_e]t+\varphi_a-\varphi_e) \\ &- \sin([\omega_a+\omega_e]t+\varphi_a+\varphi_e)\} \\ &+ 0.5\cdot\hat{S^2}_a\{1-\cos 2\cdot(\omega_a t+\varphi_a)\} \\ &+ 0.5\cdot\hat{S^2}_e\{1+\cos 2\cdot(\omega_e t+\varphi_e)\}\end{aligned} \tag{6.13}$$

Except for the constant offset parts ($0.5\cdot\hat{S^2}_a$,$0.5\cdot\hat{S^2}_e$) the cosine oscillation with twice the angular frequency $2\omega_a$ and $2\omega_e$, and with the scaling factor 0.5, one obtains the same summand as in the case of multiplication in Eq. 6.10. At the VCO entrance changes, however, the working point at the lock in. Now the input signal $s_{VCO}(t)$ does not fluctuate around the zero point any more, but around the constant fraction $0.5\cdot\left(\hat{S^2}_a+\hat{S^2}_e\right)$, i.e.

$$s_{VCO}(t) \sim \hat{S}_a\hat{S}_e\sin(\varphi_a-\varphi_e) + 0.5\cdot\left(\hat{S^2}_a+\hat{S^2}_e\right)$$

This has to be taken into account in the VCO, e.g. by using a counter signal (see offset compensation at an input voltage in Tietze, Schenk, Gamm (2019))

The purely mathematical solution of non-linear differential equation systems for non-linear models is quite difficult, even ambiguous and in many cases generally not solvable. We are left then with a numerical computation of physical parameters which are of interest, such as ion concentrations, membrane potentials or -currents. In this connection it is useful to study not only the phase shifting effect of *one* external pulse, but also the effect of a *periodic* signal, which has a different period length as compared to the Eigenperiod of the model used. It can -similar to a PLL- attune to the "foreign" period length via its non-linear behaviour (e.g. a characteristic curve). A helpful parameter in this connection is the ratio of period length T_x of the internal oscillation to the period length T_z of the external oscillation, which corresponds in the case of

infinite periods n to the *rotation number* ρ of the external oscillation, i.e.

$$\rho := \lim_{n\to\infty} \frac{\sum_{i=1}^{n} \Delta\varphi_i}{n \cdot 2\pi} = \frac{T_x}{T_z}, \quad \begin{array}{rcl} \Delta\varphi_i & : & \text{phase changes i-th period} \\ n & : & \text{number of external periods} \end{array} \tag{6.14}$$

If it stays constant, although the period length of the external oscillation changes, it means, that the oscillator has adjusted its period to the one of the external oscillation, i.e. *it is locked in* (as in a PLL). If, however, it changes, the external oscillator does not change its frequency and both oscillations can appear simultaneously at the oscillator exit (e.g. at the VP oscillator, see Pfeifer (1966) and Van der Pol (1927)).

To study this behaviour, Fig. 6.22 shows an example of a block scheme for numerical calculations with the aid of Scilab/Xcos. In principle, arbitrary oscillators can be examined in this

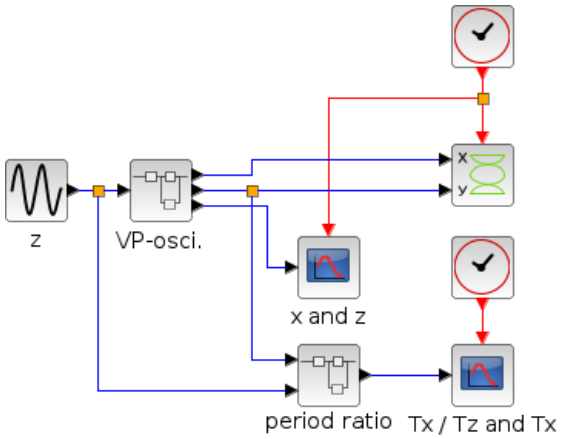

Figure 6.22: *Block diagram for general calculation of the ratio between the period Tz of an external stimulus and the period Tx of the oscillator. The superblock "VP Osci" contains the oscillator of interest (here VP, but e.g. Fitzhugh- or Integrate-And-Fire-Oszillator can be used). The corresponding ratio of the periods is calculated in the super block "period ratio", which is depicted in detail in Fig. 6.23)*

way, and the block scheme allows not only the rotation number ρ, but also the period length of the internal oscillator T_x and the signals x and z are displayed graphically. The corresponding calculation with Scilab/Xcos shows Fig. 6.23. The superblock "VP-Oszi" contains the respective oscillator to be studied (e.g. VP-, Fitzhugh- or Integrate-And-Fire-Oscillator). The present calculation is done in the superblock "period ratio". First the constant components are suppressed again by high passes, so that the oscillation to be studied oscillates around the zero point and zero crossing can occur. This is necessary, to allow an Xcos-block to recognise them. Afterwards the ratio of the periods of the two signals x and z are determined by dividing the number of zero crossings of the internal oscillator and of the external oscillation, in order to obtain the rotation number. For this purpose the number of zero crossings for both input signals are counted from minus to plus. To obtain the corresponding phase change, one should multiply with the phase change for a full period, i.e. 360°. However, since the phase changes of the external and internal

signals are divided by each other, the multiplication with 360° shorten, and we are left after the division with the number of periods of the external signal to the internal signal. The period length T_x of the internal signal is determined by starting an integrator during the zero crossing from minus to plus, and setting it back at the next zero crossing and starting it anew. However, before it the last value is sampled and stored, which corresponds to the period length, if the integration constant is One.

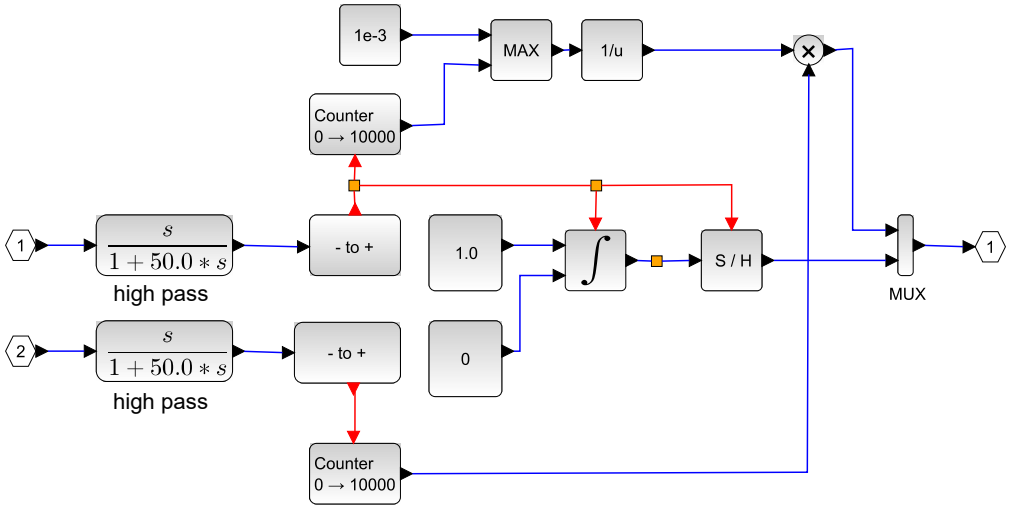

Figure 6.23: *Superblock "period ratio." in Scilab/Xcos to determine the ratio T_x/T_z between the period length T_x of the internal oscillator and the period length T_z of the external signal z according to Fig. 6.22.The two inputs (cf. Fig 6.22) are denoted 1 and 2, the output 1, all in hexagonal symbols.*

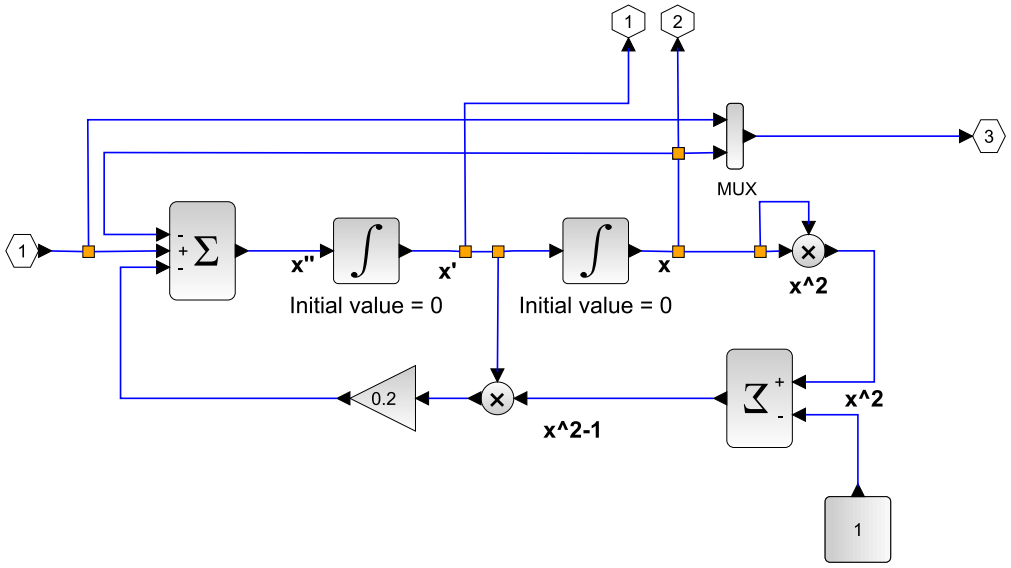

Figure 6.24: *Superblock "VP-osci" in Fig. 6.22 is the VP oscillator.Hexagonal numbers means input and output in Scilab/Xcos of this Superblock.*

An example for the simulation of a VP-oscillator with $\varepsilon = 0.2$ is shown in Fig. 6.25 and 6.26. Here a sine signal was used, which is supposed to "catch" the oscillation of the VP-oscillator. However, the external signal has a much higher frequency than as could be produced by the VP oscillator without external influence. Both oscillations, that of the VP oscillator without external influence as well as that of the external signal could principally occur at the exit of the VP-Oszillators. However, due to non-linear influences such as the non-linear characteristic curve of the VP-oscillator (see Fig. 7.30) mixed products, which can control the VP-oscillator in a certain "capture range" like a PLL (see Fig. 6.21) in such a way, that it is "locked in" to the signal of the external oscillation.

Van der Pol studied already in 1927 the entrainment by an external oscillation and obtained by assuming, that the amplitudes of the oscillations did not change much, an approximation for the "capture area" of his oscillators (Van der Pol 1927). This is not only possible close to the Eigenfrequency of an oscillator, but also at multiples or whole parts of it, which was universally found in 1961 by the mathematician V. I. Arnold (see Arnold (1961)). For its illustration an example is shown in Fig. 6.22, where a VP-oscillator with $\varepsilon = 0.2$ is influenced by an external sine wave oscillation, which has, however, a much higher frequency as the VP-oscillator. The oscillation at the exit of the VP-oscillator is therefore usually very distorted, since it contains now also frequency parts of the external signal. If, however, the external oscillation has twice the frequency, the output signal becomes sinusoidal again (see Fig. 6.25). One should note, however, that the VP-oscillator does not posses twice the frequency, but that the external oscillation has a fixed phase relation with respect to the VP-oscillator at every second period, thus leading to a phase synchronisation. In determining the period length it turns out, that the period length of the output signal x (after a certain transient time) is exactly twice the value as that of the external sine oscillation z, i.e. $T_x/T_z = 2$, see Fig. 6.26.

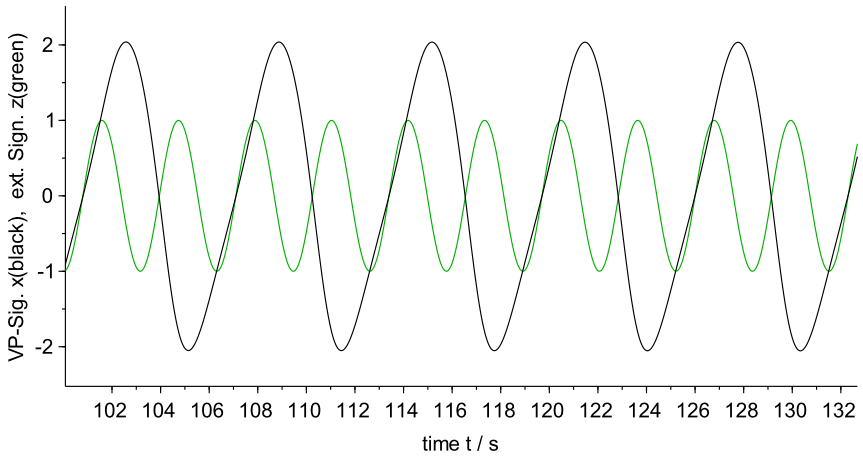

Figure 6.25: *Simulation of the output signal x (black) and an external input signal z (green) and entrainment with twice the frequency of the VP oscillator ($\varepsilon = 0.2$) using the Xcos-circuit in Fig. 6.22 and 6.24.*

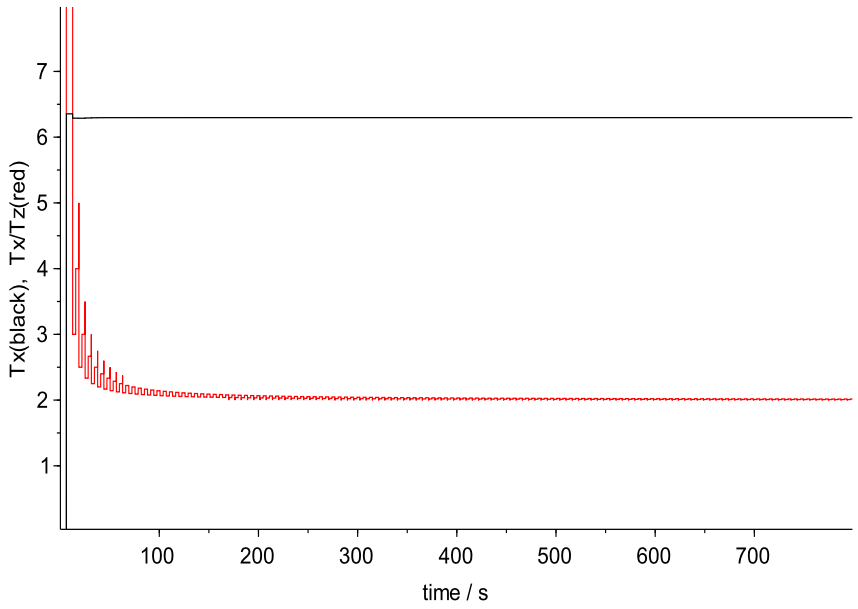

Figure 6.26: *Plot of the simulation with period length Tx of the VP-oscillator (black curve, see Fig. 6.24) with $\varepsilon = 0.2$. Tz is the period length of the perturbation, external, signal. The plotted ratio of the periods Tx/Tz (red curve) is the Xcos circuit output after Fig. 6.22. Tz is the period length of the external signal. Since this ratio is 2 (as shown after the transients), the period length Tz of the external signal is half of that of the VP oscillator*

It is entirely different, if the frequency of the external signal is smaller then the Eigenfrequency of the VP-oscillator. In this case the frequency of the VP-oscillator can change strongly. In Fig. 6.27 and 6.28 an example is shown, where the frequency of the external signal is only half of the Eigenfrequency of the VP-oscillator. Then the frequencies of the VP-oscillator and of the external signal are the same and the rotation number ρ or the ratio $T_x/T_z = 1$, see Fig. 6.28.

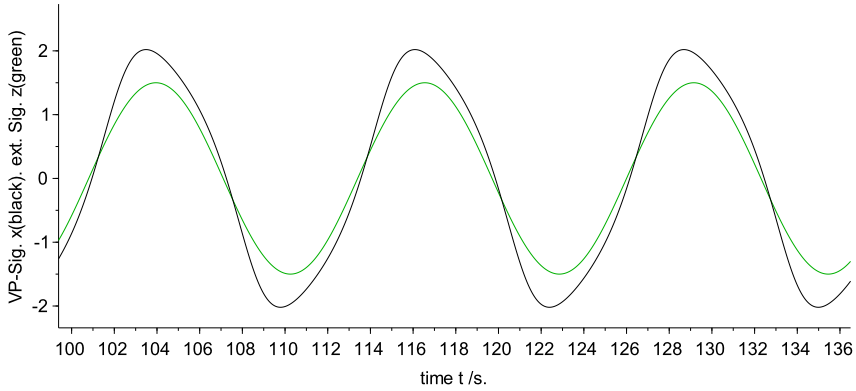

Figure 6.27: *Plot of the simulation of the output signal x (black) with an external sine signal z and entrainment with the same frequency at the VP oscillator ($\varepsilon = 0.2$) using the Xcos circuit in Fig. 6.22 and 6.24.*

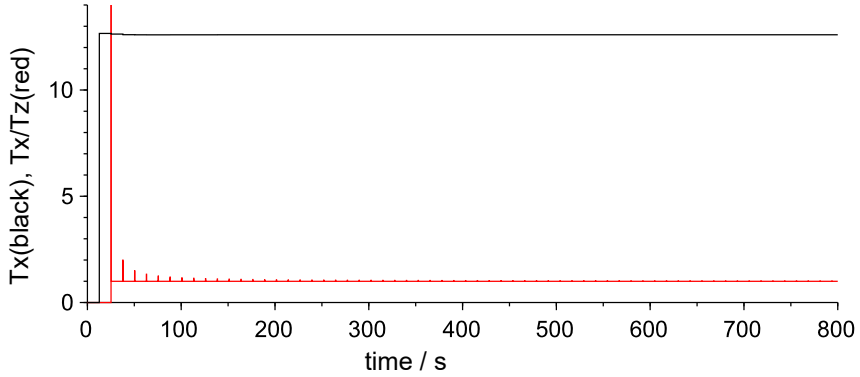

Figure 6.28: *Plot of the simulation of the period length Tx of the VP oscillator in Fig. 6.24 ($\varepsilon = 0.2$) and the ratio of the periods Tx/Tz in the Xcos circuit of Fig. 6.22, whereby Tz is the period length of the external signal. Since this ratio is 1, the period length Tz of the external signal is as large as the one of the VP oscillator*

To find out in which cases the oscillator can be entrained by an external oscillation, various parameter such as the amplitude of the oscillation, its shape (e.g. sinusoidal or triangular) or its period length can be varied. To avoid the cumbersome entering of these parameters in the

corresponding simulations of the Xcos circuit, again a script can be provided, which takes care of these tasks. In the Scilab listing 6.4 first the rotation number ρ is determined by varying the period length of the external oscillation at a given amplitude of the external oscillation, after ward this amplitude as well as the period length is varied and a broken rational rotation number colour coded (these are the ranges of entrainment).

Listing 6.4: *Scilab-Script to produce a 'devils ladder' and 'Arnold's tongues' in Fig. 6.30 and 6.31 with simulations using the Xcos circuit in Fig. 6.29*

```
// Loading the library blocks and the simulation system
loadXcosLibs(); loadScicos();
//
importXcosDiagram("Dateiname.zcos") //Xcos-Modell load
//
typeof(scs_m) //diagram structure
//
// This diagram posesses  4 context variables:
//   Amp: Amplitude (standard value: 1)
//    KreisFreq: Angular frequency (Standard value: 4*%pi*0.15873)
//    eps: Parameter VP-Oszi (Standard value: 0.2)
//    Tend: End of simulation time (Standard value: 800)
//
scs_m.props.context; //imbedded definition
//
// First batch simulation with the imbedded parameter of the diagrams
printf("First␣simulation␣with␣internal␣standard␣values␣of␣the␣Xcos␣circuit\n")
    scicos_simulate(scs_m);
Tx=TxEnd.values;
RotNr=TxDivTzEnd.values;
printf("Amplitude:␣1,␣frequency:␣0.15873␣Hz,␣period␣length:␣%6.2f␣sec.,␣rotations␣Nr.:␣
    %6.2f\n", Tx, RotNr)
//
// selected changes of amplitude, frequency and Epsilon
printf("Then␣simulation␣with␣parameter␣variation␣of␣Xcos␣circuit\n")
Tz1=2
Tz2=22
eps=4
Context.eps=eps
DTz=(Tz2-Tz1)/200
f1=[Tz1:DTz:Tz2]
f2=[0.001:0.005:1.001]
fTx=zeros(size(f2,2),size(f1,2))
fRotNr=zeros(size(f2,2),size(f1,2))
for j=1:size(f2,2)
  Context.Amp=f2(j)
  for i=1:size(f1,2)
    Context.Freq=2*%pi/f1(i)
    scicos_simulate(scs_m,Context);
    Tx=TxEnd.values;
    fTx(j,i)=Tx;
    RotNr=TxDivTzEnd.values;
    fRotNr(j,i)=RotNr;
    if modulo(i-1,4) == 0 then printf("Ampl.:␣%5.2f␣,Tz:␣%5.2f␣Sek.,Tx:␣%6.2f␣Sek.,␣Rot
        -Nr.:␣%6.2f\n", f2(j), f1(i), Tx, RotNr); end
  end
end
//
// Readout of results
//
// First plot 'devils staircase' (at half of  maximal amplitude of oscillation)
```

```
scf(1);
iAmp=size(f2,2)/2
Ampgra=iAmp*max(f2)/size(f2,2)
Ampgra10=floor(Ampgra*10)/10
plot2d(f1,fRotNr(iAmp,:))
xgrid()
title("Rot.-Nrn. for Ampl. =" +string(Ampgra10)+", eps =" +string(eps),"fontsize",5);
xlabel("Period of external sinus oscillation Tz (sec.)","fontsize",4);
ylabel("Rot.-Nr. Tx/Tz","fontsize",4)
//
// Then draw "Arnold's tongues"
scf(2);
fRotNrf=fRotNr($:-1:1,:) // Matrix-rows, reverse up and down
PlotSparse(sparse(((0.49<fRotNrf)&(fRotNrf<0.51))*1),"kD")
PlotSparse(sparse(((0.98<fRotNrf)&(fRotNrf<1.1))*1),"bD")
PlotSparse(sparse(((1.98<fRotNrf)&(fRotNrf<2.1))*1),"gD")
PlotSparse(sparse(((2.98<fRotNrf)&(fRotNrf<3.1))*1),"rD")
PlotSparse(sparse(((1.48<fRotNrf)&(fRotNrf<1.53))*1),"mD")
title("Range of entrainment, eps ="+string(eps),"fontsize",5)
xlabel("Period of external Sinus oscillation Tz (sec.)","fontsize",4)
ylabel("Ampl. of ext. Sinus osc.","fontsize",4)
hl=legend(['Tx/Tz=0.5';'Tx/Tz=1';'Tx/Tz =2';'Tx/Tz =3';'Tx/Tz =1.5'],-1);
```

In order to avoid a new oscilloscope image every time a parameter value is changed (as in the Xcos circuit in Fig. 6.22) the Xcos circuit in Fig. 6.22 was simplified by excluding the oscilloscope, see now Fig. 6.29. Instead, the period length T_x and the rotation number (ρ) are stored by using the block "To workspace" in the work area of Scilab. Later the information can be further processed by a Scilab-script and displayed at the end of all simulations. This is illustrated by the block „Peri.-Ratio." at which the oscilloscope is again replaced by the block „trash".

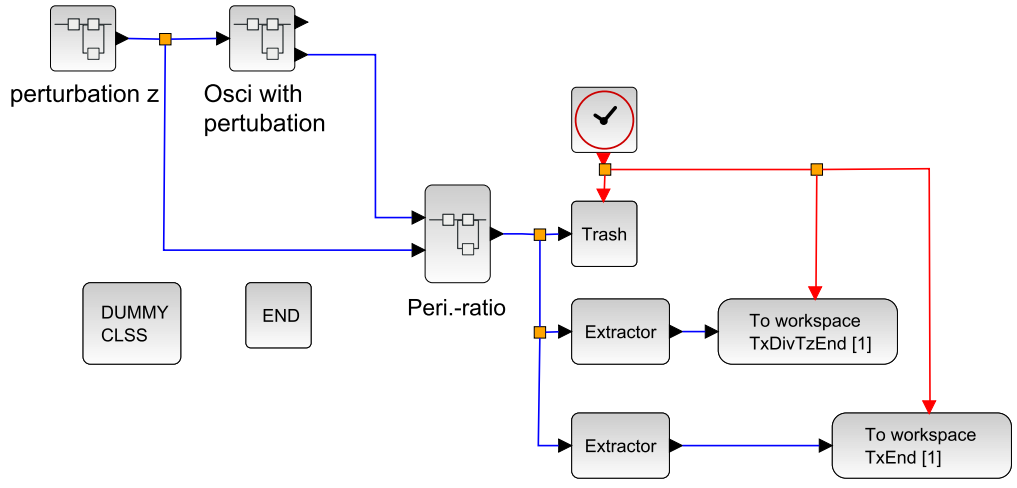

Figure 6.29: *Determination of the period ratios of period T_z of an external stimulus in the superblock "perturbation z" and of the output signals T_x of the oscillators to be studied as in Fig. 6.22, but without oscilloscope*

As a first example a VP oscillator is studied with such a Scilab/xcos method, (with $\varepsilon = 4$ and

an external sine signal with an amplitude of 0.5). The result is shown in Fig. 6.30 As can be

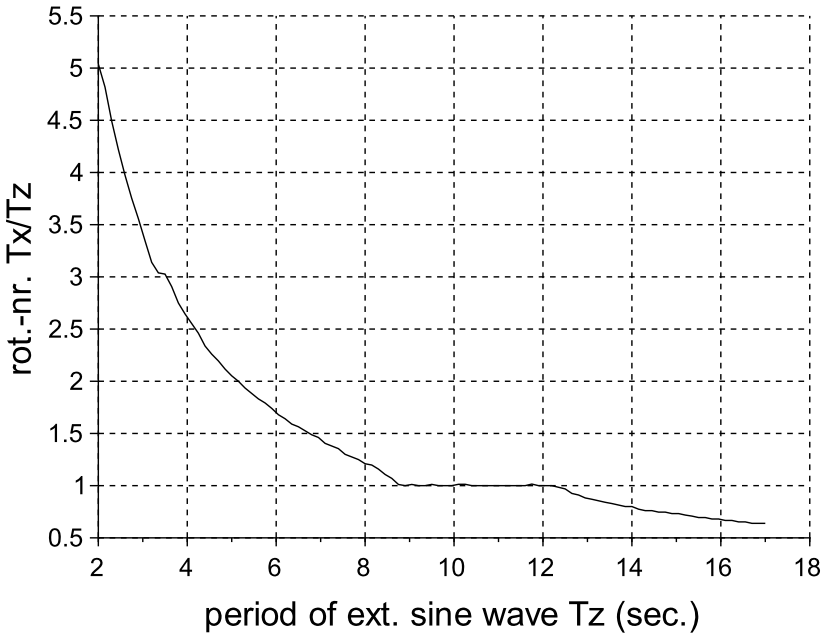

Figure 6.30: *Rotation number and its dependency on the period length of an externally effective sine oscillation with an amplitude of 0.5 of a VP oscillator with $\varepsilon = 4$ (devil's stair case) using the Xcos-circuit after Fig. 6.24 and 6.29 and the Scilab-Script 6.4.*

seen, the course of the curve is hyperbolic, however, in the range from ca. 3,2 to 3.7 and from ca. 8.5 to 12,5 sec horizontal staircases are visible, and the rotation number does not change. These are two ranges of entrainment or phase locking, and in general there are not just two, but several ranges, depending on the variation of the period length of the external oscillation. This looks like a staircase and is sometimes called "devil's stair case", see Glass, Mackey (1988) and Pikovsky, Rosenblum, Kurths (2001).

From Fig. 6.31 , where the entrainment ranges are depicted for different amplitudes of the external sine wave, one recognises, that entrainment exists at different values of the period length of the external sine oscillation, since there the rotation numbers are broken rational (cf. $\rho = T_x/T_Z$ in formula 6.14), as explained in the legend for the corresponding colour of the entrainment ranges. It is also seen that the entrainment 'window' becomes broader for stronger amplitudes of the external signal. These ranges are triangular and resemble a human tongue. They are therefore called "Arnold's tongue", see Glass, Mackey (1988) and Pikovsky, Rosenblum, Kurths (2001).

As a second example besides the VP oscillator above we discuss another simple oscillator, Neuron model, producing neuronal pulses. Its non-linearity is, however, not a non-linear, continuous, characteristic curve, but an abrupt reaction to a threshold value. In this example the parameters of the oscillation producer (e.g. the concentration of certain molecules or ions such as sodium- and potassium ions) are increased by synthesis, until a certain threshold is

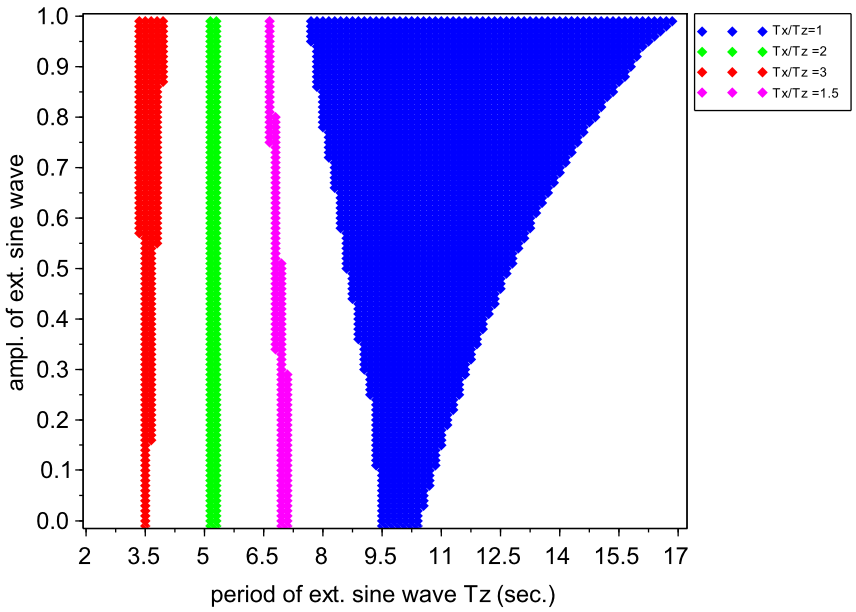

Figure 6.31: *Colour coded broken rational rotation number as a function of the amplitude and period length of an external sine oscillation on a VP oscillator with $\varepsilon = 4$, so called Arnold's tongue. The Xcos circuit in Fig. 6.24 and 6.29, and the Scilab-Script 6.4 were used to produce the curves .*

reached. At this moment the item is suddenly released to the environment, is set back to zero, and the concentration is again increased by synthesis, until the threshold is again reached, and so on. This leads to a sawtooth oscillation. If the threshold is now externally changed in time, e.g. by a sine wave, it might happen, that at certain parameter values the sawtooth top does not hit the threshold in each period of the sine oscillation, but e.g. only at every third period, as exemplified in Fig. 6.32. The corresponding Xcos model is illustrated in 6.33. It is seen that an integrator is started with the integration constant Λ and the initial value zero. Its output value x is then compared with the threshold value S(t), and if this is reached (detected by the Xcos block "Zcross" as a zero crossing), the integrator is reset to zero and the integration begins anew. The threshold S(t) consists of a constant value θ_0 and the externally applied signal.

The sawtooth oscillation can be depicted at the i-th period, starting at T_i, by an upward oblique, straight line with

$$x(t) = \Lambda(t - T_i) \text{ for } T_i < t \leq T_{i+1}$$

The threshold value S(t) can be described by an externally applied oscillation, e.g. a Sine oscillation with the amplitude K and the angular frequency ω, and a constant shift θ_0 according to

$$S(t) = \theta_0 + K \sin(\omega t) \quad \text{with } K < \theta_0$$

If the threshold S(t) is reached, the actual integration and the i-th period with duration T_{ip} ends

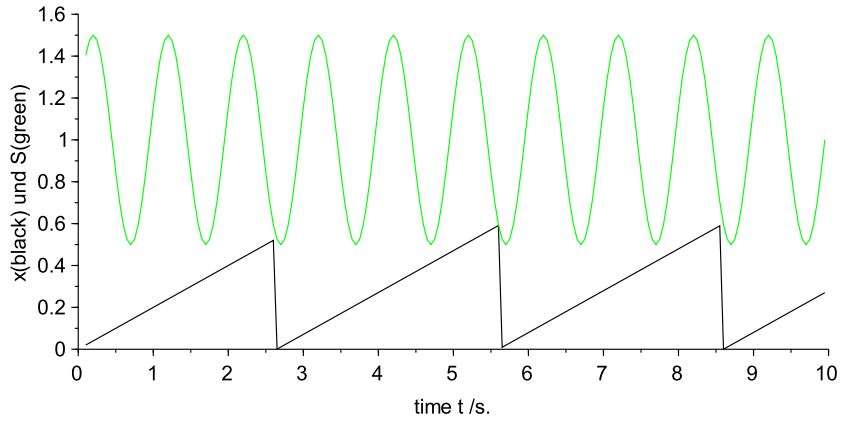

Figure 6.32: *Plot of the simulation of the exit signal x (black) with an external sine wave signal z (green curve) and entrainment at the threefold frequency of the "Integrate and Fire oscillator" using the Xcos circuit of Fig. 6.22 and 6.33.*

within the sawtooth oscillation, i.e.

$$x(T_{i+1}) = \Lambda \cdot \underbrace{(T_{i+1} - T_i)}_{T_{ip}} = S(T_{i+1}) = \theta_0 + K \sin\left(\omega \underbrace{\left[T_i + T_{ip}\right]}_{T_{i+1}}\right) \tag{6.15}$$

A special case will be treated below:

If the period length T_{ip} of the sawtooth oscillation does not change, but stays constant, i.e.

$$T_{ip} = T_p = \text{constant}$$

and if this period length is N times as large as the period length T_e of the externally applied sinus oscillation, i.e.

$$2\pi/\omega = T_e = T_p/N$$

eq. 6.15 can be simplified:

$$\Lambda \cdot (T_{i+1} - T_i) = \theta_0 + K \sin(\omega [T_i + NT_e]) = \theta_0 + K \sin(\omega T_i) \tag{6.16}$$

In this case several periods N of the external oscillation with duration T_e have already passed until the threshold S(t) is reached. In Fig. 6.32, for instance, the threshold is reached only after three periods (N=3), which corresponds to a ratio of 3:1. In this case the oscillator is "locked in" with the ratio 3:1 to the phase of the external oscillation.

The description of the oscillation according to Eq. 6.15 can be interpreted in such a way, that at the time the i-th threshold is reached the following i+1-th threshold can be determined. Thus, it is a recursion equation allowing to predict the time, at which it is "fired". The ranges of

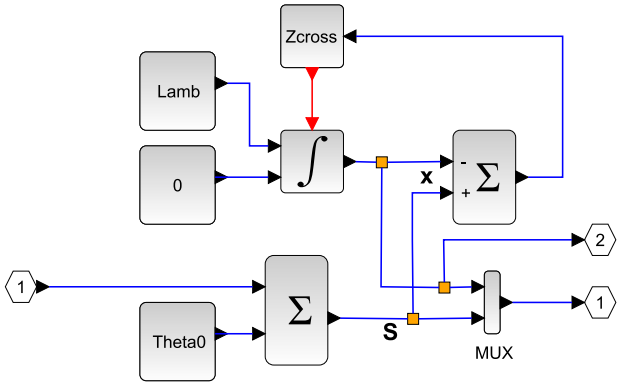

Figure 6.33: *Superblock „VP-oszi“ in Fig. 6.22 in the “Integrate and Fire oscillator”*

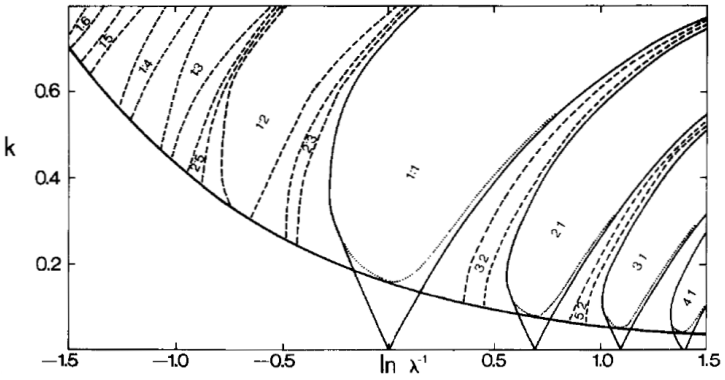

Figure 6.34: *Capture areas (’locking areas’; Arnold’s tongue) of the* “Integrate and Fire oscillator” *according to Glass, Mackey (1979) depending on the frequency of the driving sine oscillation and its amplitude with* $\lambda^{-1} = \omega\Theta_0/2\pi\Lambda$ *and* $k = K/\theta_0$

entrainment according to the special case in Eq. 6.16 can be analytically calculated, as done in detail by Glass, Mackey (1979) (see Fig. 6.34). In this case one obtains from Eq. 6.16 after resetting

$$T_{i+1} = T_i + \alpha + \varepsilon \sin(\omega T_i) \qquad (6.17)$$
$$\text{with } \alpha := \theta_0/\Lambda,\ \varepsilon := K/\Lambda$$

which can be interpreted as a change in the Fig. from T_i to T_{i+1} or by multiplication with ω as a change of phase from $\varphi_i = \omega T_i$ to $\varphi_{i+1} = \omega T_{i+1}$. That would be *a circular illustration according to Poincare*, whereby after each "firing" the phase of the driving sinus oscillation is determined, as done with the isochrons of the VP-oscillator in Fig. 6.11.

The principal capture area for the synchronised (locked in) case are shown as yellow areas

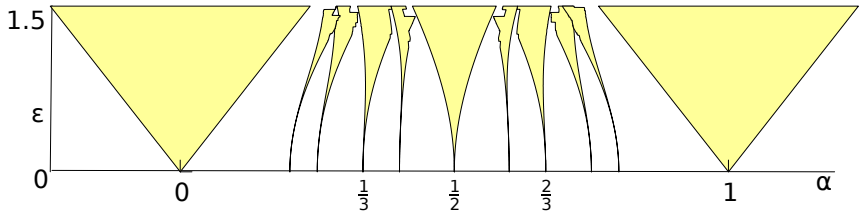

Figure 6.35: *Capture areas (Arnold's tongue) of the* Integrate and Fire oscillator *according to Eq. 6.17 if the constant threshold α and the amplitude ε ($\alpha := \Theta_0/\Lambda$, $\varepsilon := K/\Lambda$ and $\omega = 1$) are varied in the* C^{++} *program (see Arnold tongue - Wikipedia)*

if the constant threshold α and the amplitude ε of the driving sinus oscillation are varied in Fig. 6.35 according to the C^{++} program (see Arnold tongue - Wikipedia).

6.3 How to model the induction of arrhythmicity, Efforts to experimentally reach a singularity

How to stop a circadian rhythm by pulse perturbation was mentioned already in Sect. 3.1 and some examples were given. The discussion started with a description of an oscillation with two state variables showing a limit cycle in the phase plane, see Fig.6.12. A perturbation moved the oscillator from the limit cycle trajectory to a new point in the phase plane. It was assumed that the characteristics of a critical perturbation pulse could be such as to send the perturbed oscillator into a singularity area, being stopped or showing arrhyhmicity.

In the literature on biological oscillators the term arrhythmicity is usually equivalent to a 'stopped' oscillator. Arrhythmicity can also be reached in other ways – the rhythmic system can be treated in more complicated manner than above and finally end up without oscillations. We will show and discuss some of these cases reported in the literature.

In this subchapter we would like to discuss some difficulties and complications that one meets, both experimentally and theoretically, in the search for the arrhythmicity. It will be seen that it is in many cases valuable to develop a relevant model of the system under study. The topic of stopping a circadian rhythm is well covered in the book "How to stop a biological clock. Point of singularity" (Engelmann, Witte 2016).

While much of the literature on arrhythmicity of biological oscillators concentrate on ultradian oscillation in animals and plants (in fact also in our subchapter 6.1), also the circadian rhythms of humans can be perturbed and stopped. This subchapter will discuss, to some extent, the possibilities to halt the circadian rhythms of man and some effects of such an arrythmicity.

In the case of disturbances of the human heart rhythm (temporary frequency changes etc.) one often speaks about heart arrhythmia. The term is also used in the literature on other biological rhythms. The use of the terms is not consistent in the literature on biological oscillations – we will stick to the term arrhythmicity when talking about suppressed oscillations.

6.3.1 Use of single perturbation pulses

Winfree Winfree 1970 was the first one who systematically studied the possible arrhythmicity of the well-known *Drosophila* eclosion rhythm. He used blue light pulses to perturb the rhythm. And he scanned necessary pulse durations, pulse heights (i.e. light intensity) and proper phases of the rhythm to apply the critical perturbation so as to approach a singular, arrhythmic state, i.e. to stop the rhythm.

In this case the light perturbation was fairly short to get close to the singularity - with the intensity used it was of the order of seconds. In other circadian experiments (Engelmann W. 1978) red light has been used to disturb the flower movements of Kalanchoë petals. Then pulses of a duration of about two hours stopped the movements (when using proper light intensity). In both cases it was extremely important to find out at which phase of the oscillation the pulses should be given to achieve suppression.

In the case of the *Drosophila* clock the light pulse should be given in the late delay period of the phase response curve (at the transition point, see e.g. Winfree 1980). In the circadian Kalanchoë clock the light pulse should start briefly before the petal closure (phase delay region) to stop/attenuate the movements (see e.g. Engelmann W. 1978). Also for other biological oscillators, for example several short term oscillations that have been studied, it requires lots of experiments to find the proper characteristics of the perturbation to stop the oscillation. ”Trial and error” seems to be an unavoidable part of the experimental procedure when looking for the pulse conditions leading to a stopping (or at least suppression) of the clock.

An example of stopping ultradian oscillators is given in Fig 7.28. Here light/dark pulses could be given to stop a short-term transpiration rhythm in a plant leaf (Johnsson, Boström, Pedersen 1993).

Not only light pulses but also other perturbation types can evidently be used. Examples of electric pulses stopping minute-period leaf movements have been recorded. It is known that electric pulses can stop the oscillations of the human heart muscle .

6.3.1.1 Complications.

It should be mentioned that the oscillator itself might in some cases affect the receptor/transducer for the perturbation. The pulse given to the system might, therefore, be affected and modified by the oscillator itself. An example is the ultradian oscillator which moves a plant leaf up and down. If light comes from above onto a moving leaf, the absorbed light to the oscillator will be different dependent on the leaf position – which is controlled by the oscillator itself. This means that we have a feed-back link from the oscillator output to its input sensor. Such a model can be outlined as in Figure 6.36.

A second example: A human subject can be said to be studied under ’constant light conditions’. But the light hitting the retina will then be much less during the subject’s sleep periods (with closed eyes). The circadian work/sleep output will therefore affect the retina and the input transducers of the circadian system – again in a feed-back manner as sketched in Fig 6.36. The set up of the experiments must be carefully discussed.

6.3.2 Use of two or several pulses to perturb oscillators.

Extending the one-pulse experiment discussed above, one could apply two or more (interspaced) pulses. Again the use of the relevant phase response curve will be valuable.

In double pulse (8 hours part, red light) experiments on *Kalanchoë* is has been shown that arrhythmicity can be achieved when the first pulse is applied just before the rhythm minimum, and the second one 8 hours after the first pulse. The phase shifts after light pulses have been rather extensively studied in this system.

Grone et al. 2011 induced arrhythmicity of the circadian system of a rodent by giving continuous light for several weeks at a critical pulse or a short light pulse, which switched the phase of the rhythm from delay to advance. The light pulses were given in such a way that during the first night the phase was advanced and delayed during the following night. The animals were then arrhythmic. The authors tested whether the loss of rhythm in the behaviour was due to arrhythmia in the suprachiasmatic nucleus (SCN). For this purpose the expression of the mRNA of the clock proteins per1, per2, bmal1, and cry1 was measured in the SCN. The expression of these genes was indeed reduced by 18 to 40%, and the reduced amplitude was reflected in a strongly attenuated oscillation. The model of reduced amplitude due to light pulses can thus be explained by a singularity in the molecular circadian mechanism.

Similar experiments on arhythmicity were also performed on small mammals. At the Djungarian hamster Phodopus sungorus, Steinlechner, Stieglitz, Ruf (2002) showed that short light pulses during the night of a 16:8 h light-dark cycle (LD) advanced or delayed the rhythm of locomotor activity depending on the time of application; a combination of two 15 min light pulses -the first in the late night phase and the second in the early night phase of the following night- shortened the active phase significantly. In 75% of all animals the rhythm disappeared and arrhythmia occurred, which could last up to 145 days, even though the animals were still kept in LD. Since three different hands of the clock were affected, namely activity, body temperature and melatonin rhythm, the state of the central pacemaker must have changed. The authors propose a model in which two weakly coupled oscillators no longer show any phase differences and the amplitude of the output falls to zero.

In another rodent, the large Egyptian jumping mouse Jaculus orientalis3, El Moussaouiti et al. 2010 found phase shifts of the activity rhythms by giving 15 min light pulses, which caused the typical delays in the subjective evening and early night and advances in the late subjective night and early morning. Between these phases (CT3-CT8), there is a dead zone in which light does not have any effect. However, some of the animals showed a strong shift of more than 9 h at this time, indicating that the animals showed a strong response (type 0) and that there was a singular point at CT19. Therefore, it would be possible and desirable to induce arrhythmia in this time range.

Data from the eclosion rhythm in Drosophila, achieved with 15 min pulses white light (i.e. much stronger than the pulses used to create arrhythmicity as mentioned above) and given under different conditions can be found in the literature . Likewise phase shift data from caused by 30 min, 60 min pulses have been published. Under certain assumptions one can predict (out from the 15 min phase response curve) the phase shifts of multiple and combined 15 min pulses and also that the oscillation will stop at a certain phase if continuously perturbed with the white light. The strong white light cause arrhythmicity of the system if given continuously.

6.3.3 Several oscillators.

In our introduction to arrhythmicity we used one single, simple oscillator possible to describe in a phase plane. Of course, such a simple one-oscillator description is not always representative for biological oscillators which in many cases consist of several interacting cells, as in a tissue.

If we, for example, imagine a clock to be located in an excitable tissue, it is possible that the different cells act together and outwardly act as a single unit. The *Drosophila* eclosion clock and the *Kalanchoë* flower clock each consists of several cells controlling a circadian behaviour. Despite this multi-oscillatory nature of the system it is a reasonable start of modelling to look upon the system as one, over-all, 'unit oscillator' – a 'bulk' oscillator. At a later stage we might develop the model and take into account that the tissue is composed of several oscillatory cells, each an oscillatory unit. This is the progress we have followed in sec. 7.8 and chap.8 of the present book.

It is a remarkable fact that it is possible to perturb such a bulk oscillator to stop, as our examples demonstrate. Questions arise: Does it mean that each individual oscillator/cell is stopped? Or do the cells simply desynchronizes and oscillate totally out of phase with respect to each other so as to produce an arrhythmic unit, as seen from 'outside'?

6.3.4 Arrhythmicities and human circadian rhythms.

We now turn to the human circadian system. Can the human clock be stopped at all? How to search for an arrhythmicity and possibly the human circadian rhythm? And if clock is stopped, what will be the effect on the body?

The human circadian oscillator shows a period (in darkness, endogenously) just above 24 h. Czeisler, Duffy et al. 1999 specifies it to 24,18 h. Early bunker experiments to determine circadian behaviour were carried out in Erling-Andechs near Munich (see Wever 1979), from which a mean period length of 25 h for the free running of humans was concluded. But since the subjects could change the timing of the light sources the light level could affect the period time. To obtain the true endogenous period, the light intensity has to be much weaker (10-15 lux) than used by the objects in bunker experiments. The light program should, furthermore, not correspond to the period of the internal oscillator, and the experiments should run for at least 20 days (Klerman, Dijk et al. 1996).

Many features of the human clock were modelled successfully when an extended model of the van der Pol equation was used (Wever 1984, also see sec.7.7):

$$\ddot{y} + 0.5(y^2 + y^{-2} - 3)\dot{y} + (1 + 0.6)y = \ddot{z} + \dot{z} + z$$

Here y is the oscillating variable and z the intensity of the ambient light (and which must be kept within certain limits if oscillations in y should arise). However, more extended models seems necessary to develop and the modelling of the human circadian rhythms is a vivid area. It could be mentioned that in a study of the singularities (Pedersen, Johnsson 1994) of the equation above leads to unstable singularity conditions – while experimental approaches point to possibilities to stop the clock.

While it was previously assumed that in humans social contacts are more important for the synchronisation of circadian rhythms than light, Czeisler 1995 has not confirmed this. He found

that repeated daily light pulses can strongly shift the human circadian oscillator (a so-called type 0 response). This shows that the pacemaker is not only influenced by the timing of the light pulse and its strength, but also by the number of days on which it occurred. This treatment also influences the amplitude of the oscillations. A critical pulse at a particular phase brings the oscillator to a singular point, which expresses itself in the stopping of the circadian clock. This result could be important in the treatment of sleep disorders, since under these condition the human internal clock can be shifted to any phase in three days.

Jewett, Kronauer, Czeisler 1991 reported, that strong light pulses decreased amplitude of rhythms when given for some cycles at a time when the phase of the circadian pacemaker is strongly shifted. In some cases the rhythm was completely lost, as might be expected in the singularity region. In another publication (Jewett, Kronauer, Czeisler 1994) it was shown, that the pacemaker of the circadian system of humans is not simply a phase-only oscillator, but that amplitude is also important, and that a phase-amplitude model better describes the experimental data. A single 5 h pulse with strong light leads to a weak phase shift (type 1), the same pulse given on the two following days reduces the amplitude strongly, and pulses near the minimum of body temperature given for three days dampens the oscillation strongly (type 0 phase shift) or cause arrhythmia.

6.3.5 Some remarks on efforts to use models and study the singularity. Advantages with model work? Model work in general.

To have a model of the system under study is quite useful – it allows flexible perturbation studies and predictions and can be a very time saving working tool.

An introduction to some types of models was given in Chapter 5. In later chapters (7 and 8) we discuss some models published in the literature and might be those approaches can be applied in further experiments. We have also seen that despite some problems that have been mentioned, the use of pulse perturbations is very useful to get for example phase response curves.

A kind of summary of the previous subchapter has indicated that a natural starting point for studies of a biological oscillator would be to use perturbation 'pulses'. One could argue that if one administers a pulse, then it may often be transformed underway before it reaches the oscillator. It is unlikely that what is finally reaching the clock is a pulse as mostly described in the literature - with rectangular shape, defined start/end times and defined height/intensity. It will probably be delayed and smeared out before entering the clock proper. Even if this is the case, it is natural to start experiments and simulations with pulse perturbations. Might be, at a later stage, that one could improve the characteristics of the perturbation that enters the clock.

The approach from such experiments will also indicate in which phase the pulses should be applied to reach the singularities.

The problem of damping or stopping unwanted oscillations arises also in non-biological systems, e.g. in a mechanical/chemical production plant: How should one affect the system so as to achieve a steady state ?

In control theory one is often interested in controlling a complicated system in order to damp/annihilate self oscillations of the system (e.g. Åström, Wittenmark 2013). Many technical systems, e.g. in the process industry, must be controlled carefully to avoid oscillation reducing

the production. One approach used is often called dead-beat control or dead-beat strategy. In discrete-time control one looks for an input, control, signal to the process, which should bring the system to the steady state in the shortest time (with fewest steps). For linear systems this can often be accomplished, but for non-linear ones (as in biological oscillations) it is usually more complicated.

In biology Winfree 1980 explored experimentally (by varying length and intensity of blue light pulses) the possibility to stop the eclosion rhythm of Drosophila flies by a single short light pulse. This could be denoted an experimental dead-beat strategy.

An approach involving parts of the strategy has been demonstrated in the case of the circadian van der Pol model and its use by Wever (Pedersen, Johnsson 1994, see page 194).

All this focusses on the great advantage of having (or trying to develop) a model for the oscillating system. One could easily change parameter values and perturbation characteristics and see if arrhythmicity can be achieved. This is, of course, of great value for trying out the arrhythmicity predictions experimentally.

To determine correct pulse timing (phase with respect to the rhythm) and properties is difficult – it must be said to the reader that this can be a 'trial and error' exercise. From the literature it is seen that also experimentally it is difficult to find the proper perturbation characteristics that lead to a standstill (arrhythmicity) of the oscillator. It is by no means a trivial task to find the proper perturbations (e.g. Winfree!).

Kronauer, Gunzelmann et al. 2007 discuss the results of a symposium in which models for circadian rhythms in humans were presented and emphasise that a close cooperation between researchers who work experimentally and those who build mathematical models are necessary.

Furthermore, models for shift work are important. The aim is to find an optimal working schedule that takes into account the needs of shift workers and of the industry. For this purpose, schedules have been developed that avoid strong conflicts with the circadian system of the workers (Czeisler, Moore-Ede, Coleman 1982). Kostreva, McNelis, Clemens 2002 used the two-oscillator model of Kronauer, Czeisler et al. 1982 to match the requirements with the rhythm of the shift workers in the respective shifts. The most suitable shifts were those in which the shift rhythm was close to the free-run rhythm. These are slow, forward rotation patterns that alternate every two weeks with two days of recovery per week.

Here again it must be pointed out how important models are in chronobiology (see Beersma 2005). Models for circadian rhythms of humans have been proposed by the Kronauer team and have been further developed over the years. An older model describes quite accurately how strong light (over 4 000 lux) can influences phase and amplitude if administered over a longer period of time (about 5 h). However, it could not correctly describe more recent results, according to which shorter and weaker exposures were effective. Therefore the authors proposed a new model in which a dynamic stimulus processor (process L) between the light stimulus and the traditional circadian pacemaker mediated a self-excited limit cycle oscillator (process P). With this model, phase shifts could be simulated by short and long light pulses and arbitrary intensities. The model makes predictions that should be tested (Kronauer, Czeisler et al. 1982).

The VP oscillator in Kronauer's model was replaced by Jewett, Forger, Kronauer 1999 by a higher order limit cycle oscillator, whereby the amplitude near the singularity recovers more slowly, and near the limit cycle more rapidly. The maximum light sensitivity is now 4 h before

the body temperature minimum compared to Kronauer's model and the body temperature minimum and the critical phase 0.8 h later. The new model shows a direct effect of light on the circadian period: with increasing light intensity the period decreases, which is consistent with Aschoff's rule.

Special findings in the circadian system such as late sleep under free-run conditions compared to those under synchronised conditions, internal de-synchronisation between circadian rhythms and the sleep-wake wake cycle and bi-circadian (48-50 h) sleep-wake cycles could all be explained with the coupled oscillator model of Kronauer (Kronauer, Czeisler et al. 1982), but the physiological causes were unclear. Phillips, Czeisler, Klerman 2011attempted to use a physiological model of the hypothalamic and brainstem nuclei to elucidate the mechanisms responsible for internal de-synchronization using a physiological model of the hypothalamic and brainstem nuclei.

Indic et al. 2005 compared two models that compare phase and amplitude dynamics. They differ in their predictions of how quickly phase and amplitude recover when the amplitudes of the oscillation are small. When the biological processes that are responsible for the rhythms are taken into account, more computational effort is required. Two models have been published for mammals, one by Leloup, Goldbeter 2003 and Leloup, Goldbeter 2004 and the other by Forger, Peskin 2003 with 19 and 73 differential equations, respectively. It was reduced to a model with two differential equations, which shows still the most important characteristics of a biological clock, namely the approximate 24 h period, the synchronisation by the LD cycle, the phase response curve, and the amplitude recovery after an appropriate disturbance. This simplifies the mathematical analysis considerably. It can be used to couple oscillators of mammals and to understand their dynamics.

For some time, systems biology has complemented the molecular biology to understand the various components of a system and the network of interactions so that one can better control it and design new systems with appropriate structures and the underlying dynamic principles (Ueda 2007). Mammalian circadian clocks have been used as a model system for this purpose with the clock-controlled genes and cis-elements, transcriptional and post-transcriptional loops (with functional genomics), with parameter changes of the clock components, perturbations of the clock, and with the specific singular behaviour. This includes phase shifts, non-linear behaviour, temperature compensation, and synchronisation; as well as how these clocks interact with the environment, such as how light changes are represented internally, and how day-length is perceived photo-periodically. The singular behaviour of biological clocks can also be studied in systems biology (Ukai, Kobayashi et al. 2007).

To better understand how arrhythmia develops after a specific pulse at a specific time, the photoreceptor melanopsin was inserted into mammalian cells. This made them sensitive to light. The cellular clocks could actually be brought to a singular state by a critical pulse of light. Theoretical considerations indicate why the singular behaviour occurs in different organisms. It is suggested that desynchronisation is the most likely mechanism for arrhythmia. The in vitro and in silico findings were confirmed by in vivo observations that desynchronisation is responsible for the decreasing amplitude of rhythms in the suprachiasmatic nucleus after a critical light pulse (Ukai, Ueda 2010).

Another model explains how flights across time zones slowly adjust the circadian system to the new time zone (Gander, Kronauer, Graeber 1985). How fast this resynchronisation proceeds

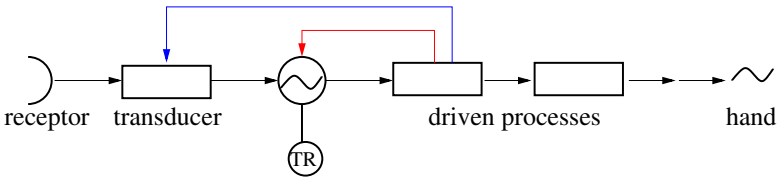

Figure 6.36: *Oscillator model scheme with various components: receptor(s), a transducer, input to the oscillator, various driven processes, and finally the observed output (*hands *such as leaf movement or O_2 production of a plant). There might exist feedback from one (or several) of the driven processes to the oscillator (red) or to the transducer (blue). After Engelmann, Schrempf 1979*

depends on the number of time zones flown over, the direction of flight (East or West), and the strength of the time cues in the country of arrival. Differences in the adaptation are mainly based on the individual period lengths of the passengers.

A practical application of arrhythmia arrhythmicity by the singular point in a bioreactor has already been mentioned in Section 3.1

6.4 Modelling temperature robustness

6.4.1 Models for temperature robustness of rhythms.

Let's see, how we can model temperature robustness. But before, we should have a look at a schematic representation of the structure of an oscillator with temperature robustness (see Fig. 6.36). Inputs such as light or temperature step ups or step downs or pulses are perceived by receptors connected with the oscillator via transducers. The oscillator (~) might or might not be temperature robust by a special mechanism (TR). Driven processes lead to observed outputs (*hands*) such as leaf movement or O_2 production of a plant. Feedback to the oscillator or to the transducer might exist, which could simulate a circadian sensitivity of the oscillator to the constant simulating agent (Engelmann, Schrempf 1979). The situation can be illustrated as in Fig. 6.36.

6.4.2 Membranes as part of oscillator

For a long time discussions have pointed at membranes as central parts in circadian oscillations. The arguments for the involvement of membranes in circadian rhythms have been compiled and discussed in Engelmann, Schrempf 1979. The long period of about 24 h could be due to membranes as diffusion barriers, slowing down reactions and transport process. Various substances affecting structure and function of membranes have been reported to influence the period and/or the phase of circadian rhythms. Membrane models for circadian rhythms were proposed by Sweeney 1976; Njus, Sulzman, Hastings 1974; Schweiger, Schweiger 1977; Burgoyne 1978 (see Fig. 6.37, 6.38, and 6.39).

Membranes were also proposed to explain temperature robustness (Njus, Sulzman, Hastings 1974). One way which has been proposed influencing membranes for the oxygen development

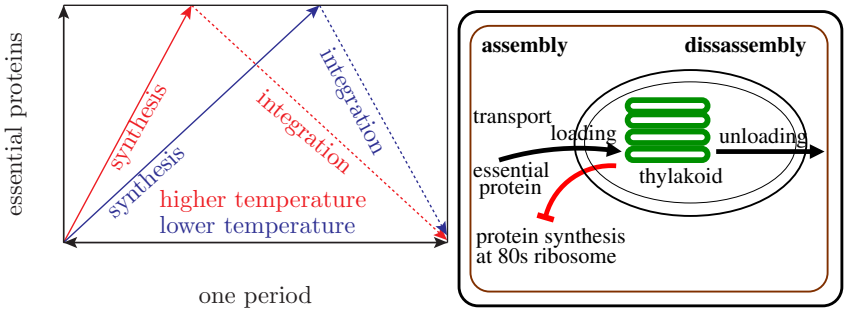

Figure 6.37: *Temperature compensation of circadian clock in* Acetabularia.
Left: At higher temperature (red) the synthesis of essential proteins (y axis) is faster, but the integration into thylakoids slower: At lower temperature (blue) the synthesis is slower, but the integration speeds up. In this way the period length depends only marginally on temperature ("one period" two-head arrow at x-axis). The speed is indicated by the slope of the straight lines.
Right: The translation-membrane model of Schweiger, Schweiger 1977. Essential proteins are translated on 80S ribosomes in the cytoplasm and transported into chloroplasts, where they are loaded on thylakoid membranes. After complete synthesis is stopped, the essential proteins disassembled until the thylakoids are unloaded. Assembly can start again. From Engelmann, Schrempf 1979; see also for N. crassa *Dunlap, Feldman 1988, based on a proposal of Hastings, Sweeney 1957 and Schweiger, Schweiger 1977*

by the photosynthetic apparatus in the thylakoids of *Acetabularia* is illustrated and explained in Fig. 6.37. There are two processes following each other during the circadian cycle, one of which (the synthesis of essential proteins) is sped up by higher temperatures, the other one (integration of the essential proteins into the thylakoid membranes) is slower at higher temperatures.

Lakin-Thomas, who has worked intensively on lipids and lipid-affecting mutants in Neurospora favours the "old membrane model" in which membrane lipids adjust to new constant temperatures. It is known that membranes do adjust their composition to compensate for changes in temperature, so one does not need to invent any new molecular mechanisms. She mentions, that not all non-canonical rhythms are temperature robust, for instance choline-depleted *Neurospora*: its period depends on the temperature. In Lakin-Thomas 2019 it is pointed out, that circadian rhythmicity intersects with fundamental metabolic processes. It is discussed if there may be circadian metabolic oscillators that exist independently but interact with the TTFLs. Questions are, whether metabolism affects circadian rhythmicity, and vice versa. Furthermore, is metabolism rhythmic, and if so, is that rhythmicity cell autonomous? PTO's might also be involved as links between the Target of Rapamycin (TOR) signalling pathway and circadian oscillators, known to generate rhythmicity independent of TTFLs.

Another example is a very simplified feedback model (see Fig. 6.41) in which the protein A is transcribed induces the production of protein B by the gene B. Since this protein B *inhibits* the transcription of the protein A by the gene A, it will break down without being replenished. Gene B will be switched off due to the lack of protein A, and protein B decreases to a point where gene A is not any more repressed. Now gene A is switched on and the whole cycle can

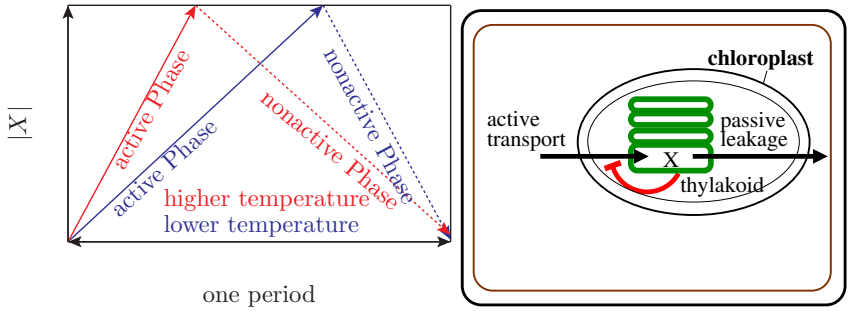

Figure 6.38: *Temperature compensation of circadian clock in* Acetabularia *according to Sweeney 1976. Left: At higher temperature (red) the synthesis of essential proteins (y axis) is faster, but the integration into thylakoids slower: At lower temperature (blue) the synthesis is slower, but the integration speeds up. In this way the period length depends only marginally on temperature ("one period" two-head arrow at x-axis). The speed is indicated by the slope of the straight lines. Right: Scheme of the model. Active transport of substance X through chloroplast envelope and thylakoid membrane increases its concentration in the thylakoid, until at a threshold the transport is stopped. Due to passive leakage X is diminished and active transport resumed, From Engelmann, Schrempf 1979; see also for* N. crassa *Dunlap, Feldman 1988, based on a proposal of Hastings, Sweeney 1957 and Schweiger, Schweiger 1977*

start again. The temperature robustness of this feedback model is shown in Fig. 6.43 (see Gibo, Kurosawa 2019).

6.4.3 Other Models

First mention three earlier hypotheses to explain temperature robustness, namely the *temperature-amplitude coupling hypothesis* (temperature-sensitive amplitudes in gene activity rhythms can result in a stable period by generating larger amplitudes at higher temperatures (Lakin-Thomas, Brody, Coté 1991)), the *balance hypothesis* (temperature robustness arises from a balance between period-shortening and period-lengthening reactions (Ruoff 1992)), and the *critical-reaction hypothesis* assuming that critical reactions govern the period which can be stable if they are insensitive to temperature (Terauchi et al. 2007).

Afterwards a new hypothesis was proposed, according to which the *waveform of the circadian oscillation* that is more non-sinusoidal at higher temperatures is essential for temperature robustness of the circadian rhythm (see Fig. 6.42). They used the TTLO oscillator model of Drosophila and mammals (see Fig. 6.43), and furthermore the PTO of cyanobacteria (three proteins KaiA, KaiB, and KaiC and ATP, Fig. 6.44) for their model. Because the structure of the PTO is different from that of the TTLO oscillator, one would expect the condition for robustness against temperature fluctuations to differ. However, the analysis again showed that temperature robustness in the PTO model needed a more non-sinusoidal waveform at higher temperatures, although the network structure of the PTO model of the cyanobacteria differs considerably from that of the TTLO model (see Fig. 6.44)

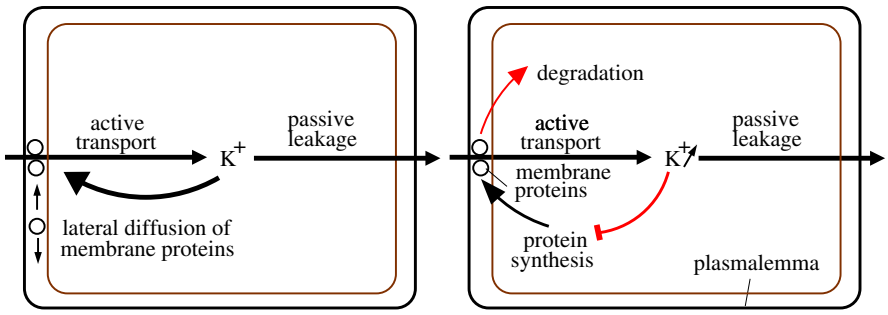

Figure 6.39:
Left: Membrane model of Njus, Sulzman, Hastings 1974. Transport of K^+ *through the plasmalemma increases the concentration, until at a threshold the composition of the membrane changes in such a way that transport stops. Due to passive leakage the concentration of* K^+ *then decreases until feedback inhibition stops and transport is resumed. Lateral diffusion of membrane proteins are involved.*
Right: Model of Burgoyne 1978 of monovalent ion-mediated translational control. Ions, e.g. Ca^{2+}, K^+ *are transported into the cell by membrane proteins (ATPases). Synthesis of these proteins on mRNA is inhibited by high concentrations. The amount of membrane proteins decreases due to normal degradation. Less ions are transported into the cell, their concentration decreases due to passive leakage. Inhibition of protein synthesis ceases, when a threshold of the intracellular ions is reached. With increasing synthesis of the proteins the transport of ions increases again, and feedback inhibition of the synthesis stops. The circadian time delay is due to the long half-life and time for synthesis and transport of the membrane proteins. From Engelmann, Schrempf 1979*

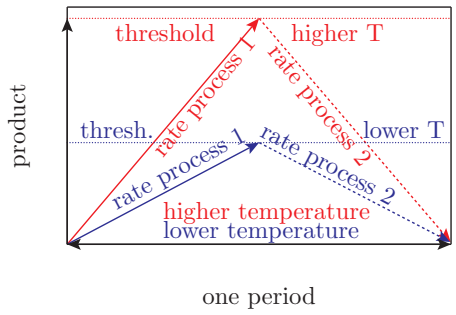

Figure 6.40: *Temperature compensation of circadian clock in* Acetabularia*: At higher temperature (red) the synthesis of essential proteins (y axis) is faster, but the integration into thylakoids slower: At lower temperature (blue) the synthesis is slower, but the integration speeds up. In this way the period length depends only marginally on temperature ("one period" twohead arrow at x-axis). The speed is indicated by the slope of the straight lines. From Engelmann, Schrempf 1979; see also for* N. crassa *Dunlap, Feldman 1988, based on a proposal of Hastings, Sweeney 1957 and Schweiger, Schweiger 1977*

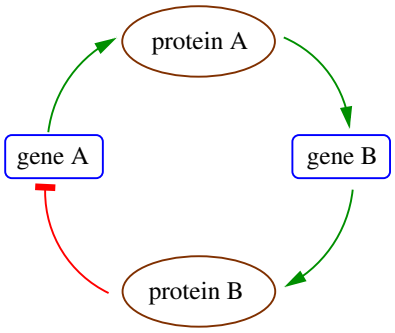

Figure 6.41: *Scheme of a feedback loop (e.g. a TTFL): At the start of a cycle, protein A accumulates and switches gene B on. Protein B is now also accumulating, until it has reached a sufficient amount to switch off (red) gene A. Protein A will be broken down without being replenished. Gene B will be switched off due to the lack of protein A. Protein B decreases to a point where gene A is not any more repressed. Gene A is switched on and the whole cycle starts again. For the temperature robustness of this feedback model see Fig. 6.43 and Gibo, Kurosawa 2019*

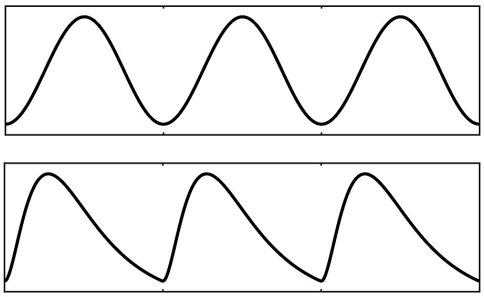

Figure 6.42: *Different wave forms of the Gibo-Kurosawa model.*
Top: Sinusoidal oscillation with NS = 1 *(NS is an index for the non-sinusoidal form of a curve;* NS = 1 *is strict sinusoidal,* NS = 2 *is skewed to the left*
x-axis is time axis, in the case of circadian rhythms 3 periods, each about 24 h. After Fig. 1 in Gibo, Kurosawa 2019. It is valid for the TTO model, as shown in Fig. 6.43, as well as for the post-translational oscillator (PTO) model (Fig. 6.44)

The waveform of the oscillation may also be important for the *entrainment* of circadian rhythms.

The historical development of mathematical models of bi-stability and oscillations in chemical reaction networks were reviewed by Tyson, Albert et al. 2008. In the 1960s and 1970s, these models were limited to well-studied biochemical examples, such as glycolytic oscillations and cyclic AMP signalling. In the 1980s and later after the rapid discoveries of molecular genetics, the field was widened by mathematical modellers to gene-protein interaction networks that control circadian rhythms, cell cycle and cell division, and the design of synthetic gene networks.

It was also experimented with synthetic biotechnology to reprogram cellular regulatory mechanisms (Hussain et al. 2014). The robustness was improved by using intrinsic properties of transcription factors within the circuit to buffer against intra- and extracellular variability. This led to the design and construction of a synthetic gene oscillator in *Escherichia coli* that maintains a constant period over a range of temperatures. They began with a synthetic dual-feedback oscillator with a temperature-dependent period. Computational modelling predicted and subsequent experiments confirmed that a single amino acid mutation to the core transcriptional repressure of the circuit results in temperature robustness[3]. A transcriptional oscillator resulted with a nearly constant period of 48 min for the temperature range from 30°C to 41°C. In the absence of

[3] Specifically, they used a temperature-sensitive lactose repressor mutant. It loses the ability to repress its target promoter at high temperatures. In the oscillator, this thermoinduction of the repressor leads to an increase

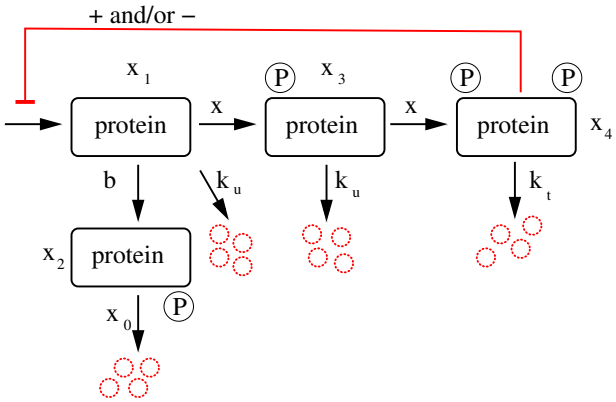

Figure 6.43: *TTO model (essential for cellular circadian oscillations in* Neurospora, Arabidopsis, Drosophila, *and mammals). A gene transcribes protein x_1 which induces another gene to transcribe the protein x_3 which becomes phosphorylated (P). This induces again another gene to transcribe protein x_4, which is more phosphorylated (P, P). This protein inhibits (red line with cross-piece) the transcription of the first gene. All proteins are slowly disintegrated (red circles) with certain reaction constants k, protein x_1 via another protein x_2. Mathematical analyses of Gibo, Kurosawa (2019) revealed that temperature robustness required waveforms that are more non-sinusoidal at higher temperatures (see Fig. 6.42).*

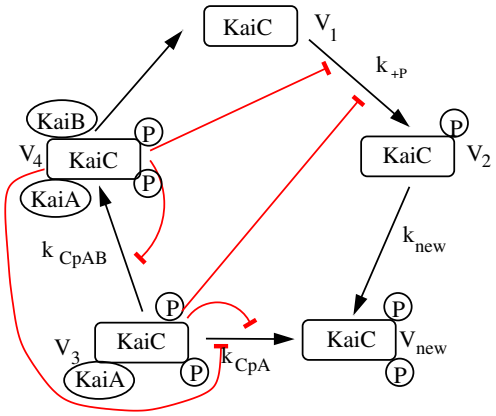

Figure 6.44: *A PTO model of a* cyanobacteria, *in which circadian oscillations can be reconstituted in vitro with three proteins (KaiA, KaiB, and KaiC) and ATP. V_1 is protein concentration of non-phosphorylated KaiC, V_2 of mono-phosphorylated KaiC, V_{new} of double-phosphorylated KaiC, V_3 of double-phosphorylated KaiC bound to KaiA, V_4 of double-phosphorylated KaiC bound to KaiA and KaiB. Increase in phosphorylated KaiC increases the complex of KaiC and KaiA, which causes sequestration of free KaiA (total amount of KaiA is conserved). This sequestration works as a negative feedback for KaiC phosphorylation, potentially resulting in limit cycles. After Gibo, Kurosawa 2019.*

the mutation the period drops from 60 to 30 min over the same temperature range. Synthetic gene circuits can thus be engineered to be robust to extracellular conditions by modifying the protein level.

As mentioned before (see page 153), the underlying mechanism for temperature robustness due to an asymmetric waveform was discussed by Gibo, Kurosawa 2020. Faster reaction rates increase the abundance of transcription factors; the degradation process requires therefore more time and consequently the waveform becomes non-sinusoidal. siRNA-mediated knock-down of the mRNA m6A methyl-transferase elongates the decrease phase of Per2 oscillations without affecting the increase phase (Fustin et al. 2013). At the same time the amplitude is increased, and amplitude is an index of period robustness (Gibo, Kurosawa 2019). The balance between period-shortening and period-lengthening effects is required for temperature robustness (Ruoff 1992). Rate limiting of the PER2 phosphorylation is contact between the circadian clock and mRNA m6A methylation via CK1δ2. This asymmetry in waveform reminds of the models of Sweeney (1976) (see Fig. 6.38) and of Schweiger, Schweiger (1977) (Fig. 6.37) which are also based on different wave forms at various temperatures.

Another mechanism for temperature robustness has been proposed by Kon et al. (2021) (see Fig. 6.45) and is due to a Ca^{2+} oscillator. This evolutionary conserved mechanism is found both in eukaryotes and prokaryotes. It consists of a Na^{+}–Ca^{2+} exchanger (NCX), which at lower temperature elevates the intracellular Ca^{2+} level. This activates the Ca^{2+}/CaM (calmodulin-dependent) protein kinase II (CaMKII) and accelerates transcriptional oscillations of clock genes, for instance in mammalian cells. The Ca^{2+} signalling is conserved among mice, Drosophila, and Arabidopsis and contributes to the temperature robustness of the transcriptional cyanobacterial clock

in period at high temperatures. That compensates for the decrease in period due to Arrhenius scaling of the reaction rates.

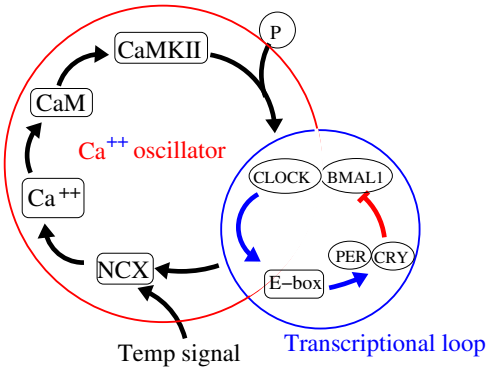

Figure 6.45: *Temperature robustness is supposed to be due to a* Ca^{++} *oscillator which is an evolutionary conserved mechanism in both eukaryotes and prokaryotes (here, in a blue circle, for eukaryotes). The* Ca^{++} *oscillator (red circle) consists of a* Na^{+}/Ca^{2+} *exchanger (NCX). At lower temperature, NCX elevates the intracellular* Ca^{++} *level. This activates the* Ca^{++}*/CaM (calmodulin-dependent) protein kinase II (CaMKII) and accelerates transcriptional oscillations of clock genes, for instance in mammalian cells (CLOCK-BMAL1 activate -blue arrows- via an E-box PER-CRY, which inhibits-red arrow- CLOCK-BMAL1). This* Ca^{++} *signalling is conserved among mice,* Drosophila, *and* Arabidopsis. *The NCX also contributes to the temperature robustness in transcriptional rhythms in the cyanobacterial clock. After Kon et al. (2021).*

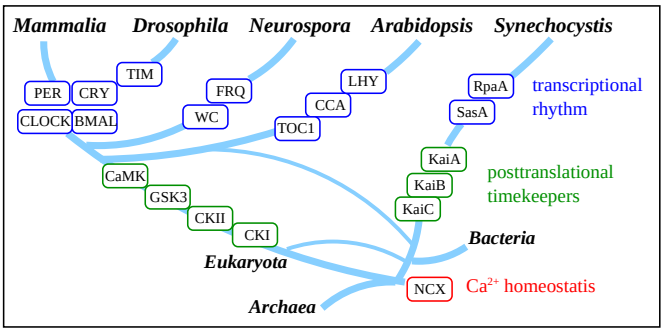

Figure 6.46: *How ancient* Ca^{2+} *signalling and temperature robust circadian rhythms might be connected (lines), according to Kon et al. (2021).*
In cyanobacteria (e.g. Synechocystis*), posttranslational timekeepers consisting of the KaiA/KaiB/KaiC drive transcriptional rhythms. NCX* Na^{+}/Ca^{2+} *exchanger) is a highly conserved molecule among the three domains of life (*Archaea, Bacteria, Eukaryota*) and a common circadian timekeeping element in eukaryotes and prokaryotes. Its original function is to regulate* Ca^{2+} *homeostasis.*
*Clock genes in transcriptional rhythms evolved independently in the diverse eukaryotes (*animals, fungi, and plants*). Multifunctional kinases, such as casein kinase I (CKI), casein kinase II (CKII), glycogen synthase kinase 3 (GSK3), or* Ca^{2+} *dependent kinase (CaMK), are involved in posttranslational regulation of clock gene products (blue boxes).*

7 Models of rhythms from the literature - *overall systems and lumped models*

In the following we have chosen models, which had to be tested, whether they described correctly the observed rhythmic events and the effect of temperature or light pulses upon them. As an especially rigorous test we used furthermore the singular state, which was found in quite a number of rhythms of various organisms

The models chosen are the following ones: a basic feedback model introducing feedback and signal delay (Johnsson, Karlsson 1972 and Karlsson, Johnsson 1972) (Sect. 7.1), the feedback model of Lewis/Saunders, which is derived from it (Sect. 7.2), the Goodwin oscillator (Sect. 7.3), the Goldbeter oscillator (Sect. 7.4), the modified VP-oscillator after Wever (Sect. 7.7) and models for heart rhythms (Sect. 2.3.1).

7.1 Simple feedback model from Karlsson/Johnsson

Johnsson and Karlsson tested a feedback model to simulate the Kalanchoë petal movement rhythm to simulate the *Kalanchoë* petal movement rhythm (Johnsson, Karlsson 1972). It can be described mathematically by a time independent set value c_{ref} of the oscillation level $c(t)$ with the differential equation

$$\frac{dc(t)}{dt} = HeV\left\{F\left[c_{ref} - c(t - t_V)\right] + c_{pert}\right\} \tag{7.1}$$

and is shown in Fig. 7.1 as a block diagram. The included functional blocks (F and HeV) are shown in Fig. 7.2.

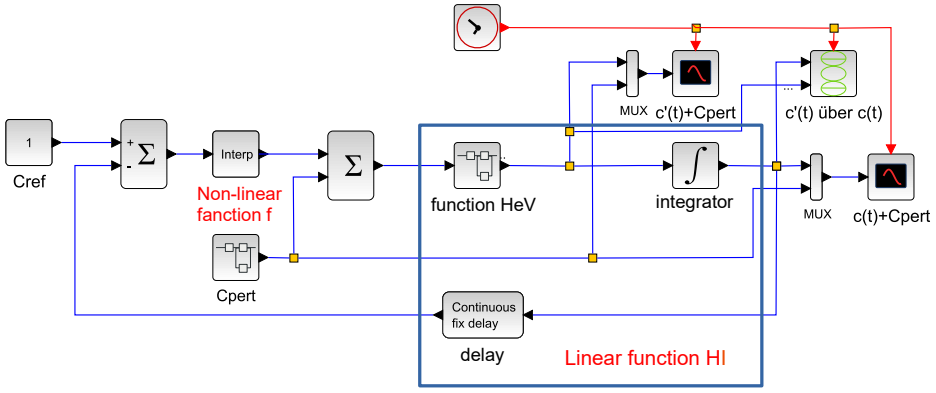

Figure 7.1: *Feedback model of Johnsson and Karlsson (see also Fig. 5.29) created with Scilab. In Fig. 7.2 the functions f and HeV (H-function with external delayer, here in superblock) are diagrammed. Disturbances (e.g. a light pulse) applied via* c(pert) *can be inserted between the function F and the function HeV. The signal is conducted via the multiplexer MUX (top) together with the signal* c(t) *to the output (top) and visualised as a curve and a pulse. Via a further MUX (right) together with the* c(ref) *signal it is conducted to another output (right). The* c(t) *signal is by the continuous-fix-delay element delayed, fed back and compared with the* c(ref) *value in the subtracter (top left). Later it passes again the loop.* c′(t) *over* c(t) *is generated by CSCOPXY at the top right (the phase diagram, shown in the lower part of Fig. 7.5) and likewise led to the output at the right. After Johnsson, Karlsson 1972; Karlsson, Johnsson 1972*

.

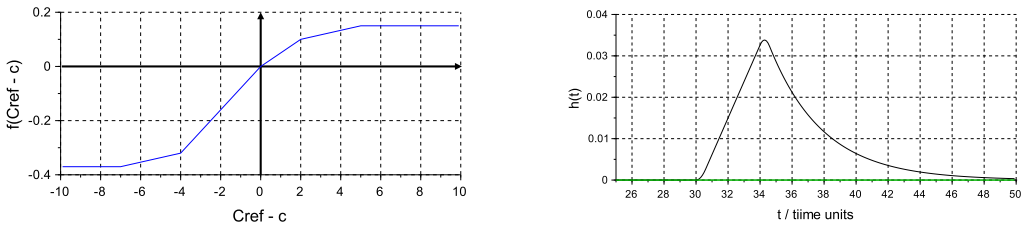

Figure 7.2: *Functional blocks of the feedback model of Karlsson and Johnsson. At the left the function f and at the right the function H are shown (in Fig. 7.1 these functions are represented by and).*
The function f shows, how the output of cref − c *depends on the feed back signal* cref. *It has an upper and a lower limit, which prevents the oscillation from building up too much.*
The function HeV represents a kind of memory: What happened until 30 time units is not remembered, what happened 32 time units ago is well remembered and afterwards memory fades towards zero.. After Johnsson, Karlsson (1972).

The usefulness of this model was tested with disturbances of the *Kalanchoë* petal movement

by applying single light pulses at various phases of the rhythm. The produced phase shifts of the rhythm could be simulated by the model. Likewise the phase shifting effect of temperature pulses could also be simulated successfully.

The principle to study the pulse response is shown in Fig. 7.3: After a period of τ time units a pulse is applied in the oscillator model T time units later with the duration S. The oscillation is disturbed in such a way, that its phase position is shifted in respect to an undisturbed oscillating plant. Θ is the distance between the end of the disturbing pulse and the next extreme point of the oscillation (e.g. maximum), when the oscillation is stable again after the disturbance. The phase shift Θ is then reduced by a multiple of the duration τ of the oscillation, which is smaller than Θ, i.e. the phase shift is $\Theta \bmod(\tau)$.

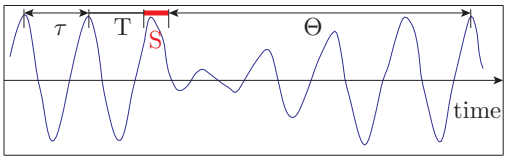

Figure 7.3: *Principle of the phase shift measurement after a disturbing pulse. τ: Period length before the pulse, T: Begin of the pulse after the end of a period, Θ: Time between the end of the pulse and the same extreme value point in the oscillation being stable again (e.g. end of period, see Johnsson, Karlsson (1971))*

If the width of the pulse S and the point in time T, at which the pulse is given, are varied and if the phase shift is plotted as a function of these phase shifts (from Θ), a three dimensional picture is obtained, which has been displayed in Fig. 7.4 in such a way, that the third dimension can be seen in form of "contour lines", i.e. in case of identical values of the phase shifts they are connected by a curve.

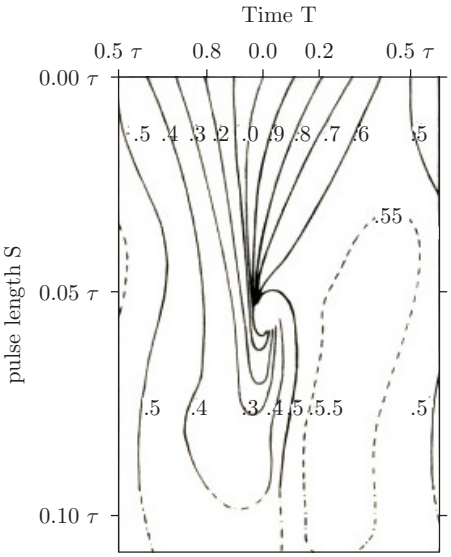

Figure 7.4: *Phase shifts of the oscillation as a function of the phase T and the duration S of a disturbing pulse. Values of the same phase shifts are connected by a "contour line". The calculations were performed only for a pulse width S smaller than 0.09τ. The guessed curves at longer pulse widths are drawn as thin lines (see Johnsson, Karlsson (1971)).*

From the course of the curves it can be seen, that a pulse with a width of about 0.05τ given at

the maximum of the oscillation ($T = 0$) attracts almost all contour lines. There the pulse time can vary much (e.g. from -0.4 to $+0.4\tau$) without a change in the phase shift. In this point the oscillation can be brought to a standstill (see Winfree (1983)).

A critical test of the Scilab/xcos build model is also the experimentally shown possibility, to induce arrhythmicity by applying a very specific light pulse at a certain phase, that is, to bring the oscillator into the singular point. For this to occur the following parameters were used in the simulation:

- a pulse with after 372 time units with 3.5 amplitude units
- a delay by 30 time units
- duration of the period about 140 time units

The period was somewhat more as the fourfold of the delay, a consequence of the integrator and the feedback with time delay (see Fig. 7.1). The curve for $c(t)$ is shown in Fig. 7.5. Compare it with the experimentally obtained curve in Fig. 3.1. If $c'(t)$ is plotted against $c(t)$, one obtains the phase diagram in the lower part of Fig. 7.5.

In contrast to the experiments the point of singularity was not stable in the simulation: After a short pause the oscillation started anew and reached amplitudes as large as before the pulse. However, the parameters of the disturbing pulses (amplitude, duration and time of disturbance) are very difficult to find. Already the smallest change can prevent arrhythmicity.

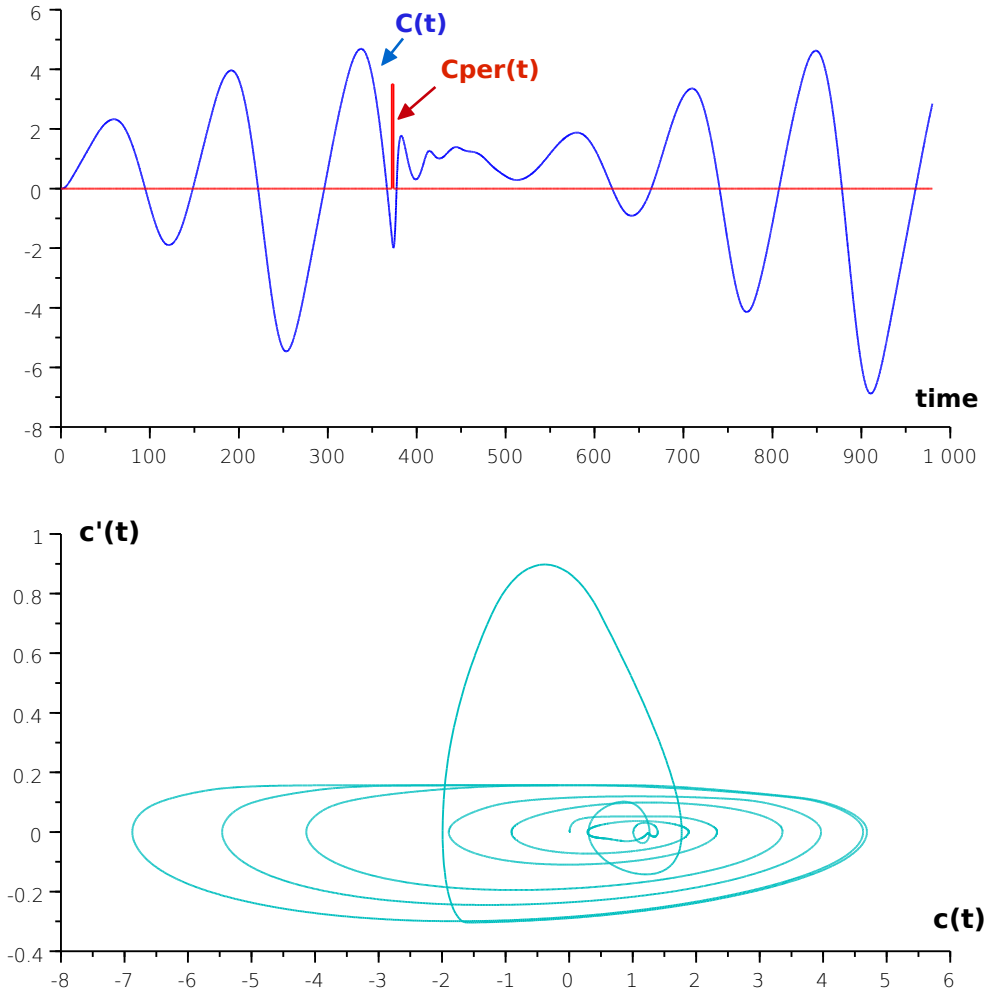

Figure 7.5: *Top: Example for arrhythmicity (staying only for a short while) by a pulse (red); simulation results of the feedback model of Johnsson and Karlsson in Fig. 7.1.. Below:Phase diagram ($c'(t)$ as a function of $c(t)$); simulation results of the feedback model of Johnsson and Karlsson in Fig. 7.1*

7.1.1 Appendix to the model of Karlsson/Johnsson Oscillator, Harmonic Balance

The stability of the Karlsson/johnsson model can be investigated not only by determining the singularity point and linearisation in the environment around it, but also with the help of linearisation in the harmonic balance according to Section 5.6.5.1. The division of the model in Fig.7.1 into a static linear and frequency-dependent part, is illustrated in Fig.7.6.

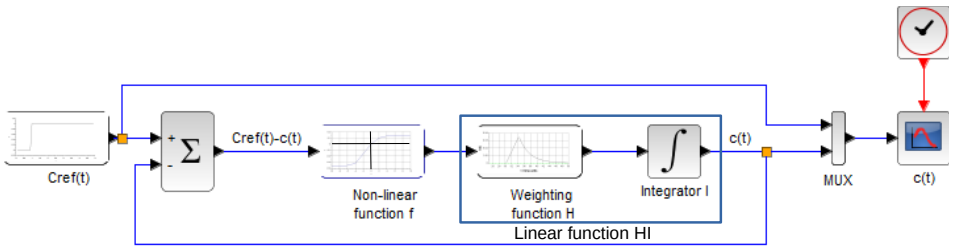

Figure 7.6: *The feedback model of Johnsson and Karlsson (see also Fig. 7.1) .*

If the non-linear part of the model is approximated by the properties of the fundamental, it can be replaced by a linear part that acts like an amplifier whose gain depends on the amplitude of the fundamental of the input signal (see subsection 5.6.5.1 and Fig.5.30). The overall system can then be regarded as linear, which is fed back and then generates independent oscillations if the condition according to the equation 5.36 is fulfilled. This means with our notation (cf. the previous equation with slightly different symbols 5.36 ($Fv(p) \cdot F(A, f) = -1$):

$$F(A, f) = -\frac{1}{HI(f)} \tag{7.2}$$

Where the two curves F(A,f) and -1/HI(f) intersect, the oscillation condition 7.2 is fulfilled.

If the saturation characteristic curve for F(A,f) shown in Fig.7.2 and the linear function HI(f) are selected, the following result is obtained as shown in Fig.7.7.

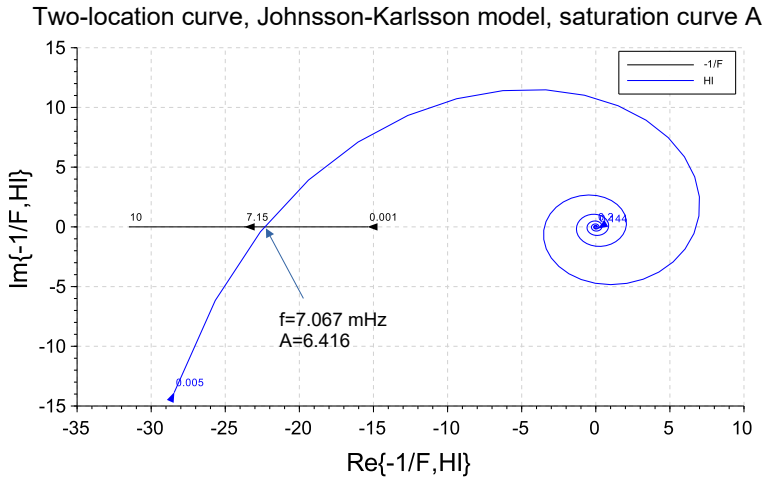

Figure 7.7: *Two-location curve diagram of the non-linear approximation -1/F(A,f) of the Saturation characteristic and the linear function HI in the Johnsson and Karlsson feedback model (see also Fig. 7.6) .*

It can be seen that the curves intersect at a frequency of 7.067 mHz at an amplitude of the fundamental wave with an amplitude of 6.416. Therefore, an oscillation can be generated under these conditions, which is also approximately confirmed by a simulation of the step response with Scilab according to the model shown in Fig.7.6.

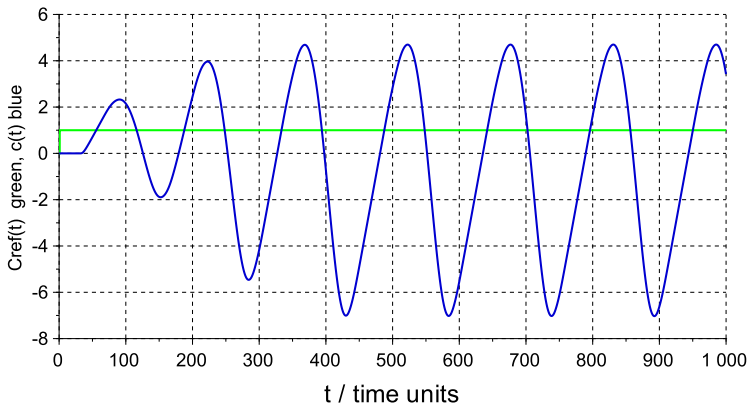

Figure 7.8: *Step response of c(t) (blue curve) in the Johnsson/Karlsson model according to Fig.7.6. Green curve represents the c_{ref} value.*

7.2 Feedback model of Lewis/Saunders

The team of Bob Lewis in Auckland (New Zealand) studied very intensively the rhythmic behaviour of the New Zealand Weta *Hemideina thoracica*. The Weta is a night active insect and its locomotor activity is controlled by a circadian clock. A model was developed (see Fig. 7.9 and Lewis (1999) and Gander, Lewis (1979)), which was derived from the feedback model of Johnsson and Karlsson (see Fig. 7.1) and is based on the assumption, that in sites of the cells a substance X is synthesised which is lost with time to the outside. The sum of X (from other cells) is -time delayed- sensed by sensors at the cell membrane and fed back to the synthesis sites (see Fig. 7.9).

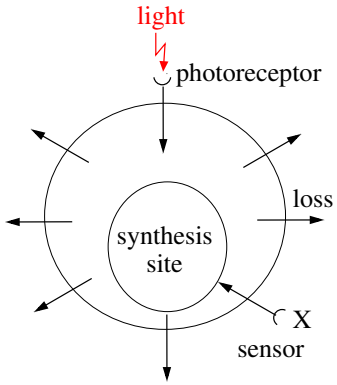

Figure 7.9: *Scheme of the feedback model of Lewis with sites of synthesis of a substance X (circle) and its loss to the outside; sensors for this substance send feedback, time delayed, signals with affect the concentration in the cell. Light acts via photoreceptors as a signal on the cell. For the model see Fig. 7.10*

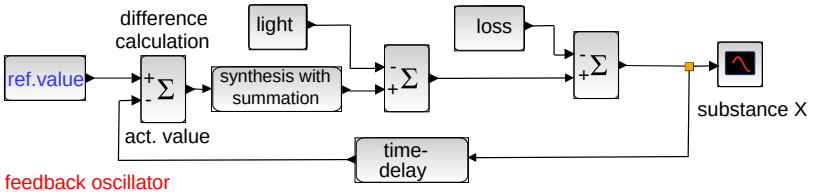

Figure 7.10: *In the feedback model of Lewis the set value* c_{ref} *is compared after a time delay with the actual value* c(t). *The difference (error) regulates the synthesis of a substance. Disturbances by light influence the oscillation. Loss of the substance via membranes is a further constituent of the system. The course of the concentration X can be seen in CFSCOPE (symbol)*  . *The delayed feedback of the current value serves to form the difference, before the loop is run through again. See Lewis 1976; Gander, Lewis 1979. The model is shown in Fig. 7.11 in a modified form (for temperature varied situations) for Scilab*

The model resembles a refrigerator: If the set point temperature is exceeded, the compressor is switched off. The temperature falls below the set point, but increases again slowly, until the cooling starts again. Disturbances such as the opening of the refrigerator influence the oscillations.

The model of Lewis simulates successfully the effect of light pulses (Lewis 1976) and temperature pulses (Gander 1976; Gander, Lewis 1979) on the rhythm. Further experimental findings

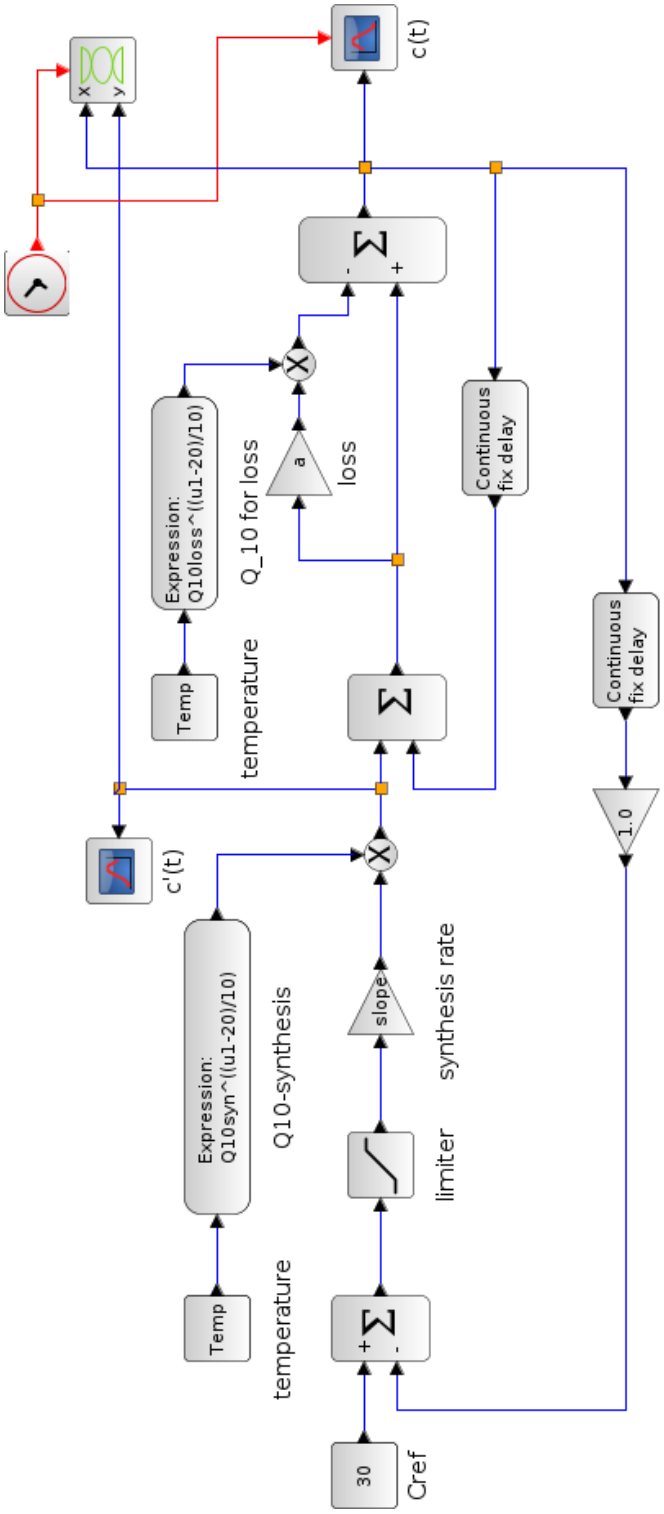

Figure 7.11: *The feedback model of Lewis (Fig. 7.9) for the activity rhythm of the Weta is displayed here in an extended form, to show besides the light effect (top centre) also the temperature influences (the two* Temp *blocks at the top left) on the substance X with an* $Q_{10} = 2$*. The dependency of the synthesis rate on temperature is given in the* Q_{10}*-synthesis block and for the loss in the* Q_{10} *block. Disturbances by light have been omitted in this version, since the influence of temperature on the oscillation was in focus. The time course of the concentration of a substance X can be seen in CFSCOPE (symbol) . A time delayed feed back of the current value serves to build the difference, before the loop is passed again. An additional feedback loop (continuous fix delay) serves to increment the steps by 1. See Lewis 1976; Gander, Lewis 1979.*

such as the *splitting* of the rhythm in several components, spontaneous changes in period length during free run (Fig. 7.12) and so called aftereffects could be simulated, if the circadian system consisted of two rhythm generators, which were mutually coupled (Lewis, Bullivant, King 1991) or if a population of weakly coupled oscillators was used (Christensen, Lewis 1983; Christensen, Lewis 1982; King 1988).

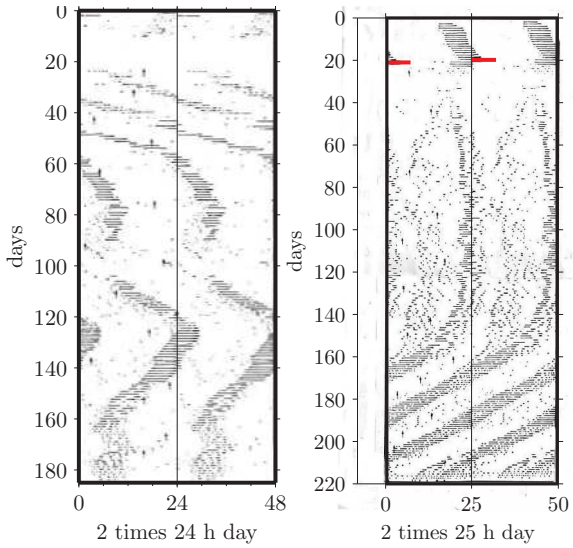

Figure 7.12: *Actograms of a Weta.*
They show spontaneous period changes (left) and splitting (right, splitting caused by an 8h light pulse, marked red; activity is here plotted in 25h grid!). Double plots: Activity of the first and second day plotted next to each other, then below the activity of the second and third day and so on. Arrows show the feeding times. From Christensen, Lewis 1982.

Such coupled oscillator nets can be displayed with Scilab/Xcos in such a way (functional diagram in Fig. 7.11), that temperature and light influences can be simulated and the amplitude of the oscillation be heavily impaired (see Fig. 7.13). Details in Engelmann-Witte 2016.

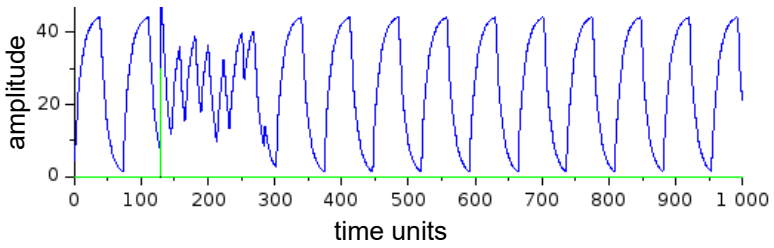

Figure 7.13: *The Lewis feedback model (Fig. 7.11) was used to simulate with Scilab the disturbance of the activity rhythm of the Weta (blue curve) by a light pulse (green vertical stroke). After Lewis, Saunders 1987 and Christensen, Lewis 1983*

7.3 The Goodwin oscillator

The Goodwin model is a 3-variable model and demonstrates how oscillations in a delayed negative feedback based system can emerge at the molecular level (Goodwin 1965). This prototypical model and its variants have been commonly used to model circadian and other genetic oscillators in biology (Gonze, Leloup, Goldbeter 2000; Bodenstein, Heiland, Schuster 2012; Bardal 2002). The model rests on the transcription and translation of a "clock gene" - in *Neurospora* the frq gene, the corresponding frq mRNA and the FRQ protein and on the subsequent formation of a transcription inhibitor which blocks the expression (see Fig. 3.4).

This oscillator with a negative feedback does not only show the correct phase position of the frq mRNA and of the FRQ protein level, but also correct phase response curves towards temperature steps and -pulses in respect to the experimental results in *Drosophila* as well as in *Neurospora*. The most important elements in the concept of a negative back coupled oscillator is the formation of frq-mRNA (variable X) by the frq-gene, see Fig. 7.15. This process, namely the transcription of the gene and the transport of the frq-mRNA in the cytosol (often denoted TTFL, transcription-translation-feedback-loop) is presented by the reaction R1 (see Fig. 7.14). In the cytosol the frq-mRNA is translated to FRQ-protein (reaction R2, variable Y). From the cytosol the FRQ-protein is transported back in the cell nucleus, where it or a modified (perhaps phosphorylated) form of it (variable Z) is assumed to inhibit the transcription of frq.

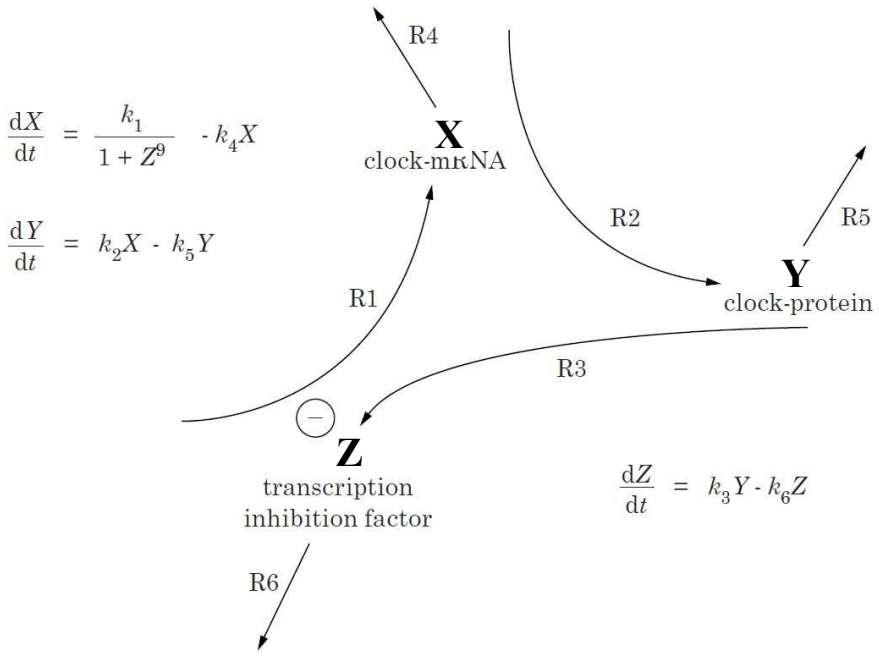

Figure 7.14: *Oscillator consisting of transcription and translation of a "clock gene" in the Goodwin model. Reaction R1 is the formation of the clock-mRNA (X); reaction R2 is the synthesis of the clock protein (Y), and R3 is the production of a transcription inhibitor (Z). R4, R5 and R6 are degradation reactions, see Ruoff, Vinsjevik et al. 1999a*

The entry of FRQ into the cell nucleus, the modification of FRQ into an inhibitory factor and the inhibition of the frq transcription are combined in the Goodwin model as reaction R3. The reactions R4, R5 and R6 represent the degradation of the frq-mRNA (X), FRQ protein (Y) respectively the inhibitory factor (Z). Mathematically seen the (non-inhibited) transcription rate is assumed to be constant and is described by the particular rate constant k_1. The translation rate depends on the amount of mRNA (X) and is written as k_2X. Likewise the rate of the formation of the inhibiting factor Z is presented by the term k_3Y. The inhibition of transcription is introduced by the factor $1/(1+Z^9)$ in relation to the uninhibited transcription rate (k_1) (see Fig. 7.14).

The model can be described by the following coupled differential equation system (Bardal, Johnsson, Chapman 2003):

$$\begin{aligned} X' := \frac{dX}{dt} &= \frac{k_1}{1+Z^9} - k_4X \\ Y' := \frac{dY}{dt} &= k_2X - k_5Y \\ Z' := \frac{dZ}{dt} &= k_3Y - k_6Z \end{aligned} \tag{7.3}$$

A corresponding Scilab/Xcos model is shown in Fig. 7.15.

The only source of non-linearity in this model is a Hill function, characterising the repression process. It was mathematically shown that to obtain limit cycle oscillations, the Hill coefficient must be larger than 8, a value often considered unrealistic. It is indeed difficult to bring such a high coefficient in agreement with simple cooperative dynamics.

The singular point X_0, Y_0 and Z_0 (no oscillation) is found by setting de derivatives X_0', Y_0' and Z_0' equal zero for the point:

$$\begin{aligned} X'|_{X_0,Y_0,Z_0} = 0 &= f_1(X,Y,Z) = \frac{k_1}{1+Z_0^9} - k_4X_0 \\ Y'|_{X_0,Y_0,Z_0} = 0 &= f_2(X,Y,Z) = k_2X_0 - k_5Y_0 \\ Z'|_{X_0.Y_0,Z_0} = 0 &= f_3(X,Y,Z) = k_3Y_0 - k_6Z_0 \end{aligned} \tag{7.4}$$

This equation system is not analytically solvable because of the high power of Z_0^9. Under the condition, that $Z^9 \gg 1$, an approximation can be found, see (Bardal 2002; Bardal, Johnsson 2001):

$$\begin{aligned} Z_0 &= \left(\frac{k_1k_2k_3}{k_4k_5k_6}\right)^{1/10} \\ Y_0 &= \frac{k_6}{k_3}Z_0 \\ X_0 &= \frac{k_5k_6}{k_2k_3}Z_0 \end{aligned} \tag{7.5}$$

Thus, one obtains e.g with the parameter values given by Ruoff, Vinsjevik et al. 1999b

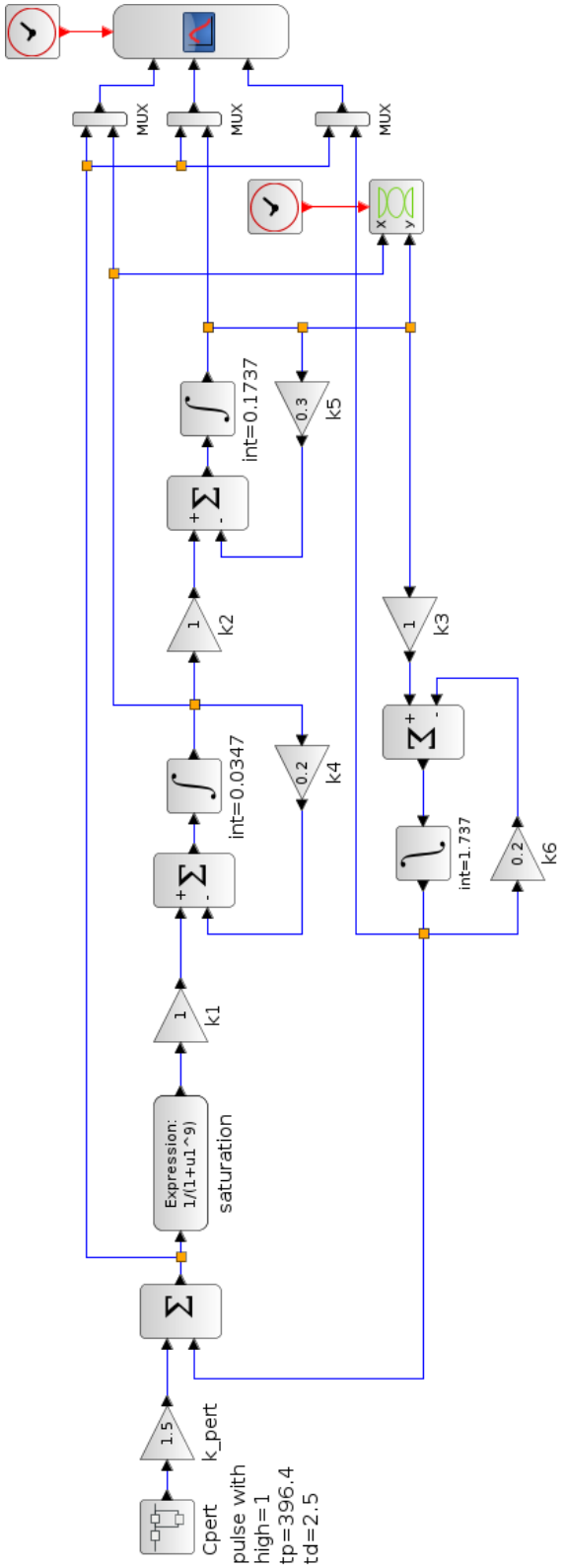

Figure 7.15: *The Goodwin oscillator, modified by Bardal-Johnsson (Bardal 2002). The initial values of the integrators with the outputs x, y and z (0.0347, 0.1737, 1.737) were selected so that no oscillation of the limit cycle type occurs at the start of the simulation, but oscillations can be initiated by a pulse.*

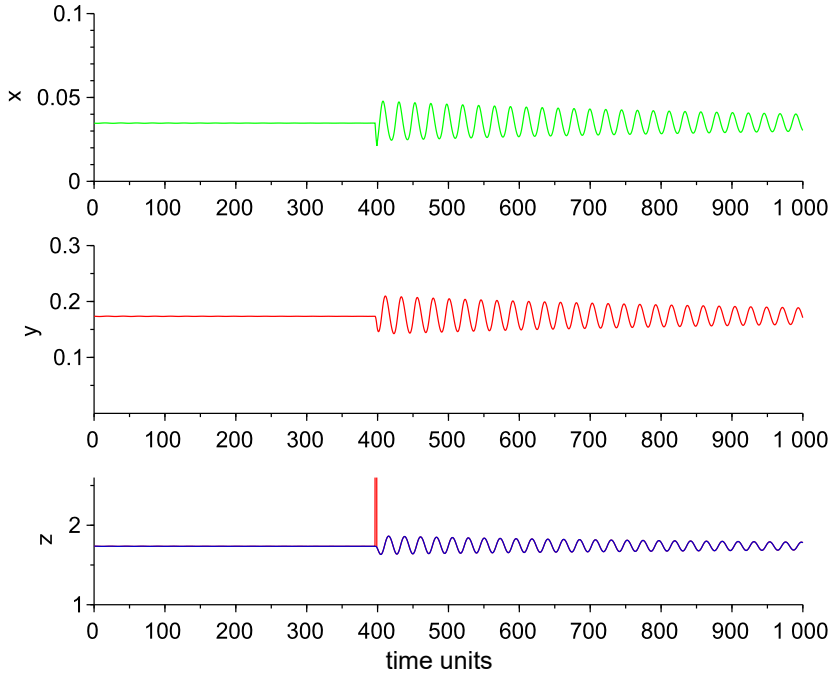

Figure 7.16: *Output signals of the Goodwin oscillator according to Fig. 7.15. The stability of this oscillation depends on the parameter values k_4, k_5 and k_6. In the case of the coefficients $k_4 = k_5 = 0.2$ and $k_6 = 0.1$ given by Ruoff, Vinsjevik et al. 1999b these oscillations fade away. The singular point x, y and z (0.0347, 0.1737, 1.737) thus remains stable.*

$k_1 = k_2 = k_3 = 1$, $k_4 = k_5 = 0,2$ and $k_6 = 0,1$ the following results for the singular point:

$$\begin{aligned} X_0 &\approx 0.03474 \\ Y_0 &\approx 0.1737 \\ Z_0 &\approx 1.737 \end{aligned}$$

(It is obvious that $Z_0^9 \gg 1$). The stability of this point can, as usual (and as used for the Goldbeter model in Sect. 7.4), be studied by a linearising procedure. For small changes x, y, z around this singularity point one obtains

$$X := X_0 + x,\ Y := Y_0 + y \text{ and } Z = Z_0 + z$$

we get around this point X_0, Y_0 and Z_0 the linear equation system:

$$\begin{aligned} x' &= \left.\frac{df_1(X,Y)}{dx}\right|_{X_0,Y_0,Z_0} x + \left.\frac{df_1(X,Y,Z)}{dy}\right|_{X_0,Y_0,Z_0} y + \left.\frac{df_1(X,Y,Z)}{dz}\right|_{X_0,Y_0,Z_0} z \\ y' &= \left.\frac{df_2(X,Y)}{dx}\right|_{X_0,Y_0,Z_0} x + \left.\frac{df_2(X,Y,Z)}{dy}\right|_{X_0,Y_0,Z_0} y + \left.\frac{df_2(X,Y,Z)}{dz}\right|_{X_0,Y_0,Z_0} z \\ z' &= \left.\frac{df_3(X,Y)}{dx}\right|_{X_0,Y_0,Z_0} x + \left.\frac{df_3(X,Y,Z)}{dy}\right|_{X_0,Y_0,Z_0} y + \left.\frac{df_3(X,Y,Z)}{dz}\right|_{X_0,Y_0,Z_0} z \end{aligned} \tag{7.6}$$

The results can be expressed in the form of a matrix:

$$\underbrace{\begin{pmatrix} x' \\ y' \\ z' \end{pmatrix}}_{\vec{x'}} = \underbrace{\begin{pmatrix} -k_4 & 0 & \frac{-k_1 9 Z_0^8}{(1+Z_0^9)^2} \\ k_2 & -k_5 & 0 \\ 0 & k_3 & -k_6 \end{pmatrix}}_{\underline{\underline{A}}} \cdot \underbrace{\begin{pmatrix} x \\ y \\ z \end{pmatrix}}_{\vec{x}} \tag{7.7}$$

Here the arrows above x' and x denote vectors and the two lines below A denote a matrix. The solution of this *linear* differential system can be carried out in the same way as we have used in Sect. 5.5 (albeit in the two dimensional case). We use the Fourier transform of $\vec{x}$ and $\vec{x'}$

$$p \cdot \vec{X} = \underline{\underline{A}} \cdot \vec{X} \tag{7.8}$$

where $\vec{X}$ is the Fourier transform of $\vec{x}$ and $p = \sigma + j\omega$ the complex frequency with the real part σ and the imaginary part ω. σ represents the damping of the solution and ω is the angular frequency of the corresponding oscillation $\sim \exp(\sigma t) \cdot \cos(\omega t)$. The Eq. 7.8 can be rewritten, as follows:

$$\left(\underline{\underline{A}} - p \cdot \underline{\underline{E}}\right) \cdot \vec{X} = \vec{0}, \ \underline{\underline{E}}: \text{ unit matrix} \tag{7.9}$$

Except for the trivial solution that $\vec{X} = \vec{0}$ which is of no interest, the equation is only fulfilled if the parenthesis disappears. This can be expressed as follows:

$$\underline{\underline{A}} - p \cdot \underline{\underline{E}} = \begin{pmatrix} -k_4 & 0 & \frac{-k_1 9 Z_0^8}{(1+Z_0^9)^2} \\ k_2 & -k_5 & 0 \\ 0 & k_3 & -k_6 \end{pmatrix} - p \cdot \begin{pmatrix} 1 & 0 & 0 \\ 0 & 1 & 0 \\ 0 & 0 & 1 \end{pmatrix} = \underline{\underline{0}}$$

The solution (often denoted the eigenvalue equation for the matrix) can be obtained from the requirement that the corresponding determinant should be = 0, i.e.

$$\det\left(\underline{\underline{A}} - p \cdot \underline{\underline{E}}\right) = \det \begin{pmatrix} -k_4 - p & 0 & \frac{-k_1 9 Z_0^8}{(1+Z_0^9)^2} \\ k_2 & -k_5 - p & 0 \\ 0 & k_3 & -k_6 - p \end{pmatrix} = 0$$

If the determinant is written explicitly one gets the following cubic equation for p

$$p^3 - rp^2 + sp + t = 0 \tag{7.10}$$

with

$$\begin{aligned} r &= k_4 + k_5 + k_6 \\ s &= k_4k_5 + k_4k_6 + k_5k_6 \\ t &= k_4k_5k_6 + k_2k_3\frac{k_1 9 Z_0^8}{(1+Z_0^9)^2} \end{aligned} \tag{7.11}$$

The last term in the expression for t in the equation can be developed, remembering our assumption that $Z^{10} \gg 1$ and that $Z^{10} = (k_1k_2k_3)/k_5k_6)$

$$t \approx k_4k_5k_6 + k_2k_3\frac{9k_1Z_0^8}{(Z_0^9)^2} = k_4k_5k_6 + \frac{9k_1k_2k_3}{Z_0^{10}} \approx 10k_4k_5k_6 \tag{7.12}$$

The resulting cubic equation

$$p^3 + (k_4 + k_5 + k_6)p^2 + (k_4k_5 + k_4k_6 + k_5k_6)p + 10k_4k_5k_6 = 0$$

can be solved in Scilab with the "roots" commands (see List. 7.1) as well as directly with an algorithm based on the Cardano equations.

Using the Cardano formula, Eq. 7.10 has first to be brought into a reduced form without the quadratic power p^2 term, i.e.

$$\tilde{p}^3 + o\tilde{p} + q = 0$$

with

$$\begin{aligned} \tilde{p} &:= p + \frac{r}{3} \\ o &:= s + \frac{r^2}{3} \\ q &:= 2\frac{r^3}{27} - \frac{sr}{3} + t \end{aligned}$$

For this equation one obtains three solutions

$$\begin{aligned} \tilde{p}_1 &= \underbrace{\sqrt[3]{-\frac{q}{2} + \sqrt{\frac{q^2}{4} + \frac{o^3}{27}}}}_{u_1} + \underbrace{\sqrt[3]{-\frac{q}{2} - \sqrt{\frac{q^2}{4} + \frac{o^3}{27}}}}_{v_1} \\ \tilde{p}_{2/3} &= -\frac{u_1+v_1}{2} \pm j\frac{u_1+v_1}{2}\sqrt{3} \end{aligned} \tag{7.13}$$

Listing 7.1: *Solution of the cubic polynomial according to the formula of Cardano in Scilab*

```
//
//Values of Ruoff 1999
k1=1; k2=1; k3=1; k4=0.2; k5=0.2; k6=0.1;
disp("parameter of the Goodwin-oscillator-model:")
mprintf("\n\r k1 = %1.1f, k2 = %1.1f, k3 = %1.1f, \n k4 = %1.1f, k5 = %1.1f, k6 = %1.1f
    \n",k1, k2, k3, k4, k5, k6)
//
//characteristic polynomial of 3rd grade
// x^3+r*x^2+s*x+t (see Bardal 2002)
r=k4+k5+k6; s=k4*k5+k4*k6+k5*k6; t=10*k4*k5*k6;
//
//zero order determination with "roots" of Scilab
xr = roots([1.0 r s t]);
disp("3 pole locations:"); disp(xr)
```

and to get the explicit p-solutions one has to use the formula $p = \tilde{p} - r/3$ again.

The algorithms give the outcome for the three roots $p = \sigma + j\omega$ in the following time dependent form:

$$x, y, z \sim e^{\alpha t} \cos(\omega t + \varphi)$$

where the exponential factor determines whether the respective coordinate increases or decreases with time, i.e. whether the singular point is unstable or not.

Specifically the algorithms give the following three solutions for the Goodwin model with the Hill parameter = 9 and the reaction rates k_1 - k_6 we have chosen to study:

1. $\alpha = -0,5$ and $\omega = 0$
2. $\alpha = +0,0$ and $\omega = 0.2828427$
3. $\alpha = +0,0$ and $\omega = -0.2828427$

Since the exponent is negative in the e-function for the first solution, the singularity (X_0, Y_0, Z_0) is stable (decreasing oscillation). In the second and third solution oscillations with the frequency $\omega = 0.2828427$ and *constant* amplitude will exist ($\alpha = 0$). In general both of these solutions can appear and add up.

However, if our parameter values k_4, k_5 or k_6 are changed, the exponent can be positive and an oscillation with increasing amplitude could arise - leading to an instability of the singular point and, possibly, to limit cycle oscillations of the system. This sensitivity of the oscillatory tendency towards changes of the parameters k_4, k_5 or k_6 can be studied with the *root locus response* (Evans 1950), as known from control theory.

We have already carried out a singularity study in a two dimensional case in Sect. 5.5. In the present section the three dimensional deviations from the singular point (i.e. x, y and z) resulted in a linear equation system of order three but solving such a system was fairly laborious. Different tools from control theory can also be used for the same purpose and are sometimes to prefer. Special algorithms of Scilab/Xcos are pertinent. The use of them will be outlined in the first part of Listing 7.1 and we will then see in detail how the properties of the singularity depend on the precise choice of parameter values in the system.

Some comments: We used a Goodwin model with six different reaction rate constants and one Hill exponent, p (which was attributed the value 9). By varying the parameters the model can be studied and one can get a "solution space" and new information, possibly leading to critical experiments and tests of the system.

The critical non-linearity in the Goodwin model is of the type $1/(1 + Z^p)$. The p coefficient has to be > 8 for oscillations to occur (Griffith 1968). The experimental support for having such a large coefficient is not published, as far as is known to the authors. Alternative "designs" of the Goodwin approach have been promoted and can be of interest to the reader; we mention papers by Richard D. Bliss 1982,Gonze, Bernard et al. (2005). Different versions of the Goodwin model were discussed in a master thesis by Conrad 1999.:

- **Introducing more variables**.
  The number of variables X, Y and Z in the Goodwin model can be increased without

changing the structure of the model. The procedure to discuss the stability can then be applied. The equations for an n-variable extension can be shown below, compared to the three variable system:

n variables:

$$\begin{aligned} X_1^{'} &= k_1/(1+X_n^p) - k_4 X_1 \\ X_2^{'} &= k_2 X_1 - k_5 X_2 \\ X_3^{'} &= k_3 X_2 - k_6 X_3 \\ \vdots &\ \vdots\ \ \vdots \\ X_n^{'} &= k_n X_{n-1} - k_{n+3} X_n \end{aligned}$$

3 variables:

$$\begin{aligned} X^{'} &= k_1/(1+Z^p) - k_4 X \\ Y^{`} &= k_2 X - k_5 Y \\ Z^{'} &= k_3 Y - k_6 Z \end{aligned}$$

-

It seems intuitively clear that the chain reactions in such a sequence could provide appreciable delays in the feedback system. This increases possibilities for oscillations even if the Hill constant p is < 8. We will discuss this later.

- **Introducing a new non-linearity**
  Leaving this extension of the model we turn our interest to a new version of the model: a further nonlinearity is introduced at another place in the equation system. We exemplify by mentioning the model presented by Richard D. Bliss 1982.

  Richard D. Bliss 1982 used another non-linear term in their three variable model, namely a non-linear breakdown reaction of the Z-variable. The reaction follows the so-called Michaelis-Menten kinetics. This kinetics is well known from enzyme reactions and relate the reactions rate v to form a product P from a substrate S as follows

$$v = d[P]/dt = V_{max} \cdot [S]/(K_M + [S])$$

  :

  In the equation V_{max} represents the maximum reaction rate achieved by the system at saturating substrate concentration. Biochemical reactions involving a single substrate are often assumed to follow Michaelis—Menten formalism (not always with regard to the underlying assumptions of the description).

  .

  The three variable model of Richard D. Bliss 1982 therefore looked like the following (we replace their constants etc. with symbols used before to facilitate a comparison with the

model discussed)

$$\begin{aligned} X^{'} &= k_1/(1+Z) - k_4 X \\ Y^{'} &= k_2 X - k_5 Y \\ Z^{`} &= k_3 Y - k_6 Z/(k_7 + Z) \end{aligned}$$

The Hill coefficient in the equation for X' is now = 1, but a new non-linearity appears in the rate constants of Z'. The structure of the Hill equation is, in fact, similar to the one for Michelis-Menten kinetics but the position in the equation system and the interpretation is different.

A study of the oscillations of the Bliss et al. model follows the outline given for the Goodwin oscillator. The singularity is easily derived and gives the coordinates

$$\begin{aligned} X_0 &= k_1/k_4(1+Z_0) \\ Y_0 &= k_2/k_5 X_0 \\ Z_0 &= k_3 k_{70}/(1 - k_3 Y_0) \end{aligned}$$

A Scilab diagram for this model version of the model is shown in Fig. 7.17. We leave it as a task for the reader to find a set of parameter values to produce oscillations.

- **Introducing discrete time lag, the Scheper model Scheper 1999**
  We have already introduced the concept of time lag in an oscillating model (see Section 7.1). Broadly speaking a feedback loop requires a sufficient phase shift of the signal in the loop in order to produce oscillations. The phase shift can arise due to discrete time lags of the signal, as was demonstrated in the discussion of the Karlsson and Johnsson model, Section 7.1.

  Scheper (Scheper 1999) used a two variable oscillator model of central pacemaker neurons of the supra-chiasmatic nucleus (SCN). This tissue plays a fundamental role in the mammal circadian system, see subsection 6.2.2. The model is based on the mRNA participating in the production of a protein, in turn acting on the mRNA production rate constant via a negative feed back loop, thus a TTFL model.

  The model contains non-linearities and a discrete time lag 1. This delay represents the duration of the so- called the 'protein synthesis cascade'. The essential parts of this model of the SCN pacemaker neurons can be schematically depicted as shown in Fig.7.18.
  The corresponding equations in a form that facilitates a comparison with the previous models:

$$\begin{aligned} dX/dt &= k_1/(1 + (Y/k)^n) - k_2 X \\ dY/dt &= k_3 X(t-\tau)^m - k_4 Y \end{aligned}$$

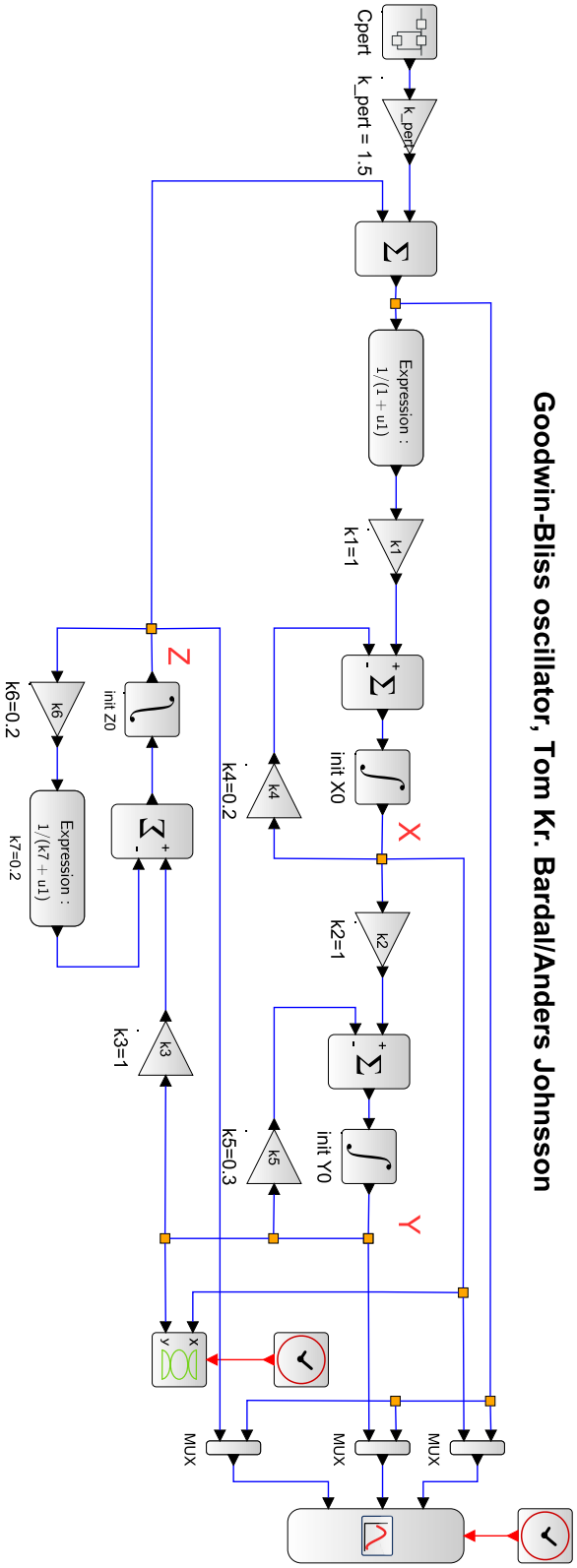

Figure 7.17: *The Goodwin oscillator, modified by Bliss (Richard D. Bliss 1982) and Bardal-Johnsson (Bardal 2002).*

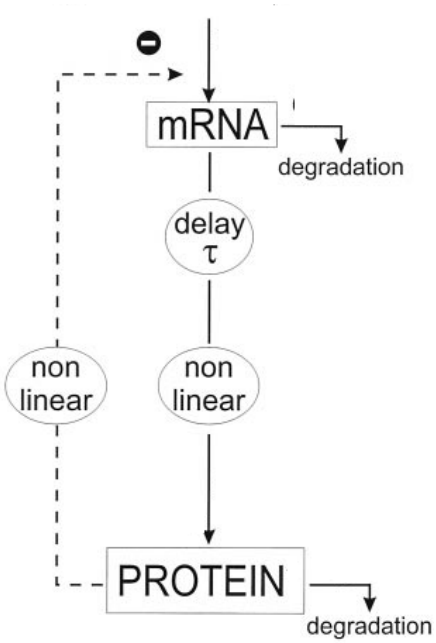

Figure 7.18: *Simplified figure after Scheper 1999 Model interpretation of the biological elements of the protein synthesis cascade, assumed to be elementary to the circadian rhythm generator. Model emphasize the delay (τ) and non-linearity in the protein production cascade, the non-linear negative feedback, as well as the mRNA and protein production and degradation.*

Observe the discrete time lag τ, the non-linearities and that the Hill coefficient — here denoted n - can attain low values without preventing oscillations. For a value of $T = 4.0$ h the parameters can be chosen so as to achieve an overall oscillatory period of 24.6 h. The Hill coefficient is then 2.0 and the non-linearity coefficient m in the protein synthesis cascade is chosen to be 3.0 (see Scheper 1999).

- **Introducing distributed time lags.**
  A basic differential equation involving a discrete time lag was mentioned earlier (see discussion point befor)

$$dX/dt = -k \cdot X(t - \tau)$$

and it appears in several chapters. The reaction rate can be said to be determined by the concentration at a certain, discrete, time τ earlier than t (as well as by the rate constant k). If one would model a reaction where the rate is determined be the concentration at several times earlier, a sort of "memory" function K(t) can be used:

$$dX/dt = \int K(\tau)X(t - \tau)\, d\tau$$

The K(t) function weighs different values of the X(t) and the integral sums them up. The shape of the K-function — often denoted the Kernel function — is usually showing a maximum and is then decays towards zero (X(t) ("values of X(t) a long time ago does influence the reaction rate less and less the bigger the τ .

We mention this since it is often natural to include discrete/distributed time lags in model simulations (see e.g. Conrad 1999).

7.3.1 Appendix to the Goodwin Oscillator

This appendix contains three parts: The first part below, the second one on page 181, and the third one on page 182.

1st part of Appendix to the Goodwin Oscillator: The root locus method introduced by Evans 1950 is an elegant method to solve algebraic equations. One can clearly deduce from a plot how the variation of a parameter affects the stability of the system under study.

In a simple feedback system according to Fig.5.12 the output signal y is the result of the forward transfer function F_v working on its *input* $= (x - y \cdot F_R)$. The transfer function of the overall feedback system $G(p)$ will therefore be

$$G(p) = y(p)/x(p) = F_v(p)/(1 + \underbrace{F_v(p) \cdot F_R(p)}_{F_0(p)}) \tag{7.14}$$

We can write the product of the forward transfer function times the backward transfer function as $F_v(p) \cdot F_R(p) = F_0(p)$, and $F_0(p)$ will be the overall amplification of the opened feedback. We see that the stability of the feedback system is determined by the zero points (or roots) of the denominator of $G(p)$. So, the overall feedback system will have **poles** or **singularities** where

$$1 + F_0(p) = 0, \text{ with } F_0(p) := K \cdot \tilde{F}_0(p) \tag{7.15}$$

where K is a new parameter we have introduced. The special case of $K = 1$ is thus embedded in the more general solution to Eq. 7.15. In the root locus method the factor K will be varied in the interval $(0, \infty)$ to evaluate and study the roots of the equation and, thus, providing clues to the singularities of $G(p)$.

In the case of the Goodwin oscillator the stability of the point of singularity was determined above by the zero points of the polynomial in Eq. 7.10:

$$p^3 + (k_4 + k_5 + k_6)p^2 + (k_4k_5 + k_4k_6 + k_5k_6)p + 10k_4k_5k_6 = 0 \tag{7.16}$$

If one can transform this polynomial into the form of equation above, i.e. $1 + K \cdot \tilde{F}_0 = 0$ the root locus method can be used here, also for studies of the Goodwin oscillator. Then the equation for the feedback system according to Eq. 7.16 is not examined directly but by a study of the zero's and poles of $F_0(p)$. This can occasionally be an easier way of analysis. We can exemplify by factoring out k_5 and rewrite Eq. 7.16:

$$k_5(p^2 + (k_4 + k_6)p + 10 \cdot k_4k_6) + p^3 + (k_4 + k_6)p^2 + (k_4k_6)p = 0$$

Further on we can introduce a general variable K instead of k_5:

$$1 + K(p^2 + (k_4 + k_6)p + 10 \cdot k_4k_6)/p^3 + (k_4 + k_6)p^2 + (k_4k_6)p = 0$$

and get the expression sought for and in accordance with Eq. 7.15.

$$1 + K \underbrace{\frac{p^2 + (k_4 + k_6)p + (10 \cdot k_4 k_6)}{p \cdot (p^2 + (k_4 + k_6)p + k_4 k_6)}}_{\tilde{F}_0(p)} = 0 \tag{7.17}$$

We have, therefore, succeeded in transforming the equation for the Goodwin oscillator into a form that is suitable for the application of the root locus method. The choice of the factor k_5 is motivated from our wish to vary the magnitude of this reaction rate and see how this affects the system properties. The rate constant k_5 from the Goodwin model will now correspond to *one* value of K. k_5 is 'embedded' in the solution to the equation for K.

From Eq. 7.16 one can see that if the parameters k_4 and k_5 are varied in the same way, the result will be identical changes in each term in Eq.7.16 due to the symmetries in the three terms. Therefore one does not need to explore the variation of k_4 if the variation of k_5 is known, and vice versa. We chose to study the solutions for the system when first k_5 (thus also k_4) and then k_6 is varied.
We should also for the following discussion remember the parameter choices made, viz.

$$k_1 = k_2 = k_3 = 1, k_4 = k_5 = 0.2 \text{ and } k_6 = 0.1$$

These root locus curves were established under Scilab using the command "evans". 7.2.

2nd part Appendix to the Goodwin Oscillator: Root loci, varying $\mathbf{k_5}$ or $\mathbf{k_4}$: We will now derive the locus diagram for the rate constant $\mathbf{k_5}$ (and $\mathbf{k_4}$ shows the same pattern, as mentioned above). In the first appendix above we factored out the variable $\mathbf{k_5}$ in the equation for the Goodwin system. The equation was transformed into the form of a feedback system

$$1 + K \cdot \tilde{F}_0 = 0 \tag{7.18}$$

and explicitly $F_0(p)$ became the values of its roots are easy to specify: From the denominator

$$p \cdot (p^2 + (k_4 + k_6)p + k_4 k_6) = 0$$

it follows that the values for the three poles p_i with i = 1, 2 and 3, are:

$$\begin{aligned} p_1 &= 0 \\ p_2 &= -k_4 \\ p_3 &= -k_6 \end{aligned} \tag{7.19}$$

For the two roots of the numerator of $\tilde{F}_0(p)$, $p^2 + (k_4 + k_6)p + (10 \cdot k_4 k_6)$, we get the zeroes denoted $p_{oi} (i = 1 \text{ and } 2)$

$$p_{01/02} = -\frac{k_4 + k_6}{2} \pm \sqrt{\left(\frac{k_4 + k_6}{2}\right) - 10 k_4 k_6} \tag{7.20}$$

First pole of the open system has then a zero point and the second and third ones contain

just one parameter, viz. k_4 or k_6. The real part of the zeros lies at the mean value of k_4 and k_6 according to formula 7.20 i.e. at $-(k_4 + k_6)/2$. One also sees that for k_4 and $k_6 > 0$ (which is to be assumed since $k_4 = 0.2$ and $k_6 = 0.1$ in the neighbourhood of $k_5 = 0.2$) the zero location of the closed system 7.18 has a real part of ≈ 0. This can also be confirmed by direct calculation using the "roots" function of Scilab of the Cardano's formula (see List. 7.2).

Listing 7.2: *Creating the root locus curve 7.19 for the solution of the polynomial*

```
//Values of Ruoff 1999
k1=1; k2=1; k3=1; k4=0.2; k5=0.2; k6=0.1;
disp("parameter␣of␣the␣Goodwin-oscillator-model:")
mprintf("\n\r␣k1␣=␣%1.1f,␣k2␣=␣%1.1f,␣k3␣=␣%1.1f,␣\n␣k4␣=␣%1.1f,␣k5␣=␣%1.1f,␣k6␣=␣%1.1f
    ␣\n",k1, k2, k3, k4, k5, k6)
//characteristic polynomial 3rd degree x^3+r*x^2+s*x+t with
// r=k4+k5+k6; s=k4*k5+k4*k6+k5*k6; t=10*k4*k5*k6;
//After factoring out k5 it follows:
//x^3+(k4+k6)x^2+k4k6x+k5[x^2+(k4+k6)x+10k4*k6]=0
//if one now divides by:=x^3+(k4+k6)x^2+k4k6x, it follows:
//1+k5[{x^2+(k4+k6)x+10k4k6}/{x^3+(k4+k6)x^2+k4k6x}] = 0
//
// 1+kF(x) = 0 with k=k5 with
//F(x):=[{x^2+(k4+k6)x+10k4k6}/{x^3+(k4+k6)x^2+k4k6x}]
//
//This can be solved with the root locus curve method after Evans by
//variing k=k5 from 0 to kmax.
x = poly(0,'x'); kmax=2.5;
num = x^2+(k4+k6)*x+10*k4*k6;
den = x^3+(k4+k6)*x^2+k4*k6*x;
sys=syslin ("c" , num/den);
evans(sys,kmax)
legend(["pole␣locations␣of␣the␣open␣circles"; "zeros␣of␣the␣open␣circles"],3)
xlabel("$\alpha$", "fontsize",5); ylabel("$\omega$", "fontsize",5);
title("root␣locus␣curve␣after␣Evans","fontsize", 5)
set(gca(),"grid",[16 16])
```

The root locus curve is the result when our amplification factor K in Eq. 7.18 is varied in the interval $(0, \infty)$ and the root coordinates are plotted in a diagram with frequency ω vs. amplitude factor α. The points are connected and Fig. 7.19 shows the result. The sensitivity in Fig. 7.19 changing the parameter K (i.e. k_5 as seen from Eq. 7.18) can be recognised if the diagram is expanded for a value of K around 0.2. This is done in Fig.7.19 and it demonstrates that a small variation in K around 0.2 can cause a slight increase of the oscillation (α is balancing at zero value). At the other ranges of the root locus the real part of the p values stays negative, which corresponds to a decreasing oscillation. Here the unperturbed system is stable without oscillation.
These root locus curves were calculated in Scilab, using the Listing 7.2.

3rd part of Appendix to the Goodwin Oscillator: Varying k_6

Analogously to the variation of k_5 in Eq. 7.16 the parameter k_6 should be factored out:

$$p^3 + (k_4 + k_5)p^2 + (k_4k_5)p + k_6(p^2 + (k_4 + k_5)p + 10 \cdot k_4k_5) = 0$$

and after a division by the sum of the terms without k6 one obtains7.33

$$1 + k_6 \cdot \frac{p^2 + (k_4 + k_5)p + (10 \cdot k_4k_5)}{p \cdot (p^2 + (k_4 + k_5)p + k_4k_5)} = 0 \tag{7.21}$$

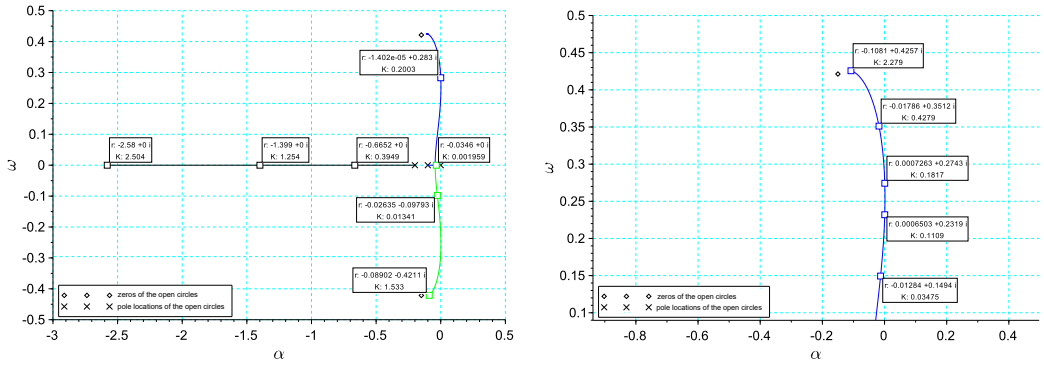

Figure 7.19: *Left: Root locus curve (after Evans) for the pole locations of the polynomial according to Eq.7.15 and Eq. 7.17 if $k = k_5$ are varied. For $k \approx 0$ the curve begins at the zeros of the open system and at $k \to \infty$ it ends at its pole locations. The parameter r at the data points on the curves shows the local values of the pole location.*
Right: Surroundings of the root locus curve in Fig. 7.19 for the pole locations of the polynomial Eq. 7.17 according to Eq. 7.15 and Eq. 7.18 in the vicinity of $k = k_5 \approx 0.2$

A comparison with Eq. 7.17 shows that now we have simply replaced k_6 with k_5 in $\tilde{F}_0(p)$. Therefore, the results after varying k_5 can now be used for the variation of k_6 if the indices are changed. For the denominator

$$p \cdot (p^2 + (k_4 + k_5)p + k_4 k_5) = 0$$

it follows for the three roots p_i with $i = 1, 2$ and 3 :

$$\begin{aligned} p_1 &= 0 \\ p_2 &= -k_4 \\ p_3 &= -k_5 \end{aligned} \tag{7.22}$$

p_2 and p_3 are of the same size since $k_4 = k_5 = 0.2$. That is, we have a simple zero at $p_1 = 0$ and a double pole located at $p_2 = p_3$, which shifts the root locus curve when comparing with the one previously treated above. For the locations of the two zeroes p_{0j} (with $i = 1$ and 2) we get from the numerator

$$p^2 + (k_4 + k_5)p + 10 \cdot k_4 k_5 = 0$$

that

$$p_{01/02} = -\frac{k_4 + k_5}{2} \pm \sqrt{\left(\frac{k_4 + k_5}{2}\right) - 10 k_4 k_5} \tag{7.23}$$

We see here too that for k_4 and $k_5 > 0$ (which is the case since $k_4 = k_5 = 0.2$ in the neighbourhood of $k_6 = 0.1$) the pole location of the closed system Eq. 7.15 has a real part of ≈ 0. The algorithm of Scilab is the same as above, if in the variable "num" and "den" k_6 is replaced by k_5. Fig. 7.20 show the corresponding root locus curve.

The sensitivity to changes in parameter k_6 can be seen if we amplify the root locus curve as shown in Fig. 7.20 for a value of $k = k_1 = 0.1$. One can recognise that a varying k_6 in the range around $k_6 = 0.1$ up to about 0.4 a small increase of the oscillatory tendency is possible. In the other ranges of this locus curve the real part α of the poles stays negative (again as in the variation of k_5), which leads to a decreasing amplitude of the oscillations.

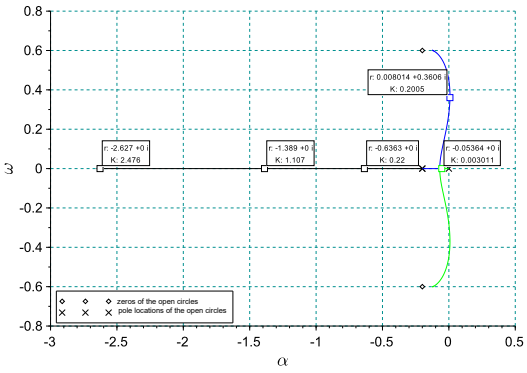

Figure 7.20: *Root locus curve after Evans for the pole locations of the polynomial according to Eq.7.15 and Eq. 7.21 if $k = k_6$ are varied. For $k \approx 0$ the curve begins at the zeros of the open system and at $k \to \infty$ it ends at its pole locations. The parameter r at the data points on the curves shows the local values of the pole*

7.4 The Goldbeter oscillator

Goldbeter developed models for various cyclic processes starting with Cyclin, a family of proteins that controls the cell cycle by activating cyclin-dependent kinase.

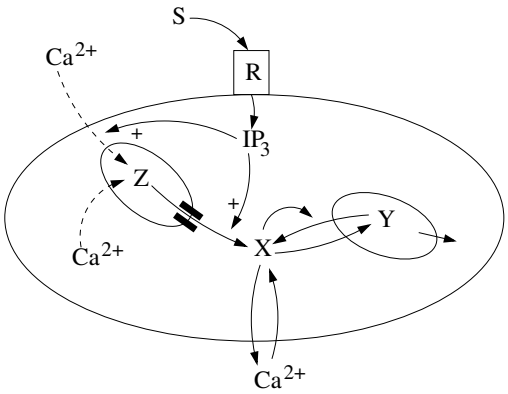

Figure 7.21: *The Goldbeter model for* Ca^{2+} *oscillations uses 3 storages for* Ca^{2+}*: X in the cell, Y and Z.* Ca^{2+} *can enter and leave the cell. Signals (S) are received by receptors (R) and influence via IP3 (inositol-1,4,5-triphosphate) positively the uptake and discharge of* Ca^{2+} *from outside and inside the cell into the IP3 sensitive* Ca^{2+}*-storage Z. Y is a IP3* insensitive Ca^{2+}*-storage which is in exchange with the cell* Ca^{2+} *X. After (Goldbeter, Dupont, Berridge 1990) from (Aanes 2011). Afterwards the model was used to simulate the glycolysis oscillation (Goldbeter, Lefever 1972)*

Afterwards the model was used to simulate the glycolysis oscillation (Goldbeter, Lefever 1972), Ca^{2+} oscillations (Goldbeter, Dupont, Berridge 1990), circadian oscillations in the *Drosophila*

period protein (Goldbeter 1995), circadian rhythms in *Neurospora* (Gonze, Leloup, Goldbeter 2000), in *Cyanobacteria* (Gonze, Roussel, Goldbeter 2002), in the mammalian circadian clock (Leloup, Goldbeter 2003; Leloup, Goldbeter 2004) and jet-lag and for sleep disorders (Goldbeter, Leloup 2021). Entrainment and the amplitude of the circadian oscillation is presented in Kurosawa, Goldbeter 2006 and the induction of arrhythmicity by a single light pulse was successfully simulated (Leloup, Goldbeter 2001; Leloup, Goldbeter 2013). For minimal models for circadian oscillations see Gérard, Gonze, Goldbeter 2009, for circadian rhythms and systems biology see Goldbeter, Gérard, Leloup 2010. A paper on biological switches and clocks is Tyson, Albert et al. 2008, and a book by Goldbeter are Goldbeter 1996, a link is Au coeur des rythmes.

The Goldbeter basic model ispresented here as a kind of unit model (valid for one cell). It will be used extensively in Chap. 8, for example to simulate circumnutations (Sect. 8.4), by extending its use in coupling several cells together. There simulations are done for one cell, two coupled cells and six cells in a ring, furthermore for cell cylinders with various numbers of cells in a ring and different numbers of rings on top of each other forming a cylinder. Our Scilab simulations are often based on reports by our graduate and master students and their extensive work on modelling – which we gratefully acknowledge. The thesis by (Aanes 2011) summarize parts of the work in our groups in the field and has been very useful.

Here we use the Goldbeter model as a minimal model for Ca^{2+} oscillations as shown in Fig. 7.21. Expressed with reaction kinetic differential equations one obtains

$$\boxed{\begin{array}{rcl} \dot{X} & = & v_0 + v_1\beta - f(X,Y) - kX \\ \dot{Y} & = & f(X,Y) \\ f(X,Y) & = & \frac{v_{M_2}X^n}{K_2^n+X^n} - \frac{v_{M_3}Y^m}{K_R^m+Y^m}\frac{X^p}{K_A^p+X^p} - k_fY \end{array}}$$

in which important variables and parameters are:

- $\dot{X}$: Alteration rate of intracellular Ca^{2+} per time unit
- $\dot{Y}$: Alteration rate of IP_3 *insensitive* Ca^{2+} per time unit
- v_0: extracellular constant influx of Ca^{2+}
- $v_1\beta$: IP_3- affected influx of Ca^{2+} storage

The singular point X_0 and Y_0 (no oscillation) is valid for:

$$\begin{array}{rcl} \dot{X}\big|_{X_0,Y_0} = 0 & = & v_0 + v_1\beta - f(X_0,Y_0) - kX_0 \\ \dot{Y}\big|_{X_0,Y_0} = 0 & = & f(X_0,Y_0) = \frac{v_{M_2}X_0^n}{K_2^n+X_0^n} - \frac{v_{M_3}Y_0^m}{K_R^m+Y_0^m}\frac{X_0^p}{K_A^p+X_0^p} - k_fY_0 \end{array}$$

as an example the following model parameters: $v_{M_2} = 20, v_{M_3} = 23, K_2 = k_f = 1, K_R = k = 0,8$, $K_A = 0,9, m = n = 1, p = 2$ and $v = v_0 + v_1\beta = 0,325$: :

$$\begin{array}{rcl} X_0 & = & v/k = 0,40625 \\ Y_0 & = & 2,75964 \end{array}$$

Result: The Ca^{2+} point of rest X_0 is *independent of the non-linearity* and depends only on the influx v and the feedback factor k.

The following ways of studying the *stability* exist:

1. *Linearisation* at the points of rest for X_0 and Y_0, i.e. $f(X,Y)$ is replaced by a flat plane and only small changes in x and y of $X = X_0 + x$ and $Y = Y_0 + y$ are studied and checked, whether they increase.
   - *Advantage:* The poles (points of instability) and zero points (no oscillations) of the system can be calculated easily.
   - *Disadvantage:* Errors in the case of large amplitudes of the oscillation, whereby the errors become too large due to linearity approximation.
2. Instead of points of singularity the Lyapunov coefficients are identified. They show, whether a stable point of attraction exists (so called attractor).
   - *Advantage*: No need to linearise the system.
   - *Disadvantage:* Calculation is difficult.

In the case of *linearisation* at the points of rest: Because of

$$X := X_0 + x \text{ and } Y := Y_0 + y$$

for small changes in x and y around the points of rest X_0,Y_0 results the *linear equation system*:

$$\begin{aligned} \dot{x} &= -\left.\frac{df(X,Y)}{dx}\right|_{X_0,Y_0} x - kx - \left.\frac{df(X,Y)}{dy}\right|_{X_0,Y_0} y \\ \dot{y} &= \left.\frac{df(X,Y)}{dx}\right|_{X_0,Y_0} x + \left.\frac{df(X,Y)}{dy}\right|_{X_0,Y_0} y \end{aligned}$$

For the changes of the Ca^{2+} concentrations x and y one obtains e.g. for the parameter values $v_{M_2} = 20$, $v_{M_3} = 23$, $K_2 = k_f = 1$, $K_R = k = 0,8$, $K_A = 0,9$, $m = n = 1$,$p = 2$:

$$x, y \sim e^{\alpha t}\cos(\omega t + \varphi), \text{ mit } \alpha = 0.092,\ \omega = 0.994$$

Since the exponent α in the e function is positive, the point of rest X_0, Y_0 becomes <u>*unstable*</u> (increasing oscillation)!
In Scilab/Xcos the model would be as shown in Fig. 7.22, and the output signals and phase diagram are presented in Fig. 7.23

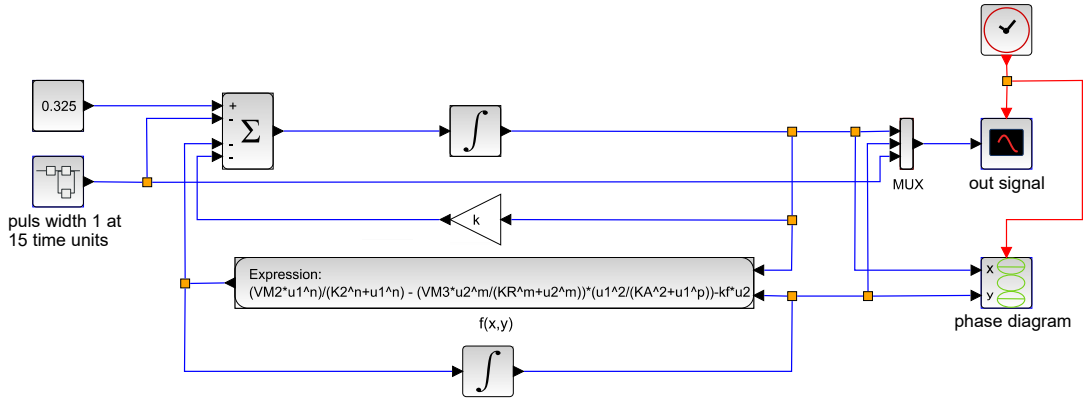

Figure 7.22: *The Goldbeter feedback model for* Ca^{2+} *oscillations is shown here for the following parameters:* $v_{M_2} = 20$, $v_{M_3} = 23$, $K_2 = k_f = 1$, $K_R = k = 0,8$, $K_A = 0,9$, $m = n = 1$, $p = 2$, $v = v_0 + v_1\beta = 0,325$. *After (Goldbeter, Dupont, Berridge 1990) in Aanes (2011)*

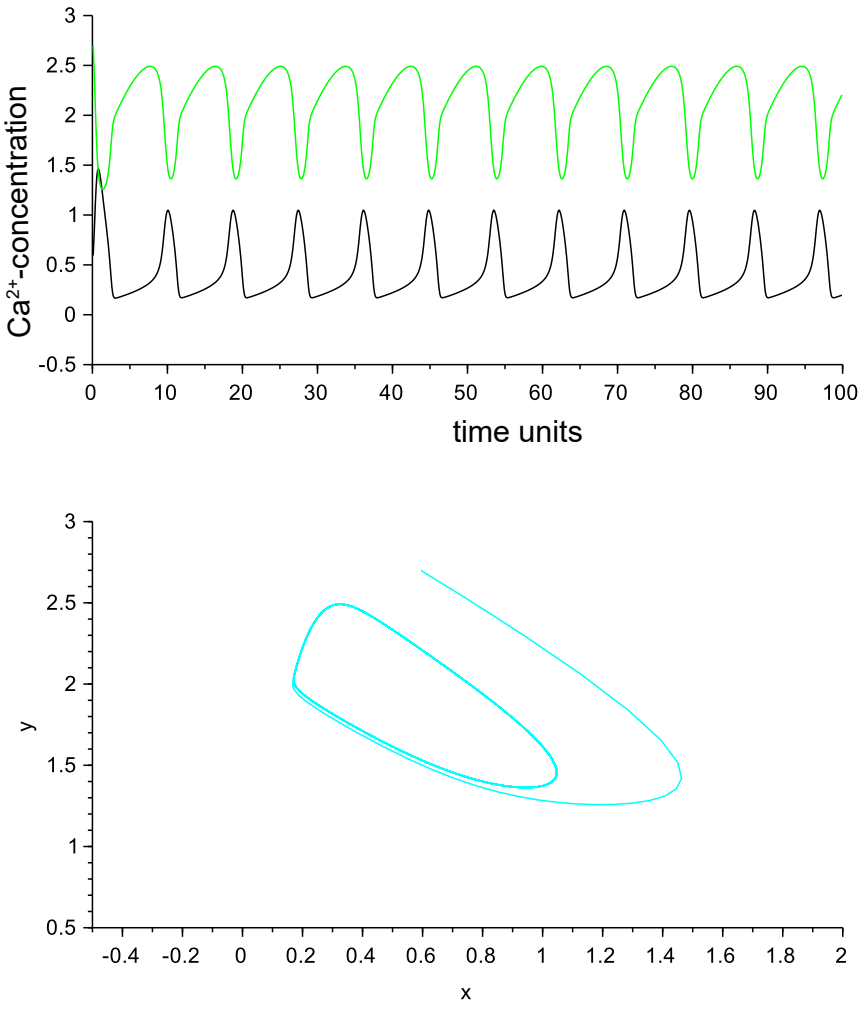

Figure 7.23: *Output signals and phase diagram from Scilab simulations on the Goldbeter model as shown in Fig.7.22 Top: Output signals from Scilab simulations of the Goldbeter model for* Ca^{2+} *concentration (black curve) and the IP3 insensitive* Ca^{2+} *concentration (green curve). Bottom: Phase diagram of the two oscillations as shown at the top.*

If a disturbing pulse is administered, the output looks like shown in Fig. 7.24. There is an immediate disturbance, but the old phase relationship is quickly reestablished.

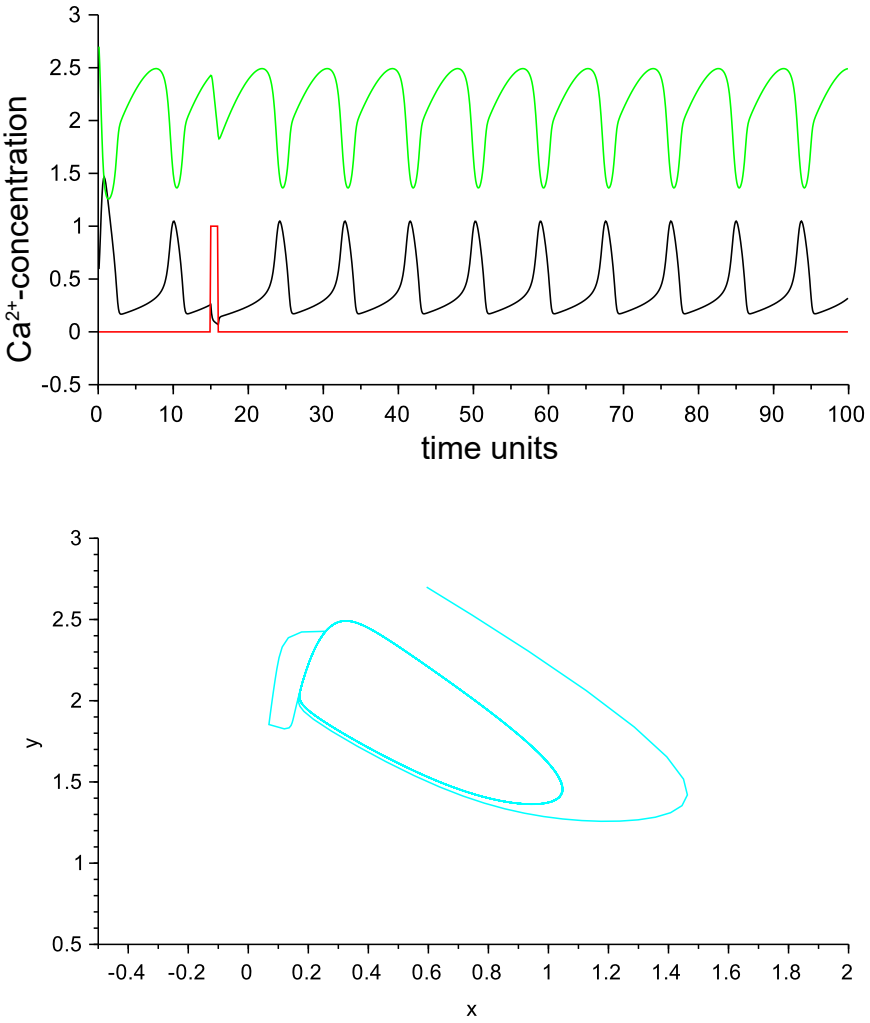

Figure 7.24: *The Goldbeter model - output signals and phase diagram with disturbing pulse (cf. Fig. 7.22) . Top:Oscillations of the* Ca^{2+} *concentration (black curve) and the IP3 insensitive* Ca^{2+} *concentration (green curve). Red pulse: perturbations. Bottom: Phase diagram of the two oscillations as shown in top figure.*

7.5 The Cowan oscillator for rhythmic transpiration in plants

In this section we would like to concentrate on the fact that oscillations occur in the transpiration of plants. The small leaf openings that allow the water flux from the inner parts of the leaf

to the atmosphere – the stomata - are regulated by volume changes of guard cells around the opening (see Fig. 3.11 in subsect. 3.3.2). It is important to understand *how* plants regulate these openings, necessary for photosynthesis and the uptake of CO_2, but also for the plant's uptake of water and its transpiration (water transports necessary substances such as minerals from the root system to the growing parts of the plants).

Thus biomass production is a matter of not only uptake of carbon dioxide but also coupled to the release of water. The so called *Water Use Efficiency* (WUE) is a measure of the relation between the biomass production of a plant relative to its *use* of water.

C3 and C4 plants have typically a WUE around 1 – 5 g dry weight biomass per 103 g water (i.e. a difference of the order of 100!). Increase of biomass production, but with less transpiration is thus preferable and connected with a higher WUE value.

To understand the intricate stomata control mechanisms we have to study *how* they proceed. But, they also present the demanding question, *why* these mechanisms show oscillations (as mentioned before). No conclusive answer seems to be given for the time being, but tentative discussions/experiments could take a starting point in the concept of WUE. Some interesting results indicate that if the transpiration oscillates, the WUE can, in fact, *increase* during temporary limitations in water supply (Upadhyaya, Rand, Cooke (1988) and see overview Yang et al. (2021) and Yoo et al. (2009)). The transpiration oscillations might, therefore, contribute to the plants ability to sustain and survive during dry periods – indicating a rationale from an evolutionary point of view and a tentative answer to the *why* question.

7.5.1 Macroscopic water transport via guard cells

The guard cells have dimensions of about 10 μm. Albeit small, they are often abundant and cover most often the lower side of leaves (sometimes also the upper side, e.g. in water plants). The density can for example be about 75 stomata per square mm (typical for a primary leaf of an oat shoot).

It can be illustrative to shortly emphasise the importance of the guard cells and mention some quantitative measures from a global point of view. The water that is evaporated from the Earth's surface in the global water cycle is to a certain extent evaporation from terrestrial plants. The overall stomata transpiration is estimated to account for 80 to 90 % of the terrestrial evaporation. This corresponds to about 60 000 cubic km water per year (i.e. about $60x10^{15}$ kg per year). Data of this order have been found by several investigators (e.g. Jasechko et al. 2013). Simultaneous with this water (vapour) stream outwards through the stomata openings the guard cells also control the CO_2 influx to the photosynthetic apparatus through the same openings. The estimated flux of CO_2 through the guard cells is of the order of $125x10^{12}$ kg per year (e.g. Beer et al. 2010).

The guard cells' importance for these essential gas transports through the stomata should be obvious. It is interesting that the water transpiration is often found to be oscillatory. The period of the transpiration varies from species to species and differs dependent on external conditions, but often found to be in the range of some minutes to a few hours.

7.5.2 Hydraulic model for oscillatory water transpiration and guard cell regulation at the organism level

Hydraulic models have been published and used in the interpretation of "overall" oscillatory plant transpiration. They can describe the water transport in an individual plant and also be used to simulate oscillations in the transpiration. An electric analogue is given in Fig. 7.25. The picture provides the basis for the modelling as proposed by Cowan (1972) and is later discussed by a.o. Gumowski 1983; Johnsson 1973; Johnsson 2015 and also Prytz 2001. Other hydraulic models have been published also by e.g. Delwiche, Cooke 1977.

In Fig. 7.25, Ψ represents water potentials (corresponding to electric potentials), R hydraulic resistances (electric resistances), i water fluxes (electric currents) and W the water content of cells ("charge" of condenser). The index g stands for guards cell, s for subsidiary cell and m for other cells (mesophyll) in the leaves. The stomata pore is regulated by the circuit in the upper right corner of the scheme and the transpiration flux i_a is a function of the water content W_g and W_s, i.e. $i_a = f(Wg, Ws + \text{other variables})$. The symbol Δ stands for applied water changes in the guard cells (which will be used later in this sub-subsection).

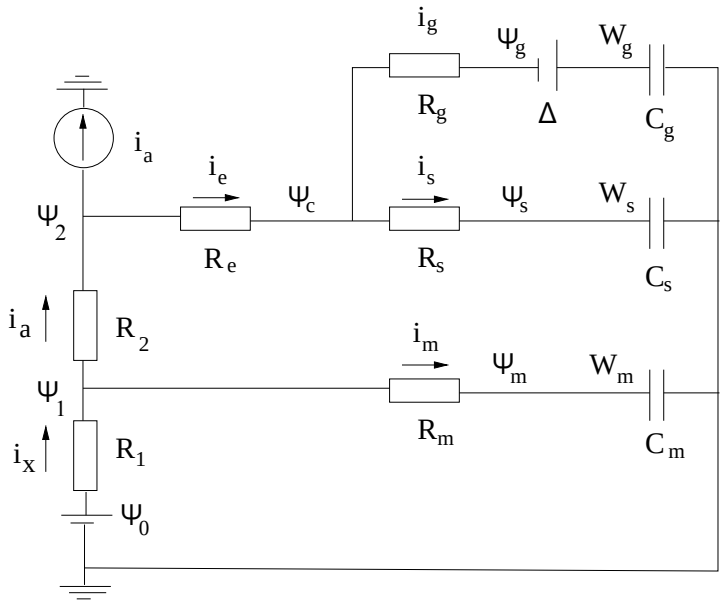

Figure 7.25: *Hydraulic model of plant water regulation (based on Cowan 1972).*
Ψ represents water potentials (corresponding to electric potentials), R hydraulic resistances (electric resistances), i water fluxes (electric currents) and W the water content of cells ("charge" of condenser). The index e stands for epidermis cell, g for guard cells for subsidiary cell and m for other cells (mesophyll) in the leaves. The stomata pore is regulated by the circuit in the upper right corner of the scheme and the transpiration flux i is a function of the water content W_g and W_s, i.e. $i_a = f(Wg, Ws + \text{other variables})$. The symbol Δ stands for applied water potential changes in the guard cells. Redrawn from Prytz 2001

The model is of course a lumped model, and can represent one whole plant on the organism level (however, it does not exclude the possibility that each stoma behaves identically).

One sees that the water (current) taken up moves through the root resistance R1 and along the stem /base into the schematically and lumped guard cells and their subsidiary cells. Ψ_x is the water potential outside the root, possible to modify osmotically, i_x stands for the water flux upwards through the stem (x for xylem vessels). The guard cells are represented by the condensers and are capable of swelling and shrinking (charging). The same is true for the subsidiary cells. The stomata opening is influenced by the volume (charge) of the cells, and the stomata opening is thus affected both by the guard cells and the subsidiary tissue. The time constants of charging the cells plays an important role in the dynamics of the model.

The stomata cavity "releases" its humid content dependent on the water vapour gradient and the opening area - meaning the external parameters (temperature, diffusion barrier, wind speed, relative humidity etc) as well as the internal conditions (the water content of the plant, the relative humidity in the stomata cavity, the rate of photosynthesis, the physiological status of the guard cells etc) plays an interacting role in the transpiration of the leaf, which can be measured with different methods.

The passive elements of this macroscopic, hydraulic model are of course represented by the water conducting elements and water-storing elements. The dynamic elements of the model are represented by the mechanisms that alter the volume changes of the guard cells and the subsidiary tissue into controlled opening of the stomata.

The model above has proved to describe several relevant experimental results in many species. Simulations with parameters given by Cowan 1972 have been used (Gumowski 1983) to produce oscillations with a relevant period, amplitude and curve form. Furthermore, light treatments as well as changes of the osmotic root medium can be simulated.

Gumowski 1983 points out that observed changes in the form of the transpiration curve can be explained under certain restrictions on the model. The model has especially been tested on smaller plants, but bushes and small trees have also been reported to show transpiration oscillations.

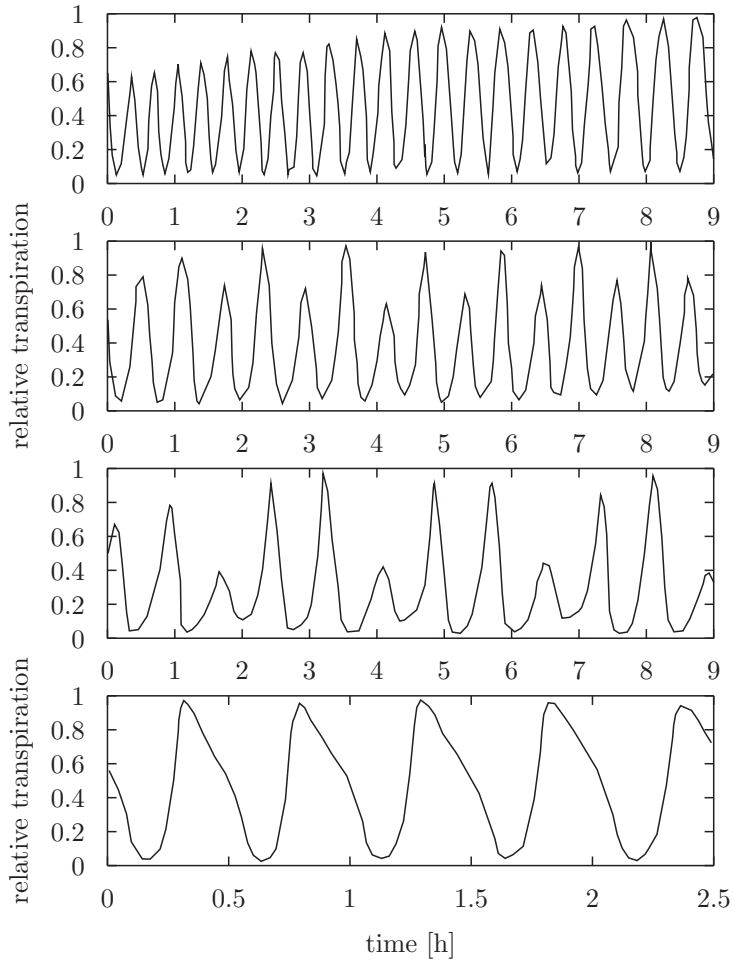

Figure 7.26: *Examples of whole leaf transpiration oscillations discussed and simulated with the model of Prytz. Top curve shows ordinary sine shaped oscillations. Second curve shows period doubling or period-2 oscillation, third curve shows period-3 oscillations, and fourth curve a slightly deformed ordinary oscillations. Redrawn from Prytz 2001*

7.5.3 Strength of coupling of oscillating stomata over leaf surface

In subsect. 8.1 *coupled* oscillators will be discussed. Calcium played a central role in each individual cell (and we choose to study oscillators of the Goldbeter model type, see sec.7.4). The simulations indicated that different patterns could arise if oscillators were coupled in a 2D area. Comparing the results of these simulations in 2D corresponding to a leaf surface with individual guard cells coupled together reveals some interesting similarities.

For the time being, we just recall that 2D-simulations of calcium sensitive units can reveal features relevant for and found also in leaves with oscillating transpiration (guard cell controlled). Conditions were also found in which different parts of an "area" of coupled cells could be synchronised but without being totally in phase over the whole area.

"Patchy" behaviour has been reported also in transpiration oscillations (e.g. Haefner, Buckley, Mott 1997) and one example can be shown in Fig. 7.27, which clearly demonstrates that not all parts of the recorded leaf are in synchrony.

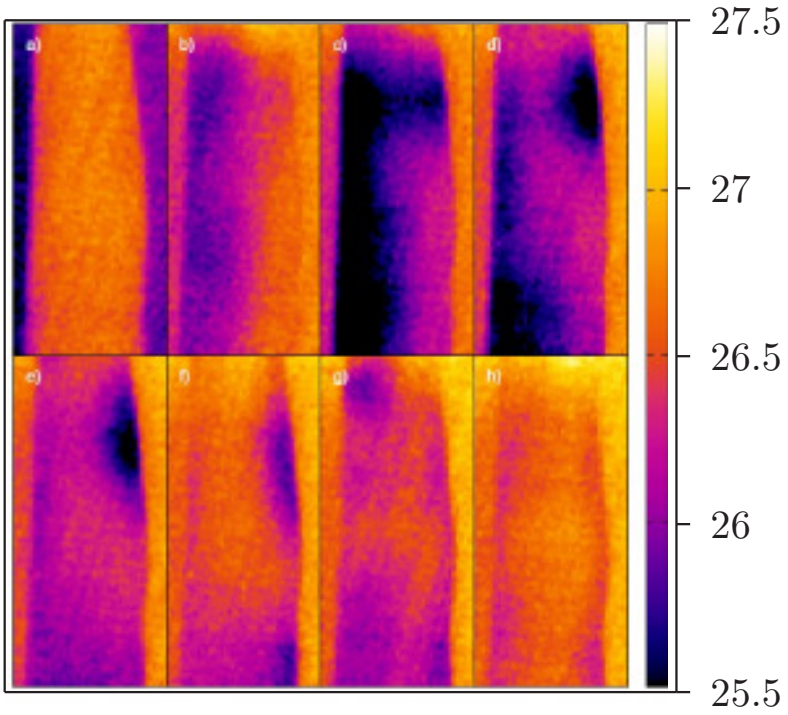

Figure 7.27: *Thermograms (camera recording temperatures between 27,5 and 22,5°C) Figures demonstrate a patch-like temperature distribution due to stomatal conductance in a leaf of* Avena. *Top row images recorded at t=0 min, 22 min 10 s, 27 min 10 s, 31 min 30 s, lower row recording 34 min, 39 min 10 s, 65 min and 91 min 50 s. Slightly changed from Prytz 2001*

Further figures from simulations will be shown in subsubsections 8.4.4 and 8.4.5.

We would like to mention the result of an experiment showing that light pulses can send a transpiration system of a leaf into a singular state (see Fig. 7.28). The experiment furthermore demonstrates that in this case subsequent smaller perturbations were not sufficient to bring the oscillation back to the limit cycle. Not before a sufficiently long pulse of darkness (pulse length in upper part of Fig. 7.28 is increasing from I $\longrightarrow$ II $\longrightarrow$ III) the oscillation started with a normal amplitude.

Here an interesting question arises: do the stomata-guard cells of the whole leaf stop oscillating in the singular state shown, or are they just totally de-synchronized and producing a constant output together?

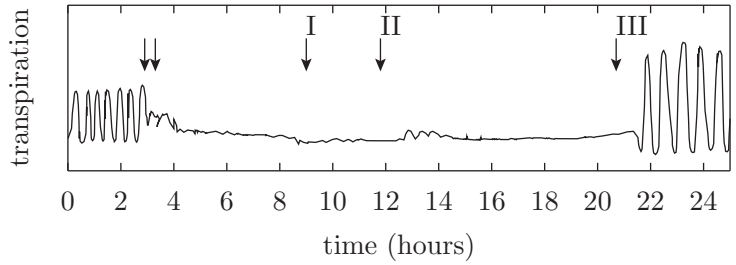

Figure 7.28: *Recording of transpiration rhythm of primary oat leaf in 20 mW/m^2 white light. x-axis shows time in h, y-axis relative transpiration from leaf. The oscillations were damped and stopped by two pulses: 30 mW/m^2 light increase for 2 min followed by 5 min darkness for 2 min. To try to induce oscillations anew, three darkness pulses were given: the first one consisted of 30 s duration, the second of 2 min duration and the third one of 10 min length. This last pulse induced again sustained oscillations (Johnsson, Brogardh, Holje 1979).*

7.6 Van der Pol Oscillator and its properties

The VP oscillator compensates the parallel-damping of the feedback model with two integrators according to Fig. 5.20 by a non-linear amplification, which balances the damping losses at first, but not any more at a larger amplitude, and so an amplitude regulation is simultaneously realised. This becomes especially obvious, if a model is constructed, in which the differential Eq. 5.10 is integrated once and in which it is taken into account, that the derivative refers to the dimension less normed time $\tau := \omega_0 t$ with the normed angular frequency ω_0, i.e.

$$x' - \varepsilon \cdot (x - \frac{x^3}{3}) + \int x \, d\tau = c \tag{7.24}$$

If in this equation the constant is set to c = 0 and if it is, as done above, arranged according to the highest derivative, we obtain

$$x' = \varepsilon \cdot (x - \frac{x^3}{3}) - \int x \, d\tau \tag{7.25}$$

Analogue to the steps 2 and 3 in Sect. 5.5 for constructing the functional diagram the Scilab diagram in Fig. 7.29 is obtained. The results of the simulation are for $\varepsilon = 0.2$ the same as in Fig. 5.9 and 5.10. In contrast to the preceding functional diagram (Fig. 5.8) now, due to the functional block "expression", a nonlinear cubic characteristic line is realised (see Fig. 7.30), which regulates the amplitude in the VP-oscillator. We are here not dealing with a saturation: For positive x-values the function $y = -x + x^3/3$ becomes initially smaller when x is increased (see again Fig. 7.30) but then from for x > 1 it becomes larger and larger. Positive changes of x lead, therefore, in the range $0 \leq |x| \leq 1$ to negative changes of y. If, however, |x| is larger than 1, positive changes at the input also leads to positive changes at the output. A positive feedback coupling is accomplished in the first case and a negative feedback coupling in the second case (the result is the same for negative x, as the reader will easily see). Altogether this

corresponds to an amplitude control, because smaller oscillations are amplified and larger ones are damped. Due to the feed back with amplification $\varepsilon = 5$ the signal can increase in a certain range of values and take a course which is not sinusoidal any more (see Fig. 7.34 and Fig. 7.33). This is, however, desired in some models e.g. in the case of action impulses of the heart beat.

This circuit of the VP-oscillator resembles strongly the feedback model with two integrators in Fig. 5.17 – provided the the amplification factor $\varepsilon = 0$! . The difference is obviosly, that there exists in the feedback branch (in parallel to the integrator) a non-linear amplification with $\varepsilon \cdot (-x + x^3/3)$. It affects the amplitude in such a way, that it is limited for small ε, but the curve shape is also, for larger values, highly deformed.

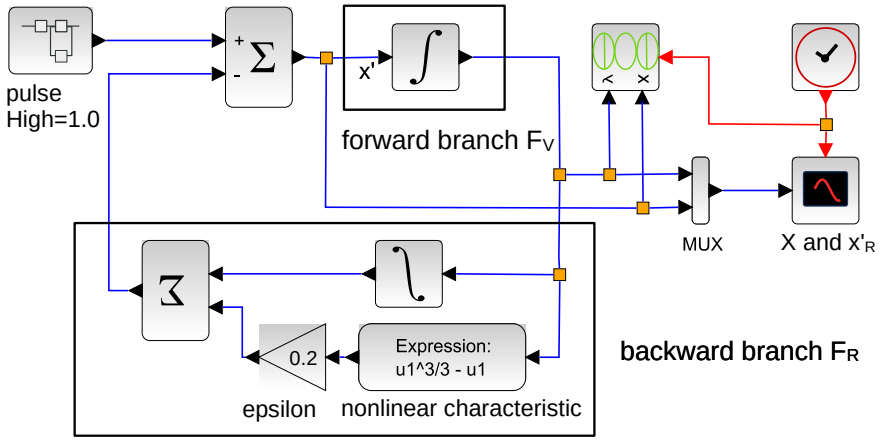

Figure 7.29: *Functional diagram of the VP-oscillator in Scilab/Xcos according to Eq. 7.25 with ε= 0.2 and an impulse with a height of 1 and a width of 1*

Without the non-linear characteristic line the VP-oscillator corresponds to the feedback model with two integrators (Fig. 5.17), which is realised at a value of $\varepsilon = 0$. Thereby it would according to Eq. 5.23 oscillate with the same frequency f_0 of 0.158 Hz. If, however, for larger values of ε the oscillation is not sinusoidal any more, the influence can still be calculated, because the still present periodic course with a period of $T_P = 1/f_P$ can be expressed as a Fourier series with

$$x(t) = \sum_{n=1}^{\infty} \hat{x}_n \cos(n\,\omega_P t) \tag{7.26}$$

and because this can be inserted in the VP differential Eq. 5.10 (see e.g. Van der Pol (1927) and Pfeifer (1966)). Before it should, however, be multiplied on both sides with $x(t)$ and integrated respectively averaged after the duration of a period $\tau_P = \omega_0 T_p$:

$$\int_0^{\tau_P} x\{x'' + \varepsilon \cdot (x^2 - 1)x' + x\}\, d\tau = 0$$

it follows:

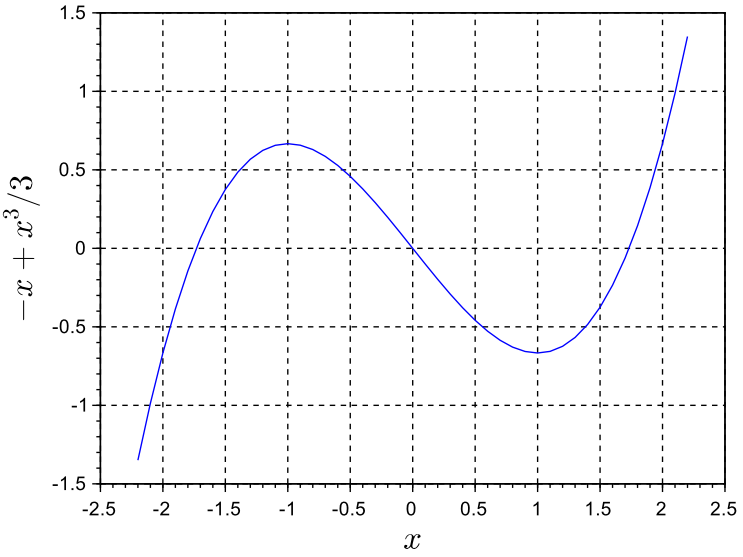

Figure 7.30: *Cubic characteristic of the VP-oscillator*

$$\int_0^{\tau_P} x\frac{d^2x}{d\tau^2}d\tau + \varepsilon \cdot \int_0^{\tau_P} x^3\frac{dx}{d\tau}d\tau - \varepsilon \cdot \int_0^{\tau_P} x\frac{dx}{d\tau}d\tau + \int_0^{\tau_P} x^2 d\tau = 0$$

After integration of the separate summands by partial integration and transliteration with

$$\underbrace{x\frac{dx}{d\tau}\Big|_0^{\tau_P}}_{=0} - \int_0^{\tau_P}\left(\frac{dx}{d\tau}\right)^2 d\tau + \varepsilon\,\underbrace{\frac{1}{4}x^4\Big|_0^{\tau_P}}_{=0} - \varepsilon\,\underbrace{\frac{1}{2}x^2\Big|_0^{\tau_P}}_{=0} + \int_0^{\tau_P} x^2 d\tau = 0$$

one obtains the following final result:

$$\int_0^{\tau_P}\left(\frac{dx}{d\tau}\right)^2 d\tau = \int_0^{\tau_P} x^2 d\tau \quad \text{respectively} \quad \frac{1}{\omega_0}\int_0^{T_P}\left(\frac{dx}{dt}\right)^2 dt = \omega_0\int_0^{T_P} x^2 dt \tag{7.27}$$

In those summands, in which the integral could be calculated, the result becomes zero, since the output signal is periodic and since the values at the begin and at the end of the period are identical (otherwise it would not be a period).

If both sides of the last equation are divided by the period τ_P respectively by T_P of the oscillation, the left side of the equation corresponds to the squared mean of the derivative of the signal and the right side corresponds to the mean of the squared signal itself. Each of the sides describe an average energy, in one case that of the signal derivative and in the other case that of the signal itself.

If in this average equation the Fourier series 7.26 is inserted, the respective energy can be expressed by the sum of the energies of the single sinus respectively cosine oscillations (Parseval

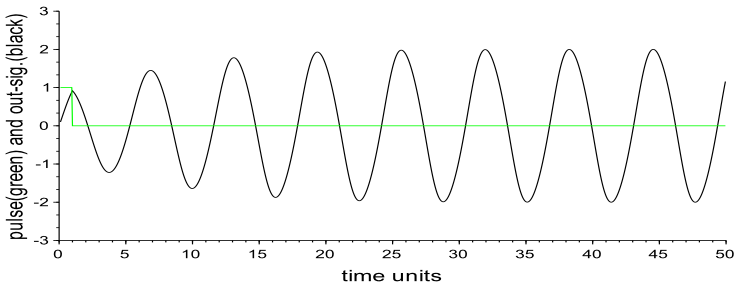

Figure 7.31: *Signal x (black) and the pertubatiom Signal (green) in an example simulation of the VP-oscillator in Fig. 7.29 with $\varepsilon = 0.2$*

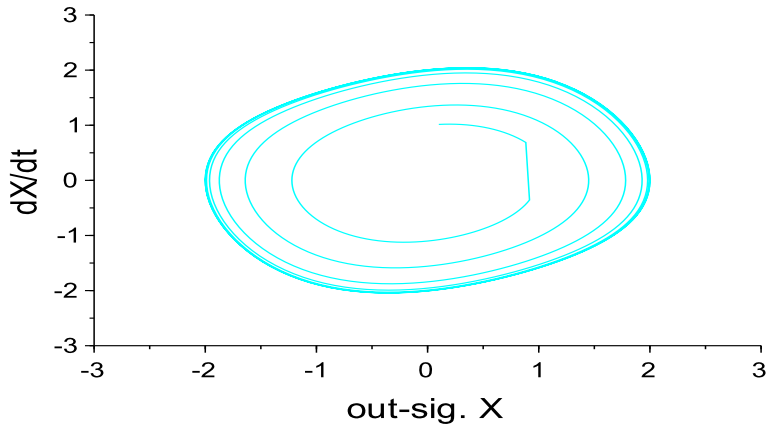

Figure 7.32: *The derivative of the signal x with respect to time as a function of x (xy-diagram) in an example simulation of the VP-oscillator in Fig. 7.29 with $\varepsilon = 0,2$*

theorem), i.e.:

$$\frac{1}{T_P}\int_0^{T_P}\left(\frac{dx}{dt}\right)^2 dt = \sum_{n=1}^{\infty} n^2\omega_P^2\hat{x}_n^2 \quad \text{und} \quad \frac{1}{T_P}\int_0^{T_P} x^2 dt = \sum_{n=1}^{\infty}\hat{x}_n^2$$

Inserting it in Eq. 7.27:

$$\sum_{n=1}^{\infty} n^2\omega_P^2\hat{x}_n^2 = \omega_0^2\sum_{n=1}^{\infty}\hat{x}_n^2$$

and in this way one obtains for the angular frequency ω_P:

$$\omega_P = \omega_0 \sqrt{\frac{\sum_{n=1}^{\infty} \hat{x}_n^2}{\sum_{n=1}^{\infty} n^2 \hat{x}_n^2}} \tag{7.28}$$

This means (see e.g. figures 5.9 and 7.31):

> The *frequency* of the initial oscillation *decreases* with increasing number of harmonics, i.e. the larger the distortion of a sinusoidal oscillation, the longer is its period!

As an example Fig. 7.31 and 7.33 show the signal and the vector diagram of the VP-oscillator in Fig. 7.29 for $\varepsilon = 0.2$. Comparing the time courses one recognises clearly, that it is at $\varepsilon = 5$ not any more sinusoidal and that the oscillation according to Eq. 7.28 has under these distortions a *lower* frequency, as without these distortions.

The non-sinusoidal oscillation for $\varepsilon = 5$ according to Fig. 7.34 reaches its maximal amplitude faster as the sinusoidal oscillation for $\varepsilon = 0,2$ according to Fig. 7.31. It has thus a shorter *setting time*, which is of advantage for a faster impulse transmission between cells (e.g. in the nervous system). If ε is further increased, the oscillation approaches more and more a square wave and is also called relaxation oscillation, because it jumps so to speak between the minimal and maximal value (see Wever (1963) and Fig. 7.34).

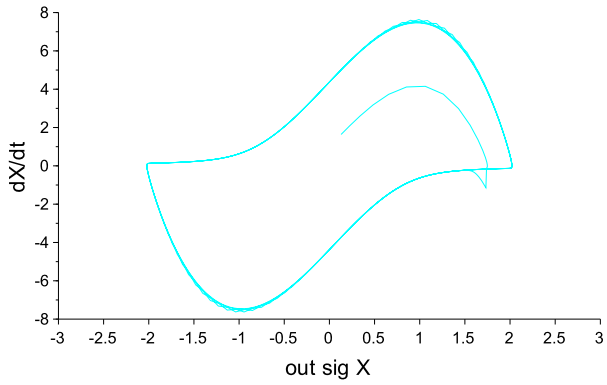

Figure 7.33: *The time derivative of the signal x with time as a function of x (xy-diagram) in an example simulation of the VP-oscillator in Fig. 7.34 with $\varepsilon = 5$*

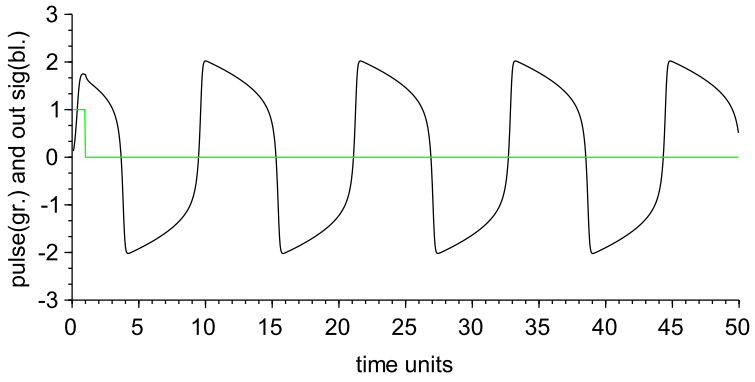

Figure 7.34: *Signal x and stimulus (green) in an example simulation of the VP-oscillator in Fig. 7.29 with $\varepsilon = 5$*

7.7 Modified Van der Pol-oscillator after Wever

A modified VP oscillator after Wever (see e.g. Wever (1979) or Pedersen, Johnsson (1994)) with the differential Eq.

$$\ddot{X} + 0.5(X^2 + X^{-2} - 3)\dot{X} + (1 + 0.6X)X = Z \tag{7.29}$$

and the perturbing signal $Z = Z0 + Z_{\text{pert}}$ is shown in the functional diagram Fig. 7.35.

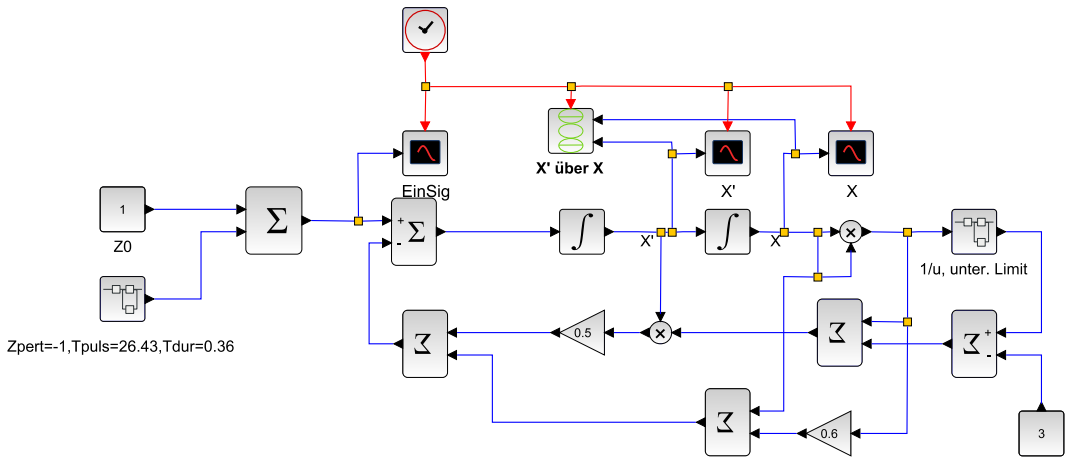

Figure 7.35: *VP oscillator with singular point after Wever (1979) and Pedersen, Johnsson (1994)*

If a disturbing pulse is given to the left integrator, the oscillation shown in Fig. 7.36 results,

in which x is plotted against time. If the derivative x' is plotted against x, we get the phase diagram in the lower part of the figure.

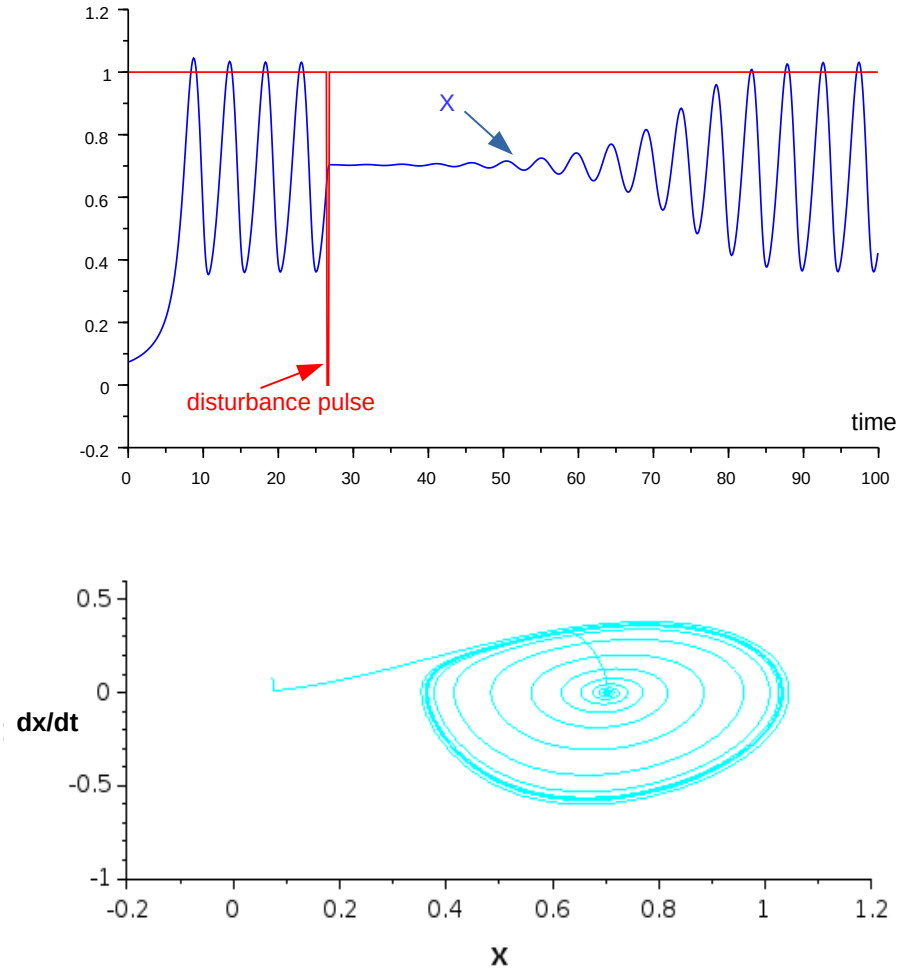

Figure 7.36: *Top: Output signal x of the modified VP-oscillator after Wever (see Fig. 7.35). After a perturbing pulse the system is pushed for about 10 time units into a singular point. Afterwards the oscillator begins to oscillate again.*
Below: If x' is plotted against x, a phase diagram demonstrates that the singular point is quickly reached and that the system returns slowly to the limit cycle, which is of no relevance here.

7.7.1 Appendix to the modified VP-Oscillator from Wever, dead-beat control:

To study the stability of the singularity in a biological oscillating system (subsect. 3.1) one has to try or perturb/force the oscillating system into its steady state. The same problem arises

when one would like to stop or damp unwanted oscillations in a mechanical system, e.g. in a chemical production plant. How should one perturb the system and send it into its steady state?

Control theory developed methods for this and one approach is often called dead-beat control or dead-beat strategy. In discrete-time control one looks for an input control signal, which should bring the system to the steady state in the shortest time (with fewest steps) when applied to the system(see Fig.7.37).

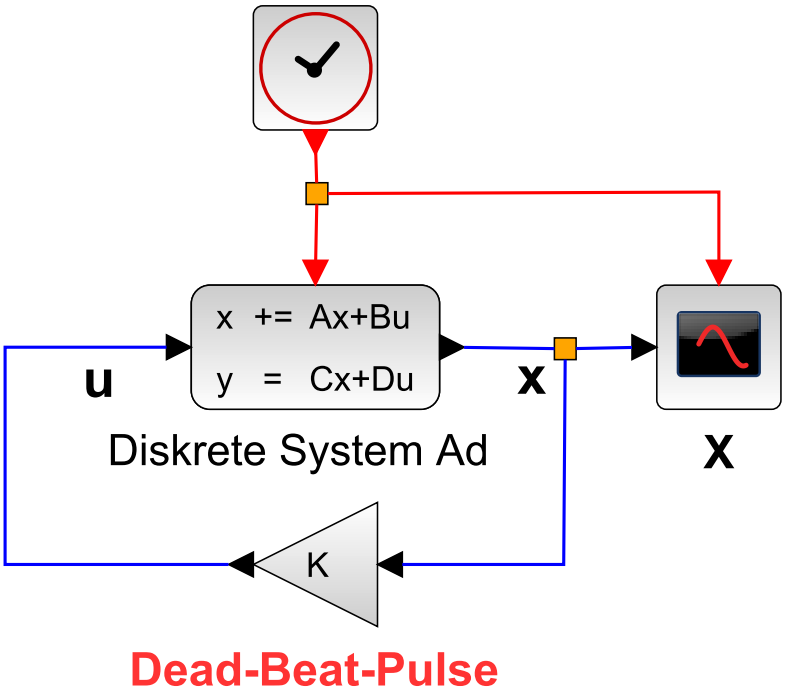

Figure 7.37: *Principle of "dead-beat control" of a discrete system. (In the icon of the system super-Block of scilab, the matrices A, B, C and D are specified without the index "d" as in Eq.7.33, e.g. the specified matrix A corresponds to the matrix in Eq.7.33. The plus sign in front of the equals sign simply corresponds to the discrete addition for the next sampling step, instead of the first derivative in the linear system)*
The method uses suitable pulses to 'kill' transients or oscillations in such a way that the system output signal stays at x_{ref} after shortest possible time. As these pulses also depend on the values of the output signal itself, a feedback system is created whose parameters in K (K: vector $\vec{k}$ with constant values) is selected that the transient processes are damped to such an extent that they disappear completely after m pulses. m is the system level (see explanation in the text and Listing7.3)
.

For linear systems this can often be accomplished, but for non-linear ones (as in the case of biological oscillation) it is more complicated and there is much research activity in the field.

In biology Winfree (1980) explored the possibility to stop the eclosion rhythm of *Drosophila* flies by a single short light pulse - this is in reality a dead-beat strategy. Pedersen, Johnsson

(1994) used in their simulations the VP equation (see Sect. 7.6) as a starting point for a direct simulation study of the dead-beat strategy in the case of a biological oscillation.

This strategy can also be applied to the modified van der Pol oscillator according to Wever as follows:

1. **Transformation into a first-order system of equations**
   The second-order differential equation 7.29 can be written as a system of first-order equations:

$$\begin{array}{rcccl} \dot{X}_1 & = & f_1(X_1, X_2) & = & X_2 \\ \dot{X}_2 & = & f_2(X_1, X_2) + Z & = & -0.5(X_1^2 + X_1^{-2} - 3)X_2 - (1 + 0.6X_1)X_1 + Z \end{array} \tag{7.30}$$

2. **Determination of the singular point**
   The singularity point is where $\dot{X}_1 = \dot{X}_2 = 0$ and $Z = Z0$. This results in (see Pedersen, Johnsson 1994):

$$\begin{array}{rcl} X_1 & = & X0_1 = -\dfrac{1}{1.2} \pm \dfrac{\sqrt{1 + 2.4Z0}}{1.2} \\ X_2 & = & X0_2 = 0 \end{array} \tag{7.31}$$

   As seen from Fig.7.36 the x-coordinate of the output signal stays at x_{ref} in steady state (here about x = 0.7). Without loosing generality we now denote the singular point by the coordinate $X0_1$ and $X0_2$.

3. **Linearisation at the point of singularity**:
   With $X_1 := X0_1 + x_1$,$X_2 := X0_2 + x_2$and $Z = Z0 + z_{pert}$ we get:

$$\begin{array}{rcccl} \dot{x}_1 & = & \left.\frac{df_1(X_1,X_2)}{dX_1}\right|_{X0_1,X0_2} x_1 + \left.\frac{df_1(X_1,X_2)}{dX_2}\right|_{X0_1,X0_2} x_2 & = & x_2 \\ \dot{x}_2 & = & \left.\frac{df_2(X_1,X_2)}{dX_1}\right|_{X0_1,X0_2} x_1 + \left.\frac{df(X_1,X_2)}{dX_2}\right|_{X0_1,X0_2} x_2 + z_{pert} & = & \mp\sqrt{1 + 2.4Z0}x_1 - (X0_1^2 + X0_1^{-2} - 3)\frac{x_2}{2} + z_{pert} \end{array}$$

   or in matrix notation:

$$\underbrace{\begin{pmatrix} \dot{x}_1 \\ \dot{x}_2 \end{pmatrix}}_{\vec{\dot{x}}} = \underbrace{\begin{pmatrix} 0 & 1 \\ \mp\sqrt{1 + 2.4Z0} & -0.5(X0_1^2 + X0_1^{-2} - 3) \end{pmatrix}}_{\underline{\underline{A}}} \cdot \underbrace{\begin{pmatrix} x_1 \\ x_2 \end{pmatrix}}_{\vec{x}} + \underbrace{\begin{pmatrix} 0 \\ 1 \end{pmatrix}}_{\vec{B}} z_{pert} \tag{7.32}$$

4. **Discretization of the linearised system**
   The linearised system should only be examined at discrete points in time t_i with the same time interval Δt and should therefore be transformed into the discrete range. For this purpose, the derivatives of $x_i, i = 1, 2$ with respect to time t are approximated by a simple Euler approximation as follows:

$$\underbrace{\begin{pmatrix} \dot{x}_1(t_i) \\ \dot{x}_2(t_i) \end{pmatrix}}_{\overrightarrow{\dot{x}(t_i)}} \Delta t \approx \underbrace{\begin{pmatrix} x_1(t_{i+1}) \\ x_2(t_{i+1}) \end{pmatrix}}_{\overrightarrow{x(t_{i+1})}} - \underbrace{\begin{pmatrix} x_1(t_i) \\ x_2(t_i) \end{pmatrix}}_{\overrightarrow{x(t_i)}}$$

If this approximation is used in 7.32 you get:

$$\begin{aligned}\overrightarrow{x(t_{i+1})} = \overrightarrow{x(t_i)} + \overrightarrow{\dot{x}(t_i)}\Delta t &= \overrightarrow{x(t_i)} + \underset{=}{A}\overrightarrow{x(t_i)}\Delta t + \vec{B}z_{pert}(t_i)\Delta t \\ &= \underbrace{\left(\underset{=}{E} + \underset{=}{A}\Delta t\right)}_{\underset{=}{A_d}}\overrightarrow{x(t_i)} + \underbrace{\vec{B}\Delta t}_{\vec{B}_d} z_{pert}(t_i)\end{aligned}$$

The discrete-time linearised system therefore results in

$$\overrightarrow{x(t_{i+1})} = \underset{=}{A_d}\overrightarrow{x(t_i)} + \vec{B}_d z_{pert}(t_i) \tag{7.33}$$

5. **Discrete control by pulses**
Suitable external pulses $z_{pert}(t_i)$ are applied to the system to stop the oscillations of the system. If we choose

$$z_{per}(t_i) = -\vec{k}'\overrightarrow{x(t_i)}, \text{ with } \vec{k}' \text{ transpose of } \vec{k} \text{ (vector with constant values)} \tag{7.34}$$

and get after insertion into eq. 7.33 :

$$\overrightarrow{x(t_{i+1})} = \underbrace{\left(\underset{=}{A_d} - \vec{B}_d\vec{k}'\right)}_{\underset{=}{F_d}}\overrightarrow{x(t_i)} = \underset{=}{F_d}\overrightarrow{x(t_i)} \tag{7.35}$$

This is a feedback control that changes the pole positions of the overall system $\underset{=}{F_d}$ and can favourably influence the system properties.

6. **Desired closed-loop poles placement for Dead-Beat control**
This requires pulses that lead the signals $\overrightarrow{x(t_i)}$ to the singularity point in the shortest possible time. This is possible if the poles z_i taking into account the control pulses $z_{pert}(t_i)$ lie in the origin of the Z-plane with $z := e^{p\Delta t}$. If this equation 7.35 is applied repeatedly, the result is

$$\begin{array}{ccccc}\overrightarrow{x(t_{i+1})} & = & \underset{=}{F_d}\overrightarrow{x(t_i)} & & \\ \overrightarrow{x(t_{i+2})} & = & \underset{=}{F_d}\overrightarrow{x(t_{i+1})} & = & \underset{=}{F_d^2}\overrightarrow{x(t_i)} \\ \vdots & \vdots & \vdots & \vdots & \vdots \\ \overrightarrow{x(t_{i+n})} & = & \underset{=}{F_d}\overrightarrow{x(t_{i+n-1})} & = & \underset{=}{F_d^n}\overrightarrow{x(t_i)}\end{array} \tag{7.36}$$

The signal $\overrightarrow{x(t_{i+n})}$ therefore disappears according to the last line of 7.36 after n pulses if $\underset{=}{F_d^n} = 0$. However, this is the case if the pole positions of the discrete system 7.35 are all zero. This can be achieved by appropriately weighting impulses $z_{per}(t_i) = -\vec{k}'\overrightarrow{x(t_i)}$.
The pole positions of the discrete system can be easily determined by transforming the linear difference equation into the frequency domain using the discrete Fourier transform, because the difference equation becomes an algebraic equation. Discrete

Fourier transformation of $\vec{x}$ and $\overrightarrow{x'}$ yields to:

$$z \cdot \vec{X} = \underline{\underline{F_d}} \cdot \vec{X} \tag{7.37}$$

where $\vec{X}$ is the discrete Fourier transformed of $\vec{x}$ and $z = e^{p\Delta t}$. with $p = \sigma + j\omega$ is the complex frequency with the real part σ and the imaginary part ω. σ is the damping and ω the angular frequency of a cosine oscillation $\sim \exp(\sigma t) \cdot \cos(\omega t)$. Rearranging Eq. 7.37 one obtains:

$$\left(\underline{\underline{F_d}} - z_{pole} \cdot \underline{\underline{E}}\right) \cdot \vec{X} = \vec{0}, \ \underline{\underline{E}} : \text{ unit matrix} \tag{7.38}$$

The eigenvalue equation 7.38 is fulfilled except for $\vec{X} = 0$ when

$$\det\left(\underline{\underline{F_d}} - z_{pole} \cdot \underline{\underline{E}}\right) = 0 \tag{7.39}$$

If all pole positions for a system of m-th degree are zero, the result is:

$$\det\left(\underline{\underline{F_d}} - z_{pole} \cdot \underline{\underline{E}}\right) = z_{pole}^m = 0$$

and since, according to the Cayley-Hamilton theorem Åström, Wittenmark 2013,Ackermann 2012, each matrix fulfils its own eigenvalue equation 7.39, the following follows:

$$z_{pole}^m = \underline{\underline{F_d^m}} = 0 \tag{7.40}$$

In this case, we actually obtain according to the **dead beat control** procedure from the equation 7.36 that the signals disappear after n=m weighted pulses, i.e..

$$\overrightarrow{x(t_{i+n})} = \underline{\underline{F_d^n}}\overrightarrow{x(t_i)} = \underline{\underline{F_d^m}}\overrightarrow{x(t_i)} = 0, n = m, \text{(system degree)}$$

The corresponding weighting vector $\vec{k}$ for the impulses can now be determined with the help of Scilab (see Listing 7.3).

Listing 7.3: *Example of a **dead-beat control** for the linearised and discrete modified Van der Pol oscillator according to Wever in Fig. 7.35*

```
// Parameters for modified van der pol oscillator from Wever
Z0 = 1;              // constant part of Z
X01 = -1/1.2+sqrt(1+2.4*Z0)/1.2 //  1. solution of the singular point
//X01 = -1/1.2-sqrt(1+2.4*Z0)/1.2 //  2. solution of the singular point
X02 = 0.0;
T_s = 0.1;           // Sampling period
// Linearized system matrices around X1=X01, X2=X20
A = [0, 1; -sqrt(1+2.4*Z0), -0.5*(X01^2+X01^-2-3)]; // for 1. solution of the
    singular point
//A = [0, 1; sqrt(1+2.4*Z0), -0.5*(X01^2+X01^-2-3)]; // for 2. solution of the
    singular point
B = [0; 1];
C = [1, 0];
//
```

```
// Discretization of the system
sys = syslin('c', A, B, C);           // Continuous-time state-space model
sys_d = dscr(sys, T_s);               // Discrete-time system
Ad = sys_d.A;
Bd = sys_d.B;
Cd = sys_d.C;
//
// Desired closed-loop poles for Dead-Beat control
desired_poles = [0, 0];               // Poles at the origin for Dead-Beat
//
// Compute Dead-Beat control gain
K = ppol(Ad, Bd, desired_poles);
//
// Simulation parameters
N = 5;                                // Number of simulation steps
x = [X01*1.0;X02*1.0];                // Initial state
r = X01;                              // reference
y = zeros(1, N);                      // System output
u = zeros(1, N);                      // Controlinput
//
// Closed-loop simulation
for k = 1:N
    y(k) = Cd * x;                    // Compute output
    u(k) = -K * x;
    x = Ad * x + Bd * u(k);           // Update state
end
//
// Plot results
scf(1);
t = (0:N-1) * T_s;                    // Time vector
plot2d3(t, u+r, style=[2], rect=[-0.05,-80.0,0.45,80.0]);     // Input pulse
plot(t, u+r, '.');
plot(t, zeros(1,N), 'g', 'LineWidth', 2)
xlabel('Time (s)','fontsize',4);
ylabel('Input-Pulse u','fontsize',4);
xgrid;
title('Dead-Beat control for linearized van der pol oscillator after Wever','
    fontsize',4);
scf(2);
plot2d3(t, y+r, style=[2], rect=[-0.05,0.0,0.45,1.6]);     // Output response
plot(t, y+r, '.');
plot(t, ones(1, N)*r,'r', 'LineWidth', 2);
xlabel('Time (s)','fontsize',4);
ylabel('Output','fontsize',4);
xgrid;
legend('','System Output y+r', 'Reference r');
title('Dead-Beat control for linearized van der pol oscillator after Wever','
    fontsize',4);
```

The listing shows the application of the dead beat method to Wever's modified Van der Pol oscillator, which is to be brought to the singularity point (see Eq.[7.31]) after only two pulses, corresponding to the system degree m=2. After calculating the corresponding values for the output signal x0, the non-linear system is approximated at this point by a linear one and discretised with a sampling interval Ts. The poles of the linearised system are then shifted to the zero point with the aid of a suitable feedback (Åström, Wittenmark 2013, Ahmad Taher Azar 2015, Ackermann 1972), whereby the singularity point can be reached after m pulses of the feedback. Fig. 7.38 shows the result for the singularity point with a positive sign in front of the root, i.e. $X0_1 = -\frac{1}{1.2} + \frac{\sqrt{1+2.4Z0}}{1.2}, X0_2 = 0$ and Z0=1.

As the result for the output signal x in the dead beat method with linearisation around the singularity point only represents the changes around this point, the reference signal r (around which linearisation is performed, in this case the singularity point) was added to the output signal.

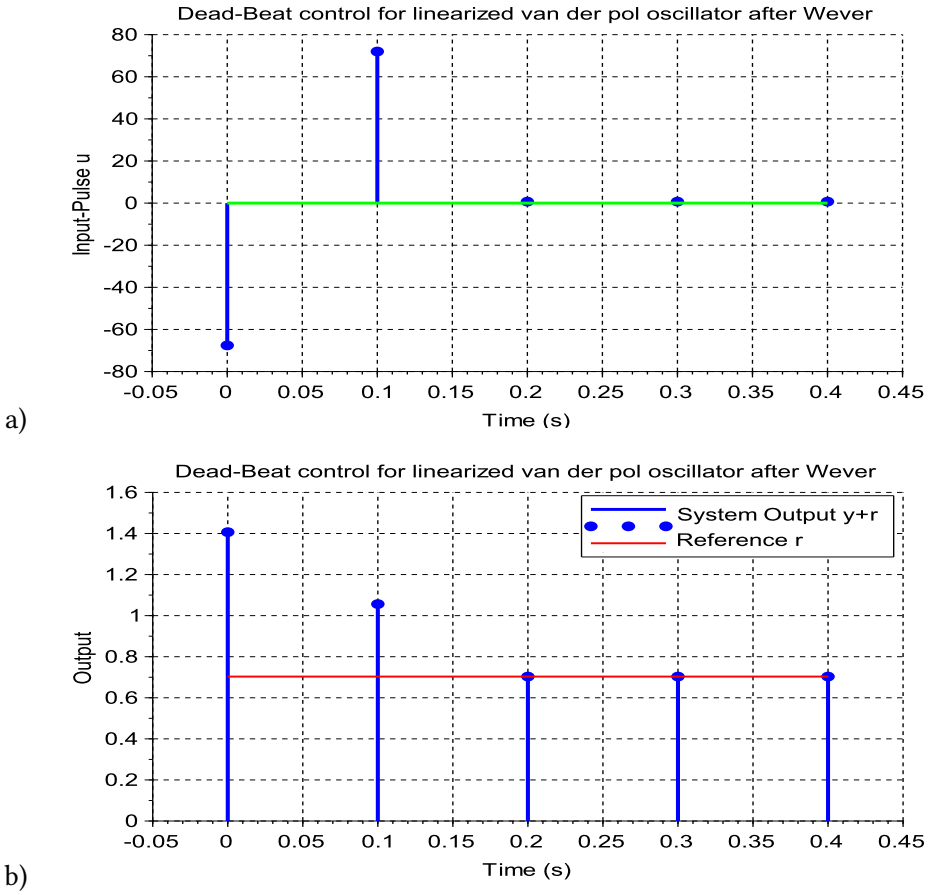

Figure 7.38: *a) Input control signal curve u and b) associated Output signal curve y+r when controlled, using the dead beat method with the Van der Pol oscillator according to Wever (see Fig.7.37). Simulation with the Scilab (see Listing 7.3). The reference signal or singularity point r is actually reached after two pulses.*

The dead beat method assumes that the system is linear and discrete. For non-linear systems, you can linearise around any state point and also apply this method in its surroundings. The modified van der Pol oscillator according to Wever is non-linear, i.e. we had to linearise above what we had carried out in the vicinity of the singularity point and then digitised. In doing so, we were able to achieve that the oscillations could actually be stopped in a very short time after two pulses, corresponding to system degree 2 (see example in fig:7.37).

The question now arises as to whether this is also possible with the original non-linear van

der Pol oscillator according to Wever as shown in Fig.7.35 For this purpose, this non-linear system is to be controlled around the state point around which it was linearised (this was the singularity point) with the same feedback as the linearised system according to Fig. 7.37. The modified functional circuit board is shown in Fig.7.39 The vector of the control gain K and the unstable singularity point (X01, Y01) were determined using the Scilab script in Listing[7.3]. (X01=0.7032574, Y01=0.0), K = [97.104222 15.034816]. The dead beat control can be switched on and off with the switch from Scilab/Xcos.

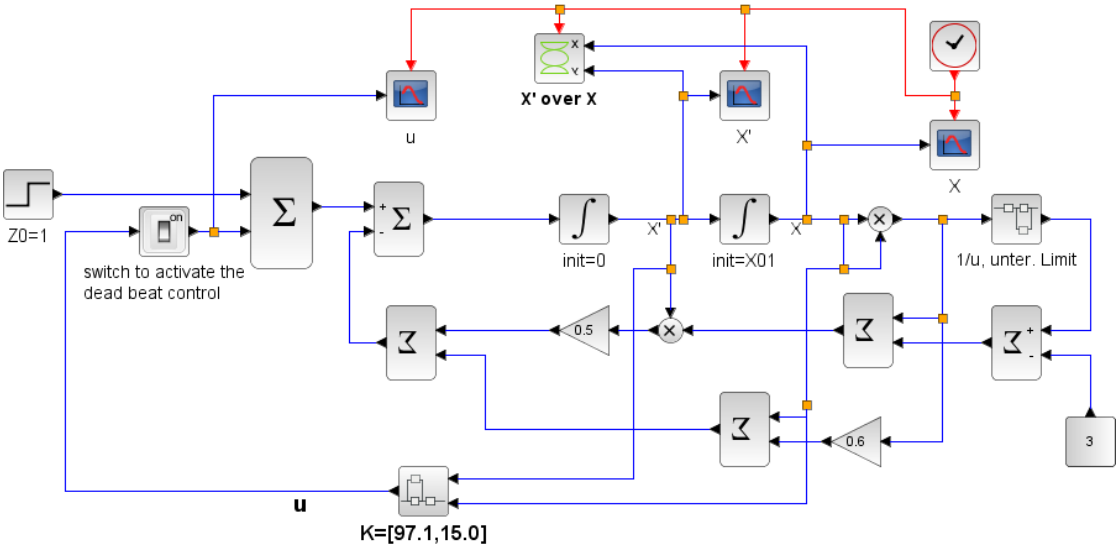

Figure 7.39: *VP oscillator after Wever (1979) and Pedersen, Johnsson (1994) with dead beat control.*

The superblock with the control constants K is shown in Fig.7.40.

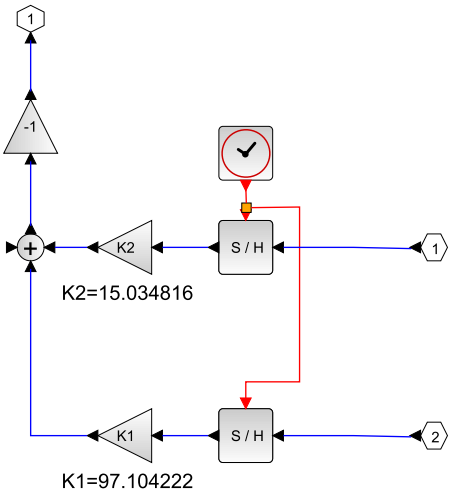

Figure 7.40: *Control amplification (superblock in Fig.7.39). A sample and hold element is used here, whereby the sampling rate is selected to be equal to the sampling interval of the digital dead beat controller in Fig.7.38 (0.1 sec.).*

Now it should be checked how stable this oscillator is at the start at the singularity point

with and without dead beat control and whether oscillations occur, which is to be expected without dead beat control, since at the singularity point the associated eigenvalue of the system matrix $\overrightarrow{A}$ has an eigenvalue with a positive real part. Fig.7.41 shows the simulation without dead beat control (switch is off), whereby after starting at the singularity point a constant oscillation occurs after approx. 3 seconds.

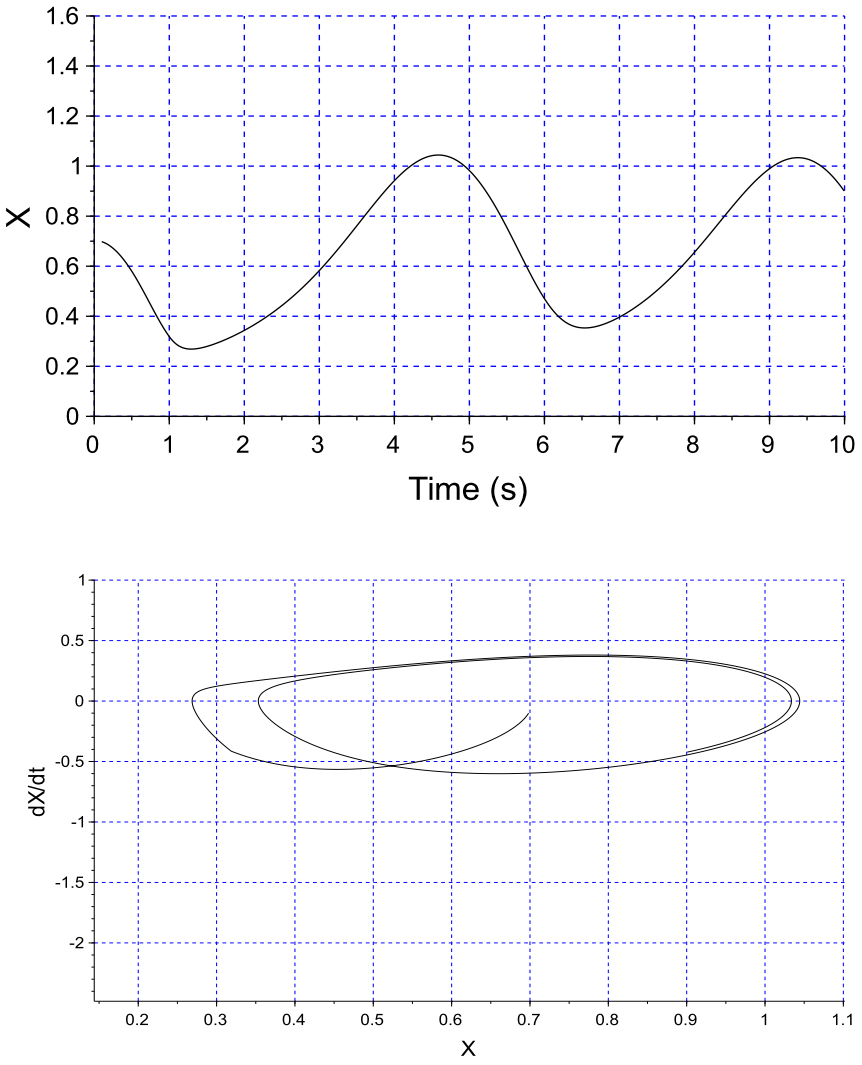

Figure 7.41: *Output of the VP oscillator Wever modification without dead beat control (**switch is off**) from Scilab simulation after Function diagram in Fig. 7.39*
Top: Output signals with oscillations.
Bottom: Phase diagram. . It is seen that the singularity point is unstable at $X = X0_1 = 0.7032574$ *and* $dX/dt = Y0_1 = 0$*, because an oscillation occurs again (after approx. 3 seconds).*

Fig.7.42 shows the simulation with dead beat control (switch is on), whereby after starting at the singularity point no oscillation arise.

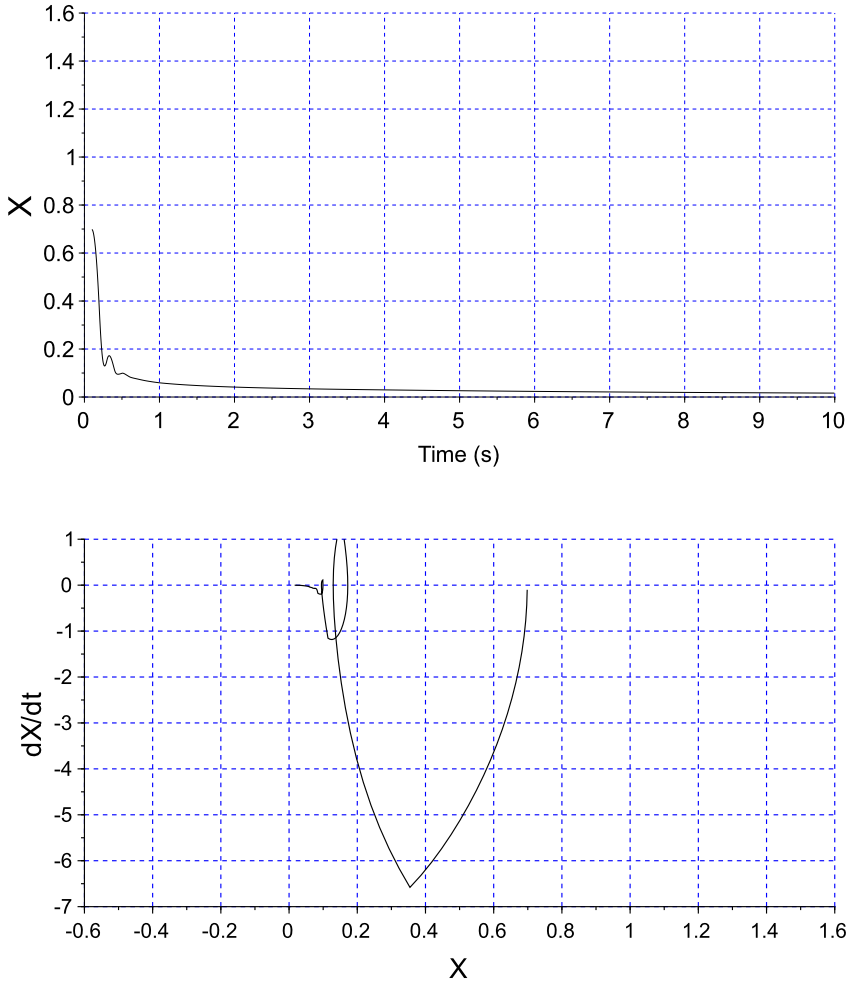

Figure 7.42: *Outputsignal X of the VP oscillator (Wever modification) with dead beat control (**switch is on**) from Scilab simulation after Function diagram in Fig. 7.39Top: Output signals X with no oscillations. Bottom: Phase diagram. . You can see that there is no longer any oscillation.*

The control signal of the deadbeat control is shown in Fig.7.43.

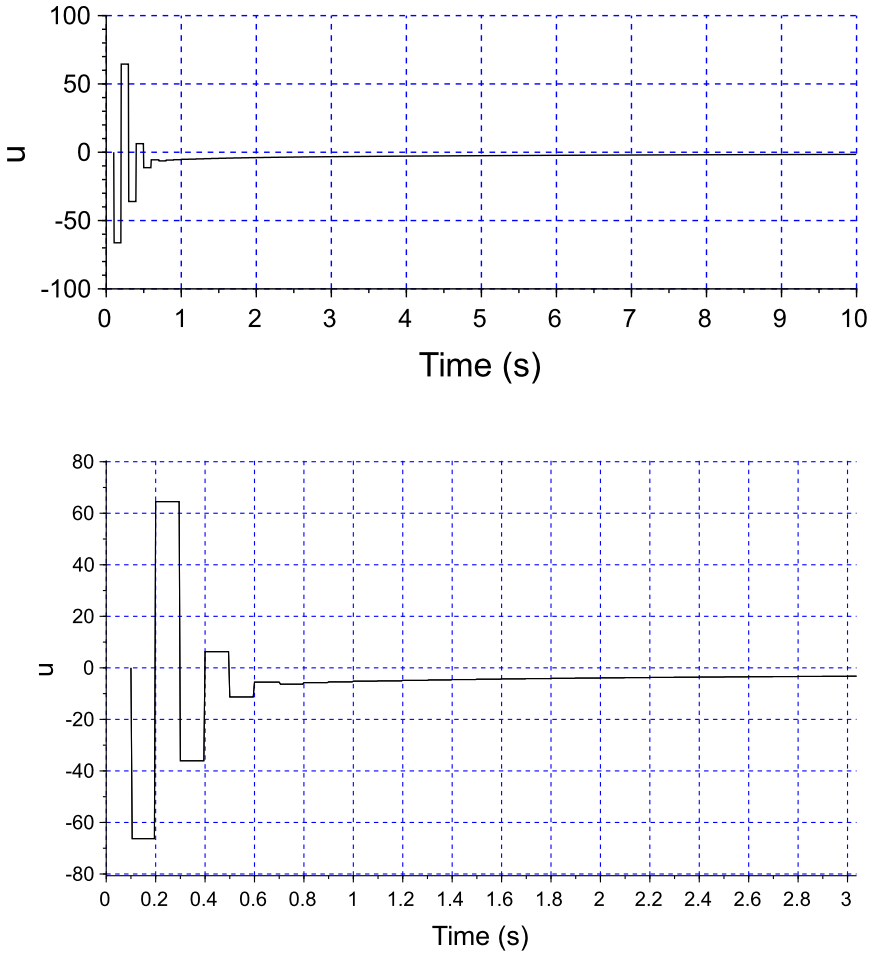

Figure 7.43: *Control signal u of VP Osci Wever modification with dead beat after Fig.7.39 (Top: time axis 10 sec., Bottom:time axis zoomed to 3 sec.)*

If you compare this dead beat signal with the controller signal of the digitised system in Fig.7.38, you can see that the oscillation cannot be suppressed with two pulses, but that four additional pulses are required, although the first two pulses are apparently repeated twice with a smaller amplitude before the controller no longer generates any pulses.

7.8 Models for heart rhythms and the cardiovascular system

In the human circulatory system, oxygen-rich blood is transported through the body to the cells, where it delivers the oxygen to them, is pumped back into the lungs via the right ventricle, where it is oxygenated again and transported on to the left ventricle, where it is passed on again to the "consumer cells". The blood pressure (force per area, measured in mm Hg[1]) is largest in the aorta and drops on the way of the blood through the circulation via artery, capillaries and veins until the heart is reached again. The heart works like two pumps in a muscle, each of which has an atrial and main chamber (see Fig.7.44).

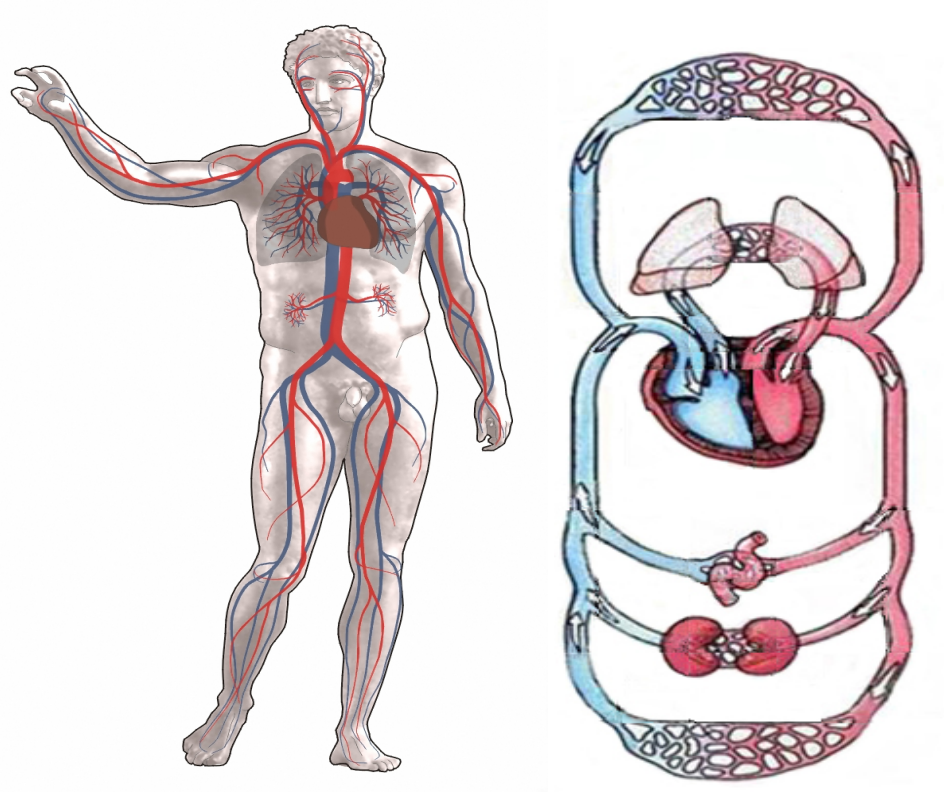

Figure 7.44: *Schematic illustration of circulatory system of the human body. Left: Some larger blood vessels within the body. Right: the oxygen depleted blood (blue) flows from the heart to the lungs and becomes oxygenated (red), enters the heart and is pumped out to tissue and organs, delivering oxygen (later again blue)*
(The left figure is from wikimedia.org. https://commons.wikimedia.org/wiki/Main_Page. The left figure is licensed under the Creative Commons Attribution-Share Alike 2.5 Generic https://creativecommons.org/licenses/by-sa/2.5/deed.en , the right figure from CVSim, an open-source cardiovascular simulator for teaching and research, freely downloadable from Physionet, see under http://physionet.org/physiotools/cvsim))

[1] millimeter mercury column

In subsect. 2.3.1 we already treated heart rhythms, how they arise and normally run In the following we are dealing with models which can also simulate these effects and how under critical circumstances the heart might stop to beat.

The heart of mammals consists how already mentioned in subsect. 2.3.1 of the two atria which serve as “injection chambers", and the two ventricles as “pumps" (see Fig. 7.45). The

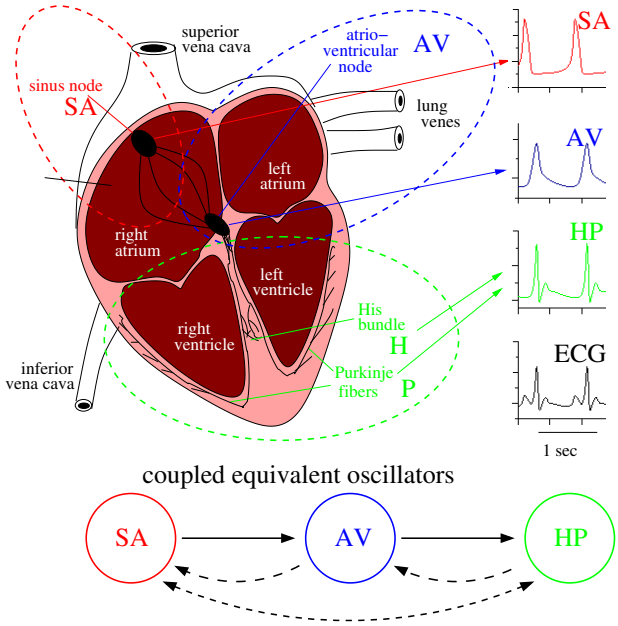

Figure 7.45: *Extended heart section figure (c.f. figure 2.7), colpeted and connected with electrical events. Top-Left: Sketch of heart section. Left and right atrium are “injection chambers" and left and right ventricles are “pumps". Blood low in oxygen reaches the heart via the inferior and superior vena cava and from there via the lung veins to the lung, where the blood is again supplied with oxygen (see Heartfunction). Right: Time coure of stimulation and electric events. Electric impulses are produced in the sinus node (SA) which is the primary pacemaker and synchronise the contractions of the atrium. The impulses reach the atrioventricular node (AV) and via the stem of His bundle (H) and the Purkinje fibres (P) the musculature of the main chambers. They make sure that they contract in the right beat rhythm (see Heart stimulation), Lower part of figure sequence with possible feed backs (dashed arrows). After Gois, Savi 2009; Zebrowski et al. 2007.*

contractions of the heart begin in the atria and take over in the ventricles. A wave of electric impulses run over the muscle cell of the heart tissue and coordinate the four chambers. The muscle fibres contract, if the internal potential of the cells is temporarily depolarised by an action potential. After a refractory phase the cells repolarise again. During this phase a normal stimulus can *not* trigger an action potential.

Especially the cells in the sinus node at the upper rim of the atrium are pacemaker for this

stimulation, and the atrioventricular node[2] serves as a further pacemaker. It triggers via the Purkinje fibres the contraction of the ventricular muscle (see Fig. 7.45).

The natural frequency of the sinus node determines the heart beat. Under resting conditions it is about 1sec. Neuronal impulses from the brain, from various ganglia, and from internal organs can speed up or speed down the heart beat. This occurs normally in the whole heart synchronously. In the case of cardiac infarction, unusual high hormone or ion concentrations, chemical stress, physical damage, or a strong electric stroke, the synchronisation might fail.

So far, we have only investigated the electrical excitation of the nervous system, which can be visualised by an ECG. This stimulates the heart muscle to contract rhythmically, which transports oxygen-carrying blood to the vital supply of the body's cells. This muscle contraction is achieved by electrically dependent channels in the cell membranes and chemical reactions, which can be explained by the sliding filament theory in muscle (see e.g. on the Internet at https://www.nature.com/scitable/topicpage/the-sliding-filament-theory-of-muscle-contraction-14567666/).

In Fig.7.46 the muscle contraction process is shown and can be described as follows :

- The action potential reaches the axon terminal (No.1).
- Voltage-dependent calcium gates open, allowing calcium to enter the axon terminal (No.2).
- Neurotransmitter vesicles fuse with the pre synaptic membrane and acetylcholine (ACh) is released into the synaptic cleft via exocytosis(No. 3).
- ACh binds to postsynaptic receptors on the sarcolemma(No.4).
- This binding causes ion channels to open and allows sodium ions to flow across the membrane into the muscle cell(No.5).
- The flow of sodium ions across the membrane into the muscle cell generates an action potential which travels to the myofibril and results in muscle contraction(No.6).

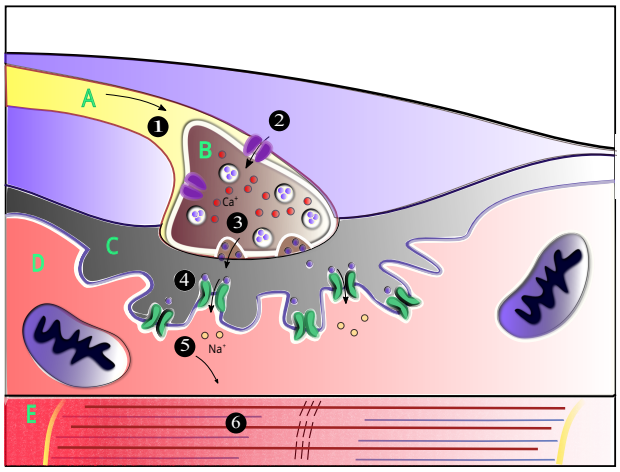

Figure 7.46: *Muscle Contraction Process,*
Labels: A: Motor Neuron Axon B: Axon Terminal C. Synaptic Cleft D. Muscle Cell, E. Part of a Myofibril (The Figure is from wikimedia.org under Creative Commons Attribution-Share Alike 4.0 https://creativecommons.org/licenses/by-sa/4.0/deed.en license)

[2] A heavily branched neuronal network with exceptional fast conduction of electric impulses

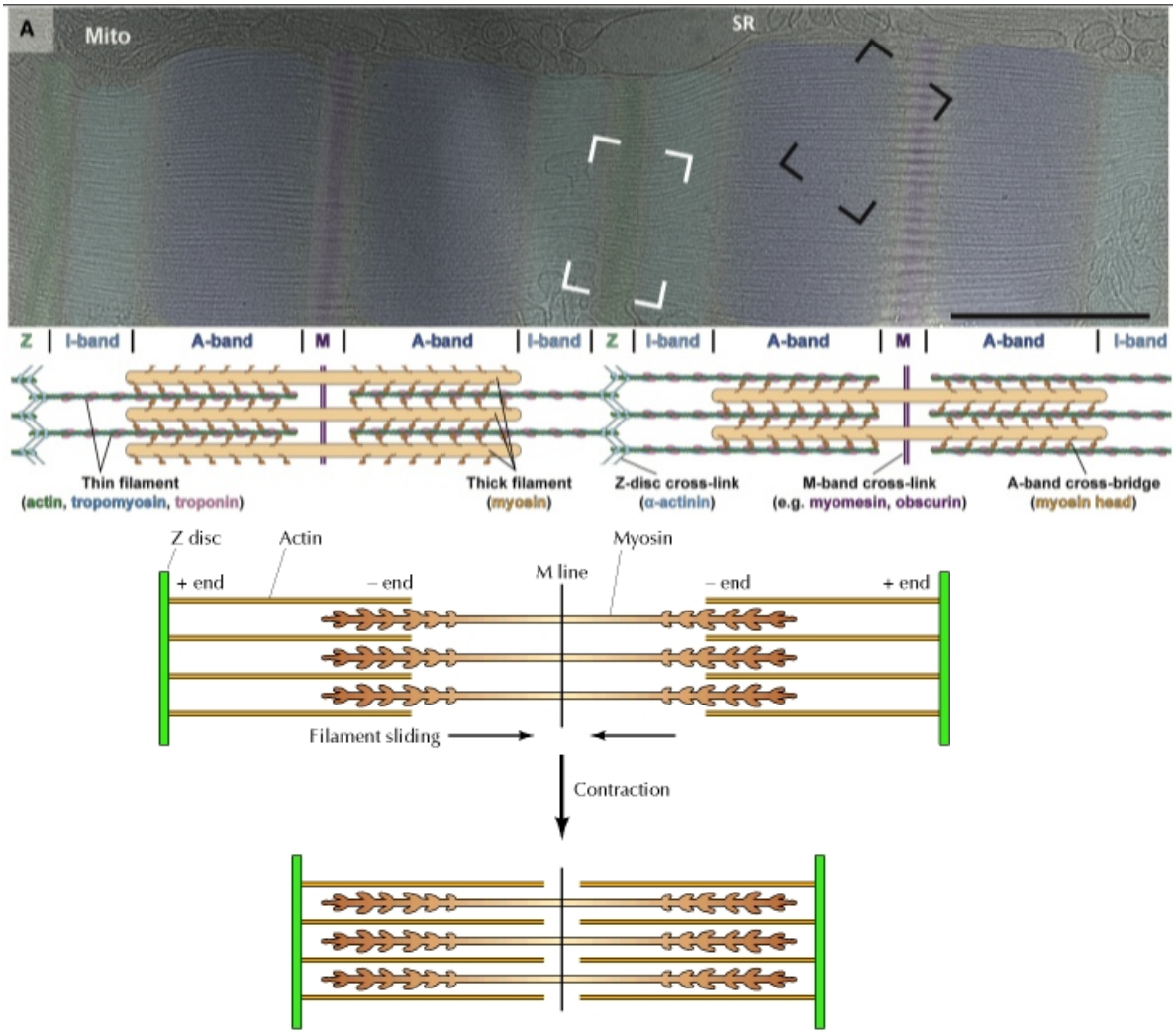

Figure 7.47: *Eenlarged image to the smallest part of a myofibril(Sarkomer) which results in muscle contraction(No. 6)*
Above: Electron microscope view of the heart muscle and schematic representation of the contraction, where the mobile, thinner myosin elements are pushed into the thicker, more immobile filaments (actin), below: Schematic representation of a relaxed and tensed muscle part(Sarcomer)
(The Figures are from wikimedia.org under the Creative Commons Attribution-Share Alike 4.0 International license)

The nervous system and the internal oscillators in the heart (sinus node, AV node, His bundle) generate electrical impulses in the heart that propagate in such a way that the areas in the heart are stimulated at the right time and the corresponding muscles are activated, including those that control the existing valves in the right way so that the "heart pump" pumps the blood in the right direction. The mechanical structure of the "heart pump" is shown in Fig.7.48.

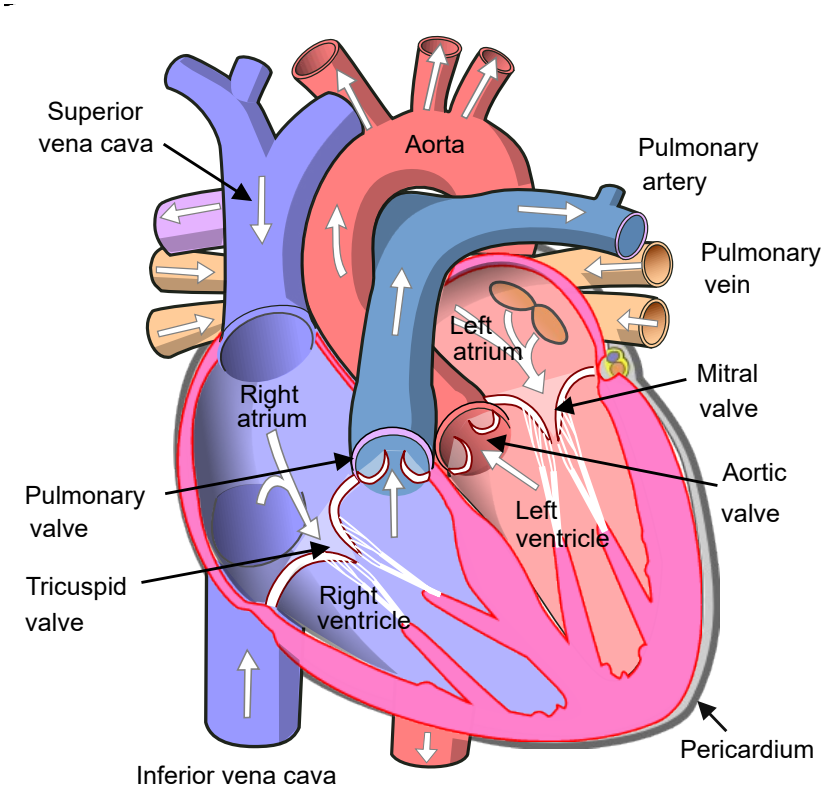

Figure 7.48: *Diagram of the human hearts mechanics with the pumping directions of the blood and the heart valves*
(The Figure is from wikimedia.org https://commons.wikimedia.org/wiki/File:Diagram_of_the_human_heart_(cropped).svg *under CC-BY-SA 3.0-*https://creativecommons.org/licenses/by-sa/3.0/deed.en *license)*

Effect of electrical excitation (ECG) on blood pressure and heart sounds The coordinated electrical excitation of the heart muscles and the heart valves (by the sinus and AV nodes and by the Purkinji bundle of His) causes the pumping properties of the heart, which periodically changes the blood pressure and flow. These effects have been measured and investigated many times (e.g. by Carl J. Wiggers, see https://en.wikipedia.org/wiki/Carl_J._Wiggers). Certain changes in the curves of blood pressure, blood flow, heart sounds and delays compared to the electrical excitation according to the ECG have been shown, which can also be explained by the heart mechanics of the heart valves, which pump the blood into the arteries like a pulse and produce sounds when they open and close (see Fig.7.49).

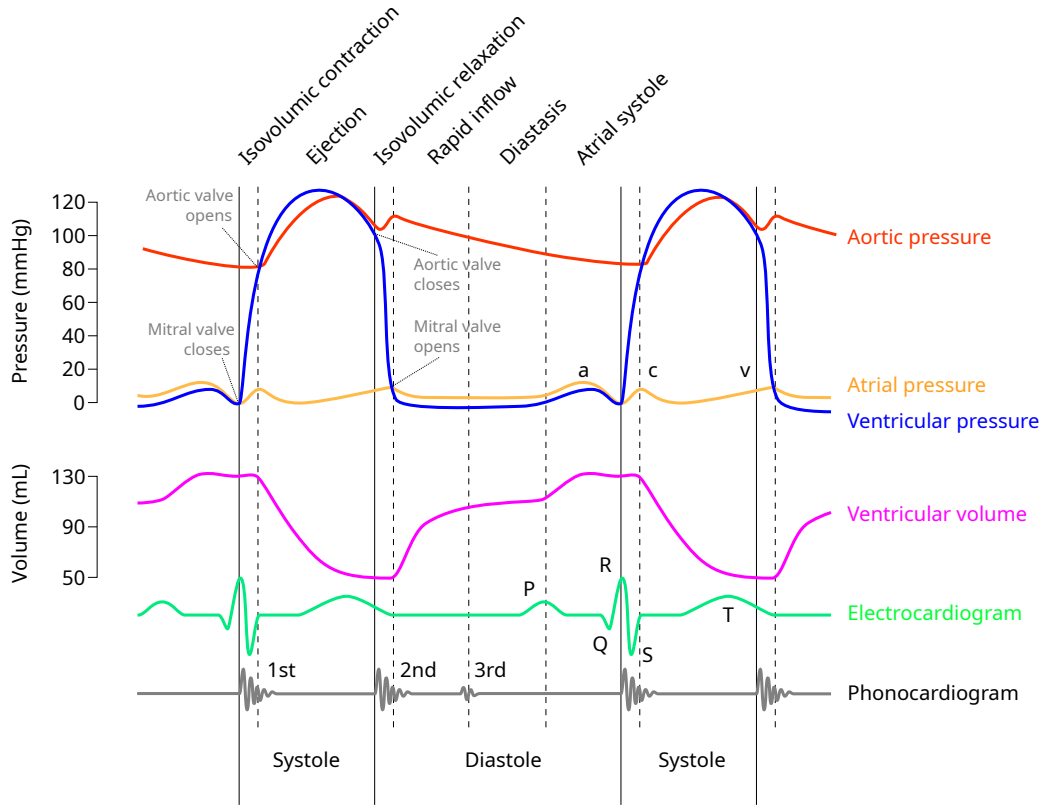

Figure 7.49: *Wiggers Diagram of several human measured variables of the human circulatory system*
(The Figures are from wikimedia.org under the Creative Commons Attribution-Share Alike 4.0 International license)

Wiggers Diagram shows

- Electrocardiogram (ECG) – electrical activation of the heart
- Aortic, ventricular, and atrial pressures – mechanical events in different chambers
- Ventricular volume – filling and ejection phases
- Heart sounds – timing of S1, S2 (and sometimes S3, S4)
- Flow events – opening and closing of heart valves

Phases in the Cardiac Cycle (Left Heart Example)

- Atrial Systole
  - Triggered by the P wave on the ECG (atrial depolarization).

  - Atria contract ⟶ last bit of blood pushed into ventricles ("atrial kick").
  - Atrial pressure rises slightly, ventricular pressure increases a bit, ventricular volume peaks.

- Isovolumetric Contraction
  - Starts after the QRS complex (ventricular depolarization).
  - Ventricles begin to contract, pressure rises sharply.
  - All valves closed ⟶ volume stays constant ("isovolumetric").
  - First heart sound S1 occurs when AV valves (mitral/tricuspid) close.

- Ventricular Ejection
  - Once ventricular pressure > aortic pressure, aortic valve opens.
  - Blood flows into the aorta, aortic pressure rises.
  - Ventricular volume drops rapidly during early ejection, then more slowly during late ejection.
  - T wave (ventricular repolarization) occurs near the end.

- Isovolumetric Relaxation
  - Ventricles relax, pressure falls quickly.
  - When ventricular pressure < aortic pressure, aortic valve closes ⟶ second heart sound S2.
  - All valves closed again ⟶ volume constant.

- Ventricular Filling
  - Ventricular pressure < atrial pressure ⟶ AV valves open.
  - Rapid filling phase (passive), then slow filling (diastasis).
  - Cycle repeats.

Sequence of a pulse beat : The course of the pumping function as a function of the electrical excitation (ECG) is shown in Fig.7.50(see Bernhard S., K.-H. 2022)

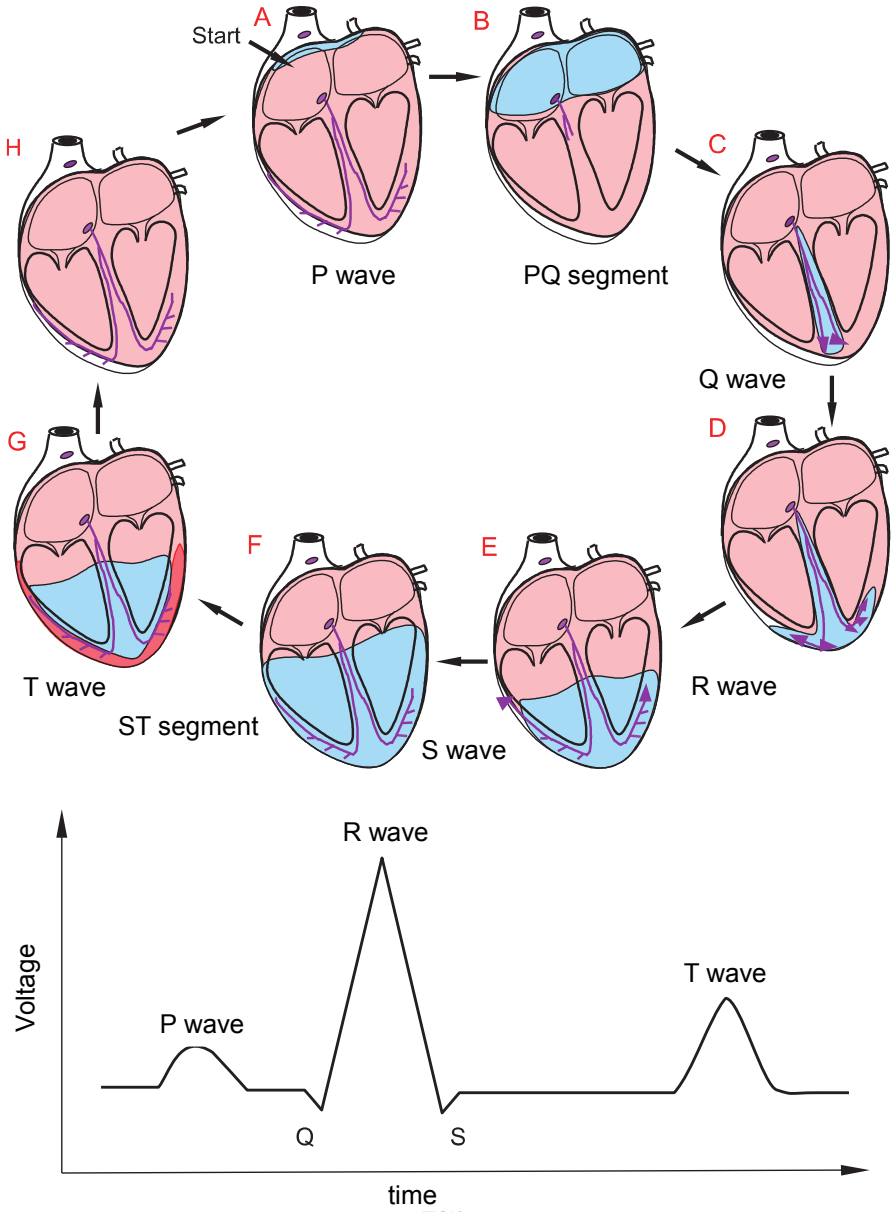

Figure 7.50: *Diagram of the human hearts mechanics with the pumping directions of the blood and the heart valves*

section A: The cardiac excitation cycle is initiated by an action potential from the pacemaker cells in the sinus node.

section B: The excitation spreads across both atria and the cell membranes of the atrial cells become depolarised, which is evident on the ECG as a P wave. In this section, the atria contract and fill the ventricles with blood, causing the leaflet valves (mitral and tricuspid valves) open between the atria and the main chamber and the semilunar valve indexes (aortic and pulmonary valves) open between the atria and the main chamber. (aortic and pulmonary valves) are closed.

section C: The excitation through the sinus node spreads to the AV node. It can only spread further into the wall between the left and right main chamber ("tawara" = thigh) via this node and the adjoining His bundle. This section can be seen as a Q wave in the ECG.

section D: At the end of the wall between the left and right main chambers, the excitation can travel further into the outer wall of the main chambers via the "Purkinje"=fibres, which generates the central R-wave in the ECG.

section E: The cardiac muscle cells of the main chambers are now excited via the Purkinje"=fibres, which can be seen as the S-wave in the ECG.

section F: Once all the cardiac muscle cells of the main chambers have been excited, the main chambers contract, which increases the pressure there, the valves open and the blood is forced out of the chambers into the aorta or the pulmonary artery. At the same time, the atria are also filled with blood during this expulsion phase. As an ST segment it is found in the ECG between the S wave and the T wave.

section G: Since in the meantime all heart cells have been excited, the conduction of impulses between the atria and the main chambers is normally only possible via the His bundle and the AV node, and the cells also need a certain time (refractory period) until they can be excited again by an action potential, the excitation from the main chambers can no longer spread back into the atria. The relaxation phase or diastole now begins, recognisable as a T-wave in the ECG.

section H: Finally, all cells of the main chamber return to their resting state by re-polarising. Now a new cardiac cycle can begin again by stimulating an action potential from the sinus node.

7.8.1 Models for pacemaker cells after Hodgkin/Huxley and FitzHugh

Neurons can produce electric impulses after stimulation or autonomously, in order to generate at the target a certain effect (e.g. contraction of muscles). The first studies and quantitative descriptions of the ion channels of a cell, which generate an impulse, were performed by Hodgkin, Huxley 1952[3] at the giant axon of the squid. Their equations described the produced impulses correctly, but were very complicated. FitzHugh 1961 and independently Nagumo,

[3] for which they obtained the Nobel Prize in Physiology or Medicine 1963

Arimoto, Yoshizawa 1962 were able to simplify these to the Fitz Hugh-Nagumo-Model. FitzHugh calls this model Bonhoeffer-Van der Pol oscillator, since the equations for $a = b = 0$ describe a special case of the VP oscillator:

$$\begin{aligned} \dot{v} &= v - \tfrac{1}{3}v^3 - w + I_{ext} \\ \tau\dot{w} &= v - a - bw \end{aligned} \tag{7.41}$$

v is the membrane potential, w and τ are auxiliary variables and I_{ext} an external current; $\dot{v}$ and $\dot{w}$ are as usual the first derivative of v and w.

Even without external stimulation oscillations occur, which simulate the potential of an oscillation producing neuron. Instead of the parameters a and b the original VP oscillator can be extended in another way, in order to describe important properties of the action potentials and to influence the frequency and the oscillation stability without changing the signal shape significantly (see Grudzinski, Zebrowski 2004).

$$\ddot{x} + \alpha(x - v_1)(x - v_2)\dot{x} + x(x + d)(x + e)/ed = 0, \quad d, e, \alpha > 0 \tag{7.42}$$

The corresponding Scilab model is shown in Fig. 7.51. This model can not only be used to describe the action potential of a single neuron, but does so for many neurons of similar type (e.g. in the sinus node).

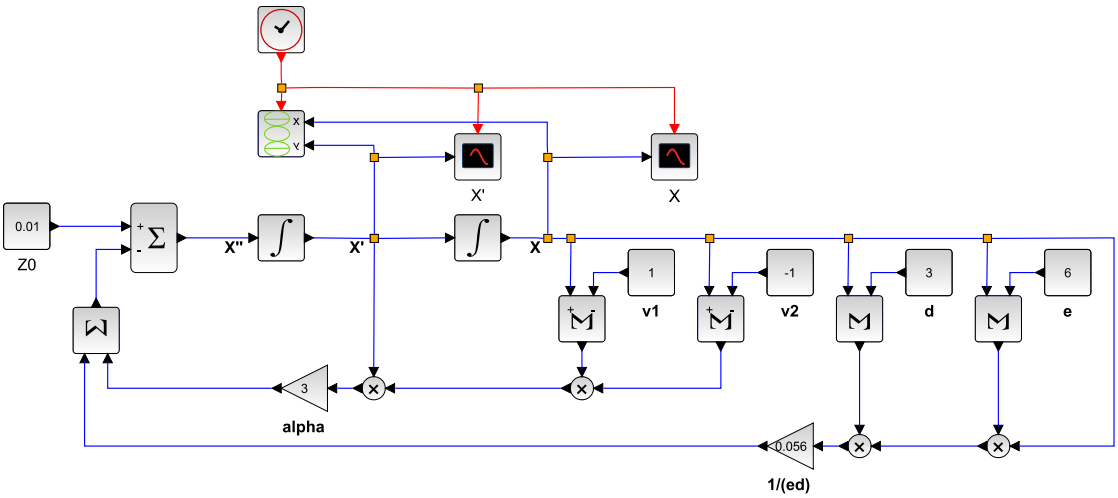

Figure 7.51: *A VP oscillator after Grudzinski, Zebrowski 2004 according to Eq. 7.42 simulates the action potential of an oscillation producing neuron or of a whole bundle of nerves of similar cell type (e.g. of the SA- or AV nodes in the heart). The parameter α changes the diastolic as well as the refractory time segment of the cardiac infarction, v_1 and v_2 changes the value of the resting potential , and the parameters e and d can be used to influence the period length of the heart beats; everything else including the shape of the ECG stay unchanged. Thus all parameters are able to change the heart beat rate, but in different ways.*

This modified VP oscillator is, however, not stable against external influences. If an impulse is

applied additionally to the entrance (a model for it in Engelmann, Witte 2016), it can, depending on the time and amplitude, at which the impulse was given, suppress the oscillation (Fig. 7.52, top curve) or stop it completely (Fig. 7.52, lower curve).

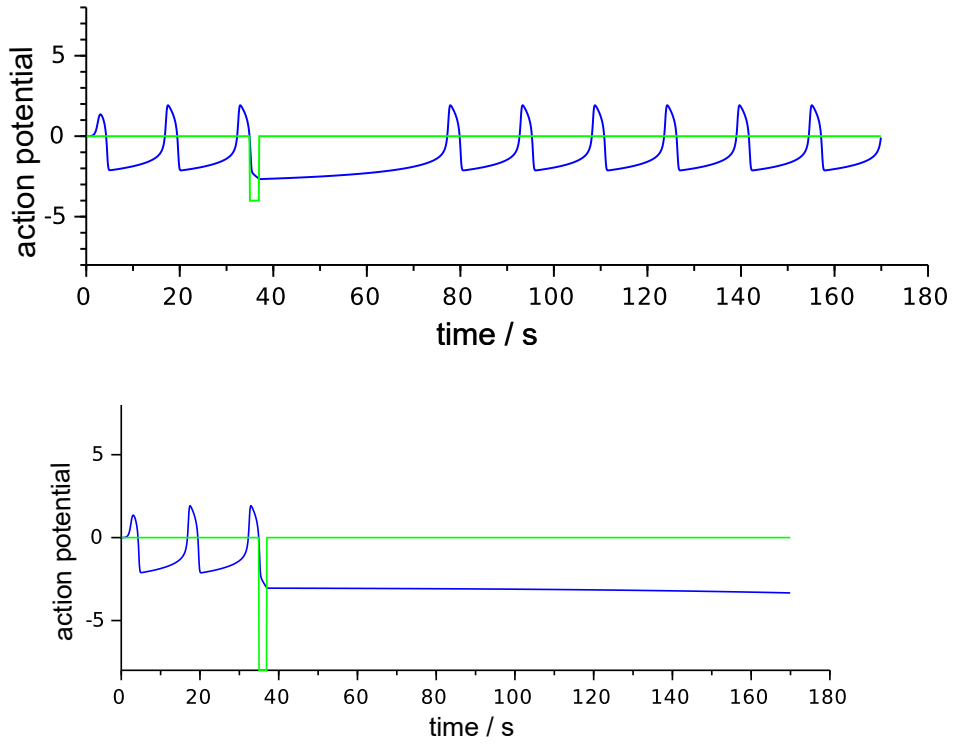

Figure 7.52: *Action potential x(t) of a VP oscillator, which stops briefly for two time units (upper curve) or completely (lower curve, see also Engelmann, Witte (2016)).*

7.8.2 One- and two oscillator model of Grudzinski and Zebrowski

The sinus node of the heart consists of uniform heart cells, which can produce oscillations autonomously. Since they correspond to the oscillation of a single heart cell, the model of (Grudzinski, Zebrowski 2004) (Fig. 7.53) is suitable also as a model for the whole sinus node. This node influences now the AV node, which consists also of uniform oscillation producing heart cells, although with a smaller Eigenfrequency. Thus the sinus node functions due to the coupling with the AV node as a pacemaker: The heart cells of the AV node produce with the same frequency as the heart of the sinus node an action potential. Both oscillations - the one of the sinus node and the delayed one of the AV node - yield an altered signal, which is able to describe also pathological properties of real ECG signals. A corresponding model in Scilab/xcos shows Fig. 7.53.

For a mathematical description the equations (analogue to Eq. 7.42) for *two* modified VP oscillators were used, which are mutually coupled.

As a start only the coupling between the sinus node and the AV nodes are considered (see Zebrowski et al. (2007)). In Eq. 7.43 the lower index SA is used for signals and parameters of the sinus node and lower index AV is used for the signals and parameters of the atrioventricular nodes. In the coupling k_{SA-AV} is the damping factor of the sinus- to the AV node and k_{AV-AV} the feedback of the AV node from its output to the input. $x_{SA}^{\tau_{SA-AV}}$ is the output signal delayed by the run time τ_{SA-AV} of the sinus node to the AV node, since the output signal of the sinus node is not directly connected to the AV node, but can reach it only via other neurons. Therefore it should generally hold: $x^{\tau}(t) = x(t-\tau)$.

$$\begin{aligned} \ddot{x}_{SA} &= -\alpha_{SA}(x_{SA} - v_{SA_1})(x_{SA} - v_{SA_2})\dot{x}_{SA} \\ &- x_{SA} f_{SA}(x_{SA} + d_{SA})(x_{SA} - e_{SA}) \\ \ddot{x}_{AV} &= -\alpha_{AV}(x_{AV} - v_{AV_1})(x_{AV} - v_{AV_2})\dot{x}_{AV} \\ &- x_{AV} f_{AV}(x_{AV} + d_{AV})(x_{AV} - e_{SA}) \\ &+ k_{SA-AV} x_{SA}^{\tau_{SA-AV}} - k_{AV-AV} x_{AV} \end{aligned} \tag{7.43}$$

The equivalent model in Scilab/xcos is shown in figures 7.52 and 7.54.

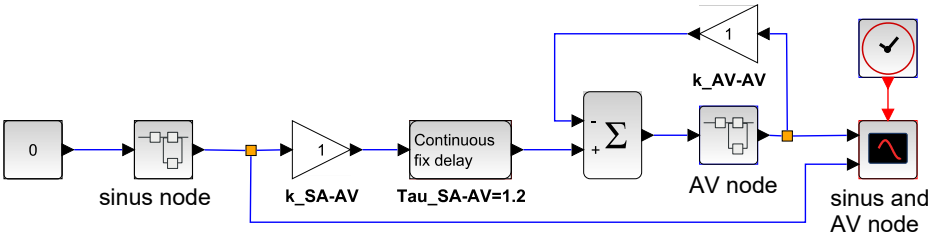

Figure 7.53: *Oscillator model with SA- and AV node of the heart according to the differential Eq. 7.43 after Zebrowski et al. (2007), where here additionally a delay $\tau_{SA-AV} = 1.2$ of the sinus node signal has been added, before it reaches the control input of the AV node. k_{SA-AV} and k_{AV-AV} are the damping factors between the sinus- and the AV node and feedback of the AV node from its output to its input. Both have the value 1. The sinus node as well as the AV node are represented in Scilab/Xcos by a small separate network (superblock). It is shown for the AV node in Fig. 7.54. For the sinus node it is the same, but with other parameters (see also Engelmann, Witte (2016).*

If the coupling factor from the sinus node to the AV node k_{SA-AV} not too big in respect to the feedback factor k_{AV-AV} of the AV oscillator, both oscillators can oscillate in their Eigenfrequencies (see Fig. 7.55). In this case each of the two oscillators can react like a single one to external influences, e.g. with a temporary or complete stop of the oscillation (see Fig. 7.52).

Is, however, the coupling factor k_{SA-AV} from the sinus to the AV node considerably larger, the signal of the sinus node has a large influence on the AV node:

- Is the Eigenfrequency of the AV nodes not substantially smaller as the one of the sinus node, the signal of the sinus node can trigger that of the AV nodes, so that both nodes oscillate with the same Frequency (see Fig. 7.56).

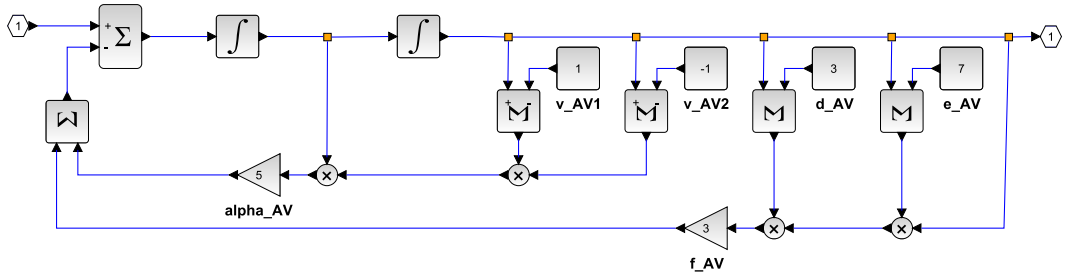

Figure 7.54: *A small separate network (superblock) of the AV node in Fig. 7.53, which corresponds to the one of the sinus node, however with other values for the parameter e, i.e. according to Zebrowski et al. (2007) the parameters for the AV node* $v_{AV_1} = 1$, $v_{AV_2} = -1$, $d_{AV} = 3$, $e_{AV} = 7$, $f_{AV} = 3$, $\alpha_{AV} = 5$ *and for the sinus node* $v_{SA_1} = 1$, $v_{SA_2} = -1$, $d_{SA} = 3$, $e_{SA} = 12$, $f_{SA} = 3$, $\alpha_{SA} = 5$ *were chosen.*

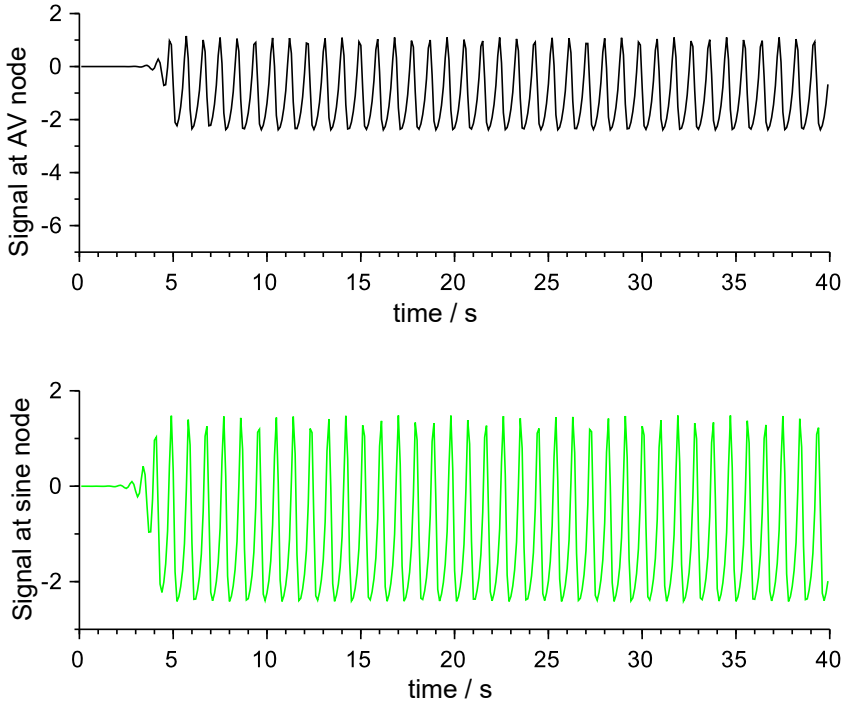

Figure 7.56: *Synchronised oscillation of the sinus- and AV nodes according to figures 7.53 and 7.54 in the case of stronger coupling of the sinus node to the AV node, if the Eigenfrequencies do not deviate much from each other* ($k_{SA-AV} = 12$, $k_{AV-AV} = 1$, $e_{SA} = 12$ *and* $e_{AV} = 11$)

- Is the Eigenfrequency of the AV nodes too low in order to follow the signal of the sinus node, interruption occur (see Fig. 7.57).

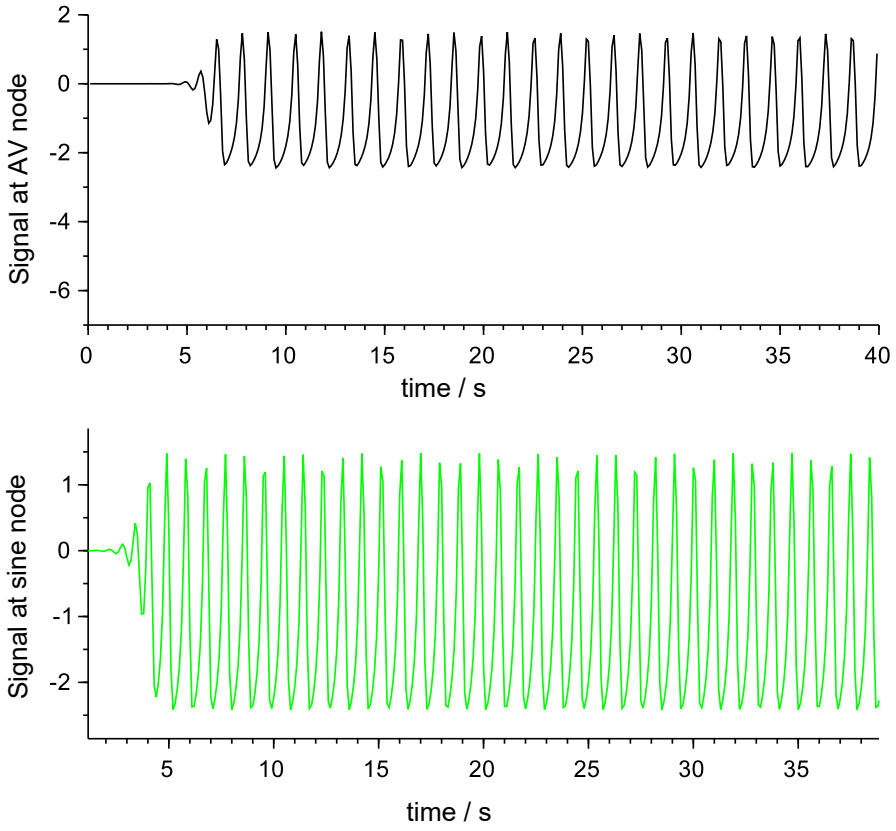

Figure 7.55: *Decoupled oscillations of the sinus- and AV node according to Fig. 7.53 and 7.54 with* $k_{SA-AV} = k_{AV-AV} = 1$, $e_{SA} = 12$ *and* $e_{AV} = 7$

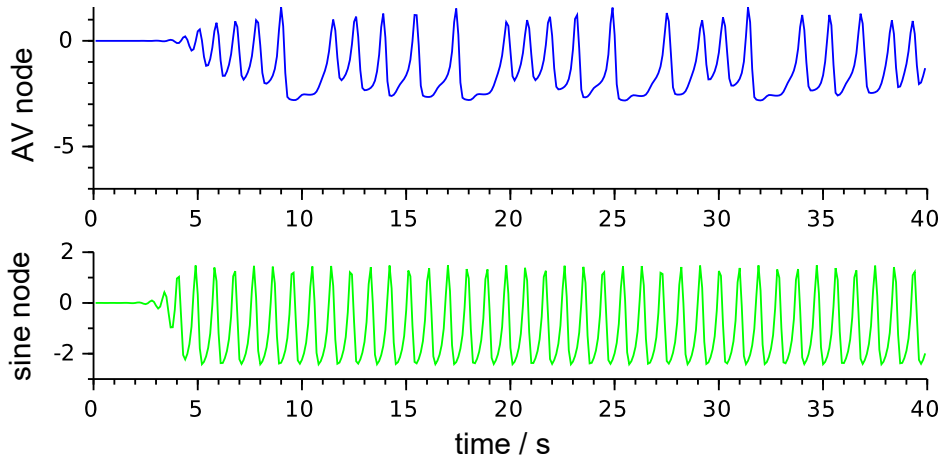

Figure 7.57: *Partly synchronised oscillations of the sinus- and AV nodes according to Fig. 7.53 and 7.54 in the case of stronger coupling of the sinus node to the AV node, and this node can not follow the signal of the sinus node because the Natural frequency is too low(*$k_{SA-AV} = 12$, $k_{AV-AV} = 1$, $e_{SA} = 12$ *and* $e_{AV} = 7$*). See also Engelmann, Witte (2016)*

- In the worst case the oscillations stop completely after a few arrhythmic oscillation of the AV node (the main chamber of the heart for pumping blood, see Fig. 2.7) if the Eigenfrequencies of sinus- and AV nodes are too different, and the heart stops beating (see Fig. 7.58).

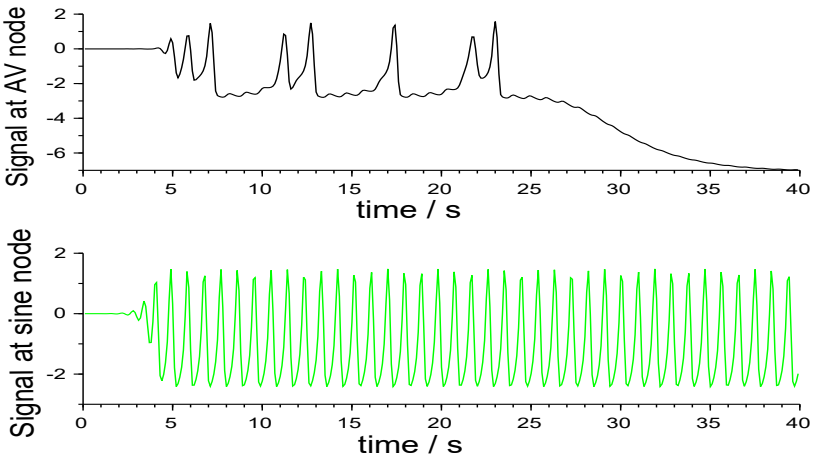

Figure 7.58: *Unsynchronisable oscillations of the AV nodes according to figures 7.53 and 7.54 in the case of stronger coupling between the sinus node an the AV node, if the oscillation of the AV nodes stops completely after irregular interruptions, i.e. if the singular point has been reached* ($k_{SA-AV} = 12$, $k_{AV-AV} = 1$, $e_{SA} = 12$ *and* $e_{AV} = 7$*).*

7.8.3 Three-oscillator model of Gois and Savi

With the two oscillators of the former section, which describe the coupling of the sinus- and the AV node, many properties of the production of oscillations by the heart can be explained. The various signals do, however, not yet resemble the ECG signals $x_{EKG}(t)$ measured at the surface of the body. The reason is, that the HIS bundle and the Purkinje fibers are also oscillators which are involved in the ECG signal (see Fig. 2.7). The output signals of the sinus node (SA) $x_{SA}(t)$, of the atrioventricular node (AV) $x_{AV}(t)$ and of the His-Purkinje complex (HP) $x_{HP}(t)$ overlay each other and act in different strength at the surface of the body. The ECG signal can be described approximately linear by a weighted addition of these signals with damping factors a_{SA}, a_{AV} and a_{HP} (see Gois, Savi (2009)):

$$x_{EKG}(t) = a_{SA}x_{SA}(t) + a_{AV}x_{AV}(t) + a_{HP}x_{HP}(t)$$

Since the excitation of the heart pump reaches the main chamber via the atrium and the AV node, the coupling of the three oscillators shall be done directional, i.e. from the SA- to the AV- and finally to the HP oscillator, as shown in the lower part of Fig. 2.7.

The mathematical equations for three oscillators are obtained from those for two by supple-

menting these with the corresponding coupling to Eq. 7.43:

$$\begin{aligned}
\ddot{x}_{SA} &= -\alpha_{SA}(x_{SA} - v_{SA_1})(x_{SA} - v_{SA_2})\dot{x}_{SA} \\
&- x_{SA} f_{SA}(x_{SA} + d_{SA})(x_{SA} - e_{SA}) \\
\ddot{x}_{AV} &= -\alpha_{AV}(x_{AV} - v_{AV_1})(x_{AV} - v_{AV_2})\dot{x}_{AV} \\
&- x_{AV} f_{AV}(x_{AV} + d_{AV})(x_{AV} - e_{SA}) \\
&+ k_{SA-AV} x_{SA}^{\tau_{SA-AV}} - k_{AV-AV} x_{AV} \\
\ddot{x}_{HP} &= -\alpha_{HP}(x_{HP} - v_{HP_1})(x_{HP} - v_{HP_2})\dot{x}_{HP} \\
&- x_{HP} f_{HP}(x_{HP} + d_{HP})(x_{HP} - e_{HP}) \\
&+ k_{AV-HP} x_{SA}^{\tau_{AV-HP}} - k_{HP-HP} x_{HP}
\end{aligned} \tag{7.44}$$

The corresponding model in Scilab/xcos is shown in Fig. 7.59. Here the disturbances due to deviations of the ECG base line (e.g. if the skin contact has changed) and due to noise (e.g. with 50Hz net hum, influences of fluorescent tubes, radio waves) have been taken into account.

The produced signals of the sinus node (SA), AV node (AV) and His bundle with the Purkinke fibers (HP) and the resulting ECG signal without disturbances is shown in Fig. 7.60. In this figure it can nicely be seen, of which parts the separate fractions of an ECG signal consist. The p waves are from the signal of the sinus node and the QRS complex is produced by the cooperation of the AV node and the HIS bundle with the Purkinje fibers. The T wave is mainly produced by the HIS bundle and the Purkinje fibres.

In Fig. 7.61 the ECG signal is shown with the additional signals due to noise and an unsteady base line.

With the three oscillator heart model of Gois, Savi (2009) the various ECGs of heart diseases can be simulated, e.g.

- AV rhythm
- His bundle rhythm
- Ventricular fibrillation and -flatter
- AV block
- Dropout of heart beats
- Extra systoles
- Sinus-bradia and tachycardia

An especially tragic case is the sudden cardiovascular collapse . It can be triggered by an external impulse and can likewise be simulated with this model. At first the figures 7.62 and 7.63 show the effect of a short negative impulse at the sinus node with a width of 0.216 and an amplitude of 1 at the 80th time unit. As shown in the figure, two heart beats drop out, before the normal sinus rhythm occurs again.

If this impulse is only slightly longer (from 0.216 to 0.21634, i.e. *0.157%!*), an asystole occurs and the heart stops beating (sudden cardiac death, see Fig. 7.64 and 7.65).

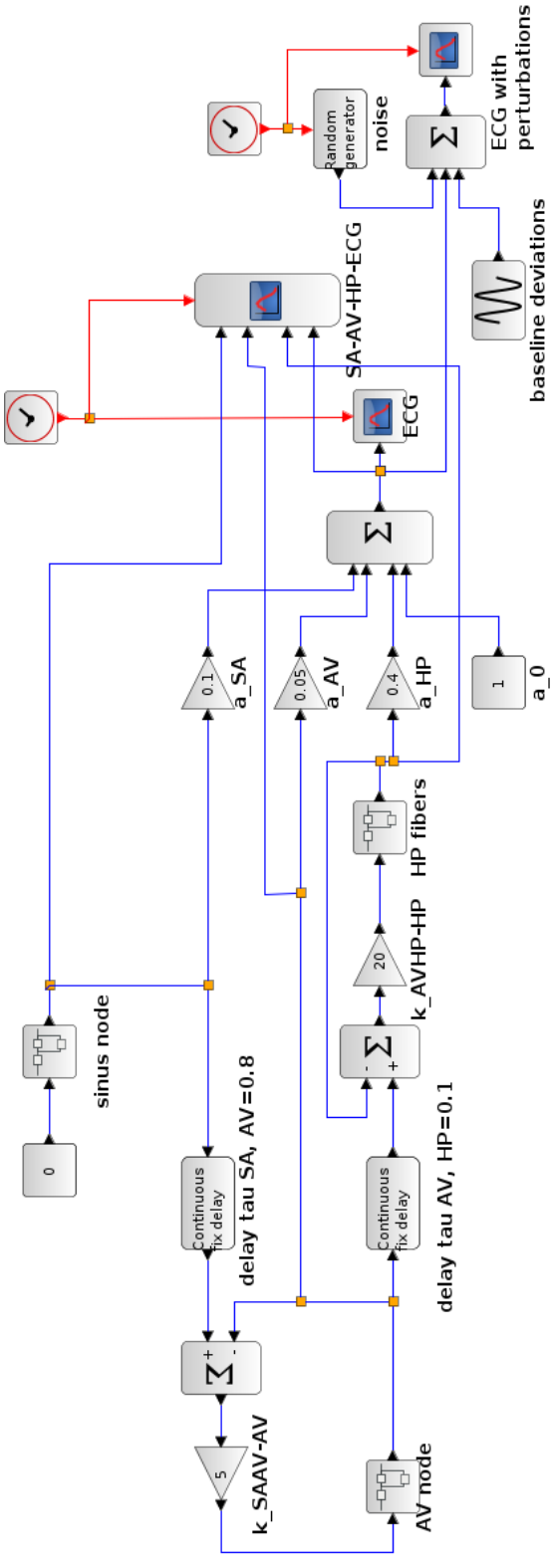

Figure 7.59: *Oscillator model of the heart with SA-, AV- and HP nodes according to Fig. 2.7 and the differential Eq. 7.44 of Gois, Savi (2009). However here a delay with $\tau_{SA-AV} = 0,8$ of the sinus node signals to the AV node and a delay with $\tau_{AV-HP} = 0,1$ from the AV node to the His-Purkinje complex was added (before these signals reach the control input of the AV nodes respectively of the HP node, they were weighted by the coupling factors $k_{SA-AV} = k_{AV-AV} := k_{SAAV-AV} = 5$ and $k_{AV-HP} = k_{HP-HP} := k_{AVHP-HP} = 20$. An oscillator node (SA-, AV- or HP node) corresponds to the one of the two oscillator models (only SA- and AV node, see Fig. 7.54). The particular parameters were chosen as in Gois, Savi (2009): In the case of the sinus node it is $v_{SA_1} = 0,2$, $v_{SA_2} = -1.9$, $d_{SA} = 3$, $e_{SA} = 4,9$, $f_{SA} = 1$, $\alpha_{SA} = 3$, in the case of the AV node $v_{AV_1} = 0,1$, $v_{AV_2} = -0,1$, $d_{AV} = 3$, $e_{AV} = 3$, $f_{AV} = 1$, $\alpha_{AV} = 3$, and in the case of the His-Purkinje complex it is $v_{HP_1} = 1$, $v_{HP_2} = -1$, $d_{HP} = 3$, $e_{HP} = 7$, $f_{SA} = 1$, $\alpha_{HP} = 5$.*

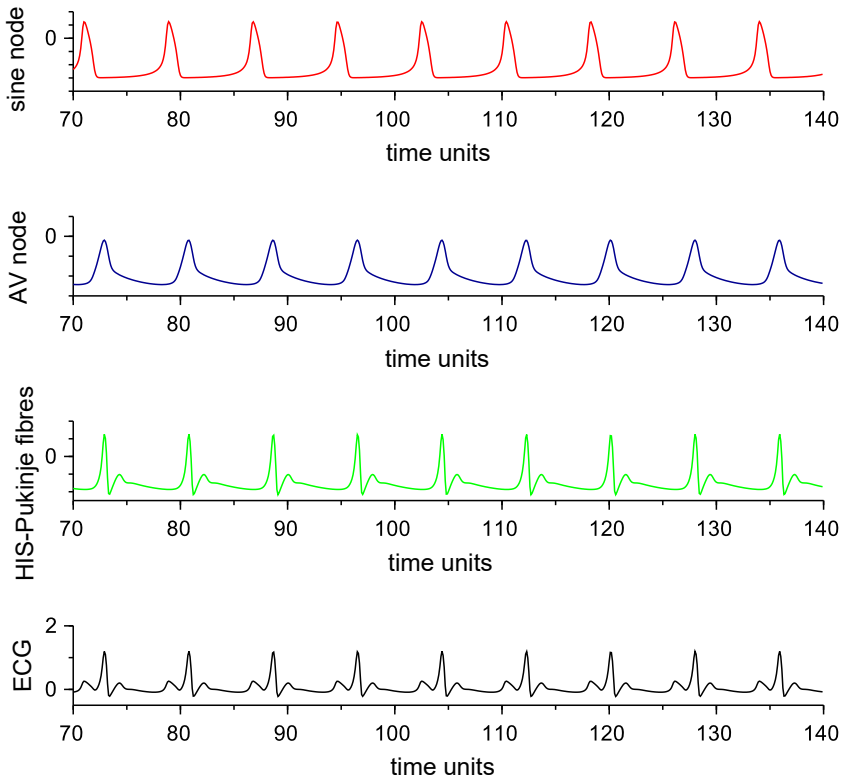

Figure 7.60: *Simulation of the signals during the ECG production by the three pacemakers sinus node (top, red), AV node (below, blue) and HP-Purkinje fibers (green) in the heart. The ECG (black) is composed of the three curves. Three oscillator heart model of Gois, Savi (2009), see also Engelmann, Witte (2016).*

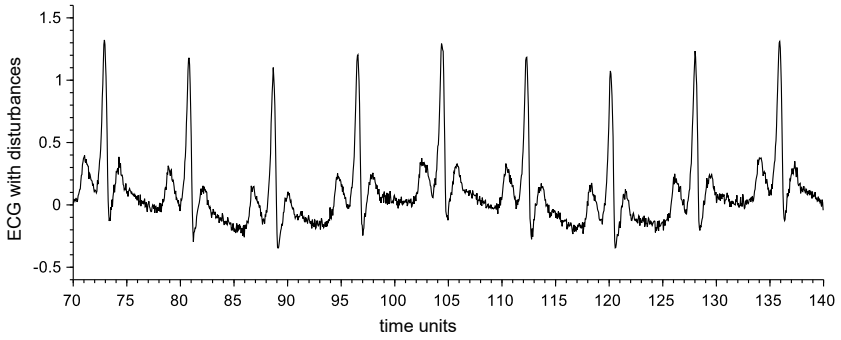

Figure 7.61: *ECG signal of Karl-Heinz Witte, own measurements. Compare with Fig. 7.60, lowermost curve*

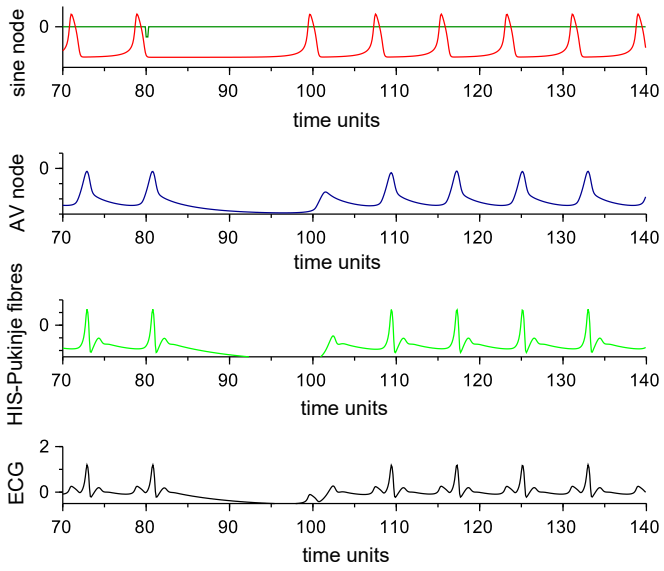

Figure 7.62: *Simulation of the signals during the ECG simulation with the three oscillator heart model of Gois, Savi (2009), see also Engelmann, Witte (2016). As in Fig. 7.60, but with an external negative impulse at the sinus node (green) at the time 80 with an amplitude of 1 and a width of 0.216 time units. At least two heart beats drop out, before the normal sinus rhythm comes back.*

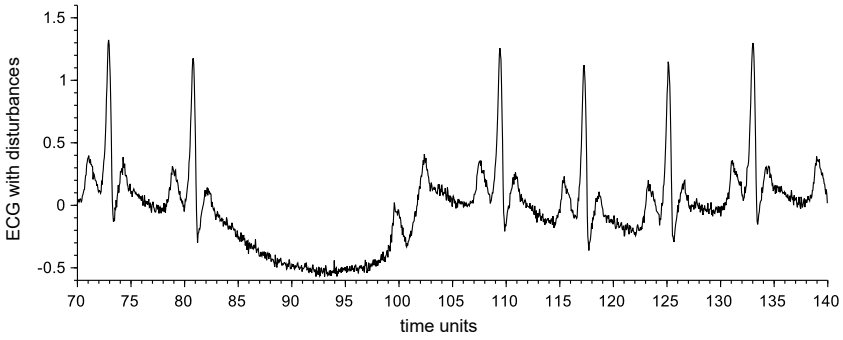

Figure 7.63: *ECG for Fig. 7.62 with noise from the three oscillator model after Fig. 7.59 and an external negative impulse at the m sinus node with an amplitude of 1 and a width of 0.216 at the time unit 80.*

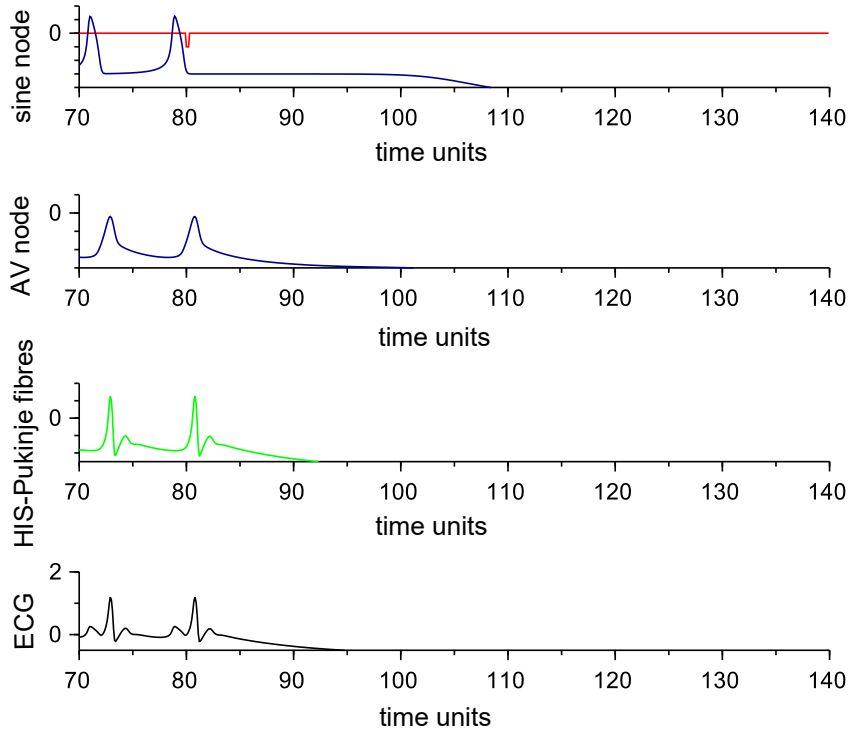

Figure 7.64: *ECG signals of the three oscillator model in Fig. 7.59 getting an external negative impulse at the sinus node with an amplitude of 1 and a width of 0.21634 time units (increased by 0,157% in respect to the previous example) at the time unit 80. An asystole arises, i.e. the heart stops beating and the singular point is reached.*

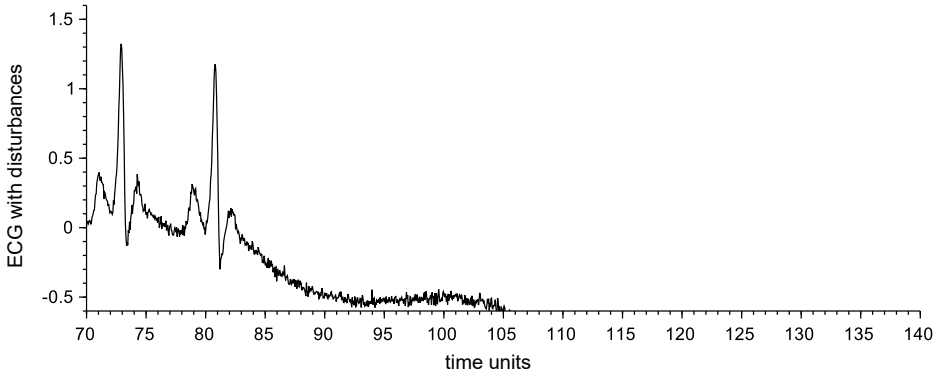

Figure 7.65: *ECG for Fig. 7.64 with noise at the three oscillator model in Fig. 7.59 receiving an external negative impulse at the sinus node with an amplitude of 1 and a width of 0.216 time units applied during the time unit 80.*

7.8.4 Heart model with only one oscillator to produce a realistic ECG

If a model is used, which describes only the electric signals of the ECG, one can take e.g. the model of Clifford (see Fig. 7.66 and the functional diagram in Fig. 7.67 (literature: McSharry, Clifford (2006), Stefanovska (2007), Stefanovska, Hocik (2000), Stefanovska, Lotric et al. (2001) and Stefanovska, Luchinsky, McClintock (2001)). Hereby the individual sections of *one* cardiac infarction (QRS complex with P and T waves) are approximated by Gauß functions, which are prompted by a *single* simplified oscillator, which describes the model for the sinus node. Hereby the influences of respiration and of the nervous system can be considered by the spectrally measured properties, which corresponds to an additional frequency modulation. Fluctuations of the ECG base line, which could arise e.g. by a varying resistance between skin and electrode are generated by a further simple sinus oscillator.

If one simulates with this model a pulse of about 60 beats per minute and breathes of air of about 15 per minute, and if the base line fluctuates with a period length of about 4 seconds, a signal course is obtain as shown in Fig. 7.68.

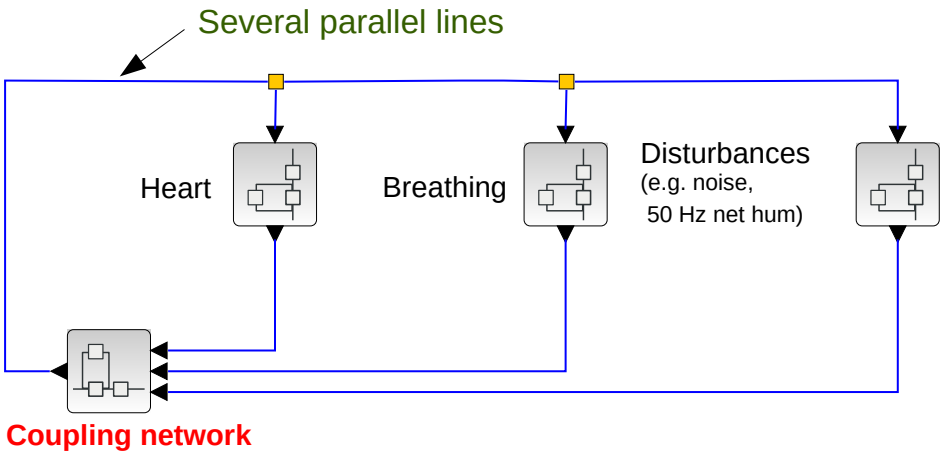

Figure 7.66: *A coupled oscillator net is the ECG oscillator of Clifford. Heart and breathing are coupled with each other via a couple network. Disturbances by noise or the 50 Hz net hum can influence it.&&&*

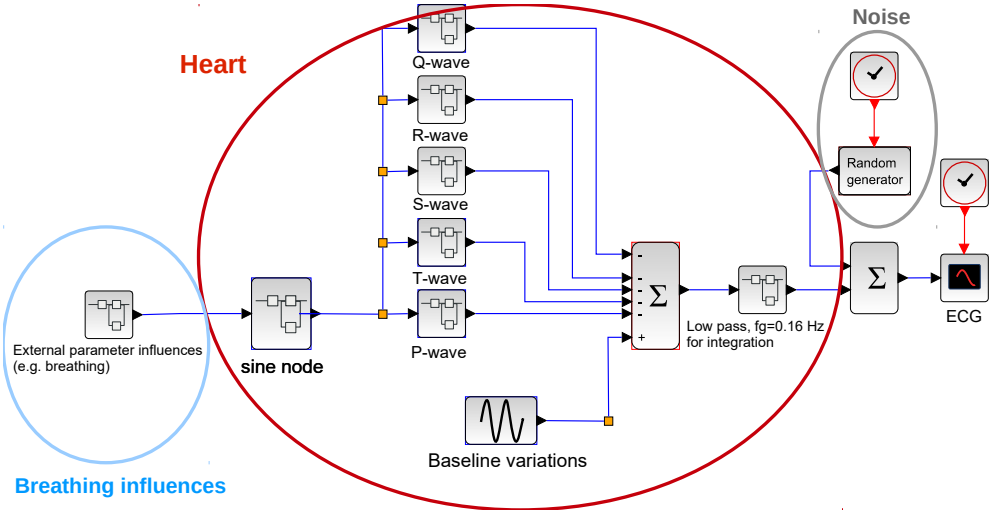

Figure 7.67: *Influencing the ECG oscillators (heart, red oval) by breathing (grey oval) and noise (blue oval), after McSharry, Clifford (2006).*

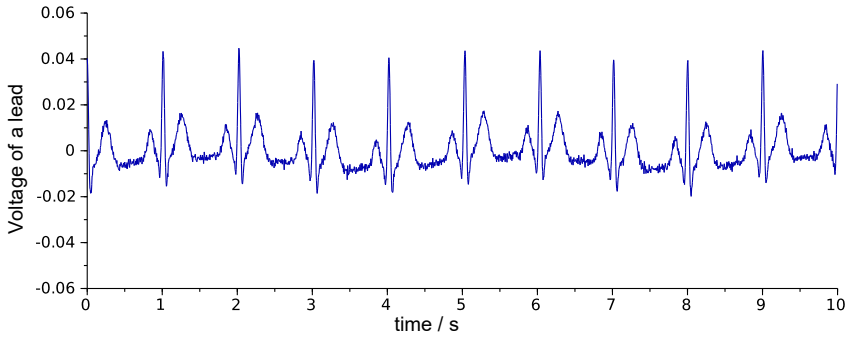

Figure 7.68: *Simulation of the ECG oscillators of McSharry and Clifford (McSharry, Clifford 2006) with a pulse of about 60 beats per minute and breathes of about 15 per minute: The base line fluctuates with a period length of about 4 s..*

In the case of the heart a model can e.g. be approached, which consists of 3 oscillators, which generates the fluctuating rhythm of the sinus node, the AV node, and eventually of the Purkinje fibers. The oscillators are mutually coupled, whereby the sinus node possesses the highest Eigenfrequency and controls thus externally the other oscillators (AV node and Purkinje fibers).

7.8.5 Models for Blood pressure and flow models in the circulation system

So far, models for the electrical excitation of the heart have been described and models for the transport of blood in the circulatory system have not been presented, although they are also

very important to understand how the blood can be transported sufficiently to the brain, lungs, organs and other muscles. It is also helpful to use models where the signal direction is not shown as in a flow diagram but where only the connections between the "components" are described (e.g. in an electrical circuit with non-active parts such as resistors (R), capacitors (C), inductors (L) and active parts such as operational amplifiers and transistors).

First, a section of an artery or vein is to be examined in general and an analogue electrical model developed for it. Fig. 7.69 shows a part of the veins (arteries in red and veins in blue) of the human circulatory system in which a piece of vein is marked. The physical quantities of e.g. flow and pressure are shown in Fig.7.70.

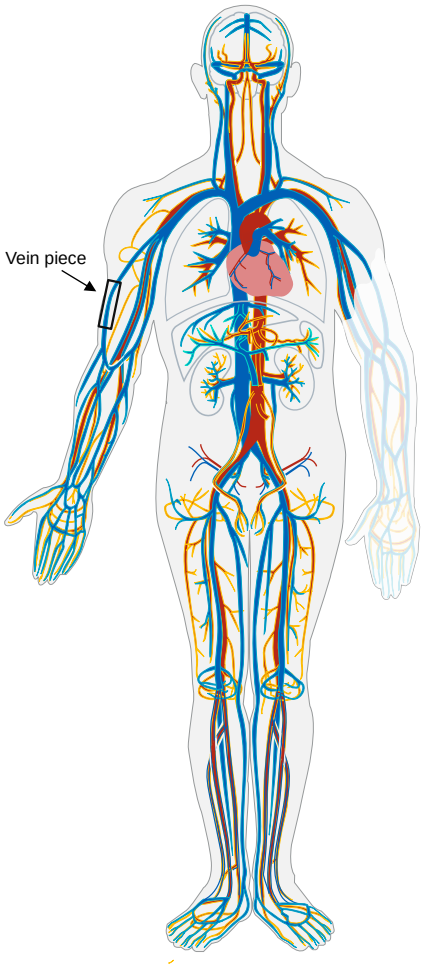

Figure 7.69: *Illustration of arteries (red) and veins (blue) of the human circulatory system, with a labelled piece of vein(Mofified Figure of the Figures from wikimedia.org. https://commons.wikimedia.org/wiki/File:Circulatory_System_no_tags.svg. This work has been released into the public domain by its author, LadyofHats. This applies worldwide. In some countries this may not be legally possible; if so: LadyofHats grants anyone the right to use this work for any purpose, without any conditions, unless such conditions are required by law.)*

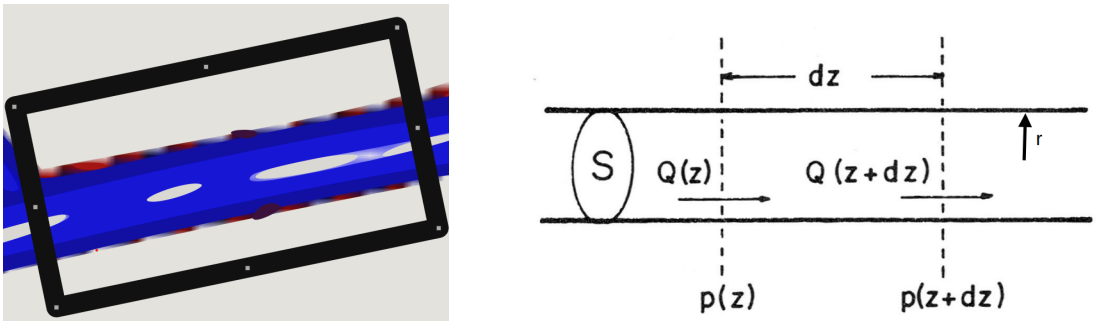

Figure 7.70: *Description of the piece of vein shown in Fig.7.69 (left) by means of a schematic representation with indication of the physical quantities (right)*
S: Area of the core cross-section of the vein, r: Radius of the blood vessel. Q: blood flow, P: blood pressure, z: length coordinate

Two equations apply to the section of length dz of the blood vessel section:

1. the sum of the acting forces is equalised (equilibrium of forces) and
2. no blood disappears in the section (conservation of mass).

Prerequisite: incompressible blood and continuous (laminar) flow (no vortices)
The following forces must be taken into account:

- External forces $S[p(z+dz)-p(z)]$ =Sdp with $S=\pi r^2$
- Inertia forces $m_B dv/dt = Sdz\rho dv/dt$ mitρ : specific density
- Frictional force $8\eta Qdz/r^2$ mit $Q=\pi r^2 v$: Flow in volume per time, η: Viscosity, v: speed (according to **Hagen-Poiseuille**,see e.g..https://de.wikipedia.org/wiki/Gesetz_von_Hagen-Poiseuille)

Since the sum of all forces in a piece of the veins must disappear, the result is

$$\pi r^2 dp + \pi r^2 dz\rho dv/dt + 8\eta Qdz/r^2 = 0$$

By substituting $v = Q/(\pi r^2)$ and dividing by $\pi r^2 dz$ the **1st relationship(Diff.-Gl.)** between pressure p and flow Q follows:

$$dp/dz + \underbrace{\left(\rho/\pi r^2\right)}_{=L'} dQ/dt + \underbrace{\left(8\eta/\pi r^4\right)}_{=R'} Q = 0 \tag{7.45}$$

Since it is assumed that the blood is not compressed as it flows through the veins, the volume in the section of vein must also be maintained during the flow. This then leads to the second differential equation. With

- the flow change due to volume change $dQ = dV/dt$,

- the change in volume due to pressure $dV/dt = (dS/dt)dz = \underbrace{(dS/dp)}_{C''}(dp/dt)dz$

  with C' Compliance per unit length,
- the change in volume when the flow passes through small branches $G'dz\,p$

results for the sum of the volume changes:

$$dQ + C'dp/dt)dz + G'dzp = 0$$

By dividing by dz, the **2nd relationship (Diff. -Gl.)** between pressure p and flow Q follows:

$$dQ/dz + C'(dp/dt) + G'p = 0 \tag{7.46}$$

Limitations in the body Hagen–Poiseuille is an idealized model:

- Blood is non-Newtonian (its viscosity changes with shear rate).
- Flow is pulsatile, not perfectly steady.
- Vessels are elastic, not rigid.
- Turbulence can occur at high flow rates or in narrowed arteries.

Still, the basic law is extremely useful for understanding how radius, viscosity, and pressure interact in controlling blood flow.

The hemodynamic behavior of the circulatory system, particularly in arteries, can be mathematically modeled using analogies to electrical circuits. This approach is called the lumped parameter model or Windkessel model when applied to vascular segments. The core idea is to draw parallels between fluid flow in vessels and current in circuits, as well as pressure and voltage (see Fig.7.71).

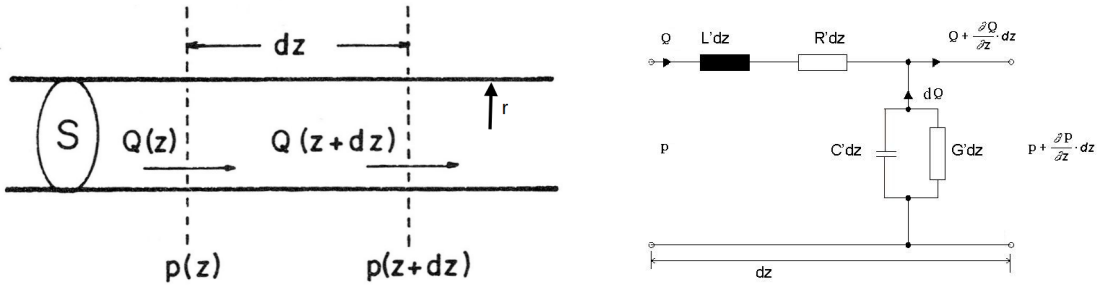

Figure 7.71: *Description of the piece of vein shown in Fig.7.70 (left) with electrical equivalent circuit diagram(right)*
S: Area of the core cross-section of the vein, r: Radius of the blood vessel. Q: flow rate, P: blood pressure, z: length coordinate, R:Vascular resistance, C: Compliance , L:Blood inertia, G:Leakage conductance. The values with a dash (e.g. R', C', L') mean values per unit length.,

Electrical circuit	Vascular/arterial system	Unit (electrical)	Unit (vascular)
Voltage (V)	Pressure (P)	V	mmHg or Pa
Current (I)	Flow rate (Q)	A	mL/s or L/min
Charge (Q_e)	Volume (V_β)	C	mL or L
Resistance (R)	Vascular resistance (R_v)	Ω	mmHg·s/mL or Pa·s/m³
Conductance(G).	Leakage conductance.	S	mL/(mmHg·s) or m^3/(Pa·s)
Capacitance (C)	Compliance (C_v)	F	mL/mmHg or m³/Pa
Inductance (L)	Inertance (L_v)	H	mmHg·s²/mL or Pa·s²/m³
Power P_{el}	Hydraulic power	W	mmHg·mL/s or W

Table 7.1: *Analogy between an electrical circuit and the arterial / vascular system:*

Table 7.1 shows the analogy between an electrical circuit and the arterial / vascular system with indication of the units: The motor for generating the blood flow, the heart, see Fig.7.48, actually consists of two pumps with an anterior and main chamber, whereby valves prevent the blood from flowing back, as the pumps only open in one direction. There are valves not only in the heart but also in the veins so that the blood does not run back towards the feet during circulation due to gravity when the deoxygenated blood is to be pumped back to the heart so that it can be further enriched with blood in the lungs.

Like the blood vessels, these heart pumps can also be described by an electrical analogue circuit. Fig.7.72 shows the pump on the left, which pumps the blood from the lungs into the Aorta, with the corresponding electrical equivalent circuit diagram, where the heart valves are replaced by switches which open when the flow is only in one direction. You could also use diodes with very steep forward characteristics..

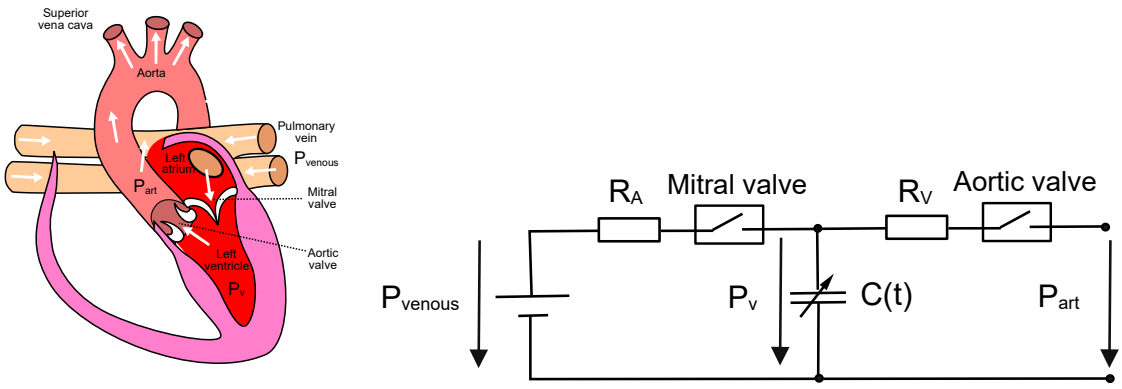

Figure 7.72: *Left ventricle of the heart in modified Fig.7.48(same license) with electri. circuit diagram Pvenous: Blood pressure in the veins in front of the mitral valve, Pv:Blood pressure behind the mitral valve, Part: Arterial blood pressure behind the aortic valve, RA:Resistance in the atrium, Rv:Resistance in the ventricle, C(t): Temporal change in the volume of the ventricle due to its pressure change (The pumping function is created by the rhythmic change of these.)*

In principle, the volume of the heart chambers changes in a similar way to the volume in a piece of vein. However, this is not caused by blood pressure but by electrical excitation of the heart muscles by the heart's internal oscillators, such as the sinus or AV node, but also by impulses from the autonomic nervous system, which can also influence blood pressure in other parts of the circulatory system.

The property of the volume change in blood vessels and ventricles is described by the **compliance**, which is determined for

- **blood vessels** per vein section dz by

$$C' = \frac{dS}{dp}, \quad \text{S: cutting surface, p: pressure}$$

- and in the **ventricle** with

$$C(t) = \frac{V_v(t) - V_0}{P(t)}, \quad V_V(t) \text{ : Ventrivular volume, } V_0 \text{ : correction Volume}$$

The inverse of this is the ventricular elastances $[E(t) = 1/C(t)]$ of the heart muscle and indicates how much the pressure changes due to volume changes (it is easier to realise the inverse E(t) of the compliance C(t), see e.g.B. Snyder, Rideout 1968; Rideout 1991) and has been analysed many times with regard to the heart muscle and described with cosine functions(see Fig. 7.73, e.g. Thomas Heldt, Kamm, G.Mark 2002 and Segers et al. 2003):

$$E(t) = \begin{cases} E_{dias} + \frac{E_{sys}-E_{dias}}{2} \cdot \left\{1 - \cos\left(\pi \cdot \frac{t}{T_S(n)}\right)\right\} & 0 \le t \le T_S \\ E_{dias} + \frac{E_{sys}-E_{dias}}{2} \cdot \left\{1 + \cos\left(2\pi \cdot \frac{t-T_S(n)}{T_S(n)}\right)\right\} & T_S \le t \le \frac{3}{2}T_S \\ E_{dias} & \frac{3}{2}T_S < t \le T(n) \end{cases} \tag{7.47}$$

E_{dias}: Elastance during diastole, E_{sys}: Elastance during systole, $T_S(n)$: Time to the end of systole at the n-th interval T(n) between two R-waves of the ECG, $T_S(n) \approx 0,3 \cdot \sqrt{T(n-1)}$.

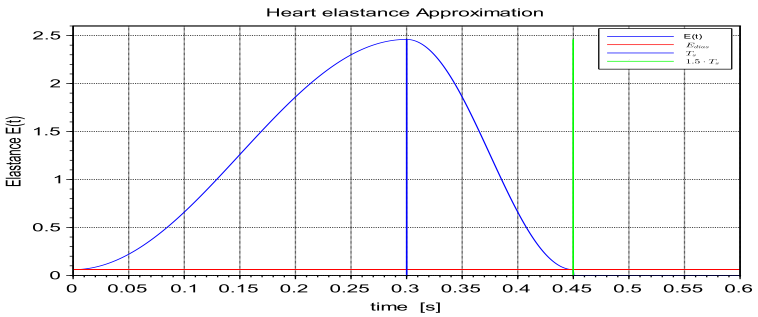

Figure 7.73: *Approximation for the elastance E(t) according to equation 7.47 and* $T(n) = 1$, $E_{dias} = 0.06$, $E_{sys} = 2.46$

> The function E(t) describes the change in the elasticity of the heart muscle during a heartbeat caused by nerve stimulation (e.g. sinus node SA). It could also be understood as an impulse response to a nerve impulse and the electrical excitation by an ECG as an input signal to a filter with this impulse response. But how do you obtain this filter?

It would be easy to realise such a filter in the digital domain, which is not recursive and generates this impulse response. However, this would require sampling the signal, feeding it to the digital filter and, after filtering, returning it to the continuous-time domain by interpolating between the discrete output values.

However, it would be more favourable to design a filter in the continuous-time domain, because this would cause the transformations to decay into the discrete-time domain and back. For example, E(t) can be transformed into the frequency domain as an impulse response by Laplace transformation and then the resulting parts can be modelled as function blocks (e.g. in Scilab). This results in the Laplace transform $\mathscr{L}\{E(t)\}(s)$ (without the constant portion E_{dias} for $t > \frac{3}{2}T_S$, since the normal one-sided Laplace transformation does not exist only for a constant fraction for a time from -infinity to plus infinity, This must be added to the filter later during realisation):

$$\begin{aligned} \mathscr{L}\{E(t)\}(s) \quad &= \quad E_m \frac{1-e^{-sT_S}}{s} - \Delta E \frac{s(1+e^{-sT_S}}{s^2+(\pi/T_S)^2} \\ &\quad + e^{-sT_S}\left[E_m \frac{1-e^{-sT_S/2}}{s} - \Delta E \frac{s(1+e^{-sT_S/2}}{s^2+(\pi/T_S)^2}\right] \qquad (7.48) \\ \text{with} \quad E_m &= \frac{E_{sys}+E_{dias}}{2}, \Delta E = \frac{E_{sys}-E_{dias}}{2} \end{aligned}$$

From this, a filter can be developed directly in Scilab and its reaction to a pulse tested (see Fig.7.74) The output signal of the test circuit is shown in Fig.7.74 As can be seen, this signal

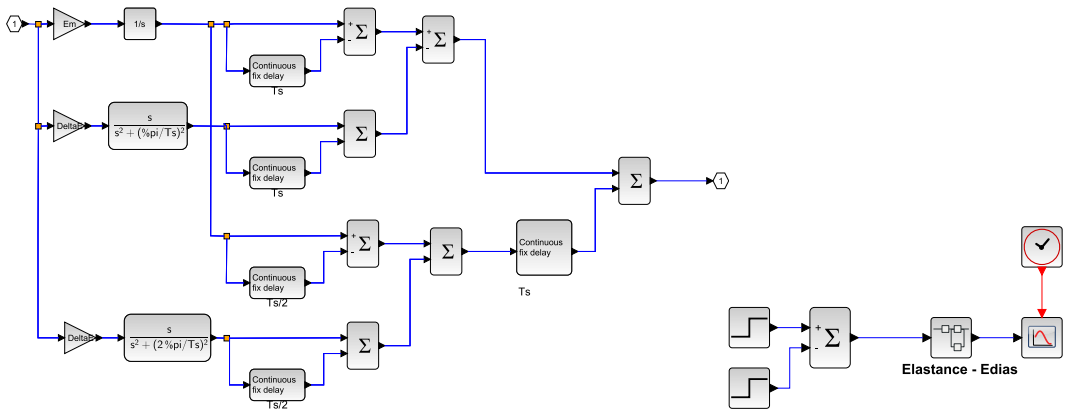

Figure 7.74: *Elastance filter after the Laplace transformation according to Eq.7.48(left) and test circuit(right), whereby a square-wave pulse is applied to the filter input.*

corresponds well with the elastance E(t) as shown in Fig.7.73 The maximum is shifted to the

right by 0.1 seconds, but this is because the square-wave pulse is not applied to the input at 0 but only after 0.1 seconds...

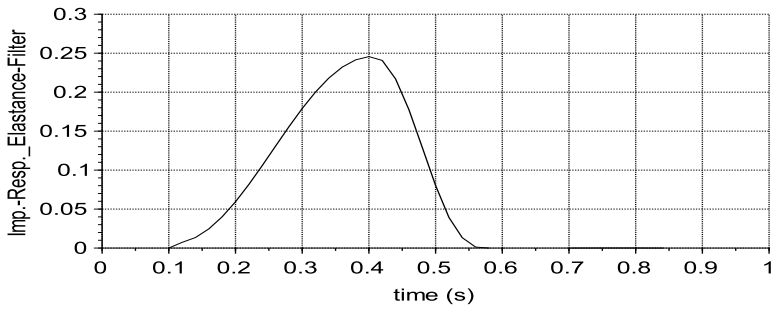

Figure 7.75: *Rectangular response of the elactance filter in Fig.7.74.*

However, it is not only possible to apply a square-wave pulse to the input and thus generate a rhythmic change in blood pressure, but also models for generating an ECG as described in the previous sections. Now it is also possible to analyse non-rhythmic excitations such as cardiac arrhythmias, since the function of the elactance E(t) in Eq.7.47 depends on the current period interval T(n) of the n-th heartbeat. For example, in the model of McSharry and Clifford according to Fig.7.67 McSharry, Clifford 2006, the rhythmic change of the pulse beat due to breathing can also be simulated.

The replacement circuit diagram with the parts for the ventricle and a vein piece can now be created in details (see Fig.7.76) or with Superblocks(see Fig7.77).

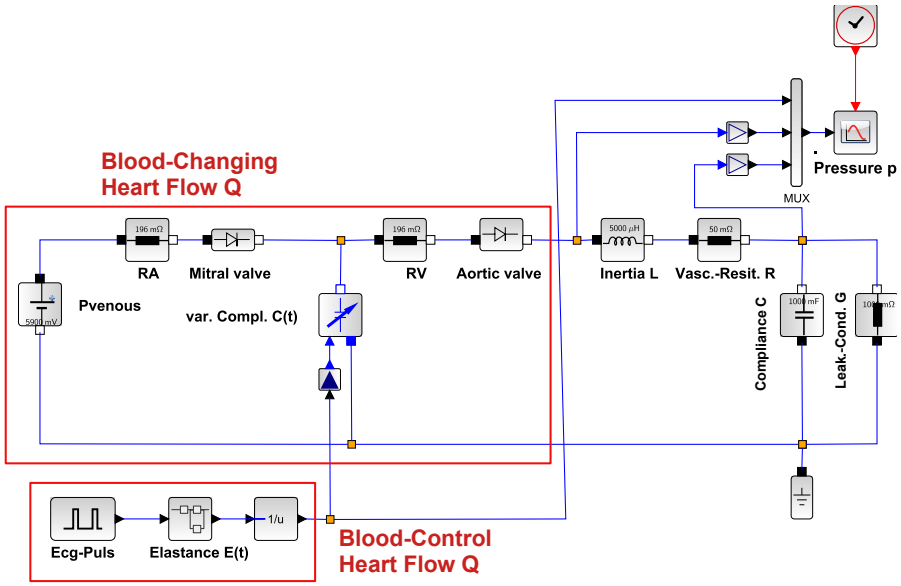

Figure 7.76: *Scilab/Xcos diagram for left ventricle and vein section, according to Fig.7.72 and 7.71.*

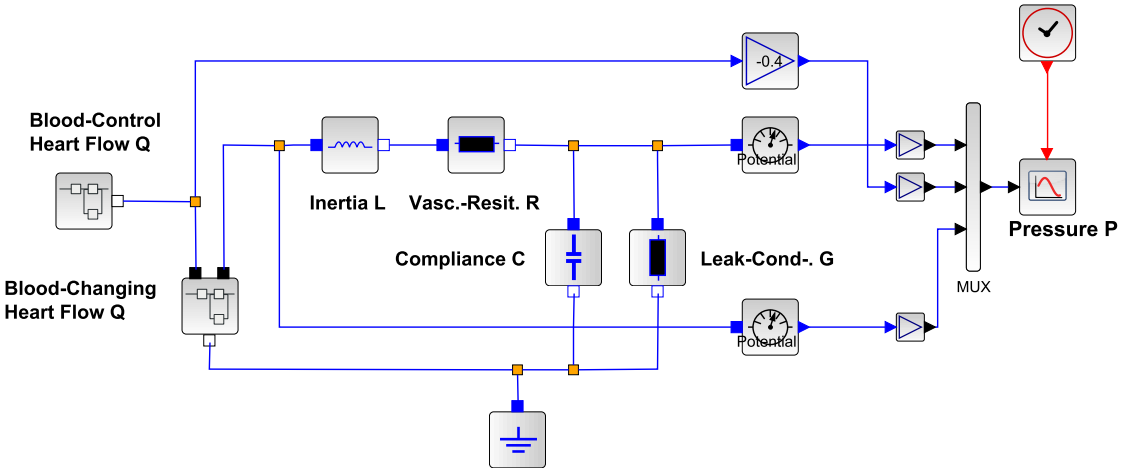

Figure 7.77: *Scilab/Xcos diagram for left ventricle and vein sectionaccording to Fig.7.76 but with superblocks.*

In order to investigate the blood pressure and volume of a blood vessel only in principle, whether the model also corresponds to the Windkessel model and provides realistic values, simpler models for the heart as a pump can also be selected, e.g. sine half-waves for the electrical excitation and a controlled current source for the pressure changes (see Fig.7.78).

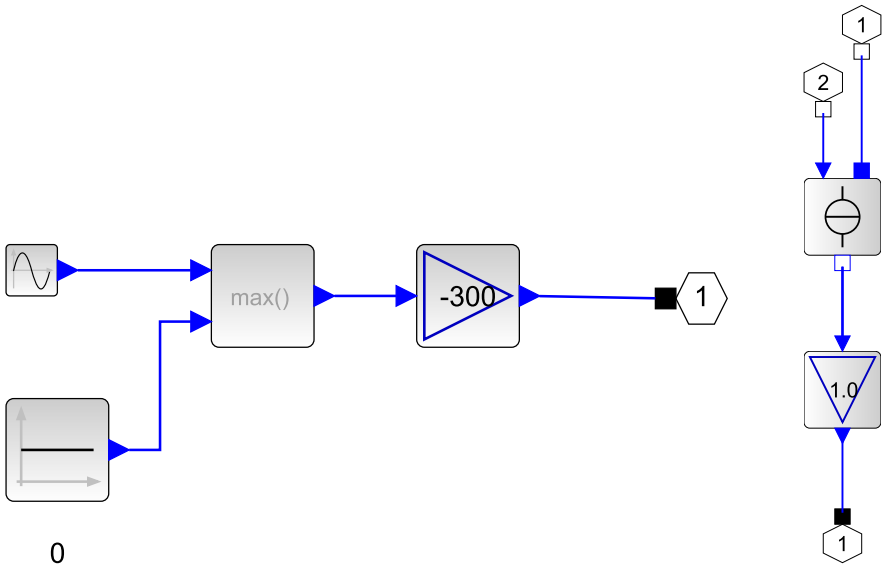

Figure 7.78: *Simpler superblocks in the Scilab/Xcos circuit according to Fig. 7.77, left for the electrical excitation and right for the pressure change.*

The result of a simulation with simplified models for the generation of the Ecg and the associated pressure change of the left heart pump is shown in Fig.7.79.

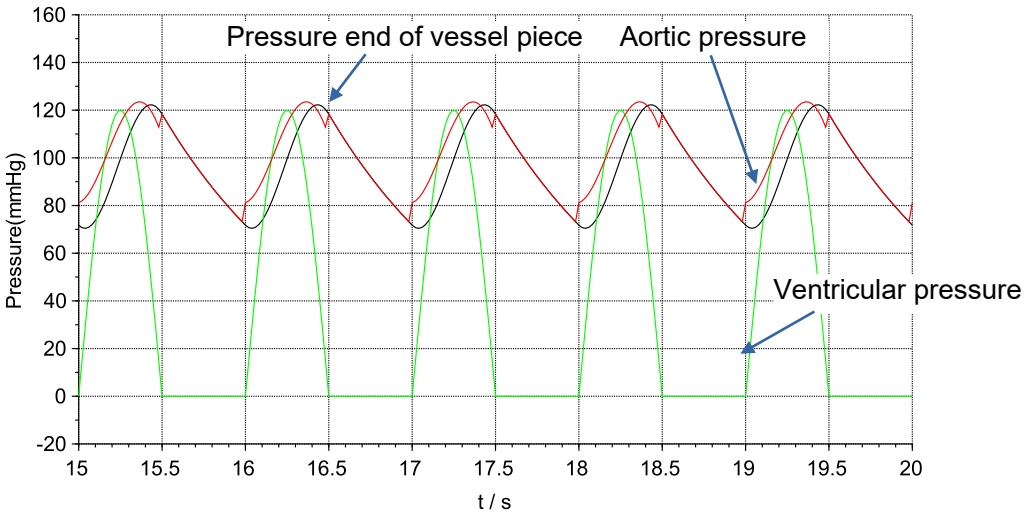

Figure 7.79: *Simulation with Scilb/Xcos of the blood pressures for a piece of vessel for the left ventricle and vein sectionaccording to Fig.7.76 but with superblocks.*
(R=0,05 mmHg·s/mL, C=1 mL/mmHg, L = 0,05 mmHg·s²/mL, G= 1 mL/(mmHg·s) , Maximum of the sine half-wave during excitation: 300)

8 Models of rhythms selected from the literature - emphasising “coupled oscillator models”

We have up to now mainly focused our attention to the structure of *single* oscillators and how to model it. We have seen that simulations can be useful in studies of parameter changes and so on. We will now approach a realistic situation when we study biological oscillators: We want to see how *several* oscillators, in several biological cells, interact and affect each other.

The following sections discuss interacting, coupled, oscillators in a *net*. The net can consist of a big amount of oscillators (Sect. 8.2). We will build models of nets, exemplifying the modelling in a row (where each oscillator couples to the neighbour in its front and its back, as in a ring). We can denoted this an *one* dimensional net.

We will also extend our models to *two*–dimensional nets. We apply the model to a flat structure in biology, namely a plant leaf surface. The surface of the leaf has openings – pores – through which water transpires. These pores are regulating the transpiration; under some conditions the pores are opening and closing rhythmically – they oscillate. We will couple several oscillating pores together in this two dimensional model and simulate some of the often very intricate oscillatory patterns that can arise (Sections 8.3 and 8.4).

We will end the sections by simulating a *three*–dimensional model of oscillators (Sect. 8.4). We simply take the two–dimensional surface model mentioned above and bend it so it becomes a cylinder or tube. It is interesting that the model now can show patterns in time and space (over the surface) that have close similarities with many phenomena in biology!

8.1 Coupled oscillator net

Already Lewis tried to describe the rhythmic behaviour of the Weta with coupled oscillators (see Sect. 7.2). The reason to do so were actograms, in which the activity rhythm of the Weta showed spontaneous alterations of the period length. The splitting of the activity in two components (see Fig. 7.12) speaks also against the assumption, that a single oscillator can describe the behaviour of the animals satisfactorily (Christensen, Lewis 1982).

Therefore we have to deal with *coupled* oscillator nets. They are connected with each other via a coupled network, need, however, not necessarily be of the same kind (see Fig. 8.1).

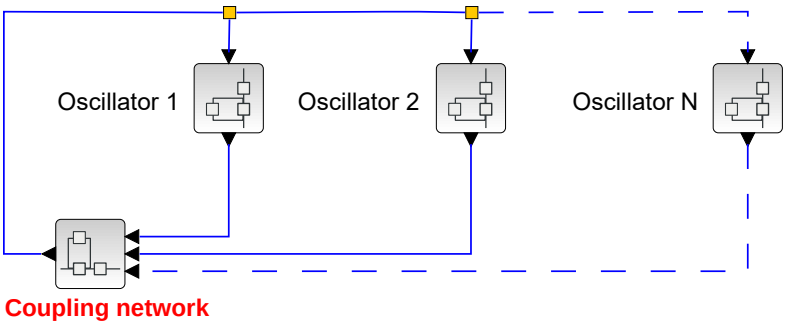

Figure 8.1: *Coupled oscillator nets are connected with each other. The individual oscillators (1, 2, N) need not be of the same kind*

Often the coupled network consists of a summing unit circuit and a single oscillator in a slightly modified feedback model (see Fig. 8.2 and 8.3).

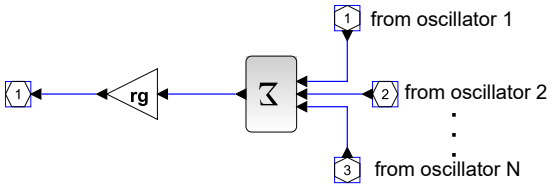

Figure 8.2: *The coupled network consists often of a summing unit-circuit*

The duration of the oscillation respectively the frequency, with which the whole oscillator network oscillates, can be find out in the event of similar individual oscillators in *homogeneous* cases, when the reference concentration in all individual oscillators is zero $(c_{ref})_i = 0$), from the signal balance at the right summing unit (see red arrow in Fig. 8.3):

$$\begin{aligned} \frac{cr_i}{Fv_i \,.\, Fr_i} &= -(1-r_i)\cdot cr_i - r_g \sum_{j=1}^{N} r_j \cdot cr_j \\ &= -[1-(1-r_g)r_i]cr_i - r_g \sum_{j=1,\neq i}^{N} r_j \cdot cr_j \end{aligned}$$

(i = 1 to N) or in matrix form:

$$\left(\underline{\underline{R}} + \underline{\underline{F}}\right) \cdot \underline{Cr} = \underline{0} \tag{8.1}$$

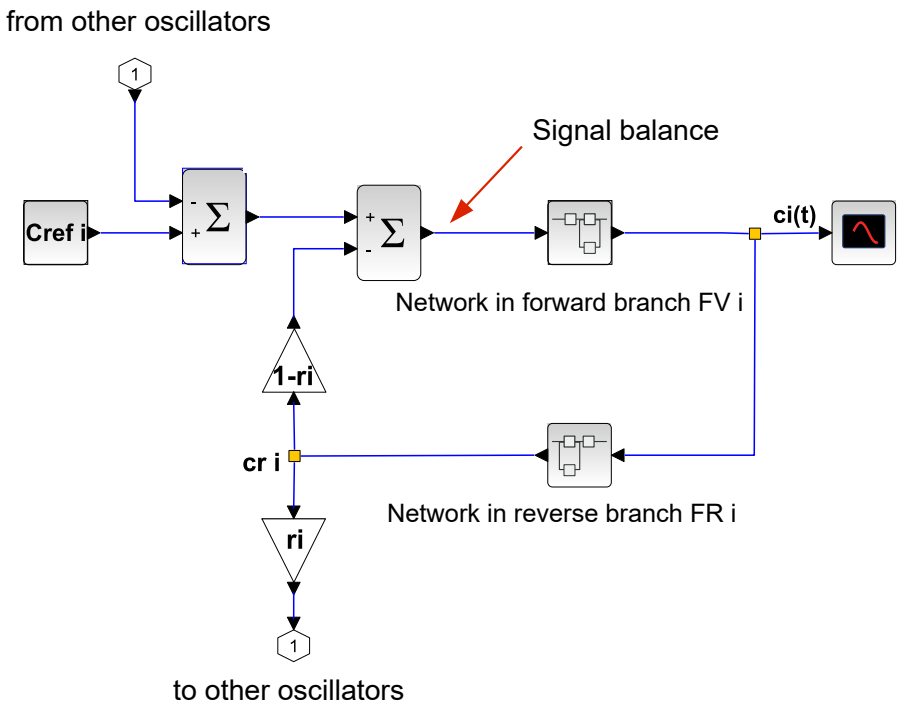

Figure 8.3: *A single oscillator consists often of a slightly modified feedback model*

with

$$\underline{\underline{R}} := \begin{bmatrix} 1-(1-r_g)r_1 & r_g \cdot r_2 & \cdots & r_g \cdot r_N \\ r_g \cdot r_1 & 1-(1-r_g)r_2 & \cdots & r_g \cdot r_N \\ \vdots & \vdots & \ddots & \vdots \\ r_g \cdot r_1 & r_g \cdot r_2 & \cdots & 1-(1-r_g)r_N \end{bmatrix} \tag{8.2}$$

and

$$\underline{\underline{F}} := \begin{bmatrix} \frac{1}{Fv_1 \cdot Fr_1} & 0 & \cdots & 0 \\ 0 & \frac{1}{Fv_2 \cdot Fr_2} & \cdots & 0 \\ \vdots & \vdots & \ddots & \vdots \\ 0 & 0 & \cdots & \frac{1}{Fv_N \cdot Fr_N} \end{bmatrix}, \underline{Cr} := \begin{bmatrix} cr_1 \\ cr_2 \\ \vdots \\ cr_N \end{bmatrix}$$

Nontrivial solutions ($cr_i = 0$) exist, if the determinant of $\underline{\underline{R}} + \underline{\underline{F}}$ disappears, i.e. for

$$\det\left(\underline{\underline{R}} + \underline{\underline{F}}\right) = \underline{0}$$

If in the special case of all individual oscillators being identical with the same transfer properties in the forward as well as in the backward branch, and if all of them are coupled with each other

in the same way ($Fv_i = Fv$, $Fr_i = Fr$ and $r_i = r$ for each individual oscillator with one of the numbers i = 1,2,3, ... N) ($r_i = r$), it follows from the last equation:

$$\det\left(\underline{\underline{R}} + \underline{\underline{F}}\right) = \det\left(\underline{\underline{R}} + \frac{1}{\underbrace{Fv \cdot Fr}_{-\lambda}}\underline{\underline{E}}\right) = \underline{0}$$

where $\underline{\underline{E}}$ stands for the unit matrix and λ is a constant.

This is, however, the Eigenwert equation for the coupling matrix $\underline{\underline{R}}$ with $\det\left(\underline{\underline{R}} - \lambda \cdot \underline{\underline{E}}\right) = 0$, which can be calculated with known mathematical procedures and analytically specified.

For N Eigenwerte follows e.g. for the *special case* of similar coupling of all individual oscillators, i.e. $r_i = r$ for all i oscillators and $r_g = 1$ for the coupling matrix $\underline{\underline{R}}$:

$$\underline{\underline{R}} := \begin{bmatrix} 1 & r & \cdots & r \\ r & 1 & \cdots & r \\ \vdots & \vdots & \ddots & \vdots \\ r & r & \ldots & 1 \end{bmatrix} \tag{8.3}$$

This is a cyclic matrix with N rows and N columns, and the Eigenwerte can be calculated with the help of the Fourier matrix with the elements

$$w_{ik} := e^{-j2\pi ik/N} \text{ with } i,k = 0,\ldots,N-1 \tag{8.4}$$

from the *first column* of the matrix $\underline{\underline{R}}$ according to

$$(\lambda_1,\ldots,\lambda_N)^T = \underline{\underline{W}} \cdot (1,r,\ldots,r)^T \tag{8.5}$$

There diag(λ_i) is a diagonal matrix with the diagonal elements λ_i,which represent the Eigenwerte, (i = 1 to N) i.e.

$$\lambda_i = 1 + r \cdot \sum_{l=1}^{N-1} e^{-j2\pi li/N} \text{ with } i = 0,\ldots,N-1 \tag{8.6}$$

It follows:

1. $\lambda_a = 1 + (N-1) \cdot r$
   (occurs once, column sum of $\underline{\underline{R}}$)
2. $\lambda_b = 1 - r$
   (occurs N-1 times, column difference of $\underline{\underline{R}}$)

This equation represents, as in the case of single oscillators, the necessary condition for the value and the phase of the needed forward amplification and the feed back and means in the case of real feed back coefficients, that the Eigenwerte λ are real constants. Forward and backward amplifications must therefore in total possess a phase shift of an uneven numbered multiple of

180° (because of the minus sign, which causes a further phase shift of 180°), i.e.

$$\begin{aligned} \varphi(Fv) + \varphi(Fr) &= (2n+1)\cdot\pi(\triangleq 180°),\ \text{n: integer} \\ \varphi(Fv) &: \text{phase of forward branch} \\ \varphi(Fr) &: \text{phase of backward branch} \end{aligned}$$

For the conditions of the absolute values of the transfer in the forward and backward branch follows:

$$\mid Fv \mid \cdot \mid Fr \mid = \mid \frac{1}{\lambda} \mid$$

In contrast to a single oscillator this product must not be ≥ 1 (see Sect. 8.4), but can correspond to the reciprocal value of an Eigenwert $\mid \frac{1}{\lambda} \mid$. This determines the conditions for the absolute values of the transfer functions in the forward and backward branches and the resulting frequency. Table 8.1 gives for some special cases the corresponding conditions.

Forward branch Fv	Backward branch Fr	frequency f / constrained conditions
const. (Fv=K])	delay td (Fr=$e^{-j2\pi f\cdot td}$)	$f = (2n+1)/(2\cdot td)$, n: digit $K_a = 1/[1+(1-N)r]$ $K_b = 1/(1-r)$
integr. (Fv=$K/(j2\pi f)$)	delay td (Fr=$e^{-j2\pi f\cdot td}$)	$f = (4n+1)/(4\cdot td)$, n: digit $K_a = 2\pi f/[1+(1-N)r]$ $K_b = 2\pi f/(1-r)$
integr. (Fv=$K/(j2\pi f)$)	integr. (Fr=$K/(j2\pi f)$)	$f_a = \frac{K}{2\pi}\sqrt{1+(N-1)r}$ $f_b = \frac{K}{2\pi}\sqrt{1-r}$

Table 8.1: *Examples for forward and backward amplification in the frequency domain (after Fourier transformation) of a single oscillator in a coupled Net of similar oscillators with conditions for oscillations given for $r_g = 1$. The index a (e.g. K_a) gives the conditions for the Eigenwert λ_a, the index b (e.g. K_b) analogue for the Eigenwert λ_b. If the backward branch contains a delay unit, the oscillator frequency is determined by this one only. If there is an integrator for the forward as well as for the backward branch, the frequency is determined directly by the Eigenwerte, and the amplification factor K is principally freely eligible.*

Thus, in a coupled oscillator system different frequencies can occur, with which the whole system oscillates, even in the case of similar oscillators. The diversity is larger compared to a single oscillator. Which oscillation is prompted, depends on the initial conditions, but also on disturbances, which can offset the whole system into another rhythm. If the coupling between the oscillators is unequal, whole subnetworks can oscillate against each other and extinguish every collective rhythm.

If the common coupling factor between the individual oscillators is $r_g \neq 1$, the solution can be found by dividing the Eq. 8.1 by $1-(1-r_g)r$. One obtains (for definition of matrix $\underline{Cr}$ see formulae 8.2):

$$\left(\underline{\underline{\tilde{R}}} + \underline{\underline{\tilde{F}}}\right) \cdot \underline{Cr} = \underline{0}$$

with

$$\underline{\underline{\tilde{R}}} := \begin{bmatrix} 1 & \frac{r_g r}{1-(1-r_g)r} & \cdots & \frac{r_g r}{1-(1-r_g)r} \\ \frac{r_g r}{1-(1-r_g)r} & 1 & \cdots & \frac{r_g r}{1-(1-r_g)r} \\ \vdots & \vdots & \ddots & \vdots \\ \frac{r_g r}{1-(1-r_g)r} & \frac{r_g r}{1-(1-r_g)r}_g & \cdots & 1 \end{bmatrix}$$

and

$$\underline{\underline{\tilde{F}}} := \frac{1}{1-(1-r_g)r} \begin{bmatrix} \frac{1}{Fv_1 \cdot Fr_1} & 0 & \cdots & 0 \\ 0 & \frac{1}{Fv_2 \cdot Fr_2} & \cdots & 0 \\ \vdots & \vdots & \ddots & \vdots \\ 0 & 0 & \cdots & \frac{1}{Fv_N \cdot Fr_N} \end{bmatrix}$$

The Eigenwerte are obtained in analogy to the Eigenwerte above for the special case $r_g = 1$, if the coupling factor of an individual oscillator r is replaced by $\frac{r_g r}{1-(1-r_g)r}$, i.e.

1. $\tilde{\lambda}_a = 1 + (N-1) \cdot \frac{r_g r}{1-(1-r_g)r}$
   (occurs once, column sum of $\underline{\underline{R}}$)
2. $\tilde{\lambda}_b = 1 - \frac{r_g r}{1-(1-r_g)r}$
   (occurs N-1 times, column difference of $\underline{\underline{R}}$)

An example for two of those coupled oscillators is shown in Fig. 8.4.

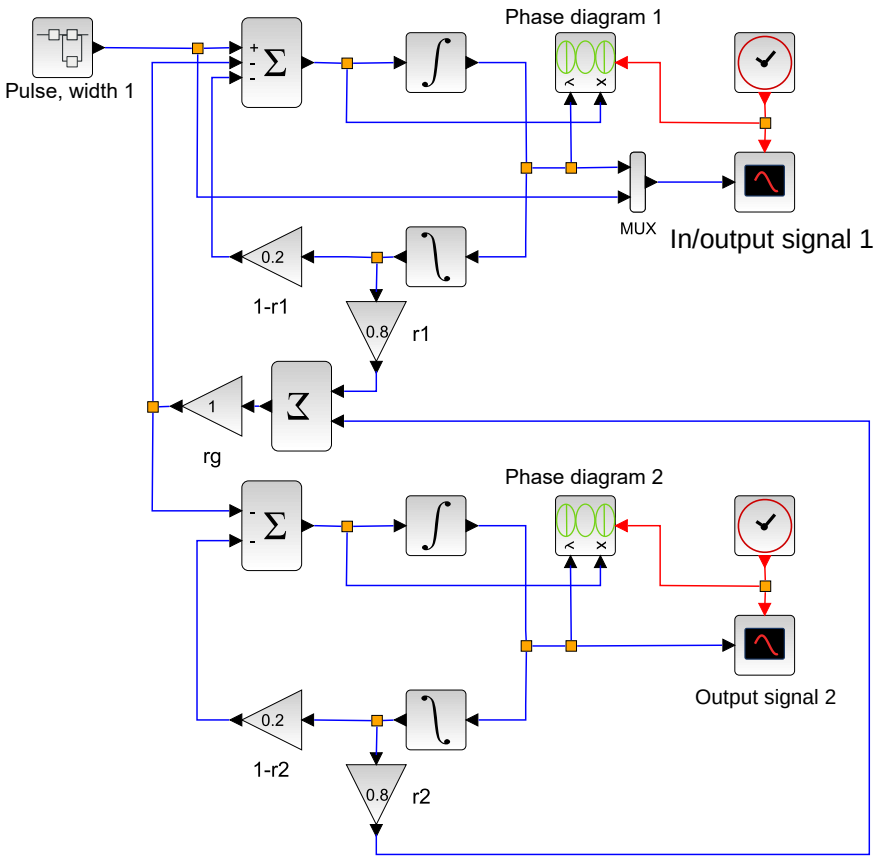

Figure 8.4: *Two coupled feedback oscillators with two integrators, after Fig. 5.17*

Each oscillator is a feedback model according to Fig. 5.17 with the same oscillation frequency f_0 of 0.159 (see Eq. 5.23). Due to the coupling of the two similar oscillators they are now able to oscillate together with two different frequencies. According to the last line in table 8.1 one obtains for N=2, K=1 and a coupling strength of $r_1 = r_2 = r = 0.8$:

$$\begin{aligned} f_a &= \frac{1}{2\pi}\sqrt{1+(N-1)r} = \frac{1}{2\pi}\sqrt{1+(2-1)0.8} = 0.2135 \\ f_b &= \frac{1}{2\pi}\sqrt{1-r} = \frac{1}{2\pi}\sqrt{1-0.8} = 0.0712 \end{aligned}$$

The resulting oscillations with the frequencies of 0.0712 and 0.2135 are larger or smaller as the frequency of a single oscillator. They can be recognised in the output signals of the two oscillators even without frequency analysis (see Fig. 8.5). In contrast to the phase diagram 5.19 with *one* circle of an oscillator with two integrators in Fig. 5.17 one now sees in the phase diagram 8.6 *three* circles in each oscillator output signal. One lies in the origin of the coordinate

system, the two others are symmetrically shifted at the abscissa by +0.4 or -0.4. They represent the additional oscillations due to the coupling of the two oscillators. As the oscillation with the circle in the origin of the phase diagram has another frequency than those shown by the two oscillators, when uncoupled.

Altogether is can be stated, that the frequency of the oscillation with the circle in the origin of the phase diagram respectively the primary oscillation has declined. The amplitude of this primary oscillation is maximal. This network shows, that due to the coupling the main oscillation has become smaller as compared to the oscillation of a single oscillator.

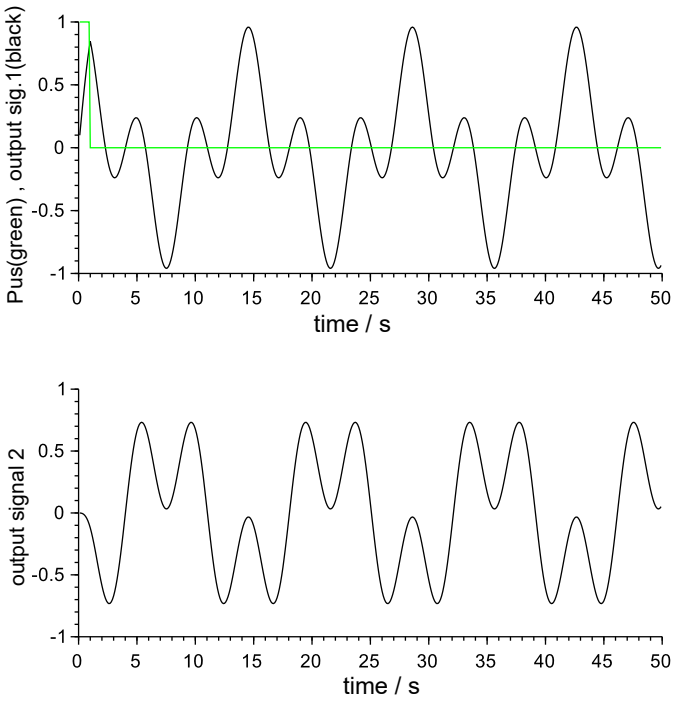

Figure 8.5: *Output signal of two coupled oscillators as shown in Fig. 8.4 with K=1, N=2 and r=0.8. They contain two frequency fractions with* $f_a = 0.2135$ *and* $f_b = 0.0712$

8.2 General: Several coupled oscillators

We generalise now the coupling of single oscillators in such a way, that not all oscillators are fed from outside by the same storage as done by Lewis in Fig. 8.1, but that each oscillator can be individually coupled with another oscillator and that furthermore the oscillator in the superblock can be changed in a general way. The corresponding block diagram is shown in Fig. 8.7 and the content of a single oscillator superblock in Fig. 8.8.

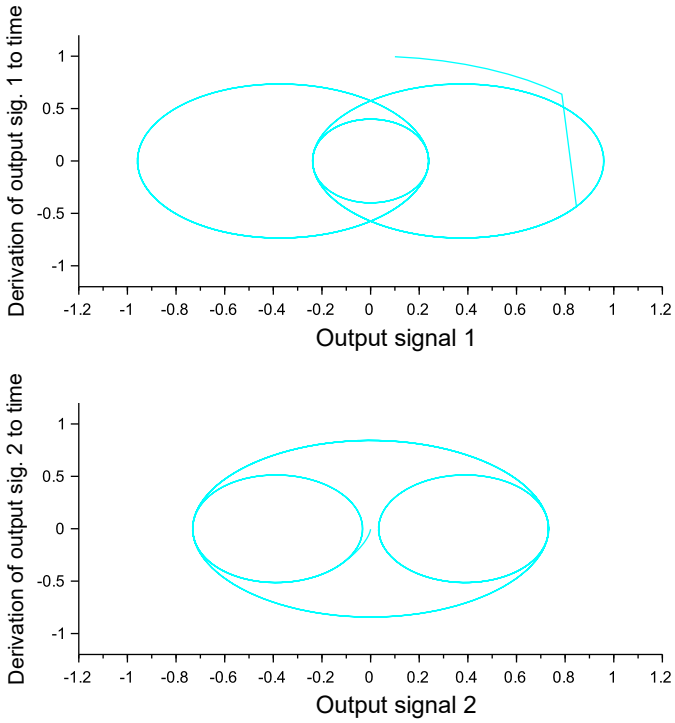

Figure 8.6: *Phase diagram of two coupled oscillators as shown in Fig. 8.48.4 with K=1, N=2 and r=0.8*

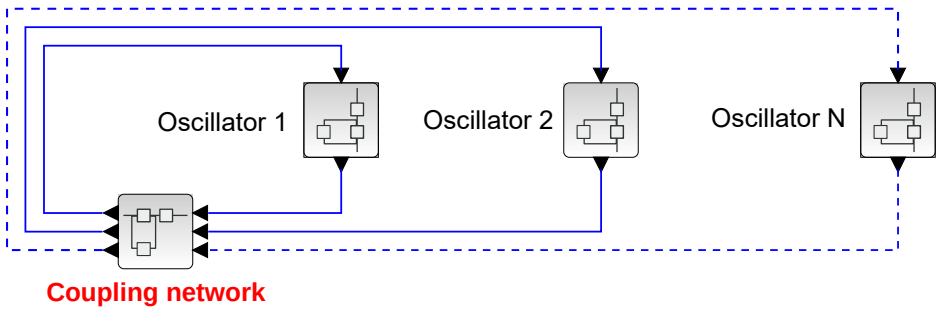

Figure 8.7: *Several coupled oscillators (1, 2, ... N) are coupled in this block diagram, where N is the number of cells.*

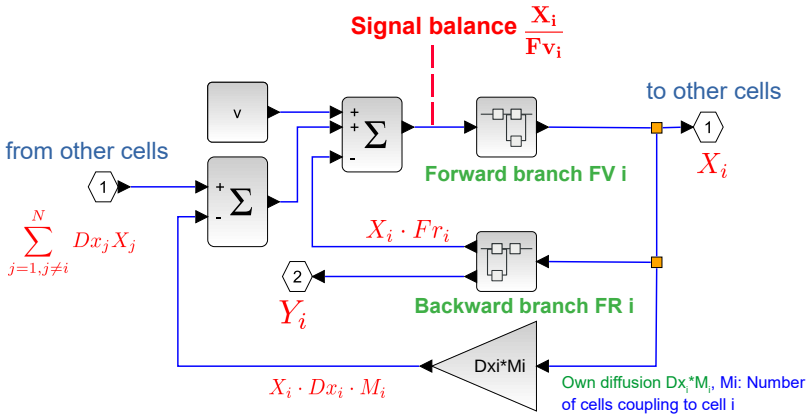

Figure 8.8: *Content of the superblock in Fig. 8.7.*

From the signal balance of Fig. 8.8 one obtains behind the summation:

$$\frac{X_i}{Fv_i} = v - X_i\, Fr_i - X_i \cdot Dx_i M_i + \sum_{j=1,j\neq i}^{N} Dx_j X_j, \quad i = 1, \ldots, N$$

or written in matrix form:

$$\left(\underline{\underline{Dx}} + \underline{\underline{F}}\right) \cdot \underline{X} = \underline{v}$$

with

$$\underline{\underline{Dx}} := \begin{bmatrix} Dx_1 M_1 & -Dx_2 & \cdots & -Dx_N \\ -Dx_1 & Dx_2 M_2 & \cdots & -Dx_N \\ \vdots & \vdots & \ddots & \vdots \\ -Dx_1 & -Dx_2 & \cdots & Dx_N M_N \end{bmatrix} \text{ and } \underline{v} := \begin{bmatrix} v \\ v \\ \vdots \\ v \end{bmatrix} \tag{8.7}$$

$$\underline{\underline{F}} := \begin{bmatrix} \frac{1}{Fv_1} + Fr_1 & 0 & \cdots & 0 \\ 0 & \frac{1}{Fv_2} + Fr_2 & \cdots & 0 \\ \vdots & \vdots & \ddots & \vdots \\ 0 & 0 & \cdots & \frac{1}{Fv_N} + Fr_N \end{bmatrix} \text{ and } \underline{X} := \begin{bmatrix} X_1 \\ X_2 \\ \vdots \\ X_N \end{bmatrix}$$

In the special case of uniform cells and without influx one obtains $Fv_i = Fv$, $Fr_i = Fr$, $v_i = 0$ and

$$\left(\underline{\underline{Dx}} + \underbrace{\frac{1 + FvFr}{Fv}}_{-\lambda} \cdot \underline{\underline{E}}\right) \cdot \underline{X} = \underline{0}, \qquad \begin{array}{lll} \underline{\underline{E}} & : & \text{unit matrix} \\ \lambda & : & \text{Eigenvalue (constant)} \end{array}$$

The result of the Eigenvalue equation is

- $\underline{\underline{Dx}} - \lambda \cdot \underline{\underline{E}}$ for the matrix $\underline{\underline{Dx}}$ with its Eigenvalue λ

- With the help of the transfer functions Fv and Fr the frequencies of the oscillations can be determined, which can spread over the cells coupled in space and time.

A special case is the uniform diffusion, i.e. $Dx_i = Dx$, $M_i = N$

One obtains two Eigenvalues at

$$\begin{aligned} \lambda_a &= 0 \text{ and} \\ \lambda_b &= Dx \cdot N \end{aligned}$$

For the resonance frequency ω_r follows:

1. for $\lambda_a = 0$ at $Fv(\omega_r) \neq 0$ the product is

$$1 + Fv(\omega_r) \cdot Fr(\omega_r) = 0 \quad \text{and}$$

2. for $\lambda_b = Dx \cdot N$

$$\frac{1 + Fr(\omega_r)Fv(\omega_r)}{Fv(\omega_r)} = Dx \cdot N$$

respectively

$$1 + Fv(\omega_r) \cdot \underbrace{(Fr(\omega_r) - Dx \cdot N)}_{\widetilde{Fr}(\omega_r)} = 0 \tag{8.8}$$

- In the first case for $\lambda_a = 0$ a resonance frequency results, which corresponds to that of the single oscillator, i.e. the oscillators oscillate in the same frequency as if they would not be coupled mutually.

- In the second case for $\lambda_b = Dx \cdot N$ another common resonance frequency is additionally possible, where oscillators with the help of other oscillators produce a mostly smaller oscillation frequency. The transfer function of the feedback $Fr(\omega_r)$ of a single oscillators has thereby seemingly changed, which reduces in the case of a positive coupling Dx according to $Dx \cdot N$ the feedback $Fr(\omega_r)$, if it is positive. The result is understandable: If each individual oscillator couples with every other one with the same strength, then the individual oscillator needs less feedback, since this is provided also from the other oscillators, which oscillate with the same frequency.

- The pole positions of these coupled oscillators can also be determined analogue to a single oscillator using the **root locus method** according to Eq.7.15 as a function of a specific parameter, with the only difference that the feedback polynomial must be modified according to Eq. 8.8. If

$$Fr(\omega_r) \ll Dx \cdot N \tag{8.9}$$

Eq. 8.8 can approximated by

$$1 + Fv(\omega_r) \cdot (F_r(\omega) - Dx \cdot N) \approx 1 - \underbrace{Dx \cdot N}_{-K} \cdot F_V(\omega_r) \approx 0 \tag{8.10}$$

The factor -$K = Dx \cdot N$ corresponds to the factor K in Eq.7.15 for the root locus method. In this case, the root locus method can be used directly to analyse the extent to which the coupling Dx between the oscillators influences the overall frequency.

8.3 Simulating transpiration oscillations

We will now go into more details on the transpiration oscillations which we have mentioned in the introduction to Chap. 8. It illustrates the usefulness of understanding modelling and simulation of complex systems. And, furthermore, we have chosen this example since it comes from the important processes of plant water regulation and photosynthesis - with their enormous importance for life on the Earth. We are going to model and discuss the oscillations of the many coupled openings on leaf surfaces – they control the flux of water out of plants, simultaneously with the control of the uptake of carbon dioxide for photosynthesis. This is surely an important and formidable task!

The typical dimensions of such valves – the proper scientific term is *stomata* – are about $10\mu m$. It sounds like a contradiction that such small openings can play a so fundamental role - but we know that globally stomata regulate every year an amount of water into the atmosphere corresponding to a volume of about $60\,000\,km^3$. Observe the dimension – cubic kilometer! Evidently there are many stomata globally and on all leaves on the Earth surface (density about 50 stomata per square millimeter of a common oat leaf)! Not difficult to understand that many reseachers are interested in studying these processes and the oscillations of the transpiration and the stomata cells.

We start by describing, to some extent, the leaf valves, the stomata structures (see subsect. 3.3.2), their coupling and oscillations (subsect. 8.3.1). We give an overall – description in physical terms of the leaf system (subsect. 8.3.2) and sketch parts of the molecular mechanisms involved (subsect. 8.3.3).

Then we construct and discuss a two-dimensional model of the oscillations on the surface. The surface can be bent to a cylinder and used to study how the coupled oscillations now show complicated structures relevant for different phenomena in plant physiology (Sect. 8.4).

8.3.1 Coupling of oscillating guard cells over leaf surface

The stomata over a leaf surface must, in order to show a synchronous oscillation in transpiration, be coupled. Assuming all stomata to be almost identical, the discussion in Chap. 8 on coupling between oscillators is highly relevant. If the stomata on the surface are strongly coupled (via diffusion of substances but also via other extracellular influences, for example via the availability of water in the leaf, via electric cell potentials etc), they will then likely be synchronous, as demonstrated in Fig. 8.9.

If "looser" coupled they could still oscillate but now out of phase with each other, or only in phase with the nearest neighbours.

Since water loss through the stomata means a phase transition, the temperature of the stomata that evaporates humidity will decrease. It it therefore possible to see oscillatory water transpiration as oscillatory temperature changes of the surface. An example of the use of this technique is given in Fig. 8.9. The temperature at several points along the leaf has been recorded

in time (left) by thermography, and simultaneously the overall water transpiration has been measured in the air passing the leaf (see curve at bottom). To the right of figure: leaf measured with recording points in greenish colour, and colour/temperature code.

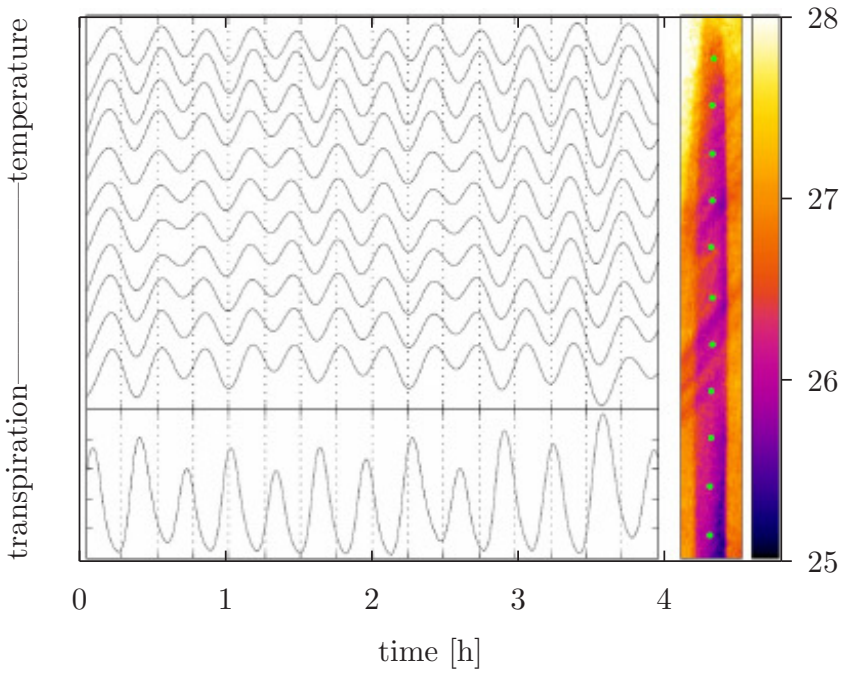

Figure 8.9: *Overall transpiration measured by the surface temperature of a primary oat leaf (thermogram at the right with colour coded temperature, coding shown in the very right box in degrees). At 11 positions (indicated by greenish dots) the time course was obtained and shown in the left part of the figure. The lowest curve is the simultaneously recorded overall water transpiration and shows two distinct peak heights corresponding to periods of about 20 and 40 min. Modified from Fig. 5 in Prytz 2001*

The example shows that the transpiration is synchronised by and large but that in this recording a period doubling (a subharmonic component) is also present.

Studies were also performed with pulses of different osmotica in the root medium. The oscillations were then affected and phase and amplitude changes were successfully predicted.

Changing light conditions of course changes transpiration (and photosynthesis). Pulses of light could easily be administered to perturb amplitude and phase of the oscillations. Such perturbation studies might also show that the oscillations could be brought into a stable singular point, as discussed in Sect. 3.1.

The hydraulic model discussed earlier (Fig.7.25) could produce simulation in accordance with these and other experimental results on the transpiration at an organism level. The symbol (Δ) in the figure 7.25 was used to simulate light pulses (light perceived by chromophores in the guard cells).

An approach to vary the root resistance (R1 in Fig. 7.25) was introduced by Brogårdh, Johnsson

(1973) who replaced/added mechanical compression of the transport vessels. The method allowed entrance of ions from a medium to arrive at the stomata - ions which otherwise had to pass or be stopped at the root membrane system. In this way it was e.g. demonstrated that the period of the transpiration oscillations increased when calcium ions were added to the root medium and could be transported to the external medium of guard cells.

8.3.2 Coupling of hydraulic oscillations and guard cell oscillations

We have discussed hydraulic models (see Sect. 7.5) which could explain transpiration oscillations with periods around 1-2 h. We have also mentioned stomata oscillations, showing shorter periods. Ions reaching the stomata seem to directly influence the period and the pattern of the oscillations. Altogether, experimental results point to an interaction between the hydraulic components and guard cell oscillations.

Experimentally it is found that rather complicated patterns in the leaf transpiration can occur - some examples are shown in Fig. 8.10, where potassium ions have been added to the medium of a xylem compressed oat plant. The patterns show subharmonics, period-3 and different patterns which are published by Prytz 2001 in his biophysics thesis. He discussed the results when one assumes that the guard cell oscillations introduced a water potential difference Δ in the hydraulic part of Fig. 7.25. If one uses parameter values on the hydraulic system and introduces the potential difference as a sine wave the resulting output shows features which reflects the mutual coupling. Of course, the resulting oscillations are dependent on the amplitudes of the two oscillatory systems, on their frequencies etc.

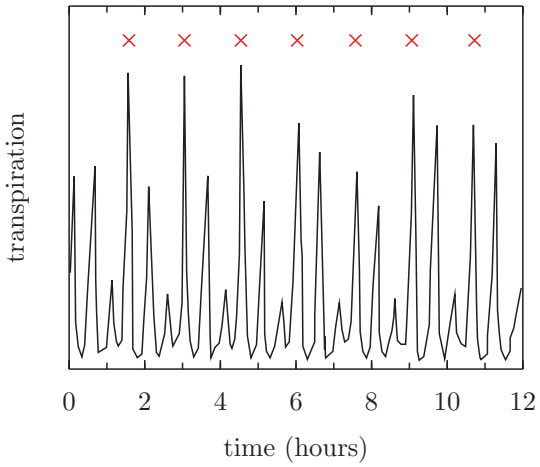

Figure 8.10: *Example of transpiration of an* Avena *seedling. x-axis: time in h. y-axis: relative transpiration. Red crosses mark higher amplitudes. Redrawn after Prytz 2001*

Transpiration simulations could then produce results, similar to those of Fig. 8.10. The result is a complicated coupling between two different types of oscillations - or it can also be seen as an example of an experiment where the two frequencies of the oscillators are too different to produce a simple phase lock.

8.3.3 Molecular level of guard cell regulation

We have not gone into details on the molecular regulation of the guard cell regulation of the transpiration oscillations. Many fascinating aspects have been revealed during the last years on the ion transport over the guard cell membranes. It is well known that potassium ions play a crucial role in the regulation of the cell's osmotic swelling and shrinking. Anion channels regulate e.g. the transport of chloride, being activated by the calcium level and by abscissic acid. Electric membrane potentials are affected by the transport and participate in the control.

It should be mentioned that the calcium ions play important role(s) in the guard cell reactions. Interestingly Allen et al. 2001 found oscillations in cytosolic calcium concentrations which are central regulators of signal transduction cascades, although the roles of individual $[Ca^{2+}]_{cyt}$ oscillation parameters in regulating downstream physiological responses remain largely unknown. However, this vivid field of research is beyond the scope of the present discussion and the interested reader may consult the special literature (e.g. Allen et al. 2001; Smedler, Uhlen 2014).

8.4 Simulating oscillations in cylindrical systems

Oscillators in a population of cells can affect each other in many ways - they could e.g. exchange molecules that are transported via diffusion, or by bulk transport, in the medium. The interacting oscillators/cells are said to be coupled.

In this section we will model and simulate a cylindrical structure of coupled oscillators. In order to build up the model we start with modelling and simulating only two coupled oscillations (subsect. 8.4.1) and discuss how the coupling will affect the resulting oscillations.

Then we will consider coupling between several cells/oscillators. In one case the cells will couple only to their neighbours in a ring – arranged for example like beads in a necklace. Although such «onedimensional» cases look fairly simple, the coupling can produce very different oscillatory patterns. The simulations will be carried out for both 6 and for 50 oscillators in a ring (subsections 8.4.2 and 8.4.3).

A further extension can be made when looking at coupling of cells/oscillators arranged in a surface structure, a «twodimensional case». In nature, this type of coupling is relevant when treating, for example, the biological cells of a flat plant leaf or cells in the skin of an animal. The individual oscillator is then assumed to couple to several neighbouring cells, e.g. four or six neighbours (or more, depending on symmetry required). The oscillatory patterns can now reach a very high degree of complexity. For example, cells in one part of the area can oscillate differently from the those in another one; one speaks about so-called 'patchy areas' or 'cluster areas' (as shown in subsect. 8.4.4).

We will finally use the tools achieved to model cell coupling in a cylinder structure. The cylinder consists of several rings of oscillators, stacked above each other - like stacking several necklaces upon each other! Thus oscillators in a ring can couple to neighbours not only in the same ring but also to neighbours in the rings stacked above and below. The surface of the cylinder will be a curved/bent two - dimensional structure which was used in the simulations just mentioned above. One could say that the cylinder is a simple 3-dimensional model. Despite many obvious model simplifications we will see that the oscillations in the structure cylinder can

produce intriguing patterns in time and space (subsect. 8.4.4). It is fascinating that many features in growth phenomena and electrical phenomena in nature can be found in the simulations - like growth oscillations and electrical waves in cylindrical plant stems and roots etc.

The models have to be further extended if cellular oscillations in, e.g. biological tissues like glands and tumours should be modelled. This will, however, be too complicated for our purpose here. But the future is full of exciting problems!

8.4.1 Two oscillators

The case of *two* oscillators of the type described in Fig.7.22 is shown with Scilab/Xcos in Fig. 8.11, and its output and phase diagram in Fig. 8.14. By putting each oscillator and the coupling network in superblocks, the structure of the model is easier to recognise (see Fig. 8.12). Clicking on the superblock in the Scilab/xcos model shows the oscillator structure respectively the coupling network (see Fig. 8.13).

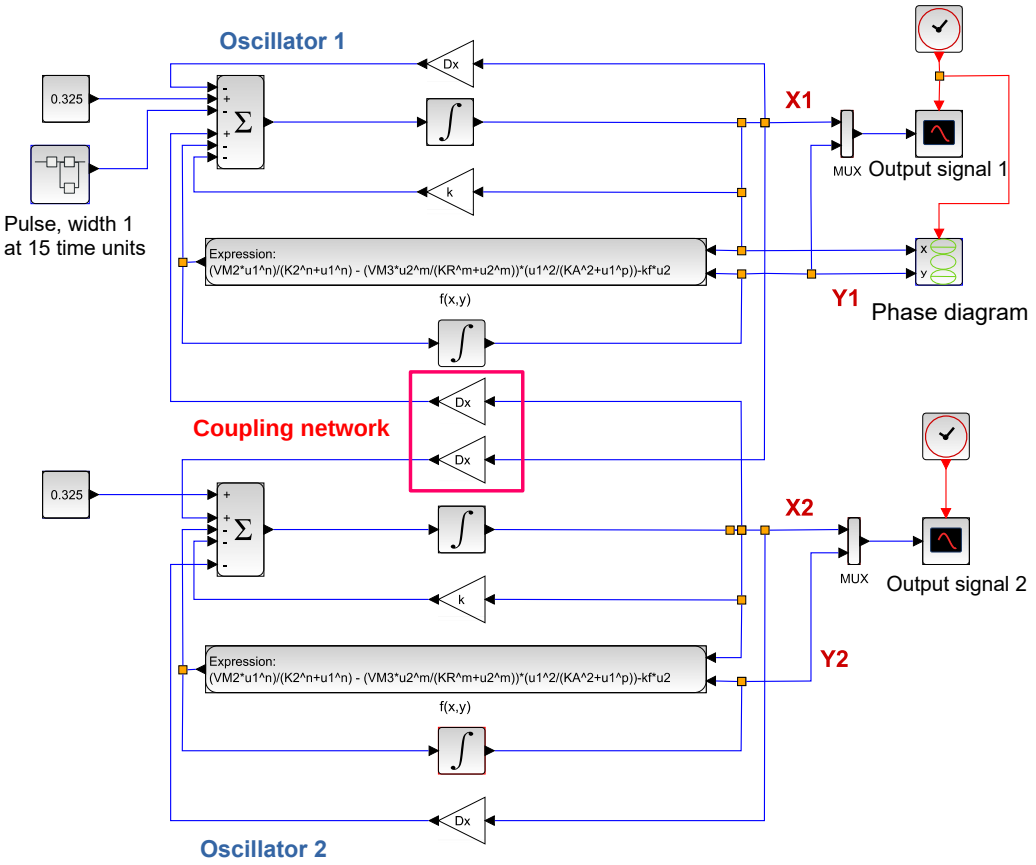

Figure 8.11: *Two oscillators discussed before (see Fig.7.22) coupled with each other.*

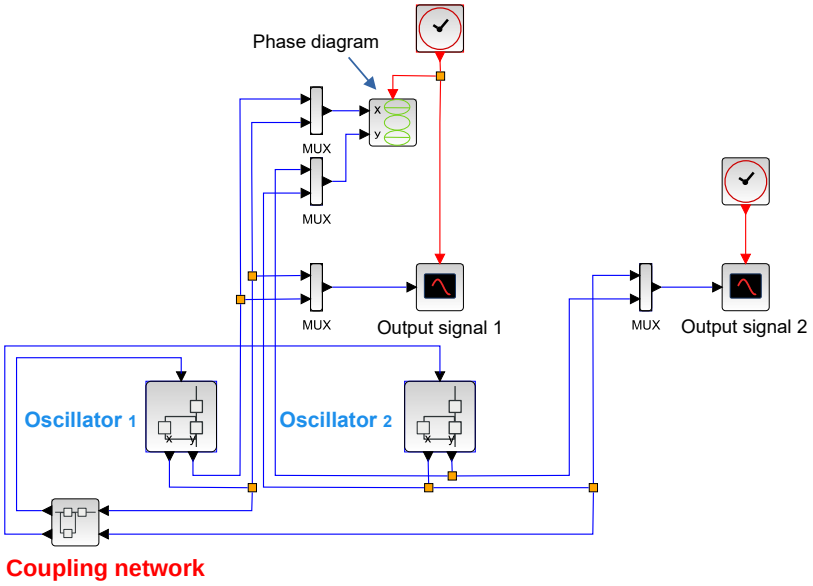

Figure 8.12: *Each of the two oscillators of the model in Fig. 8.11 was hidden in superblock oscillator 1 and superblock oscillator 2. The couple network is thus now represented by a superblock. In this way the Scilab/Xcos model is more compact and the structure of the model is easier to recognise.*

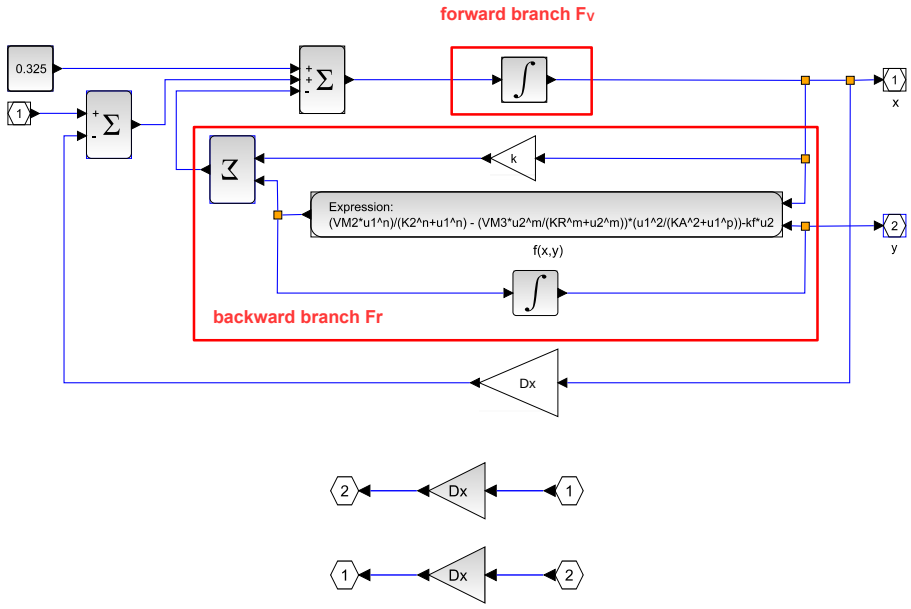

Figure 8.13: *A click on the superblock in Fig. 8.12 opens the contained oscillator structure (top) respectively the contained couple network (bottom)*

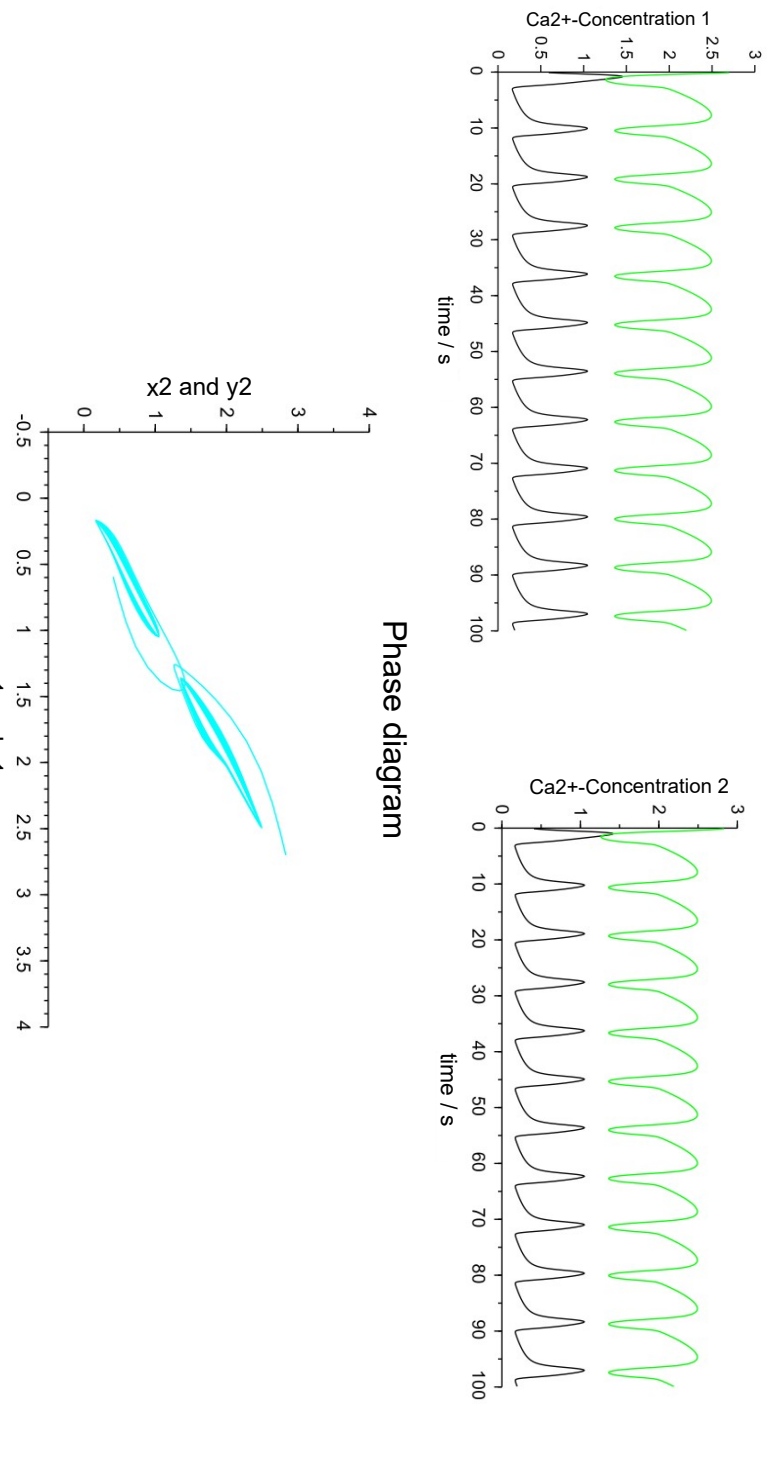

Figure 8.14: *Two coupled oscillators of the model in Fig. 8.12, output of oscillators 1 and 2, and phase diagram x2/y2 versus x1/y1*

8.4.2 Ring with 6 cells

The general block diagram for 6 oscillators (cells) coupled in a ring is shown in Fig. 8.15 and the content of a superblock for an oscillator in Fig. 8.16. How the 6 oscillators are coupled with each other, is shown in Fig. 8.17.

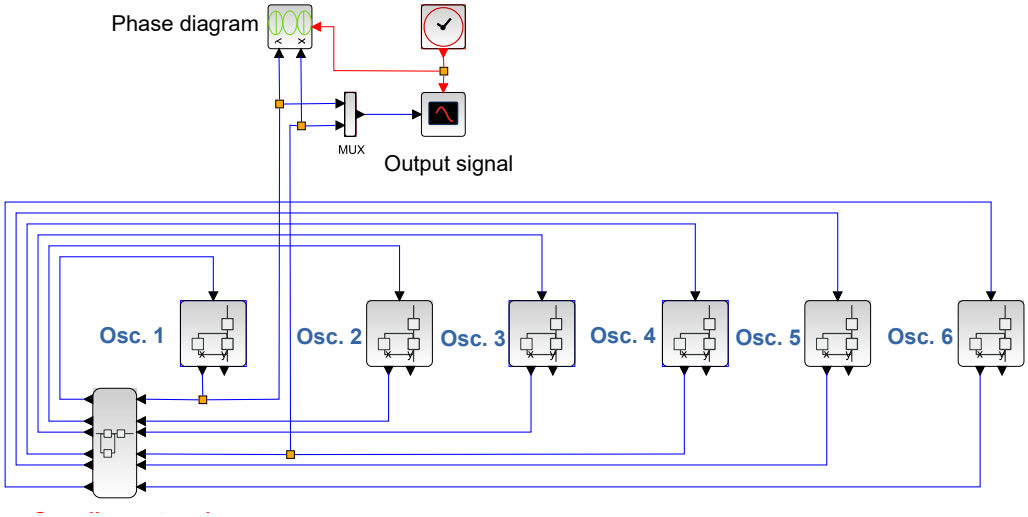

Figure 8.15: *Six coupled oscillators in a ring.*

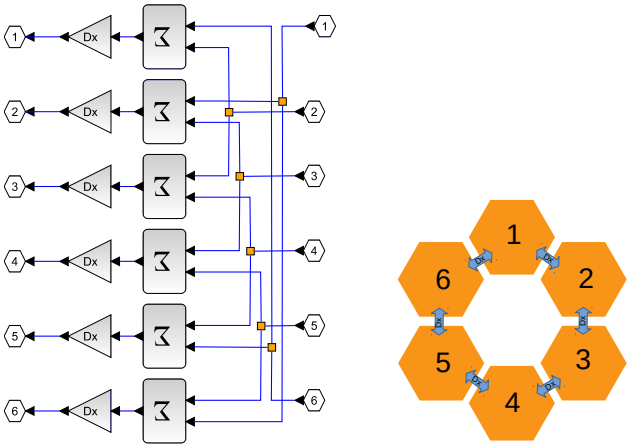

Figure 8.17: *The left part shows the neighbouring cells for each of the 6 oscillators, and the right part shows the same in a simplified version. Thus, cell 1 is coupled with cell 2 and 6, cell 2 with cell 3 and 1 and so on.*

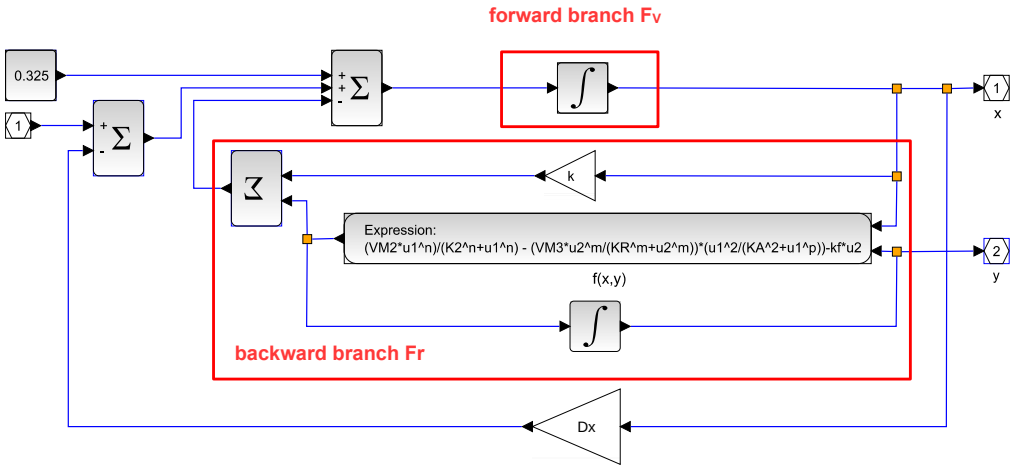

Figure 8.16: *Content of the oscillator superblock in a ring of six cells.*

Since $N = 6$ and $M_i = 2$, the corresponding coupling matrix $\underset{=}{Dx}$ is

$$\underset{=}{Dx6} := Dx \cdot \begin{bmatrix} 2 & -1 & 0 & 0 & 0 & -1 \\ -1 & 2 & -1 & 0 & 0 & 0 \\ 0 & -1 & 2 & -1 & 0 & 0 \\ 0 & 0 & -1 & 2 & -1 & 0 \\ 0 & 0 & 0 & -1 & 2 & -1 \\ -1 & 0 & 0 & 0 & -1 & 2 \end{bmatrix} \tag{8.11}$$

This is likewise a cyclic matrix with 6 cells and 6 columns, the Eigenwert of which can be calculated with the help of a Fourier matrix according to the Eq. 8.4 and analogue to the Eq. 8.5 with the Fourier matrix

$$\underset{=}{W} = (e^{-j2\pi ik/6})_{i,k=0,\ldots,5} \tag{8.12}$$

from the first column of the matrix $\underset{=}{Dx}$ according to

$$(\lambda_0, \ldots, \lambda_5)^T = \underset{=}{W} \cdot Dx \cdot (2, -1, 0, 0, 0, -1)^T \tag{8.13}$$

. Thereby the diag(λ_i) is a diagonal matrix with the diagonal elements λ_l, which specify the Eigenwerte, (l = 0 to 5) i.e.

$$\lambda_i = Dx \cdot \left(2 \cdot 1 - 1 \cdot e^{-j2\pi l/6} - 1 \cdot e^{-j2\pi 5l/6}\right), \; i = 0, \ldots, 5 \tag{8.14}$$

It follows:

$$\begin{array}{lllllllll} \lambda_0 & = & 0 & , & \lambda_1 & = & Dx & , & \lambda_2 = 3Dx \\ \lambda_3 & = & 4Dx & , & \lambda_4 & = & 3Dx & , & \lambda_5 = Dx \end{array} \tag{8.15}$$

The result is, that each cell in the ring can oscillate with its own resonance frequency (for $\lambda_d = 0$), but in addition with at least three further resonance frequencies.

We are now dealing with a ring with 6 cells, which are *synchronised in time*. The result of the simulation is shown in Fig. 8.18 for cell 1 (black curve) and 4 (green curve) at the start (time unit 4 to 104) and 700 time units later (time unit 699 to 800). Fig. 8.19 demonstrates the phase diagram when oscillator #4 is plotted against oscillator #1

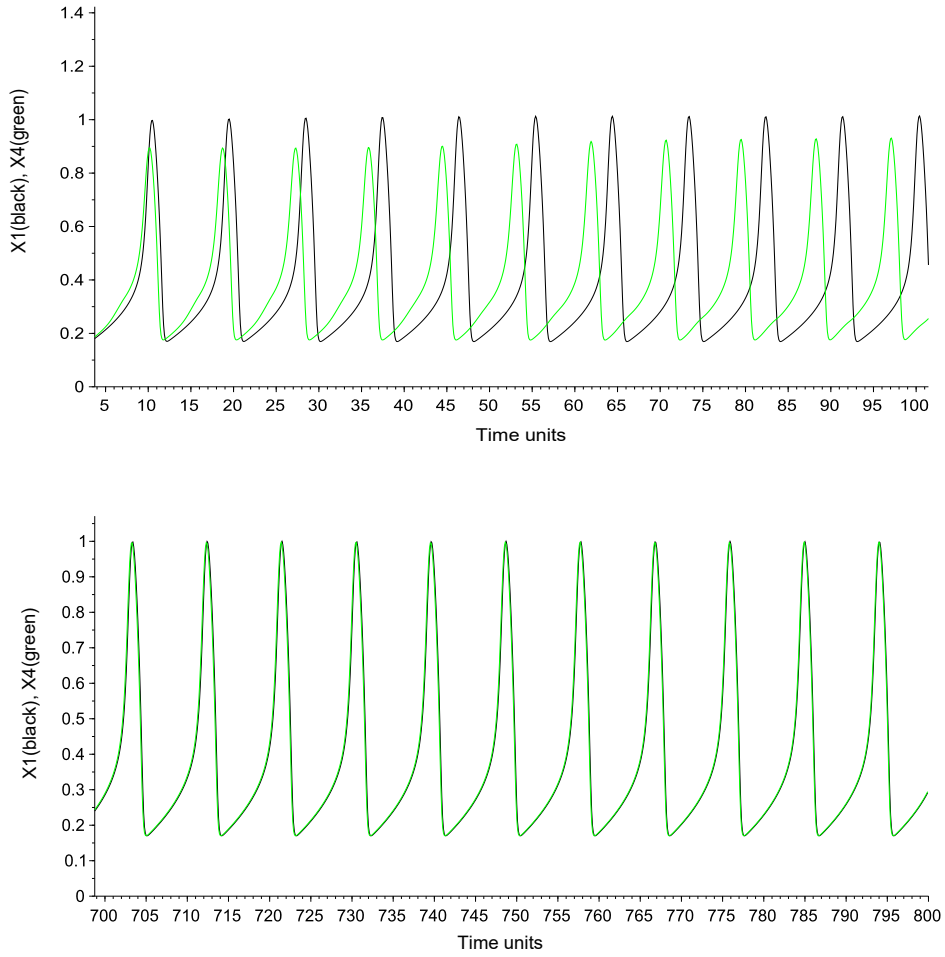

Figure 8.18: *The upper part shows the oscillation of cell 1 (black) and cell 4 (green) at the begin of simulation (time unit 4 to 104) and the lower part 700 time units later (time unit 699 to 800). The two curves drift away at the begin of the recording (upper part, but are in phase at a later time (lower part).*

Now we extend the system and look at rings with 6 cells also synchronising *in space* A 2D

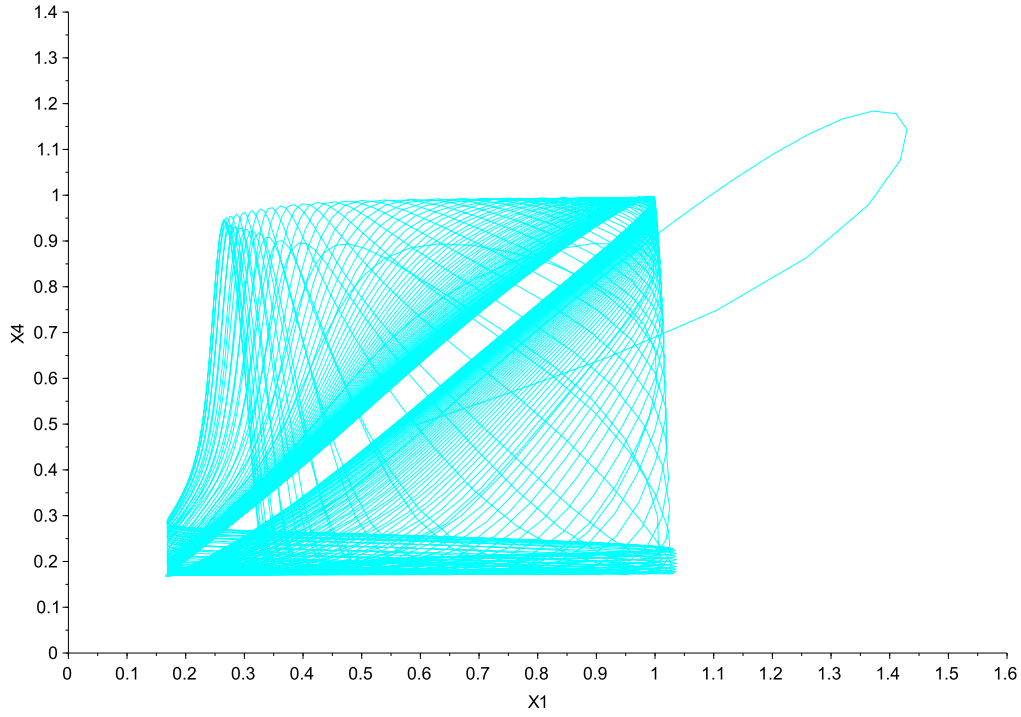

Figure 8.19: *Phase diagram of oscillator 4 (x4, abscissa) over oscillator 1 (x1, ordinate) of a simulation of 6 cells coupled in a ring.*

contour presentation of the results is used a simulation time is 5000 time units (see Fig. 8.20). However, after some time the synchronisation among the 6 cells fails.

A longer simulation time for 50000 time units shows again, that the 6 cells are no longer synchronised in space (see Fig. 8.21).

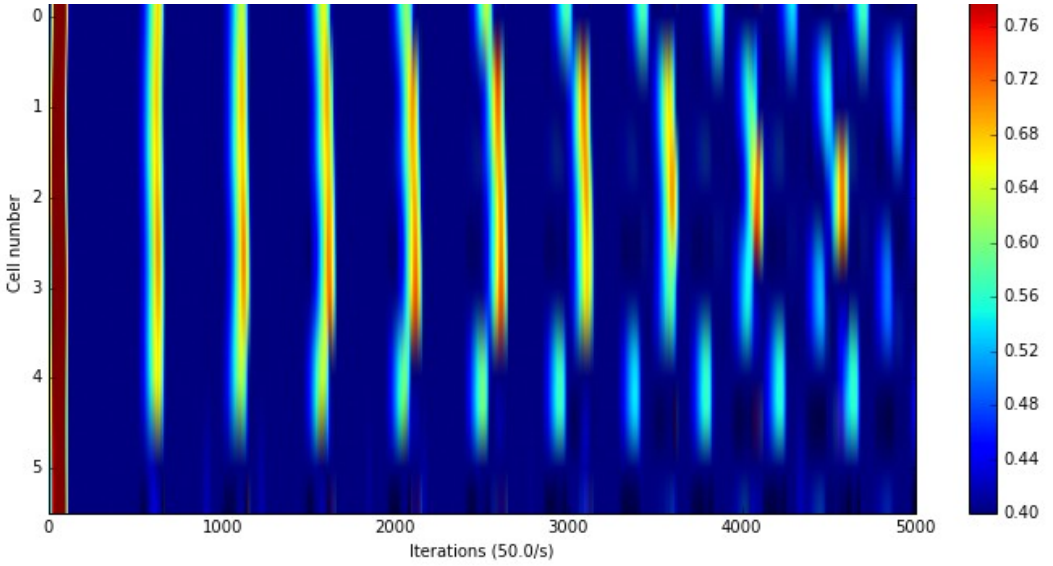

Figure 8.20: *Oscillations of 6 coupled cells in one ring (ordinate) are simulated over 5000 time units. Synchronisation breaks up and the concentrations of* Ca^{2+} *varies (see the different colours and the colour code 0.4 (blue) to 0.8 (dark red) in steps of 0.04)*

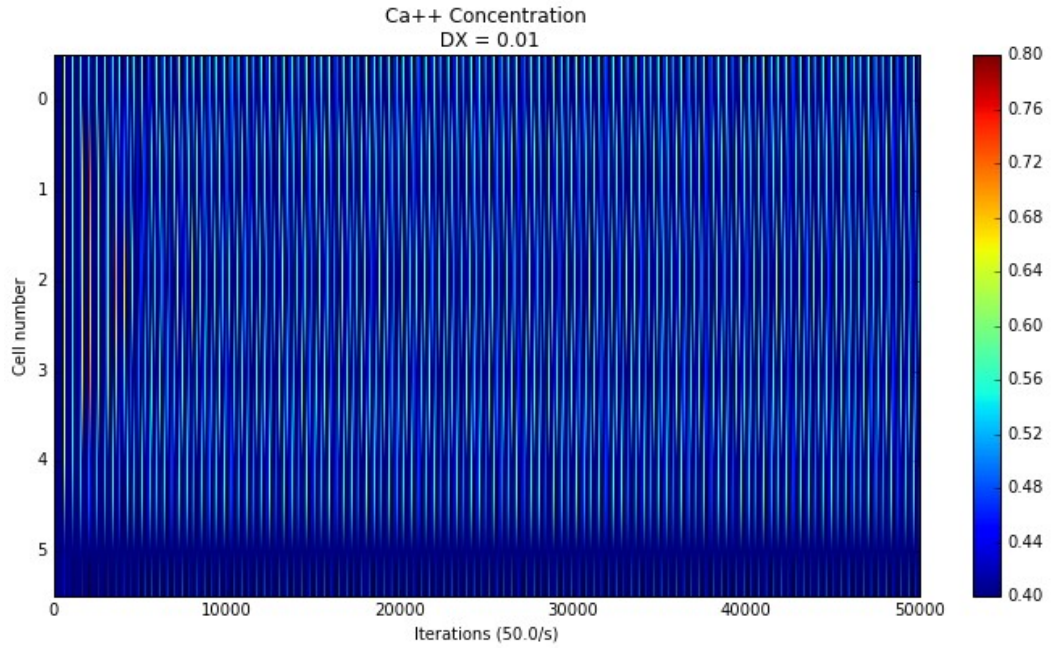

Figure 8.21: *Oscillations of 6 coupled cells in one ring (ordinate) are simulated over 50 000 time units. Coupling coefficient Dx = 0.01. Synchronisation breaks up and the concentrations of* Ca^{2+} *varies (see the different colors and the colour code 0.4 (blue) to 0.8 (dark red) in steps of 0.04)*

8.4.3 Ring with 50 cells

If the number of coupled cells in a ring is increased from 6 to 50, the breakdown of local synchronisation is even more pronounced (see Fig. 8.21).

Since $N = 50$ and $M_i = 2$, the corresponding couple matrix $\underline{\underline{Dx}}$ is

$$\underline{\underline{Dx}}50 := Dx \cdot \begin{array}{c} \begin{array}{ccccccc} 0 & 1 & 2 & 3 & 4 & \dots & 49 \end{array} \\ \begin{bmatrix} 2 & -1 & 0 & 0 & 0 & \cdots & -1 \\ -1 & 2 & -1 & 0 & 0 & \cdots & 2 \\ 0 & -1 & 2 & -1 & 0 & \cdots & -1 \\ 0 & 0 & -1 & 2 & -1 & \cdots & 0 \\ 0 & 0 & 0 & -1 & 2 & \cdots & 0 \\ \vdots & \vdots & \vdots & \vdots & \vdots & \ddots & \vdots \\ -1 & 2 & -1 & 0 & 0 & \cdots & 0 \end{bmatrix} \\ \uparrow row - Nr. \end{array} \quad \begin{array}{c} \leftarrow col. - Nr. \\ 0 \\ 1 \\ 2 \\ 3 \\ 4 \\ \vdots \\ 49 \end{array} \tag{8.16}$$

This is likewise a cyclic matrix with 50 cells and 50 columns, the Eigenwert of which can be calculated with the help of a Fourier matrix according to the Eq. 8.4 and analogue to the Eq. 8.5 with the Fourier matrix

$$\underline{\underline{W}} = (e^{-j2\pi ik/50})_{i,k=0,\dots,49} \tag{8.17}$$

from the first column of the matrix $\underline{\underline{Dx}}$ according to

$$(\lambda_0, \dots, \lambda_{49})^T = \underline{\underline{W}} \cdot Dx \cdot (2, -1, 0, 0, 0, \cdots, -1)^T \tag{8.18}$$

. Thereby the diag(λ_i) is a diagonal matrix with the diagonal elements λ_i, which specify the Eigenwerte, (i = 0 to 49) i.e.

$$\lambda_i = Dx \cdot \left(2 \cdot 1 - 1 \cdot e^{-j2\pi i/50} - 1 \cdot e^{-j2\pi 49i/50}\right),\ i = 0, \dots, 49 \tag{8.19}$$

It follows:

$$\begin{array}{lllllll} \lambda_0 = 0 & , & \lambda_1 = 0.0157706Dx & , & \lambda_2 = 0.0628337Dx \text{ usw.} \\ \lambda_{25} = 4Dx & \text{usw.} & \lambda_{48} = 0.0628337Dx & , & \lambda_{49} = 0.0157706Dx \end{array} \tag{8.20}$$

The result is, that each cell in the ring can oscillate with its own resonance frequency (for $\lambda_0 = 0$), but in addition with at least 24 further resonance frequencies.

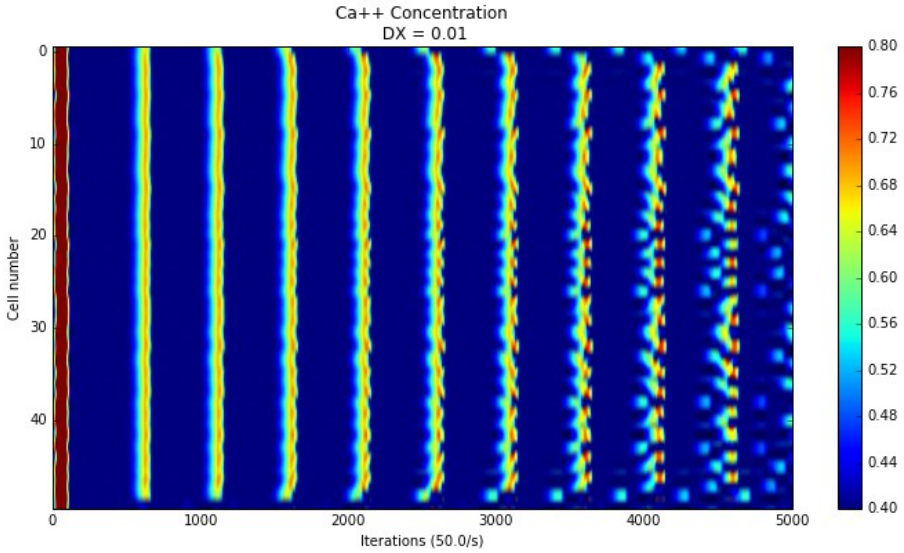

Figure 8.22: *50 coupled cells in ring (ordinate) are simulated over 5000 time units. Synchronisation breaks up and the concentrations of* Ca^{2+} *varies (see the different colours and the color code 0.4 (blue) to 0.8 (dark red) in steps of 0.04). Coupling coefficient Dx = 0.01 .*

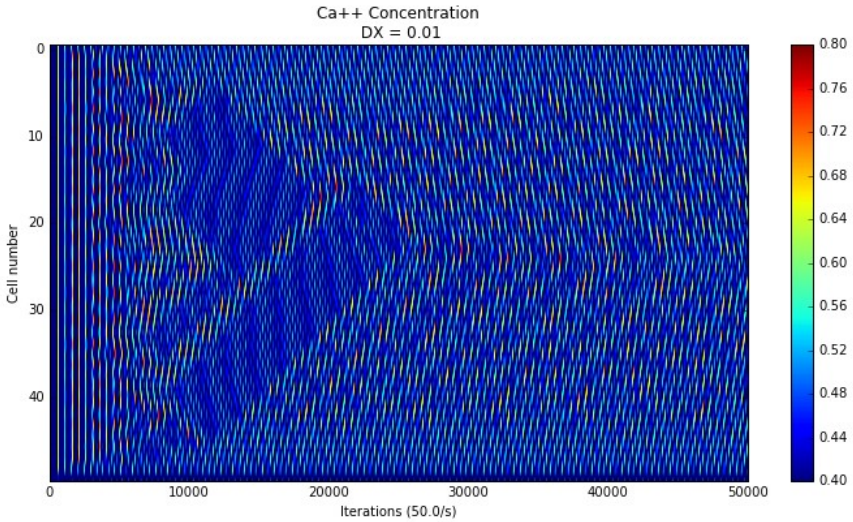

Figure 8.23: *Simulation of oscillations 50 coupled cells in one ring (ordinate from 0 to 50 downward) over 50 000 time units (abscissa from 0 to 50 000). Colour code 0.4 (blue) to 0.8 (dark red) in steps of 0.04. After a chaotic spreading of waves at the start, regular oscillations occur after a certain time due to synchronisation. Coupling coefficient Dx = 0.01*

8.4.4 Cylinder with 50 rings and 50 stacked rings and 50 cells per ring

To match the real situation in an extending hypocotyl (a scheme of a cross section is shown in the left part of Fig. 8.24), 50 rings were used instead of one, thus simulating a cylinder composed of rings on top of each other. The cells are again coupled by diffusion of the Ca^{2+} and the direction of the diffusion is shown in the scheme at the right of the figure with cell numbers horizontally and ring numbers vertically. We thus end up with 2500 oscillators and the general structure of the model is shown in the block diagram of figure 8.25 in superblocks and a couple matrix.

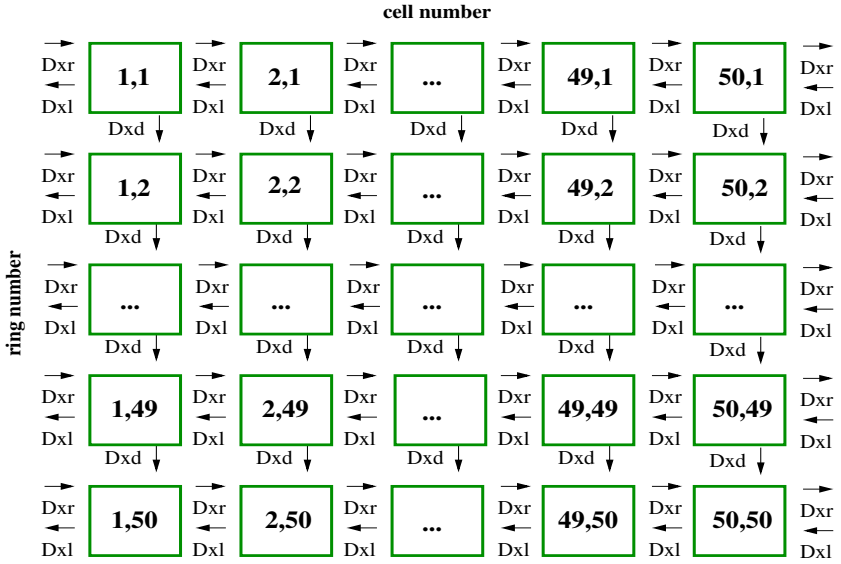

Figure 8.24: *Left: Figure of schematic cross section of a stalk.. Right: Matrix with 1-50 cells horizontally in ring, (Index j$\epsilon\{1,\ldots,50\}$ in the cell i,j for the jth row) and 1-50 rings vertically (Index i$\epsilon\{1,\ldots,50\}$, in the cell i,j for the ith column). Simulation of oscillatory patterns were made for 50 000 time units (see Fig. 8.26 and 8.27). Diffusion coupling horizontally in rings, either left direction Dxl or right direction Dxr. Diffusion coupling downwards Dxd.*

For a cylinder with 50 rings and 50 cells per ring you get with different diffusions in horizontal Dxr and vertical directions Dxd the corresponding couple matrix $\underset{=}{Dx50X50}$ is:

$$\underset{=}{Dxrl50X50} := \begin{array}{c} \begin{matrix} 0-49 & 50-99 & 100-149 & \cdots & 2350-2399 & 2400-2449 & 2450-2499 \end{matrix} \\ \begin{bmatrix} \underset{=}{Dxrl50} & \underset{=}{0} & \underset{=}{0} & \cdots & \underset{=}{0} & \underset{=}{0} & \underset{=}{0} \\ \underset{=}{\text{diag}(-Dxd)} & \underset{=}{Dxrl50} & \underset{=}{0} & \cdots & \underset{=}{0} & \underset{=}{0} & \underset{=}{0} \\ \underset{=}{0} & \underset{=}{\text{diag}(-Dxd)} & \underset{=}{Dxrl50} & \cdots & \underset{=}{0} & \underset{=}{0} & \underset{=}{0} \\ \underset{=}{\vdots} & \underset{=}{\vdots} & \underset{=}{\vdots} & \ddots & \underset{=}{\vdots} & \underset{=}{\vdots} & \underset{=}{\vdots} \\ \underset{=}{0} & \underset{=}{0} & \underset{=}{0} & \cdots & \underset{=}{Dxrl50} & \underset{=}{0} & \underset{=}{0} \\ \underset{=}{0} & \underset{=}{0} & \underset{=}{0} & \cdots & \underset{=}{\text{diag}(-Dxd)} & \underset{=}{Drl50} & \underset{=}{0} \\ \underset{=}{0} & \underset{=}{0} & \underset{=}{0} & \cdots & \underset{=}{0} & \underset{=}{\text{diag}(-Dxd)} & \underset{=}{Dxrl50} \end{bmatrix} \end{array} \begin{array}{l} \leftarrow col.-Nr. \\ 0-49 \\ 50-99 \\ 100-149 \\ \vdots \\ 2350-2399 \\ 2400-2449 \\ 2450-2499 \\ \uparrow row-Nr. \end{array} \tag{8.21}$$

with $\text{diag}(Dxd)$ is a 50X50 diagonal matrix with elements Dxd, $\underset{=}{0}$ is a 50X50 matrix with zero

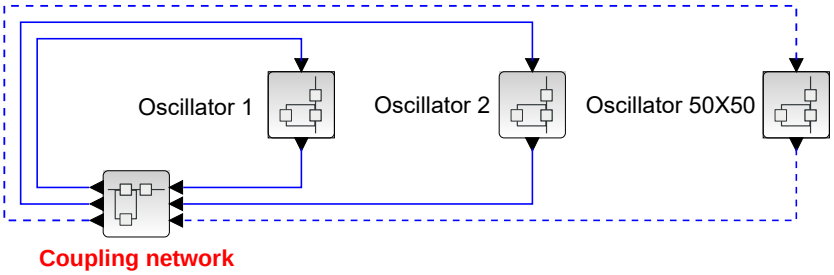

Figure 8.25: *Block diagram of 50 cell rings on top of each other forming a cylinder. The coupling network adds up the various rings.*

elements , $row-Nr.=n-1+(m-1)\cdot 50$, $col.-Nr.=m-1+(n-1)\cdot 50$, m and n are the row and column numbers of the sub-matrices $\underset{=}{Dxrl50}$.

$$\underset{=}{Dxrl50} = \begin{array}{c} \begin{matrix} 1 & 2 & 3 & 4 & 5 & \dots & 50 & \leftarrow m \end{matrix} \\ \left[\begin{matrix} Dxr+Dxl+Dxd & -Dxr & 0 & 0 & 0 & \cdots & -Dxr & 1 \\ -Dxl & Dxr+Dxl+Dxd & -Dxr & 0 & 0 & \cdots & Dxr+Dxl & 2 \\ 0 & -Dxl & Dxr+Dxl+Dxd & -Dxr & 0 & \cdots & -Dxl1 & 3 \\ 0 & 0 & -Dxl & Dxr+Dxl+Dxd & -Dxr & \cdots & 0 & 4 \\ 0 & 0 & 0 & -Dxl & Dxr+Dxl+Dxd & \cdots & 0 & 5 \\ \vdots & \vdots & \vdots & \vdots & \vdots & \ddots & \vdots & \vdots \\ 0 & 0 & 0 & -Dxl & Dxr+Dxl+Dxd & \cdots & 0 & 50 \end{matrix}\right] \\ \uparrow n \end{array}$$

Unfortunately, the matrix Dxrl50X50 is no longer cyclic because the first ring lacks the coupling to a ring below it and the last ring lacks the coupling to a ring above it. Therefore, the corresponding eigenvalues can no longer be calculated as easily as e.g. according to eq. 8.19 .

However, if the first ring were also to couple to the last ring and vice versa, a **torus** would be created whose matrix $\underset{=}{Dxrl50X50T}$ would become cyclic again:

$$\underset{=}{Dxrl50X50T} := \begin{array}{c} \begin{matrix} 0-49 & 50-99 & 100-149 & \cdots & 2350-2399 & 2400-2449 & 2450-2499 & \leftarrow col.-Nr. \end{matrix} \\ \left[\begin{matrix} \underset{=}{Dxrl50} & \underset{=}{0} & \underset{=}{0} & \cdots & \underset{=}{0} & \underset{=}{0} & \underset{=}{\mathrm{diag}(-Dxd)} & 0-49 \\ \underset{=}{\mathrm{diag}(-Dxd)} & \underset{=}{Dxrl50} & \underset{=}{0} & \cdots & \underset{=}{0} & \underset{=}{0} & \underset{=}{0} & 50-99 \\ \underset{=}{0} & \underset{=}{\mathrm{diag}(-Dxd)} & \underset{=}{Dxrl50} & \cdots & \underset{=}{0} & \underset{=}{0} & \underset{=}{0} & 100-149 \\ \vdots & \vdots & \vdots & \ddots & \vdots & \vdots & \vdots & \vdots \\ \underset{=}{0} & \underset{=}{0} & \underset{=}{0} & \cdots & \underset{=}{Dxrl50} & \underset{=}{0} & \underset{=}{0} & 2350-2399 \\ \underset{=}{0} & \underset{=}{0} & \underset{=}{0} & \cdots & \underset{=}{\mathrm{diag}(-Dxd)} & \underset{=}{Dxrl50} & \underset{=}{0} & 2400-2449 \\ \underset{=}{0} & \underset{=}{0} & \underset{=}{0} & \cdots & \underset{=}{0} & \underset{=}{\mathrm{diag}(-Dxd)} & \underset{=}{Dxrl50} & 2450-2499 \end{matrix}\right] \\ \uparrow row-Nr. \end{array} \tag{8.22}$$

This is likewise a cyclic matrix with 2500 cells and 2500 columns, the Eigenwert of which can be calculated with the help of a Fourier matrix according to the Eq. 8.4 and analogue to the Eq. 8.5 with the Fourier matrix

$$\underset{=}{W} = (e^{-j2\pi ik/2500})_{i,k=0,\dots,2499} \tag{8.23}$$

from the first column of the matrix $\underset{=}{Dxrl50X50T}$ according to

$$(\lambda_0,\dots,\lambda_{2499})^T = \underset{=}{W}\cdot(Dxr+Dxl+Dxd,-Dxl,48*(0,)-Dxd,2402*(0,)0)^T \tag{8.24}$$

. Thereby the diag(λ_i) is a diagonal matrix with the diagonal elements λ_l, which specify the Eigenwerte, (i = 0 to 2499) i.e.

$$\lambda_i = Dxr + Dxl + Dxd - Dxl - Dxd \cdot e^{-j2\pi i/2500} - Dxd \cdot e^{-j2\pi 50i/2500},\ i = 0, \ldots, 2499 \quad (8.25)$$

However, due to the large number of 2500 eigenvalues and the dependence on the diffusion parameters Dxr, Dxl and Dxd, we will not list them here.

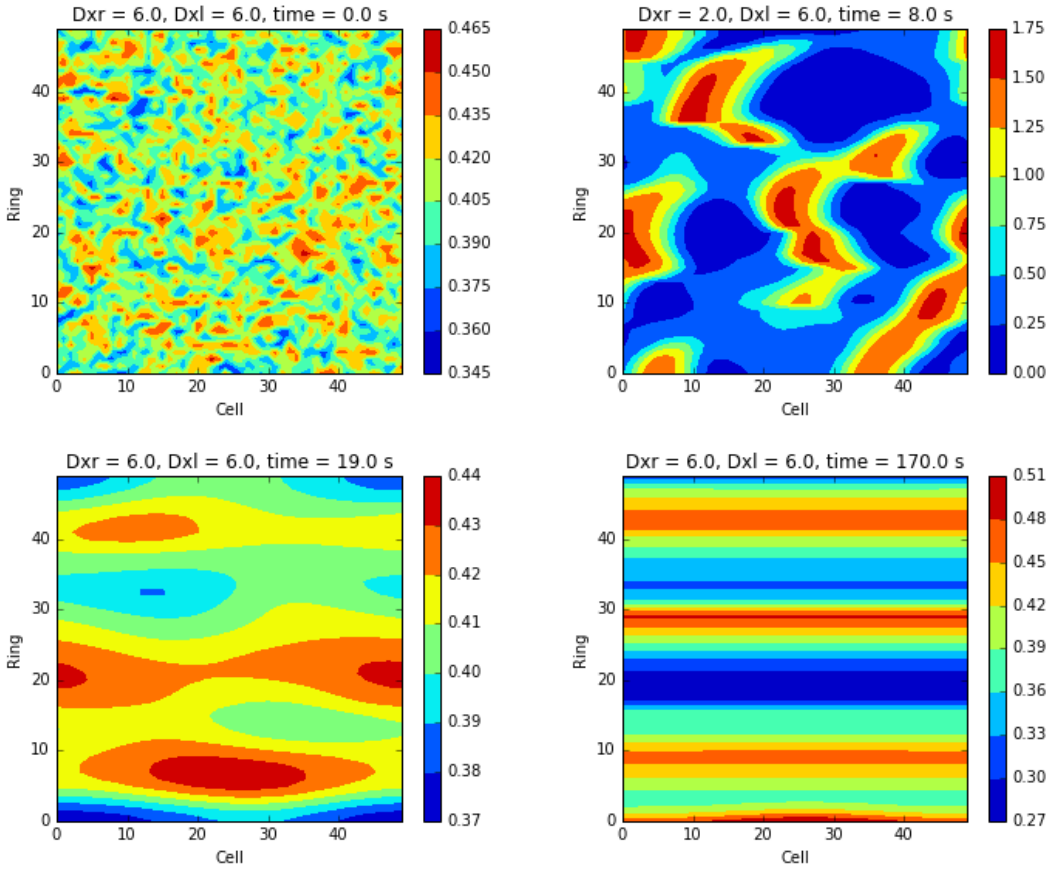

Figure 8.26: *Result of simulations with 50 cells in a ring, 50 rings on top of each other thus forming a cylinder.*
Uniform diffusion *Dx=6.0 and random concentration at the begin of the simulations. Then Dxr=6.0, Dxl=2.0,Dxd=1.0. Cluster formation after 4 time units, stronger horizontal cluster formation after 19 time units, one stripe cluster formation after 170 time units (final situation).*
x-axis cell number from 0 to 50 (steps 10), y-axis ring number from 0 to 50 (steps 10). Colour code 0.345 (blue) to 0.465 (dark red) in steps 15

Another simulation was performed with diffusion in different directions and the results are shown in Fig. 8.27.

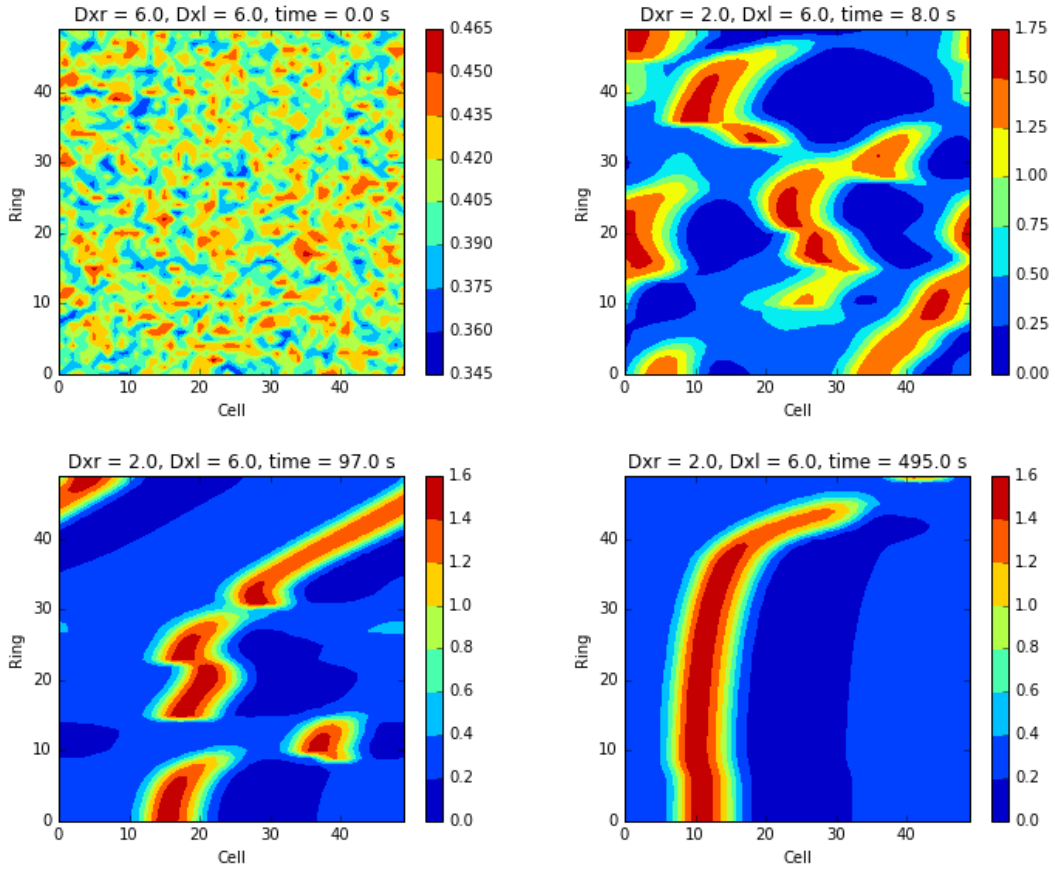

Figure 8.27: *Result of simulations with 50 cells in a ring, 50 rings on top of each other thus forming a cylinder. Diffusion Dx=6.0 in different directions and random concentration at the begin of the simulations.*
Cluster formation after 8 time units, stripe cluster formation after 97 time units, one stripe cluster formation after 495 sec. Dxr=6.0, Dxl=2.0. x-axis cell number from 0 to 50 (steps 10), y-axis ring number from 0 to 50 (steps 10). Colour code 0.345 (blue) to 0.465 (dark red) in steps 15.

8.4.5 Cylinder with 200 rings and 50 cells per ring

The length of the cylinder was now increased to 200 rings with 50 cells each. The general block diagram is shown in Fig. 8.28. It consists of 10000 oscillators in superblocks and one couple matrix.

The results of these simulations were plotted in 3D by joining the begin and the end of the plane data of Fig. 8.30 in Fig. 8.31.

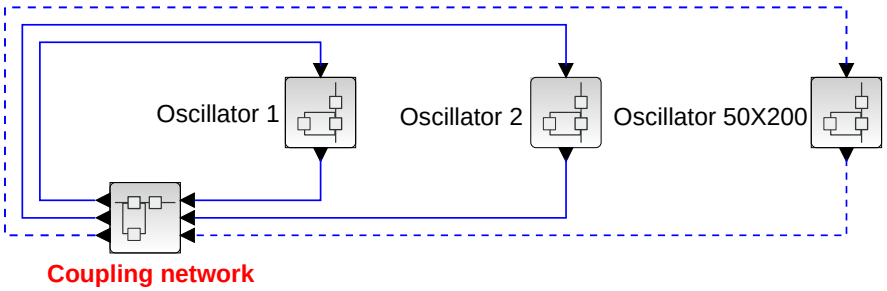

Figure 8.28: *Block diagram of 200 cell rings on top of each other forming a cylinder. The couple network adds up the various rings.*

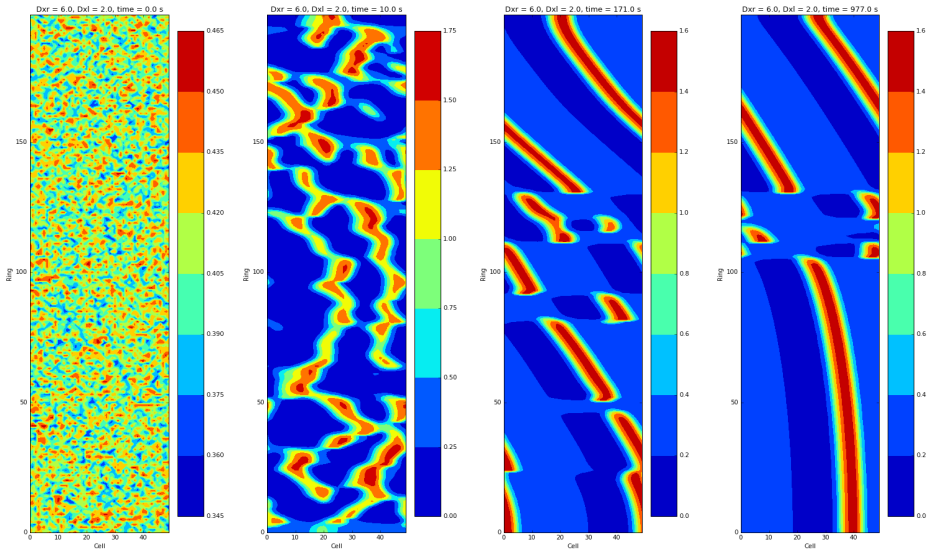

Figure 8.29: *Result of simulations with 50 cells in a ring, 200 rings on top of each other thus forming a cylinder.*
Diffusion in different directions (Dxr=6.0, Dxl=2.0 and random concentration at the start of the simulations. Results of the simulation at 0, 10, 171, and 977 time units.. x-axis cell number from 0 to 50 (steps 10), y-axis ring number from 0 to 200 (steps 50). Colour code 0.345 (blue) to 0.465 (dark red) in steps 15

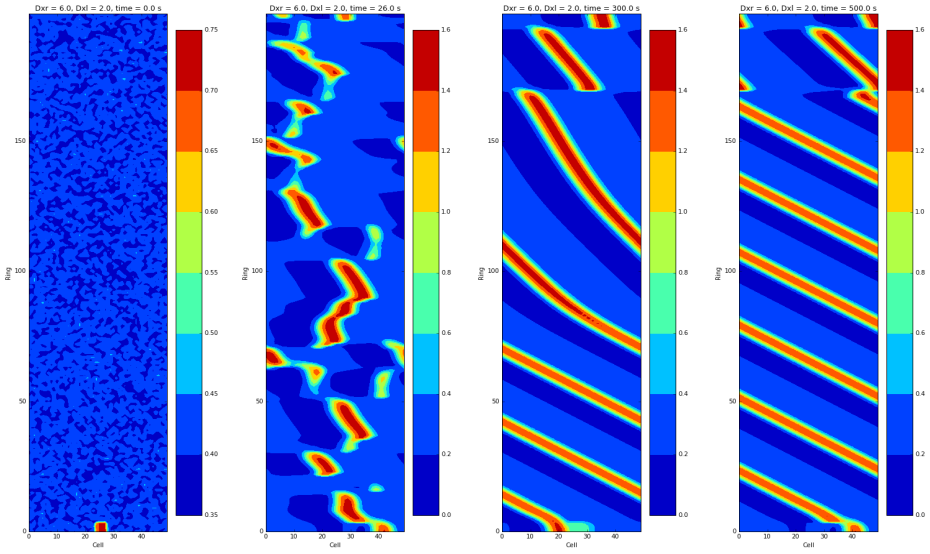

Figure 8.30: *Result of simulations with 50 cells in a ring, 200 rings on top of each other thus forming a cylinder.* Diffusion in different directions *(Dxr=6.0, Dxl=2.0) and random concentration at the begin of the simulations. Additionally a sinusoidal excitation was applied in the first ring and the 25th cell with an amplitude of 0.7 and an angular frequency ω of 1,047. The figure shows the results of the simulation for 0, 26, 300 and 500 time units. Axes and colour as in Fig. 8.29*

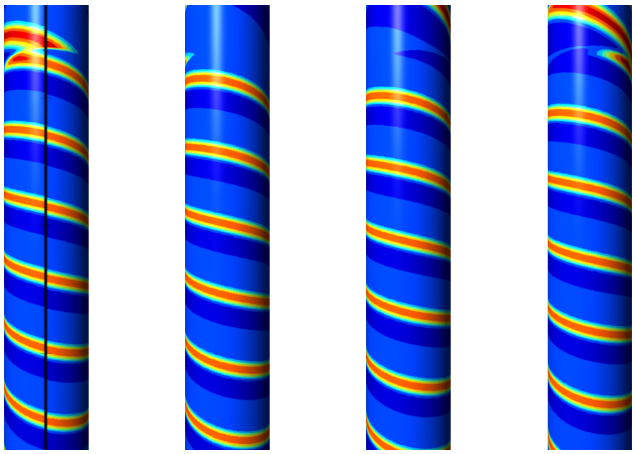

Figure 8.31: *Result of simulations with 50 cells in a ring, 200 rings on top of each other thus forming a cylinder.* Diffusion in different directions *Dxr=6.0, Dxl=2.0 and random concentration at the begin of the simulations. The 3D presentation shows the results of the simulation in 0, 26, 300, and 500 time units. Axes and colour coding description as in Fig. 8.30*

9 Appendices

9.1 Playground - Modeling and Simulations

You might like to start your own simulations of rhythmic phenomena after having gone through this book. As a start, a "playground" with the description of some interesting phenomena as we found in the literature will be given.

We have already (chapter 5) discussed a population oscillation that was studied in biomattematics by Lotka and Volterra (wikipedia: see Lotka-Volterra equations, or for example: https://en.wikipedia.org/wiki/Lotka%E2%80%93Volterra_equations). It is often denoted “The Volterra-Lotka” model or, by its popular name “The Predatur-Prey”.

In this chapter we first study this Predator-Prey model as a fairly simple example of a biological oscillator (see subsect. 9.1.1) followed by examples of models with coupled oscillators (see subsect. 9.1.2). We then discuss some different features of biological oscillators, for example their period length, possible perturbation agents and phase shifts and so on.

9.1.1 Single Oscillator: Predator-Prey model

We repeat the outline:

If in an area many prey animals exist, the predators are well off and can reproduce at a high rate. The increasing predator population however reduces the prey population. Finally there is not enough food left, the number of predators increases less strongly and the prey population can recover. The time course of such an interaction is shown in Fig. 9.1. There are programs which graphically display the interplay between the sizes of the populations of predator and prey.

Long period oscillations The population oscillations modeled in the literature by the Predator-Prey model are usually of ecological type and showing fairly long period, e.g. one year. But there are several examples of biological oscillations – many not yet modelled satisfactorily - with much longer period. Those can be an interesting topic for a discussions.

Among extreme rhythms are the periodicity in the mass blossom of bamboo species which can be mentioned - with interval of 65 years or even longer. As mentioned before in this book the duration necessary to observe and determine a precise value of a very long period in rhythms can be prohibitive.

We would like to mention the interesting and long term observations of the life-cycle control of periodic cikadas: Magicicada exhibits a spectacular life-cycle phenomenon, with periodic mass emergence (documented for a long time) every 13 or 17 years in the eastern United States. It is unclear how the cikadas’ periodical life cycle is controlled, but Sota (2022) proposes a model where an internal 4-year period oscillator is gating processes in the larvae to control

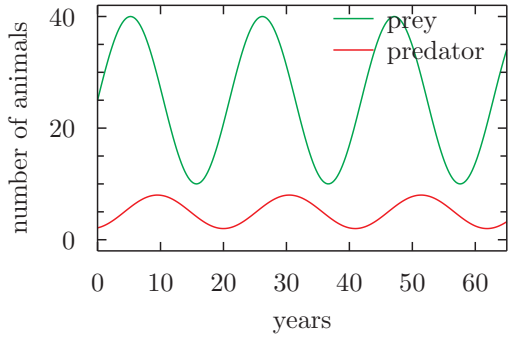

Figure 9.1: *Time course of the interaction of predator-prey populations. The prey population (green curve) is increasing during the first years, followed by an increasing predator population (red curve) with a lag of several years. For a model to simulate these data see Fig. 5.26.*

the outbursts. This could be part of the explanation for the fascinating prime number periods recorded (13 and 17 years!):

https://en.wikipedia.org/wiki/Magicicada_septendecim

How should one achieve and save time series long enough in order to be able to predict long term oscillatory phenomena (climate, pandemics etc)?

9.1.2 Multiple oscillators: Playing in a clock shop

We will turn to coupled oscillators and discuss how the number of cells in a tissue can affect the frequency of rhythm (Pavlidis approach).

In the literature on oscillators, the subtle concept of clock shop has been used by e.g. Pavlidis (Pavlidis 1971) and Winfree (Winfree 1967), to discuss the behaviour of several oscillators – physical clocks or biological ones. If we start with the well-known (simplified) differential equation describing oscillations of a physical pendulum (clock!) it can be written as::

$$d^2x/dt^2 + c \cdot dx/dt + \omega_0^2 \cdot x = 0$$

Here x is the pendulum angle, c is presenting friction and ω_0 is the pendulum frequency. The solution is oscillatory for small x, as we remember, and can be written

$$x(t) = x_0 e^{-t \cdot c/2} \cdot sin(\omega t + \varphi), \text{ where } \omega^2 = \omega_0^2 - (c/2)^2$$

(for $c = 0$ we have of course the simple harmonic oscillator with constant amplitude and the basic frequency ω_0). For $c < 0$ the amplitude of the oscillation increases, and to prevent "explosive solutions" one can introduce, for example, a limitation on dx/dt, requiring it to be limited by a constant $-H$, i.e.

$$\begin{aligned} d^2x/dt^2 + c \cdot dx/dt + \omega_0^2 x &= 0 \text{ when } dx/dt \geq -H \\ dx/dt &= -H \text{ otherwise} \end{aligned}$$

The system has now been changed into a non-linear one. This new system can describe sustained, limited oscillations. The reader might find it useful to implement this in Scilab (the program can be also be used in the following).

The differential equation can be applied to different problems. Pavlidis (Pavlidis 1971) started with this 2nd order differential equation to describe a network of oscillating cells, each of them following the equation and each of them 'coupled to' all the others. The variable x could then stand for a variable concentration of a molecule, which is essential for the biological rhythm mechanism.

Now, assume that we have a wall with n such pendulums. Through vibrations in the wall they might affect each other and we assume that this takes such a form that the amplitude x_j of $(pendulum)_j$ affects the x-values of all other pendulums with a coupling factor $r \cdot \omega_0^2$. Here the *r-symbol* denotes an interaction or coupling between the pendulums. Pavlidis showed how the number of cells in such an oscillating network can affect the frequency of rhythm (Pavlidis 1973).

When we have N equal pendulums or oscillatory cells (all with the same r and ω_0) we finally reach the expression for pendulum 'k' in our cluster or network

$$d^2x_k/dt^2 + c \cdot dx_k/dt + \omega_0^2 \cdot x_k = r \cdot \omega_0^2 \sum_{j=1,\neq k}^{N} x_j$$

This is a coupled oscillator network which we have already discussed in a slightly different context: see Fig.8.1 , Fig.8.2 and Fig. 8.3 with

$$\begin{aligned}
c_i &= x_j \\
Fr_i &= 1 \\
Fv_i &= \mathcal{F}\{d^2x_k/dt^2 + c \cdot dx_k/dt + \omega_0^2 \cdot x_k\}/\mathcal{F}\{x_k\} \\
&= p^2 + c \cdot p + \omega_0^2, \text{ with } p := \sigma + j\omega \\
r_i &= 1 \\
r_g &= r \cdot \omega_0^2 \\
\mathcal{F}(x_k) &: \text{complex Fourier transformation from } x_k
\end{aligned}$$

We can now study, for example, the average output signal of the cluster. Denoting this average 'y' we get

$$y := \frac{1}{N} \sum_{j=1}^{N} x_j$$

Now if our pendulum system could be regarded as a model for a rhythmic cell system (following Pavlidis) y might be looked upon as an average signal from a cluster of identical cells, a type of biological tissue.

Rewriting the second order differential equation we can get

$$d^2x_k/dt^2 + c \cdot dx_k/dt + \omega_0^2 \cdot x_k - r \cdot \omega_0^2 \sum_{j=1,\neq k}^{N} x_j = 0$$

or for the cluster

$$d^2y/dt^2 + c \cdot dy/dt + \omega_0^2 \cdot (1-r)y = 0$$

Thus the frequency of the cluster would change and becomes moderated by the factor $\sqrt{1-r}$ in the case of the linear cluster.

If we include the limitations of -H, and thus study a non-linear corresponding cluster model it would be of great interest to see if the frequency change we calculated above, is also valid for the non-linear model.

There are now many problems to play around with, once we have implemented the model. Some of the can be mentioned:

1. What is the frequency of y ? How does the coupling influence the frequency? Study first the linear system (i.e. without the y) by adding all the differential equations, introduce y and give an expression for the frequency of y as a function of N. The number of oscillators, N is certainly positive, but can one imagine negative values of r ?

2. If one studies $N = 6$ and still keep r constant, now denoted r_g, the coupling situation can be described by the matrix R, see Eq.8.2 ,

$$\underline{\underline{R}} = \begin{pmatrix} 1 & r_g & r_g & r_g & r_g & r_g \\ r_g & 1 & r_g & r_g & r_g & r_g \\ r_g & r_g & 1 & r_g & r_g & r_g \\ r_g & r_g & r_g & 1 & r_g & r_g \\ r_g & r_g & r_g & r_g & 1 & r_g \\ r_g & r_g & r_g & r_g & r_g & 1 \end{pmatrix}$$

   We see that the elements in the matrix are all equal = r_g except for the (diagonal) trace elements. It means that an individual cell is coupled with r_g to all the other five cells (but not to itself). Use Scilab to implement the 6-element network!

3. Introduce, for comparison, another coupling matrix $R1$:

$$\underline{\underline{R1}} = \begin{pmatrix} 1 & r_{g1} & 0 & 0 & 0 & r_{g1} \\ r_{g1} & 1 & r_{g1} & 0 & 0 & 0 \\ 0 & r_{g1} & 1 & r_{g1} & 0 & 0 \\ 0 & 0 & r_{g1} & 1 & r_{g1} & 0 \\ 0 & 0 & 0 & r_{g1} & 1 & r_{g1} \\ r_{g1} & 0 & 0 & 0 & r_{g1} & 1 \end{pmatrix}$$

   In this case, we see that each oscillator couples only to its neighbours (coupling coefficient r_{g1}) and the oscillators can be depicted to be joined in a ring (a similar situation has been treated, in another context, in Sect. 8.4 and there in subsect.8.4.2 and the following of the present book.
   Try to simulate different behaviour of the oscillators on the ring. What happens if the starting phases of the oscillators are different? If the frequency of the individual oscillator is slightly different?

4. It might be interesting for the reader to introduce a perturbation into the system, for example by adding a pulse of the substance x to one or more oscillators in the system. Then one would be able to study how the perturbation affects the phase and the amplitude of the network oscillation. A phase response curve would then be possible to construct.

5. One could speculate about the nature of the coupling factor:
   Is it likely that the coupling is constant throughout a biological tissue which has 2 or 3 dimensions? Or in a liquid solution with interacting cells? Should the r_g-values be dependent on the spacial *distances* between the oscillators, e.g. in a liquid cell solution? How should one interpret negative r-values?

9.2 Modeling at different organizational levels.

We have seen in previous chapters that models for 'lumped' or overall systems can be developed to describe relevant features of the oscillating system. We discussed oscillating water transpiration from a plant leaf – being the overall result of the water vapour transport through many oscillating pore openings. Of course the overall oscillations are useful for discussion of the individual plant, or the canopy etc. – simultaneously as one would like to model the oscillations of the individual pore opening.

Of course, one would in most cases like to describe the different and more detailed parts/mechanisms that constitute the overall oscillatory system. Then the model must be refined. In our chapters we have discussed how individual detailed oscillators, for example in cells, couple to each other to produce a bigger, overall, oscillating system.

And the modelling does not stop there. One would probably like to know how the molecules interact in a single cell to create an oscillating system. We are then on a still more detailed level. And we have seen that here the biochemical properties and reactions come explicitly into play.

Further on: in several cases the modelling has led to genetically based models where modern biotechnological methods from chemistry, biology and biophysics cooperate to find details in the oscillators.

9.3 Some discussion points and open questions

9.3.1 Introduction

Oscillatory biological rhythms provide a fascinating multitude of questions and unsolved problems. Discussions around their properties can be fruitful and interesting and we just want to hint at some subjects.

9.3.2 Discussions

1. *Ultradian rhythms* are very frequent in biology (as partly reflected in previous chapters). Most work has probably been concentrated on rhythms with a period of about 1 – 2 hours (see e.g. references Brodsky (2022) and Lloyd, Nanjundiah, Engelmann and Johnsson (2023)).

In the case of circadian rhythms, the rhythms have probably an adaptive value to the light/darkness changes in Nature. Let us say that the circadian rhythms have an evolutionary advantage for the organisms. The same can be said of annual rhythms – they allow the organism to adapt to variations of the climate throughout the year. But why are there so many ultradian rhythms in the period region of one-two hours?

2. *Lithium ion.* It turns out that the Li+ ion lengthens the period of the circadian clocks in many organisms (all?). At the same time it is used in treatment of patients with certain forms of depressive disorders. Is there a causal connection between lithium effects on circadian rhythms and on depressions? Discuss the newest results in the literature on lithium effects in manic-depressive disorders and on circadian rhythms.
   It is remarkable that many of the *ultradian* oscillations discussed in the present book also lengthen their period after lithium addition (e.g. oscillatory water evaporation in plants). Are biological oscillations – circadian as well as ultradian ones – involving same, lithium sensitive, mechanisms?
   Discuss if this indicates that the lithium ion acts as a general slowing down in oscillatory systems,

3. *Minute period oscillations of plant leaves.* Rapid leaf oscillatory movements exist in some plants (minute range, see chapter 2). Scientists have studied how their mechanisms and the electrical waves that accompany them have been studied and discussed. But any answer to the why question "what is the advantage of these oscillations?" has not been agreed upon.

4. *Three dimensional tissue.* We have used models that show oscillatory behaviour on two-dimensional surfaces or cylinders (see chapter 8.4). However, three dimensional structures – e.g. 3 dimensional tissue where oscillating cells are in contact with several neighbours – have not been discussed. The corresponding modelling and simulation studies of possible oscillations offer several problems that can be interesting to discuss.

5. *Time series and Signal analysis.* In modern science, studies of time varying phenomena usually mean that one ends up with time series, i.e. measurement data, sampled at time intervals and successively stored. The sampling processes are digital and there exist important issues regarding e.g. sampling rate, regarding precision of period possible to achieve etc. Usually the effective techniques are developed and work in the frequency domain.
   Altogether this makes the applications of signal analysis to the results very important. It can be very fruitful if cooperation between biologists and expertise on signal analysis is established in the research group.

6. *Electromagnetic fields* can affect biological oscillators (obviously so in the case of the heart oscillations). We have mentioned some examples in this book. Discussions of how the fields penetrate tissue and affect oscillatory reactions are certainly needed. A fairly recent paper points at the formation of chemical radical pairs could be affected by both electromagnetic fields and lithium ions, which are both known to interact with circadian

clocks (Zadeh-Haghighi, Simon 2022). It is predicted that stronger magnetic fields would shorten the clock's period.

7. Both lumped models and multi-oscillator models are useful

8. *Molecular mechanism and genetics of models:* The molecular basis of cR is thought to be due to a negative transcriptional feedback with sufficient time delay. Several authors have tried to model cR on this basis, such as Tyson, Hong et al. 1999; Hong, Conrad, Tyson 2007; Brown, Doyle 2020; Goldbeter, Leloup 2021, and we mentioned this issue at several placed in the book (see Fig. 3.3 for Drosophila, and Sect. 7.3 and 7.4). Yao et al. 2022 used bifurcation theory to explore mathematical models of the circadian clock in mammals, with which Kim, Forger 2012 tried to simulate the inhibitory binding of PER proteins to their transcription activator BMAL1. Since the binding affinity between PER and BMAL1 was much to high, they introduced
(1) a multistep reaction chain for post-transcriptional modifications of Per mRNA and post-translational photostimulations of PER, and
(2) replaced the first-order rate law for degradation of PER by a Michaelis-Menten rate law, and
(3) included a second negative feedback loop with REV-ERB and a positive feedback loop involving ROR (see also Patton, Hastings 2023). The resulting model rectified the problem.

9. *Chaos theory* was introduced by Strogatz 1991 as a new approach in non-linear dynamics. Normally the circadian cycling follows 24 h limit cycle oscillations. But under some circumstances, more complex non-linear phenomena are observed at the organismic and tissue level, such as the emergence of chaos, or the splitting of oscillations with two different periods. Results of Soest et al. 2020 show that period doubling, chaos and splitting appear in different feedback models of the mammalian circadian clock without external forcing. The authors found that changes in the degradation of clock genes and proteins might alter the dynamics of the system and induce complex non-linear events.

10. *Long period rhythms* have not been discussed in the book. tidal rhythms, (lunar influence), weekly rhythms? Annual rhythms.
Prime numbers and rhythms in cicadas (13 and 17 years rhythms):

11. *Conclusion*: The area of biological oscillation is exciting, open for many new studies etc. and so on!

9.3.2.1 Perturbation of oscillators. Perturbing agents.

In several chapters we have discussed perturbations of the oscillators, demonstrated, i.e., by phase shifts of the oscillations.

One can discuss many types of perturbations. Change of environmental parameters like temperature, light, humidity etc. can per definition be regarded as perturbations of the biological oscillators. Other perturbations can be administrated to the oscillatory system, as singular treatments or repeatedly or with different shapes. However, in the literature one often uses the

concept in the more restricted meaning and specify the administered perturbation treatment as pulses, sine wave perturbations, step perturbations etc.

Such administered perturbations can reveal many important properties of the system (as we have tried to show in different chapters in this book). Phase or amplitude changes might be general key words here. To find resonances in a system one could give repeated pulse perturbations with different frequencies and record the amplitude of the system. This can reveal filter effects, time delays etc. of the system. (It can be time consuming and require a series of experiments to vary period of the pulse treatment and swept frequency techniques can in some cases provide an alternative method).

Some relevant perturbing agents are mentioned below, but a deeper discussion will be rewarding

- *Light* perturbations have often been used and discussed in the previous book chapters. They can reveal many properties of the basic oscillator – but they must be absorbed by a relevant chromophore in order to act on/in the oscillator. The absorption spectrum and photo-properties of the absorbing chromophores should not be interpreted as properties of the oscillator system itself (in humans e,g, the retinal photosensitivity is different from that of the circadian clock). Darkness could also be of interest to apply to the oscillator.

- *Temperature* perturbations (increased or decreased temperature) are often studied. But temperature is a rather unspecific parameter that is likely to affect many steps in the oscillating system, thus difficult to use for detailed mechanism studies.

- *Humidity* perturbations can be of interest, for example, in plant oscillations.

- *Electromagnetic fields* can affect biological oscillators (obviously so in the case of the heart oscillations). We have mentioned some examples in this book. Discussions of how the fields penetrate tissue and affect oscillatory reactions are certainly needed. A fairly recent paper points at the formation of chemical radical pairs could be affected by both electromagnetic fields and lithium ions, which are both known to interact with circadian clocks (see Zadeh-Haghighi, Simon 2022). It is predicted that stronger magnetic fields would shorten the clock's period.

Adding special chemical substances to the biological organism could be efficient in revealing details of the oscillatory mechanism. The mechanisms can, for example, be dependent on certain ions, and administrating a higher/lower dose/concentration can then give clues as to the oscillatory mechanism.

- *Heavy water.* Since water is involved in all biological oscillating systems, perturbation by administrating a heavy water isotope – so-called deuterium – is likely to affect the period of a biological oscillator. This has been shown in several systems – but since the heavy water has general effects, like changing diffusion processes, it might not lead to further detailed chemical knowledge about the oscillator mechanisms.

- *Lithium ions.* It turns out that the Li+ ion lengthens the period of the circadian clocks in many organisms. It should be noted that also non-circadian biological oscillators

(plant leaf movements, plant transpiration and others) have been demonstrated to have a period sensitive to lithium administration. One must discuss and consider the question if biological oscillations – circadian as well as ultradian ones – are involving the same, lithium sensitive, mechanisms?
Lithium salts are well knows in treatment of patients with certain forms of depressive disorders . Is there a causal connection between lithium effects on circadian rhythms and on depressions?

- *Different chemical agents* can influence circadian rhythms but in most cases the specific action site and mechanisms should be further studied. Melatonin (and synthetic compounds) modify clock controlled reactions. Examples of the work in this intense research field can be found in Lin et al. 2020,Zheng et al. 2021 and other reports.

9.3.2.2 Difference between a compact light pulse and one consisting of flashes of light

Fairly long duration light pulses have often been used to study, for example, phase changes of the circadian rhythms (to obtain a Phase Response Curve). A typical duration of such a compact pulse can be, say, 15 min. Several pulses of the same length are also given repetitively to study entrainment phenomena, as discussed in chapter 6.2.

When giving light pulse perturbations it is, as we have noted, important to specify the wavelength of the light, the intensity of the light, and the pulse duration. The intensity of the light (i.e. radiant flux received by a surface per unit area, W/m^2) multiplied with the pulse duration is often denoted light dose. The light used in experiments has to be absorbed by pigments, with a subsequent reaction chain to the oscillator mechanism proper. Spectral light studies, therefore, shows properties of the light perceiving system, as well as properties of the oscillators themselves.

Only in experiments involving the human visual system and its perception mechanisms one uses photometric units, among which lux is frequently used (= luminous flux incident on a surface).

The effects of several light pulses can in some cases be added up so that, for example, an exposure to a compact 30 min light pulse can be the same as the results for two subsequent individual 15 min pulses. Such experiments have been conducted and discussed e.g. in the case of the Drosophila eclosion rhythm (Pittendrigh, Minis 1972, Johnsson, Karlsson 1972, Nunes 1981 and others). Approaches have also allowed to discuss how short pulses (< 15 min) added up to produce identical phase shifts as shown by a compact pulse.

Lately it was tried, whether and how very short pulses flashes of light in the millisecond (msec) range are able to phase shift the rhythm (Kaladchibachi et al. 2019). They showed for Drosophila ananassae, that 8, 16 or 120 msec flashes shift the phase of the locomotor activity of the adult flies. The pulse irradiance and the number of stimuli given during 15 min were varied. The following physical characteristics of the flashes (blue LED) were checked:

- The spectrum,
- the intensity of the light and
- the duration of the flashes.

It was found, that the Drosophila pacemaker integrates these photonic information. Flash duration is important for the amount of phase shifts. Shorter msec pulses were more effective than longer ones (8 msec more effective than 16 and 120; but phase shift was diminished with shorter than 8 msec pulses). Apparently the pacemaker's photosensitivity is instantaneously reduced by the blue light in msec (photopigments: cryptochrome, melanopsin).

If the findings are applicable to humans, phototherapy for affective disorders or for sleep disorder and shift work might be improved.

Since rodents also respond to sequences of millisecond light flashes (Vidal, Morin 2007), it was tested whether humans respond to a sequence of 60 2 msec pulses (473 lux, produced by a tungsten lamp with a broad emission spectrum). The pulses were given once per minute over an hour (i.e., 0.12 s of light over an hour) in two sequential nights at a phase of the circadian cycle, at which a delay of the circadian rhythm occurs (Zeitzer, Ruby et al. 2011). Sleepiness, polysomnograms, and onset of melatonin secretion (via collected saliva) were measured to determine the phase delay. As a control, subjects experienced no light treatment at an earlier or later setting (randomly determined). A 45±13 min ($p<0.01$) delay of the measured items was observed, showing, that these light flashes increased subjective and objective alertness while suppressing delta and sigma activity in the EEG.

The circadian system of humans is apparently able to respond to a sequence of msec flashes of light exposures. Other studies (Chang, Santhi et al. 2011) had shown, that 1 h of LL (10 000 lux) during a similar phase produces an 82 min phase delay. Although that light was considerably brighter and continuously offered (3600 sec vs. 0.12 sec) the flashes used here resulted in 45% of the phase shift when compared with the Vidal Morin(2007) set-up (assuming roughly the same spectral composition of the white light) Vidal, Morin 2007. That is, light 30 000 times briefer and more than 20 times dimmer, led to almost half the phase shift. In another study (Zeitzer, Dijk et al. 2000), it was found that 6.5 h of light of the same intensity used here delayed the rhythm by 154 min. With the light exposure 195 000 times briefer lead to 29% of the phase change. This indicates that a sequence of light flashes is not "seen" by the circadian clock as a continuous stimulation, but as a series of discrete stimulations. This temporal integration could occur either in the ipRGC or in the SCN neurons (or in both).

10 Epilog

I keep six honest serving-men
(They taught me all I knew);
Their names are What and Why and When
And How and Where and Who.
I send them over land and sea,
I send them east and west;
But after they have worked for me,
I give them all a rest

The Elephant's Child (from "Just
So Stories", Rudyard Kipling 1912)

The reader of the present book might have been overwhelmed by the many questions that have been raised – and to a large extent even left unanswered! But the six questions in Kipling's verse – What, Why, When, How, Where and Who - might be relevant to keep in mind, not only for a newborn elephant child who should grasp and learn about all problems in the world around him/her, but also for the very interested student/reseacher who will learn about biological oscillations and how to simulate them! Please, dear reader, try to contribute to the solution of some questions in the field!

One aim of this book was not to answer all questions, but to give the reader an overview of the different rhythms found among organisms, including humans, by offering various examples and describe how they are affected by external events. Another object was to show, how important it is to model those rhythms, and to introduce the reader to a program allowing them to build and use models for biological rhythms.

The choice of the examples is given by the research experiences and preferences of the authors and is thus subjective. Some of them might therefore be quite detailed, other fields omitted or only marginally covered. But if the reader is able to reproduce the simulations, and, more important, to simulate own examples, one purpose of our book would be reached.

Many books have appeared and is continuously published on the fields of biological rhythms, signal analysis, oscillatory systems and so on – it is not possible here to try to give a complete list of references, and the libraries with good search systems should be consulted For an overview of some recent and more classical books on rhythms see Sect. 12.

We hope that it has been evident from the text that the area of biological rhythms and oscillations is exciting, important, covering many fields of both practical and theoretical interests and offering a wealth of intricate problems. The importance of the field and of circadian rhythms

has been emphasized by the Nobel Prize in Physiology or Medicine in 2017 that was given to three researchers for their work on biological clocks (see Osterkamp 2017 and Young 2018).

Those, which are not yet familiar with the broad field of chronobiology, might like to become familiar with the various groups and we recommend to have a look at the journals for publications in this area (e.g. *Chronobiology International*, *Chronobiology*, *Journal of Biological Rhythms*) and the meetings, conferences (*Gordon Research Conference on Chronobiology*), and symposia of the societies (e.g. the *European Biological Rhythm Society* EBRS, *Society for Research on Biological Rhythms*). *Research Gate* (see ResearchGate[1]) is another way to get informed by and in touch with workers in the field. For an overview of recent and more classical books on rhythms see Sect. 12.

Much of the work with this book is due to late professor Wolfgang Engelmann, Tübingen, the primus motor in creating the book. Mistakes and errors in the text which are often impossible to avoid, are however the responsibility of the two authors below.

Karl-Heinz Witte and Anders Johnsson

[1] a European commercial social network for scientists and researchers to find and share papers, ask and answer questions

What do we learn from it?

To hope for a change without doing something for it
is like staying on the railway station and waiting for a ship

Albert Einstein

There is nothing good
unless you do it

Erich Kästner

11 Acknowledgements

We would like to thank all students, colleagues and the Lyx user group who have supported us in the production of this book and especially Winfried Hellung for his critical review of the manuscript.

We would appreciate hints for mistakes, shortages, incomprehensible or mistakable in the book. Our addresses are:

Karl-Heinz Witte, Hochschule RheinMain, Fachbereich Ingenieurwissenschaften, Am Brückweg 26, 65428 Rüsselsheim, Germany, Tel. +49 (0) 6142-898-4234, E-Mail: karl-heinz.witte@hs-rm.de

Anders Johnsson, Norwegian University of Science and Technology, NTNU, Department of Physics, N-7491 Trondheim, Norway, Tel. +47 9067 2213, E-Mail: anders.cg.johnsson@gmail.com

12 Recommended further readings

Bünning E (1983) *The physiological clock*. 2nd ed. Heidelberg Science Library Springer New York

Forger DB (2017) *Biological clocks, rhythms, and oscillations - The theory of biological timekeeping*. MIT Press

Glass L, Mackey MC (1988) *From Clocks to Chaos, the Rhythms of Life*. Princeton University Press, Princeton, N. J.

Honma S (2018) The mammalian circadian system: a hierarchical multi-oscillator structure for generating circadian rhythm. *J Physiol Sci* 68: 207–218

Hoppensteadt FC (1997) *An Introduction to the Mathematics of Neurons*. Cambridge University Press, Cambridge

Hoppensteadt FC, Prescin CS (2010) *Modeling and Simulation in Medicine and the Life Sciences*.

Mieda M (2020) The central circadian clock of the suprachiasmatic nucleus as an ensemble of multiple oscillatory neurons. *Neurosci Res* 156: 24–31

Pilz LK et al. (2018) Sleep and light exposure across different levels of urbanisation in Brazilian communities. *Sci Rep* 8: 11389

Roenneberg T, Winnebeck EC, Klerman EB (2019) Daylight saving time and artificial time zones - a battle between biological and social times. *Front Physiol* 10: 944

Winfree AT (2001) *The geometry of biological time*. 2nd ed. Springer, New York

Yan L (2009) Expression of clock genes in the suprachiasmatic nucleus: effect of environmental lighting conditions. *Rev Endocr Metab Disord* 10: 301–310

Subject index

Name index

Nomenclature

Behind the normal glossary items follows abbreviation -in red- and the corresponding items, and mathematical symbols -in red- with its items

action potential occurs when the membrane potential of a cell membrane rapidly rises and falls (depolarization)

Actograms are a plot that shows rhythms in biological variables throughout the day as a function of the time of day (x-axis) and the respective day (y-axis), see e.g. on the Internet under the link https://en.wikipedia.org/wiki/Actogram

amplitude of an oscillation is a measure of its change in a single period; it is also used for the differences between the extreme values

angular frequency is a scalar measure of rotation rate. It refers to the angular displacement per unit time or the rate of change of the phase of a sinusoidal waveform (for example, in oscillations and waves)

anisomycin is an antibiotic, which interferes with the protein- and DNA synthesis. Inhibits the peptidyltransferase or the 80S ribosome system.

annual rhythm a rhythm with a period length of about a year

aorta is the main and largest artery in the human body, originating from the left ventricle of the heart and extending down to the abdomen, where it splits into two smaller arteries (the common iliac arteries). The aorta distributes oxygenated blood to all parts of the body

Aplysia californica Aplysia is a genus of medium-sized to extremely large sea slugs, specifically sea hares, which are one clade of large sea slugs, marine gastropod mollusks (Opisthobranchia).

arrhythmicity is the loss or strong damping of an oscillation

Aschoff rule the free run period in night active animals is longer in continuous light LL as it is in continuous darkness DD; in day active animals it is shorter

atrium is the upper chamber through which blood enters the ventricles of the heart. There are two atria in the human heart – the left atrium receives blood from the pulmonary (lung) circulation, and the right atrium receives blood from the venae cavae (venous circulation)

atrium is the upper chamber through which blood enters the ventricles of the heart. There are two atria in the human heart – the left atrium receives blood from the pulmonary (lung) circulation, and the right atrium receives blood from the venae cavae (venous circulation)

attractor a set of states to which a model tends toward as time increases.

axon or nerve fiber is a long, slender projection of a neuron in vertebrates that conducts electrical impulses (=action potentials) away

from the nerve cell body, thus transmitting information to other neurons, muscles, and glands

bioreactor refers to any manufactured device or system that supports a biologically active environment

block diagram is a grafical diagram of a system describing its function

BMI Body mass index is a value derived from the mass (weight in kg) and height (in metres) of a person. The body mass is divided by the square of the body height (kg/sqm)

Bonhoeffer-Van der Pol oscillator is a special case of the Van der Pol oscillator and describes the activation- and deactivation dynamic in a firing neuron

Bulla gouldiana Bulla (bubble snail) is a genus of medium to large hermaphrodite sea snails, marine opisthobranch gastropod molluscs. Suborder Cephalaspidea, headshield slugs, and order Opisthobranchia.

cellulose microfibrils are embedded in the wall matrix of plant cells and consist of hemicellulose and protopectins

characteristic curve in mathematics, used in the method of characteristics for solving partial differential equations

chronobiology (greek: chronos = time) studies the temporal organisation of physiological processes and rhythmic patterns of behaviour in organisms

chrononutrition combines the results of nutritional research with chronobiology

circumnutation circular movements often exhibited by the tips of growing plant stems, caused by repeating cycles of differences in growth around the sides of the elongating stem

coefficient changes with time

coefficient matrix helps to treat linear equation systems. All coefficients are combined in a matrix

compressor is a mechanical device that increases the pressure of a gas by reducing its volume, e.g. in refrigerators

conidia are spores of fungi, which are asexually formed in the conidiophores. In higher fungi (Asco- and Basidiomycetae) for asexual propagation

continuous darkness DD conventional notation for an environment maintained in continuous darkness, i.e. dark-dark conditions without light exposure

contour lines are best known as level curves in maps. Here lines of identical > phase shifts, which result from pulses of different length (x-axis) and at different timing (y-axis)

cooperative dynamics xx

coordinate sytem serves to define unambiguously the position of points and objects in a geometric space

cosine is a trigonometric function

coupling matrix helps to understand the coupling mechanism between the components of a system. It consists of rows and columns, and in their intersection the kind of influence is shown

CRISPR/Cas9 technology clustered regularly interspaced short palindromic repeats/CRISPR associated nucleases system was originally discovered to be an acquired immune response mechanism used by archaea and bacteria. It has since been adopted for use as a tool in the genetic engineering of higher organisms

critical phase if a pulse of light, temperature, chemical, or an electrical current etc is applied at a certain phase of the oscillation, the rhythm disappears if the strength of the pulse is appropriate

cuticle = pupal case, covers an insect during its >metamorphosis from the last larval stage to the adult (imago)

cyanobacteria or cyanophyta, blue-green algae, belonging to the prokaryots. A phylum of bacteria that obtain energy via photosynthesis

depolarisation is the change of the membrane potential towards more positiv (= less negativ) values

depolarisation is the change of the membrane potential towards more positiv (= less negativ) values

dormancy is a period in an organism's life cycle when growth, development, and (in animals) physical activity are temporarily stopped

e-function or exponential function is important to describe growth processes (e.g. exponential growth)

ECG or electrocardiogram is the recording of the sum of the electrical activities of all heart muscle fibers

efferent conveying away from a center, e.g. neuronal signals from the brain to other parts

entrainment Body mass index is a value derived from the mass (weight in kg) and height (in metres) of a person. The body mass is divided by the square of the body height (kg/sqm)

entrainment range or range of entrainment: a circadian rhythm can be locked to a non-24-h zeitgeber cycle (e.g., light-dark cycles, temperature cycles or cycling social cues), but only within given limits

enzymes are proteins that act as biological catalysts (biocatalysts). Catalysts accelerate chemical reactions

equation, algebraic in a wider sense: in contrast to differential equations. In a more specific sense: An equation in the form of Pn(x)=0 (polynomial)

feedback is a connection, a loop, between the cause and effect of a process

Fourier row (after Joseph Fourier) is the series expansion of a periodic, sectionwise static function in a function series of sinus- and cosinus functions

frequency range of a system is the range over which it is considered to provide satisfactory performance, such as a useful level of signal with acceptable distortion characteristics

functional block describes the functions and interrelationships of a block diagram system

functional diagram allows a simple grafic presentation of the sequential control

functional equation describes the assignement between the domain of definition and the domain of the values, in which the unknown represents a function. The term functional equation usually refers to equations that cannot be simply reduced to algebraic equations or differential equations

ganglion (plural ganglia) are the accumulated neural cell bodies in the peripheral nervous system. In lower animals the central nervous system consists of differenciated larger ganglia

ganglion (plural ganglia) are the accumulated neural cell bodies in the peripheral nervous system. In lower animals the central nervous system consists of differenciated larger ganglia

genotype-phenotype distinction is drawn in genetics; genotype is an organism's full hereditary information, phenotype is an organism's actual observed properties, such as morphology, development, or behavior

giant axon in squids are 100 to 1000 times thicker as in mammals (up to 1 mm diameter), allows a fast synaptic efficacy

Gleichanteile is the constant portion in a signal; not necessarily the mean value

Goldbeter, Albert a Belgian theoretical biologist, professor and leader of the research group theoretical chronobiology at the Free Universityt Brussels. He developed mathematical models for various periodical biological systems

Goodwin, Brian Carey was a Canadian mathematician and biologist at the open University. Founder of theoretical biology and biomathematics. He introduced complex systems and generative models in the evolutionary biology

gravitropism or geotropism is a coordinated process of differential growth by a plant in response to gravity

guard cells form the stomate of plants, which are pores for exchanging gas with the surrounding

harmonic is an oscillation, the frequency of which is a whole-number multiple of a basic frequency

heliotropism a form of tropism. Diurnal or seasonal motion of plant parts (flowers or leaves) in response to the direction of the sun

high pass filter passes frequencies above the cut-off frequency almost unweakened and damps lower frequencies

Hill function a Belgian theoretical biologist, professor and leader of the research group theoretical chronobiology at the Free University in Brussels. He developed mathematical models for various periodical biological systems

His bundle are special heart muscle cells, which transfer electric impulses from the atrioventricular nodes to the Purkinje fibers

Hodgkin and Huxley described experiments for the ion movements in a neuron during an action potential and formed from the Informations a mathematical model.\{}\{}Sir Andrew Fielding Huxley, born November 22, 1917, English physiologist and biophysisist. Fellow of the Royal Society of London. 1963 Nobel price together with Hodgkin and Eccles

homology is similarity due to shared ancestry between a pair of structures or genes in different taxa (e.g. the forelimbs of vertebrates, where the wings of bats and birds, the arms of primates, the front flippers of whales and the forelegs of four-legged vertebrates like dogs and crocodiles are all derived from the same ancestral tetrapod structure)

hyperpolarisation is the change of the membrane potential towards more positiv (= less negativ) values

hypocotyl is the stem of a germinating seedling, found below the cotyledons

integrator is an element, the outgoing signal of which is the time integral of the input signal

lateral leaflet the lateral leaf-like part of a compound leaf

Lewis Robert Lewis, zoologist at the University of Auckland, New Zealand. Circadian rhythms in insects, models

limit cycle a cycle which nearby trajectories spiral toward or away from

linearising The result of a network analysis could be a nonlinear equation system. Under certain conditions it can be transferred to a linear system. Linearising in a working point is the simplest method for it

Lingulodinium polyedra belongs to the genus of dinoflagellates (family Gonyaulacaceae). The genus has cosmopolitan distribution

luciferase is an oxidative enzyme that produce bioluminescence. Luciferin is the substrate. Luciferases are widely used in biotechnology, e.g. as reporter genes

matrix is a rectangular array or table of numbers, symbols, or expressions, arranged in rows and columns. One application of matrices is for instance to represent linear transformations (that is, generalizations of linear functions such as f(x) = 4x)

matrix, cyclic their rows and columns fullfill a certain permutation condition; connected with discret fast Fourier transformation

membrane potential is the difference in electric potential between the interior and the exterior of a biological cell

mercury column blood pressure is usually measured in mm Hg; legal measure in the EU

metabolism is the entity of the chemical processes in organisms

metamorphosis is a form of holometabolic insect development which includes four life stages: egg, larva, pupa and imago (=adult)

molecular biology deals with the structure, biosynthesis, and function of DNA and RNA at the molecular level, and their interaction with proteins. Overlaps with further fields of biology and chemistry such as genetics and biochemistry

natural frequncy of an oscillating system is the frequency, at which the system oscillates after a single excitation

natural frequncy of an oscillating system is the frequency, at which the system oscillates after a single excitation

net, linear is a network in which the current or voltage in any element that results from two sources of energy acting together is equal to the sum of the currents or voltages that result from each of the sources acting alone.

net, nonlinear is a network in which the current or voltage in any element that results from two sources of energy acting together is not equal to the sum of the currents or voltages that result from each of the sources acting alone.

network is a system, the structure of which can be mathematically modelled as a graph. A graph consists of elements (>nodes), which are connected with each other via edges

network element a limitable functional unit in a network with at least one input and output

neuropil is a neuronal network system forming in invertebrates the central part of the ganglia

Neurospora crassa a fungus belonging to the Ascomycetae (=sac fungi)

nodes are a batch of elements (=nodes), which are connected with each other in functional circuit (>network)

pacemaker normally pacemaker of the heart, but also used as a synonym for oscillator

pacemaker normally pacemaker of the heart, but also used as a synonym for oscillator

pharmacology is concerned with the study of drug or medication action

phase the instantaneous state of an oscillation relative to a reference point within a cycle

phase-response curve a plot of the effect of a stimulus such as light exposure or pharmacological treatment, as a function of when the stimulus is applied > PRC

photoperiodism is the physiological reaction of organisms to the length of a night or a dark period.

photoreceptor specialised light sensitive sensory cell of eyes, but also pigments in organisms such as phototropines, phytochromes and cryptochromes

phototaxis is the directed reaction of organisms to light (positiv: in direction of higher, negative: in direction of lower illumination values)

plaster epithelium at the upper side of the petals of plants with papilla like cells

prokaryot is a cellular organism that lacks a nucleus. In the three-domain system, based upon molecular analysis, prokaryotes are divided into two domains: Bacteria (formerly Eubacteria) and Archaea (formerly Archaebacteria).

promoter is a sequence of DNA to which proteins bind that initiate transcription of a single RNA from the DNA downstream of it. This RNA may encode a protein, or can have a function in itself. Promoters are located near the transcription start sites of genes

pseudopodium is a temporary arm-like projection of a eukaryotic cell membrane that are developed in the direction of movement. Filled with cytoplasm, pseudopodia primarily consist of actin filaments and may also contain microtubules and intermediate filaments; used for motility and ingestion. Often found in amoeba

pulvinus is a joint-like thickening at the base of a plant leaf or leaflet that allows growth-independent movement. Common in members of the bean family Fabaceae

puparium =pupal case, covers an insect during its >metamorphosis from the last larval stage to the adult (imago)

Purkinje fibers excitations are passed from the AV-node to the His-bundle and further to the Purkinje fibers at the top of the heart. They are connected with the muscle fibers of the heart

Purkinje fibers excitations are passed from the AV-node to the His-bundle and further to the Purkinje fibers at the top of the heart. They are connected with the muscle fibers of the heart

quinine acid is an alcaloid from the chinchona bark. Medication against malaria

radiofrequency is the oscillation rate of radio frequency electromagnetic waves (radio waves) between 3 and 30 megahertz (MHz)

reaction kinetic desribes the course of chemical reactions

reentrainment or re-entrainment is the entrainment after it was lost. Same as resynchronisation

refractory period or exponent of a dynamical system is a quantity that characterises the rate of separation of infinitesimally close trajectories

repolarisation is the change of the membrane potential towards more positiv (= less negativ) values

repolarisation is the change of the membrane potential towards more positiv (= less negativ) values

resonance frequency is the frequency, at which the amplitude of an oscillating system is largest as compared with neighboring frequencies

resting potential or resting membrane potential, as opposed to action potential, can be defined as a relatively stable, ground value of transmembrane voltage in animal and plant cells

resynchronisation a second or subsequent synchronisation to a new time cue, e.g. after a time zone flight

retina the neuronal tissue of the interior of eyes of vertebrates, some squids, and snails

rhizopods belong to the protista and are naked or testate amoeba, some slime molds, foraminiferae. Characterised by pseudopodia used for feeding and locomotion

Saunders David Saunders, zoologist in Edinburgh, photoperiodism and circadian rhythms in insects

Scilab/xcos comprehensive and powerful program for usage in numeric mathematics and for simulation of dynamic systems. It was developed at the Institut National de Recherche en Informatique et en Automatique (INRIA) in France since 1990 and in 2003 taken over by the Scilab Consortium. In July 2008 the Scilab Consortium united with the Digiteo Foundation; since July 2012 the edition and development is in the hands of Scilab Enterprises.

self excited for oscillators: the system begins to (re)oscillate even without external influences

singular state or > singularity

singularity or singular point is a point at which a given mathematical object is not defined, or a point where the mathematical object ceases to be well-behaved in some particular way, such as by lacking differentiability or analyticity

sinus node is the primary electric pacemaker of the heart action. Positioned in the right atrium close to the orifice of the upper vena cava and part of the excitation system

sinus node is the primary electric pacemaker of the heart action. Positioned in the right atrium close to the orifice of the upper vena cava and part of the excitation system

sinus-bradia denotes a heart beat below 60 beats per minute in an adult person

state variable is one of the set of variables that are used to describe the mathematical 'state' of a dynamical system

stimulus processor device to handle stimuli

subjective day time the section under >freerun conditions, at which normaly day (i.e. light) prevails

superblock combines certain parts of a >block diagram, so that it is better arranged

superposition principle is the superposition of the same physical variable, whereby they do not obstruct each other. Used in linear problems in many fields in physics

synchronisation is the coordination of events, clocks and time cues to operate a system in unison. The events can occur at the same time (synchronously) or in a certain series

synchronisation is the coordination of events, clocks and time cues to operate a system in unison. The events can occur at the same time (synchronously) or in a certain series

system parameter changes with time

systole is the part of the cardiac cycle during which some chambers of the heart muscle contract after refilling with blood

tachycardia denotes a heart beat below 60 beats per minute in an adult person

time domain refers to the analysis of mathematical functions, physical signals or time series of economic or environmental data, with respect to time

transfer function also known as system function or network function of a control system component is a mathematical function which models the output for each possible input. In its simplest form, this function is a two-dimensional graph of an independent scalar input versus the dependent scalar output, called a transfer curve or characteristic curve. Transfer functions are used to design and analyse systems assembled from components, particularly using the block diagram technique in electronics and control theory

ventricle is one of two large chambers toward the bottom of the heart that collect and expel blood received from an atrium towards the peripheral beds within the body and lungs

ventricle is one of two large chambers toward the bottom of the heart that collect and expel blood received from an atrium towards the peripheral beds within the body and lungs

Wever, Rütger physisist at the Max-Planck-Institute for behavioural physiology in Andechs, Germany. Coworker of Aschoff and Gwinner. Research on circadian rhythms of humans and animals in a subterranean bunker since the early 1960th

xenobiotic A xenobiotic is a chemical substance found within an organism that is not naturally produced or expected to be present within the organism

Zeitgeber or time cue, timer, synchronises an oscillation

Zeitgeber time (ZT) or timer time is a unit of time based on the period of a zeitgeber, such as the 12:12LD cycle. In free-running, constant conditions, the onset of activity of day-active organisms is circadian time zero (CT0) and the onset of activity of night-active organisms is CT12. In an LD cycle, for diurnal organisms ZT0 (lights on) is the time of activity onset and ZT12 (lights off) defines activity onset for nocturnal animals.

ABBREVIATIONS

a.o. among others

ATP adenosine triphosphate provides energy to drive many processes in living cells, often referred to as the 'molecular unit of currency' of intracellular energy transfer

ATPase adenosine triphosphatase, are a class of enzymes that catalyze the decomposition of ATP into ADP and a free phosphate ion

BRN basic retinular neuron in the eye of marine snails such as Aplysia or Bulla

CAP compound action potential recordable from the eye nerve of marine snails

CET Central European Time is a standard time which is 1 hour ahead of Coordinated Universal Time (UTC). It is used in most parts of Europe and in a few North African countries. CET is also known as Middle European Time (MET, German: MEZ) and by colloquial names such as Berlin Time, Warsaw Time, Paris Time, and Rome Time

chr is the gene for coding the chron protein

CO_2 carbon dioxid

DD continuous darkness

ELF4 is the gene for coding the chron protein

FRQ protein of the gene frq, frequency

frq is the gene for coding the FRQ protein

h hour

ipRGC intrinsically photosensitive retinal ganglion cells), also called photosensitive retinal ganglion cells, or melanopsin-containing retinal ganglion cells, are a type of neuron in the retina of the mammalian eye

KaiC is a gene belonging to the KaiABC gene cluster (with KaiA, and KaiB) that, together, regulate bacterial circadian rhythms, specifically in cyanobacteria

km kilometer

LD light-dark changes, e.g. an LD 12:12 means 12h L and 12hD follow each other

LP light pulse applied for a short time to influence a system. The term impulse is used in technic (and occassionaly also here in the book)

LUX is a gene that codes for LUX ARRHYTHMO, a protein necessary for circadian rhythms in Arabidopsis thaliana; associates with Early Flowering 3 (ELF3) and Early Flowering 4 (ELF4) to form the Evening Complex (EC), a core component of the Arabidopsis repressilator model of the plant circadian clock. The LUX protein functions as a transcription factor that negatively regulates Pseudo-Response Regulator 9 (PRR9), a core gene of the Midday Complex, another component

lux (symbol: lx) is the SI derived unit of illuminance, measuring luminous flux per unit area. It is equal to one lumen per square metre. Measure of the intensity, as perceived by the human eye. It is analogous to the radiometric unit watt per square metre, but with the power at each wavelength weighted , a standardised model of human visual brightness perception

mm millimeter

mRNA messenger ribonucleic acid. Agenome is transcribed to produce various RNAs, which are necessary for the function of the organism. Precursor mRNA is transcribed by RNA polymerase II in the nucleus, then processed by splicing to remove introns, leaving the exons in the mature mRNA, which may then be transported to the cytosol and translated by the ribosome into a protein

MUX this block merges inputs in an single output vector. Input and Output port sizes are determined by the context.

nM nanoMol

NS This index is to weight harmonics (m > q). If the time series of gene activity simply has a sinusoidal waveform, NS=1. When a time series is nonsinusoidal in shape, NS=2 (in the figure below NS=2)

PER mutation PERIODE, gene is per

PRR Pseudo-Response Regulator is a core gene of the Midday Complex, another component of the Arabidopsis repressilator model

PTO is casein kinase 1 belonging to a family of protein kinases. Serine/threonine selective enzymes which regulate signal transduction pathways in most eukaryotic cell types. CK1 isoforms are involved in circadian rhythms, nucleo-cytoplasmic shuttling of transcription factors, DNA repair, and DNA transcription

Q10 Q_{10} is a measure of how a reaction rate changes with increasing temperature. It is the ratio of the reaction rate when the temperature is increased by 10°C to the original rate

RBC red blood cell

SA sinus node of the heart

SA sinus node of the heart

SCN suprachiasmatic nucleus or nuclei is a tiny region of the brain in the hypothalamus, situated directly above the optic chiasm; responsible for controlling circadian rhythms at many different body sites. It contains several cell types and several different peptides (including vasopressin and vasoactive intestinal peptide) and neurotransmitters

sec second

TIM protein associated with the Arabidopsis clock

TTFL transcription-translation feedback loop

Bibliography

Aanes G (2011) "Modelling of oscillative, rotational plant movements" MA thesis Norwegian University of Science and Technology

Abbott SM, Reid KJ, Zee PC (2015) Circadian rhythm sleep-wake disorders. *Psychiatr Clin North Am* 38: 805–823

Abraham U et al. (2010) Coupling governs entrainment range of circadian clocks. *Mol Syst Biol* 6: 438

Ackermann J (1972) Der Entwurf linearer Regelungssysteme im Zustandsraum. *Oberpfaffenhofen*:

Ackermann J (2012) *Abtastregelung*.

Ahmad Taher Azar SV (2015) *Chaos Modeling and Control Systems Design*.

Akman OE et al. (2008) Isoform switching facilitates period control in the *Neurospora crassa* circadian clock. *Mol Syst Biol* 4: 164

Allen GJ et al. (2001) A defined range of guard cell calcium oscillation parameters encodes stomatal movements. *Nature* 411: 10053–1057

An Z et al. (2021) A two-step model of human entrainment: a quantitative study of circadian period and phase of entrainment. *Bull Math Biol* 83: 12

Angelousi A et al. (2019) Clock genes and cancer development in particular in endocrine tissues. *Endocr-relat Cancer* 26: R305–R317

Aoki T et al. (2020) The relationship between sleep habits, lifestyle factors, and achieving guideline-recommended physical activity levels in ten-to-fourteen-year-old Japanese children: A cross-sectional study. *PloS One* 15: e0242517

Arendt J (2018) Approaches to the pharmacological management of jet lag. *Drugs* 78: 1419–1431

Arnold V (1961) Small denominators in mappings of the circumference onto itself. *Izv Akad Nauk SSSR Ser Mat*:

Aronson BD et al. (1994) Negative feedback defining a circadian clock: autoregulation of the clock gene frequency. *Science* 263: 1578–1584

Aschoff J (1981) Biologische Uhren. *Giessener Universitätsblätter* 9: 9–20

Asgari-Targhi A, Klerman EB (2019) Mathematical modeling of circadian rhythms. *Wiley Interdiscip Rev Syst Biol Med* 11 (2): e1439

Ashok Kumar PV et al. (2019) It's about time: advances in understanding the circadian regulation of DNA damage and repair in carcinogenesis and cancer treatment outcomes. *Yale J Biol Med* 92: 305–316

Åström, Wittenmark (2013) *Computer-controlled systems*.

Avello P, Davis SJ, Pitchford JW (2021) Temperature robustness in *Arabidopsis* circadian clock models is facilitated by repressive interactions, autoregulation, and three-node feedbacks. *J Theor Biol* 509: 110495

Avello PA, Davis SJ, Ronald J et al. (2019) Heat the clock: entrainment and compensation in *Arabidopsis* circadian rhythms. *J Circadian Rhythms* 17: 5

Bae S-A et al. (2019) At the interface of lifestyle, behavior, and circadian rhythms: metabolic implications. *Front Nutrition* 6: 132

Baker CL, Loros JJ, Dunlap JC (2012) The circadian clock of *Neurospora crassa. FEMS Microbiol Rev* 36: 95–110

Barclay JL et al. (2012) Circadian desynchrony promotes metabolic disruption in a mouse model of shiftwork. *PLoS One* 7: e37150

Bardal TK, Johnsson A, Chapman DK (2003) Short-period circumnutations found in sunflower hypocotyls in satellite orbit. A reappraisal of data from spacelab-1. *J Gravit Physiol* 10: 1–10

Bardal Tea (2002) Stability of the steady state for a realisation of the Goodwin oscillator using linear analysis. *Dept of Physcis NTNU*:

Bardal T, Johnsson A (2001) Stability of the fixed point for a realisation of the Goodwin oscillator. Project draft. *Dept of Physics. NTNU*:

Baron KG et al. (2017) Circadian timing and alignment in healthy adults: associations with BMI, body fat, caloric intake and physical activity. *Int J Obes* 41: 203–209

Basnet S et al. (2017) Associations of common noncommunicable medical conditions and chronic diseases with chronotype in a population-based health examination study. *Chronobiol Int* 34: 462–470

Beale AD et al. (2019) Casein kinase 1 underlies temperature compensation of circadian rhythms in human red blood cells. *J Biol Rhythms* 34: 144–153

Beer CB et al. (2010) Terrestrial gross carbondioxide uptake:global distribution and covariation with climate. *Science* 329: 834–838

Beersma DGM (2005) Why and how do we model circadian rhythms? *J Biol Rhythms* 20: 304–313

Benson JA, Jacklet JW (1977) Circadian rhythm of output from neurones in the eye of Aplysia. IV. A model of the clock: Differential sensitivity to light and low temperature pulses. *J Exp Biol* 70: 195–211

Bergman O, Johnsson A, Karlsson HG (1973) Models in circadian rhythms and rhythmic phenomena in high northern latitudes. *Ber ökol Station Messaure*:

Bernhard S. BA, K.-H. W (2022) *Biosignal Processing*.

Best R (2003) *Phase-locked Loops*. Mc McGraw Hill London

Bhadra U Thakkar N DP, MP B (2017) Evolution of circadian rhythms: from bacteria to human. *Sleep Med.*:

Bick C et al. (2020) Understanding the dynamics of biological and neural oscillator networks through exact mean-field reductions: a review. *J Math Neurosci* 10: 9

Bin YS, Postnova S, Cistulli PA (2019) What works for jetlag? A systematic review of non-pharmacological interventions. *Sleep Med Rev* 43: 47–59

Bittman EL (Apr. 2021) Entrainment is NOT synchronization: an important distinction and its implications. *J Biol Rhythms* 36 (2): 196–199 ISSN: 1552-4531

Bjorvatn B, Pallesen S (2009) A practical approach to circadian rhythm sleep disorders. *Sleep Med Rev* 13: 47–60

Block GD et al. (1984) Cellular analysis of the Bulla ocular circadian pacemaker system: I. A model for retinal organization. *J Comp Physiol A* 155: 365–378

Bodenstein C, Heiland I, Schuster S (2012) Temperature compensation and entrainment in circadian rhythms. *Phys Biol* 9: 036011

Borbely AA et al. (2016) The two-process model of sleep regulation: a reappraisal. *J Sleep Res* 25: 131–143
Bradshaw WE, Holzapfel CM (1990) "Evolution of phenology and demography in the pitcher-plant mosquito, *Wyeomyia smithii*" *Insect Life Cycles* Springer, London
Brainard GC, Hanifin JP (2005) Photons, clocks, and consciousness. *J Biol Rhythms* 20 Grant numbers: NASA NSBRI NCC 9-58.: 314–325
Brogårdh T, Johnsson A (1973) A flexible apparatus for continuous recording of water uptake by plants. *Med Biol Engng* 11: 286–292
Brown JP, Martin D et al. (2020) Mental health consequences of shift work: an updated review. *Curr Psychiatry Rep* 22: 7
Brown LS, Doyle FJ (Nov. 2020) A dual-feedback loop model of the mammalian circadian clock for multi-input control of circadian phase. *PLoS Comput Biol* 16 (11): e1008459 ISSN: 1553-7358
Brum MCB et al. (2020) Night shift work, short sleep and obesity. *Diabetol Metab Syndr* 12: 13
Bünning E (1936) Die endonome Tagesrhythmik als Grundlage der photoperiodischen Reaktion. *Ber Deutsch Bot Ges* 54: 590–607
Burgoyne RD (1978) A model for the molecular basis of circadian rhythm involving monovalent ion-mediated translational control. *FEBS Lett* 94: 17–19
Burman D (2017) Sleep disorders: circadian rhythm sleep-wake disorders. *FP Essentials* 460: 33–36
Cajochen C (2005) Sleep disruption in shift work and jet lag: the role of the circadian timing system. *Praxis (Bern 1994)* 94: 1479–1483
Campbell SL, Chancelier J-P, Nikoukhah R (2006) *Modeling and simulation in Scilab/Scicos*. Springer Science and Business Media, Inc.
Cardon JH et al. (2018) Interacting circadian and homeostatic processes with opportunity cost: A mathematical model of sleep with application to two mammalian species. *PloS One* 13: e0208043
Chance B, Pye K, Higgins J (1967) Waveform generation by enzymatic oscillators. *IEEE Spectrum* 4: 79–86
Chang A, Santhi N et al. (2011) Duration response curve to bright light in humans. *Sleep* 34: A162
Chang A-M, Duffy JF et al. (2019) Chronotype genetic variant in PER2 is associated with intrinsic circadian period in humans. *Sci Rep* 9: 5350
Chaput J-P et al. (2020) Sleep timing, sleep consistency, and health in adults: a systematic review. *Appl Physiol Nutr Metab* 45 (Suppl. 2): S232–S247
Chellappa SL (2020) Circadian misalignment: A biological basis for mood vulnerability in shift work. *Eur J Neurosci* 52: 3846–3850
Christensen ND, Lewis RD (1982) The circadian locomotor rhythm of *Hemideina thoracica* (Orthoptera; Stenopelmatidae): The circadian clock as a population of interacting oscillators. *Physiol Entomol* 7: 1–1–13
– (1983) The circadian locomotor rhythm of *Hemideina thoracica* (Orthoptera; Stenopelmatidae): a population of weakly coupled feedback oscillators as a model of the underlying pacemaker. *Biol Cybern* 47: 165–172
Cingi C, Emre IE, Muluk NB (2018) Jetlag related sleep problems and their management: A review. *Travel Med Infect Dis* 24: 59–64 ISSN: 1873-0442

Cockrell AL et al. (2015) Suppressing the *Neurospora crassa* circadian clock while maintaining light responsiveness in continuous stirred tank reactors. *Sci Rep* 5: 10691

Colwell CS, Khalsa SB, Block GD (1992) Cellular mechanisms of entrainment. *Chronobiol Int* 9: 163–179

Conrad ED (1999) "Mathematical models of biochemical oscillations" MA thesis Virginia Polytechnic Institute and State University URL: URI%20http://hdl.handle.net/10919/32781

Corrent G, Eskin A, Kay I (1982) Entrainment of the circadian rhythm from the eye of *Aplysia*: role of serotonin. *Am J Physiol* 242: R326–R332

Cowan IR (1972) Oscillations in stomatal conductance and plant functioning associated with stomatal conductance: observations and a model. *Planta* 106: 185–219

Crosthwaite SK, Dunlap JC, Loros JJ (1997) Neurospora wc-1 and wc-2: Transciption, photoresponses, and the origin of the circadian rhythmicity. *Science* 276: 763–769

Crowley SJ, Eastman CI (2015) Phase advancing human circadian rhythms with morning bright light, afternoon melatonin, and gradually shifted sleep: can we reduce morning bright-light duration? *Sleep Med* 16: 288–297

– (2017) Human adolescent phase response curves to bright white light. *J Biol Rhythms* 32: 334–344

– (2018) Free-running circadian period in adolescents and adults. *J Sleep Res* 27: e12678

Crowley SJ, Fournier CL, Eastman CI (2018) Late bedtimes prevent circadian phase advances to morning bright light in adolescents. *Chronobiol Int* 35: 1748–1752

Czeisler CA (1995) The effect of light on the human circadian pacemaker. *Ciba Found Symp* 183: 254–290 ISSN: 0300-5208

Czeisler CA, Dijk DJ (1995) Use of bright light to treat maladaptation to night shift work and circadian rhythm sleep disorders. *J Sleep Res* 4: 70–73

Czeisler CA, Duffy JF et al. (1999) Stability, precision, and near-24-hour period of the human circadian pacemaker. *Science* 284: 2177–2181

Czeisler CA, Moore-Ede MC, Coleman RH (1982) Rotating shift work schedules that disrupt sleep are improved by applying circadian principles. *Science* 217: 460–463

Daan S, Beersma DG, Borbely AA (1984) Timing of human sleep: recovery process gated by a circadian pacemaker. *Am J Physiol* 246: 161–183

Daan S, Beersma DGM (1984) "Circadian gating of human sleep-wake cycles" *Mathematical models of the circadian sleep-wake cycle* ed. by MC Moore-Ede, CA Czeisler Raven Press, New York

Darwent D, Dawson D, Roach GD (2012) A model of shiftworker sleep/wake behaviour. *Accid Anal Prev* 45 Suppl: 6–10

Darwin CR, Darwin F (1880) *The power of movement in plants*. Murray London

Davis K et al. (2019) The tumour suppressing role of the circadian clock. *IUMBM Life* 71: 771–780

Degn H (1972) Oscillating chemical reactions in homogeneous phase. *J Chem Educ* 49: 302–307

Delwiche MJ, Cooke JR (1977) An analytical model of the hydraulic aspects of stomatal dynamics. *J Theor Biol* 69: 113–141

Deng F, Yang K (2019) Current status of research on the period family of clock genes in the occurrence and development of cancer. *J Cancer* 10: 1117–1123

Deng N, Kohn TP et al. (2018) The relationship between shift work and men's health. *Sexual Med Rev* 6: 446–456

Devlin PF (2002) Signs of the time: environmental input to the circadian clock. *J Exp Bot* 53: 1535–1550
Di Stefano A et al. (2019) Social dynamics modeling of chrono-nutrition. *Plos Comput Biol* 15: e1006714
Diekman CO, Bose A (2018) Reentrainment of the circadian pacemaker during jet lag: East-west asymmetry and the effects of north-south travel. *J Theor Biol* 437: 261–285
Dixon LE et al. (2014) Light and circadian regulation of clock components aids flexible responses to environmental signals. *New Phytol* 203: 568–577
Dodson ER, Zee PC (2010) Therapeutics for circadian rhythm sleep disorders. *Sleep Med Clin* 5: 701–715
Doyle S, Menaker M (2007) Circadian photoreception in vertebrates. *Cold Spring Harb Symp Quant Biol* 72: 499–508
Dubowy C, Sehgal A (2017) Circadian rhythms and sleep in *Drosophila melanogaster. Genetics* 205: 1373–1397
Duffy JF, Czeisler CA (2009) Effect of light on human circadian physiology. *Sleep Med Clin* 4 (2): 165–177
Duffy JF, Wright KP (2005) Entrainment of the human circadian system by light. *J Biol Rhythms* 20: 326–338
Dunlap J, Feldman J (1988) On the role of protein synthesis in the circadian clock of *Neurospora crassa. Proc Natl Acad Sci U S A* 85: 1096–1108
Duysens LN, Amesz J (1957) Fluorescence spectrophotometry of reduced phosphopyridine nucleotide in intact cells in the near-ultraviolet and visible region. *Biochim Biophys Acta* 24: 19–26
Edmunds LN (1988) *Cellular and molecular bases of biological clocks. Models and mechanisms for circadian timekeeping*. Springer
Eelderink-Chen Z et al. (2021) A circadian clock in a nonphotosynthetic prokaryote. *Sci Adv* 7: 2086
El Moussaouiti R et al. (2010) Phase and period responses of the jerboa *Jaculus orientalis* to short light pulses. *Chronobiol Int* 27: 1348–1364
Ellingsrud S, Johnsson A (1993) Perturbations of plant leaflet rhythms caused by electromagnetic radio-frequency radiation. *Bioelectromagnetics* 14: 257–271
Engelmann W, Schrempf M (1979) Membrane models for circadian rhythms. *J. Photochem. Photobiol. C: Photochem. Rev.* 5: 49–86
Engelmann W, Witte K-H (2016) *Wie man eine biologische Uhr stoppen kann: Singularitätspunkt.* http://nbn-resolving.de/urn:nbn:de:bsz:21-dspace-677983, Universität Tübingen
Engelmann W. JA (1978) Attenuation of the petal movement rhythm in Kalanchoe with light pulses. *Physiol. Plantarum*:
Erren TC, Lewis P (2019) Hypothesis: ubiquitous circadian disruption can cause cancer. *Eur J Epidemiol* 34: 1–4
Erzberger A et al. (2013) Genetic redundancy strengthens the circadian clock leading to a narrow entrainment range. *J R Soc Interface* 10: 20130221
Evans WR (1950) Control system synthesis by root locus method. *Trans Am Inst Electr Eng* 69: 66–69

Fahey CD, Zee PC (2006) Circadian rhythm sleep disorders and phototherapy. *Psychiatr Clin North Am* 229: 989–1007

Figueiro MG, Rea MS (2010) Lack of short-wavelength light during the school day delays dim light melatonin onset (DLMO) in middle school students. *Neuro Endocrinol Lett* 31: 92–96

Fischer D et al. (2020) Irregular sleep and event schedules are associated with poorer self-reported well-being in US college students. *Sleep* 43:

FitzHugh R (1961) Impulses and physiological states in theoretical models of nerve membrane. *Biophys J* 1: 445–466

Forger DB (2017) *Biological clocks, rhythms, and oscillations - The theory of biological timekeeping*. MIT Press

Forger DB, Jewett ME, Kronauer RE (1999) A simpler model of the human circadian pacemaker. *J Biol Rhythms* 14: 532–537

Forger DB, Peskin CS (2003) A detailed predictive model of the mammalian circadian clock. *Proc Natl Acad Sci U S A* 100: 14806–14811

Förster C, Engelmann W (1988) *Thalassomyxa australis* rhythmicity III. Entrainment by combination of different Zeitgeber. *J Interdisc Cycle Res* 19: 275–288

Foster RG, Argamaso S et al. (1993) Photoreceptors regulating circadian behavior: A mouse model. *J Biol Rhythms Suppl* 8: S17–S23

Foster RG, Hughes S, Peirson SN (2020) Circadian photoentrainment in mice and humans. *Biology* 9: 2079–7737

Francois P, Despierre N, Siggia ED (2012) Adaptive temperature compensation in circadian oscillations. *PLoS Comput Biol* 8: e1002585

Fritschi L et al. (2018) Shift work that involves circadian disruption and breast cancer: a first application of chronobiological theory and the consequent challenges. *Occup Environ Med* 75: 231–234

Fustin J-M et al. (2013) RNA-methylation-dependent RNA processing controls the speed of the circadian clock. *Cell* 155: 793–806

Gander PH (1976) "A model for the circadian pacemaker of *Hemideina thoracica* derived from the effects of temperature on its activity rhythm" PhD thesis Auckland University, New Zealand

Gander PH, Kronauer RE, Graeber RC (1985) Phase shifting two coupled circadian pacemakers: implications for jet lag. *Am J Physiol* 249: R704–R719

Gander PH, Lewis RD (1979) The circadian locomotor activity rhythm of Hemideina thoracica (Orthoptera): a feedback model for the underlying clock oscillator. *Int J Chronobiol* 6: 263–280

Gandhi AV et al. (2015) Melatonin is required for the circadian regulation of sleep. *Neuron* 85: 1193–1199

Geerdink M et al. (2016) Short blue light pulses (30 min) in the morning support a sleep-advancing protocol in a home setting. *J Biol Rhythms* 31: 483–497

Gérard C, Gonze D, Goldbeter A (2009) Dependence of the period on the rate of protein degradation in minimal models for circadian oscillations. *Philos Trans R Soc Lond A* 367: 4665–4683

Gibo S, Kurosawa G (2019) Non-sinusoidal waveform in temperature-compensated circadian oscillations. *Biophys J* 116: 741–751

– (2020) Theoretical study on the regulation of circadian rhythms by RNA methylation. *J Theor Biol* 490: 110140

Giuntella O, Mazzonna F (2019) Sunset time and the economic effects of social jetlag: evidence from US time zone borders. *J Health Econ* 65: 210–226
Glass L, Mackey MC (1979) A simple model for phase locking of biological oscillators. *J Math Biol* 7: 339–352
Glass L, Mackey MC (1988) *From Clocks to Chaos, the Rhythms of Life*. Princeton University Press, Princeton, N. J.
Goheer A et al. (2021) What influences the "when" of eating and sleeping? A qualitative interview study. *Appetite* 156: 104980
Gois S, Savi MA (2009) An analysis of heart rhythm dynamics using a three-coupled oscillator model. *Chaos, Solitons and Fract* 41: 2553–2565
Goldbeter A (Sept. 1995) A model for circadian oscillations in the *Drosophila* period protein (PER). *Proc Biol Sci* 261: 319–324
– (1996) *Biochemical oscillations and cellular rhythms: the molecular bases of periodic and chaotic behaviour*. Cambridge University Press
Goldbeter A, Dupont G, Berridge MJ (1990) Minimal model for signal-induced Ca^{2+} oscillations and for their frequency encoding through protein phosphorylation. *Proc Natl Acad Sci U S A* 87: 1461–1465
Goldbeter A, Lefever R (1972) Dissipative structures for an allosteric model. Application to glycolytic oscillations. *Biophys J* 12: 1302–1315 ISSN: 0006-3495
Goldbeter A, Gérard C, Leloup J-C (2010) Circadian rhythms and systems biology. *Med Sci (Paris)* 26: 49–56
Goldbeter A, Leloup J-C (2021) From circadian clock mechanism to sleep disorders and jet lag: Insights from a computational approach. *Biochem Pharmacol* 191: 114482
Golden SS, Ishiura M. JCH, Kondo T (1997) Cyanobacterial circadian rhythms. *Ann Rev Plant Physiol* 48: 327–354
Gonze D, Leloup JC, Goldbeter A (2000) Theoretical models for circadian rhythms in *Neurospora* and *Drosophila*. *C R Acad Sci III* 323: 57–67
Gonze D, Roussel MR, Goldbeter A (2002) A model for the enhancement of fitness in cyanobacteria based on resonance of a circadian oscillator with the external light-dark cycle. *J Theor Biol* 214: 577–297
Gonze D, Bernard S et al. (2005) Spontaneous synchronization of coupled circadian oscillators. *Biophys J* 89: 120–129
Goodwin BC (1965) "Oscillatory behavior in enzymatic control processes" *Advances in Enzyme Regulation* ed. by G Weber vol. 3 Pergamon, Oxford, UK: 425–438
Gooley JJ (2008) Treatment of circadian rhythm sleep disorders with light. *Ann Acad Med Singapore* 37: 669–676
Gould PD et al. (2018) Coordination of robust single cell rhythms in the *Arabidopsis* circadian clock via spatial waves of gene expression. *eLife* 7:
Grell KG (1985) Der Formwechsel des plasmodialen Rhizopoden Thalassomyxa australis n. G., n. Sp. *Protistologica* 21: 215–233
Griffith JS (1968) Mathematics of cellular control processes. I. Negative feedback to one gene. *J Theor Biol* 20: 202–208
Grone BP et al. (2011) Acute light exposure suppresses circadian rhythms in clock gene expression. *J Biol Rhythms* 26: 78–81

Grudzinski K, Zebrowski JJ (2004) Modeling cardiac pacemakers with relaxation oscillators. *Physica A Stat Mech Appl* 336: 153–162

Gu C, Yang H, Ruan Z (2017) Entrainment range of the suprachiasmatic nucleus affected by the difference in the neuronal amplitudes between the light-sensitive and light-insensitive regions. *Phys Rev E* 95: 042409

Gu C, Yang H, Wang M (2017) Dispersion of the intrinsic neuronal periods affects the relationship of the entrainment range to the coupling strength in the suprachiasmatic nucleus. *Phys Rev E* 96: 052207

Gu X, Le C et al. (2013) *Arabidopsis* FLC clade members form flowering-repressor complexes coordinating responses to endogenous and environmental cues. *Nat Commun* 4: 1947

Guerrero-Vargas NN et al. (2018) Shift-work: is time of eating determining metabolic health? Evidence from animal models. *Proc Nutr Soc* 77: 199–215

Gumowski I (1983) Analysis of oscillatory plant transpiration II. *J Interdisc Cycle Res* 14: 33–41

Guo J-H et al. (2020) Circadian misalignment on submarines and other non-24-h environments - from research to application. *Milit Med Res* 7: 39

Gupta A, Roth T et al. (2019) Shift work: a perspective on shift work disorder-is prevention the answer? *J Clin Sleep Med* 15: 1863–1865

Gupta CC, Centofanti S et al. (2019) Altering meal timing to improve cognitive performance during simulated nightshifts. *Chronobiol Int* 36: 1691–1713

Haefner JW, Buckley TN, Mott KA (1997) A spatially explicit model of patchy stomatal responses to humidity. *Plant, Cell Environ* 997: 1087–1097

Hamaguchi Y et al. (2015) Entrainment of mouse peripheral circadian clocks to <24 h feeding/-fasting cycles under 24 h light/dark conditions. *Sci Rep* 5: 14207

Hannay KM, Booth V, Forger DB (2019) Macroscopic models for human circadian rhythms. *J Biol Rhythms* 34: 658–671

Harrison EM, Gorman MR (2015) Rapid adjustment of circadian clocks to simulated travel to time zones across the globe. *J Biol Rhythms* 30: 557–562

Hastings JW, Sweeney BM (1957) On the mechanism of temperature independence in a biological clock. *Proc Natl Acad Sci U S A* 43: 804–811

Hastings MH, Maywood ES, Brancaccio M (2019) The mammalian circadian timing system and the suprachiasmatic nucleus as its pacemaker. *Biology* 8: 2079–7737

Heller HC, Ruby NF (2019) Functional interactions between sleep and circadian rhythms in learning and learning disabilities. *Handb Exp Pharmacol* 253: 425–440

Henslee EA et al. (2017) Rhythmic potassium transport regulates the circadian clock in human red blood cells. *Nat Commun* 8:

Hepler P, Lovy-Wheeler A (2006) "Calcium gradients and oscillations in the growing pollen tube" *Plant Physiol Biochem* ed. by L Taiz et al. 6th ed. chap. 14.1

Héricé C, Patel AA, Sakata S (2019) Circuit mechanisms and computational models of REM sleep. *Neurosci Res* 140: 77–92

Hernández-Rosas F, López-Rosas CA, Saavedra-Vélez MV (2020) Disruption of the molecular circadian clock and cancer: an epigenetic link. *Biochem Genet* 58: 189–209

Herzog ED, Block GD (1999) Keeping an eye on retinal clocks. *Chronobiol Int* 16: 229–247

Hess B, Boiteux A (1971) Oscillatory phenomena in biochemistry. *Ann Rev Biochem* 40: 237–258

Hess WR (2011) Cyanobacterial genomics for ecology and biotechnology. *Curr Opin Microbiol* 14: 608–614
Hodgkin AL, Huxley AF (1952) A quantitative description of membran current and its application to conduction and exitation in nerve. *J Physiol* 117: 50–544
Holdaway-Clarke TL et al. (2003) Effect of extracellular calcium, pH and borate on growth oscillations in *Lilium formosanum* pollen tubes. *J Exp Bot* 54: 65–72
Hong CI, Conrad ED, Tyson JJ (2007) A proposal for robust temperature compensation of circadian rhythms. *Proc Natl Acad Sci U S A* 104: 1195–1200
Hoppensteadt FC (1997) *An Introduction to the Mathematics of Neurons*. Cambridge University Press, Cambridge
Huang G, Wang L, Liu Y (Nov. 2006) Molecular mechanism of suppression of circadian rhythms by a critical stimulus. *EMBO J* 25: 5349–5357
Hulsegge G et al. (2019) Shift work, chronotype and the risk of cardiometabolic risk factors. *Eur J Public Health* 29: 128–134
Hurley J, Loros JJ, Dunlap JC (2015) Dissecting the mechanisms of the clock in *Neurospora*. *Meth Enzymol* 551: 29–52
Hussain F et al. (2014) Engineered temperature compensation in a synthetic genetic clock. *Proc Natl Acad Sci U S A* 111: 972–977
Ichiki A, Okumura K (2020) Diversity of dynamical behaviors due to initial conditions: Extension of the Ott-Antonsen ansatz for identical Kuramoto-Sakaguchi phase oscillators. *Phys Rev E* 101: 022211
Indic P et al. (2005) Comparison of amplitude recovery dynamics of two limit cycle oscillator models of the human circadian pacemaker. *Chronobiol Int* 22: 613–629
Ito-Miwa K et al. (2020) Tuning the circadian period of cyanobacteria up to 6.6 days by the single amino acid substitutions in KaiC. *Proc Natl Acad Sci U S A* 117: 20926–20931
Izhikevich EM (2007) *Dynamical Systems in Neuroscience*. MIT Academic Press, London, New York
Jacklet JW (1969) Electrophysiological organization of the eye of *Aplysia*. *J General Physiol* 53:
– (1989) *Neuronal and cellular oscillators*. vol. 2 Cellular clock Series Marcel Dekker NY
Jankowski KS, Linke M (2020) Angry night birds: Emotionality, activity and sociability temperament in adolescent chronotypes. *Chronobiol Int* 37: 652–659
Jasechko S et al. (2013) Terrestrial water flux dominated by transpiration. *Nature* 496: 347–350
Jessen NA et al. (2015) The glymphatic system: a beginner's guide. *Neurochem Res* 40: 2583–2599
Jewett ME, Forger DB, Kronauer RE (1999) Revised limit cycle oscillator model of human circadian pacemaker. *J Biol Rhythms* 14: 493–499
Jewett ME, Kronauer RE (1998) Refinement of a limit cycle oscillator model of the effects of light on the human circadian pacemaker. *J Theor Biol* 192: 455–465
Jewett ME, Kronauer RE, Czeisler CA (1991) Light-induced suppression of endogenous circadian amplitude in humans. *Nature* 350: 59–62
– (1994) Phase-amplitude resetting of the human circadian pacemaker via bright light: a further analysis. *J Biol Rhythms* 9: 295–314
Johnson CH, Kondo T (1992) Light pulses induce 'singular' behavior and shorten the period of the circadian phototaxis rhythm in the CW15 strain of *Chlamydomonas*. *J Biol Rhythms* 7: 313–327

Johnson CH, Egli M (2014) Metabolic compensation and circadian resilience in prokaryotic cyanobacteria. *Annu Rev Biochem* 83: 221–247

Johnson CH, Mori T, Xu Y (2008) A cyanobacterial circadian clockwork. *Curr Biol* 18: R816–R825

Johnson DA, Reid M et al. (2020) Associations of sleep duration and social jetlag with cardiometabolic risk factors in the study of Latino youth. *Sleep Health* 6: 563–569

Johnsson A (1973) Oscillatory transpiration and water uptake of Avena plants. I. Preliminary observations. *Physiol Plant*:

– (2015) Oscillations in Plant Transpiration. In Mancuso A and Shabala S (eds) "Rhythms in plants, 2nd ed. *Springer*:

Johnsson A, Boström A-C, Pedersen M (1993) Perturbation of the *Desmodium* leaflet oscillation by electric current pulses. *J Interdisc Cycle Res* 24: 12–32

Johnsson A, Brogardh T, Holje O (1979) Oscillatory transpiration rhythm of *Avena* plants: Perturbation experiments provide evidence for a stable point of singularity. *Physiol Plant* 45: 393–398

Johnsson A, Israelsson D (1968) Application of a theory for circumnutations to geotropic movements. *Physiol Plant* 21: 282–291

Johnsson A, Karlsson G (1971) "Biological rhythms: singularities in phase-shift experiments as predicted from a feedback model" *First European Biophysics Congress, 14 to 17 September, 1971, Baden near Vienna, Austria* Verlag der Wiener Medizinischen Akademie: 263–267

Johnsson A, Karlsson HG (1972) A feedback model for biological rhythms. I. Mathematical description and basic properties of the model. *J Theor Biol* 36: 153–174

Johnsson A, Solheim BGB, Iversen T-H (2009) Gravity amplifies and microgravitydecreases circumnutations in *Arabidopsis thaliana* stems: results from a spaceexperiment. *New Phytol* 182: 621–629

Jones MA et al. (2019) Arabidopsis JMJD5/JMJ30 acts independently of LUX ARRHYTHMO within the plant circadian clock to enable temperature compensation. *Front Plant Sci* 10:

Julius AA, Yin J, Wen JT (2019) Time optimal entrainment control for circadian rhythm. *PloS One* 14: e0225988

Kaladchibachi S et al. (2019) Optimization of circadian responses with shorter and shorter millisecond flashes. *Biol Lett-uk* 15: 20190371

Kalmus H (1935) Periodizität und Autochronie als zeitregelnde Eigenschaften der Organismen. *Biologia Generalis* 11: 93–114

– (1940) Jiurnal rhythms in the axolotl larva and in *Drosophila*. *Nature* 145: 72–73

Karlsson HG, Johnsson A (1972) A feedback model for biological rhythms. II. Comparisions with experimental results, especially on the petal rhythm of *Kalanchoe*. *J Theor Biol* 36: 175–194

Kerkhof GA (2018) Shift work and sleep disorder comorbidity tend to go hand in hand. *Chronobiol Int* 35: 219–228

Kervezee L, Cermakian N, Boivin DB (2019) Individual metabolomic signatures of circadian misalignment during simulated night shifts in humans. *PloS Biol* 17: e3000303

Keshvari M et al. (2020) Exploring the role of circadian clock gene and association with cancer pathophysiology. *Chronobiol Int* 37: 151–175

Kidd P, Young MW, Siggia ED (2015) Temperature compensation and temperature sensation in the circadian clock. *Proc Natl Acad Sci U S A* 112: E6284–E6292

Kim JK, Forger DB (2012) A mechanism for robust circadian timekeeping via stoichiometric balance. *Molecular systems biology* 8: 630 ISSN: 1744-4292 DOI: 10.1038/msb.2012.62
Kim P, Kaur M et al. (2020) The circadian clock-a molecular tool for survival in cyanobacteria. *Life (Basel)* 10: 365
King VM (1988) "Advances in the model for the circadian organisation of the Weta *Hemideina thoracica*" MA thesis Auckland University, New Zealand
Kinouchi K, Sassone-Corsi P (2020) Metabolic rivalry: circadian homeostasis and tumorigenesis. *Nat Rev Cancer* 20: 645–661
Kippert F, Lloyd D (1995) Rhythmic CO_2 formation in fermentizing and in respiring *Saccharomyces pombe* cultures. *Microbiol* 141: S888
Kleitman N (1939) *Sleep and Wakefulness*. University of Chicago Press
Klerman EB, Dijk DJ et al. (1996) Simulations of light effects on the human circadian pacemaker: implications for assessment of intrinsic period. *Am J Physiol* 270: R271–R282
Klerman EB, Brager A et al. (2022) Keeping an eye on circadian time in clinical research and medicine. *Clin Transl Med* 12:
Klerman EB, Rahman SA, St Hilaire MA (2020) What time is it? A tale of three clocks, with implications for personalized medicine. *J Pineal Res* 68: e12646
Kolbe I, Oster H (2019) Chronodisruption, metabolic homeostasis, and the regulation of inflammation in adipose tissues. *Yale J Biol Med* 92: 317–325
Kon N et al. (2021) Na+/Ca2+ exchanger mediates cold Ca2+ signaling conserved for temperature-compensated circadian rhythms. *Sci Adv* 7: eabe8132
Kostreva M, McNelis E, Clemens E (2002) Using a circadian rhythms model to evaluate shift schedules. *Ergonomics* 45: 739–763
Koumenis C, Eskin A (1992) The hunt for mechanisms of circadian timing in the eye of *Aplysia*. *Chronobiol Int* 9: 201–221
Krasnow R et al. (1981) "Measurements of *Gonyaulax* bioluminescence, including that of single cells" *Bioluminescence: Current Perspectives* ed. by K Nealson Burgess Publ. Minneapolis: 52–63
Krietsch KN et al. (2019) Sleep and weight-related factors in youth: A systematic review of recent studies. *Sleep Med Rev* 46: 87–96
Kronauer RE, Czeisler CA et al. (1982) Mathematical model of the human circadian system with two interacting oscillators. *Am J Physiol* 242: 3–17
Kronauer RE, Gunzelmann G et al. (2007) Uncovering physiologic mechanisms of circadian rhythms and sleep/wake regulation through mathematical modeling. *J Biol Rhythms* 22: 233–245
Kuramoto Y (1984) Cooperative dynamics of oscillator community, a study based on lattice of rings. *Prog Theor Phys Supp* 79: 223–240
Kurosawa G, Goldbeter A (2006) Amplitude of circadian oscillations entrained by 24-h light-dark cycles. *J Theor Biol* 242: 478–488
Kurosawa G, Iwasa Y (2005) Temperature compensation in circadian clock models. *J Theor Biol* 233: 453–468
Kutschera U, Briggs WR (Jan. 2016) Phototropic solar tracking in sunflower plants: An integrative perspective. *Ann Bot* 117: 1–8
Kuula L et al. (2018) Development of late circadian preference: sleep timing from childhood to late adolescence. *J Pediatr* 194: 182–189

Lakin-Thomas PL, Brody S, Coté GG (1991) Amplitude model for the effects of mutations and temperature on period and phase resetting of the *Neurospora* circadian oscillator. *J Biol Rhythms* 6: 281–297

– (1997) Temperature compensation and membrane composition in *Neurospora crassa*. *Chronobiol Int* 14: 445–454

Lakin-Thomas P (2019) Circadian rhythms, metabolic oscillators, and the target of rapamycin (TOR) pathway: the *Neurospora* connection. *Curr Genet* 65: 339–349

Lakin-Thomas PL (2006) Transcriptional feedback oscillators: maybe, maybe not... *J Biol Rhythms* 21: 83–92

Lakin-Thomas PL, Bell-Pedersen D, Brody S (2011) The genetics of circadian rhythms in *Neurospora*. *Adv Genet* 74: 55–103

Land MF, Fernald RD (1992) The evolution of eyes. *Annu Rev Neurosci* 15: 1–29

Leloup JC, Goldbeter A (Apr. 2001) A molecular explanation for the long-term suppression of circadian rhythms by a single light pulse. *Am J Physiol* 280: R1206–R1212

Leloup J-C, Goldbeter A (2003) Toward a detailed computational model for the mammalian circadian clock. *Proc Natl Acad Sci U S A* 100: 7051–7056

– (2004) Modeling the mammalian circadian clock: sensitivity analysis and multiplicity of oscillatory mechanisms. *J Theor Biol* 230: 541–562

– (2013) Critical phase shifts slow down circadian clock recovery: Implications for jet lag. *J Theor Biol* 333: 47–57 ISSN: 1095-8541

Lewis R, Saunders D (1987) A damped circadian oscillator model of an insect photoperiodic clock I. Description of the model based on a feedback control system. *J Theor Biol* 128: 47–59

Lewis RD (1976) The circadian rhythm of the weta *Hemideina thoracica* (Orthoptera): Free running rhythms, circadian rule and light entrainment. *Int J Chronobiol* 3: 241–254

– (1999) Control systems models for the circadian clock of the New Zealand weta, *Hemideina thoracica* (Orthoptera: Stenopelmatidae). *J Biol Rhythms* 14: 480–485

Lewis RD, Bullivant AG, King VM (1991) A dual pacemakers model for the circadian system of the insect *Hemideina thoracica*. *J Interdisc Cycle Res* 22: 293–309

Li H-X (2019) The role of circadian clock genes in tumors. *Oncotargets Ther* 12: 3645–3660

Liberman AR et al. (2018) Modeling strengthens molecular link between circadian polymorphisms and major mood disorders. *J Biol Rhythms* 33: 318–336

Lin H-H et al. (2020) Chemical modulation of circadian rhythms and assessment of cellular behavior via indirubin and derivatives. *Methods Enzymol*:

Lok R et al. (2020) Gold, silver or bronze: circadian variation strongly affects performance in Olympic athletes. *Sci Rep* 10: 16088

Lone SR et al. (2010) Circadian resonance in the development of two sympatric species of *Camponotus* ants. *J Insect Physiol* 56: 1611–1616

Loshchilov I et al. (2021) Conditions for the emergence of circumnutations in plant roots. *PloS One* 16: e0252202

Lu Z et al. (2016) Resynchronization of circadian oscillators and the east-west asymmetry of jet-lag. *Chaos* 26: 094811

Lunn RM et al. (2017) Health consequences of electric lighting practices in the modern world: a report on the national toxicology program's workshop on shift work at night, artificial light at night, and circadian disruption. *Sci Total Environ* 607: 1073–1084

Lutz H, Wendt W (2021) *Taschenbuch der Regelungstechnik*.
M. S (2022) Role of the reaction-structure coupling in temperature compensation of the KaiABC circadian rhythm. *PLoS Comput Biol.*:
Machado PB, Faria RB (May 2009) Modeling the complex bromate-iodine reaction. *J Phys Chem A* 113: 5338–5341
Mackey SR, Golden SS (2007) Winding up the cyanobacterial circadian clock. *Trends Microbiol* 15: 381–388
Malaguarnera R et al. (2020) Thyroid cancer and circadian clock disruption. *Cancers* 12: 3109
Malinowski JR, Laval-Martin DL, Edmunds LN (1985) Circadian oscillators, cell cycles, and singularities: light perturbations of the free-running rhythm of cell division in *Euglena*. *J Comp Physiol B* 155: 257–267
Martinez D, Carmo Sfreddo Lenz M do (2010) Circadian rhythm sleep disorders. *Indian J Med Res* 131: 141–149
Martino TA et al. (2008) Circadian rhythm disorganization produces profound cardiovascular and renal disease in hamsters. *Am J Physiol* 294: R1675–R1683
Mathew GM, Hale L, Chang A-M (2020) Social jetlag, eating behaviours and BMI among adolescents in the USA. *Br J Nutr* 124: 979–987
Maukonen M, Havulinna AS et al. (2020) Genetic associations of chronotype in the finnish general population. *J Biol Rhythms* 35: 501–511
Maukonen M, Kanerva N et al. (2016) The associations between chronotype, a healthy diet and obesity. *Chronobiol Int* 33: 972–981
McMahon DM, Burch JB et al. (2019) Relationships between chronotype, social jetlag, sleep, obesity and blood pressure in healthy young adults. *Chronobiol Int* 36: 493–509
McMahon DG, Iuvone PM, Tosini G (2014) Circadian organization of the mammalian retina: from gene regulation to physiology and diseases. *Prog Retin Eye Res* 39: 58–76
McSharry PE, Clifford GD (2006) "Models for ECG and RR interval processes" *Advanced Methods and Tools for ECG Data Analysis* ed. by GD Clifford, FJ Azuaje, PE McSharry Artech House Publishers: London
Melo MCA et al. (2017) Chronotype and circadian rhythm in bipolar disorder: A systematic review. *Sleep Med Rev* 34: 46–58
Merikanto I, Partonen T (2020) Increase in eveningness and insufficient sleep among adults in population-based cross-sections from 2007 to 2017. *Sleep Med* 75: 368–379
Mithani S, Fink AM (2019) Mathematical models of sleep and circadian rhythms: A case for using the 2-process model in neuroscience nursing. *J Neurosc Nurs* 51: 48–53
Miyazaki Y, Nisimura T, Numata H (2009) A circadian system is involved in photoperiodic entrainment of the circannual rhythm of *Anthrenus verbasci*. *J Insect Physiol* 55: 494–498
– (2012) Circannual rhythm in the varied carpet beetle, *Anthrenus verbasci*. *Prog Brain Res* 199: 439–456
– (2014) "Circannual rhythms in insects" *Annual, lunar, and tidal clocks* ed. by H Numata, B Helm Springer Japan chap. 3: 333–350
Mohd Azmi NAS et al. (2020) Consequences of circadian disruption in shift workers on chrononutrition and their psychosocial well-being. *Int J Environ Res Public Health* 17:
Morgan MN et al. (2019) The cancer clock is (not) ticking: links between circadian rhythms and cancer. *Clocks & Sleep* 1: 435–458

Morgenthaler TI et al. (2007) Practice parameters for the clinical evaluation and treatment of circadian rhythm sleep disorders. an american academy of sleep medicine report. *Sleep* 30: 1445–1459

Morin LP, Allen CN (2006) The circadian visual system, 2005. *Brain Res Rev* 51: 1–60

Mota MC et al. (2019) Association between social jetlag food consumption and meal times in patients with obesity-related chronic diseases. *PloS One* 14: e0212126

Mrosovsky N (1999) Masking: history, definitions, and measurement. *Chronobiol Int* 16: 415–429 ISSN: 0742-0528

Mukherji A et al. (2015) Shifting eating to the circadian rest phase misaligns the peripheral clocks with the master SCN clock and leads to a metabolic syndrome. *Proc Natl Acad Sci U S A* 112: E6691–E6698

Mullineaux CW (2014) Co-existence of photosynthetic and respiratory activities in cyanobacterial thylakoid membranes. *Biochim Biophys Acta* 1837: 503–511

Münch M et al. (2020) The role of daylight for humans: gaps in current knowledge. *Clocks & Sleep* 2: 61–85

Nagumo J, Arimoto S, Yoshizawa S (1962) An active pulse transmission line simulating nerve axon. *Proc IRE* 50: 2061–2070

Nakajima M Imai K IH et al. (2005) Reconstitution of circadian oscillation of cyanobacterial KaiC phosphorylation in vitro. *Science*:

Nanda KK, Hamner KC (1962) Investigations on the effect of "light break" on the nature of the endogenous rhythm in the flowering response of Biloxi soybean (*Glycine max* L. Merr.) *Planta* 58: 164–174

Nayak SK, Jegla T, Panda S (2007) Role of a novel photopigment, melanopsin, in behavioral adaptation to light. *Cell Mol Life Sci* 64: 144–154

Njus D, Sulzman FM, Hastings JW (1974) Membrane model for the circadian clock. *Nature* 248: 116–119

Noguchi T, Harrison EM et al. (2020) Circadian rhythm bifurcation induces flexible phase resetting by reducing circadian amplitude. *Eur J Neurosci* 51: 2329–2342

Noguchi T, Leise TL et al. (2017) Calcium circadian rhythmicity in the suprachiasmatic nucleus: cell autonomy and network modulation. *eNeuro* 4:

Numata H, Miyazaki Y, Ikeno T (2015) Common features in diverse insect clocks. *Zool Letters* 1: 10

Nunes MV (1981) A 'Simple Clock' Approch of Circadian Rhythms: An Easy Way to Predict the Clocks's Singularity. *J. theor. Biol.*:

O'Neill JS, Ooijen G van et al. (2011) Circadian rhythms persist without transcription in a eukaryote. *Nature* 469: 554–558

O'Neill JS, Reddy AB (Jan. 2011) Circadian clocks in human red blood cells. *Nature* 469 (7331): 498–503

Onai K Morishita M IS, K O, M I (2004) Circadian Rhythms in the ThermophilicCyanobacterium Thermosynechococcus elongatus: Compensation of Period Length over a WideTemperature Range. *J Bacteriol.*:

Oosterman JE, Wopereis S, Kalsbeek A (2020) The circadian clock, shift work, and tissue-specific insulin resistance. *Endocrinol* 161: 1–11

Oster H, Maronde E, Albrecht U (2002) The circadian clock as a molecular calendar. *Chronobiol Int* 19: 507–516
Osterkamp J (2017) *Medizin-Nobelpreis für die innere Uhr.* research rep. Spektrum der Wissensshaften
Ouyang Y et al. (1998) Resonating circadian clocks enhance fitness in cyanobacteria. *Proc Natl Acad Sci U S A* 95: 8660–8664
Palafox ML et al. (2019) Identification of metabolic indicators for cardiovascular risk in schoolchildren. *Rocz Panstw Zakl Hig* 70: 89–96
Patton AP, Hastings M (2023) The mammalian circadian time-keeping system. *J Huntingtons Disease*:
Pavlidis T (1971) Populations of biochemical oscillators as circadian clocks. *J Theor Biol* 33: 319–338
– (1973) *Biological oscillators: Their mathematical analysis.* Academic Press
Pedersen M, Johnsson A (1994) A study of the singularities in a mathematical model for circadian rhythms. *Biosystems* 33: 193–201
Pfeifer H (1966) *Elektronik für den Physiker III.* Akademie-Verlag Berlin
Phillips AJK, Clerx WM et al. (2017) Irregular sleep/wake patterns are associated with poorer academic performance and delayed circadian and sleep/wake timing. *Sci Rep* 7: 1–13
Phillips AJK, Czeisler CA, Klerman EB (2011) Revisiting spontaneous internal desynchrony using a quantitative model of sleep physiology. *J Biol Rhythms* 26: 441–453
Phillips DJ, Savenkova MI, Karatsoreos IN (2015) Environmental disruption of the circadian clock leads to altered sleep and immune responses in mouse. *Brain Behav Immun* 47: 14–23
Pikovsky A, Rosenblum M, Kurths J (2001) *Synchronization.* Cambridge University Press, Cambridge
Pilz LK et al. (2018) Sleep and light exposure across different levels of urbanisation in Brazilian communities. *Sci Rep* 8: 11389
Pittendrigh (1967) Circadian systems. I. The driving oscillation and its assay in Drosophila pseudoobscura. *Proc Nat Acad Sci 58(4)*:
Pittendrigh CS (1954) On temperature independence in the clock system controlling emergency time in *Drosophila. Proc Natl Acad Sci U S A* 40: 1018–1029
Pittendrigh CS, Caldarola PC (1973) General homeostasis of the frequency of circadian oscillations. *Proc Natl Acad Sci U S A* 70: 2697–701
Pittendrigh CS, Minis DH (1964) The entrainment of circadian oscillations by light and their role as photoperiodic clocks. *Amer Nat* 98: 261–294
– (1972) Circadian systems: Longevity as a function of circadian resonance in *Drosophila melanogaster. Proc Natl Acad Sci U S A* 69: 1537–1539
Plog BA, Nedergaard M (2018) The glymphatic system in central nervous system health and disease: past, present, and future. *Annu Rev Pathol* 13: 379–394
Postnova S, Lockley SW, Robinson PA (2018) Prediction of cognitive performance and subjective sleepiness using a model of arousal dynamics. *J Biol Rhythms* 33: 203–218
Pot GK (2018) Sleep and dietary habits in the urban environment: the role of chrono-nutrition. *Proc Nutr Soc* 77: 189–198
Potter GDM, Wood TR (2020) The future of shift work: circadian biology meets personalised medicine and behavioural science. *Front Nutrition* 7: 116

Prytz G (2001) "A biophysicsl study of oscillatory water regulation in plants. Measurements and models" PhD thesis Dept of Physics, Norwegian University of Scienc and Technology, Trondheim, Norway

Qiu M et al. (2019) Research on circadian clock genes in non-small-cell lung carcinoma. *Chronobiol Int* 36: 739–750

Raman S, Coogan AN (2020) A cross-sectional study of the associations between chronotype, social jetlag and subjective sleep quality in healthy adults. *Clocks & Sleep* 2: 1–6

Rangroo Thrane V et al. (2020) Twists and turns of ocular glymphatic clearance - new study reveals surprising findings in glaucoma. *Acta Ophthalmol* 99: e283–e284

Reeth O van et al. (1997) Comparative effects of a melatonin agonist on the circadian system in mice and Syrian hamsters. *Brain Research* 762: 185–194

Reid KJ et al. (2018) Impact of shift work schedules on actigraphy-based measures of sleep in hispanic workers: results from the Hispanic community health study/study of latinos ancillary sueño study. *Sleep* 41: 1–8

Rempe MJ et al. (2018) Mathematical modeling of sleep state dynamics in a rodent model of shift work. *Neurobiol Sleep Circadian Rhythm* 5: 37–51

Richard D. Bliss Page R. Painter AGM (1982) Role of feedback inhibition in stabilizing the classical operon. *Journal of Theoretical Biology*:

Richter K et al. (2020) Shiftwork and alcohol consumption: a systematic review of the literature. *Eur Addict Res*: 1–7

Rideout WC (1991) *Mathematical and Computer Modeling of Physiological Systems.*

Roach GD et al. (2018) 23rd International Symposium on Shiftwork and Working Time: Towards a Global Consensus. *Chronobiol Int* 35: 739–745

Roenneberg T, Colfax GN, Hastings JW (1989) A circadian rhythm of population behavior in *Gonyaulax polyedra*. *J Biol Rhythms* 4: 201–216

Roenneberg T, Allebrandt KV et al. (2012) Social jetlag and obesity. *Curr Biol* 22: 939–943

Roenneberg T, Winnebeck EC, Klerman EB (2019) Daylight saving time and artificial time zones - a battle between biological and social times. *Front Physiol* 10: 944

Rogers VE et al. (2020) A morning bright light therapy intervention to improve circadian health in adolescent cancer survivors: methods and preliminary feasibility. *J Pediatr Oncol Nurs* 38: 70–81

Ruoff P (1992) Introducing temperature-compensation in any reaction kinetic oscillator model. *J Interdisc Cycle Res* 23: 9–99

Ruoff P, Vinsjevik M et al. (1999a) The Goodwin modell Simulation the Effect of Cycloheximide and Heat Shok on the Sporulation of Neurospora crassa. *J. Theor. Biol[ogie* 196: 483–494

– (1999b) The Goodwin oscillator: on the importance of degradation reactions in the circadian clock. *J Biol Rhythms* 14: 469–479

Ruoff P, Christensen MK, Sharma VK (2005) PER/TIM-mediated amplification, gene dosage effects and temperature compensation in an interlocking-feedback loop model of the *Drosophila* circadian clock. *J Theor Biol* 237: 41–57

Ruoff P, Zakhartsev M, Westerhoff HV (2007) Temperature compensation through systems biology. *FEBS J* 274: 940–950

Samuelsson LB et al. (2018) Sleep and circadian disruption and incident breast cancer risk: An evidence-based and theoretical review. *Neurosci Biobehav Rev* 84: 35–48

Sancar G, Sancar C, Brunner M (2012) Metabolic compensation of the *Neurospora* clock by a glucose-dependent feedback of the circadian repressor CSP1 on the core oscillator. *Genes Dev* 26: 2435–2442

Scammell TE, Arrigoni E, Lipton JO (2017) Neural circuitry of wakefulness and sleep. *Neuron* 93: 747–765

Scheer FAJL et al. (2007) Plasticity of the intrinsic period of the human circadian timing system. *PLoS One* 2: e721

Scheper (1999) A Mathematical Model for the Intracellular Circadian Rhythm Generator. *The Journal of Neuroscience*:

Schuster M, Oberlinner C, Claus M (2019) Shift-specific associations between age, chronotype and sleep duration. *Chronobiol Int* 36: 784–795

Schweiger HG, Schweiger MFW (1977) Circadian rhythms in unicellular organisms: an endeavour to explain the molecular mechanism. *Int Rev Cytol* 51: 315–342

Segers P et al. (2003) Systematic ans pulmonary hemodynamics assed with a lumped-parameter heart-arterial interaction model. *Journal of Engineeing Mathematics*:

Serkh K, Forger DB (2014) Optimal schedules of light exposure for rapidly correcting circadian misalignment. *PloS Comput Biol* 10: e1003523

Shalit-Kaneh A et al. (2018) Multiple feedback loops of the *Arabidopsis* circadian clock provide rhythmic robustness across environmental conditions. *Proc Natl Acad Sci U S A* 115: 7147–7152

Shilts J, Chen G, Hughey JJ (2018) Evidence for widespread dysregulation of circadian clock progression in human cancer. *Peerj* 6: e4327

Silva CM et al. (2016) Chronotype, social jetlag and sleep debt are associated with dietary intake among Brazilian undergraduate students. *Chronobiol Int* 33: 740–748

Silyn-Roberts H, Engelmann W (1986) *Thalassomyxa australis*: A model organism for the evolution of circadian rhythms? *Endocyt C Res* 3: 239–242

Singh S et al. (2019) New *Drosophila* circadian clock mutants affecting temperature compensation induced by targeted mutagenesis of timeless. *Front Physiol* 10:

Skeldon AC, Derks G, Dijk D-J (2016) Modelling changes in sleep timing and duration across the lifespan: Changes in circadian rhythmicity or sleep homeostasis? *Sleep Med Rev* 28: 96–107

Skeldon AC, Dijk D-J, Derks G (2014) Mathematical models for sleep-wake dynamics: comparison of the two-process model and a mutual inhibition neuronal model. *PLoS One* 9: e103877

Skjåkødegård HF et al. (2020) Beyond sleep duration: Sleep timing as a risk factor for childhood obesity. *Pediatric Obes* 16: e12698

Skornyakov E et al. (2019) Cardiac autonomic activity during simulated shift work. *Ind Health* 57: 118–132

Smedler E, Uhlen P (2014) Frequency decoding of calcium oscillations. *Biochim Biophys Acta* 1840: 964–969

Smietanko A et al. (1988) *Thalassomyxa australis* rhythmicity II. No entrainment by light-dark-cycles and temperature cycles? *J Interdisc Cycle Res* 19: 235–240

Snyder MF, Rideout V (1968) Computer modeling of the human systemic arterial tree. *J. Biomechanics*:

Soest I van et al. (2020) Nonlinear phenomena in models of the circadian clock. *J R Soc Interface* 17: 20200556 ISSN: 1742-5662

Spoelstra K et al. (2016) Natural selection against a circadian clock gene mutation in mice. *Proc Natl Acad Sci U S A* 113: 686–691

St Hilaire MA et al. (2020) Prediction of individual differences in circadian adaptation to night work among older adults: application of a mathematical model using individual sleep-wake and light exposure data. *Chronobiol Int*: 1–8

Stefanovska A, Hocik M (2000) Spatial synchronization in the human cardiovascular system. *Prog Theor Phys Supp* 139: 270–282

Stefanovska A, Lotric MB et al. (2001) The cardiovascular system as coupled oscillators? eng *Physiol Meas* 22: 535–550

Stefanovska A, Luchinsky DG, McClintock PV (2001) Modelling couplings among the oscillators of the cardiovascular system. *Physiol Meas* 22: 551–564

Stefanovska A (2007) Coupled oscillators. Complex but not complicated cardiovascular and brain interactions. *IEEE Eng Med Biol Mag* 26: 25–29

Stehle JH et al. (2011) A survey of molecular details in the human pineal gland in the light of phylogeny, structure, function and chronobiological diseases. *J Pineal Res* 51: 17–43

Steinlechner S, Stieglitz A, Ruf T (2002) Djungarian hamsters; a species with a labile circadian pacemaker? Arrhythmicity under a light-dark cycle induced by short light pulses. *J Biol Rhythms* 17: 248–259

Stolarz M (2009) Circumnutation as a visible plant action and reaction: physiological, cellular and molecular basis for circumnutations. *Plant Signal Behav* 4: 380–387

Stoner L et al. (2018) Sleep and adiposity in preadolescent children: the importance of social jetlag. *Child Obes* 14: 158–164

Stothard ER et al. (2020) Early morning food intake as a risk factor for metabolic dysregulation. *Nutrients* 12:

Strogatz SH (1991) *Nonlinear Dynamics and Chaos – with applications to Physics, Biology, Chemistry and Engineering*. ed. by AWP Company

Sulli G, Lam MTY, Panda S (2019) Interplay between circadian clock and cancer: new frontiers for cancer treatment. *Trends Cancer* 5: 475–494

Swaminathan K, Klerman EB, Phillips AJK (2017) Are individual differences in sleep and circadian timing amplified by use of artificial light sources? *J Biol Rhythms* 32: 165–176

Sweeney BM (1976) "Evidence that membranes are components of circadian oscillators" *The molecular basis of circadian rhythms* ed. by JW Hastings, HG Schweiger Dahlem Konferenzen: 267–281

Takahashi M et al. (2018) Chronotype and social jetlag influence human circadian clock gene expression. *Sci Rep* 8: 10152

Taylor BJ, Hasler BP (2018) Chronotype and mental health: recent advances. *Curr Psychiatry Rep* 20: 59

Taylor WR, Dunlap JC, Hastings JW (1982) Inhibitors of protein synthesis on 80S ribosomes phase shift the *Gonyaulax* clock. *J Exp Biol* 97: 121–136

Tempaku PF et al. (2017) Characterization of bimodal chronotype and its association with sleep: A population-based study. *Chronobiol Int* 34: 504–510

Terauchi K et al. (2007) ATPase activity of KaiC determines the basic timing for circadian clock of cyanobacteri. *Proc Natl Acad Sci U S A* 104: 16377–16381

Thomas JM et al. (2020) Circadian rhythm phase shifts caused by timed exercise vary with chronotype. *JCI insight* 5: e134270
Thomas Heldt aEBS, Kamm RD, G.Mark R (2002) Computational modeling of cardiovascular response to orthostatic stress. *J Appl Physiol*:
Tietze U, Schenk C, Gamm E (2019) *Halbleiter-Schaltungstechnik*. Springer Berlin, Heidelberg
Torquati L et al. (2019) Shift work and poor mental health: a meta-analysis of longitudinal studies. *Am J Public Health* 109: e13–e20
Tortonese DJ et al. (2011) Experimental jetlag disrupts circadian clock genes but improves performance in racehorses after light-dependent rapid resetting of neuroendocrine systems and the rest-activity cycle. *J Neuroendocrinol* 23: 1263–1272
Touitou Y, Point S (2020) Effects and mechanisms of action of light-emitting diodes on the human retina and internal clock. *Environ Res* 190: 109942
Tseng Y-Y et al. (2012) Comprehensive modelling of the *Neurospora* circadian clock and its temperature compensation. *PloS Comput Biol* 8: e1002437
Tsuchiya Y et al. (2016) Effect of multiple clock gene ablations on the circadian period length and temperature compensation in mammalian cells. *J Biol Rhythms* 31: 48–56
Tyson JJ, Hong CI et al. (1999) A simple model of circadian rhythms based on dimerization and proteolysis of PER and TIM. *Biophys J* 77: 2411–2417
Tyson JJ (2022) From the Belousov-Zhabotinsky reaction to biochemical clocks, traveling waves and cell cycle regulation. *Biochem J* 479: 185–206
Tyson JJ, Albert R et al. (2008) Biological switches and clocks. *J R Soc Interface* 5: S1–S8
Ueda HR (2007) Systems biology of mammalian circadian clocks. *Cold Spring Harb Symp Quant Biol* 72: 365–380
Ukai H, Kobayashi TJ et al. (2007) Melanopsin-dependent photo-perturbation reveals desynchronization underlying the singularity of mammalian circadian clocks. *Nat Cell Biol* 9: 1327–1334
Ukai H, Ueda HR (2010) Systems biology of mammalian circadian clocks. *Annu Rev Physiol* 72: 579–603
Upadhyay A, Brunner M, Herzel H (2019) An inactivation switch enables rhythms in a *Neurospora* clock model. *Int J Mol Sci* 20: 2985
Upadhyaya SK, Rand RH, Cooke JR (1988) Role of stomatal oscillations ontranspiration. Assimiliation and water-use efficiency of plants. *Ecol Model* 41: 27–40
Van der Pol B (1927) Erzwungene Schwingungen in einem Kreis mit nichtlinearem Widerstand. *Philos Mag* 3:
Van Gelder RN, Buhr ED (Oct. 2016) Ocular photoreception for circadian rhythm entrainment in mammals. *Annu Rev Vision Sci* 2: 153–169
Verlande A, Masri S (2019) Circadian clocks and cancer: timekeeping governs cellular metabolism. *Trends Endocrinol Metab* 30: 445–458
Versteven M, Ernst K-M, Stanewsky R (2020) A robust and self-sustained peripheral circadian oscillator reveals differences in temperature compensation properties with central brain clocks. *Science* 23: 2873–2881
Vidal L, Morin LP (2007) Absence of normal photic integration in the circadian visual system: response to millisecond light flashes. *J Neurosci* 27: 3375–3382

Vitale JA et al. (2018) Biological rhythms, chronodisruption and chrono-enhancement: The role of physical activity as synchronizer in correcting steroids circadian rhythm in metabolic dysfunctions and cancer. *Chronobiol Int* 35: 1185–1197

Voigt RM et al. (2014) Circadian disorganization alters intestinal microbiota. *PloS One* 9: e97500

Walbeek TJ et al. (2019) Physiological, behavioral and environmental factors influence bifurcated circadian entrainment in mice. *Physiol Behav* 210: 112625

Walker M (2018) *Why we sleep*. Penguin

Wang R et al. (2004) Modelling periodic oscillation of biological systems with multiple timescale networks. *Syst Biol* 1: 71–84

Wehrens SMT et al. (2012) Mood, alertness, and performance in response to sleep deprivation and recovery sleep in experienced shiftworkers versus non-shiftworkers. *Chronobiol Int* 29: 537–548

Westerterp-Plantenga MS (2016) Sleep, circadian rhythm and body weight: parallel developments. *Proc Nutr Soc* 75: 431–439

Wever RA (1979) *The circadian system of man*. Springer, New York

Wever RA (1984) Towards a Mathematical Model of Circadian Rhythmicity. *Mathematical Models of the Circadian Sleep-Wake Cycle*:

Wever R (1963) Zum Mechanismus der biologischen 24-Stunden -Periodik, II. Mitteilung. Der Einfluss des Gleichwertes auf die Eigenschaft selbsterregter Schwingungen. *Kybernetik*:

Whitmore D, Block GD (1996) Cellular aspects of molluskan biochronometry. *Semin Cell Dev Biol* 7: 781–789

Wiegard A et al. (2020) Synechocystis KaiC3 displays temperature- and KaiB-dependent ATPase activity and is important for growth in darkness. *J Bacteriol* 202: 41

Wilson J et al. (2018) Habitual light exposure relative to circadian timing in delayed sleep-wake phase disorder. *Sleep* 41: 41

Winfree A (1970) Integrated view of resetting a circadian clock. *Journal of Theoretical Biology*:

Winfree AT (1967) Biological rhythms and the behavior of populations of coupled oscillators. *J Theor Biol* 16: 15–42

– (1980) *The geometry of biological timing*. Springer, New York, Heidelberg, Berlin

– (1983) Sudden cardia death: a problem in topology. *Sci Am* 248: 144–149

– (2001) *The geometry of biological time*. 2nd ed. Springer, New York

Wittmann M et al. (2006) Social jetlag: Misalignment of biological and social time. *Chronobiol Int* 23: 497–509

Woelders T et al. (2017) Daily light exposure patterns reveal phase and period of the human circadian clock. *J Biol Rhythms* 32: 274–286

Woelfle MA et al. (2004) The adaptive value of circadian clocks: an experimental assessment in cyanobacteria. *Curr Biol* 14: 1481–1486

Woller A, Gonze D (2013) The bird circadian clock: insights from a computational model. *J Biol Rhythms* 28: 390–402

– (2018) Modeling clock-related metabolic syndrome due to conflicting light and food cues. *Sci Rep* 8: 13641

Wong PM et al. (2015) Social jetlag, chronotype, and cardiometabolic risk. *J Clin Endocrinol Metab* 100: 4612–4620

Woolum J (1991) A re-examination of the role of the nucleus in generating the circadian rhythm in *Acetabularia*. *J Biol Rhythms* 6: 129–136
Yang Y-J et al. (2021) Evolution of stomatal closure to optimize water-use efficiency in response to dehydration in ferns and seed plants. *New Phytol* 230: 2001–2010
Yao X et al. (2022) Mathematical analysis of robustness of oscillations in models of the mammalian circadian clock. *PLoS Comput Biol* 18: e1008340
Ye Y et al. (2018) The genomic landscape and pharmacogenomic interactions of clock genes in cancer chronotherapy. *Cell Syst* 6: 314–328
Yokawa K, Baluška F (2018) Sense of space: Tactile sense for exploratory behavior of roots. *Commun Integr Biol* 11: 1–5
Yong M et al. (2016) Are chronotype, social jetlag and sleep duration associated with health measured by work ability index? *Chronobiol Int* 33: 721–729
Yoo CY et al. (2009) Regulationof transpiration to improve crop water use. *Crit Rev Plant Sci*: 410–431
Young MW (2018) Time travels: a 40-year journey from *Drosophila*'s clock mutants to human circadian disorders (Nobel Lecture). *Angew Chem-ger Edit* 57: 11532–11539
Zadeh-Haghighi H, Simon C (2022) Radical pairs can explain magnetic field and lithium effects on the circadian clock. *Sci Rep* 12: 269
Zebrowski JJ et al. (2007) Nonlinear oscillator model reproducing various phenomena in the dynamics of the conduction system of the heart. *Chaos* 17: 015121
Zeitzer JM, Dijk D-J et al. (2000) Sensitivity of the human circadian pacemaker to nocturnal light: melatonin phase resetting and suppression. *J Physiol* 526: 695–702
Zeitzer JM, Ruby NF et al. (2011) Response of the human circadian system to millisecond flashes of light. *PLoS One* 6(7): e22078
Zerbini G, Merrow M (2017) Time to learn: How chronotype impacts education. *Psych Journal* 6: 263–276
Zerón-Rugerio MF, Cambras T, Izquierdo-Pulido M (2019) Social jet lag associates negatively with the adherence to the Mediterranean diet and body mass index among young adults. *Nutrients* 11: 1756
Zerón-Rugerio MF, Hernáez Á et al. (2019) Eating jet lag: a marker of the variability in meal timing and its association with body mass index. *Nutrients* 11: 2980
Zhao Y et al. (2019) Shift work and mental health: a systematic review and meta-analysis. *Int Arch Occup Environ Health* 92: 763–793
Zheng et al. (2021) Environmental chemicals affect circadian rhythms: An underexplored effect influencing health and fitness in animals and humans. *Environment International*:
Zuraikat FM et al. (2020) Sleep regularity and cardiometabolic heath: is variability in sleep patterns a risk factor for excess adiposity and glycemic dysregulation? *Curr Diab Rep* 20: 38
Zwart BJ de et al. (2018) Pilot data on the association between social jetlag and obesity-related characteristics in Dutch adolescents over one year. *Sleep Med* 47: 32–35